Identifying and targeting LIM-domain loss in clear cell renal cell carcinoma

Dr. Katherine Jane Smith

MACantab, MBBS, MRCP

Submitted in partial fulfillment of the requirements of the
Degree of Doctor of Philosophy
March 2018

Statement of Originality

I, Katherine Jane Smith confirm that the research included within this thesis is my own work or that where it has been carried out in collaboration with, or supported by others, that this is duly acknowledged below and my contribution indicated. Previously published material is also acknowledged below.

I attest that I have exercised reasonable care to ensure that the work is original, and does not to the best of my knowledge break any UK law, infringe any third party's copyright or other Intellectual Property Right, or contain any confidential material.

I accept that the College has the right to use plagiarism detection software to check the electronic version of the thesis.

I confirm that this thesis has not been previously submitted for the award of a degree by this or any other university.

The copyright of this thesis rests with the author and no quotation from it or information derived from it may be published without the prior written consent of the author.

Signature:

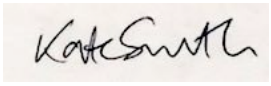

Date: 23.5.18

Publications

1 **Loss of LIM-domain proteins LIMD1, Ajuba and WTIP as a novel molecular mechanism for disease aetiology in clear cell renal cell carcinoma.**

Smith K, Sheaff M, Elia G, Clear A, Trevisan G, Foxler D, Bridge K, Shepherd S, Powles T, Sharp T.V. EJC 2016: 61, S1, S206.

Acknowledgements

I would like to thank Cancer Research UK for funding my PhD and making it possible to spend three years at Barts Cancer Institute.

Many people have helped me over the last few years. Firstly I would like to thank Dr. Tyson Sharp and Professor Tom Powles for supervising me and for their support direction.

The members of the Sharp lab were patient and understanding and I am very grateful for all of their input. In particular, thanks go to Dr. Dan Foxler, Dr. Katherine Bridge, Dr. John Foster, Dr. Kunal Shah, Dr. Dan Worth and Dr. Katy Davidson who were always generous with their time and knowledge.

Mr. George Elia and Dr. Andrew Clear provided invaluable advice and help with the immunohistochemistry. Many thanks to the consultant histopathologists and medical oncology colleague who reviewed my staining and helped me score what at times seemed like unending immunohistochemistry: Professor Mike Sheaff, Dr. Giorgia Trevisan and Dr. Scott Shepherd, your help was very much appreciated.

I must acknowledge my twin girls, Chloe and Scarlett who arrived towards the end of the PhD and temporarily derailed progress and put writing on hold. Finally, thank you to my husband Alastair and my mum Sue for providing support and looking after the girls at times so I could get on and write.

Abstract

Sequential use of targeted therapies has significantly improved overall survival in metastatic clear cell renal cell carcinoma (ccRCC) but durable responses remain rare. Improved prognostic and predictive algorithms are required.

3p loss is near ubiquitous in ccRCC. Functions of LIMD1 include regulation of hypoxia-inducible factors and microRNA-mediated gene silencing. LIMD1 loss/deregulation contributes to lung tumour formation and is associated with poor prognosis in breast cancer. The closely related family members, WTIP and Ajuba also regulate the hypoxic response and mediate micro-RNA silencing. Ajuba regulates the Hippo signaling pathway, controlling cell cycle and proliferation.

In vivo, loss of LIMD1 was observed in 49% of ccRCC samples. 76% of ccRCC tumours demonstrated reduced Ajuba staining and nuclear WTIP staining was reduced in 73% of tumours compared to matched control. Co-loss of LIMD1/Ajuba/WTIP was common. Using patient-derived tumour tissue from two prospective clinical trials, LIMD1, Ajuba and WTIP staining was correlated with clinico-pathological outcome data. With the exception of loss of Ajuba staining and tumour stage, staining and outcome data did not correlate.

The effects of LIMD1 loss on tumourigenesis were investigated using a paired lentiviral transduction system in ccRCC lines. LIMD1 loss did not affect cell migration, or cell cycle, however loss of LIMD1 was associated with greater hypoxic deregulation. A CRISPR-Cas-9 gene editing system was used to successfully knockout LIMD1 and Ajuba in a renal primary cell line.

Using a drug-screening platform, the topoisomerase-I inhibitor irinotecan was identified as a potentially synthetically lethal drug in association with LIMD1 loss. This was validated in a further ccRCC line and in non-renal lines.

Exploiting synthetic lethal approaches in ccRCC treatment has not been widely explored. Our data suggests that loss of LIMD1/Ajuba/WTIP is common and could

represent a predictive biomarker such that tumours with loss/low expression could be selectively targeted.

Table of Contents

List of Abbreviations

ABC	Activated B cell
ADC	Adenocarcinoma
Ago	Argonaute
AP-1	Activator protein-1
APS	Ammonium persulphate
ASXL	Additional sex comb-like
BEGM	Basal epithelial growth medium
BMI-1	Polycomb complex protein-1
BSA	Bovine serum albumin
C3CER1	Chromosome three commonly eliminated region 1
CAF	Cytokine and angiogenic factor
CBP	CREB-binding protein
ccA	Clear cell type A
ccB	Clear cell type B
ccRCC	Clear cell renal cell carcinoma
CRISPR	Clustered regularly interspaced palindromic repeat
crRNA	CRISPR-RNA
CSS	Cancer-Specific survival
CT	Computerised tomography
CTAD	C-terminal transactivation domain
CTLA-4	Cytotoxic T lymphocyte associated antigen-4
CUL2	Complex containing cullin 2
DAB	Diaminobenzadine
DC	Dendritic cells
DLBCL	Diffuse Large B-Cell Lymphoma
DMEM	Dulbecco's Modified Eagle Medium
DMSO	Dimethyl sulphoxide
ECL	Enhanced chemiluminescence
ECOG	Eastern Cooperative Oncology Group
ELISA	Enzyme-linked immunosorbant assay
EMT	Epithelial-mesenchymal transition

EPO	Erythropoeitin
ERK	Extracellular signal-regulated protein kinase
EtOH	Ethanol
FACS	Fluorescent Activated Cell Sorter
FBS	Foetal-bovine serum
FDA	Federal Drug Agency
GCB	Germinal Centre-B
GLUT-1	Glucose transporter-1
gRNA	Guide RNA
GWAS	Genome wide-association study
H_2O_2	Hydrogen peroxide
HAF	Hypoxia associated factor
HEPES-BSS	Hepes buffered saline solution
HHT	Homoharringtoine
HIF	Hypoxia inducible factor
HR	Hazard ratio
HR	High risk
HRE	Hypoxia response element
HRP	Horseradish peroxidase
IARC	International Agency for Research on Cancer
IFN	Interferon
IHC	Immunohistochemistry
IL-2	Interleukin-2
IL6	Interleukin-6
IP	Immunoprecipitation
IPAS	Inhibitory PAS domain protein
IR	Intermediate risk
IRF4	Interferon regulatory factor 4
JNK	C-Jun-NH2 kinase
LAR	Luciferase assay reagent
LATS	Large tumour suppressor 1
LAW	LIMD1/Ajuba/WTIP
LLN	Lower limit of normal
LOH	Loss of heterozygosity

LMP-1	Latent membrane protein-1
LR	Low risk
MAPK	Mitogen activated protein kinase
MAT	Matched adjacent tissue
mccRCC	Metastatic clear cell renal cell carcinoma
MDR	Multi-drug resistance
MeOH	Methanol
miRNA	MicroRNA
MKK	MAPK pathway kinases
mRNA	Messenger RNA
MRI	Magnetic resonance imaging
MSKCC	Memorial Sloan-Kettering Cancer Center
mTORC	mTOR complex
MVD	Microvessel density
NES	Nuclear export signal
NF2	Neurofibromin 2
NFκB	Nuclear factor kappa-light-chain enhancer of activated B cells
NHGRI	National Human Genome Research Institute
NK	Natural killer
NLS	Nuclear localisation signal
NO	Nitric oxide
NPI	Nottingham Prognostic index
NTAD	N-terminal transactivation domain
ODD	Oxygen dependent degradation
OS	Overall survival
PAM	Protospace adjacent motif
PARP	PolyADP-ribose polymerase
PAS	PER-ARNT-SIM
PBS	Phosphate-buffered saline
PD-1	Programmed death receptor-1
PDGF	Platelet derived growth factor
PDGF-RTK	PDGF receptor tyrosine kinase
PDL-1	Programmed death receptor-1 ligand
PET	Positron emission tomography

PFS	Progression free survival
PHD	Prolyl hydroxylase
PLB	Passive lysis buffer
PN	Partial nephrectomy
pRB	Retinoblastoma protein
PRISMA	Preferred reporting items for systematic review
PS	Performance status
PTH-RP	Parathyroid hormone related protein
PVDF	Polyvinylidene fluoride
RCC	Renal cell carcinoma
RFS	Relapse free survival
RISC	RNA silencing construct
RN	Radical nephrectomy
RPMI	Roswell Park Memorial Institute-1640 medium
RPTEC	Renal proximal tubular epithelial cell
SCC	Squamous cell carcinoma
SCID	Severe combined immune deficiency
SCNA	Somatic copy number alteration
SDS-PAGE	Sodium dodecyl sulphate polyacrylamide gel electrophoresis
SEER	Surveillance, epidemiology and end results
shRNA	Short hairpin RNA
siRNA	Short interfering RNA
SNP	Single nucleotide polymorphism
T-reg	Regulatory T cell
TCGA	The Cancer Genome Atlas
TEMED	N,N,N',N'-tetramethylethylenediamine
TGF	Transforming growth factor
TK-Renilla	Thymidine kinase Renilla
TKI	Tyrosine kinase inhibitor
TMA	Tissue microarray
TMB	Tetramethylbenzidine
TNM	Tumour/node/metastasis
TNS	Tissue neutralising solution

TNS	Trypsin neutralising solution
TRAF	TNF-receptor associated factors
TSG	Tumour suppressor gene
TSP	Tumour suppressor protein
UISS	University of California Los Angeles Integrated Staging System
ULN	Upper limit of normal
US	Ultrasound
VEGF	Vascular epithelial growth factor
VEGF-R	Vascular epithelial growth factor receptor
VEGF-RTK	VEGF receptor tyrosine kinase
VHL	Von Hippel Lindau
wGII	Weighted genomic instability
WTI	Wilm's tumour protein 1
WTIP	Wilms tumour-1 interacting protein
YAP	Yes-associated protein

Chapter 1 Introduction

1.1 LIM proteins

The LIM domain is a tandem zinc-finger structure that functions as a modular protein-binding interface (Kadrmas and Beckerle 2004). Rich in cysteine and histidine residues, and common to a small group of homeo-domain transcription factors, the LIM domain is known to be critical in mediating protein-protein interactions and is present in a wide variety of eukaryotic proteins with diverse biological functions (Feuerstein, Wang et al. 1994, Pawson and Nash 2003). Specificity of binding of target proteins enables LIM proteins to fulfil a wide array of biological functions (Wu, Durick et al. 1996).

Individual LIM domains are made up of approximately 55 amino acids with 8 highly conserved predominantly cysteine and histidine residues located at defined intervals (Kadrmas and Beckerle 2004). Several LIM proteins are localised only in the nucleus and have clear transcriptional roles during development, most however can interact with the actin cytoskeleton and shuttle between the nucleus and the cytoplasm modulating communication between cytoplasmic and nuclear compartments (Nix, Fradelizi et al. 2001, Kadrmas and Beckerle 2004).

LIMD1, Wilms tumour-1 interacting protein (WTIP) and Ajuba are members of the Zyxin family of LIM-domain containing proteins, proteins with both nuclear and cytosolic localisation domains that function as important scaffold proteins (Kadrmas and Beckerle 2004).

1.2 The Zyxin family of LIM domain containing proteins

There are seven members of the Zyxin family of LIM-domain containing proteins. Phylogenetic analysis sub-divides the family into the Ajuba sub-family, comprising LIMD1, Ajuba and WTIP, and the Zyxin sub-family, LPP, Trip6, Zyxin and migfilin Proteins in each sub-family have differential roles, with members of the Zyxin family preferentially localising to sites of cell adhesion, where they play a critical role in mediating cytoskeletal arrangements (Kadrmas and Beckerle 2004). Members of the Ajuba family localise to both the cytoplasm and the nucleus (Kadrmas and Beckerle 2004).

1.2.1 LIMD1, Ajuba and WTIP

Located on chromosome 3p21.3, *LIMD1* has eight exons, encoding a 676 amino-acid protein with a pre-LIM and LIM domain-containing region. The proline/serine rich pre-LIM region contains a nuclear export signal (NES), whilst the LIM domain region retains conserved LIM domain regions required for nuclear localisation properties (**Figure 1.1**). (Sharp, Munoz et al. 2004, Sharp, Al-Attar et al. 2008).

LIMD1, like other LIM domain containing proteins shuttles between the nucleus and cytoplasm, the equilibrium of which is towards nuclear export (Kadrmas and Beckerle 2004). Its stable structural core helps facilitate high-affinity binding to specific protein partners, facilitating its role as an adapter protein (Kadrmas and Beckerle 2004).

Ajuba, located on chromosome 14q11.2, encodes a 538-amino acid protein, which shares considerable homology with LIMD1. Ajuba contains the characteristic tandemly arranged LIM domains in the C-terminus and has both a pre-LIM encoded NES and a LIM domain encoded nuclear localisation signal (NLS) critical for its role in signal transduction (**Figure 1.1**).

The 430 amino acid protein WTIP is 19q13.1 encoded and acts as a binding partner of the Wilms tumour protein (WT1), a transcription factor essential for normal nephron formation. Again, WTIP contains both NES and NLS and shuttles between the nucleus and cytoplasm, the C terminal PDZ domain, plays a key role in the formation and function of signal transduction complexes (**Figure 1.1**). Within the nucleus, WTIP represses WT1 activated transcription (Srichai, Konieczkowski et al. 2004).

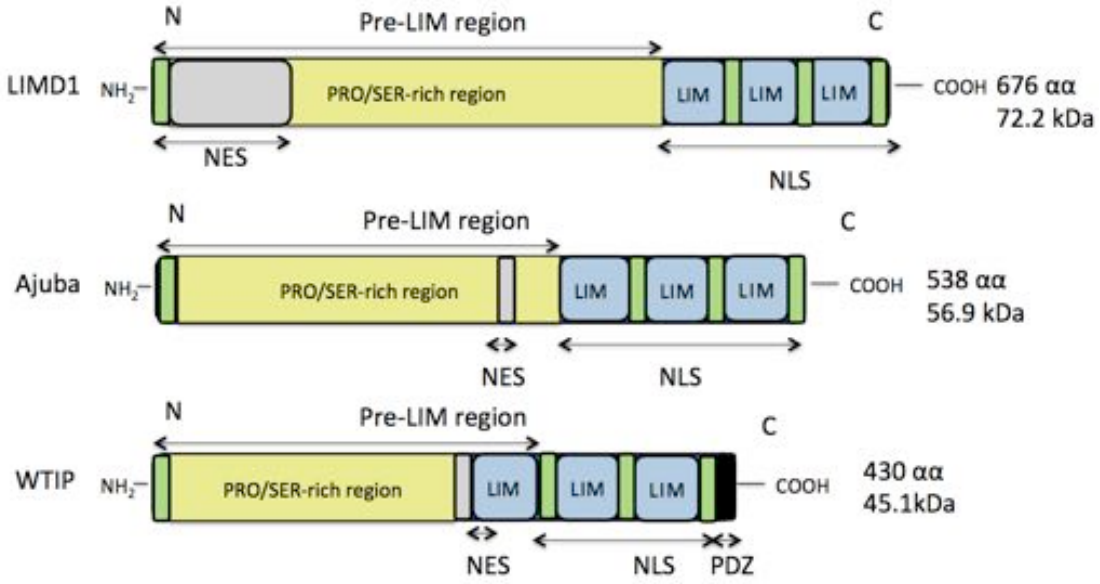

Figure 1.1: Schemata of LIMD1, Ajuba and WTIP structure. The pre-LIM region is proline/serine rich and encodes a nuclear export signal (NES). The LIM domain region contains a NLS and tandem zinc-finger motifs critical in mediating protein-protein interactions. WTIP contains a PDZ domain, a common structural domain that plays a key role in the formation and function of signal transduction complexes.

1.3. Loss of chromosome 3 commonly eliminated region (C3CER1) in tumourigenesis

Imrie *et al* used an elimination test assay to demonstrate that 3p21.3 chromosomal loss is frequent through loss of heterozygosity (LOH), driving malignant growth in severe combined immuno-deficiency (SCID) mice. After four passages in SCID mice, microcell hybrids originally containing an intact chromosome 3 generated from two alternative donors were analysed by comparative chromosome painting, reverse painting and polymerase chain reaction (PCR) marker analysis. Analysis demonstrated frequent loss of 3p with associated preservation of 3q (Kholodnyuk, Kost-Alimova et al. 1997).

More recent studies have demonstrated that the 3p21.3 region is frequently lost by LOH in many human tumours, in particular breast, lung, gastric, colorectal, ovarian, renal and head and neck carcinomas and it has consequently become known as the chromosome 3, commonly eliminated region 1 (C3CER1) (Lerman and Minna 2000, Yang, Yoshimura et al. 2002, Chakraborty, Dasgupta et al. 2003, Petursdottir, Thorsteinsdottir et al. 2004). The C3CER1 spans approximately 2.4 Mega bases and contains 32 genes, including the tumour suppressor gene *LIMD1* (Kost-Alimova and

Imreh 2007). Although a number of roles for LIMD1 have been characterised, relatively little is known about how loss/deregulation contributes to cellular transformation and tumourigenesis.

1.4 LIMD1 loss/deregulation is associated with tumourigenesis in a number of solid malignancies

1.4.1 LIMD1 loss in lung carcinoma

In lung carcinoma, LIMD1 loss has been characterised as playing a critical role in tumourigenesis (Sharp, Al-Attar et al. 2008). In a panel of 100 human lung squamous cell carcinomas (SCCs), the majority of tumours stained immunohistochemically for LIMD1 had reduced LIMD1 staining compared to matched non-cancerous, control tissue (Sharp, Al-Attar et al. 2008). In lung adenocarcinoma (ADC), comparison of LIMD1 mRNA levels between ADC and adjacent normal alveolar epithelium demonstrated lower levels of LIMD1 mRNA in tumour compared to the matched, control tissue (Sharp, Munoz et al. 2004).

Limd1^{-}/$^{-}$ mice challenged with the carcinogen urethane developed more tumours, which were also of increased size compared to wild type *Limd1* proficient mice (Sharp, Al-Attar et al. 2008). When *Limd1*$^{-/-}$ mice were bred with mice expressing oncogenic *K-Ras*^{G12D}, mice heterozygous for *K-Ras*^{G12D} developed a greatly increased tumour number and tumour volume compared to control *Limd1*$^{+}$/$^{+}$ mice heterozygous for *K-Ras*^{G12D} when exposed to the carcinogen urethane. Loss of *Limd1* in these mice increased mortality: at 12 months *K-Ras*^{G12D}/*Limd1*$^{-}$/$^{-}$ mice had a 90% mortality rate compared to 30% in the *K-Ras*^{G12D}/*Limd1*$^{+}$/$^{+}$ *mice* (Sharp, Al-Attar et al. 2008) (**Figure 1.2**).

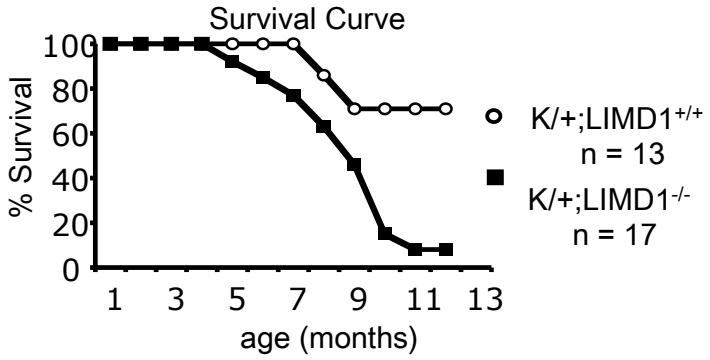

Figure 1.2 Deletion of *Limd1* increases mortality in K-Ras^{G12D} mice. *Limd1*$^{-/-}$ mice heterozygous for *K-Ras*^{G12D} developed more tumours than *Limd1*$^{+/+}$ mice expressing oncogenic *K-Ras*^{G12D} after urethane challenge. *Limd1* deficient mice had a significantly shorter OS compared to *Limd1* proficient control. Taken from (Sharp, Al-Attar et al. 2008)

In lung ADC, interrogation of the National Human Genome Research Institute (NHGRI) sponsored tumour sequencing project revealed that copy number alterations of *LIMD1* were common, with *LIMD1* deletions occurring in 32% of tumours compared to matched control tissue. However, sequencing of all 8 exons and intron-exon boundaries revealed no *LIMD1* mutations in the 188 ADC samples. Deletion of *LIMD1* was observed more commonly than for some other frequently deleted genes in the C3CER1 region and occurred more commonly than that observed for known lung tumour suppressor genes e.g. *p53* (**Figure 1.3)** (Sharp, Al-Attar et al. 2008).

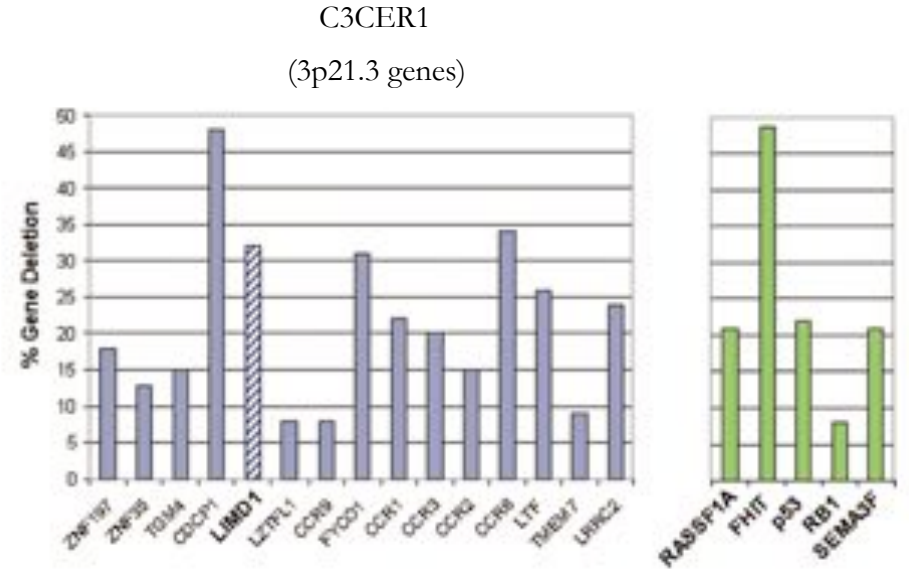

Figure 1.3 *LIMD1* gene deletion and surrounding 3p21.3 genes in human lung adenocarcinomas

Histogram demonstrating the percentage gene deletion for the indicated *C3CER1* gene cluster as determined by interrogation of the NHGRI-sponsored tumour suppressor protein (TSP) dataset of lung adenocarcinoma tumour compared to matched, normal tissue. Indicated genes are arranged relative to their 3p21.3 spatial location. For reference, other known tumour suppressor genes (TSGs) (*p53* and *Rb)* and putative 3p TSG deletions are shown. Taken from (Sharp, Al-Attar et al. 2008).

Recent as yet, unpublished work by our group in lung adenocarcinoma, re-analysing data from the TCGA Research Network using new data available via cBioportal suggests that LIMD1 deletion is much more common than previously described. cBioportal (http://cbioportal.org) is web resource that helps facilitate the analysis and visualisation of cancer genomic data (Gao, Aksoy et al. 2013).

The cBioportal platform now allows the interrogation of gene copy number at an individual sample level, enabling the investigation of both deep and shallow gene deletions, rather than deep deletion data only as was previously available. Copy number analysis assigns a predicted copy number value according to the following key:

-2	Deep deletion. Possibly a homozygous deletion
-1	Shallow deletion. Possibly a heterozygous deletion
0	Diploid
1	Low-level gain
2	High-level amplification.

Analysis of 516-lung adenocarcinoma samples and 501 lung squamous cell carcinomas identified shallow and deep combined *LIMD1* deletions and this combined analysis demonstrated that gene deletion was much higher than previously identified and comparable to known highly mutated driver mutations (**Figure 1.4**). Both shallow and deep LIMD1 deletions are likely to contribute to loss of gene expression, albeit to different degrees.

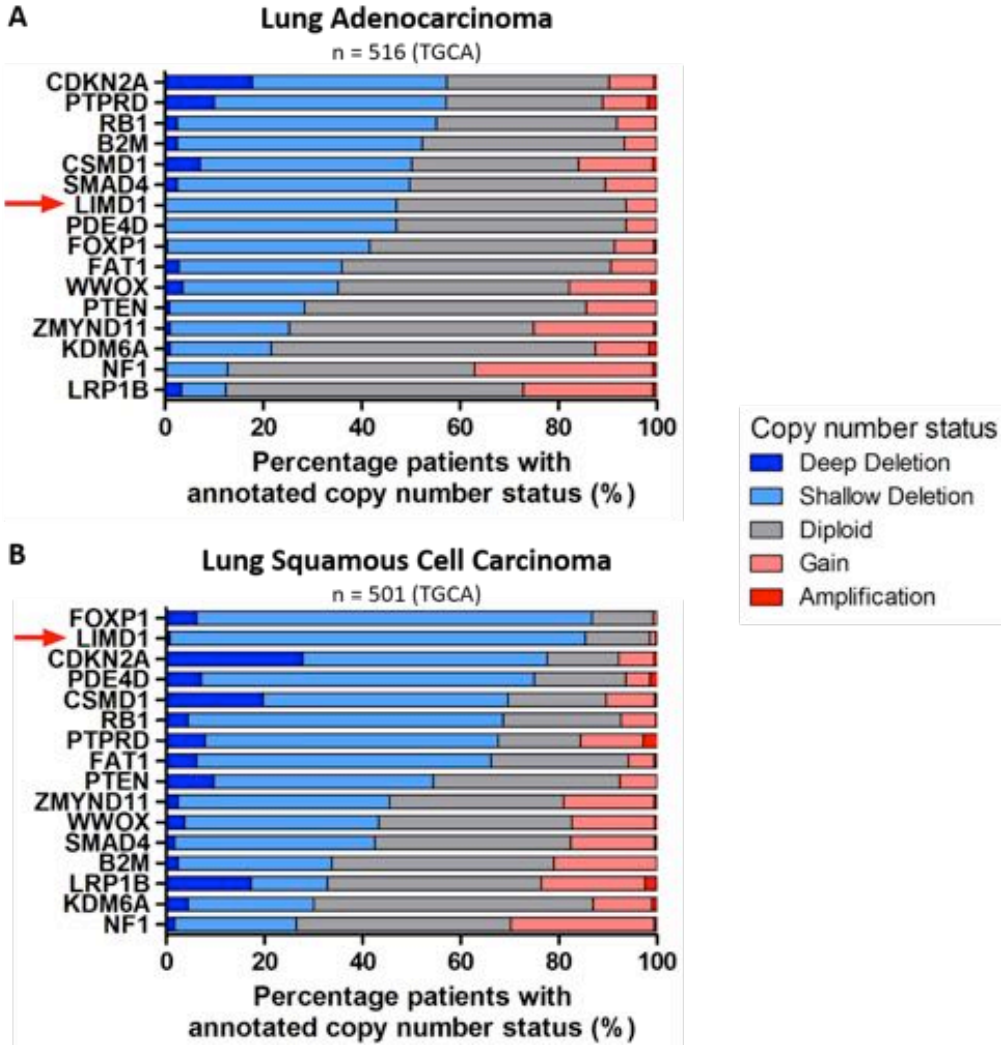

Figure 1.4. cBioPortal analysis of LIMD1 loss in adenocarcinoma and squamous cell carcinoma of the lung. Genes are ordered by percentage loss from greatest to smallest. **(A)** In lung adenocarcinoma, 0.2% of tumours contain a deep *LIMD1* deletion and 46.9% contain a shallow *LIMD1* deletion. **(B)** In squamous cell carcinoma, 0.8% of tumours contain a deep *LIMD1* deletion and 84.6% contain a shallow *LIMD1* deletion. Graphs generated by Dr John Foster (2017, unpublished).

1.4.2 LIMD1 loss in breast carcinoma

Using a tissue microarray (TMA) containing breast cancer tissue and self-matched adjacent normal and distal normal tissue, Spendlove *et al* demonstrated that intense LIMD1 staining was observed in the epithelial cells of terminal duct lobular units and that reduced LIMD1 staining was common in breast tumour (Spendlove, Al-Attar et al. 2008). Using TMAs constructed using tissue obtained from patients with operable breast carcinoma, LIMD1 immunohistochemistry (IHC) was correlated with clinico-pathological data with 495 histospots valid for analysis. Interestingly, subcellular localisation of LIMD1 appeared important in driving breast cancer tumourigenesis. Absence of nuclear LIMD1 staining strongly correlated with reduced patient survival, increased tumour size, higher histological grade and worse Nottingham Prognostic Index (NPI) score, a classification that stratifies tumours from excellent prognosis type to poor prognosis type. The authors hypothesised that this was related to reduced overall total LIMD1 staining (Sharp, Munoz et al. 2004, Spendlove, Al-Attar et al. 2008).

1.4.3 LIMD1 loss in head and neck carcinoma

Chakraborty *et al* had previously identified that LOH at 3p21.3 was common in head and neck carcinomas (Chakraborty, Dasgupta et al. 2003) and that *LIMD1* deletion/changes in methylation patterns were significantly associated with the development of dysplastic head and neck lesions (Ghosh, Ghosh et al. 2008). Analysis of 25 dysplastic head and neck lesions and 58 head and neck squamous cell carcinomas (SCCs) revealed that 94% of samples contained *LIMD1* alterations, predominantly deletions and changes in methylation patterns, with mutations more commonly observed in the SCC samples than the dysplastic lesions. Most of the mutations were present in and around the retinoblastoma protein (pRb)-binding domain of exon 1 and most resulted in truncated, non-functional LIMD1 (Ghosh, Ghosh et al. 2008).

1.4.4 LIMD1 expression in Diffuse Large B-Cell lymphoma (DLBCL)

Gene expression profiling has enabled the division of DLBCL into two major cell- of origin phenotypes, germinal centre B (GCB) cell like, which typically have a favourable prognosis and poorer prognosis, activated B cell (ABC) like (Wright, Tan et al. 2003).

Use of such gene expression based subtype analysis in the routine clinical setting is however expensive, time consuming and rarely practical. Xu *et al* identified a two-gene signature the LIMD1-MYBL1 index, which they compared against the gold standard Affymetrix-based standard. *MYBL1* belongs to the Myb oncogene family of transcription factors, which regulate the proliferation and differentiation of different haematopoeitic cells (Golay, Basilico et al. 1996).

Xu *et al* demonstrated that ABC tumours typically demonstrated high *LIMD1* expression, and GCB tumours high *MYBL1* expression. Tested against the gold standard Affymetrix method, the Index achieved excellent sensitivity for both ABC and GCB subgroups and Overall Survival (OS) rates were significantly different between the two groups stratified using this index, with highly expressing LIMD1 tumours demonstrating poor prognosis as expected. This simple analysis platform stratifies tumours into two prognosis groups, without the need for a gene expression based platform, which may not be routinely practical in clinical practice. The author hypothesised that given LIMD1's role as a positive regulator of Nuclear Factor-kappa-light chain enhancer of activated B cells (NF-κB) in osteoclast differentiation that over-expression of LIMD1 may contribute to the upregulation of the NF-κB pathway in ABC-DLBCL (Xu, Tan et al. 2015).

1.5 Ajuba deregulation in tumourigenesis

1.5.1 Ajuba loss in malignant mesothelioma

In a panel of 24 malignant mesothelioma cell lines, Tanaka *et al* demonstrated by Western blotting that 18 of the 24 cell lines (75%) demonstrated significant reduction in

Ajuba expression compared to an immortalised control mesothelial cell line, with 15 cell lines demonstrating no Ajuba expression. The immunohistochemical analysis of 20 malignant mesothelial specimens also demonstrated frequent reduction in staining for Ajuba with 5 samples (25%), demonstrating no Ajuba staining and 11 (55%), demonstrating little staining for Ajuba (Tanaka, Osada et al. 2015).

1.5.2. Ajuba expression in oesophageal squamous cell carcinoma

Ajuba overexpression has been associated with tumourigenesis in oesophageal SCC. Analysis of 179 oesophageal SCC samples compared to matched adjacent tissue (MAT), demonstrated significant Ajuba overexpression within the tumour samples, with mean expression levels 2.15 times greater than those in the MAT ($p<0.001$). Analysis of immunohistochemical (IHC) staining for Ajuba in 81 tumour samples from the same cohort compared to corresponding non-tumour, demonstrated high Ajuba staining in 70% of tumour samples compared to only 20% of non-tumour samples ($p<0.001$). Associated *in vitro* experiments demonstrated that Ajuba overexpression promoted oesophageal SCC colony formation and cell growth as well as cell migration (Shi, Chen et al. 2016).

1.5.3 Ajuba deregulation in colorectal carcinoma

A similar observation of Ajuba upregulation was noted in colorectal cancer specimens and cell lines. Analysis of Ajuba levels in a high-throughput microarray dataset of 34, tumour samples demonstrated significant Ajuba up-regulation compared to non-tumour control. *In vitro*, Western blot analysis of 7 colorectal cancer cell lines compared to non-tumour control demonstrated Ajuba overexpression in all cancer cell lines, with an associated upregulation of Ajuba mRNA levels. In this cohort, no significant differences in LIMD1 or WTIP levels were observed compared to control (Liang, Zhang et al. 2014).

1.6. WTIP loss in human disease

No studies to data have demonstrated a clear role for WTIP deregulation in tumourigenesis. 19q13.11 deletion syndrome is associated with developmental delay and intellectual disabilities, speech disturbance, growth retardation and hypospadias with WTIP identified as the most likely candidate gene (Gana, Veggiotti et al. 2012).

1.7 Characterised functions of LIM-domain containing proteins

1.7.1 LIMD1 is required for microRNA-mediated gene silencing

MicroRNAs (miRNAs) are small, non-coding RNA molecules, of approximately 22 nucleotides that function as post-transcriptional silencers of gene expression by forming base pair interactions with messenger RNA (mRNA) (Filipowicz, Bhattacharyya et al. 2008).

MiRNAs are critical in the temporal regulation of development (He and Hannon 2004) and in addition changes in miRNA expression patterns are implicated in driving tumourigenesis in a range of human malignancies with both over-expression and down-regulation contributing to malignant transformation (Cummins, He et al. 2006, Roldo, Missiaglia et al. 2006). In ccRCC for example miR-16, miR-452 and miR-224 are frequently up regulated (Jung, Mollenkopf et al. 2009).

MiRNAs are generated in a two-step pathway. Most reside in inter-genic or intronic gene regions and are transcribed into primary-miRNA (pri-miRNA) transcripts by RNA polymerase II (James, Wong et al. 2012). These pri-miRNA transcripts are then processed into hairpin precursor miRNA molecules (pre-miRNA) 70-100 nucleotides in length by a complex containing the Drosha RNase and the double strand RNA-binding protein DGCR8 (Han, Lee et al. 2006) (James, Wong et al. 2012). The pre-miRNA then translocates to the cytoplasm in an exportin-5 dependent manner and the complex is processed by DICER into ~20 nucleotide duplexes with 2 nucleotide 3' overhangs. One strand of the duplex is selected as the mature miRNA and the remaining strand degraded (James, Wong et al. 2012).

Specifically, miRNAs regulate gene expression by assembling alongside the Argonaute (Ago) protein into miRNA induced silencing complexes (miRISCs). The specific miRNA, guides the bound Ago protein to complementary mRNA target sequences, which results in post-transcriptional mRNA silencing and/or degradation of the mRNA sequence (Filipowicz, Bhattacharyya et al. 2008). The microRNA-induced silencing complex (miRISC) is a large multi-subunit complex, in which AGO drives the recruitment of GW182/TNRC6 proteins, scaffold proteins critical for the formation of the miRISC and their downstream effector complexes (Braun, Huntzinger et al. 2013) . In turn, translational repression, mRNA destabilisation and degradation of target mRNAs is achieved by the recruitment of effector proteins to the miRISC such as those involved in de-capping, DCP1/2, RNA unwinding, DDX6, and de-adenylation, CCR4-NOT (**Figure 1.5**) (Chekulaeva, Parker et al. 2010, Chekulaeva, Mathys et al. 2011, Chen, Boland et al. 2014).

There are four human AGO proteins (AGO1-4) which appear to demonstrate a degree of functional redundancy with respect to miRNA loading/target recognition with the functionally dominant AGO determined by protein expression levels (Dueck, Ziegler et al. 2012). Recent work however suggests that differential regulation of the AGOs by signalling pathways is important and that the AGOs are not fully interchangeable.

LIMD1, Ajuba and WTIP localise to cytoplasmic P-bodies, sites of miRNA/mRNA interaction where mRNAs accumulate and are subjected to degradation or storage (James, Wong et al. 2012). These LIM-domain proteins facilitate miRNA-mediated silencing through their interaction with components of the miRISC (James, Zhang et al. 2010) (Bridge, Shah et al. 2017).

James *et al* identified LIMD1, Ajuba and WTIP co-localisation in cytoplasmic P-bodies alongside components of the miRISC, specifically eIF4E, DCP-2 and RCK/p54, AGO2 and GW182. Subsequent immunoprecipitation (IP) experiments demonstrated that all three proteins interact with components of the miRISC: AGO2, RCK, DCP2 and eIF4E (James, Zhang et al. 2010).

Using LIMD1 short hairpin (shRNA)-directed knockdown and rescue lines, James *et al* demonstrated that LIMD1, Ajuba and WTIP are critical effectors of miRNA-mediated

gene silencing, with siRNA-targeted depletion resulting in significant de-repression of miRNA mediated silencing. In addition, all three proteins were able to bind to the mRNA 5' m^7GTP cap structure and could be co-purified with endogenous eIF4E using m^7GTP-Sepharose beads, leading them to propose that all three proteins act as a molecular scaffold protein, facilitating an association between the core miRISC and the eIF4E/m^7GTP-cap structure of the mRNA (James, Zhang et al. 2010)

Recent work by Bridge *et al* has updated this model with the demonstration that the Akt3-mediated phosphorylation of AGO2 (S387) promotes an interaction with LIMD1, which acts as a molecular 'clamp' facilitating the interaction of AGO2 with TNRC6A and the miRISC (**Figure 1.5**) ((Bridge, Shah et al. 2017).

Using a Renilla luciferase reporter construct with five targeted or non-targeted miR-99/100 binding sites in the 3' UTR, siRNA-mediated knockdown of AGO2, TRNC6A or LIMD1 all resulted in significant de-repression of the reporter construct whereas knockdown of AGO1, 3 or 4 did not. Interestingly, by using a CRISPR-Cas-9 system to genetically ablate LIMD1 in HELA cells, repression of the miR99/100 reporter was equivalent in the paired LIMD1 proficient and deficient cells. Further analysis demonstrated that there was a switch in AGO utilisation in the LIMD1$^{-/-}$ line to AGO-3, and that AGO-3 depletion produced an equivalent de-repression in this reporter in the LIMD1 deficient compared to proficient line. In the LIMD1 deficient HELA cell line, AGO3 interaction with GWI82 was achieved through a switch in LIM protein to WTIP (Bridge, Shah et al. 2017). A diagram of the proposed interaction of LIMD1/WTIP with components of the miRISC is shown in **Figure 1.5**.

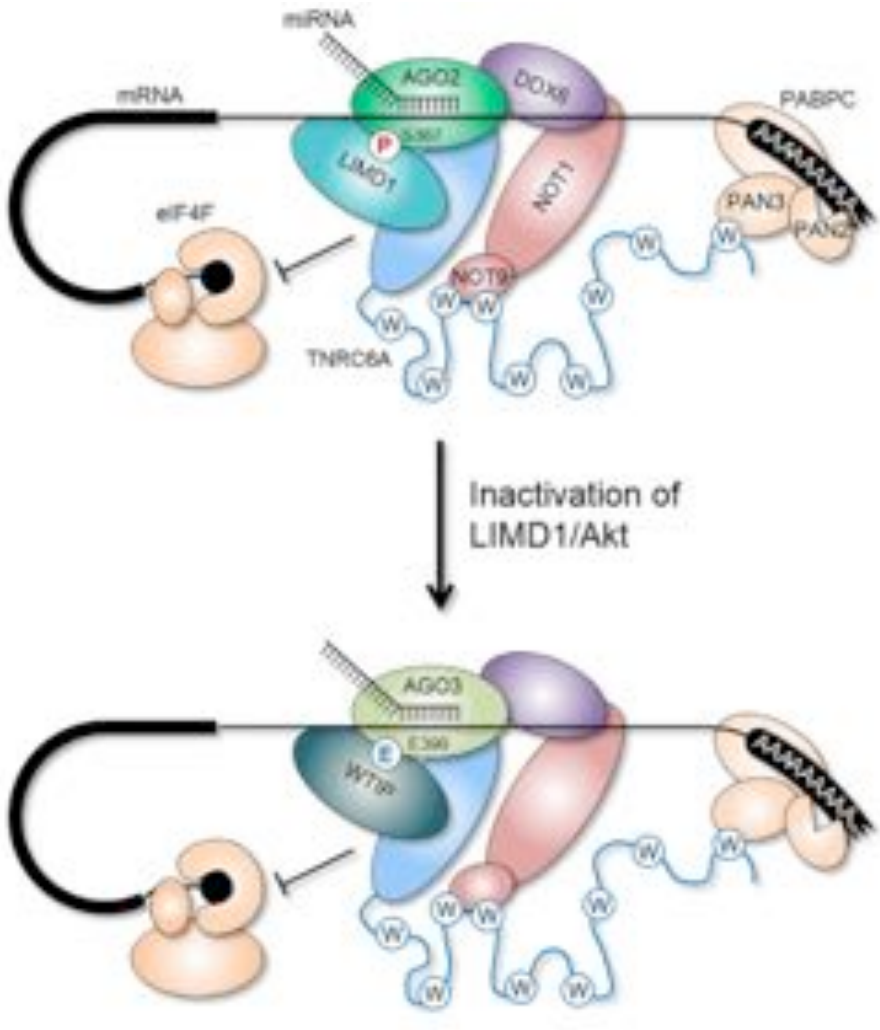

Figure 1.5. Proposed model for the formation of an inhibitory closed-loop complex mediating miRNA mediated silencing. In LIMD1 proficient cells, LIMD1 phosphorylation at S387 by Akt3 facilitates the interaction of AGO2 with TNRC6A and the downstream effector DDX6. In the absence of LIMD1, there is a switch in LIM protein and AGO, with WTIP forming a complex with AGO3 and TNRC6A. Taken from (Bridge, Shah et al. 2017)

miRNA downregulation can drive tumourigenesis in multiple tumour types including ccRCC, through the deregulation of gene expression (He and Hannon 2004, Huang, Dai et al. 2009). Loss of LIMD1/WTIP with consequent deregulation of the miRISC and reduced miRNA induced post-transcriptional gene silencing, could be an important mechanism for driving tumourigenesis in ccRCC.

1.7.2 LIMD1 regulation of hypoxia inducible factors (HIF)

Hypoxia is a common consequence of the rapid growth of many solid tumours including ccRCC and functions as a critical driver and regulator of a network of gene expression, at both translational and post-translational levels (Hockel and Vaupel 2001) (Schito and Semenza 2016). HIFs are transcriptional regulators that regulate oxygen-dependent gene expression resulting in the expression of genes that are critical for the regulation of cell survival and angiogenesis (Carroll and Ashcroft 2005) (Poon, Harris et al. 2009, Schito and Semenza 2016).

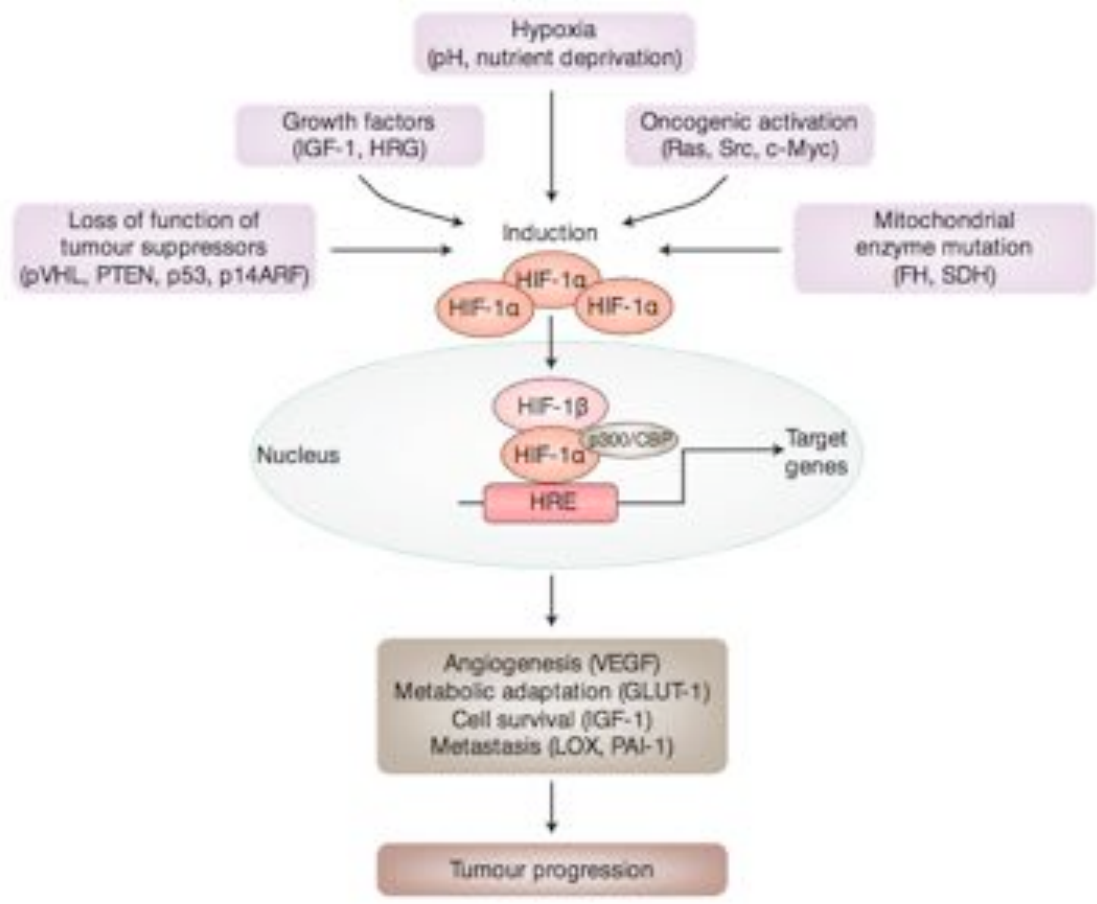

Figure 1.6 Activation of the HIF pathway in renal cell carcinoma.

Micro-environmental changes such as hypoxia, changes in pH and nutrient deprivation, changes in growth factors and genetic changes can lead to a loss of function of tumour suppressors and oncogenic activation in turn driving tumourigenesis. Increased HIFα translocates to the nucleus, heterodimerises with HIFβ and recruits co-activators e.g. p300/CBP, which in turn activate the transcription of multiple genes involved in angiogenesis, metabolic adaptation, cell survival and metastases. Adapted from (Poon, Harris et al. 2009).

There are three prolyl hydroxylases PHD1, 2 and 3 that regulate HIF. A further critical oxygen dependent regulator of HIF-α is factor inhibiting HIF (FIH-1), which acts independently of the HIF regulation by PHDs (Webb, Coleman et al. 2009).

In normoxia, the PHDs hydroxylate two conserved proline residues on HIF-α, which leads to the binding of the von Hippel-Lindau (VHL) tumour suppressor and subsequent VHL mediated poly-ubiquitylation and degradation of HIF-α via the proteasome (**Figure 1.7**) (Jaakkola, Mole et al. 2001). Of the three PHDs, PHD2 is thought to represent the more critical oxygen sensor in the regulation of HIFα (Appelhoff, Tian et al. 2004). Work by the Sharp group has demonstrated that LIMD1 is a critical regulator of the hypoxic response through HIF1α regulation (Foxler, Bridge et al. 2012).

Co-immunoprecipitation (IP) assays with X-press tagged LIMD1, Ajuba and WTIP proteins and PHDs 1, 2 and 3 demonstrated that LIMD1 bound to all three of the PHDs, with WTIP and Ajuba binding only to PHD1 and 3. In a direct binding assay, recombinant LIMD1 was found to bind directly to glutathione-S-transferase (GST)-PHD-2. Hypothesising that LIMD1 formed a PHD-LIMD1-VHL active complex to regulate HIF-1α, the group demonstrated that endogenous LIMD1 co-immunoprecipitated with PHD2 whilst IP of endogenous VHL resulted in co-immunoprecipitation of elongin B and cullin 2, (adapter proteins that help facilitate proteasomal degradation via VHL), as well as co-immunoprecipitation of LIMD1 and PHD2. *In vivo* co-immunoprecipitation studies with the pre-LIM region of LIMD1 (LIMD1Δ472-676) and LIM-domain region LIMD1Δ1-467) revealed PHD2 bound to the pre-LIM region and VHL to the LIM-domain region.

As predicted, overexpression of LIMD1 resulted in significantly reduced hypoxic response element (HRE) driven luciferase reporter assay and this was further increased with co-expression of exogenous PHD2. In hypoxia, LIMD1-depleted cells exhibited an exaggerated increase in HIF1α protein levels.

Given that in normoxia degradation of HIF1α is the result of hydroxylation and ubiquitylation within the oxygen-dependent degradation domain (ODD) of HIF1α, the relationship between increased LIMD1 expression and levels of ODD were investigated

and as predicted, increased LIMD1 expression resulted in reduced levels of ODD whilst LIMD1 depletion resulted in increased ODD expression.

Given the PHD2-LIMD1-VHL binding model hypothesis, PHD2/VHL non-binding LIMD1 mutants would be expected to be unable to induce ODD or HIF degradation and this was confirmed *in vitro*, confirming that associated PHD hydroxylase and/or VHL ubiquitin-ligase is required for functional LIMD1 regulation of this pathway (Foxler, Bridge et al. 2012).

An overview of the role of LIMD1 in this pathway in both normoxia and hypoxia is shown in **Figure 1.7**.

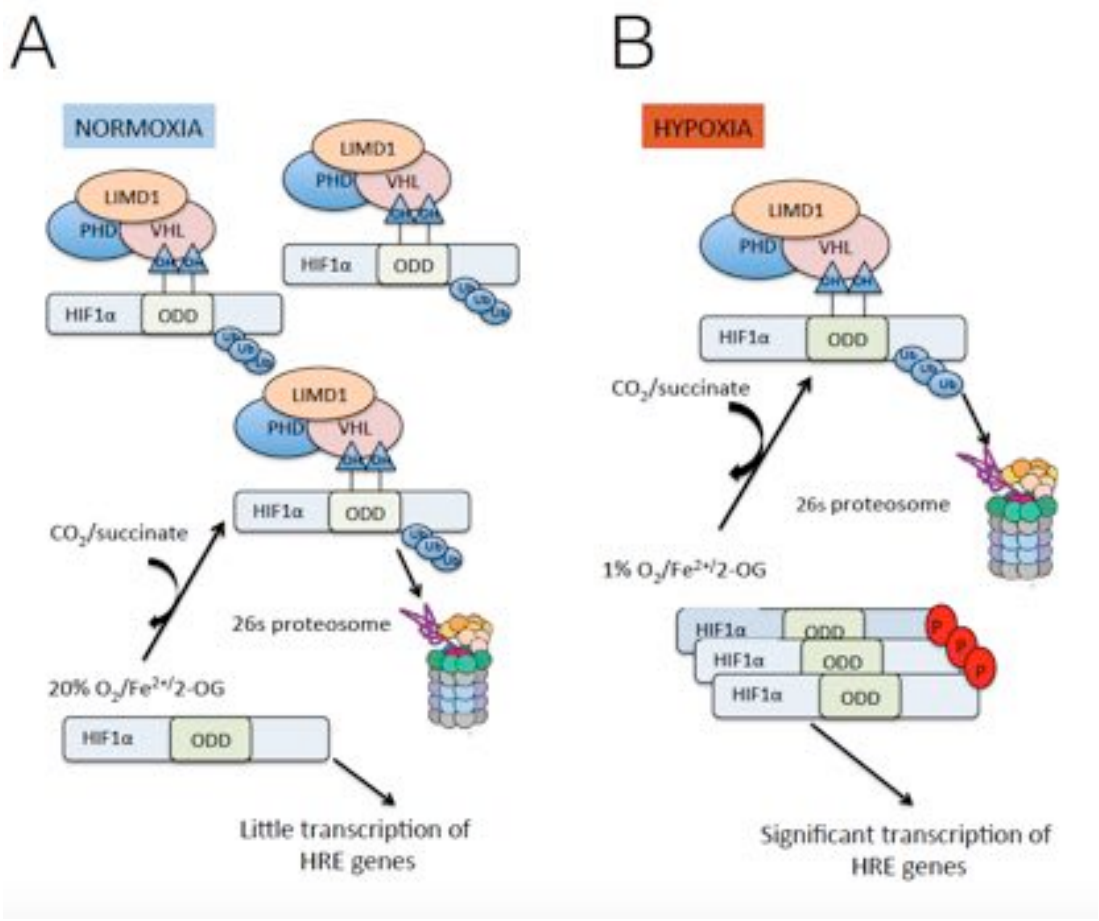

Figure 1.7 LIMD1 forms a molecular scaffold to simultaneously bind VHL and PHD to form a VHL-LIMD1-PHD complex that targets HIF1α for degradation via the proteasome **A** In normoxia, a significant proportion of HIF1α is hydroxylated and LIMD1 interacts with PHD2 through its pre-LIM region and with VHL through the LIM domain to link the proteins into one complex and promote significant HIF1α degradation via the proteasome. **B** In hypoxia, LIMD1 still engages an active pool of PHD2 and VHL to enable a degree of HIF1α modification and

degradation but there is a significant increase in HIF1α, a proportion of which becomes phosphorylated and transcriptionally active. Adapted from (Foxler, Bridge et al. 2012)

1.7.3 LIMD1 interacts with the retinoblastoma protein and represses E2F-driven transcription

The retinoblastoma 1 gene *RB1* is an archetypal tumour suppressor (Knudson 1971). pRb binds to the E2F family of transcription factors and upon binding acts as a critical negative regulator of the cell cycle, controlling entry into S-phase through the regulation of the G1/S checkpoint (Dimova and Dyson 2005). In addition, E2F family members play a critical role in the regulation of genes with other cell cycle functions, notably DNA repair and recombination, differentiation and development, and the regulation of apoptosis (Dimova and Dyson 2005).

LIMD1 has been characterised as a binding partner for pRb leading in turn to the repression of E2F-driven transcription (Sharp, Munoz et al. 2004). Sharp *et al* performed a yeast two-hybrid screen to identify binding partners of pRb using full-length pRb fused to the GAL4 DNA binding domain. This interaction was confirmed with the use of an *in vitro* pull-down assay with [S^{35}] methionine-labelled LIMD1, confirming that amino acids 326-628 of LIMD1 interact with amino acids 763-928 in the C-terminus of pRb. E2F luciferase reporter assays were then undertaken in HEK-293-T cells to assess LIMD1 regulation of E2F1-driven transcription. This demonstrated that LIMD1 represses E2F1 driven transcription in a LIMD1 concentration-dependent manner. LIMD1 deletion mutants were then examined for their ability to repress E2F driven transcription. Deletion of the pRb-binding domain resulted in a greater than 50% reduction in the ability of LIMD1 to repress E2F mediated transcription (**Figure 1.8**) (Sharp, Munoz et al. 2004).

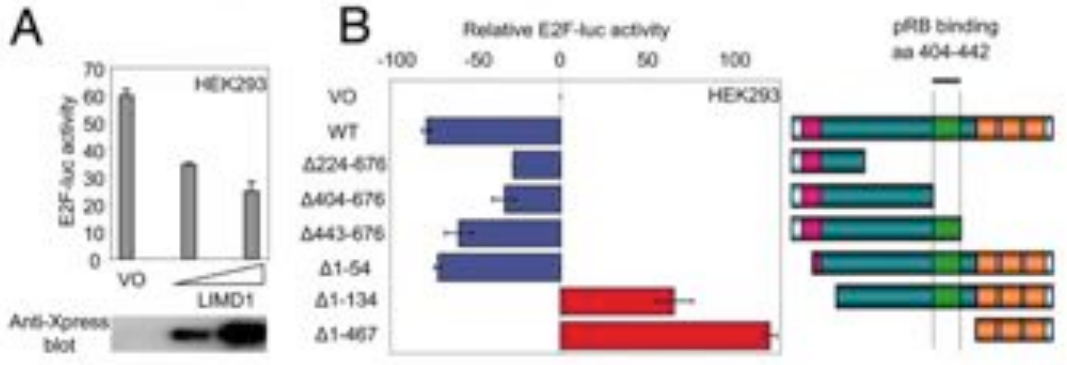

Figure 1.8. LIMD1 represses E2F driven transcription. A. HEK-293 cells were transiently transfected with an empty vector or LIMD1 expression vector and luciferase activity determined 48 hours later in the presence of the E2F luciferase reporter. Western blotting for LIMD1 was undertaken. **B.** The ability of LIMD1 to repress E2F-luciferase driven transcription depends on the presence of the pRB-binding domain. Adapted from (Sharp, Munoz et al. 2004),

1.7.4 LIMD1 is a regulator of bone remodelling

Bone homeostasis is maintained by the balance between osteoclast mediated bone resorption and osteoblast mediated bone formation (Tanaka, Nakayamada et al. 2005). Crosstalk between these two processes is critical for maintaining this homeostatic relationship. Both osteoblasts and osteoclast progenitors are localised in the bone marrow: osteoblasts derive from the mesenchymal bone marrow stromal cell lineage and osteoclasts from bone marrow derived macrophages (Tanaka, Nakayamada et al. 2005). Osteoclast differentiation is regulated by a number of proteins: in particular by the receptor activator of NF-kB ligand RANK-L. Activation of NF-kB through the binding of RANK-L facilitates the association with TNF-receptor associated factors (TRAFs) in particular TRAF6 which in turn bind to proteins within a multiprotein complex known as the sequestrome which includes the protein p62, leading to the activation of a signalling cascade which activates genes critical for osteoclast development (Feng, Zhao et al. 2007). LIMD1 can bind to both p62 and TRAF6 and in addition during osteoclast differentiation LIMD1 levels are induced (Feng, Zhao et al. 2007)(**Figure 1.9**). Work by Luderer *et al* has also demonstrated that LIMD1 influences osteoblast progenitor numbers, differentiation and function with *LIMD1*$^{-/-}$ osteoblasts displaying increased mineralisation and differentiation (Luderer, Bai et al. 2008).

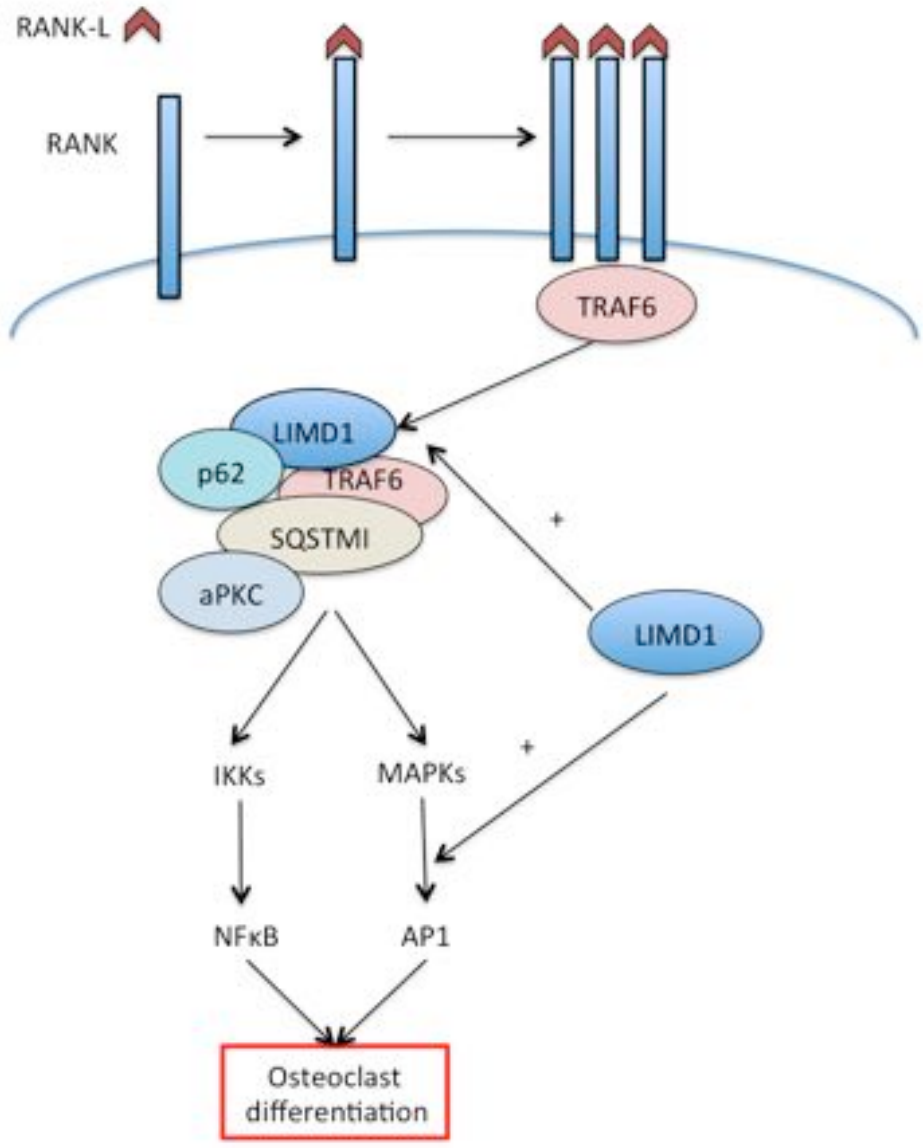

Figure 1.9 RANK-L mediated osteoclast differentiation is regulated by LIMD1. RANK-L binding to its receptor, results in receptor activation and trimerisation. In turn this facilitates an association with TRAF proteins, in turn facilitating the formation of a sequestrome, a multiprotein complex including p62 and atypical protein kinase C (aPKc). Activation of the enzyme IκB kinase (IKK) phosphorylates IκBα, which leads to its dissocation from NFκB and degradation via the proteasome. The activated NFκB translocates to the nucleus and binds and activates DNA response elements. MAPK pathway activation activates Activator protein-1 (API)/Fos, and influences downstream transcription and osteoclast differentiation. LIMD1 can bind TRAF6 and p62 and acts as a positive regulator of AP1.

1.7.5 LIMD1 and Latent membrane protein 1 (LMP-1) in EBV latency

The Epstein Barr virus (EBV) is a powerful driver of malignancy, particularly in HIV-associated cancers and head and neck cancers (Boshoff and Weiss 2002). The EBV

Latent membrane protein 1 (LMP-1) is a pleiotrophic growth factor that promotes cell growth and transformation *in vitro* and in transgenic mice (Thornburg, Kulwichit et al. 2006). This oncogenicity is in part mediated through the activation of NFkB pathways and LIMD1 as outlined is known to bind TRAF6 and enhances the ability of TRAF6 to activate AP1 in osteoblasts (Feng, Zhao et al. 2007). The oncogenic transcription factor Interferon regulatory factor 4 (IRF4), is a transcription factor essential for the development of T cells and is a marker of the ABC subtype of DLBCL-considered to be of poorer prognosis. IRF4 and LIMD1 levels have been shown to correlate in a range of haematological malignancies, including EBV-driven ones (Wang, Yao et al. 2014). Wang *et al* demonstrated that IRF-4 and NFkB bind to the LIMD1 promoter in EBV transformed cells, and that LIMD1 expression is up-regulated by IRF-4 and NFkB downstream of LMP1. In EBV transformed cells, co-immunoprecipitation assays with LMP1 deletion mutants confirmed that the cytoplasmic activating domains, CTAR1 and CTAR2 of LMP-1 interact with LIMD1 and as expected with TRAF-6 and that deletion of both domains ablated its ability to interact with LIMD1. Interestingly, over-expresison of full length LMP1 resulted in significantly lower levels of LIMD1, which occurred at the post-translational level, thought to result in LIMD1 degradation through a proteasome dependent pathway. Knockdown of LIMD1 resulted in reduced activity of NFkB and AP1 indicating that LIMD1 is required for LMP1/TRAF6-mediated signal transduction and also resulted in the downregulation of the LMP1 target genes, IRF4, IRF7 and Bcl-6. Finally, LIMD1 depletion increased DNA damage associated cell death and inhibited autophagy, suggesting that LIMD1 protects EBV-transformed cells from DNA damage but makes them more susceptible to autophagy (Wang, Howell et al. 2018).

1.7.6 Ajuba regulates the Hippo signalling pathway

The Hippo signalling pathway controls organ size, through the regulation of the cell cycle, proliferation and apoptosis (Huang, Wu et al. 2005). A number of mammalian regulators of this pathway have been characterised including the serine/threonine kinase large tumour suppressor 1 and 2 (LATS1/2) (Zeng and Hong 2008). Increasing evidence is emerging that deregulation of the Hippo pathway occurs in a broad range of human carcinomas including colorectal, lung, liver and ovarian cancer (Harvey, Zhang et al. 2013). Interestingly, somatic or germline mutations in genes that regulate the Hippo signalling pathway are uncommon: mutations in *neurofibromin 2* (*NF2*) encoding

merlin are described, but mutations in other pathway genes are rare (Harvey, Zhang et al. 2013).

In Drosophila *Djub* is the sole orthologue of the Ajuba subfamily of LIM proteins (Renfranz, Siegrist et al. 2003) functioning as an essential negative regulator of the conserved Hippo signalling pathway (Das Thakur, Feng et al. 2010). In mammalian cells, activation of the Hippo signalling pathway induces the activation of LATS1/2 which phosphorylates and inactivates the transcriptional co-activator Yes-associated protein (YAP) and its paralogue TAZ, excluding YAP/TAZ from the nucleus with consequent down-regulation of genes driving cell growth (Zhao, Tumaneng et al. 2011). Ajuba LIM proteins are important negative regulators of the Hippo signalling pathway. In mammalian cells, Ajuba, LIMD1 and WTIP strongly associate with LATS1/2, preventing LATS1/2 mediated YAP/TAZ phosphorylation therefore functioning as negative regulators of YAP activity (**Figure 1.10**). (Das Thakur, Feng et al. 2010) (Tanaka, Osada et al. 2015)

Zhao *et al* have demonstrated that in sub-confluent non-contacted cells, Ajuba LIM proteins are predominantly cytosolic, resulting in the inhibition of LATS1/2 mediated YAP phosphorylation and activated YAP therefore accumulates in the nucleus and cells proliferate, but once confluent, Ajuba proteins are recruited to adherens junctions in turn releasing LATS1/2 resulting in YAP phosphorylation and subsequent cell inactivation and growth arrest (Zhao, Wei et al. 2007).

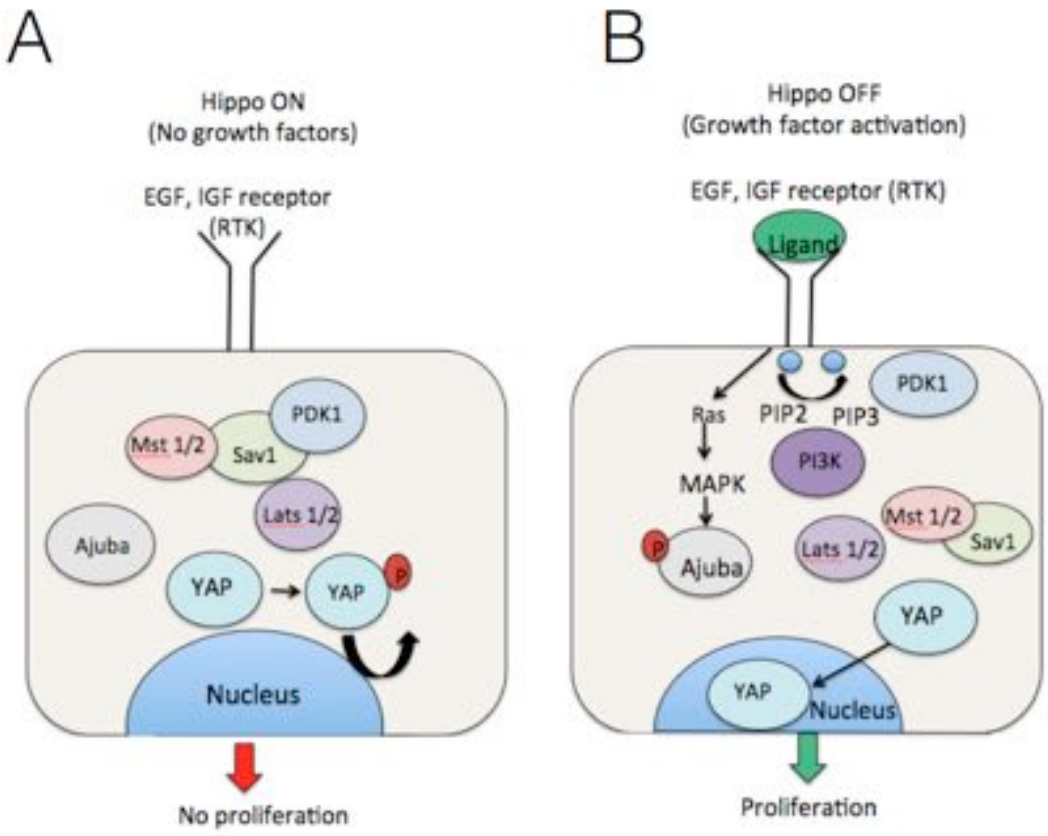

Figure 1.10 Ajuba proteins regulate the Hippo signalling pathway. A In confluent cells in the absence of growth factors, PDK1 forms a complex with Hippo pathway components (Lats, Mst, PDK1 and Sav1) and the Hippo pathway is active, YAP remains phosphorylated and excluded from the nucleus resulting in cell growth arrest. **B** Activation of the Ras/MAPK pathways through growth factor activation results in phosphorylation of Ajuba and disassociation of the PDK1/Hippo complex. Growth factors can also activate PI3K and recruit PDK1 to the cell membrane, resulting in further disassociation of the PDK1-Hippo complex. This results in YAP de-phosphorylation, which accumulates in the nucleus, driving transcription of pro-proliferative genes. Adapted from (Gumbiner and Kim 2014).

1.7.7 Ajuba regulates epithelial-mesenchymal transition (EMT)

EMT is fundamental for tumour invasion and metastasis (Thiery 2003). During EMT, epithelial cells lose contact with their neighbours and gain mesenchymal properties, enabling them to break through the basement membrane: a critical component of this pathway is the functional loss of E-cadherin (Onder, Gupta et al. 2008). Snail proteins contain conserved SNAG (Snail/Gfi) domains, essential for the binding of transcriptional co-repressor complexes, and in turn target the downregulation of E-cadherin expression, thereby driving EMT (Onder, Gupta et al. 2008).

In Xenopus, Ajuba can act as a transcriptional co-repressor alongside Snail by binding the SNAG transcriptional repressor domain on *E-cadherin*, in turn repressing E-cadherin transcription (Langer, Feng et al. 2008).

In colorectal cell lines, the ectopic expression of Ajuba induces EMT, enhancing cell motility and invasiveness through Snail upregulation (Wang, Shi et al. 2013). In clinical colorectal specimens, an inverse correlation between Ajuba and E-cadherin expression is observed (Wang, Shi et al. 2013).

1.7.8 Ajuba proteins stabilise adherens junctions

The regulation of stable cadherin-dependent junctions between neighbouring cells is fundamental to ensure epithelial cell differentiation; deregulation of such interactions can promote tumour growth and metastasis (Onder, Gupta et al. 2008). The small GTPase Rac1 (Rac) is a critical signalling pathway co-ordinating cadherin-F actin association at the plasma membrane and therefore mediating the recruitment of actin to clustered cadherin complexes (Ratheesh, Priya et al. 2013). Upon cell-cell contact, Ajuba and Rac are both recruited independently to cell junctions, and upon Rac activation, the Rac effector PAK1 is activated by auto-phosphorylation, in turn phosphorylating Ajuba and increasing its affinity to activate Rac; essentially Ajuba acts as a scaffold to concentrate active Rac. In the absence of Ajuba, Rac can still be recruited and activated by junction assembly, but cannot resist mechanical stress (Nola, Daigaku et al. 2011).

1.7.9 Ajuba proteins localise to centrosomes and are required for mitotic commitment

Aurora family kinases are critical regulators of mitosis (Goldenson and Crispino 2015) . Aurora-A is required for mitotic entry with activation of Aurora-A in late G2 phase essential for the recruitment of the cyclin B1-Cdk1 complex to centrosomes and upon activation of this complex, cells are committed to mitosis (Hirota, Kunitoku et al. 2003). In a two-hybrid screen Ajuba has been characterised as binding Aurora-A and Ajuba induces the auto-phosphorylation and consequent activation of Aurora-A (Hirota,

Kunitoku et al. 2003). Depletion of Ajuba prevents the activation of Aurora-A at centrosomes in late G2 phase and associated entry into mitosis is inhibited (Hirota, Kunitoku et al. 2003).

1.7.10 WTIP regulates podocyte function

Podocytes are highly specialised glomerular epithelial cells that help maintain the normal function of the glomerular filtration barrier in the kidney. WTIP has been shown to regulate podocyte-actin dynamics and therefore maintain stable cell contact (Sedor, Madhavan et al. 2011). After glomerular injury, WTIP shuttles to the podocyte nucleus and effects changes in gene transcription that enable podocyte remodelling (Sedor, Madhavan et al. 2011). WTIP also interacts with additional sex comb-like (ASXL) family proteins; chromatin factors that are involved in transcriptional activation and repression and in combination with ASXL proteins play an important role in kidney podocyte development (Moon, Um et al. 2015).

1.7.11 WTIP inhibits Wnt signalling

Deregulated Wnt signalling is common in cancer pathways (Polakis 2012) . Ror2 is a receptor tyrosine kinase, involved in the development of multiple tissue types including skeletal and heart muscle, lung and kidney formation. In mice, Wtip and Ror2 have been shown to interact with Ror2 recruiting Wtip to the cell membrane with both genes and proteins demonstrating overlapping expression in the mouse embryo (van Wijk, Witte et al. 2009). Wtip can inhibit Wnt signalling in both mammalian cells and Xenopus embryos, through an interaction with the receptor tyrosine kinase Ror2 (van Wijk, Witte et al. 2009).

1.8. Summary of the function of the Ajuba proteins

The mammalian Ajuba proteins LIMD1, Ajuba and WTIP participate in a diverse array of cellular processes (Kadrmas and Beckerle 2004). All three proteins contain the characteristic C-terminal LIM domains, which facilitate protein-protein interactions and can shuttle between the nucleus and the cytoplasm, functioning as important signalling transducers relaying signals between the cell surface and the nucleus (Kadrmas and Beckerle 2004), playing for example a critical role in the regulation of EMT via E-cadherin expression (Wang, Shi et al. 2013). Ajuba proteins are negative regulators of the Hippo signalling pathway (Das Thakur, Feng et al. 2010), upregulation of which is implicated in driving tumourigenesis in multiple tumour types. Other roles include the stabilisation of adherens junctions (Nola, Daigaku et al. 2011). LIMD1 is a regulator of pRb, in turn repressing E2-F mediated transcription and acts as an important regulator of bone remodelling through its effects on osteoclast differentiation (Luderer, Bai et al. 2008).

Ajuba proteins are essential components of the miRISC, facilitating miRNA mediated gene silencing (Bridge, Shah et al. 2017). Acting as scaffold proteins, all three proteins regulate the hypoxic response, targeting HIFα for VHL mediated polyubiquitylation and degradation via the proteasome (Foxler, Bridge et al. 2012).

Deregulation of the pathways described is frequently implicated in driving tumourigenesis and metastasis. LIMD1, Ajuba and WTIP demonstrate considerable functional redundancy as demonstrated for example in the regulation of the hypoxic response and in miRNA silencing via the miRISCs.

A number of studies have implicated Ajuba protein deregulation as important in driving tumourigenesis *in vivo*. LIMD1 loss is common in lung carcinoma and drives tumourigenesis in a mouse model, whilst in breast cancer LIMD1 loss contributes to tumourigenesis and is associated with worse prognosis disease (Sharp, Al-Attar et al. 2008, Spendlove, Al-Attar et al. 2008). LIMD1 expression levels are also associated with subtypes of DLBCL (Li, Wang et al. 2015). Ajuba upregulation has also been associated with colorectal carcinoma and oesophageal squamous cell carcinoma (Liang, Zhang et

al. 2014, Shi, Chen et al. 2016). Ajuba loss in malignant mesothelioma has been described and is related to deregulation of the Hippo signalling pathway (Tanaka, Osada et al. 2015).

To date, LIMD1, Ajuba and WTIP have not been characterised in ccRCC. Hypoxic deregulation is a critical driver of tumourigenesis in ccRCC and deregulation of miRNA mediated silencing is commonly observed (Biswas, Troy et al. 2010). Dysfunctional Hippo signalling can mediate proliferation, invasiveness and the metastatic potential of ccRCC (Schutte, Bisht et al. 2014). It was therefore hypothesised that deregulation of the LIM domain containing proteins LIMD1, Ajuba and WTIP may contribute to tumourigenesis in ccRCC.

1.9 Overview of Clear cell renal cell carcinoma

Renal cell carcinoma (RCC) accounts for 3.8% of adult malignancies globally and is the eighth leading cause of cancer-related death (Rathmell and Godley 2010). The commonest RCC, clear cell renal cell carcinoma (ccRCC), accounts for 70-80% of cases and has the greatest potential for recurrence and distant metastatic spread (Escudier, Szczylik et al. 2012).

Patients with organ-confined RCC may be cured with nephrectomy, however approximately 30% of patients have metastatic disease at the time of initial presentation and 40% of patients with localised disease, will recur post nephrectomy (Koul, Huh et al. 2011). Metastatic RCC will progress in almost all patients and is often accompanied by significant morbidity (Escudier, Porta et al. 2014).

Since 2007, the prognosis of metastatic RCC has improved dramatically with the development of targeted agents which target complex pathways regulating RCC tumourigenesis (Escudier, Szczylik et al. 2012). In addition, the use of immune checkpoint inhibitors to enhance anti-tumour immunity offers a promising novel therapeutic approach (Massari, Santoni et al. 2015).

Currently with sequential and repeated use of targeted agents, patients with intermediate-prognosis disease have an overall survival of 25-30 months compared to

10 months in the pre-targeted therapy era (Motzer, Mazumdar et al. 1999, Heng, Xie et al. 2009) and this may increase further with the use of novel therapeutic options. Nonetheless, the natural history of ccRCC can be highly unpredictable, between 4.2% and 7.1% of patients with small tumours less than 4cm in diameter have metastatic disease at presentation (Lughezzani, Jeldres et al. 2009), and conversely up to 40% of patients with lymph node metastases diagnosed at nephrectomy are alive five years after surgery (Mekhail, Abou-Jawde et al. 2005).

1.10 Epidemiology of ccRCC

Incidence of ccRCC is highest in North America and Northern Europe and the disease is over-represented in men, with a male to female ratio of 1.5-2:1 (Levi, Ferlay et al. 2008). Incidence of RCC is substantially lower amongst Asians, both within Asian countries and in Western countries (Ljungberg, Campbell et al. 2011). Prevalence increases with increasing age and most tumours are diagnosed in those aged 60-64; nonetheless 7% of sporadic tumours are diagnosed in patients under the age of 40 (Rodriguez, Patard et al. 2002). The incidence of all stages continues to increase and although there has been a decrease in overall mortality rates for RCC in many Western countries, this is not true globally (Levi, Ferlay et al. 2008) (**Figure 1.11**).

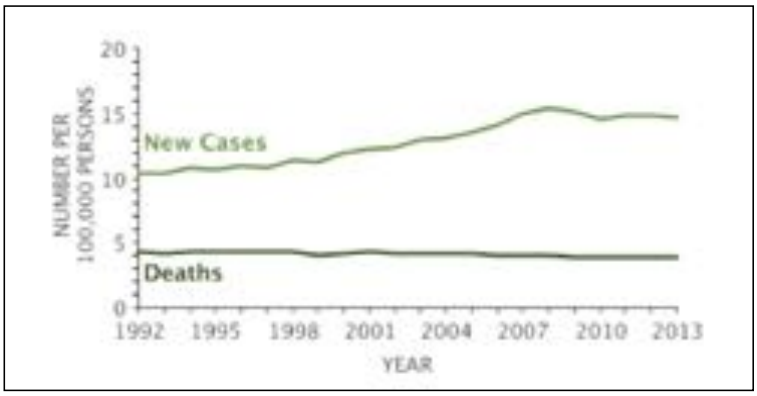

Figure 1.11 Number of new cases of RCC and deaths per 100,000 of the population in the USA. The number of age-adjusted new cases per 100,000 has continued to increase between 1992 and 2013 whilst the number of deaths per 100,000 has remained constant, likely representing an increase in early tumour diagnosis in combination with increasing all stage incidence related to environmental factors with improved outcomes for patients with metastatic disease. **Adapted from Surveillance, epidemiology, and end results (SEER) program.**

A number of identified risk factors contribute to a significantly increased risk of sporadic ccRCC and the environmental factors best characterised are obesity and smoking (Ljungberg, Campbell et al. 2011). Hypertension and advanced kidney disease necessitating dialysis also increase risk (Ljungberg, Campbell et al. 2011). Dietary habits, particularly red meat intake and occupational exposure to specific carcinogens have been implicated, although evidence for this in the literature is inconclusive (Daniel, Schwartz et al. 2011). Moderate alcohol consumption appears to have a protective effect and reasons for this are unknown (Bellocco, Pasquali et al. 2012). In up to 50% of cases, renal masses are diagnosed incidentally on ultrasound (US) or computed tomography (CT) conducted for other medical reasons (Gill, Aron et al. 2010). This has increased the incidence of small renal masses, defined as contrast enhancing masses with a maximum dimension of 4cm or less (Gill, Aron et al. 2010).

In 1-5% of cases, ccRCC may arise as part of a hereditary syndrome, the most common of which is Von-Hippel Lindau syndrome, characterised by germ-line mutations in the tumour suppressor gene *Von-Hippel Lindau* (*VHL*) (Sudarshan and Linehan 2006). Associated focal lesions arise from the inactivation or silencing of the remaining wild type allele (Latif, Tory et al. 1993).

For a first-degree relative of a patient with RCC the increased risk of RCC is roughly two-fold (Ljungberg, Campbell et al. 2011). Genetic susceptibility and its interaction with environmental exposure is thought to influence renal cell cancer risk but limited studies identifying candidate genes have thus far proved inconclusive (Chow, Dong et al. 2010). However, a large genome-wide association study (GWAS) led by the International Agency for Research on Cancer (IARC) and the US National Cancer Institute has provided stronger evidence of the association between genetic variants and risk of sporadic RCC, identifying for example an association between genetic variants of the gene encoding hypoxia-inducible factor-2α (HIF2α) and increased risk of renal carcinoma (Purdue, Johansson et al. 2011).

1.11 Pathology of clear cell renal cell carcinoma

Clear cell renal cell carcinoma (ccRCC) is the commonest RCC, identified in 75-80% of cases (Frew and Moch 2015). ccRCCs are renal cortical tumours characterised by malignant epithelial cells with clear or eosinophilic cytoplasm and a compact-alveolar or acinar growth pattern: tumours are typically highly vascular (Aydin and Zhou 2008). The name 'Clear Cell' reflects the finding that the cytoplasm is commonly filled with glycogen and lipids which are lost upon tissue fixation (Frew and Moch 2015) (**Figure 1.12**). In the main, the literature supports the view that most ccRCCs arise from the renal proximal tubules with most tumours staining positively for proximal tubule markers including CD10 and villin, however some ccRCC can also express distal tubule and collecting duct markers such as cytokeratin 19 and CD24 (Frew and Moch 2015).

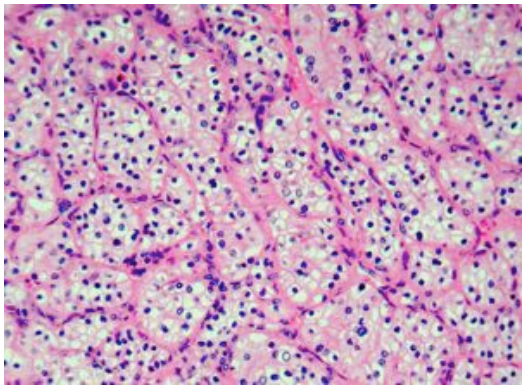

Figure 1.12 Typical histological appearance of clear cell renal cell carcinoma. Haematoxylin and eosin staining is demonstrated with nests of epithelial cells with clear cytoplasm and a distinct cell membrane, separated by a delicate branching network of vascular tissue. **Taken from Medscape**.

1.12 Genetics of clear cell renal cell carcinoma

1.12.1 Clear cell renal cell carcinoma is a disease of 3p loss

Hereditary ccRCC typically occurs in patients with germline mutations in the tumour suppressor gene *VHL*, a classic tumour suppressor and regulator of HIF1α, located on the short arm of chromosome 3 (3p25.3) (Latif, Tory et al. 1993, Crossey, Foster et al.

1994). For decades, sporadic ccRCC was defined by the biallelic loss of function of *VHL*, which occurs through a combination of 3p loss and *VHL* mutation or changes in promoter methylation status with such changes observed in over 90% of ccRCC tumours Such an early event is designated a trunk event, with loss/mutation, an early driver of tumourigenesis. (Zbar, Brauch et al. 1987, Gnarra, Tory et al. 1994, Kaelin 2007, Sato, Yoshizato et al. 2013).

However, it is clear that biallelic loss of *VHL* function is not sufficient for ccRCC formation. The study of kidneys of patients with VHL disease, i.e. germline mutations in one copy of *VHL*, has demonstrated that these patients probably have hundreds of thousands of functional VHL null single cells or multi-centre clusters of cells, despite no evidence of ccRCC (Montani, Heinimann et al. 2010).

Comprehensive large-scale sequencing projects using highly integrative analysis of The Cancer Genome Atlas (TCGA) and work undertaken by Sato *et al* analysed over 400 and 240 cases of ccRCC respectively. In the ccRCC samples, whole-genome and/or whole exome expression was undertaken, RNA sequencing and array-based gene expression was analysed as well as gene copy number and methylation status (Cancer Genome Atlas Research 2013, Sato, Yoshizato et al. 2013).

Work by the TCGA Research Network identified that recurrent arm-level and focal somatic copy number alterations (SCNAs) occurred at fewer sites than observed for other cancers. The SCNAs that did occur, however, more commonly involved entire chromosomes or chromosome arms compared to focal events: in 17% of cases compared to 0.4% of cases respectively (Cancer Genome Atlas Research 2013). In over 90% of cases, this chromosomal loss involved loss of chromosome 3p, which incorporates *VHL*, *PBRM1*, *SETD2* and *BAP1* genes (Cancer Genome Atlas Research 2013) (**Figure 1.12**). Sato *et al* observed similar levels of 3p LOH in 94% of ccRCC specimens analysed, with 77.6% occurring through simple 3p loss or copy neutral LOH (uniparental disomy in 22.4%) (Hakimi, Pham et al. 2013, Sato, Yoshizato et al. 2013).

Intriguingly, when whole-exome sequencing and large-scale targeted sequencing studies of these tumours were undertaken, four of the top five significantly mutated genes were

located between 3p21 and 3p25 in *VHL*, *PBRMI*, *SETD2* and *BAP1* genes (Hakimi, Pham et al. 2013, Sato, Yoshizato et al. 2013) (**Figure 1.13**).

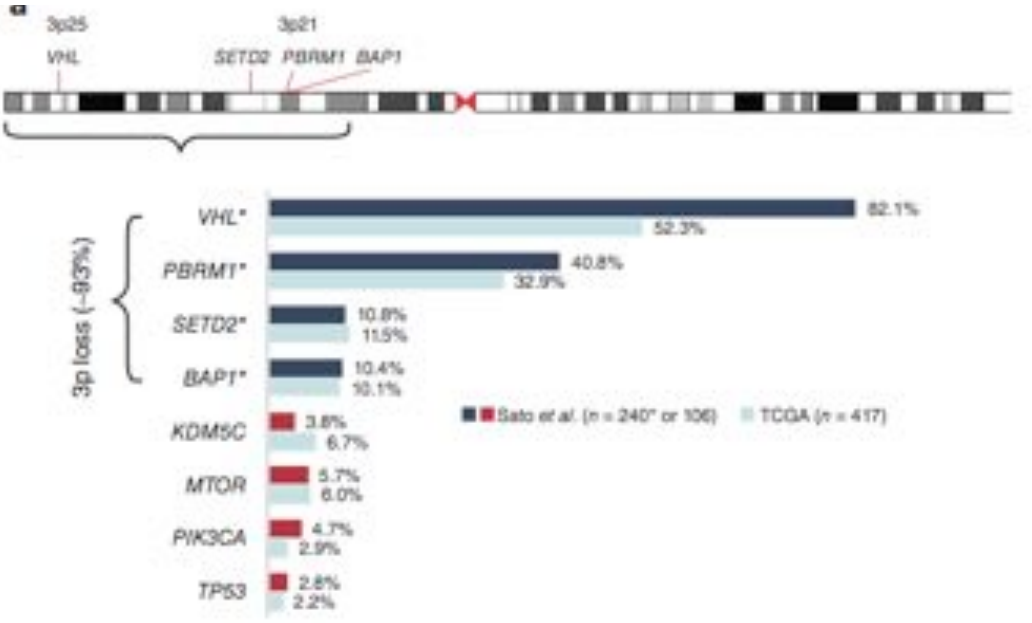

Figure 1.13 Frequency of mutated genes identified in studies by both interrogation of the TCGA and by Sato *et al*. The relationship between the *VHL*, *PBRM1*, *SETD2* and *BAP-1* loci on 3p is outlined and the frequency of mutation of commonly mutated genes in ccRCC tumours identified by the TCGA investigators and by Sato *et al* indicated. Asterisks indicate selective deep sequencing of frequently mutated tumour suppressors in addition to samples in the study by Sato *et al* (n=240). Adapted from **(Hakimi, Pham et al. 2013)**

PBRM1, SETD2 and BAP1 all function as chromatin and/or histone modifiers. (Dalgliesh, Furge et al. 2010, Varela, Tarpey et al. 2011). *PBRM1* encodes the Polybromo1 (BAF180) protein, which functions as the chromatin targeting subunit of the Polybromo complex SW1/SNF (Gossage, Murtaza et al. 2014). *SETD2* encodes a protein responsible for methylation/demethylation of histone residues whilst *BAP1* encodes a nuclear de-ubiquitylase, which mediates de-ubiquitylation of histones (Gossage, Murtaza et al. 2014).

Given that 3p LOH is so commonly observed in ccRCC, loss of function mutations of any of these four genes is highly likely to result in complete inactivation of one of four tumour suppressors that may be functionally linked. Interestingly, Sato *et al* demonstrated that almost all mutations involving *PBRMI*, *SETD2* and *BAP1* occurred in a subset of *VHL* inactivated cases. In addition, the allelic frequency of mutations of *SETD2* and *BAP1* was significantly less than that for *VHL*. This indicates that *SETD2* and *BAP1* mutations are acquired and selected for from within pre-existing *VHL*

mutated clones and/or *PBRM1* mutated clones, in turn potentially contributing to further tumour progression. *BAP-1* mutations were also mutually exclusive with *PBRM1* mutations (Sato, Yoshizato et al. 2013).

There is emerging evidence that these genes function as important tumour suppressors in a range of malignancies, with *BAP1* for example implicated in mesothelioma tumourigenesis (Bott, Brevet et al. 2011) and *SETD2* in breast carcinoma tumourigenesis (Al Sarakbi, Sasi et al. 2009). In addition, Hakimi *et al* have demonstrated that BAP1 mutations are associated with worse cancer specific survival in ccRCC, (**Section 1.20**) (Hakimi, Pham et al. 2013)

1.12.2 Copy number alterations at other loci in ccRCC

Sato *et al* and the TCGA Research Network investigators observed frequent copy number alterations at other chromosome loci, often involving large chromosome segments. Gain of 5q was observed in 67% of samples tested by the TCGA network, and further analysis refined this area to the 5q35 region (Cancer Genome Atlas Research 2013). Sato *et al* observed gain of 5q in 65% of samples (Sato, Yoshizato et al. 2013). The relevant target(s) of this amplification are not known, although 5q amplification does lead to overexpression of the *SQSTM1* oncogene, also known as the ubiquitin-binding protein p62, an autophagosome carrier protein that can target proteins that bind to it for selective autophagy (Cassidy and Narita 2015) and known to promote resistance to redox stress *in vitro* (Li, Shen et al. 2013). Interestingly as outlined in Section 1.7.4, LIMD1 can bind to p62, and in osteoclasts leads to the activation of a signalling cascade activating genes critical in normal bone development (Feng, Zhao et al. 2007).

Gain of 7q (41%), loss of 8p and or 8q (20%) and loss of heterozygosity at 9p were all commonly observed in samples tested by Sato *et al* (Sato, Yoshizato et al. 2013). Arm level losses on chromosome 14q were also common, seen in 45% of samples tested by the TCGA research network (Cancer Genome Atlas Research 2013).

Loss of 14q has been described in other studies. Kroeger *et al* analysed 288 ccRCC tumours and identified loss of 14q in 28% of tumours. Of note HIF1α is 14q encoded

and Kroeger *et al* hypothesised that 14q loss was a surrogate marker for HIF1α loss (Kroeger, Klatte et al. 2013).

In ccRCC with intact *VHL*, Sato *et al* observed mutations in *TCEBI* in 36-42% of cases (Sato, Yoshizato et al. 2013). *TCEB1*, located on chromosome 8q21, encodes Elongin C, a subunit of the heterotrimeric RNA polymerase II elongation factor and a vital component of the VHL complex, important in accomplishing ubiquitylation of VHL-bound HIF proteins (Aso, Lane et al. 1995). Sato *et al* demonstrated that mutations in *TCEBI* were always accompanied by LOH at 8q21. In addition, there were no significant differences in the clinico-pathological characteristics of cases with *VHL* mutations and those with mutations in *TCEB1* (Sato, Yoshizato et al. 2013), suggesting that loss of functional TCEB1 or VHL have an equivalent role in driving ccRCC tumourigenesis.

Other frequently identified mutational targets in ccRCC include *TET2* (mutated or deleted in 16% of tumours), *KEAP1* and *MTOR*. TET2 is believed to play a critical step in DNA demethylation (Tahiliani, Koh et al. 2009) whilst KEAP1 is a key component of a cullin-RING ubiquitin ligase complex involved in the oxidative stress response (Kansanen, Kuosmanen et al. 2013). Sato *et al* identified that including *MTOR*, 26% of tumours had mutations that involved the PI3K-AKT-mTOR signalling pathway (Hakimi, Pham et al. 2013, Sato, Yoshizato et al. 2013) and this closely correlates with the figure of 28% observed by the TCGA investigators (Cancer Genome Atlas Research 2013).

1.13 Hypoxia inducible factors in ccRCC

Rapid tumour cell proliferation often results in tumour outgrowth of vascular supply and disorganised neo-angiogenesis with resultant areas of tumour hypoxia (Carroll and Ashcroft 2005, Pal and Figlin 2011).

Such hypoxia results in tumour adaptations with consequent pro-tumourigenic effects. The transcription factor and regulator of tumour oxygen homeostasis HIF, is the major protein up-regulated by tumour hypoxia (Schito and Semenza 2016). Tumour hypoxia also results in relative resistance to apoptosis through for example loss of functional p53 (Graeber, Osmanian et al. 1996). In addition mechanisms that include NFκB and

activator protein 1 (AP-1) up-regulation initiate pro-survival mechanisms that increase cell proliferation, migration and invasion (Dong, Venkatachalam et al. 2001, Pennacchietti, Michieli et al. 2003, Eales, Hollinshead et al. 2016). Deregulation of such pathways drives tumourigenesis and thus pathogenesis of cancer (Pantuck, Zeng et al. 2003, Pouyssegur, Dayan et al. 2006, Koul, Huh et al. 2011, Eales, Hollinshead et al. 2016).

1.13.1 Overview of hypoxia inducible factors

Heterodimeric HIFs are DNA binding complexes that direct the transcription of genes with HREs. There are three isoforms of the HIF-α subunit, HIF1-α, HIF-2α and HIF-3α that form heterodimers with a constitutively expressed, stable β subunit (**Figure 1.14**) (Loboda, Jozkowicz et al. 2010). The HIFα/β heterodimer binds HREs in the promoters of target genes. HIF-1α and HIF-2α are critical mediators of the hypoxic response, whilst the role of HIF-3α is less well characterised (Loboda, Jozkowicz et al. 2010). Both HIF1α and HIF2α are closely related at a protein level with a similar domain structure and activate a similar broad pattern of genes, although there are some critical differences (Hu, Wang et al. 2003, Hu, Sataur et al. 2007, Webb, Coleman et al. 2009). HIF3α, has six splice variants, one of which can function in a dominant negative role to impair the induction of hypoxia inducible genes and when co-expressed with HIF1α, prevents HIF1α DNA/HRE interaction (Loboda, Jozkowicz et al. 2010). In addition HIF3α lacks a C-terminal activation domain and therefore cannot function as an effective transcriptional activator (Pasanen, Heikkila et al. 2010) (**Figure 1.14**).

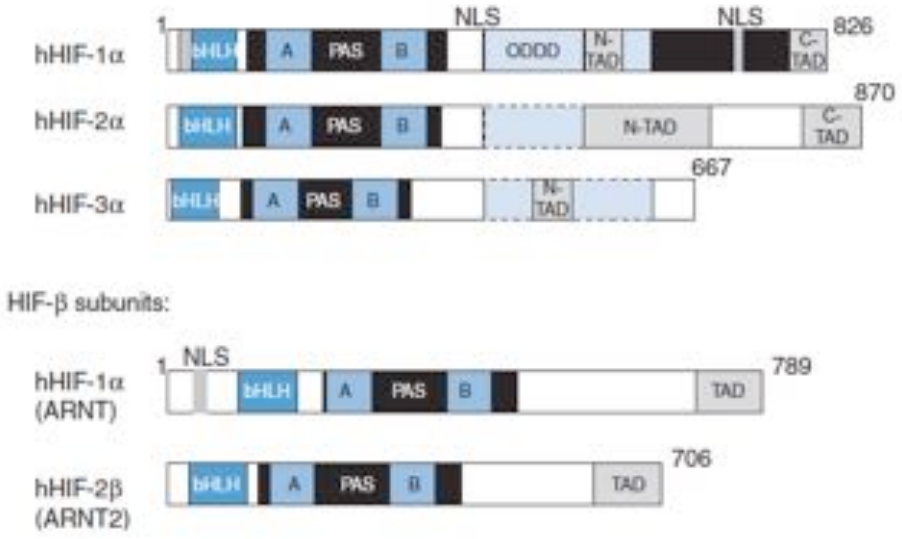

Figure 1.14 HIFα and HIFβ subunits.

HIFs consist of an α and a β subunit which share considerable homology. There are three human isoforms of the α subunit and two of the β-subunit. The functional domains include a basic helix-loop-helix (bHLH) domain that mediate DNA binding and two per-ARNT-pas (PAS) domains that mediate interaction with the HIFα/β subunit. The α-subunits contain an ODDD domain that is required for oxygen dependent hydroxylation and subsequent degradation via the proteasome. Proline hydroxylase proteins (PHDs) facilitate hydroxylation of the ODDD and this in turn can be inhibited by factor inhibiting HIF (FIH). C and N-terminal transactivation domains (TADs) are identified in both HIF-1α and HIF-2α and facilitate interaction with the p300/DBP transcriptional co-activator. HIF3α lacks a CTAD. Nuclear localisation signals (NLS) target HIF proteins to the nucleus. Adapted from (Brahimi-Horn and Pouyssegur 2007)

1.13.3 The von Hippel-Lindau (VHL) protein

Loss of and mutations in the *VHL* gene in both hereditary and sporadic ccRCC have been described. The *VHL* gene encodes two isoforms of pVHL, one a 213-amino acid, 30kDa isoform ($pVHL_{30}$) and the second a 160-amino acid 19kDa form ($pVHL_{19}$) (Blankenship, Naglich et al. 1999) $pVHL_{19}$ is the isoform that predominates in many tissues and lacks a 53 amino-acid terminal pentameric acid repeat domain (Gossage, Eisen et al. 2015). Functional studies suggest that both forms have broadly equivalent effects in driving tumourigenesis *in vitro* and tumour suppressor activity *in vivo* (Iliopoulos, Ohh et al. 1998) (Schoenfeld, Davidowitz et al. 1998) although some differences are apparent with only one isoform, regulating microtubule function (Ratcliffe 2003).

pVHL is composed of an α and β domain which are closely coupled, with the α-domain consisting of three α helices and the β-domain, two β-sheets with an α-helix on top (Gossage, Eisen et al. 2015). Work in VHL deficient RCC lines demonstrated constitutively high expression of genes containing HRE elements including VEGF and GLUT1 and following re-expression of function VHL, expression levels were significantly downregulated. VHL was shown to bind to HIF1α and decrease protein levels without affecting its mRNA expression suggesting that it played a critical role in the regulation of HIFα (Gnarra, Zhou et al. 1996, Iliopoulos, Levy et al. 1996)

Work in the 1990s, demonstrated that the VHL complex forms a ternary complex by binding to transcription elongation factors C and B to form the VCB complex, a

functional E3 ligase critical for pVHL function (Kibel, Iliopoulos et al. 1995). The VCB complex in turn nucleates a complex containing cullin 2 (CUL2) and the RING finger protein (RBX1), to form the VCB-CR complex (Stebbins, Kaelin et al. 1999). Elongin B and C act as adapters that link pVHL in the VCB-CR complex to heterodimers of CUL2 and RBX1 and this interaction stabilises pVHL and elongin B and C, with the resultant complex resistant to degradation via the proteasome (Schoenfeld, Davidowitz et al. 2000). By contrast, pVHLs that harbour mutations disrupting elongin binding undergo rapid proteasome mediated degradation (Stebbins, Kaelin et al. 1999).

1.13.4 Prolyl hydroxylases (PHDs)

Subsequent work demonstrated that the HIFα domain bound exclusively to the β-domain of pVHL and that this binding is dependent on the hydroxylation of two, conserved proline resides within HIFα by PHD1, PHD2 or PHD3. Mutational mapping identified the proline residues 402 and 564 within HIF1α as the targets for PHD hydroxylation with mutation of either residue leading to a stabilisation of HIF1α protein levels (Brahimi-Horn and Pouyssegur 2007). PHD mediated hydroxylation of HIFα requires oxygen as a co-substrate and PHDs are therefore normally only active in normoxia and PHD proteins are the major oxygen sensors of the cell (Brahimi-Horn and Pouyssegur 2007).

Prolyl hydroxylation of HIFα by PHD leads to HIF recognition and ubiquitylation by the VCB-CR complex and in turn polyubiquitylated HIFs are recognised and degraded by the cellular proteasome. However, under hypoxic conditions, or in the absence of functional pVHL, HIFα accumulates and transcriptional regulation of genes with HIF-responsive elements result (**Figure 1.14**) (Pantuck, Zeng et al. 2003, Brahimi-Horn and Pouyssegur 2007).

1.13.5 HIF-1 and HIF2 regulation

In hypoxia or where hypoxic deregulation has occurred, HIF1α/2α heterodimerises with HIFβ and the complex in turn recognises a conserved DNA consensus sequence

within the promoters of target gene HREs. In turn the HIFα/β complex recruits the transcriptional co-activators p300 and CREB-binding protein (CBP). HIF1α contains two transcriptional co-activator domains, the N-terminal transactivation domain (NTAD) and C-terminal transactivation domain (CTAD), linked by an inhibitory domain. The NTAD overlaps with the oxygen-dependent degradation domain (ODD) (Brahimi-Horn and Pouyssegur 2007)).

Hydroxylation of conserved proline residues in the ODD domain and lysine acetylation confers recognition by the VHL-ubiquitin E3 ligase complex under normal oxygen tension (Ke and Costa 2006). In hypoxia, however inhibition of hydroxylation by the PHDs results in stabilisation of HIFα/β and subsequent transcriptional activation of target genes.

Factor inhibiting HIF (FIH-1)

Asparaginyl hydroxylation of HIF-α by FIH-1 prevents the interaction of the C-TAD with the transcriptional co-activator CBP/p300 (Webb, Coleman et al. 2009) and provides a further oxygen-dependent mechanism in the control of HIF that is independent of HIF-α stability regulation by HIF PHDs (**Figure 1.15**). FIH-1 and the PHDs belong to the same superfamily of dioxygenases and in general require the same set of cofactors (oxygen, 2-oxoglutarate and ferrous iron), but there are differences between these enzymes. Firstly, FIH-1 has a higher affinity for molecular oxygen relative to the PHDs, and this suggests that in mild hypoxia FIH-1 can remain active while the PHDs are inactivated (**Figure 1.15**) (Webb, Coleman et al. 2009). This is potentially important because not all HIF target genes are equally dependent on the function of the C-TAD (Ke and Costa 2006)

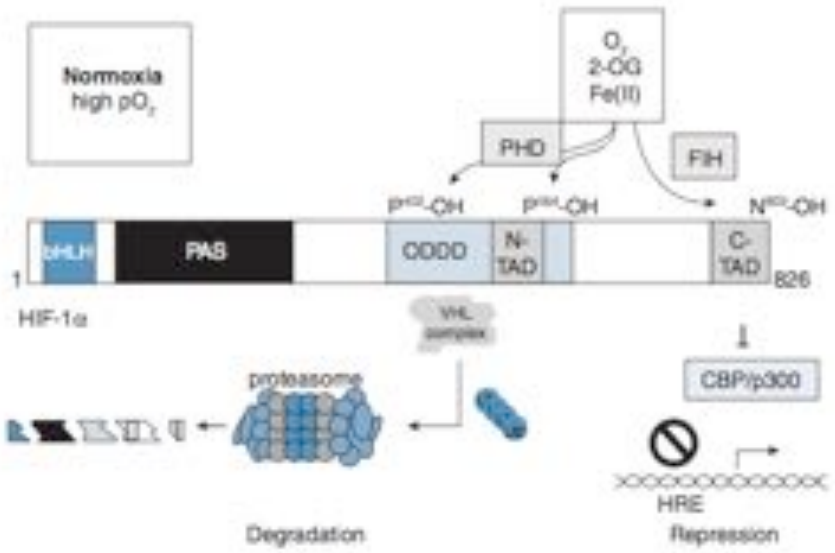

Figure 1.15 HIF-1α regulation by proline hydroxylation. In normoxia, HIF1α is hydroxylated by PHDs 1, 2 and 3 in the presence of O_2, Fe^{2+}, 2-oxoglutarate (2-OG) and ascorbate. Consequently hydroxylated HIF-1α is inactivated through its interaction with the VHL-ubiquitin E3-containing complex that ubiquitinates HIF1α targeting it for degradation via the proteasome and abrogating interaction with the co-activator p300/CBP. In hypoxia or in the absence of a function VHL complex, HIF1α is stabilised and interacts with HIF1β leading to transcriptional activation of genes containing HRE elements. Adapted from (Brahimi-Horn and Pouyssegur 2007)

1.14 HIF1α and HIF2α regulate the transcription of different genes

HIF1α and HIF2α can regulate the expression of many of the same hypoxia-induced genes but also have unique transcriptional targets. This transcriptional specificity resides in differences in the N-TAD domain, and subsequent differential interactions with transcriptional co-factors (Hu, Sataur et al. 2007, Loboda, Jozkowicz et al. 2010, LaGory and Giaccia 2016). For example *SLC2A1,* which encodes GLUT1 and *CA12* which encodes CAXII are target genes of both HIF1α and HIF2α, whilst genes that play an important role in mediating glycolysis such as *PFK* (encoding phosphofructokinase), and *HK1/2* (encoding hexokinase 1 and 2) are solely HIF1α target genes. In contrast, *EPO*, encoding erythropoeitin and *POU5F1* encoding the stem cell identify factor OCT4 are predominantly regulated by HIF2α (Keith, Johnson et al. 2012).

There are also clear differences in the patterns of expression of HIF-1α and HIF-2α. In normal tissue, HIF-1α is ubiquitously expressed whilst HIF-2α expression is less ubiquitous, predominating in the kidney, lung, heart, and small intestine (Gordan, Bertout et al. 2007, LaGory and Giaccia 2016). Differential expression of HIF-1α and HIF-2α are also key in driving key development processes with HIF-1α for example playing a key central role in early vascular and bone development, a role that is subsequently assumed by HIF-2α as oxygen tension increases (Koh and Powis 2012). HIF-1α and HIF-2α additionally have play different roles in the regulation of myeloid gene function with HIF-1α upregulation associated with anti-microbial effector function of myeloid cells and the pathophysiology of sepsis. HIF-1 drives the upregulation of macrophage derived VEGF, whilst HIF-2α drives macrophage production of soluble VEGFR-1, suggesting specific and independent roles for HIF-1α and HIF-2α (Eubank, Roda et al. 2011).

HIF-1α and HIF-2α levels are regulated by differential post-transcription and post-translational modulation. For example, hypoxia-associated factor (HAF), an ubiquitin ligase that functions in an oxygen independent fashion, targets HIF1α but not HIF2α for proteolytic degradation (Koh and Powis 2009), HAF can bind HIF-2α, but at a different site to HIF-1α, increasing HIF-2α transactivation without causing its degradation (Koh and Powis 2009). In addition, specific PHD enzymes have differential effects on HIF-1α/HIF-2α with for example PHD3 preferentially hydroxylating HIF-2α in multiple cell lines (Appelhoff, Tian et al. 2004)

1.14.1 HIF1α and HIF2α in tumourigenesis

Increased HIF-1α and HIF-2α expression has been observed in a broad range of human cancer cell types including bladder, breast, gastric, head and neck, ovarian and renal cell carcinomas (Keith, Johnson et al. 2012). For most tumour types both HIF-1α and HIF-2α over-expression appear to result in worse prognosis although this is not the case for some tumour types. In neuroblastoma for example HIF-1α overexpression is associated with a better prognosis and HIF-2α over-expression with a worse prognosis (Keith, Johnson et al. 2012).

Comparison of HIF1α and HIF2α functions in a KRAS driven mouse model of lung tumourigenesis demonstrated that *Hif1a* deletion had little effect on tumour burden and tumourigenesis whilst overexpression of a stabilised HIF-2α protein promoted tumour angiogenesis and invasion through the expression of VEGFA and SNAIL (Kim, Perera et al. 2009).

In ccRCC, VHL inactivation is observed in over 90% of tumours. In tumours with wild type pVHL, biallelic inactivation of *TCEB1*, (which encodes elongin C), is observed in 42% of tumours. This in turn leads to constitutive HIF-α activity, suggesting that there is a strong selective pressure to inactivate the normal controls that result in HIF-α degradation (Sato, Yoshizato et al. 2013, Frew and Moch 2015).

HIF-1α and HIF-2α are not equivalent in driving ccRCC tumourigenesis and increasing evidence supports the observation that HIF-2α plays a more critical pro-tumourigenic role: HIF-1α may in fact function as a tumour suppressor (Raval, Lau et al. 2005). Raval *et al* demonstrated that in VHL-defective RCC cells, enhanced expression of HIF-2α resulted in reduced HIF-1α expression and the reverse was also observed: this may be related to a reverse hypoxia response element in the *HIF1A* promoter region resulting in epigenetic silencing of HIF1A mRNA expression. Raval *et al* also demonstrated that in VHL-defective RCC lines, HIF-1α and HIF-2α have contrasting effects on the biology of RCC with HIF2α but not HIF-1α driving the expression of cyclin D1, TGFα and VEGF, whilst the pro-apoptotic gene encoding BNip3 is promoted positively by HIF-1α and negatively in HIF-2α (Raval, Lau et al. 2005).

The balance between HIF1-α and HIF2-α activation also appears important in ccRCC tumourigenesis. In an RCC tumourigraft model, HIF-1α overexpression retarded tumour growth whilst HIF-2α overexpression enhanced growth (Raval, Lau et al. 2005), similar results were also observed by Biswas *et al* in 786-0 xenografts (Biswas, Troy et al. 2010).

HIF-1α can oppose the activity of the cell cycle promoting protein MYC through direct binding to MYC (Koshiji, Kageyama et al. 2004) and by the upregulation of proteasome-dependent MYC degradation (Zhang, Gao et al. 2007). HIF-2α on the other hand enhances MYC activity resulting in cell cycle progression through the

upregulation of cell-cycle promoting genes such as *CYCLIN D1* and *CYCLIN D2* (Gordan, Bertout et al. 2007). In sporadic ccRCC cases that express both HIF-1α and HIF-2α, MYC activity is reduced with lower frequencies of proliferating tumour cells in comparison to tumours that express only HIF-2α (Frew and Moch 2015).

In ccRCC cell lines, HIF-1α and HIF-2α expression levels are differentially dependent on the activities of the mammalian target of rapamycin complex 1 (mTORC1) and mTORC2 as well as the AKT-1, AKT2 and AKT3 kinases (Toschi, Lee et al. 2008). Since mutational activation of the PI3K-mTOR pathways is common in ccRCC, it may be that deregulation of this pathway contributes to the differential expression of HIF1α and HIF-2α (Frew and Moch 2015).

In addition, HAF can regulate the differential expression of HIF-1α and HIF-2α driven genes, trans-activating HIF-2α and targeting HIF-1α for degradation. This is turn up-regulates HIF-2α mediated gene expression with upregulation of genes involved in invasion such as MMP9, PAI-1 and the stem cell factor OCT-3/4 and also promoting EMT. Chronic hypoxia up-regulates HAF transcription, potentially further driving a switch from a HIF-1α to HIF-2α dependent response to hypoxia (Koh, Lemos et al. 2011).

In patients with VHL-disease where tumour cells are VHL-null, early kidney lesions tend to express more HIF-1α and more advanced lesions more HIF-2α (Raval, Lau et al. 2005). This may result from chromosomal changes that occur during ccRCC progression. Single copy loss of 14q, which harbours the *HIF1A* locus predicts worse outcome and biallelic loss of function of HIF-1α is common (Shen, Beroukhim et al. 2011). Certainly *in vivo* analysis of HIF-1α overexpression in some series has correlated with both favourable and unfavourable prognostic features (Lidgren, Hedberg et al. 2005, Klatte, Seligson et al. 2007), whilst HIF-2α overexpression has generally correlated with worse clinico-pathological parameters, with subcellular localisation implicated in prognosis (Kroeger, Seligson et al. 2014).

1.14.2 Activation of the PI3K-AKT-mTORC1 signalling pathway in ccRCC through HIF activation

The HIFα/β complex drives the transcription of growth factors such as VEGF, platelet derived growth factor (PDGF) and transforming growth factor-α (TGF-α) (Oosterwijk, Rathmell et al. 2011). VEGF binds and activates the VEGF receptors 1 and 2 (VEGF-R1 and 2), which stimulates angiogenesis through the downstream activation of the PI3K-AKT-mTORC1 signalling pathway (de Vries, Escobedo et al. 1992, Millauer, Wizigmann-Voos et al. 1993) (**Figure 1.16**). VEGFR-2 activation promotes endothelial cell proliferation, migration and vascular permeability whilst activation of VEGFR-1 results in neo-vascularisation through the organisation of new capillaries, and the recruitment of vascular smooth muscle cells and pericytes (de Vries, Escobedo et al. 1992, Millauer, Wizigmann-Voos et al. 1993, Sakamoto, Ryan et al. 2008). Tyrosine-kinase inhibitors (TKIs) used in the treatment of metastatic ccRCC effect responses through the targeting of VEGF receptor tyrosine kinases, whilst the monoclonal antibody bevacizumab targets the VEGF-R preventing VEGF binding (Oosterwijk, Rathmell et al. 2011) (**Figure 1.16**).

VEGF, PDGF and TGF-β activation in addition activate the mTOR pathway, which in turn generates a positive feedback loop to increase cellular HIFα levels (Cho, Signoretti et al. 2007). mTOR, forms a complex with a regulatory-associated protein to form mTORC1 and with a separate complex to form mTORC2 (Faivre, Kroemer et al. 2006, Koul, Huh et al. 2011). Downstream activation of mTORC1 results in upregulation of protein synthesis, entrance into the G1 phase of the cell cycle and down-regulation of proteins that regulate apoptosis (Faivre, Kroemer et al. 2006). mTOR inhibitors such as everolimus predominantly mediate their effects through the downregulation of anti-angiogenic pathways and in particular effects on endothelial cells and pericytes (Le Tourneau, Faivre et al. 2008) (**Figure 1.16**)

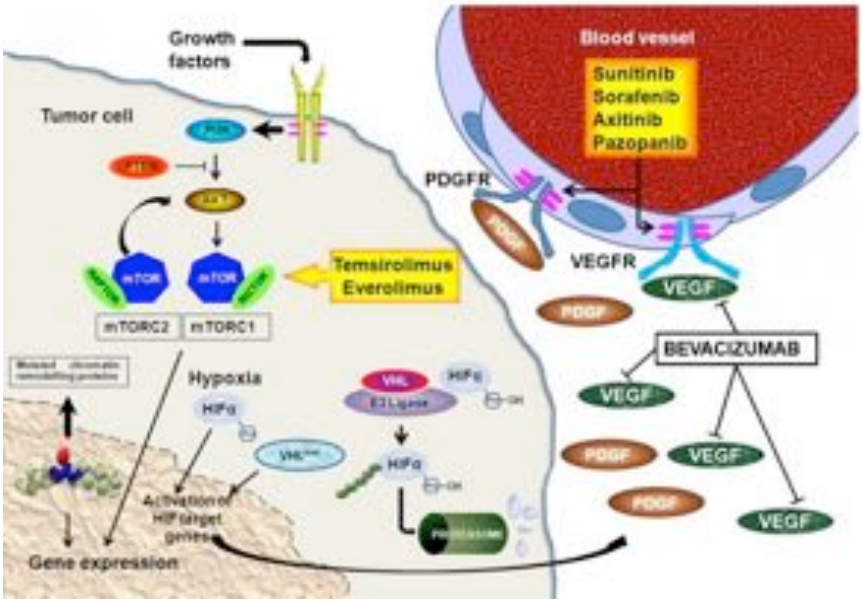

Figure 1.16 Schematic overview of hypoxic deregulation in ccRCC and the mechanism of action of targeted therapies. Sunitinib, sorafenib, axitinb and pazopanib are small molecular inhibitors of multiple receptor tyrosine kinase receptors including VEGF-R and PDGF-R. Temsirolimus and everolimus inhibit the kinase activity of the mTOR complex 1. Bevacizumab is a VEGF ligand-binding monoclonal antibody. Adapted from (Oosterwijk, Rathmell et al. 2011)

Additional genomic mutations of genes that regulate the PI3K-mTORC1 signalling cascade are common and observed in approximately 20% of all ccRCC cases and such mutations often occur in a mutually exclusive fashion. Such mutations include 'loss of function' mutations of negative regulators of the pathway such as *PTEN*, and *TSC1* and activation mutations of positive regulators such as *PIK3CA*, *PIK3CB*, and *AKT1/2/3* (Cancer Genome Atlas Research 2013). In a subset of ccRCCs, in addition to loss of function mutations of *VHL*, it appears that there is a selective advantage obtained from additional co-operating mutations that generate further deregulation of the PI3K signalling pathways (Frew and Moch 2015).

1.14.3 HIF-1α and HIF-2α as central metabolic regulators in ccRCC

HIF-α activation results in the upregulation of the expression of glucose transporters and almost all glycolytic enzymes and also induces pyruvate dehydrogenase kinase 1 and lactate dehydrogenase A (Iyer, Kotch et al. 1998), causing a Warburg-like metabolic shift, driving pyruvate away from mitochondrial oxidation. Reactive oxygen species play

an important role in signalling cascades that stimulate malignant cell growth. Cells that are VHL-deficient have increased level of NOX_4 and NADPH-dependent superoxide. Reactive oxygen species in turn regulate hypoxia-dependent and hypoxia-independent activation of HIF-2α (Block, Gorin et al. 2007). In addition, alterations in other genes such as *p53*, *MYC* and *PI3K-mTORC1* pathway components will result in significant changes in cellular metabolism (Frew and Moch 2015).

1.14.4 Hypoxic deregulation affects cell cycle regulation in ccRCC

Loss of VHL function in primary mouse cells appears to engage cell cycle checkpoint and/or senescence pathways and impair cellular proliferation. In sporadic ccRCC in around 40% of tumours, mutations or copy number deletions of genes that encode components of cell-cycle and senescence regulatory networks such as *CDKN2A*, *TP53*, *RB1* and *ATM*, or copy number gains of chromosomal regions that span *MYC* or *MDM4* are observed (Cancer Genome Atlas Research 2013, Sato, Yoshizato et al. 2013). HIF-α activation also induces the expression of transforming growth factor alpha (TGF-α), which results in activation of an EGF-R/PI3K/AKT/IκB-kinase-α/NFκB signalling cascade (An and Rettig 2005). NFκB activation increases cell cycle transition through the induction of cyclin D1, driving cell transition from G1 to S, in addition, upregulation is association with an increase in cell proliferation, tissue invasion, angiogenesis and apoptosis inhibition (Guttridge, Albanese et al. 1999).

1.14.5 Loss of pVHL affects microtubule function

pVHL regulates the orientation of mitotic cell division and ensures the fidelity of the mitosis spindle checkpoint in a HIF-α independent fashion. Loss of pVHL leads to reduced MAD2 expression (Thoma, Toso et al. 2009), a key component of the mitotic spindle checkpoint that prevents onset of anaphase until all chromosomes are correctly aligned (Thoma, Toso et al. 2009). Microtubules are crucial for the maintenance of cell shape and polarity, and in addition critical for cilia maintenance: pVHL plays an important role in cilia maintenance and in human cells lacking pVHL, cilia formation does not occur which in adult kidney cells results in the formation of pre-cancerous renal cysts (Schermer, Ghenoiu et al. 2006).

1.14.6 Mitogen-activated protein kinase (MAP-K) deregulation in ccRCC

Mitogen-activated protein kinase (MAPK) pathway kinases (MKK) play a critical role in the regulation of cell differentiation, survival and proliferation (Pearson, Robinson et al. 2001). Upon activation, MKKs phosphorylate MAPKs such as the extracellular signal-regulated protein kinase (ERK), c-Jun-NH2 kinase (JNK) and p38 MAP-K (Robinson and Cobb 1997). Sustained activation of ERK is an established requirement for angiogenesis and overexpression of MKK has been described in RCC (Oka, Chatani et al. 1995).

1.15 MiRNA deregulation in ccRCC

The role of LIMD1, Ajuba and WTIP in the regulation of miRNA mediated mRNA silencing has been outlined (James, Zhang et al. 2010, Bridge, Shah et al. 2017). Chen *et al* performed systematic and integrative analysis of 5 public miRNA expression datasets in ccRCC comparing expression profiles with that of normal renal tissue. This identified eleven deregulated miRNAs shared by five independent datasets that could distinguish normal kidney from ccRCC. Differentially enriched miRNA target genes played a critical role in cell cycle and transcription regulation, particularly the G1/S transition. Other pathways that demonstrated differential enrichment were involved in receptor mediated HIF regulation, as well as PTEN, TGF, and WNT pathways and the control of cytoskeletal remodelling (Chen, Zhang et al. 2013).

Increasing evidence supports the role of miRNAs in the regulation of the VHL/HIF axis with for example miR-17-5p and miR-224 acting as direct targets of both *VHL* and *HIF1α*. miR-138 was identified as a negative regulator of HIF1α with upregulation associated with increased apoptosis and migration of ccRCC cells (Song, Zhang et al. 2011). miR-210 has been shown to be expressed at higher levels in tumours with *VHL* mutations and is strongly regulated by both HIF-1α and to a lesser extent HIF-2α (McCormick, Blick et al. 2013) Overexpression of miR-210 has been shown to correlate with better clinico-pathological features, low tumour grade, stage and Ki-67 levels. Patients undergoing nephrectomy for localised RCC with tumours expressing high miR-210 had significantly longer OS than those with tumours with low miR-210 levels

(McCormick, Blick et al. 2013, Samaan, Khella et al. 2015). miR-122 upregulation has also been shown to play an important role in RCC progression by activating the PI3K/Akt signalling pathways. Numerous miRNAs are also downregulated in ccRCC with for example miR-187, miR215, miR-217, miR-155 and miR1826 associated with poorer prognosis (shorter survival or early recurrence) (Li, Wang et al. 2015).

In an analysis of 316 patients with RCC, genetic variations in microRNA-related genes notably *DICER* and *DROSHA* have been shown to associate with worse survival and increased risk of tumour recurrence. Interestingly in this same cohort, cumulative effects of multiple SNPs impacted on RCC survival, with patients carrying six or more unfavourable SNPs demonstrating a 6.66 fold increased risk of death compared to those with two or fewer unfavourable SNPs (95% confidence interval (CI) 2.49-17.86) (Lin, Horikawa et al. 2010).

1.16 Hippo pathway deregulation in ccRCC

Schütte *et al* have demonstrated that aberrant Hippo signaling is important in driving ccRCC proliferation and invasiveness. Immunohistochemical staining of 31 ccRCC tumours demonstrated nuclear overexpression of the Hippo target YAP, which was particularly prominent at the tumour edge suggesting that overexpression was driving tumour invasion. *In vitro*, shRNA mediated knockdown of YAP significantly inhibited the proliferation and migration of ccRCC cells in soft agar assays, whilst in a mouse xenograft ccRCC model, YAP knockdown significantly reduced tumour growth. Microarray analysis of YAP knockdown versus mock-transduced ccRCC cells demonstrated the down-regulation of endothelin 1 and 2 and the angiogenic inducer CYR61 as well up-regulation of the cell adhesion molecule cadherin 6 and c-myc (Schutte, Bisht et al. 2014).

1.17 Presentation of renal cell carcinoma

Historically a classic triad of haematuria, palpable abdominal mass and flank pain has been described, however fewer than 10% of patients now present in this manner and such symptoms are associated with advanced disease and consequent poor prognosis (Patard, Leray et al. 2003). Up to 50% of patients are diagnosed incidentally on imaging

for other medical reasons (Gill, Aron et al. 2010). Paraneoplastic syndromes are common and occur in approximately 30% of patients and are related to tumour-mediated cytokine release, in particular interleukin-6 (IL-6), erythropoietin (EPO), parathyroid related peptide (PTH-RP) and nitric oxide (NO) production and can result in constitutional syndromes such as weight loss, fever and malaise. Other paraneoplastic syndromes results in specific metabolic and biochemical abnormalities, such as hypercalcaemia as a result of PTH-RP production and erythrocytosis related to EPO production (Palapattu, Kristo et al. 2002).

1.18 Diagnosis of renal cell carcinoma

US and CT are commonly undertaken to detect and evaluate renal masses with CT playing an important role in the staging of RCC (Israel and Bosniak 2005). The presence of a contrast enhancing mass on CT is highly suggestive of malignancy (Israel and Bosniak 2005). Renal ultrasonography can be useful for the further evaluation of questionable cystic renal masses if CT imaging is inconclusive but large papillary tumours may be overlooked by renal ultrasonography (Israel and Bosniak 2005). Positron emission tomography (PET) is not a standard imaging modality of choice (Ljungberg, Bensalah et al. 2015). Further characterisation of possible lung metastases or enlarged mediastinal lymph nodes should be undertaken with contrast enhanced CT scan of the chest (Ljungberg, Bensalah et al. 2015). Most individuals with bone or brain metastases are symptomatic and in such patients further appropriate targeted imaging should be undertaken with for example bone scan or MRI of the brain (Ljungberg, Bensalah et al. 2015).

Following the identification of a renal mass, most renal masses will be further evaluated with a percutaneous renal biopsy. At least two quality cores (non-fragmented and >10mm in length) should be taken and peripheral biopsies are preferable to central to avoid the issue of central necrosis (Ljungberg, Bensalah et al. 2015).

1.19 Treatment of clear cell renal cell carcinoma

1.19.1 Treatment of organ-confined ccRCC

Treatment of organ-confined disease is typically with partial nephrectomy (PN) or radical nephrectomy (RN): this is the only curative treatment with associated high-quality evidence. Smaller T1a-b tumours should be managed by PN if technically feasible as there is no difference in cancer-specific relapse between a PN or RN approach, but all-cause mortality is increased in patients undergoing RN where tumours are less than four centimetres (MacLennan, Imamura et al. 2012). PN can be performed using an open or laparoscopic or robot-assisted laparoscopic approach (Ljungberg, Bensalah et al. 2015). For larger tumours, lower morbidity is associated with a laparoscopic, compared to open RN approach and this approach is therefore preferable where technically possible (Ljungberg, Bensalah et al. 2015).

Radiofrequency ablation or cryo-ablation remain alternative validated approaches in patients with small tumours; particularly in those not fit enough to undergo surgery (Escudier, Porta et al. 2014). Microwave ablation, laser ablation and high intensity focused US ablation are considered experimental approaches and are not routinely recommended (Ljungberg, Bensalah et al. 2015).

1.19.2 Treatment of metastatic ccRCC (mccRCC)

1.19.2.1 Surgery in mccRCC

Cytoreductive nephrectomy is recommended in patients with good PS and a large primary tumour with limited volume of metastatic disease and in those with a symptomatic primary tumour, for example causing significant pain or haematuria (Escudier, Porta et al. 2014). Two large multi-centre phase III trials, the CARMENA and Surtime EORTC-GU 30073 evaluated the role of upfront nephrectomy versus TKI treatment with Overall Survival (OS) and Progression Free rate at 28 weeks as their respective primary endpoints. The CARMENA trial, a randomised multi-centre trial of

patients with synchronous mRCC randomised patients 1:1 to either 12 weeks of neo-adjuvant suntinib prior to nephrectomy or sunitinib alone without nephrectomy. This non-inferiority trial demonstrated no statistically significant difference in OS for sunitinib along compared to sunitinib prior to nephrectomy (Hazard ratio (HR) for death 0.89, 95% CI 0.71-1.10)) (Mejean, Ravaud et al. 2018). The EORTC-GU 30073 study (SURTIME) randomised patients with resectable, synchronous metastatic ccRCC to either immediate nephrectomy followed by sunitinib or deferred nephrectomy with neo-adjuvant sunitinib for twelve weeks. Results demonstrated that there was no difference in progression free rate at 28 weeks between the two arms but strikingly, although the sample size was small, OS stratified by the intention to treat population was significantly increased in the deferred nephrectomy group at 32.4 months (95% confidence interval (CI) 14.5-63.5 months) versus 15.1 months (95% CI 14.5-63.5 months). In addition, there were fewer surgical complications in the deferred arm at 27.5%, versus 43.5% (Bex, Mulders et al. 2017). Such practice changing clinical trials are redefining the role of upfront nephrectomy in this patient group.

Metastatectomy with resection of metastatic lesions can play in role in fit patients with a limited burden of disease, e.g. solitary or easily accessible pulmonary metastases and tumour characteristics suggesting reasonably indolent disease (Ljungberg, Bensalah et al. 2015). Resection of solitary lung metastases may provide a survival benefit in a subgroup of patients without aggressive tumour characteristics (Karam, Rini et al. 2011).

1.19.2.2 Chemotherapy and radiotherapy in mccRCC

Chemotherapy and radiotherapy play a limited role in the treatment of metastatic ccRCC. Most ccRCC tumours demonstrate a degree of chemotherapy resistance, in part related to tumour production of large amounts of a multi-drug resistance protein, leading to cellular cytotoxic drug efflux (Tobe, Noble-Topham et al. 1995). Relative tumour hypoxia and disorganised angiogenesis, impairing tumour-associated drug delivery are also likely to contribute (Karakashev and Reginato 2015). Combination chemotherapy with irinotecan, cisplatin and mitomycin-C (IPM) does for example demonstrate some efficacy: in a retrospective analysis of 62 patients, 64% of patients derived some benefit following the failure of cytokine therapy (Shamash, Powles et al.

2005). The role of chemotherapy is however increasingly diminishing since the introduction of effective targeted therapy.

RCCs have traditionally been considered relatively radioresistant, defined as a poor clinical response to conventional radiotherapy doses. The radiobiologic characteristics of *in vitro* survival curves are considered important determinants of tumour response to conventional radiotherapy with the classic measure of radiosensitivity defined as the survival fraction of cells in a clonogenic survival curve after a 2 Gy radiation exposure (Ning, Trisler et al. 1997). *In vitro* assays demonstrate that RCC lines are relatively insensitive to 2 Gy radiation, although they do show sensitivity to higher doses of radiotherapy, particularly doses of over 6 Gy (Ning, Trisler et al. 1997).

Given the relative tumour insensitivity to conventional RT doses and inherent limited radiation tolerance of the normal kidneys and surrounding tissues, fractionated radiotherapy is rarely used to treat primary renal tumours. Several clinical studies have however reported excellent control of brain metastases in patients treated with >10 Gy fractions delivered through stereotactic radiosurgery (Sheehan, Sun et al. 2003) and good control of spinal metastases and pain relief in patients treated with a 20 Gy single RT fraction (Gerszten, Burton et al. 2007).

1.19.2.3 Interleukin-2 (IL-2) and interferon-α (IFN-α) in mRCC

Prior to the introduction of TKIs, IFN-α and high dose IL-2 were the mainstay of treatment, associated with a modest at best response. High dose IL-2 is only appropriate in a small subset of very fit patients with good prognosis disease and since the introduction of checkpoint inhibition has become increasingly redundant. In patients with good prognosis disease, response rates to IFNα are in the region of 10-20% with an associated survival benefit of only a few months (Coppin, Porzsolt et al. 2005). In the SELECT trial, high dose IL-2 was associated with a durable complete response in less than 10% of cases, however most patients do not benefit and the median PFS of patients in the study was short at only 4.4 months (Clement and McDermott 2009).

1.19.2.4 Targeted therapy for metastatic RCC

Angiogenesis is a critical step in ccRCC tumour progression with multiple kinases such as VEGF-receptor tyrosine kinases (VEGF-R-TKs) and PDGF-receptor-tyrosine kinases (PDGF-RTK) up-regulating angiogenesis and maintaining tumour growth (Gotink and Verheul 2010) (**Figure 1.15**)

Currently eight targeted drugs are approved in the USA and Europe for treating metastatic ccRCC and with sequential and recurrent use of such drugs, median OS is around 27 months in patients with Memorial Sloan-Kettering Cancer Cancer (MSKCC) intermediate prognosis disease compared to 9 months in the pre-TKI era (this is a prognostic scoring system that stratifies patients according to clinico-pathological parameters) (Motzer, Hutson et al. 2013) and immune checkpoint inhibitors may extend this figure further. Most targeted agents target VEGF/PDGF-mediated angiogenesis either directly blocking VEGF/VEGFR interaction, as in the case of the humanised monoclonal antibody bevacizumab, or indirectly, as multi-tyrosine kinase inhibitors in the case of sunitinib, pazopanib, sorafenib, axitinib and cabozantinib (Gotink and Verheul 2010, Tannir, Schwab et al. 2017) (**Figure 1.15**). Temsirolimus and everolimus are analogues of rapamycin that inhibit the kinase activity of the mTOR complex 1 (mTORC1) resulting in reduced translation of cell-cycle regulatory proteins and suppressed angiogenesis (Rini 2011) (**Figure 1.15**).

Multi-targeted TKIs have conventionally been used as first-line agents, and most are small-molecule kinase inhibitors that compete with ATP to prevent ATP binding and kinase activation. Their dominant molecular targets are the VEGF receptor TK, in particular, VEGFR-1, 2, and 3 TKs but other pro-angiogenic pathways are also affected, particularly the PDGF-R and c-KIT pathways (Gotink and Verheul 2010, Rini 2011). Sunitinib for example targets VEGFR, PDGFR, FLT-3 and c-KIT and off-target effects can contribute to drug-associated side effects (O'Farrell, Abrams et al. 2003).

Pivotal phase III randomised controlled trials had established the use of sunitinib and pazopanib as first-line treatment in mccRCC although novel immunotherapy agents are changing the treatment paradigm (Motzer, Hutson et al. 2007, Sternberg, Davis et al. 2010, Escudier, Porta et al. 2014). Bevacizumab in combination with IFN-α has a role in

favourable and intermediate prognostic groups, although it is not generally used in the United Kingdom (Rini, Halabi et al. 2010).

The potent, orally available TKI axitinib is not recommended as first line therapy in metastatic ccRCC as the primary end-point of PFS was not met in the pivotal trial evaluating the role of axitinib in this setting (Hutson, Lesovoy et al. 2013).

mTOR inhibitors have conventionally been used after the failure of VEGF-targeted therapy. In the phase III randomised controlled trial RECORD-1, patients who had progressed after first line VEGF-targeted therapy were randomised 2:1 to everolimus or placebo with crossover to everolimus permitted upon progression. In the intention to treat analysis, the PFS was significantly improved in the everolimus arm at 5.4 versus 1.9 months (Stein, Bellmunt et al. 2013).

The majority of patients will initially obtain clinical benefit with VEGF-targeted therapy, however acquired resistance invariably develops, variable both in timing and clinical pattern. Some mechanisms such as angiogenic escape are described, whereby with time the initial targeted therapy becomes ineffective at blocking the VEGF axis, but switching to a more potent VEGF targeted agent may result in a further response (Motzer, Escudier et al. 2013). In addition, the restoration of angiogenesis may result through the activation of VEGF-independent pathways, for example FGF-2, tie2/Ang2, IL8 and Src upregulation (Powles, Chowdhury et al. 2011). MET and AXL up-regulation are also increasingly implicated in resistance to VEGF-TKI. MET is a receptor tyrosine kinase which after binding to its ligand, hepatocyte growth factor, activates pro-tumourigenic pathways, which regulate cell proliferation, motility, migration and invasion, MET upregulation in ccRCC is a poor prognostic indicator. AXL is another RTK, which binds to the ligand GAS6, in turn stimulating multiple pro-tumourigenic signalling cascades (Zhou, Liu et al. 2016). AXL upregulation is associated with worse outcome in ccRCC and upregulation is also an established mechanism for resistance to VEGF TKIs (Zhou, Liu et al. 2016).

Cabozantanib is on oral TKI that targets the VEGF-TKI as well as the MET and AXL signalling pathways. In the metastatic RCC phase III study evaluating cabozantinib versus everolimus (METEOR) study, patients who had received at least one prior

VEGFR-TKI and had progressed within 6 months of the most recent dose of VEGFR-TKI were randomised to either cabozantinib or everolimus. The PFS in patients receiving cabozantinib was 7.4 months versus 3.8 months in those receiving everolimus, (HR 0.58, 95% CI 0.51-0.89) (Choueiri, Escudier et al. 2016).

More recently the role of cabozantinib in patients with poor and intermediate prognosis mRCC has been evaluated in the first line setting. In a multi-centre phase III trial, patients were randomised either to receive sunitinib or cabozantinib with crossover not permitted. A significant improvement in PFS was observed in association with cabozantinib treatment of 8.2 versus 5.6 months for sunitinib, median OS was also improved, at 30.3 months versus 21.8 months although this did not meet statistical significance (Choueiri, Halabi et al. 2017).

The multi-tyrosine kinase inhibitor lenvatinib, is a potent VEGF-R TKI, and also acts on the FGF-R pathways, a common mechanism for tumour escape and TKI resistance. In a randomised phase II study, patients randomised to the combination treatment compared to everolimus alone, demonstrated a 9-month improvement in PFS (O'Reilly and Larkin 2017).

Studies such as the phase II study of axitinib in patients with metastatic RCC unsuitable for nephrectomy (A-PREDICT) are making use of sequential tissue before and after VEGF-targeted therapy to help improve our understanding of possible mechanisms of tumour escape. Predictive biomarkers that establish the likely therapeutic benefit of targeted agents are being evaluated and are discussed further in section 1.21. Single nucleotide polymorphisms (SNPs) appear particularly promising, however intra-tumoural heterogeneity undoubtedly has hampered biomarker identification (Section 1.22).

1.19.2.5 Novel immune therapy in metastatic ccRCC

The natural history of RCC suggests that the immune system can play a powerful role in controlling tumour growth, as disease regression can occur in the absence of treatment. RCC typically has a prominent immune cell infiltrate with high levels of T cells, natural killer (NK) cells, dendritic cells (DCs) and macrophages, but often demonstrates a high level of immune dysfunction. This ultimately promotes cell growth and immune evasion

(Porta, Bonomi et al. 2007). Mechanisms for immune escape include T-cell down-regulation through anergy-associated gene upregulation (Noessner, Brech et al. 2012) and disturbance of the circulating lymphocyte and dendritic cell subpopulations (Porta, Bonomi et al. 2007).

Novel immune modulating agents act predominantly as immune checkpoint blocking antibodies, blocking in particular the cytotoxic T-lymphocyte-associated antigen 4 (CTLA-4) and programmed death receptor-1 (PD-1)/programmed death receptor ligand-1 (PDL1) (Mataraza and Gotwals 2016). CTLA-4 inhibits T-cell activation during the priming phase of T-cell activation whilst PD-1, expressed on B, T and NK cells, exerts its inhibitory activity predominantly during the effector phase of T-cell activation within the tumour microenvironment (Topalian, Drake et al. 2015). PD-1 and PD-L1 are also both expressed on regulatory T-cells (Tregs) and Treg upregulation can promote a pro-angiogenic RCC phenotype (Facciabene, Motz et al. 2012).

Multiple trials have evaluated anti-PD-1 and anti PDL-1 therapy in RCC. In the phase III Checkmate-025 trial, patients with advanced metastatic ccRCC who had received previous targeted therapy, were randomised to either the PD-1 blocking drug nivolumab, or the mTOR inhibitor everolimus until progression or unacceptable toxicity. Nivolumab improved OS, with a median OS of 25 months compared to 19.6 months in patients receiving everolimus (Motzer, Rini et al. 2015). Studies have also demonstrated that blocking PDL-1 in mRCC is also effective. In a phase 1a study of the humanised anti-PDL-1 antibody atezolizumab, a reduction in tumour burden was observed in 46% of patients with an associated manageable safety profile (McDermott, Sosman et al. 2016).

CTLA-4 blockade in metastatic RCC has also been evaluated. In a phase II study, 5 out of 40 patients receiving high dose ipilumimab responded compared to 1 response out of 20 patients in the low dose group (Yang, Hughes et al. 2007).

In the Checkmate-214 trial presented at ESMO in September 2017, treatment naïve patients with mRCC were randomised to combination therapy with nivolumab and ipilumimab versus sunitinib monotherapy (Rexer 2015). Overall there was an improvement in both objective response rate (ORR) and PFS in association with the

combination of nivolumab and ipilumimab: 41.6% versus 26.5% (p<0.0001) for ORR and a PFS of 11.6 versus 8.2 months (HR 0.82, p=0.03). More striking however was the subgroup analysis of patients with poor and intermediate prognosis disease with tumours demonstrating positivity for PDL-1 expression (≥1%). In these patients the ORR was 58.5% versus 25% and median PFS was 22.8 months versus 5.9 months (HR 0.48, p=0.0003). In patients with good prognosis disease however, the reverse association was seen irrespective of tumour PDL-1 expression. The ORR was 29% with nivolumab/ipilimumab versus 52% with sunitinib (p = 0.0002) and median PFS was 15.3 months versus 25.1 months, respectively, HR 2.17, p < 0.0001. This study is therefore potentially practice changing (Rexer 2015, Rexer, Steiner et al. 2017).

1.20 Prognostic factors in clear cell renal cell carcinoma

An on-going challenge in an era of personalised and molecularly targeted medicine is to identify biomarkers that assist diagnosis, determine prognosis and predict how patients will respond to treatment. Such a targeted approach can result in a stratified patient-centred focus, with the aim of maximising therapeutic efficacy for that individual.

Prognostic factors are objectively measurable clinical or biological characteristics that provide information on the likely outcome for that patient based on the factor identified. This can provide important patient-relevant information, such as giving an estimate of OS, which in turn may dictate how that patient is treated. For example, active surveillance may be inappropriate in a patient with a tumour with poor prognostic features. A predictive factor is a clinical or biological characteristic that provides information on the likely benefit of treatment i.e. whether a patient will respond to a particular treatment.

For ccRCC, a number of clinical prognostic algorithms exist and numerous prognostic biomarkers have been identified. Few of these however have been externally validated and currently there are no validated predictive biomarkers (Gulati, Martinez et al. 2014).

1.20.1 TNM stage classification

The tumour/node/metastasis (TNM) staging is a validated prognostic scoring system, first described in 2001, which should be used for clinical and scientific staging purposes. Updated in 2010, accurate staging is crucial to aid decision-making related to for example the surgical management of localised disease. In addition this classification provides important prognostic information on the likelihood of local recurrence and long-term overall survival. The 2010 TNM staging classification is prognostic and has undergone validation in both single institution and multi-institution analyses (Zisman, Pantuck et al. 2001, Edge and Compton 2010, Kim, Alt et al. 2011, Ljungberg, Bensalah et al. 2015).

1.20.2 Grading of ccRCC

The pathological grading of ccRCC is based on the microscopic morphology after haematoxylin and eosin (H and E) staining. The most popular grading system was described in 1982 by Fuhrman *et al* (Fuhrman, Lasky et al. 1982). This system defines four nuclear grades on the basis of increasing nuclear size, irregularity and nucleolar prominence. In patients with localised disease, Fuhrman grade is strongly predictive of the likelihood of distant metastases following nephrectomy (Fuhrman, Lasky et al. 1982). Recently a simplified nuclear grading system has been proposed based solely on nucleoli size and shape: this correlates with prognosis and demonstrates good inter-observer reproducibility and increasingly is recommended as the grading system of choice (Srigley, Delahunt et al. 2013, Escudier, Porta et al. 2014).

1.20.3 Clinical prognostic factors in ccRCC

There are several prognostic, validated scoring systems in routine use in both localised and metastatic ccRCC. Whilst giving an indication of likely prognosis within the population as a whole, the accuracy of outcome-prediction is limited at an individual patient level (Motzer, Mazumdar et al. 1999, Frank, Blute et al. 2002, Heng, Xie et al. 2009, Tang, Vickers et al. 2011).

The SSIGN score incorporates the stage, size, grade and presence/absence of necrosis and generates a score of between 0 and 15, which correlates well with 5-year metastasis-free survival. Patients designated 0-2 are considered low risk with a 97.1% 5 year-metastasis-free survival whilst those scoring ≥6 are considered high risk with a 31.2% 5 year-metastasis-free survival (Leibovich, Blute et al. 2003). The SSIGN score has subsequently undergone validation in a European single centre cohort of >1800 patients with scores found to correlate with Cancer- Specific Survival (CSS). Combining scores into five categories improved discrimination with respect to CSS (Zigeuner, Hutterer et al. 2010).

The University of California Los Angeles Integrated Staging System (UISS) incorporates prognostic models for both localised and metastatic RCC and has been validated in an international multi-centre study of over 4000 patients in the pre-TKI era (**Figure 1.17**) (Patard, Kim et al. 2004). The original UISS score was modified into an algorithm that stratified patient survival into low (LR), intermediate (IR) and high risk (HR) groups for both localised and metastatic disease based on the 1997 TNM stage, Fuhrman grade and Eastern Cooperative Oncology Group (ECOG) performance status (PS). In the cohort described, significant differences in 3-year OS were observed in patients with localised disease depending on their risk group with 3-year OS of 92%, 67% and 44% for LR, IR and HR groups respectively. In patients with metastatic disease, the 3-year survival rates were 37%, 23% and 12% for LR, IR and HR groups respectively (**Figure 1.17**) (Patard, Kim et al. 2004).

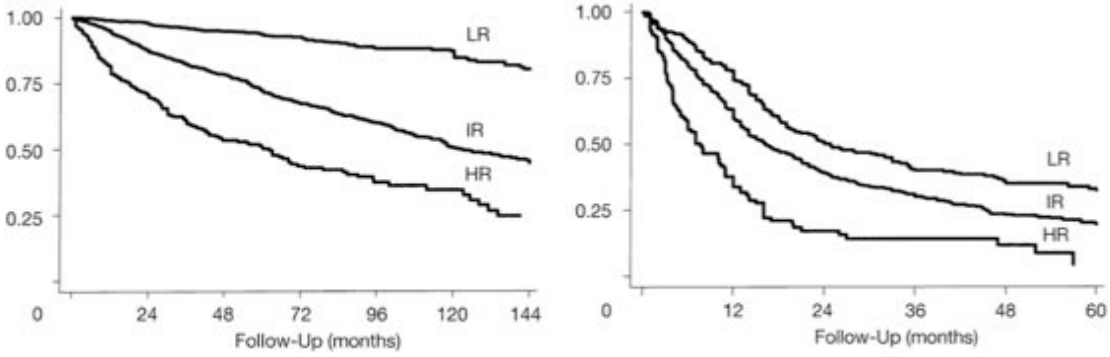

Figure 1.17 Kaplan-Meier survival estimates according to University of California Los Angeles Integrated Staging System in 3,119 patients with localised disease

(left panel), and 1,083 patients with metastatic disease (right panel). LR, low-risk; IR, intermediate-risk; HR, high-risk. Adapted from (Patard, Kim et al. 2004)

In the metastatic setting, one of the most widely used predictive models to predict OS is the MSKCC tool developed by Motzer *et al*. This was developed in patients receiving IFN-α (Motzer, Bacik et al. 2002) and independently validated in 2005 in patients receiving a variety of single and combination agents (Mekhail, Abou-Jawde et al. 2005) before undergoing validation in patients receiving targeted therapy (sunitinib) (Motzer, Hutson et al. 2009). The components of the MSKCC score are (1) KPS less than 80%, (2) time from diagnosis of RCC to treatment of less than one year, (3) serum lactate dehydrogenase greater than 1.5x upper limit of normal (ULN), (4) corrected serum calcium greater than 10mg/dL and (5) haemoglobin concentration less than the lower limit of normal (LLN).

Favourable prognosis is defined as no poor prognostic factors, intermediate as one or two poor prognostic factors and poor, as more than two poor prognostic factors (Motzer, Bacik et al. 2002). In the validation study by Mekhail *et al*, median OS stratified for the three prognostic groups was 28.6, 14.6, and 4.5 months respectively (P<0.0001) (**Figure 1.18**) (Mekhail, Abou-Jawde et al. 2005).

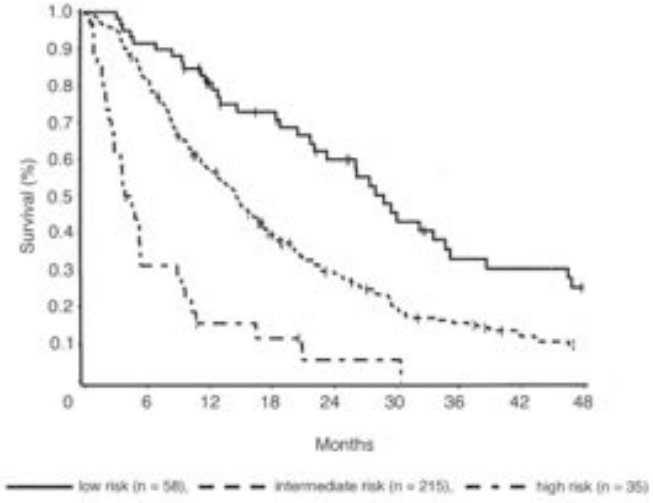

Figure 1.18 Kaplan-Meier survival estimates by MSKCC risk groups in the cohort of 353 previously untreated patients with mRCC. Patients were stratified in to high, intermediate and low risk groups on the basis of their pre-treatment MSKCC score. Adapted from (Mekhail, Abou-Jawde et al. 2005)

Heng *et al* identified prognostic factors predictive of OS in 645 patients with mRCC receiving 1st line VEGF-targeted therapy. Four of the five adverse prognostic factors form part of the MSKCC score: (1) haemoglobin less than lower limit of normal (LLN), (2) corrected calcium > upper limit of normal (ULN), (3) KPS<80%, and (4) time from diagnosis to treatment of <1 year. In addition neutrophil count >ULN and platelet count >ULN were identified as independent adverse prognostic factors. Patients were stratified in to three-risk groups, favourable, (0 risk factors), intermediate, (1-2 risk factors) and poor risk (3 or greater risk factors). Median OS strongly corresponded with prognostic group at 43, 27 and 8 months respectively (**Figure 1.19**) (Heng, Xie et al. 2009).

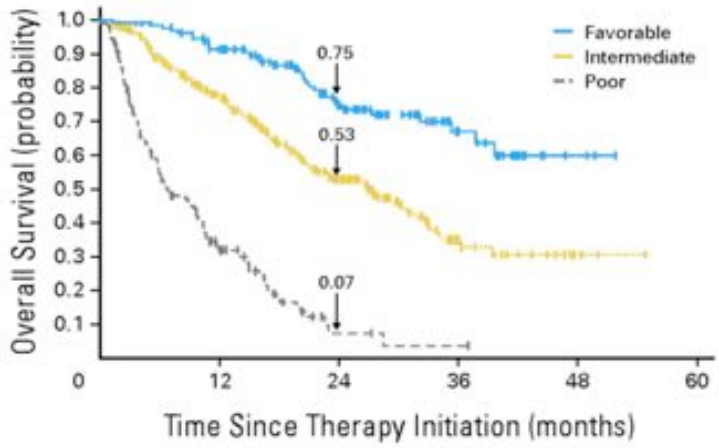

Figure 1.19 Kaplan-Meier survival estimates stratified according to Heng risk group with proportion of patients in each group alive at 24 months post therapy initiation. Adapted from (Heng, Xie et al. 2009)

1.20.4 Molecular biomarkers for ccRCC

Molecular biomarkers may be prognostic and, or predictive in nature and can be grouped according to their physiological location, defined as either circulating or tissue based.

1.20.4.1 Circulating ccRCC biomarkers

VEGF and VEGF related proteins

VEGF is a potent mediator of angiogenesis in ccRCC, facilitating tumour growth and metastases. Expression is regulated by HIFα and enhanced VEGF concentration correlates with *VHL* gene inactivation (Gnarra, Zhou et al. 1996). Jacobsen *et al*, found that elevated serum VEGF levels were prognostic and associated with a shorter survival time in the pre-TKI era (Jacobsen, Rasmuson et al. 2000). Other studies have however demonstrated opposite associations, correlating high baseline VEGF-A concentrations with shorter OS and PFS (Tran, Liu et al. 2012).

Escudier *et al* found that higher serum VEGF levels were predictive and correlated with a better response to sorafenib (Escudier, Eisen et al. 2009). Studies have however also demonstrated that low baseline levels of soluble VEGFR-3 and VEGF-C levels are associated with longer PFS in patients receiving sunitinib treatment compared to IFN-α (Deprimo, Bello et al. 2007).

Cytokine and angiogenic factors (CAFs)

Other circulating cytokine and angiogenic factors have been evaluated as potential prognostic and predictive indicators. In a phase III trial Tran *et al* found that higher baseline plasma interleukin-8, HGF and osteopontin levels were associated with shorter PFS in patients receiving pazopanib and that high concentrations of six CAF signatures, IL-6, IL-8, HGF, osteopontin, VEGF-A and TIMP-1 correlated with shorter PFS whilst higher baseline IL-6 levels were prognostic for OS (Tran, Liu et al. 2012).

1.20.4.2 Tissue based ccRCC biomarkers

VHL

Multiple biomarkers for ccRCC have been identified and many are hypoxically regulated. Most studies correlating *VHL* gene status and common clinical prognostic factors have not found an association: this may be related to the near universality of *VHL*-inactivation (Kondo, Yao et al. 2002, Gimenez-Bachs, Salinas-Sanchez et al. 2006) (Maroto and Rini 2014).

HIF

HIF1α is frequently over-expressed in ccRCC. Klatte *et al* found that in patients with metastatic ccRCC, high HIF-1α expression was independently associated with shorter OS (Klatte, Seligson et al. 2007). However other groups have not observed the same association. Lidgren *et al* for example reported no survival difference between patients with high and low HIF-1α expression (Lidgren, Hedberg et al. 2005).

HIF1α and HIF2α have some overlapping functions but can regulate distinct sets of genes with increasing evidence that HIF2α plays a more critical role in mediating tumourigenesis in ccRCC (Biswas, Troy et al. 2010). In addition, some reports have suggested that HIF1α acts as a tumour suppressor in ccRCC with overexpression associated with better prognostic outcomes (Gossage, Eisen et al. 2015). There is also conflicting evidence as to the prognostic effects of the overexpression of genes regulated downstream of *HIF1α* such as *VEGF* and *CAIX*.

Fan *et al* undertook a Preferred Reporting Items for Systematic Review (PRISMA)-compliant systematic review and meta-analysis of the prognostic significant of HIF1α and HIF2α immunohistochemical expression in renal cell carcinoma. In view of studies that have demonstrated that sub-cellular HIF localisation may be important in driving ccRCC tumourigenesis (Kroeger, Seligson et al. 2014), analysis was undertaken both for total HIF and with stratification according to sub-cellular localisation. 14 studies were

included. Total HIF1α and HIF2α expression did not correlate with PFS or OS, however sub-cellular HIF localisation was prognostic with high nuclear HIF1α expression correlating with worse OS and high cytoplasmic HIF2α with worse CSS (Fan, Li et al. 2015).

Increasing evidence is emerging that ccRCC can be subdivided into tumours with (1) wild type (WT) *VHL*, (2) *VHL*-deficient tumours that overexpress both *HIF1α* and *HIF2α* and (3) *VHL*-deficient tumours that only overexpress *HIF2α* and that such sub-classification may be prognostic. It has been suggested that this last subtype of tumours are particularly aggressive with enhanced c-MYC activity and enhanced activation of the MAPK/ERK pathway resulting in increased cell proliferation and metastases (Gordan, Lal et al. 2008).

Kroeger *et al* undertook cytogenetic analysis on 345 ccRCC tumours with abnormal karyotype, sub-classifying tumours according to the loss of the *VHL* gene (3p loss), *HIF1-α* (14q loss) and HIF2α overexpression. They concluded that tumours that demonstrated loss of 3p i.e. those with loss of *VHL* had more favourable clinico-pathological features and patients with such tumours had improved CSS compared to those with VHL-proficient tumours. In addition, loss of 14q (*HIF1α*) was associated with worse relapse-free survival (RFS) and CSS. In tumours that overexpressed *HIF2α* and had lost 3p (*VHL*), 14q loss (*HIF1α*) was the most important predictor of RFS (Kroeger, Klatte et al. 2013).

Carbonic anhydrase IX (CAIX)

CAIX is a HIF1α regulated protein involved in regulating intracellular and extracellular pH in response to hypoxic stress (Dorai, Sawczuk et al. 2006) and is up-regulated in approximately 70% of ccRCCs (Choueiri, Regan et al. 2010). In both localised and metastatic ccRCC, low CAIX staining has been shown in several series to serve as an independent poor prognostic factor for survival (Bui, Visapaa et al. 2004, Phuoc, Ehara et al. 2008). However, data from the treatment approaches in renal cancer global evaluation (TARGET) trial, evaluated CAIX expression in patients with mRCC treated with either sorafenib or placebo and demonstrated neither prognostic nor predictive value for CAIX staining (Jonasch, Corn et al. 2010). Similarly no association was observed between CAIX staining and clinical outcomes in patients receiving treatment with temsirolimus (Cho, Signoretti et al. 2007).

VEGF and VEGF-related proteins

In some studies, elevated VEGF has been shown to correlate with increasing tumour size, Fuhrman grade, tumour necrosis and tumour stage (Paradis, Lagha et al. 2000) (Yildiz, Gokce et al. 2004). VEGF-A overexpression has also been associated with shorter OS in patients receiving first line sunitinib (Garcia-Donas, Leandro-Garcia et al. 2013). This same study also found that VEGFR-3 overexpression was associated with a longer PFS and that VEGFR3 overexpression demonstrated a negative correlation with the VEGFR3 polymorphism RS307826, a predictor of sunitinib resistance (Garcia-Donas, Leandro-Garcia et al. 2013).

Chromatin remodelling genes

Loss of, and mutations in the newly identified chromatin remodelling genes *PBRM1*, *SETD2* and *BAP1* in ccRCC has been described (Sato, Yoshizato et al. 2013) (Cancer Genome Atlas Research 2013). Sato *et al* investigated the effects of these mutations on survival and tumour recurrence and found that *PBRMI* mutations had no impact on OS or disease-free survival (DFS), but that *BAP1* mutations were associated with a significantly shorter OS ($p=0.0203$). Tumours with *SETD2* mutations demonstrated a very high relapse rate (HR=3.38, $p=6x10^{-4}$) compared to *SETD2* proficient tumours but

this did not correlate with OS (Sato, Yoshizato et al. 2013). Hakimi *et al* described the outcome associated with *BAP1* and *SETD2* mutations in 609 patients with ccRCC from two distinct cohorts (an MSKCC and TCGA cohort). They observed that *BAP1* mutations were associated with worse CSS in both cohorts. *SETD2* mutations were associated with worse CSS in the TCGA cohort but not in the MSKCC cohort, whilst *PBRM1* mutations, observed with the highest frequency of the three TS, had no impact on CSS (Hakimi, Pham et al. 2013).

Single nucleotide polymorphisms

SNPs are the commonest type of genetic variation. Genome-wide association studies (GWAS) can be used to identify germline polymorphisms associated with clinical outcome. There is increasing evidence that SNPs may function as useful predictive biomarkers in ccRCC. Several studies have investigated SNPs as predictors of drug efficacy, with certain polymorphisms predicting sunitinib efficacy e.g. SNPs in the *CYP3A5*, *NR1/3* and *ABCB1* genes. Patients with favourable polymorphisms in these genes had a significantly improved median PFS when treated with sunitinib compared to those without (13.1 versus 7.5 months, p=0.009) (van der Veldt, Eechoute et al. 2011).

Genetic analysis from the comparison of pazopanib versus sunitinib in metastatic renal cell carcinoma (COMPARZ) trial, comparing upfront pazopanib versus sunitinib demonstrated a significant association between IL-8 polymorphisms in patients treated solely with sunitinib but not pazopanib with respect to both PFS and OS (Maroto and Rini 2014).

1.20.5 Clear cell type A (ccA) and clear cell type B (ccB) subtypes

In the past few years, gene expression microarray data has been analysed using software that uses iterative consensus clustering algorithms to identify distinct subtypes of ccRCC. Most previous prognostic stratification approaches relied on preselected molecular features or clinical outcomes to distinguish tumour types but with this approach there is no inherent pre-selection, and tumours are classified based on their underlying tumour biology.

By applying consensus clustering to the gene expression data of ccRCC tumours without first applying clinical or biological information, two subtypes of ccRCC designated ccA and ccB were identified. Analysis of these subsets identified a small core of highly predictive genes that can be used to classify tumours individually. The investigators found that several of the pathway genes overexpressed in ccA tumours, were strongly correlated with *VHL* inactivation and the overexpression of HIF signalling components such as *EPAS1*, *EGNL3*, *PDGFC*, *HIG2* and *CA9*. However, VHL inactivation in both ccA and ccB tumours occurred with similar frequency. Other pathways deregulated in ccA tumours are involved in fatty acid and organic acid metabolism. For ccB tumours, pathway analysis demonstrated that genes that regulate EMT, the cell cycle and wound healing were overexpressed. A third group of tumours that shared pattern features with both ccA and ccB tumours was identified, and Brannon *et al* speculated that this group may represent an intermediate group undergoing progress from one subtype to the other, or share common characteristics of both groups (Brannon, Reddy et al. 2010).

Notably when analysis of CSS and OS was undertaken for the two groups and subtype correlated with the covariates in the UISS score (Fuhrman grade, tumour size and PS), there was a significant difference. Patients with ccA tumours had a median survival of 8.6 years versus 2 years in those with ccB tumours. In addition, molecular classification strongly correlated with tumour stage and grade, with ccA tumours demonstrating lower stage and grade (Brannon, Reddy et al. 2010).

Despite attempts to stratify patient risk on the basis of biomarkers, most molecular ccRCC biomarkers have not been independently validated and validated biomarkers have not entered clinical practice. In a recent study by Gulati *et al*, ccRCC prognostic biomarkers validation was undertaken in an independent patient cohort and intra-tumour heterogeneity of the most promising biomarkers also assessed. A total of 17 out of 28 biomarkers were validated as predictors of poor CSS on univariate analysis, but only tumour stage and the ccB signature were independent predictors in multivariate analysis (Gulati, Martinez et al. 2014).

The group identified a number of somatic copy number alterations (SCNAs) as poor prognostic markers on univariate analysis, e.g. chromosome 8q and 12 amplification and chromosome 9p and 22q deletions. Given these findings the group asked whether the ccB expression signature reflected the transcriptomic impact of these poor risk genetic alterations and identified that several of these SCNAs were over-represented in the ccB samples. By calculating the weighted Genomic Instability (wGII) a measure of overall copy number aberrations, they found that ccB samples had significantly higher wGIIs compared to ccA samples. They therefore hypothesised that the ccB phenotype is partially driven by these poor prognosis SCNAs in association with a cancer genomic background of elevated chromosomal instability (Gulati, Martinez et al. 2014).

1.20.6 Biomarkers in ccRCC for predicting response to immunotherapy

Programmed death ligand-1 (PDL-1)

Drugs that enhance anti-tumour immune responses through the targeting of the PDL1-/PD1 pathways have demonstrated promising results in RCC resulting in durable responses in a subset of patients (McDermott, Sosman et al. 2016) (Herbst, Soria et al. 2014).

PDL1 is expressed on both tumour cells and also tumour-infiltrating immune cells within the tumour microenvironment where it acts as a negative regulator of T-cell proliferation and function and therefore facilitates tumour evasion of immune surveillance. Higher PDL-1 expression in tumour-infiltrating immune cells has been associated with worse outcome in RCC (Thompson, Dong et al. 2007). It appears increasingly that PDL-1 expression on tumour-infiltrating immune cells may be more important than on tumour cells.

McDermott *et al* undertook subgroup analysis for PFS and OS in patients with metastatic RCC receiving the PDL-1 inhibitor atezolizumab and found a trend towards lower anti-tumour activity in patients with tumours with low PDL1 expression compared to patients with tumours with higher PDL1 expression(McDermott, Sosman et al. 2016). In addition, a number of immunologic correlates were observed which were associated with response, such as a fall in plasma VEGFA and on-treatment falls in the

acute-phase proteins ferritin and macrophage inflammatory protein-1α. McDermott *et al* also found that a higher ratio of effector T cells to regulatory T cells as represented by FOXP3 expression was associated with atezolizumab response (McDermott, Sosman et al. 2016).

1.21 Tumour heterogeneity in ccRCC

As outlined, the clinical behaviour of both localised and metastatic ccRCC is highly variable. A major difficulty in the identification of effective biomarkers is that individual tumours are often genetically heterogeneous both within the primary tumour and in metastases from the same patient (Gerlinger, Rowan et al. 2012, Gulati, Martinez et al. 2014). Such tumour heterogeneity may be of particular relevance in the development of drug resistance, where drug-selection pressures facilitate the faster growth of drug-resistant clones, which may ultimately result in treatment failure (Campbell, Yachida et al. 2010).

Gerlinger *et al* analysed multiple samples of primary ccRCC tumours and metastatic deposits in four patients with metastatic RCC, undertaking exome sequencing, chromosome aberration analysis and ploidy profiling on multiple spatially separated samples. Biopsy samples were obtained before the initiation of six weeks of everolimus, after which period a nephrectomy was undertaken and everolimus then restarted until tumour progression. Mutations were sub-classified into those that were ubiquitous, those that were shared by several but not all regions and mutations that were unique to specific regions (designated private mutations).

For patient 1, mutational intra-tumour heterogeneity was observed in multiple driver tumour-suppressor genes in particular in, *SETD2*, *PTEN* and *KDM5C* with only *VHL* mutated ubiquitously in all analysed regions. Mutations were distinct and spatially separated, suggesting convergent phenotypic evolution with 'Darwinian selection' for mutations conferring a phenotypic advantage. Ploidy profiling and allelic analysis revealed extensive divergent allelic-imbalance profiles and ploidy heterogeneity (Gerlinger, Rowan et al. 2012) (**Figure 1.20**). Interestingly the metastatic sites and one region of the primary tumour segregated together and were enriched for genes in the ccA subgroup in contrast to the remaining tumour regions that enriched for the ccB

subgroup. This highlights a significant issue associated with biomarker prediction, whereby samples obtained from a single biopsy may not be predictive of the tumour as a whole (Gerlinger, Rowan et al. 2012).

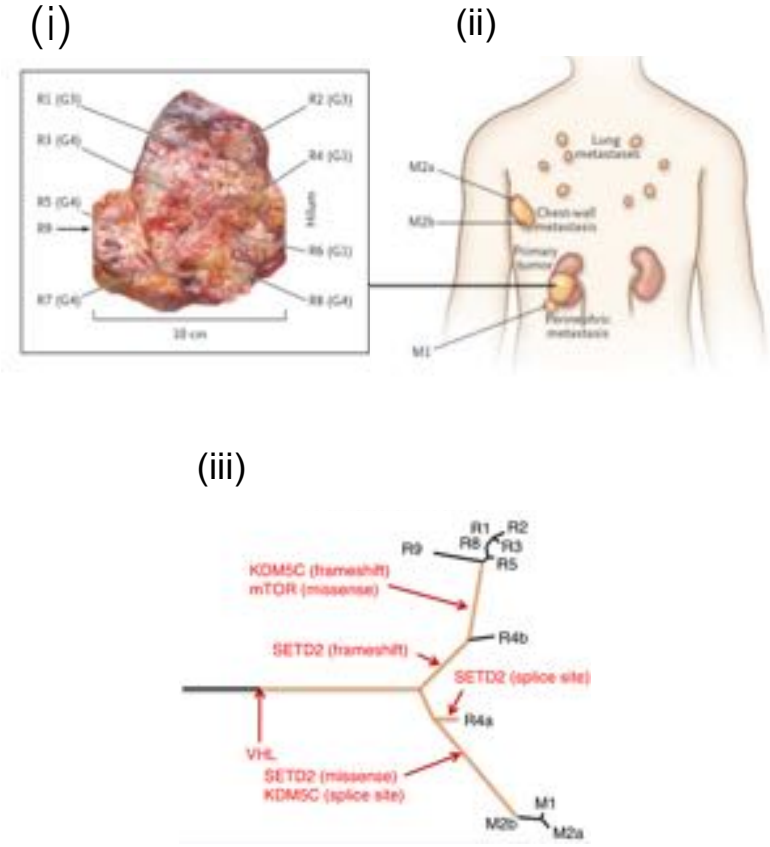

Figure 1.20 ccRCC demonstrates significant tumour heterogeneity both within the primary tumour and in metastatic deposits. Multiple samples of a primary ccRCC tumour and metastatic deposits in a patient were analysed by exome sequencing, chromosome aberration analysis and ploidy profiling on multiple spatially separated samples as indicated in **(i)** and **(ii).** This revealed a trunk-branch model of tumour heterogeneity for this patient, with ubiquitous driver events common to all components of the tumour, and heterogeneous passenger mutations, driving further tumour evolution and metastases **(iii)** Adapted from (Gerlinger, Rowan et al. 2012)

Gulati *et al* analysed 63 tumour regions from ten ccRCCs and found that only two tumours homogeneously expressed the ccA signature with the eight other tumours expressing both ccA and ccB signatures within different tumour regions (Gulati, Martinez et al. 2014). This highlights the need to sample multiple tumour regions in order to draw meaningful conclusions as to ccRCC tumour behaviour

Epigenetic events are also likely to be heterogeneous within a tumour. For example, changes in DNA methylation and repressive chromatin modifications have been found to restrict the expression of HIFα-targeted genes driving metastasis. In a ccRCC line, a subpopulation of cells were found to have a metastatic expression programme, supporting the idea that epigenetic modification of gene expression in a subset of cells drives metastasis (Vanharanta, Shu et al. 2013). It is unclear whether such changes arise stochastically or as a consequence of changes in the expression of genes that control cellular epigenetic status such as *PBRM1*, *SETD2* and *BAP1*. It is perhaps not coincidental that mutations in such genes occur so frequently in ccRCC with *BAP-1* mutations for example associated with worse clinico-pathological indices (Gossage, Murtaza et al. 2014).

Circulating blood biomarkers such as circulating tumour cells and cell-free plasma DNA may provide a non-invasive real-time surrogate for tissue based biomarkers and overcome some of the issues associated with tumour heterogeneity.

1.22 The concept of synthetic lethality and exploiting synthetically lethal relationships to target ccRCC

ccRCC displays limited chemotherapy and radiotherapy sensitivity and therefore conventional anti-cancer therapies used in many tumour types have limited efficacy. Current targeted treatments have improved OS and novel immune checkpoint therapies offer a promising new approach.

Nonetheless, most patients eventually develop resistance to targeted therapy and the identification of novel drugs or the use of existing drugs either alone or in combination with existing therapy is critical for improving patient outcome. Increased knowledge of the genetic drivers of ccRCC in particular can be exploited to specifically target tumours with such mutations.

The concept of synthetic lethality is being successfully exploited in oncology to identify drugs that specifically target cancer cells but spare healthy non-cancer cells. Synthetic lethality arises when a combination of mutations in two or more genes leads to cell death, whereas a mutation in only one of these genes does not and the cell remains

viable. In cancer cells where a particular cancer-specific gene inactivation has occurred, targeting a second gene may result in cancer-specific cell death whilst sparing non-cancerous cells (Nijman 2011). This principle is shown in **Figure 1.21**.

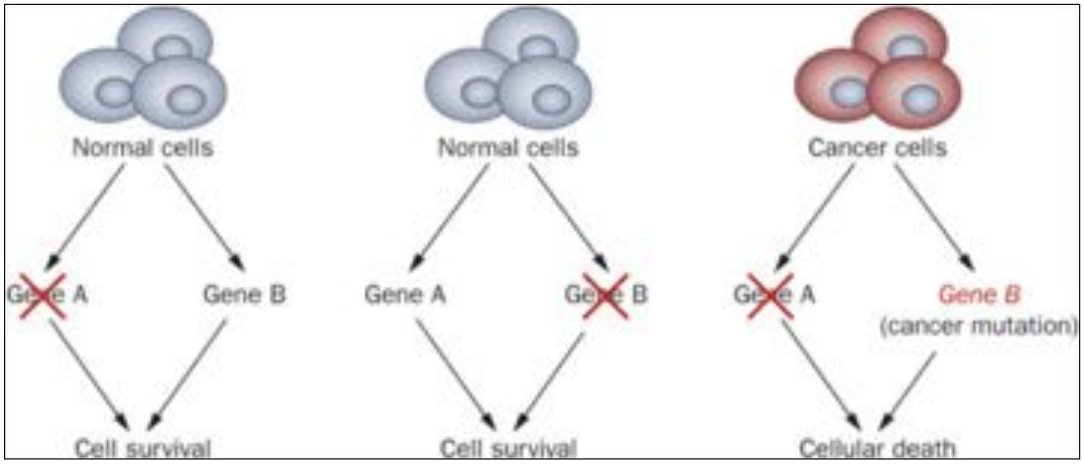

Figure 1.21 Schematic representation of synthetic lethality.

Two genes are synthetically lethal when their simultaneous inactivation results in cell death. Here, inactivation of gene A or gene B alone does not affect cell viability whereas inactivation of both genes results in cell death. Taken from Rehman *et al.* Synthetic lethal approaches to breast cancer, Nat Rev Clin Oncol 2010.

Probably the best known example of a synthetic lethal approach has come from the treatment of BRCA1/2 mutated breast and ovarian cancer with PolyADP-ribose polymerase (PARP) inhibitors (Yap, Sandhu et al. 2011). Here the BRCA1/2 mutation results in deficiency in the homologous recombination (HR) DNA repair pathway, leading to a dependency on error-prone DNA repair mechanisms and consequent genomic instability. PARP activation is largely driven by DNA damage and by targeting the BRCA1/2 mutated cancer cells and their error-prone DNA repair mechanisms, PARP inhibitors are largely selective only for cancer cells since non-cancer cells still have one functioning BRCA1/2 copy and therefore intact homologous recombination pathways (Livraghi and Garber 2015).

For many tumours, multiple anti-cancer drugs exist that effectively kill cancer cells but are not therapeutically useful due to toxic side effects in non-cancerous cells. Most chemotherapeutic drugs have very low therapeutic indices and windows. The therapeutic index is defined as the dose required for toxic effects divided by the dose required for therapeutic effect, whilst the therapeutic window refers to the concentration range over which therapeutic effects can be expected (Kaelin 2005). The

therapeutic window is affected by 'on target' pharmacokinetic properties that relate to the intended biological effect of the drug on its intended target and by 'off target' effects i.e. the propensity of the drug to affect unintended targets. This has significant implications as one of the most important factors limiting effective anti-cancer treatment relates to drug toxicity in normal cells, in particular those that are rapidly dividing such as bone-marrow haematopoietic precursors (Kaelin 2005). Synthetic lethality therefore provides a conceptual framework, by which cancer cells can be selectively targeted.

There are a number of approaches by which this can be achieved. 1) A target-driven approach such as that seen for PARP-I in BRAC1/2 mutated cancers where the target is uniquely present in cancer cells or (2) a context driven approach, related to for example epigenetic gene silencing in different tissues (Reddy and Kaelin 2002).

A number of approaches to targeting renal cell carcinoma using a synthetic lethal approach have been tried particularly through the targeting of pathways associated with VHL deficiency. Targeting VHL loss represents a particularly attractive approach as it represents a 'trunk mutation/ 'trunk event' where loss/mutation occurs at an early stage of tumour formation and is therefore present in all cells, therefore overcoming some of the issues associated with tumour heterogeneity. However, targeting 'non-trunk' mutations may also be important as these non-ubiquitous mutations may function as powerful drivers of tumour progression and metastasis and contribute to the emergence of clonal populations of drug-resistant cells (Gerlinger, Catto et al. 2015).

Chan *et al* made use of a synthetic lethal approach to target VHL mutated RCC, targeting VHL-deficient RCC cells through their reliance on the high-affinity glucose transporter 1 and aerobic glycolysis (the Warburg effect). They screened ~64,000 small molecules using a RCC cell line with a naturally occurring VHL mutation and a genetically matched cell line with reintroduced wild-type VHL. This identified two groups of drugs, one the pyridyl aniline thiazoles (e.g. STF-62247), previously characterised as demonstrating autophagic cell death in VHL-deficient RCCs (Turcotte, Chan et al. 2008) and a second class of drugs the '3-series' typified by the drug STF-31 that selectively target VHL deficient RCCs by targeting glucose uptake through GLUT1

and exploiting the dependence of VHL deficient RCCs on this mechanism for glucose uptake for survival (Chan, Sutphin et al. 2011).

Targeting ccRCC tumours in association with loss of a tumour suppressor, using a synthetically lethal approach therefore represents an attractive strategy, potentially maximising therapeutic effect in ccRCC cells whilst minimising toxicity in non-tumour cells where the tumour suppressor of interest is still expressed.

1.23 Summary

LIMD1, Ajuba and WTIP (LAW) are Zyxin family members, characterised by tandem zinc-finger motifs that facilitate protein-protein interactions enabling them to act as adaptor proteins. The LAW proteins have both nuclear and cytoplasmic localisation domains and shuttle between the nucleus and cytoplasm functioning as important signalling transducers, relaying signals between the cell surface and the nucleus (Kadrmas and Beckerle 2004). This for example facilitates a critical role in the regulation of EMT via E-cadherin expression (Wang, Shi et al. 2013). Ajuba proteins are negative regulators of the Hippo signalling pathway (Das Thakur, Feng et al. 2010), and are essential components of the miRISC, facilitating miRNA mediated gene silencing (Bridge, Shah et al. 2017). Acting as scaffold proteins, they regulate the hypoxic response targeting HIFα for VHL mediated polyubiquitylation and degradation via the proteasome (Foxler, Bridge et al. 2012). All three proteins demonstrate considerable homology (Kadrmas and Beckerle 2004).

A number of studies have implicated Ajuba proteins in tumourigenesis. LIMD1 loss is common in lung carcinoma and drives tumourigenesis in a mouse model (Sharp, Al-Attar et al. 2008), whilst in breast cancer, LIMD1 loss contributes to tumourigenesis and is associated with worse prognosis disease (Spendlove, Al-Attar et al. 2008). In head and neck cancer, *LIMD1* deletion and changes in methlylation patterns are common (Chakraborty, Dasgupta et al. 2003). Studies have also demonstrated LIMD1 up-regulation in association with DLBCL subtypes (Xu, Tan et al. 2015) and in oesophageal squamous cell carcinoma and in colorectal carcinoma Ajuba upregulation has been described (Liang, Zhang et al. 2014, Xu, Tan et al. 2015, Shi, Chen et al. 2016). Ajuba loss in malignant mesothelioma has been characterised and is related to deregulation of the Hippo signalling pathway (Tanaka, Osada et al. 2015).

To date, LIMD1, Ajuba and WTIP have not been characterised in ccRCC. Hypoxic deregulation is a critical driver of tumourigenesis in ccRCC and deregulation of miRNA-mediated silencing commonly observed (Biswas, Troy et al. 2010). Dysfunctional Hippo signalling can also mediate proliferation, invasiveness and increase the metastatic potential of ccRCC (Schutte, Bisht et al. 2014).

ccRCC is a complex tumour type that is increasing in incidence: approximately 1.6% of the population will be diagnosed with kidney cancer at some point in their lifetime (Ljungberg, Campbell et al. 2011). The genetics of ccRCC are complex. Although biallelic loss of *VHL* function occurs as a tumour initiating event in over 90% of ccRCC causing resultant hypoxic deregulation through HIFα upregulation (Frew and Moch 2015), recent genetic analysis has identified that other 3p locus genes play an important role in driving tumourigenesis, in particular the chromatin remodelling genes *PBRM1*, *SETD2* and *BAP1 (*Sato, Yoshizato et al. 2013). Further underscoring the importance of hypoxic deregulation as a critical driver of tumourigenesis in ccRCC is the observation that the deregulation of downstream targets of HIFα such as components of the PI3K-mTORC1 pathway is also common (Sato, Yoshizato et al. 2013).

Non-metastatic ccRCC is potentially curable with nephrectomy but metastatic disease is considerably harder to control. Although novel targeted agents that act as multi-tyrosine kinase inhibitors targeting VEGF pathways and inhibitors of mTOR have significantly improved overall survival, individual prognosis remains variable and reasons for this are not fully understood (Ljungberg, Bensalah et al. 2015). Immune checkpoint inhibition offers the possibility of a durable response in a sub-set of patients, although clinical trial readouts of long-term survival are not yet mature.

Clinical outcomes remain very difficult to predict and although clinical prognostic indicators can help stratify patients, most prognostic and predictive biomarkers have not been independently validated with the exception of the ccA/ccB tumour subgrouping and tumour stage and grade (Gulati, Martinez et al. 2014). Undoubtedly the development of prognostic and predictive biomarkers is hampered by intra-tumoural heterogeneity and there is currently insufficient knowledge of the effects of different combinations of mutations on the initiation and progression of ccRCC (Gerlinger, Rowan et al. 2012). Intra-tumoural heterogeneity also potentially contributes to resistance to targeted therapy with the selection of drug-resistant clones driving tumour progression and metastases (Gerlinger, Rowan et al. 2012).

Targeting tumour suppressors, which are associated with a loss of function phenotype is difficult. Using a synthetic lethal approach to selectively target another gene in a

pathway upon which the tumour cells are dependent can overcome this. Importantly such an approach can result in tumour-selective cell death with relative sparing of non-cancerous cells (Chan and Giaccia 2011, Nijman 2011).

LIMD1, WTIP and Ajuba remain uncharacterised in ccRCC. The three proteins demonstrate considerable homology and functional redundancy as shown for example in the regulation of the hypoxic response and in miRNA silencing via the miRISCs.

Given their role in multiple pathways that can drive tumourigenesis in ccRCC, particularly the regulation of the hypoxic response, miRNA silencing and Hippo signalling and the association between their loss and tumourigenesis in several tumour types it was hypothesised that loss/deregulation could drive tumourigenesis in ccRCC and, that the three proteins were likely to demonstrate a degree of functional redundancy in this tumour type.

It was also hypothesised that a synthetically lethal approach could represent an attractive therapeutic approach and be used to target ccRCC tumours that had demonstrated loss of these proteins.

1.24 Thesis aims and objectives

1. Characterisation of LIMD1, Ajuba and WTIP (LAW) expression in ccRCC and matched adjacent tissue (MAT)
2. Correlation of the relationship between expression levels of LAW proteins in ccRCC and MAT
3. Correlation of expression of LAW proteins with other hypoxically regulated proteins in ccRCC and MAT
4. Investigation of the relationship between LAW expression and clinico-pathological data in ccRCC
5. Characterisation of the effects of LIMD1 loss on cellular transformation/tumourigenesis in ccRCC *in vitro*.
6. The use of CRISPR-Cas-9 gene editing system to achieve knockout of Ajuba proteins in Renal proximal tubular epithelial cells (RPTEC)
7. Identification of anti-cancer drugs demonstrating synthetic lethality in association with LIMD1 loss in ccRCC using a drug-screening platform
8. Investigation of the effects of LIMD1 loss on the sensitivity to drugs commonly used to treat metastatic ccRCC

2 Materials and Methods

2. 1 Immunohistochemistry

2.1.1 Human tumour Samples

The GSK TMAs were constructed from archived biopsy tissue or nephrectomy specimens obtained from a prospective randomised clinical trial of the tyrosine kinase inhibitor lapatinib versus placebo (Ravaud, Hawkins et al. 2008): 145, paraffin-embedded RCC histospots of 0.6mm diameter and 4μm thickness were represented on the TMAs in triplicate with placenta and healthy kidney tissue included as control.

Further ccRCC TMAs were made by Dr Daniel Worth at Barts Cancer Institute. TMA histospots were generated from core biopsies and nephrectomy samples from a study evaluating the role of the TKI pazopanib prior to nephrectomy (Powles, Sarwar et al. 2016). Samples were represented at least in duplicate and tumours from a total of 104 patients included on the TMAs with samples taken from both baseline biopsy and nephrectomy samples (63 patients underwent nephrectomy). Histospots were paraffin-embedded, 2mm in diameter and 4μm in thickness. Both TMAs were obtained from the Orchid tissue bank and Barts Cancer Institute.

In addition, commercially available TMAs containing 75 ccRCC histospots with matched adjacent tissue were purchased from US Biomax (H-Kid-CRCC150C2-02s). A single histospot from each tumour was represented on the array with a corresponding matched adjacent tissue sample from each patient. Histospots were paraffin embedded, 1.5mm in diameter and 4μm in thickness.

Control tissue for antibody optimisation was obtained from Mr George Elia and Dr Andrew Clear at Barts Cancer Institute. Full ethical approval for the use of the tissue for non-diagnostic purposes had previously been obtained where appropriate.

2.1.2 Solutions for Immunohistochemistry

Endogenous peroxide blocking solution: 3% H_2O_2 (w/v) or 2% H_2O_2 (w/v) was added to 100% methanol (MeOH). The solution was made up freshly each time.

Antibody dilution buffer: 1% BSA (w/v) and 0.1% Sodium Azide (w/v) was added to PBS and allowed to fully dissolve prior to storage at 4°C.

Blocking horse serum: Four drops of horse serum in 5 mls PBS

Avidin/Biotinylated enzyme complex (ABC): Two drops of reagent A and 2 drops of reagent B (Universal ABC horseradish peroxidase (HRP) Kit, Vectastain PK-6200) were added to 5mls PBS and allowed to equilibrate at room temperature for at least 30 minutes prior to incubation.

3,3'-Diaminobenzidine (DAB): 1 drop of DAB chromogen was added to each ml of DAB buffer (Biogenex HK542-XAK).

1% acid alcohol: 10mls of 10mM HCL was added to 990mls of 70% ethanol (EtOH) and stored at room temperature.

TBS-T (0.05%): Pre-mixed 10x TBS buffer pH 7.4 (Severn Biotech Ltd, 20-730-10) was diluted to 1x with distilled water and stored at room temperature. 500µl of Tween®-20 (Sigma-Aldrich-P9416) was added to 1 litre of 1xTris-buffered saline (TBS)

PBS-T (0.05%): 10x PBS powder pH 7.4 (Severn Biotech Ltd, 20-730-10) was diluted to 1x with distilled water and stored at room temperature. 500µl of Tween®-20 (Sigma-Aldrich-P9416) was added to 1 litre of 1xTBS.

2.1.3 Antibodies used for Immunohistochemistry

Antigen	Catalogue Number	Dilution for IHC	Primary Species
LIMD1	(Sharp *et al*, 2004, 2008, 2009)	1:40-1:200	Mouse
HIF2α	Novus Biologicals NB100-122	1:50-1:200	Mouse
HIF1α	Novus Biologicals NB100-105	1:50-1:200	Mouse
VHL	BD Biosciences 556347	1:50-1:200	Mouse
Ajuba	Sigma Aldrich HPA006171	1:50-1:100	Rabbit
WTIP	LS Bio C160645	1:50-1:100	Rabbit
CD34	DAKO M7165	1:50	Rabbit
VEGFA	Thermoscientific RB-9031-P1	1:300	Rabbit

Table 2.1: Antibodies used for immunohistochemistry. Catalogue number, dilution and primary species detailed.

2.1.4 Manual Immunohistochemistry for LIMD1

Cut sections were dried overnight at 60°C to help section adhesion. Slides were de-paraffinised in xylene for 2x5-minutes and immersed in 70% industrial methanol solution (IMS) (Sigma-458600) for 2 minutes prior to blocking endogenous peroxidase activity with 2% H_2O_2 for 2x5-minute incubations. Slides were transferred to 70% IMS for a further 2 minutes and rinsed in running tap water for 2 minutes. Epitope retrieval was performed using a pressure cooker at maximum temperature and pressure for 10 minutes in 1% Tris based low pH antigen unmasking solution (pH 6) (Vector Labs-H3300). Once the pressure cooker had cooled in running tap water, the slides were

further cooled in running tap water for 5 minutes. Slides were washed briefly with TBS-T (0.05%) and dried briefly. Primary antibody diluted at least 30 minutes prior to application in Zytomed antibody diluent (ZUC025-100) was applied for 40 minutes, slides washed for 2 minutes with TBS-T (0.05%) and primary antibody staining detected using the Biogenex-SuperSensitive™ polymer-HRP system (QD440-XAKE): the super-enhancer was applied for 20 minutes, washed with TBS-T (0.05%) and the SS-label then applied for 30 minutes.

Slides were then washed in TBS-T (0.05%) for 2 minutes and the peroxidase reaction detected by incubation with the DAB chromogen solution for 10 minutes (Biogenex-HK542-XAK). Slides were then washed in running tap water for 2 minutes, counterstained in haematoxylin (Gill's No 2 Haematoxylin solution, (Sigma GH-S216) for 5 minutes and then rinsed in tap water for 2 minutes. Slides were differentiated in 1% Acid Alcohol with four, one-second washes and rinsed in tap water for 2 minutes. Slides were then rinsed in 1x Scott's tap water substitute (Sigma S-5134) for 3 minutes, rinsed in tap water for 2 minutes prior to dehydration through three, 2-minute changes of IMS prior to clearing in xylene for two, 2-minute washes. Slides were mounted with a DPX-xylene based permanent mount (Sigma 06522).

2.1.5 Manual Immunohistochemistry for HIF1α

Sections were de-paraffinised in xylene for two, 5-minute incubations and then in 70% ethanol for two-five minute incubations prior to blocking endogenous peroxide activity with 3% hydrogen peroxide (H_2O_2) in methanol for 10 minutes. Antigen retrieval was performed by microwave heating in pre-heated 1% Tris based low pH antigen unmasking solution (pH 6) (Vector Labs-H3300) prior to passive cooling for 10 minutes and active cooling in running water for 5 minutes.

Slides were washed with TBS for two, 3-minute washes and non-specific binding blocked with 400µl diluted horse serum per slide for thirty minutes (Universal ABC HRP Kit-Vectastain).

Slides were washed for two, 2-minutes with TBS prior to the addition of 400µl of Avidin blocking solution (Vector Laboratories SP-2001) for 15 minutes, the wash repeated and Biotin blocking solution (Vector Laboratories SP-2001) added for 15 minutes. After washing with two, 2-minute TBS washes: slides were incubated with 200µl of the diluted primary HIF1α antibody (Novus Biologicals NB-100-105) overnight in a moist humidity chamber at 4°C.

The following morning, slides were allowed to equilibrate to room temperature for 30 minutes, then washed with two, 2-minute TBS washes prior to incubation with the Universal biotinylated Secondary antibody for 30 minutes (Universal ABC Kit, Vectastain). The TBS wash was repeated and the slides incubated with 350µl of the ABC complex for 30 minutes (Universal ABC HRP Kit, Vectastain). After washing with TBS for three, 2-minute washes, 350µl of diluted DAB chromogen (Biogenex HK542-XAK) was added to each slide for 10 minutes, the slides washed with TBS (two, 2-minute washes).

Slides were counterstained with haematoxylin for 2 minutes, washed in tap water for 1 minute prior to differentiation for 1 second in 1% acid alcohol and rewashing in tap water for 1 minute. Dehydration was undertaken in increasing ethanol concentrations (2 minutes in 70% EtOH, 2 minutes in 90% EtOH, two, 3-minutes incubations in 100% EtOH) prior to clearing in xylene (two, 3-minute incubations) and mounting with DPX mountant (Sigma 06522).

2.1.6 Manual Immunohistochemistry for Ajuba and WTIP and VEGFa

Antigen retrieval was performed as described for HIF1α. Slides were then washed with three, 3-minute TBS washes and non-specific binding blocked with 5% goat serum in PBS (DAKO-X0907) for one hour. The antibody was diluted to the correct dilution in antibody dilution buffer at least 30 minutes prior to using, slides dried briefly and then incubated with the primary antibody for one hour.

Samples were washed with TBS for 5 minutes and primary antibody staining detected using the Envision Plus Detection System (K4002) with application of the labelled

polymer-HRP directly to the slide for 30 minutes. After washing with TBS for 5 minutes, 350µl of diluted DAB chromogen (Biogenex HK542-XAK) was added to each slide for 10 minutes to detect the peroxidase reaction. Slides were washed with 1xTBS (three, 2- minute washes) prior to counterstaining, clearing and mounting as for HIF1α.

2.1.7 Automated immunohistochemistry for LIMD1, VHL, HIF2α and CD34

An automated IHC system using the Ventana Discovery system was employed according to the manufacturer's specifications. Staining was undertaken with LIMD1 antibody at dilutions of between 1:40 and 1:100. Non-specific binding was blocked with an avidin and a biotin-blocking step. The primary antibody was visualised using an ABC system with a universal mouse/rabbit secondary antibody prior to incubation with an avidin/biotin complex and visualisation with a DAB chromogen. This same protocol was utilised for VHL staining, with an antibody concentration of between 1:50 and 1:400, and for HIF2α with an antibody concentration of between 1:50 and 1:400. For CD34, an antibody concentration of between 1:25 and 1:50 was utilised.

2.1.8 Manual scoring of immunohistochemistry

IHC of control and tumour samples were reviewed by either Professor Michael Sheaff of Barts Health NHS Trust, or Dr Georgia Trevisan of University College London Hospital, both experienced consultant histopathologists, in order to establish antibody specificity, help define appropriate positive and negative controls and to agree on appropriate antibody concentrations after IHC optimisation and on manual scoring systems where appropriate. All TMA histospots were only scored if the core was intact and where appropriate tumour present.

All TMAs were double scored, either by Professor Sheaff or Dr Trevisan and myself or Dr Scott Shepherd of Royal Free Hospital, an oncology specialist registrar. Intra-class correlation coefficient analysis was undertaken using SPSS-16 to assess inter-observer scoring agreement.

2.1.9 ARIOL Imaging of immunohistochemistry

Antibody staining of the commercially available TMAs was quantified using the ARIOL imaging system (Genetix, San Jose, CA). The slides were loaded in the automated slide loader (Applied Imaging SL50) prior to scanning at low resolution (1.25x) and at high resolution (20x) using the Olympus Bx61 microscope with an automated platform. After high resolution scanning, the images were reviewed for training and quantification purposes to differentiate the stained and the unstained cells by the colour of staining and the shape of the nuclei whereby brown staining was considered positive and blue staining negative. For the tumour histospots, areas of tumour were manually identified with masking of the stroma and of the normal/benign tissue from image analysis. Scores were generated using a modified automated scoring system: this generates an output score based on the combined score for the average staining intensity of the protein of interest throughout the analysed area within the histospot as a function of the area of positive staining throughout the analysed area of each histospot.

2.2 Cell Culture Techniques

2.2.1 Renal cell carcinoma cell lines

The human renal cell carcinoma lines were provided by Dr Jong-Jie Lu of Barts Cancer Institute and had been derived from patient tumours at Barts and the London NHS Trust or were commercially available. All cell lines were routinely tested for mycoplasma infection and the commercially available lines had previously undergone genetic profiling using polymorphic short tandem repeat loci analysis.

Renal cell carcinoma line	**Renal cell carcinoma subtype**	**Wild type VHL present?**
RCC4 (Va)	ccRCC	X
RCC4 (VHL)	ccRCC	X
RCC7	ccRCC	√
RCC10	ccRCC	X
RCC11	ccRCC	X

RCC12	ccRCC	X
RCC17	Papillary	X
RCC29	ccRCC	X
RCC45	ccRCC	X
RCC48	ccRCC	X
RCC59	ccRCC	X
RCC88	ccRCC	X
RCC912	ccRCC	X
CAKI1	ccRCC	X
CAKI2	ccRCC	X
ACHN	ccRCC	X
786-0	ccRCC	X

Table 2.2: RCC lines used in assays with detail of RCC subtype and wild type VHL status

2.2.2 Cell maintenance and passaging of adherent cancer cells

Adherent monolayer human cancer cell lines were cultured in Roswell Park Memorial Institute-1640 medium (RPMI-1640) (Sigma) or Dulbecco's Modified Eagle Medium (DMEM) (Sigma), supplemented with 10% heat inactivated foetal bovine serum (FBS) (Gibco) and 1% penicillin/streptomycin (PAA Laboratories) and maintained at 37°C in a humidified atmosphere with 5% CO_2 or where appropriate serum starved with culture in 1-2% FBS. When cells reached 80% confluency, they were passaged through trypsinisation (1xTrypsin-EDTA, Sigma). Lentiviral-transduced renal cell lines expressing a puromycin resistance construct, were grown in media supplemented with puromycin 0.5-3ug/ml (Invivogen (ant-pr-1)). Penicillin/streptomycin was omitted from the media in cells undergoing transfection or transduction.

2.2.3 Cell freezing of cancer cells

For long-term storage, cells of a low passage number were trypsinised and re-suspended in media, then re-pelleted by centrifugation (1200rpm, for 3 minutes) and washed with phosphate-buffered saline (PBS) before re-pelleting. The washed cell pellet was re-suspended in freezing mix (90% FBS and 10% (v/v) dimethyl sulphoxide (DMSO)) and aliquots transferred to cryovials for storage. The cryovials were stored at -80°C for 24 hours prior to transfer to liquid nitrogen for long-term storage.

2.2.4 Renal proximal tubular epithelial cells (RPTEC) and cell culture

Healthy renal proximal tubular epithelial cells obtained from Lonza (CC-2553) were cultured in renal basal epithelial growth medium (BEGM) supplemented with human epidermal growth factor 0.1%, hydrocortisone 0.1%, epinephrine 0.1%, insulin 0.1%, tri-iodothyronine 0.1%, transferrin 0.1%, fetal calf serum 0.5%, gentamicin 30μg/ml and amphotericin 15ng/ml (Clonetics™ REGM™ BulletKit™ Lonza CC-3190). Cells were maintained at 37°C in a humidified atmosphere with 5% CO_2. When cells had reached 70-80% confluency they were passaged by trypsinisation. For a 25cm^2 flask, cells were washed with 5mls of room temperature HEPES-buffered saline solution (HEPES-BSS) (Lonza-CC5022), the HEPES-BSS aspirated and cells gently trypsinised with 2mls of trypsin/EDTA solution (Lonza-CC5012). Cells were examined microscopically until 90% of the cells were rounded up, the cells gently detached and the trypsin/EDTA solution neutralised with 4mls of room temperature trypsin neutralising solution (TNS) (Lonza-CC5022). The cells were pelleted by centrifugation at 220g for 5 minutes and re-suspended in an appropriate volume of media.

2.2.5 Cell counting and cell seeding

Cells were counted using the automated TC20™ Biorad cell counter. Cells were trypsinised as described and 10μl of the carefully mixed cell suspension pipetted in to the haemocytometer slide. Each slide was read twice and a mean cell count per ml of cell suspension calculated.

Cells were seeded into sterile tissue culture plates or dishes. Lentiviral-transduced cells expressing a puromycin-resistance construct were taken out of selection 24 hours prior to seeding. Cells were plated such that they would be at the desired density at the relevant time-point as required by the protocol.

2.2.6 Hypoxic treatment of cells

Cells were exposed to 1% oxygen and maintained at 37°C and at 5% CO_2 within a hypoxic workstation for the time period required by the particular experiment.

2.2.7 Lentiviral-transduction of renal cell carcinoma cell lines

The ccRCC lines RCC11 and RCC48 were transduced with lentivirus constructs containing either knockdown LIMD1 (shLIMD1), rrLIMD1 (LIMD1 knockdown with concomitant rescue) or control, non-targeting siRNA (scr), in order to generate lines with 1) effective LIMD1 knockdown 2) effective knockdown with concomitant rescue of LIMD1 and 3) control cells transduced with non-targeting siRNA.

The lentivirus was obtained from Dr John Foster of Barts Cancer Institute who had packaged the expression vector of interest into an attenuated second-generation lentivirus with a puromycin resistance construct in HEK293T cells using the packaging plasmids pCMVO2.4 and pMDE2. The vector expresses a Flag-His tag (**Figure 2.1**). The viral supernatant was collected at 48 hours and 72 hours and kept frozen at -80°C.

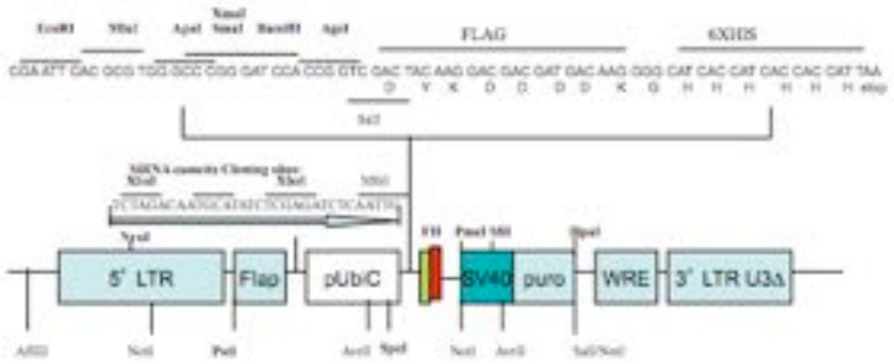

Figure 2.1. shRNA expression vector demonstrating shRNA cassette cloning site in to which the scr (control, non-targeting siRNA), short hairpin LIMD1 (shLIMD1) and rrLIMD1 (LIMD1 knockdown with concomitant rescue) were cloned. The vector expresses a Flag-His tag and a puromycin resistance construct.

RCC11 and RCC48 cell lines were seeded in to 6-well plates at different seeding densities to assess optimal seeding density for viral transduction: seeding $1x10^5$ cells/well resulted in 50% confluency at 24 hours, considered optimal for lentiviral transduction. 24 hours post seeding, a puromycin kill curve was established with cells in separate wells treated with varying puromycin concentrations: 0, 0.5, 1, 3, 5, 7.5 and 10 μg/ml (Invivogen anti-pr-1) for 48 hours, in order to identify a puromycin concentration to use to subsequently select for RCC cells that had undergone lentiviral transduction

RCC11 and RCC48 cells were seeded in to 6-well plates at $1x10^5$ cells/well. At 24 hours, the media was changed and 1ml of the appropriate thawed viral supernatant added to each 6-well plate. The virus was removed from the cells after 24 hours and fresh media added. Cells were puromycin selected from 72 hours after the addition of virus and cells used in assays after 2-3 passages. All viral waste and virally contaminated equipment was carefully decontaminated by soaking in 1% Virkon for at least 12 hours.

2.2.8 Polycomb complex protein-1 (BMI-1) immortalisation of RPTEC

Prior to BMI-1 transduction of RPTECs a puromycin-kill curve was undertaken to determine an appropriate puromycin concentration to use for selection of the BMI-1

transduced RPTECs: the lentiviral construct contains a puromycin resistance antibiotic selection marker.

RPTEC were seeded in to a 6-well plate at a seeding density of $1x10^5$ cells per well. After 24 hours, cells in separate wells were treated with varying puromycin concentrations, 0, 0.5, 1, 3 and 5μg/ml (Invivogen anti-pr-1) for 48 hours, to select an appropriate puromycin concentration to select for the lentiviral transduced RPTECs.

pFLRu and pLVX multifunctional lentivirus systems into which BMI-1 had been cloned were utilised. RPTECs were seeded into a 6-well plate at $1x10^5$ cells/well and 24 hours after seeding, 10 or 20μl of concentrated pFLRu-BMI-1 virus or, 10 or 20μl of concentrated pLVX-BMI-1 virus added to separate wells within the plate. Two control wells, where no virus was added were included. 72 hours after seeding, puromycin selection at 0.5μg/ml was started and media containing no puromycin added to one of the control wells.

2.3 CRISPR (Clustered regularly interspaced palindromic repeat)-Cas-9 system for gene editing in RPTEC (renal proximal tubular epithelial cells)

2.3.1 Edit-R DharmaFECT™ Duo gene engineering CRISPR-Cas-9 Transfection system in RPTEC

Cleavage of the complementary target for LIMD1 and Ajuba in the *BMI-1* transduced RPTEC cells was undertaken using the DharmaFECT™ Duo Transfection system.

Three 20-nucleotide target CRISPR RNAs (crRNAs), complementary to the genomic target sequence for LIMD1, and three for Ajuba, were selected by Dr Daniel Foxler (**Figures 2.2** and **2.3**). Dharmacon manufactured custom crRNAs through the addition of the required *S.pyogenes* repeat sequence to the 3' end of the target sequence resulting in a custom 42-nucleotide crRNA.

1. CTTCCAAGATCAAACTC
2. CCGAGTTTGAGGAAACTCGC
3. ATGGATAAGTATGACGACCT

Figure 2.2 gRNAs selected for LIMD1 CRISPR using the DharmaFECT™ Duo Transfection system. 20-nucleotide target guide RNAs (gRNAs) complementary to the genomic target sequence for LIMD1 were selected. All contained protospace adjacent motif (PAM) sequences and were complementary to coding sequences in exon 1 of LIMD1.

1. GGACGGCTTGCTCGCGTCGC
2. GCAAAGCTGTTAGCTCGTCC
3. GTTGCCCCCCGATTTTCGGC

Figure 2.3 gRNAs selected for Ajuba CRISPR using the DharmaFECT™ Duo Transfection system. 20-nucleotide target gRNAs complementary to the genomic target sequence for Ajuba were selected. All contained PAM sequences and were complementary to coding sequences in exon 1 of Ajuba.

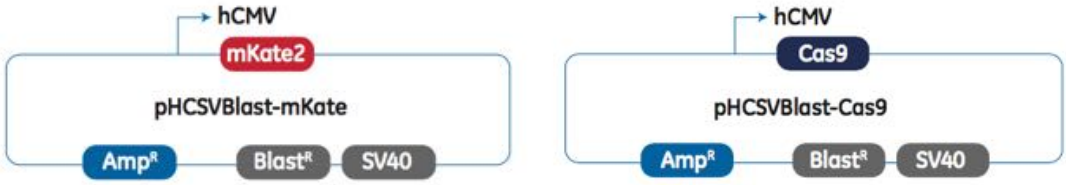

Figure 2.4. mKate2 and Cas-9 plasmids. A plasmid with an mKate2 fluorescent reporter, blasticidin resistance marker and hCMV promoter element was used to assess transfection efficiency. A Cas9 Nuclease Expression plasmid, with a Blasticidin resistance antibiotic selection marker and hCMV promoter element was used for transfection. **Taken from Dharmacon™ Edit-R™ CRISPR-Cas9 Gene Engineering with Cas9 Nuclease Expression Plasmids and synthetic RNAs.**

Since the *BMI-1*transduced cells expressed a puromycin-resistance construct, a Cas9 Nuclease Expression plasmid with a blasticidin resistance antibiotic selection marker was used to ensure that transfected cells could be selected. An mKate2 fluorescent reporter with a blasticidin resistance marker and an hCMV promoter element was used to assess transfection efficiency (Evrogen, Moscow, Russia, DharmaFECT™) (**Figure 2.4**)

BMI-1 transduced RPTEC were seeded in to a 24-well plate at a seeding density at both $5x10^4$ cells/well and $7.5x10^4$ cells/well. At 24 hours blasticidin selection in separate wells was started at 0, 2, 5, 7.5, 10, 12.5, 15 and 20μg/ml and continued for 72 hours, in order

to identify a blasticidin concentration to use to select RPTEC that had undergone transfection.

Transfection efficiency was optimised using the EditR mKATE2 optimisation plasmid, with blasticidin resistance marker. *BMI-1* transduced RPTEC cells were taken out of puromycin selection 24 hours prior to seeding and seeded in to 24 well plates in growth factor-supplemented REGM at a seeding density of either $5x10^4$ and $7.5x10^4$ cells/well.

A 10µM crRNA working solution was prepared by adding 2mls of nuclease-free10mM Tris pH 7.4 buffer to 20nmol crRNA and a 10µM tracr RNA working solution by adding 500µl of nuclease-free, 10mM Tris pH 7.4 butter to 5nM of tracr RNA. A 100ng/µl SMART Cas9 plasmid working solution was prepared by adding 1.2mls of nuclease-free, 10mM Tris pH 7.4 buffer to 120µg of plasmid.

2.3.2 Transfection protocol for the DharmaFECT™ Duo CRISPR Transfection system in RPTEC

Optimem® reduced serum medium was warmed at 37°C. A mastermix of Optimem® and Dharmafect Duo™ transfection reagent was made in an autoclaved 1.5ml eppendorf tube by adding 38.4µl of Dharmafect Duo™ transfection reagent to 601.6µl of Optimem® reduced serum medium, mixing well and then aliquoting 50µl in to 12 sterile 1.5ml eppendorf tubes and leaving for five minutes. This resulted in a final Dharmafect Duo™ concentration of 3µl/500µl.

For the knockout transfection mix:

Cas-9 plasmid	1µg (10µl)
tracrRNA	2.5µl
gRNA1	0.8µl
gRNA2	0.8µl
gRNA3	0.8µl
Optimem® reduced serum medium	37.5µl
	50µl

This resulted in a 50nm final concentration of the crRNA: tracrRNA mix.

For the control transfection mix:

Cas-9 plasmid	1µg (10µl)
tracrRNA	2.5µl
Optimem® reduced serum medium	37.5µl
	50µl

For the efficiency transfection mix:

mKATE2 plasmid	1µg (10µl)
tracrRNA	2.5µl
gRNA1	0.8µl
gRNA2	0.8µl
gRNA3	0.8µl
Optimem® reduced serum medium	37.5µl
	50µl

This resulted in a 50nm final concentration of the crRNA: tracrRNA mix.

Each of the transfection mixes was added to the 50µl dharmafect duo™/Optimem reduced serum medium, mixed well, and left for 20 minutes before adding in a drop-wise fashion to 400µl of fresh media in each well of RPTECs in a 24 well plate.

At 48 hours, the cells were examined microscopically to determine which cells had the highest fluorescent intensity and thus best transfection efficiency. The transfection mix was removed and cells transiently selected with blasticidin at 12.5µg/ml for 72 hours and then allowed to recover in antibiotic free media until confluency was reached prior to passaging. Two control un-transfected wells were also included: blasticidin at 12.5µg/ml was added to one well and antibiotic free media to the other well. All RPTEC cells in the untransfected, blasticidin treated well were dead after 72 hours in selection.

2.4 Migration as assessed through scratch assays

The lentiviral-transduced RCC cell lines were plated in to 6-well plates with seeding density of $2x10^5$/well in RPMI supplemented with 10% FCS and 1% penicillin/streptomycin.

Once 100% confluent a horizontal and vertical cross was made to transect and bisect each well using a p200 tip. Plates were then carefully washed with five changes of PBS to remove any floating cells and cells serum starved with RPMI supplemented with 2% FCS and 1% penicillin/streptomycin to encourage cell migration. Puromycin selection was maintained throughout the assay with media changed every 24 hours.

Images were taken immediately after creation of the scratch and at 24 hours and 48 hours. The size of the remaining scratch was calculated using Image-J software.

2.5 Clonogenic assays

The lentiviral transduced RCC cell lines were plated in to 6-well plates with a seeding density of 100 or 200 cells/well. Media was changed every 72 hours and puromycin selection maintained throughout. Once clear colonies were visible (approximately 14-20 days post seeding), cells were washed three times with ice cold PBS prior to fixation with ice cold 100% Methanol overnight. Cells were then counterstained with crystal violet (0.5% w/v) for 20 minutes with gentle rocking. Excess crystal violet was washed from the plates and the plates allowed to air dry. Colony number was counted manually. In order to read the absorbance of the crystal violet, crystal violet was solubilised in 2% Triton (v/v) in PBS prior to incubation on a rocker overnight at room temperature. Absorbance was then read at 540nm using the Wallac 1420 Multilabel counter plate reader.

2.6 Hypoxic response element (HRE) assay

2.6.1 HIF1α HRE-reporter assay principle

Luciferase dual-reporter assays are widely used to study transcriptional activation. The two different types of luciferase used commonly have distinct substrate requirements, which produce different wavelengths of fluorescence, thus enabling quantification from a single sample. In this assay, cells were simultaneously transfected with a thymidine kinase-Renilla (TK-Renilla) luciferase reporter (thymidine kinase is constitutively expressed) and a pGL3-(6x) HRE-firefly luciferase plasmid (whereby the promoter response element for HIF1-α had been cloned upstream of the pGL3 basic firefly luciferase plasmid). Differences in transfection efficiency could then be accounted for by normalising the luminescence obtained for the experimental reporter (Renilla) to the luminescence obtained for the constitutive reporter (Firefly). The normalised reporter luminescence in the experimental cell line of interest/experimental condition can then be normalised to the control.

2.6.2 HIF1α HRE-reporter plasmid construct

The pGL3-(6x)HRE-firefly luciferase plasmid was obtained from Dr Daniel Foxler who had cloned six copies of the promoter response element for HIF1α upstream of the pGL3 basic firefly luciferase plasmid (**Figure 2.5**) (Promega-E1751), pGL3Vo plasmid lacking the HRE construct was used as vector only control and the thymidine kinase-*Renilla* (TK-*Renilla)* luciferase reporter used as an internal control value to enable normalisation of the experimental firefly luciferase activity and to account for differences in transfection efficiency.

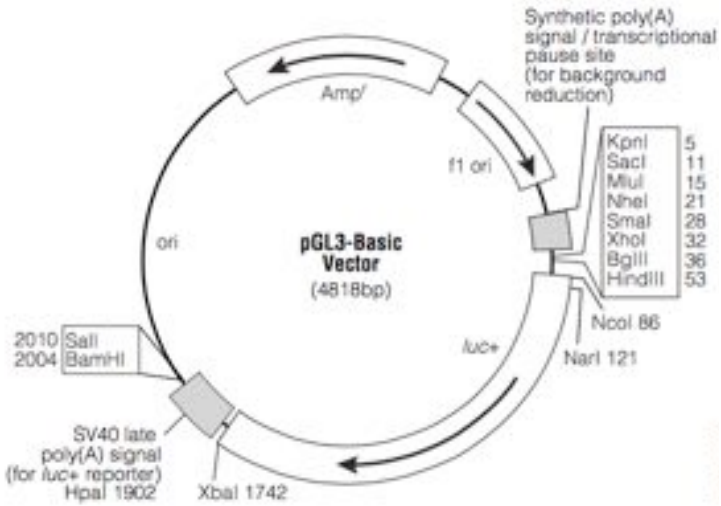

Figure 2.5. Schemata of the pGL3-Basic Vector. 6 copies of the promoter response element for HIF1α were cloned upstream of the pGL3 basic firefly luciferase plasmid. **Adapted from pGL3 Luciferase Reporter Vectors www.promega.com**.

2.6.3 Optimisation of transfection efficiency for the HIF-1α HRE-reporter system

Optimisation of the transfection conditions for the HRE reporter assay was undertaken in RCC11 and RCC45 cell lines. $3.5x10^5$ of each cell line in 500µl of RPMI were seeded in to 24 well plates. Each transfection was done in triplicate with incubation in both normoxia (20% O_2) and hypoxia (1% O_2). Cells were co-transfected in triplicate with either the pGL3-(6x)HRE-firefly luciferase or pGL3Vo firefly luciferase in combination with the TK-*Renilla* luciferase reporters. Transfection was undertaken 24 hours after the cells were seeded. Using autoclaved eppendorfs, a mastermix of the pGL3-(6x)HRE-firefly DNA or pGL3 Vo-firefly DNA in combination with the TK-*Renilla* luciferase DNA was made, adding the DNA to 50µl per well transfected of pre-warmed reduced serum media (Opti-MEM®), and mixing gently with a pipette. Viafect transfection reagent™, equilibrated to room temperature, was added to the mix at a ratio of 3:1 relative to the total amount of DNA added and mixed well by pipetting. The transfection mix was left to incubate at 20 minutes at room temperature, prior to adding 50µl of the mix dropwise directly to the media. The following combinations of pGL3-(6x)HRE or pGL3Vo in combination with the TK-*Renilla* luciferase were transfected.

TK-*Renilla* Luciferase (ng)	pGL3Vo (ng)	pGL3-(6x)HRE (ng)
30	50	50
30	100	100
30	200	200
50	50	50
50	100	100
50	200	200

Table 2.3: Optimisation of transfection for HIF-1α HRE-reporter system protocol.

Seven hours after transfection, one plate was incubated in the hypoxic workstation (1% O_2 at 37°C in a humidified atmosphere with 5% CO_2) for 16 hours and the second plate left for 16 hours in normoxia (20% O_2 at 37°C in a humidified atmosphere with 5% CO_2).

2.6.3.1 HIF1α Dual luciferase reporter assay reagent preparation

1. **Passive Lysis Buffer (PLB):** 1 volume of 5x PLB (Promega-E1941) was added to 4 volumes of distilled water, mixed well and stored at 4°C
2. **Luciferase Assay Reagent (LAR):** The lyophilised Luciferase Assay Substrate was re-suspended in Luciferase Assay Buffer II (Promega E1910) and stored at -20°C
3. **Stop and Glo Reagent ®**: 0.2 mls of 50x Stop and Glo substrate (Promega E2920) was added to 10 mls of Stop and Glo Buffer® (Promega E2920) and vortexed for 10 seconds

2.6.3.2 Cell lysis for HIF1α dual luciferase reporter assay system

Cells were lysed in 80µl 1x passive lysis buffer 24 hours post transfection and snap frozen on dry ice. Samples were thawed and allowed to equilibrate at room temperature,

with gentle rocking for fifteen minutes prior to assessing luciferase activity using the dual luciferase reporter assay system.

2.6.3.3 Protocol for readout of Luciferase reporter assay

10µl of each lysate was pipetted in triplicate in to a white-bottomed 96-well plate. 100µl of the luciferase assay reagent was added to each sample prior to gentle mixing on an orbital plate shaker for two minutes. Firefly luminescence was then read using the Wallac 1420 Multilabel Counter Plate reader. 100µl of diluted room temperature Stop and Glo® was then added to each well to quench firefly activity and the Renilla luciferase activity read using the Wallac 1420 Multilabel Counter Plate reader. The luminescence for the Renilla reporter was then normalised to the Firefly reporter for each reading and the normalised shLIMD1 values then normalised to the scr control values in both normoxia and hypoxia.

2.7 Synthetic lethality Drug screen

2.7.1 Synthetic lethality Drug screen background

A cancer-therapeutic drug library containing five hundred and eighty four Federal Drug Agency (FDA) approved, cancer-therapeutic drugs was obtained from the Institute of Cancer Research. All drugs included in the screen are either already in clinical use as cancer-therapeutic drugs, or have been evaluated within a clinical trial setting as showing potential cancer-therapeutic effects. The drug library incorporated five, 96-well plates and included empty wells in row 7 and further empty rows on plate five for the addition of further controls.

2.7.2 Optimisation of RCC11 seeding density prior to drug screen

RCC11 scr and RCC11 shLIMD1 cells of early and identical passage were taken out of puromycin selection 24 hours prior to seeding. Cells were seeded in to 96-well plates in 100µl of media with six replicates for each seeding density at a range of different

seeding densities: 800,100,1200 and 1500 cells/well for both cell lines. The media was changed at 24 and 48 hours to replicate the conditions of the drug screen and the plates manually inspected on day 6 to determine cell confluency. A seeding density that resulted in 90-95% cell confluency on day 6, considered optimal for 2-dimensional drug screens was selected for each cell line: this was 1000 cells/well and 1200 cells/well for RCC11 scr and RCC11 shLIMD1 cells respectively.

2.7.3 Seeding of RCC11 scr and RCC11 shLIMD1 cells for the drug screen

RCC11 scr and RCC11 shLIMD1 cells of early and identical passage were taken out of puromycin selection 24 hours prior to seeding. Seeding of the RCC11 scr cells was at 1000 cells/well and the RCC11 shLIMD1 cells at 1200 cells/well. 6, 96 well plates for RCC11 scr and 6, 96-well plates for RCC11 shLIMD1 cells were seeded.

2.7.4 Preparation of the drug plates

The drug library was stored in the -20°C freezer. For all five 96-well plates row 7 was empty and for the fifth plate, there were no drug compounds in rows 8-12, allowing the incorporation of additional control wells. A number of controls were added to these rows. For row 6 for all wells, a media only control was added to the top three wells (7A, B and C) and 5µl of DMSO to the 3 wells underneath (7D, E and F). We had observed activity with the tyrosine kinase inhibitor sunitinib in these cell lines and 5µl of sunitinib at a concentration of 20µM was added to well 7G and H on each plate. In addition, on the 6th plate, 5µl of sunitinib at a concentration of 20µM was added to rows 8A-E and 5µl of sunitinib at a concentration of 40µM to rows 9A-E and 5µl of sunitinib at a concentration of 60µM to rows 10A-E. Using fresh RPMI, supplemented with 10% FCS, (but containing no penicillin/streptomycin), 95µl of media was carefully aliquoted in to each well of each drug plate

Dilution of the drug library was carried out on the day drugging of the cells was undertaken.

2.7.5 Drugging of the RCC11 scr and RCC11 shLIMD1 plates

24 hours after seeding, media was aspirated from the RCC11 scr and RCC11 shLIMD1 cells and replaced with 95µl of RPMI supplemented with 10% FCS but containing no

antibiotics and plates carefully labelled. 5µl of each compound from the compound library/control wells was carefully transferred to the corresponding RCC11scr/RCC11 shLIMD1 plate using a p20 multichannel pipette and the drug carefully mixed with the media by pipetting up and down 5 times. This resulted in a final drug concentration of 1µM for all compounds in the drug library, with 0.5% DMSO control and between 1µM and 3µM of sunitinib control.

48 hours after the first drugging, the media was carefully aspirated from the 96 well plates and replaced with 95µl of RPMI supplemented with 10% FCS. The drugging process described above was repeated.

On day 6, 48 hours after the second drugging, drug assays were read using a Cell-Titer-Glo® luminescence cell viability assay.

A further drug screen was undertaken, with drugging of the cells with 2µM of the drug library. The protocol was as described, but 90µl of media was added to each well prior to drugging with 10µl of the drug library.

2.7.6 Cell-Titer-Glo® Luminescence cell viability assay

The Cell-Titer-Glo® Luminescence cell viability assay is an ATP based assay where the luminescence signal is directly proportional to the amount of ATP present, which in turn is directly proportional to the number of viable cells present in culture.

The Cell-Titer-Glo® reagents were prepared by reconstituting the lyophilised enzyme/substrate mixture according to the manufacturers instructions, and mixing well to obtain a homogenous solution prior to aliquoting and storing at -20^{o}C. Stored, thawed aliquots were diluted 1 in 4 with PBS prior to use.

Media was aspirated from the 96 well plates, and 100µl of diluted Cell-Titer-Glo® reagent pipetted in to each plate prior to mixing on an orbital shaker for 2 minutes: plates were then incubated at room temperature in the dark for 10 minutes to stabilise luminescent signal. Luminescence was read using the Wallac 1420 Multilabel counter plate reader.

2.7.7 Drug screen output analysis

The 'Z score' method was used to compare the relative cell killing for each drug between the scr and shLIMD1 plates. This method excludes control measurements altogether under the assumption that most compounds are inactive and can serve as controls. The scoring system rescales the output of the Cell-Titre Glo™ assay relative to the within plate variation by subtracting the median of the plate values from each drug assay result and dividing the difference by the median absolute deviation calculated from all measurements within the plate. This generates a readout whereby the more negative the Z-score the greater the degree of cell killing relative to the plate as a whole and the more positive the Z-score the greater the cell viability relative to the plate as a whole (Malo, Hanley et al. 2006). The outputs of the Z-scores were then plotted graphically using Prism 6. Drug 'hits' from the screen were subsequently validated using short-term cell-viability assays.

2.8 Drug-sensitivity assays

2.8.1 Drugs used in the drug sensitivity assays

All drugs were diluted to a stock concentration of 10mM in DMSO, prior to dilution to the relevant drug concentration in RPMI/DMEM media as appropriate, supplemented with 10% FCS.

Drug Name	**Drug concentration range**	**Company/Catalogue Number**
Sunitinib	0.1μM-10μM	Santa Crusz Biotechnology, 220177
Temsirolimus	0.5μM-30μM	Cambridge Bioscience, CAY11590
Irinotecan	0.1μM-60μM	LKT Laboratories, I6932

Pazopanib	0.1μM-60μM	Cambridge Bioscience, 1916-5
Dorzolamide	0.1μM-60μM	Sigma-Aldrich, SML0468
Selumetinib	0.1μM-60μM	Santa Crusz Biotechnology, sc-364613

Table 2.4: Drugs used in drug sensitivity assays. Drug name, drug concentration range and catalogue number detailed.

2.8.2 Seeding density for different cell lines for drug sensitivity assay

Early passage cells were taken out of puromycin selection 24-hours prior to plating. Seeding optimisation was undertaken such that confluency when assessed manually was at between 90-95% on day 6 (**Table 2.5**). Cell lines e.g. scr and shLIMD1 were seeded on to the same 96-well plate and each cell line dosed at each drug concentration in triplicate. At 24 and 72 hours, the media was aspirated and replaced with media containing the appropriate concentration of drug.

Cell line	**Seeding density in 96 well plate (cells/well)**
RCC11 scr	1000
RCC11 shLIMD1	1200
RCC48 scr	800
RCC48 shLIMD1	1000
HEK-293T	2000
A549	1500
HELA	1500

Table 2.5 Optimal seeding densities for a range of cell lines in a 96 well plate. Cells were seeded at a range of seeding densities in a 96 well plate and a seeding density associated with 90-95% confluency on day 6 selected.

2.8.3 Drug-sensitivity protocol

24 hours post cell seeding cells were drugged with increasing doses of the drugs listed in **Table 2.4**. Drugs were diluted in the appropriate media for optimal cell growth (RPMI or DMEM) supplemented with 10% FCS just prior to cell drugging. The dose range was chosen to give a dose response with cell death of between 0 and 95% where possible and all drugging at each dose concentration was undertaken in triplicate. Media was aspirated using a multichannel aspirator and replaced with the appropriate drug concentration. Drugging of cells in the outer wells was avoided to overcome the effects of 'edge effects', whereby evaporation of media is more likely to occur in the outermost wells.

48 hours after the first drugging, the media was carefully aspirated from the 96-well plates and the drugging process described above was repeated.

On day 6, 48 hours after the second drugging, drug assays were read using the Cell-Titer-Glo® luminescence cell viability assay described in section 2.7.6. The Luminescence was read using the Wallac 1420 Multilabel counter plate reader and the mean for each reading for each drug concentration normalised to the DMSO control and a drug dose-response curve constructed using Prism 6.

2.9. Fluorescent associated cell-sorting (FACS) protocol for the analysis of cell viability using propidium iodide (PI) staining

PI staining and FACS analysis of paired RCC11 scr/shLIMD1 and RCC48 scr/shLIMD1 cells was undertaken to assess differences in cell cycle associated with LIMD1 proficiency/deficiency.

2.9.1 Preparation of cells for FACS analysis and propidium iodide (PI) staining

RCC11 scr/shLIMD1 and RCC48 scr/shLIMD1 cells were seeded in to 6-well plates such that cell confluency was approximately 70% 24 hours post seeding. Cells were lysed and cell number counted as described in Section 2.2. $5x10^5$ cells of each cell type and a further $5x10^5$ cells (as an unstained control) were pelleted by centrifugation (300g

for five minutes at 4°C). The pellet was washed once with ice cold PBS prior to permeabilisation/fixation in 700µl of ice cold 70%-ethanol. Cells were incubated on ice for 30 minutes prior to re-pelleting (13,000g for one minute at 4°C). Cells were further permeabilised by re-suspending the pellet in 700µl of 0.1% Triton X100 in PBS on ice for five minutes prior to re-centrifugation (13,000g for one minute at 4°C). RNA was cleaved by re-suspending the pellet in 50µl of a 100µg/ml RNAse solution in PBS and shaking at 37°C at 100rpm for one hour prior to re-centrifugation (300xg for 8 minutes at 4°C). Cells were stained with 200µl of a 50µg/ml solution of propidium iodide in PBS and incubated on ice for 30 minutes. 800µl of Hank's buffered saline solution/2% FCS was added prior.

2.9.2 FACS analysis of PI staining

Fluorescence was read using a Fluorescence Activated Cell Sorter (FACS Caliber B) using the YG-610/20 excitation-emission filters with the appropriate gates set around the G0/G1, S and T2/M phase peaks. Results were analysed using Flowjo 7.6.5 software.

2.10 Enzyme linked immuno-absorbant assay (ELISA) of RCC11 and RCC48 proficient/deficient cells

2.10.1 Quantikine ELISA background

A Quantikine VEGF ELISA kit (R&D Systems) was used to measure levels of VEGFA in the supernatant. This is a sandwich immunoassay, using a prepared 96-well plate, pre-coated with capture antibody. Samples/standard are added to the plate, with analyte bound by the immobilised antibody with unbound material washed away. The substrate solution tetramethylbenzidine (TMB) is added to the well, with a blue colour developing in proportion to the amount of analyte added. Colour development is then stopped and absorbance read at 450nm.

2.10.2 Cell Preparation of RCC11 and RCC48 for ELISA

Paired RCC11 scr/shLIMD1 and RCC48 scr/shLIMD1 cells were taken out of

puromycin selection 24 hours prior to seeding in to 12-well plates at a density to ensure 50-60% confluency at 24 hours. Media was supplemented with 10% FBS but penicillin/streptomycin omitted. Plates were seeded for incubation in both normoxia (20% O_2 at 37°C in a humidified atmosphere with 5% CO_2) and in a hypoxic workstation (1% O_2 at 37°C in a humidified atmosphere with 5% CO_2). 24 hours post-seeding, cells were either transferred to the hypoxic workstation or left to remain in a normoxic environment. Cell culture media was then aliquoted 16 hours later.

2.10.3 Reagent preparation and VEGFa assay procedure

All reagents were allowed to equilibrate to room temperature prior to use. Cell culture media was pipetted in to an autoclaved eppendorf and spun at 13,000rpm for one minute before aliquoting in to a clean eppendorf. VEGF controls of known concentration supplied in the Quantikine ELISA kit were also included. The ELISA was performed in duplicate for each sample/control. 50µl of assay diluent RD1W was added to each microplate well and 200µl of the standard or sample added to the assay diluent. The microplates were then covered with an adhesive strip and incubated for two hours at room temperature. Each well was aspirated and washed three times with 400µl of wash buffer and any remaining wash buffer removed by inverting the plate and blotting against clean paper towels. 200µl of VEGF conjugate was then added to each well, covered with an adhesive strip and incubating for two hours at room temperature. Each well was then aspirated and the wash with wash buffer repeated as detailed above. The substrate solution was then made up by mixing equal quantities of colour reagent A and B and adding 200µl of the substrate solution to each well prior to incubation at room temperature for 25 minutes. 50µl of stop solution was added to each well and the optical density read using the Wallac 1420 Multilabel counter plate reader with absorbance read at both 450nm and at 540nm to account for background absorbance. Background absorbance was subtracted for each sample/control and mean values for both controls and samples calculated. Using the readout for the control samples, a corrected absorbance/VEGF concentration graph was calculated and the VEGF concentrations for the samples determined.

2.11 Western blot analysis

2.11.1. Solutions used for cell lysis

RIPA: 150 mM NaCl, 1% (v/v) IGEPAL-630, 0.5% (w/v) sodium deoxycholate, 0.1% (w/v) SDS and 50mM Tris dissolved in distilled water, pH adjusted to 8.

Protease and Phosphatase Inhibitors: (Roche). One Complete™ Protease Inhibitor Cocktail tablet and one PhosStop™ tablet were dissolved in 10mls of lysis buffer and stored at -20°C for < 6 weeks.

MG-132 Proteasome Inhibitor: (Cell Signalling). A 10mM stock solution was obtained by dissolving the MG-132 powder into sterile DMSO and stored at -20°C for < 2 months. A working concentration of 10μM was used.

2.11.2 Preparation of cell lysates for Western blot analysis

Cells were washed three times with ice cold PBS and scraped gently into ice cold RIPA lysis buffer containing protease/phosphatase inhibitor and MG132. Samples were sonicated three times for 3 seconds and centrifuged at 13,000rpm for 10 minutes at 4°C to clear insoluble cellular debris. The supernatant was transferred to a clean eppendorf tube and stored at -80°C

2.11.3 Protein concentration evaluation

Protein concentration of the cell lysates was measured using either the Bio-Rad or Sigma Bradford assay.

2.11.3.1 Bio-Rad DC ™ protein assay

Bovine serum albumin (BSA) (20mg/ml) was diluted in distilled water to generate protein standard positive controls ranging in concentration from 0.1mg/ml to 1.5mg/ml. Reagent A' was prepared by adding 20μl of Bio-Rad DC™ reagent S to 1ml of Bio-Rad DC™ reagent A (Bio-Rad 500-0116).

5µl aliquots of the control samples, a dH_20 control, and the thawed lysate samples were pipetted in triplicate in a 96-well plate. 25µl of A' and 200µl of Reagent B was then added to each sample, the plate incubated at room temperature for 10 minutes and absorbance measured at 630nm using the Wallac 1420 Multilabel counter plate reader.

2.11.3.2 Sigma Bradford Assay

Dilutions of protein standard positive controls, ranging from 0.15625mg/ml to 5mg/ml were made by diluting BSA in distilled water. 2µl of each control (including a distilled water sample as background control) and lysate sample were added in triplicate to a 96 well plate. 8µl of distilled water was added to each well to reduce the concentration of the RIPA buffer, followed by 250µl of the Bradford reagent. The plate was incubated at room temperature for 15 minutes and absorbance measured at 530nm using the Wallac 1420 Multilabel counter plate reader.

For both assays, the absorbance of the protein standards was used to construct a standard curve, using Prism 6 and the equation for this curve used to determine the sample concentrations.

2.11.4. Solutions for sodium dodecyl sulphate polyacrylamide gel electrophoresis (SDS-PAGE) and Immunoblotting

5x SDS-PAGE Sample buffer: (50% (v/v) glycerol, 250mM Tris-HCL pH 6.8, 5% (w/v) SDS, 5% (v/v), β-Mercaptoethanol and 0.05% (w/v) Bromophenol Blue) were dissolved in distilled water and stored at -20°C

Transfer buffer: Blocking Solution: 5% (w/v) dried skimmed milk powder was dissolved in 1x PBS-Tween (0.05% v/v) or 5% (w/v) dried skimmed milk powder was dissolved in 1x-TBS-Tween (0.05% v/v).

Resolving gel: ddH_2O was added to bis-acrylamide (30% stock solution, National Diagnostics EC890) of the desired volume to achieve the correct percentage gel prior to

the addition of resolving buffer (0.375M Tris pH 8.8 and 0.1% SDS) (National Diagnostics). 0.1% ammonium persulphate (APS) was added to crosslink the acrylamide, catalysed by the addition of 0.01% N,N,N',N'-tetramethylethylenediamine (TEMED) immediately prior to pouring. 100% ethanol was added immediately after pouring to achieve a straight horizontal gel during resolving.

Stacking gel: Stacking buffer (0.125M Tris pH 6.8, 0.1% SDS) was added to 4% bis-acrylamide (National Diagnostics). Crosslinking of the acrylamide was achieved with the addition of 0.1% APS and 0.01% TEMED. Gel combs were inserted straight after pouring the stacking gel.

2.11.5 Western Blot protocol

Samples were run on poured 8% to 12% polyacrylamide gels. Generally 8% gels were used to resolve proteins between 50 and 150 kDa and 10% gels for proteins between 30 and 50 kDa.

Cell lysates were denatured in 1x SDS-PAGE Sample buffer by heating at 95°C for 5 minutes. Samples were cooled on ice and centrifuged briefly prior to loading. 5µl of molecular weight marker was loaded alongside the protein samples to enable band size estimation. Typically 15-20µg of protein sample was loaded with 5µg for the β-actin control.

Proteins were resolved by SDS-PAGE at 80 Volts for 20 minutes and then at 120 Volts until fully resolved. Gels were transferred on to methanol permeabilised, Polyvinylidene fluoride (PVDF) membranes using the Trans-Blot Turbo™ system (Bio-Rad) for 20 minutes at 25 Volts and 2.5 Amps. Membranes were blocked in blocking buffer for 1 hour and then incubated with the required primary antibody diluted in blocking buffer at 4°C overnight with gentle agitation.

Antigen	**Company (Catalogue Number)**	**Dilution for immunoblotting**	**Host species**
Primary Antibodies			
LIMD1	(Sharp *et al*, 2004, 2008, 2009)	1:500	Mouse
HIF1α	BD Transduction Laboratories 610959	1:500	Mouse
HIF2α	Novus Biologicals NB100-132	1:500	Rabbit
Ajuba	Cell Signaling 4897	1:500	Mouse
WTIP	Santa Crusz SC241737	1:500	Goat
β-Actin	Sigma-Aldrich A5316	1:50,000	Mouse
Secondary Antibodies			
Mouse	Dako 2019-10	1:2,500	Goat
Rabbit	Dako 2019-03	1:2,500	Goat
Goat	Dako 2018-11	1:2,500	Rabbit

Table 2.6: Antibodies used for Immunoblot analysis. Primary antibody, catalogue number, antibody dilution, and host species listed.

Membranes were then washed with three, 5-minute washes in PBS-Tween 0.05% prior to incubation with secondary antibody (horse-radish peroxidase conjugated, diluted in blocking buffer to concentration 1:2,500) for 1 hour at room temperature with gentle agitation. Membranes were washed with three, 5-minute washes in PBS-Tween 0.05%, prior to incubation with Enhanced Chemiluminescence (ECL) Plus Western Blotting Detection Reagent (Thermo Scientific 80196) at room temperature for 5 minutes to initiate an HRP-catalysed luminescent reaction. Membranes were exposed to chemiluminescent detection film (UltraCruz autoradiography film) for between 5 seconds and up to 2 hours and the film developed in a Curix 60 Developer (Agfa, Middlesex, UK).

Chapter 3.

LIMD1, WTIP and Ajuba (LAW) expression is reduced in clear cell renal cell carcinoma

3.1 Introduction

Sharp *et al* demonstrated that LIMD1 is downregulated and contributes to tumourigenesis in lung carcinoma (Sharp, Al-Attar et al. 2008). In breast carcinoma, Spendlove *et al* showed not only frequent loss of LIMD1 expression in tumour compared to normal adjacent and distant tissue but that absence/loss of nuclear staining strongly correlated with worse patient survival and a more aggressive tumour phenotype (Spendlove, Al-Attar et al. 2008).

LIMD1, Ajuba and WTIP (LAW) are closely homologous members of the larger Zyxin family, characterised by triple tandem C-terminal zinc finger motifs which facilitate protein-protein interactions (Kadrmas and Beckerle 2004). Tanaka *et al* have recently demonstrated that in malignant mesothelioma cells, Ajuba downregulation is common and that *Ajuba* re-expression abrogated some aspects of tumourigenesis (Tanaka, Osada et al. 2015). In addition, *Ajuba* is 14q expressed and work by Kroeger *et al* has demonstrated a strong association between 14q loss and worse clinical outcome in ccRCC. Kroeger *et al* hypothesised that this could be related to HIF1α loss, which is 14q expressed, although this has not been established and other candidate genes remain uncharacterised (Kroeger, Klatte et al. 2013). Conversely, work by Shi *et al*, has demonstrated that Ajuba is frequently up-regulated in oesophageal SCC compared to non-cancerous tissue at both the mRNA and protein level (Shi, Chen et al. 2016).

All three LIM-domain proteins interact with components of the RISC and the mRNA m^7 GTP cap-protein complex required for miRNA-mediated silencing (Bridge, Shah et al. 2017). Of note, alterations in a number of hypoxically regulated miRNAs are implicated in ccRCC tumourigenesis and miRNAs are often aberrantly expressed in carcinomas with consequent oncogenic and loss of tumour suppressive functions (Li, Wang et al. 2015). In addition, all three proteins play a critical role in the regulation of the hypoxic response functioning as a molecular scaffold simultaneously binding VHL and PHDs to regulate HIF-1α (Foxler, Bridge et al. 2012). Ajuba LIM proteins are negative regulators of the Hippo signalling pathway, a critical regulator of epithelial organ size (Zeng and Hong 2008), deregulation of which is implicated in driving tumourigenesis in multiple tumour types including ccRCC (Harvey, Zhang et al. 2013) .

All three family members remain uncharacterised in ccRCC. It was hypothesised that loss of LAW is common in ccRCC and could contribute to tumourigenesis: given the close homology of the three proteins and their overlapping functionality, a degree of functional redundancy may also exist such that a second LAW protein could compensate in part for the loss of a first LAW protein. It was also hypothesised that loss of several LAW proteins may coexist and further contribute to tumourigenesis

To this end, LAW levels were characterised *in vitro* in a panel of ccRCC lines prior to assessing immunohistochemical staining in a range of normal tissues and tumours before characterising staining in ccRCC and matched adjacent tissue (MAT). The relationship between the levels of the three proteins in ccRCC and MAT was investigated: establishing if tumours that had low levels of LIMD1 for example were also more likely to have low Ajuba and or WTIP staining.

In addition, staining for LAW proteins was correlated with staining for VEGFa and CD34. Both VEGFa and CD34 are markers of hypoxic deregulation, a critical driver of ccRCC (Pouyssegur, Dayan et al. 2006) and validated prognostic indicators in ccRCC. In some studies, VEGF-A overexpression is associated with a more aggressive ccRCC subtype (Patard, Rioux-Leclercq et al. 2009) and targeted therapy with tyrosine-kinase inhibitors down-regulates angiogenesis predominantly through VEGF-R and PDGF-R pathways (Dorevic, Matusan-Ilijas et al. 2009). CD34 is an established marker for capillary endothelia and hence micro-vascular density (MVD). Tumour MVD has been shown to correlate with the aggressiveness of renal cell carcinoma: in an analysis of 57 RCC tumours, adjusted MVD was associated with shorter disease-free survival on univariate and multivariate analysis (Iakovlev, Gabril et al. 2012) (Yao, Qian et al. 2007).

3.2 Aims and Objectives

The aims and objectives of this chapter are:

1. To assess the protein levels of LAW family members in a panel of ccRCC cell lines *in vitro* by immunoblot
2. To optimise immunohistochemical staining for LAW family members in a range of normal and tumour tissues
3. To characterise the expression and relationship between LAW family members immunohistochemically in ccRCC and matched adjacent tissue (MAT)
4. To characterise the relationship between LAW family members and established markers of hypoxic deregulation in ccRCC

3.3 Expression of LIMD1 and its family members Ajuba and WTIP is reduced/absent in a significant proportion of ccRCC lines

Firstly the expression of LIMD1, Ajuba and WTIP was characterised in a panel of ccRCC lines relative to expression in renal proximal tubular epithelial cells (RPTEC), the cells from which ccRCC is thought to derive (Frew and Moch 2015) (**Figure 3.1**). Western blot analysis demonstrated good specificity of the antibodies *in vitro* with band sizes corresponding to that predicted. The Sharp lab had also used siRNA directed against the proteins of interest to knock down LAW expression, with consequent abrogation of the Western blot signal thus further confirming antibody specificity.

Blots were not run with an RPTEC-BMI-1 control included concurrently as this was not available at the time. Protein levels were analysed using Image-J and normalised to the β-actin control**.** A separate blot was run for Ajuba, LIMD1 and WTIP, which included lysate from RPTEC cells, BMI-1-transduced RPTEC and RCC45 (**Figure 3.1**). This enabled the levels of Ajuba, LIMD1 and WTIP in the RPTEC line to be normalised to the RCC45 line, and LAW levels in the panel of ccRCC line could then be normalised to this figure, allowing the comparison of LAW expression in the ccRCC lines compared to RPTEC control.

LIMD1 expression was reduced or absent in ten out of the twelve cell lines characterised (88%). Eleven of the twelve lines (92%) demonstrated low or absent Ajuba expression and for WTIP, four out of the twelve lines (33%) demonstrated low or absent WTIP expression, with the remaining eight lines (67%) demonstrating increased expression. Some lines showed high levels of expression of all three family members e.g. RCC11, whilst others had low levels of two family members e.g. RCC38, which expressed very low Ajuba and reduced LIMD1 with increased WTIP compared to the RPTEC-BMI-1 control. RCC12 was the only ccRCC line tested that expressed low levels of all three family members, although some signal was present for all three proteins (**Figure 3.1**).

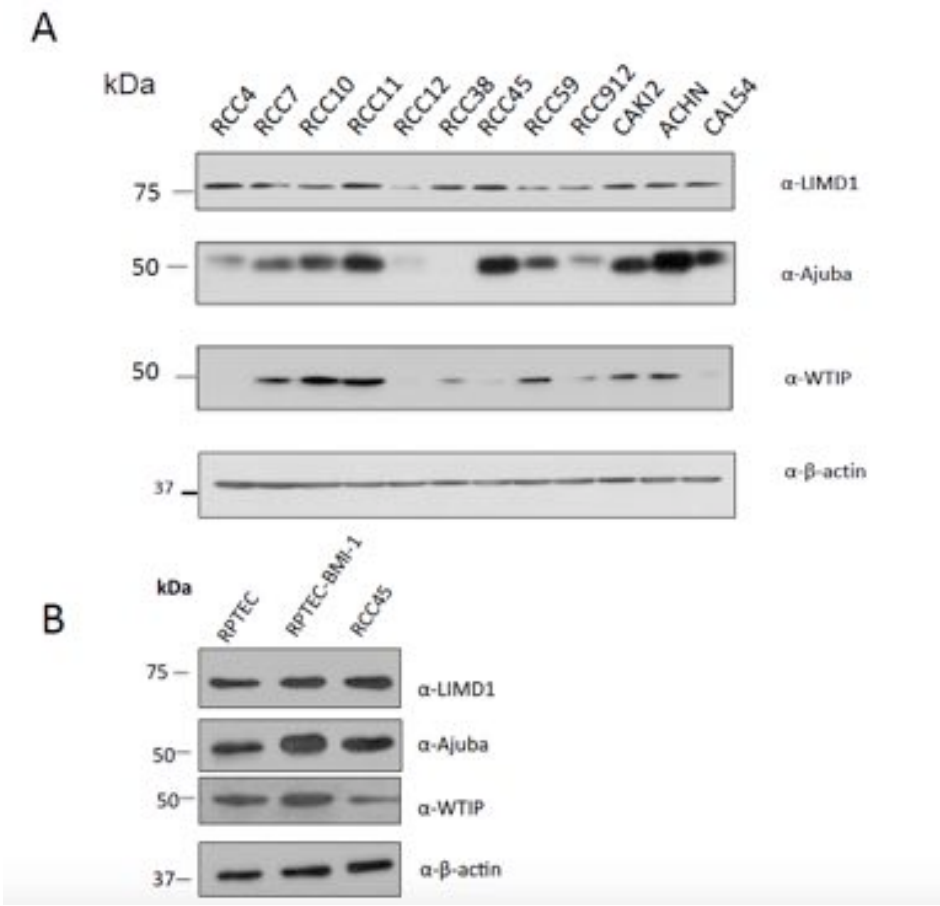

(iii)

ccRCC line	Ajuba	LIMD1	WTIP
RPTEC	1.00	1.00	1.00
RCC4	0.14	0.79	0.02
RCC7	0.31	0.57	4.30
RCC10	0.50	0.56	8.95
RCC11	0.76	1.08	9.87
RCC12	0.07	0.29	0.13
RCC38	0.00	0.76	1.90
RCC45	0.88	1.03	0.43
RCC59	0.46	0.43	4.67
RCC912	0.18	0.41	1.12
CAKI2	0.60	0.68	3.44
ACHN	1.12	0.80	3.68
CAL54	0.65	0.74	0.27

Figure 3.1 Expression of LIMD1 and family members WTIP and Ajuba is lost/reduced in ccRCC lines *in vitro*.

Immunoblots of whole cell ccRCC extracts showing the protein expression of (i) HIF2α, LIMD1, Ajuba, WTIP, VHL and β-actin as loading control. Loading protein concentrations were normalised after determination of lysate protein concentration using a Bradford assay. **(ii)** Whole cell extract immunoblots to show the protein expression of LIMD1, Ajuba and WTIP in RPTEC and BMI-1 transduced RPTEC with the ccRCC line RCC45 for comparison. Loading protein concentrations were normalised after determination of lysate protein concentration using a Bradford assay and β-actin included as a loading control. **(iii)** Western blot signal for LIMD1, Ajuba and WTIP was compared in the ccRCC lines with expression levels in RPTEC. Analysis was undertaken using Image J.

3.4 LIMD1 staining in tumours and pre-invasive tissue is specific and demonstrates predominantly cytoplasmic staining patterns

LIMD1 expression has not been characterised in most normal human tissues or carcinomas. Work by Sharp *et al* and Spendlove *et al*, characterising LIMD1 staining in breast and lung carcinoma demonstrated predominant cytoplasmic staining with some nuclear staining in breast tissue, and in both tissues little stromal staining (Sharp, Al-Attar et al. 2008, Spendlove, Al-Attar et al. 2008).

Firstly TMAs containing a range of tumour samples and pre-invasive tissue were stained, in order to demonstrate IHC antibody specificity and identify positive and negative control tissue for use when staining the ccRCC samples. Optimal staining was obtained with a manual staining protocol (LIMD1 antibody concentration 1:50). Professor Mike Sheaff of Barts Health NHS Trust reviewed all staining to define appropriate antibody concentrations, confirm that staining appeared specific and identify appropriate controls. Staining patterns were heterogeneous with a variety of cytoplasmic expression patterns in different tissues, little nuclear staining and little stromal staining. Staining was felt to be specific with little background staining observed in a range of normal and malignant tissues (**Figure 3.2**).

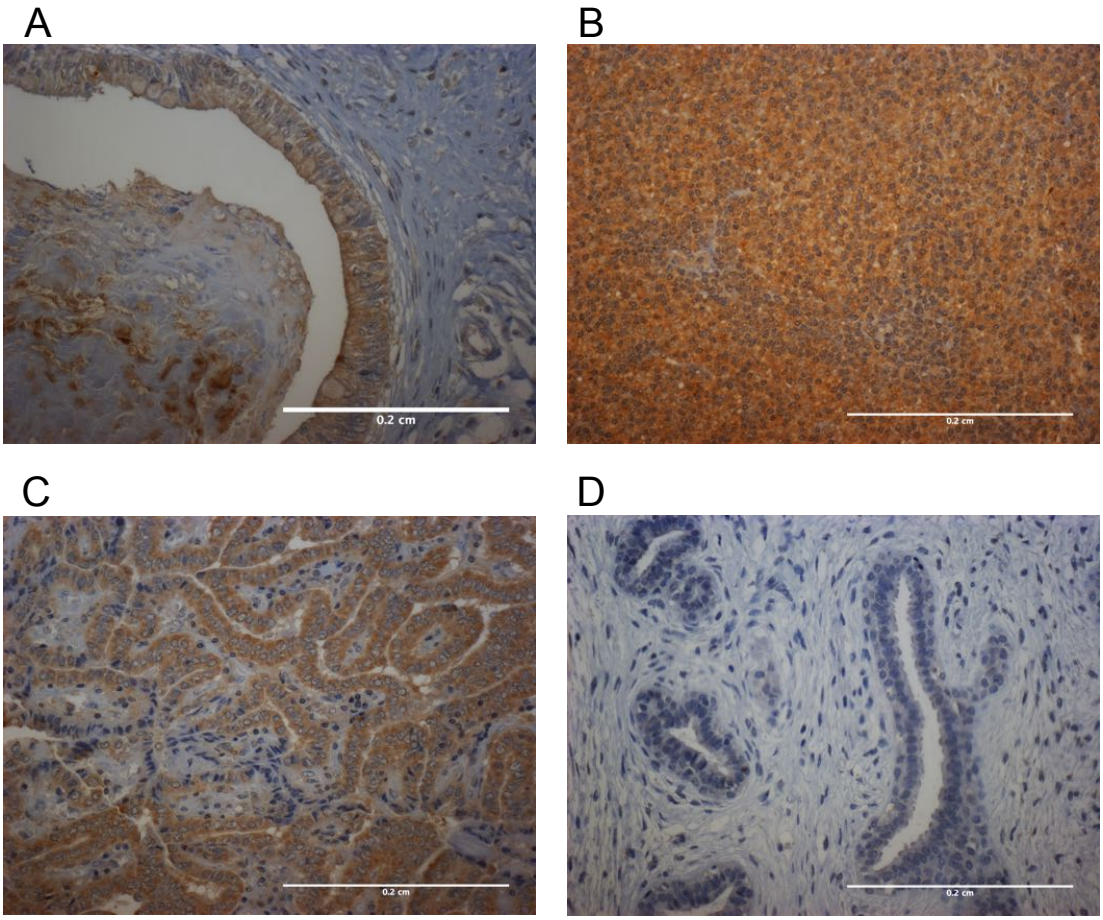

Figure 3.2: IHC staining using an optimised manual staining protocol demonstrates specific and heterogeneous LIMD1 staining in a range of tumour types.

TMAs printed with histospots from a range of tumour types were stained using an optimised manual staining protocol with LIMD1 antibody concentration 1:50, and visualisation using the Avidin-biotin peroxidase method with haematoxylin counterstaining. **(A)** Testis teratoma (strong cytoplasmic epithelial staining but little stromal staining), **(B)** thymoma (strong tumour cytoplasmic LIMD1 staining), **(C)** thyroid papillary carcinoma (strong cytoplasmic tumour staining with little stromal staining), **(D)** phylloides breast carcinoma (no LIMD1 staining). Scale bars corresponding to 200μm are shown for size comparison.

In addition, healthy breast tissue and lung tissue, where staining patterns for LIMD1 had previously been published were stained (Sharp, Al-Attar et al. 2008, Spendlove, Al-Attar et al. 2008). The antibody used for this IHC was derived from the same hybridoma used by Sharp *et al* and Spendlove *et al* (Sharp, Al-Attar et al. 2008, Spendlove, Al-Attar et al. 2008). Sharp *et al* had described the staining pattern in lung tissue, demonstrating high level, predominantly cytoplasmic expression in ciliated

pseudostriated epithelia of bronchial epithelial tissue with weaker staining in distal alveolar epithelia, and this correlated with Western blot analysis of protein extracts from these cells (Sharp, Al-Attar et al. 2008). IHC staining patterns in lung tissue were similar to that described by Sharp *et al* (Sharp, Al-Attar et al. 2008) (**Figure 3.3**). In breast tissue Spendlove *et al* had found that LIMD1 was specifically expressed in the epithelial cells of terminal duct lobular units (Spendlove, Al-Attar et al. 2008), a staining pattern we also identified, although less nuclear staining was noted (**Figure 3.3**). The control TMA described, containing a range of pre-invasive and tumour histospots was included as a positive/negative control when other tissue types were stained. For all staining, an additional negative control was included, where the primary antibody was omitted to account for non-specific antibody binding.

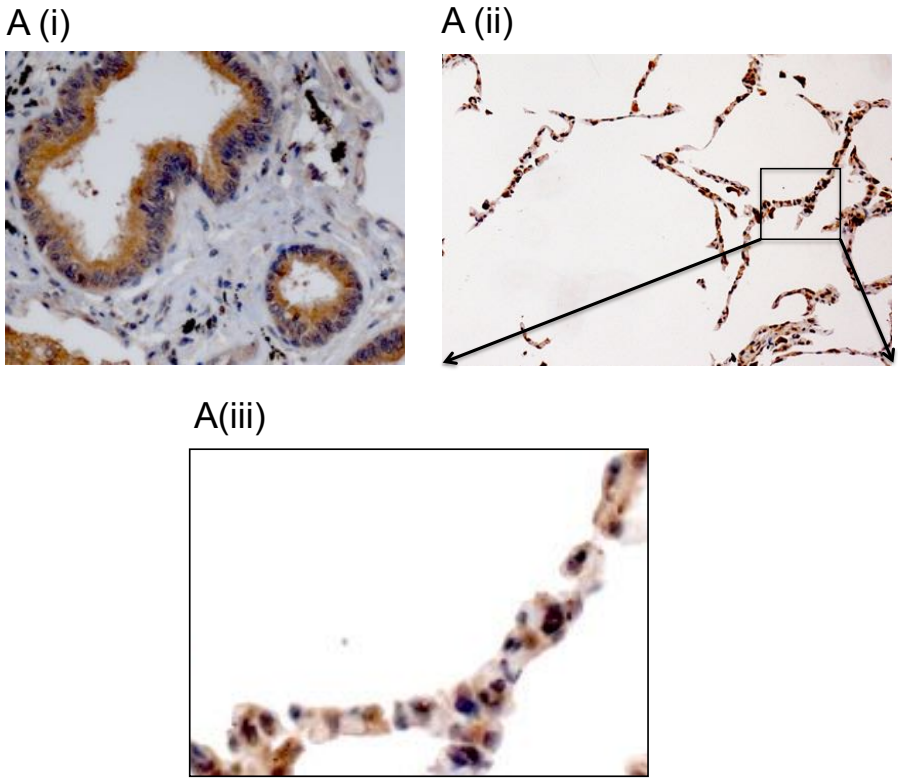

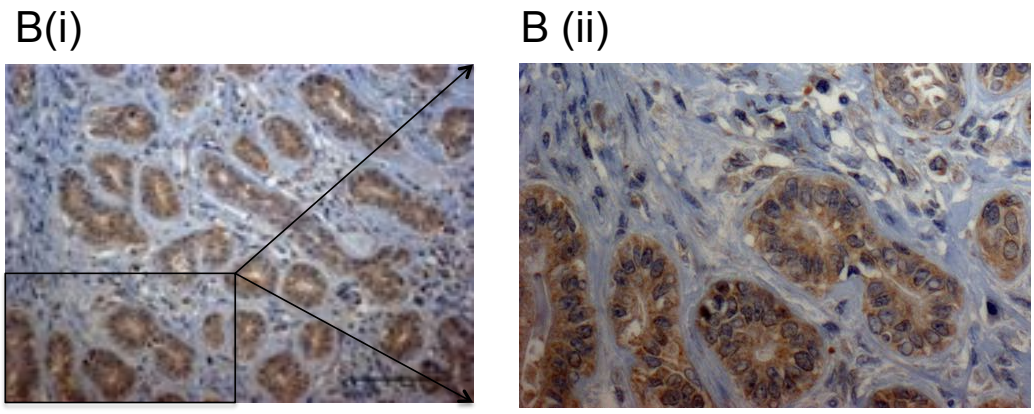

Figure 3.3: IHC staining using an optimised manual staining protocol in lung tissue and breast tissue demonstrates specific LIMD1 staining that corresponds to the pattern observed previously by Sharp *et al*.

Paraffin embedded lung tissue and breast tissue was stained using an optimised manual staining protocol with LIMD1 antibody concentration 1:50, and visualisation using the Avidin-biotin peroxidase method with haematoxylin counter staining. **(Ai)** Staining of bronchial epithelial tissue with staining of the ciliated pseudostratified epithelium (**Aii)** Staining of the distal alveolar epithelium **(Aiii)** Magnified image of the distal alveolar epithelium **(Bi)** Staining of breast tissue demonstrates staining of epithelial cells only with no stromal staining. A scale bar corresponding to 200μm is shown **(Bii)** Magnified image of breast tissue staining.

3.5 LIMD1 staining in kidney tissue

Prior to staining the ccRCC TMA histospots, the specificity of the LIMD1 antibody for kidney tissue was established and the expected staining patterns defined. Staining patterns had not previously been characterised in ccRCC or healthy renal tissue. IHC for LIMD1 in healthy renal tissue demonstrated specific staining of the proximal and distal convoluted tubules with very little staining of the glomeruli. Staining was cytoplasmic with no nuclear staining observed (**Figure 3.4**).

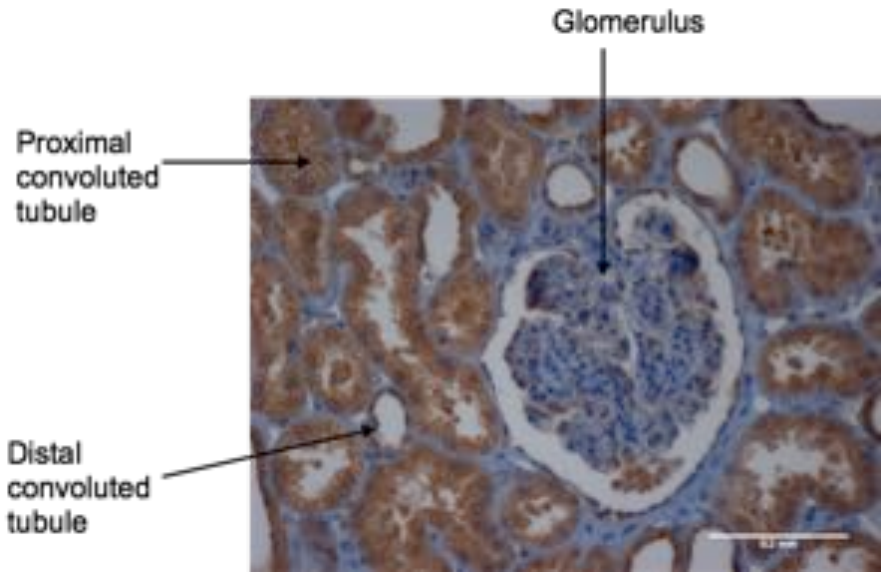

Figure 3.4: IHC in health kidney tissue is specific with staining of the proximal and distal convoluted tubules but not the glomeruli.

Healthy paraffin embedded kidney tissue was stained using an optimised manual staining protocol with LIMD1 antibody concentration 1:50, and visualisation using the Avidin-biotin peroxidase method with haematoxylin counterstaining. A scale bar corresponding to 200μm is shown for size comparison.

3.6 Ajuba and WTIP staining in a range of normal tissues

The normal staining patterns for Ajuba and WTIP are largely uncharacterised. Data sheets for the Ajuba antibody and the Protein Atlas website demonstrate strong staining of tissues of the gastrointestinal tract and this has also been described in the literature (Shi, Chen et al. 2016). Tanaka *et al* stained malignant mesothelioma tissue for Ajuba and demonstrated variable expression patterns with both cytoplasmic and nuclear staining patterns (Tanaka, Osada et al. 2015). Given that neither protein has been extensively evaluated, TMAs with histospots derived from a range of normal tissues were stained, in order to define normal staining patterns and identify positive and negative controls to include when staining our ccRCC cohort. All staining was reviewed by Professor Mike Sheaff and once optimised felt to be specific. An optimal antibody concentration of 1:50 was identified for Ajuba following review of staining in normal stomach and renal tissue using a range of antibody concentrations. Staining was strongly positive in tissue of the gastrointestinal tract in both cytoplasmic and nuclear compartments: healthy stomach tissue was subsequently used as a positive control. Optimal staining of stomach tissue for Ajuba is shown in **Figure 3.5**, and optimal staining of renal tissue in **Figures 3.7, 3.8 and 3.9.**

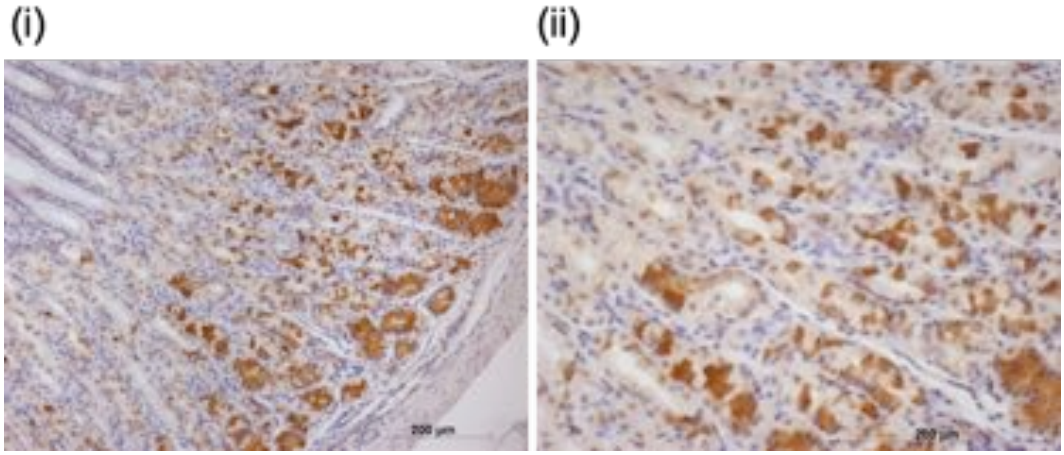

Figure 3.5. Representative staining for Ajuba in normal stomach tissue

Staining was undertaken using an optimised, manual staining protocol with visualisation using the avidin-biotin peroxidase method and haematoxylin counterstaining. Representative images of healthy stomach stained with Ajuba antibody at 1:50 are shown above at 10x and 20x magnification with both cytoplasmic and nuclear staining demonstrated (Figures **(i-ii).** Scale bars corresponding to 200μm are shown

For the normal renal tissue and ccRCC samples, Ajuba staining was predominantly nuclear with little cytoplasmic staining (**Figures 3.7, 3.8 and 3.9**). Professor Sheaff felt that only the nuclear Ajuba staining should be characterised in the ccRCC and MAT histospots and this staining pattern was consistent with that described on Protein Atlas. Review of the literature did not identify any studies characterising Ajuba staining in ccRCC.

WTIP staining was both cytoplasmic and nuclear in ccRCC and MAT histospots and staining in both compartments felt by Professor Sheaff to be a true result and scorable. Optimised WTIP staining is demonstrated in small bowel and placenta in **Figure 3.6** and in ccRCC/MAT in **Figures 3.7, 3.8 and 3.9**. Review of the literature did not identify any WTIP staining in ccRCC for comparison. For all staining a negative control was included where the primary antibody was omitted to account for non-specific binding for both the WTIP and Ajuba antibodies.

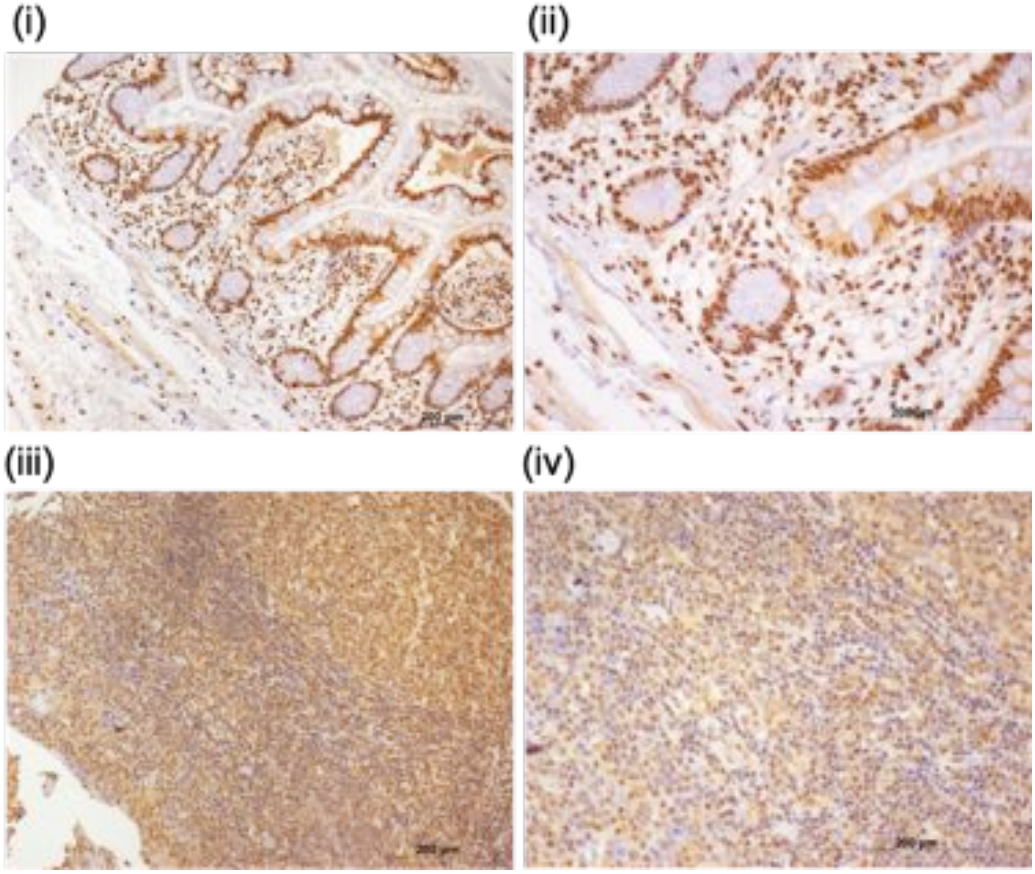

Figure 3.6 Representative images of staining for WITP in small bowel and placenta

Staining was undertaken using an optimised, manual staining protocol with visualisation using the avidin-biotin peroxidase method and haematoxylin counterstaining. **(i-ii)** Representative images of small bowel stained with WTIP antibody at 1:50 are shown above demonstrating predominantly nuclear staining patterns at 10x and 20x magnification respectively. **(iii and iv)** Representative images of lymph node tissue stained with WTIP antibody at 1:50 are shown above demonstrating lower levels of nuclear and cytoplasmic staining at 10x and 20x magnification. Scale bars corresponding to 200μm are shown for size comparison

3.7 Immunohistochemistry demonstrates loss of LAW family members in over 50% of ccRCC histospots

Having established the specificity of staining for LIMD1, WTIP and Ajuba in a range of tissue samples/tumours, immunohistochemical staining for LAW was undertaken, using a commercially available TMA purchased from US Biomax incorporating 75 ccRCC histospots, each with a MAT histospot.

Tissue micro-arrays allow for the immunohistochemical analysis of large number of tumour samples in a high-throughput manner, a particular advantage in a clinical trial setting and for research methodological studies where a large number of samples need to be analysed to identify a relationship, for example correlating tumour suppressor/oncogene expression with clinico-pathological data (Fiore, Bailey et al. 2012). It can however be difficult to set an appropriate quantitative scale that can accurately be followed by the observer, particularly when staining for proteins previously uncharacterised (Hsi 2001). Correlating staining manually between ccRCC samples and MAT using a TMA where MAT is adjacent to each ccRCC sample may also be associated with an unconscious observer bias. In addition, when attempting to identify a correlation between levels of two different proteins, scoring manually using a quantitative scale, which may only have three or four values, may make evaluation of correlation patterns difficult and a small but nonetheless significant correlation may be overlooked (Matos, Trufelli et al. 2010).

Images were therefore acquired and analysed using an automated image acquisition/analysis system. High-resolution images were obtained of each histospot and areas of tumour/normal tissue quantitatively scored using the Ariol SL-50 system (Genetix). Areas of tumour were manually identified with masking of the stroma and of the normal/benign tissue from image analysis in the ccRCC samples. Stroma was also excluded with masking in the MAT samples. Scores were generated using a modified automated scoring system: this generates an output score as a function of the average staining intensity and the area of positive staining of the protein of interest throughout the tissue. This is a validated method for the assessment of IHC staining (Yaziji and Barry 2006) (Rizzardi, Johnson et al. 2012).

Tumours were separated in to those showing a reduction in IHC staining (**Figure 3.7**), similar levels of staining (**Figure 3.8**) and increased staining (**Figure 3.9**) in the ccRCC histospots compared to MAT for each of the LAW proteins.

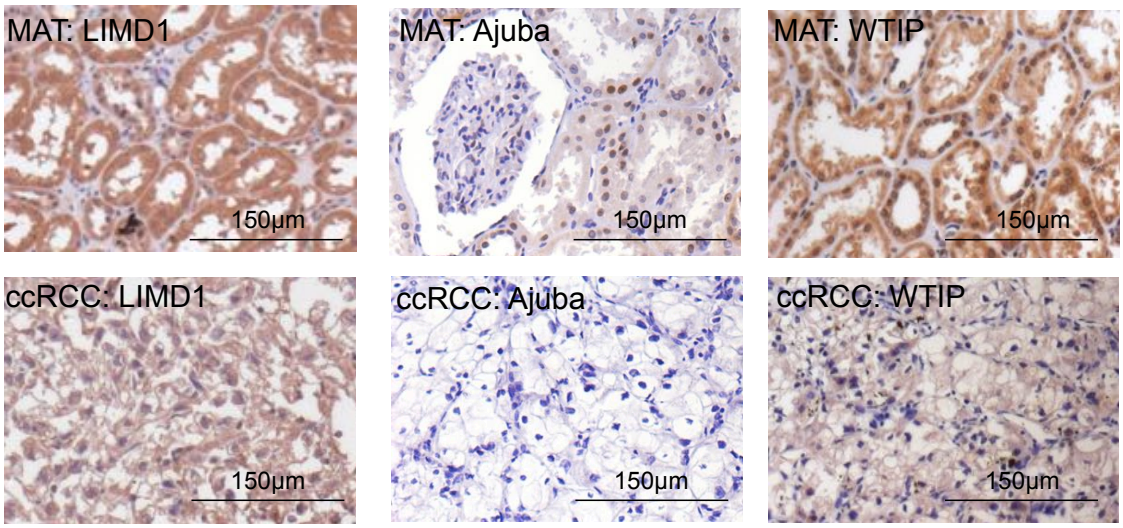

Figure 3.7 Representative images of Immunohistochemical staining in ccRCC demonstrating reduction in staining of LAW family members compared to matched adjacent tissue (MAT)

Commercially available TMAs with 75 ccRCC histospots and contiguous MAT were stained for LIMD1, Ajuba and WTIP. Staining was undertaken using an optimised, manual staining protocol with visualisation using the avidin-biotin peroxidase method and haematoxylin counterstaining. LIMD1 antibody concentration of 1:50, Ajuba antibody concentration of 1:50 and WTIP antibody concentration of 1:100 were utilised. Images demonstrate reduced staining for LIMD1, Ajuba and WTIP in the matched ccRCC samples compared to matched-adjacent tissue control. Scale bars corresponding to 150µm are shown for size comparison.

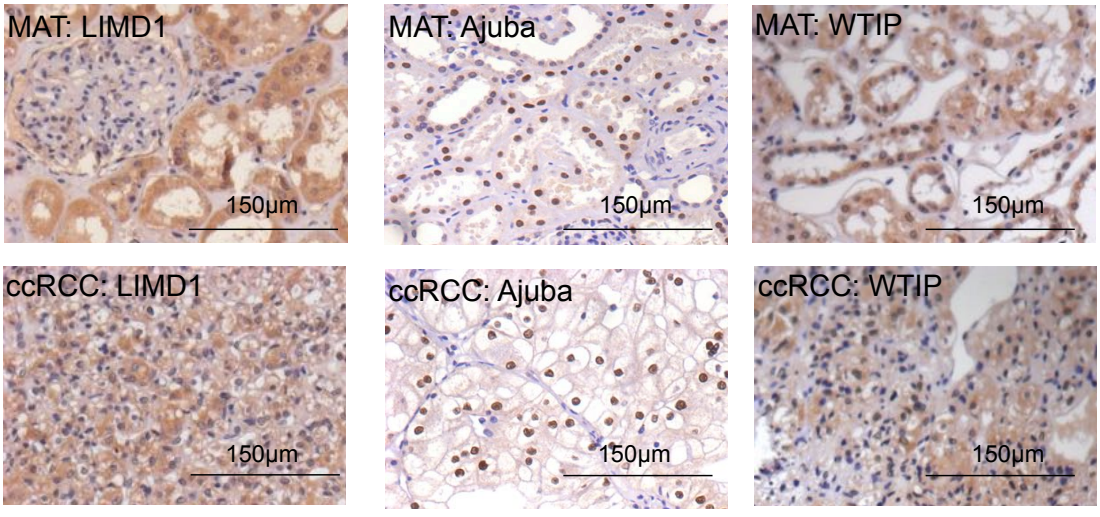

Figure 3.8 Representative images of Immunohistochemical staining in ccRCC demonstrating similar levels of staining of LAW family members compared to matched adjacent tissue (MAT)

Commercially available TMAs with 75ccRCC histospots and contiguous MAT were stained for LIMD1, Ajuba and WTIP. Staining was undertaken using an optimised, manual staining protocol with visualisation using the avidin-

biotin peroxidase method with haematoxylin counterstaining. LIMD1 antibody concentration of 1:50, Ajuba antibody concentration of 1:50 and WTIP antibody concentration of 1:100 were utilised. Images demonstrate similar levels of staining for LIMD1, Ajuba and WTIP in the matched ccRCC histospots, compared to matched-adjacent tissue control. Scale bars corresponding to 150µm is shown for size comparison.

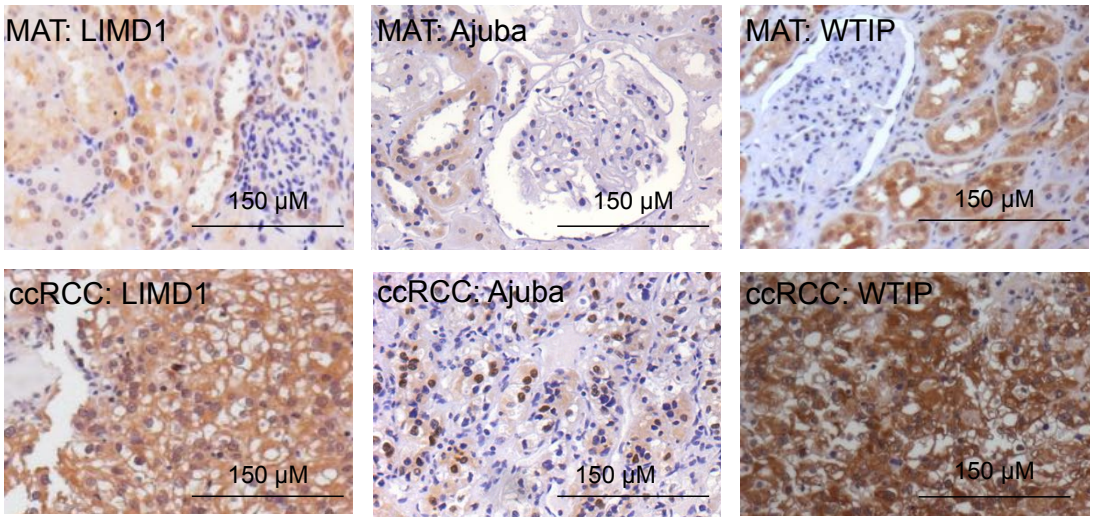

Figure 3.9 Representative images of immunohistochemical staining demonstrating increased levels of staining for LAW family members compared to matched adjacent tissue (MAT)

Commercially available TMAs with 75ccRCC histospots and contiguous MAT were stained for LIMD1, Ajuba and WTIP. Staining was undertaken using an optimised, manual staining protocol with visualisation using the avidin-biotin peroxidase method with haematoxylin counterstaining. LIMD1 antibody concentration of 1:50, Ajuba antibody concentration of 1:50 and WTIP antibody concentration of 1:100 were utilised. Images demonstrate increased levels of staining for LIMD1, Ajuba and WTIP in the matched ccRCC histospots, compared to matched-adjacent tissue control. Scale bars corresponding to 150µm are shown for size comparison.

For the Ariol SL-50 analysis, a 10% increase or decrease in combined modified automated score was deemed to represent a significant difference in staining. This cutoff was chosen, as there was little difference in the proportion of tumours in each category when this cutoff was increased to 20%. TMA histospots were also manually scored and differences in scoring between the automated and manual scoring correlated.

The manual tumour scoring system for the LAW family members was adapted from one used by Spendlove *et al* in the analysis of breast carcinoma (Spendlove, Al-Attar et al. 2008). A four-point scoring system was adopted where zero represented no staining, one weakly positive staining, two, moderately positive staining and three, strongly positive staining. Good concordance in identifying tumours with reduced, similar and

increased staining for LAW family members was seen when the manual and automated image acquisition/analysis system scores were compared particularly where loss of staining was observed (data not shown). Given the increased objectivity of the Ariol SL-50 scoring and the increased potential for discrimination between variable levels of staining, the automated modified staining score was predominantly used for subsequent comparison of staining within this TMA.

3p loss of heterozygosity is an early event in renal cell carcinoma (Clifford, Prowse et al. 1998). In a study by Kanu *et al*, 98.8% of RCC tumours that demonstrated LOH at the 3p25.3 *VHL* locus also displayed LOH at the *SETD2* locus, a 3p21.3 encoded gene (**Figure 3.10**) (Kanu, Gronroos et al. 2015).

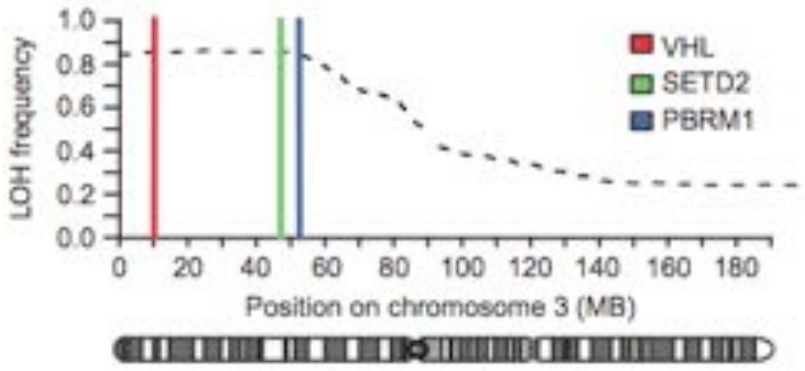

Figure 3.10. Proportion of samples showing LOH along chromosome 3 using SNP 6.0 array data in 450 RCCs from TCGA. Taken from (Kanu, Gronroos et al. 2015).

Ajuba is 14q encoded and 14q deletions are commonly seen in ccRCC. In a study by Kroger *et al,* 81/288 (28%) of tumours demonstrated loss of 14q: this was hypothesised to be associated with HIF1α loss but other candidate genes which could include Ajuba have not been characterised (Kroeger, Klatte et al. 2013).

Given that biallelic inactivation of a tumour suppressor is necessary to drive tumourigenesis, reduced expression of both 3p (e.g. LIMD1) and 14q-encoded genes (e.g. Ajuba) may be seen in tissue adjacent to a ccRCC tumour compared to that observed in tissue taken from a healthy kidney without evidence of ccRCC. WTIP is 19q13.11 encoded and 19q loss has not been implicated in ccRCC. Therefore it might

be expected that there would be some reduction in staining for the 3p encoded LIMD1 and the 14q encoded Ajuba in ccRCC histospots compared to MAT but that an absence staining would be rare in the MAT samples. Therefore comparison of staining in both ccRCC and MAT histospots was undertaken and the number of histospots with no staining for each of the three proteins also characterised. Manual scoring was used to identify tumours/MAT that demonstrated no LAW staining, as it was difficult to establish an appropriate cut off for no staining using the modified ARIOL scoring system.

49.3% of ccRCC tumours demonstrated reduced LIMD1 staining compared to MAT as assessed using the modified automated staining score (**Figures 3.7 and 3.10**), with 13/75 (17%), of the ccRCC histospots demonstrating no LIMD1 staining when scored manually, compared to 2/75 (3%) of the MAT histospots (X^2 test=13.891, p=0.0002**). 76% of tumour histospots demonstrated less Ajuba staining compared to MAT as assessed using the modified automated staining score (**Figures 3.7** and **3.10**). 26/75 (35%) ccRCC histospots demonstrating no Ajuba staining compared to 6/75 (8%) of the MAT histospots when scored manually (X^2 test=91.848, p<0.0001***).

IHC staining for WTIP demonstrated both significant cytoplasmic and nuclear staining (**Figure 3.7**). For WTIP, using the modified automated staining score, only 20% of tumours had reduced total WTIP staining compared to MAT with 63% of tumours showing increased total WTIP staining compared to MAT (**Figures 3.7** and **3.10**).

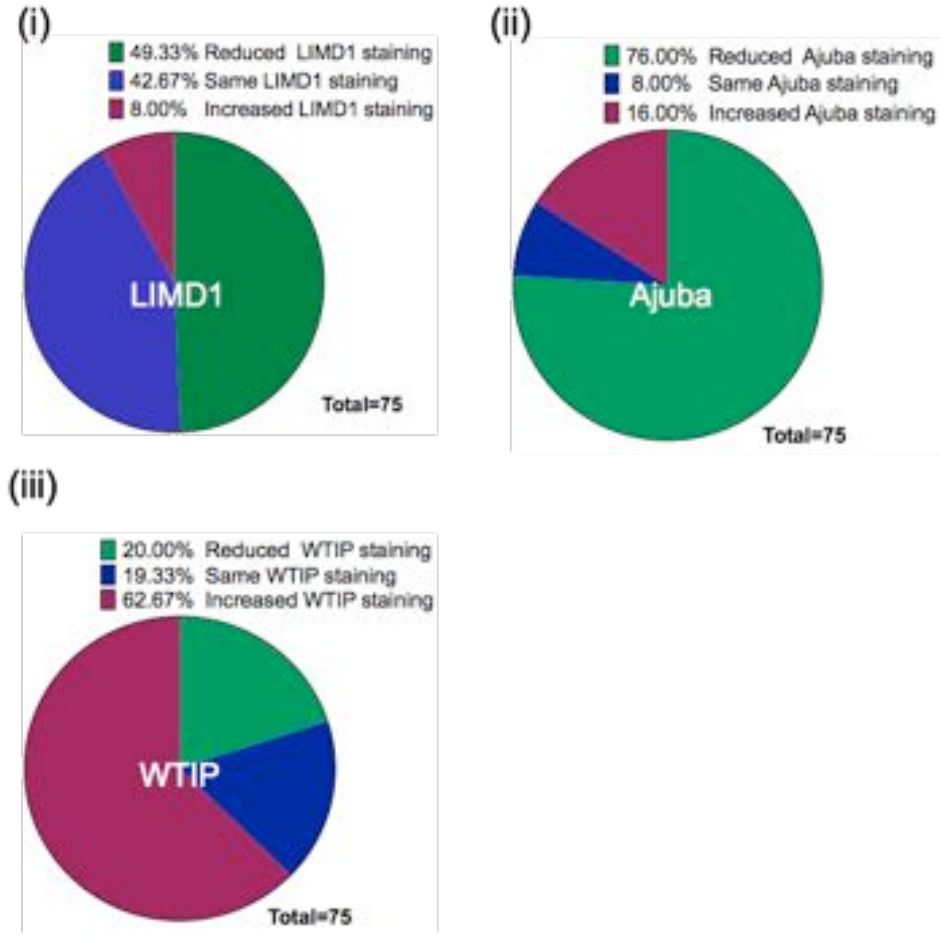

Figure 3.10 Relative differences in staining for LAW family members in ccRCC compared to MAT as assessed using the Ariol SL-50 scanning system

Antibody staining of the commercially available TMAs was quantified using the ARIOL imaging system (Genetix, San Jose, CA). After high resolution scanning, the images were reviewed for training and quantification purposes to differentiate the stained and the unstained cells by the colour of staining and the shape of the nuclei whereby brown staining was considered positive and blue staining negative). Areas of tumour were manually identified with masking of the stroma and normal/benign tissue from image analysis of the ccRCC samples and masking of the stroma in the MAT. Scores were generated using a modified automated scoring system: this generates an output score based on the combined score for the average staining intensity for the protein of interest throughout the histospot and the area of positive staining of each histospot. Tumours were divided in to three groups on the basis of differences in staining patterns between ccRCC tumours and MAT for all three family members using the Ariol output scoring system. A reduction in staining was defined as <10% reduction in ccRCC staining compared to MAT, similar staining as between ≤10% and ≥10% difference between ccRCC and MAT and increased staining as >10% staining in ccRCC compared to MAT.

(i) Pie chart to illustrate the relative differences in staining between ccRCC and MAT for LIMD1, **(ii)** Pie chart to illustrate the relative differences in staining between ccRCC and MAT for Ajuba, **(iii)** Pie chart to illustrate the relative differences in staining between ccRCC and MAT for WTIP

One disadvantage of using the automated image analysis described is that it was not possible to discriminate between nuclear and cytoplasmic staining using this system: staining for WTIP was strongly positive in both compartments. Manual scoring however allowed for the separate scoring and evaluation of nuclear and cytoplasmic staining. This demonstrated a significant reduction in nuclear staining for WTIP in over 73% of tumours with 31% of tumours demonstrating reduced cytoplasmic staining (**Figure 3.11**). 43/75 (58%) of tumours demonstrated no nuclear staining compared to 7/75 (9%) of MAT histospots, (X^2 test=293.16, p=<0.0001***). 3/75 (4%) of tumours demonstrated no cytoplasmic staining compared to 3% of MAT (X^2 test=0.344, p=0.577). This would imply that although loss of total WTIP staining was not commonly observed in ccRCC compared to MAT histospots, sub-cellular WTIP localisation differed between tumours and MAT, with significantly less nuclear staining observed in the ccRCC samples.

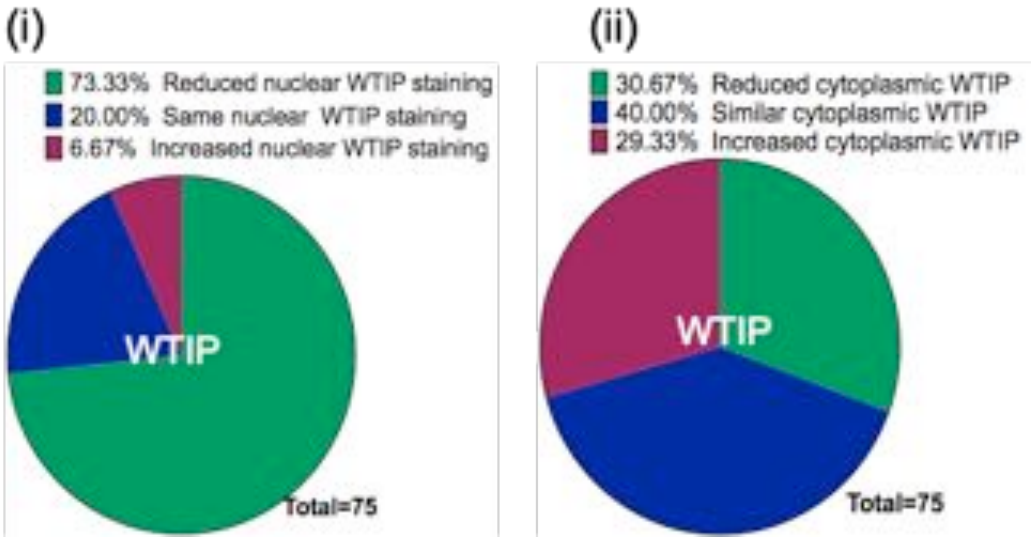

Figure 3.11 Relative differences in staining patterns for WTIP compared to MAT between ccRCC and MAT as assessed using a manual scoring system

Scoring was undertaken using a 4-point scoring system from 0-3 for both cytoplasmic and nuclear components by an experienced urology histopathologist and counter scored by myself blinded to the initial scoring: tumour only was scored in the ccRCC histospots and stroma excluded in the MAT and ccRCC histospots. **(i)** Pie chart to illustrate differences in nuclear WTIP between ccRCC and MAT. **(ii)** Pie chart to illustrate differences in cytoplasmic WTIP between ccRCC and MAT

3.8 Correlation of the relationship between LAW levels assessed immunohistochemically in ccRCC

Given the close structural homology between LAW family members and the characterised overlapping functions, particularly with respect to the regulation of HIF1α, microRNA function, and regulation of the Hippo pathway, it was hypothesised that a degree of functional redundancy may exist between LAW family members. Expression of at least one family member is likely to be a requirement for cell viability and this was observed when immunoblotting a panel of ccRCC lines (**Figure 3.1**). It was also hypothesised that loss of more than one family member may contribute to increased tumourigenesis compared to the loss of one family member alone. The relationship between staining levels for LAW in both the ccRCC and MAT was therefore characterised.

3.8.1 Levels of LIMD1 and Ajuba expression closely correlate in ccRCC but not in matched adjacent tissue (MAT)

Levels of staining for Ajuba and LIMD1 strongly associated in the ccRCC samples (Spearman-Rank correlation coefficient p=0.0012**) but not in the MAT (Spearman-Rank correlation coefficient p=0.335) (**Figure 3.12)**. This suggests that in ccRCC tumours, Ajuba and LIMD1 loss frequently co-exists. Given that LIMD1 and Ajuba levels in MAT do not correlate, this would imply that the correlation in ccRCC is not simply the result of an association whereby tumours with more LIMD1 staining also have more Ajuba staining but could suggest co-loss of both tumour suppressors, potentially functioning as a mechanism for increased tumourigenesis.

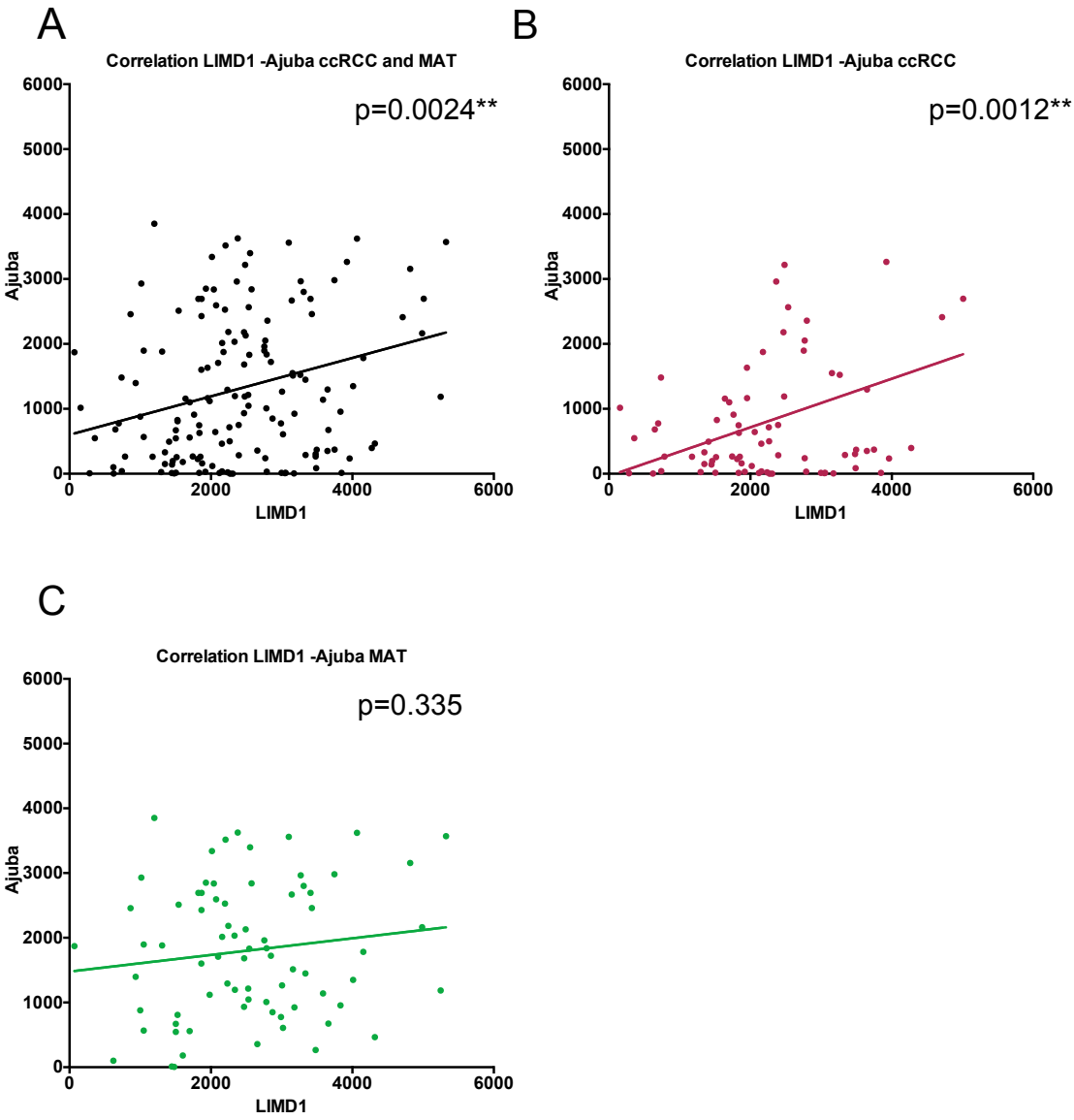

Figure 3.12. Levels of LIMD1 and Ajuba expression closely correlate in ccRCC but not MAT

The relationship between modified automated ARIOL score for Ajuba and LIMD1 were plotted graphically using Prism 6 and correlation calculated using the Spearman-Rank correlation coefficient**. A** ccRCC and MAT, **B**. ccRCC and **C**. MAT

3.8.2 Levels of LIMD1 and WTIP expression closely correlate in ccRCC and MAT

The correlation of total WTIP and LIMD1 showed a strong positive association in both ccRCC and MAT histospots as assessed using the modified automated ARIOL scoring system (Spearman-Rank correlation coefficient $p<0.0001$***) i.e. respective high or low

WTIP is associated with respective high or low LIMD1 expression in both tissues (**Figure 3.13)**. Given that WTIP staining is observed in both the cytoplasm and nucleus and the automated scoring system did not allow for the discrimination of differences in localisation of staining, manual LIMD1 staining was correlated with manual nuclear and manual cytoplasmic WTIP scoring. This was felt to be of particular relevance as 73% of tumours demonstrated reduced nuclear WTIP staining compared to MAT (**Figure 3.11)**.

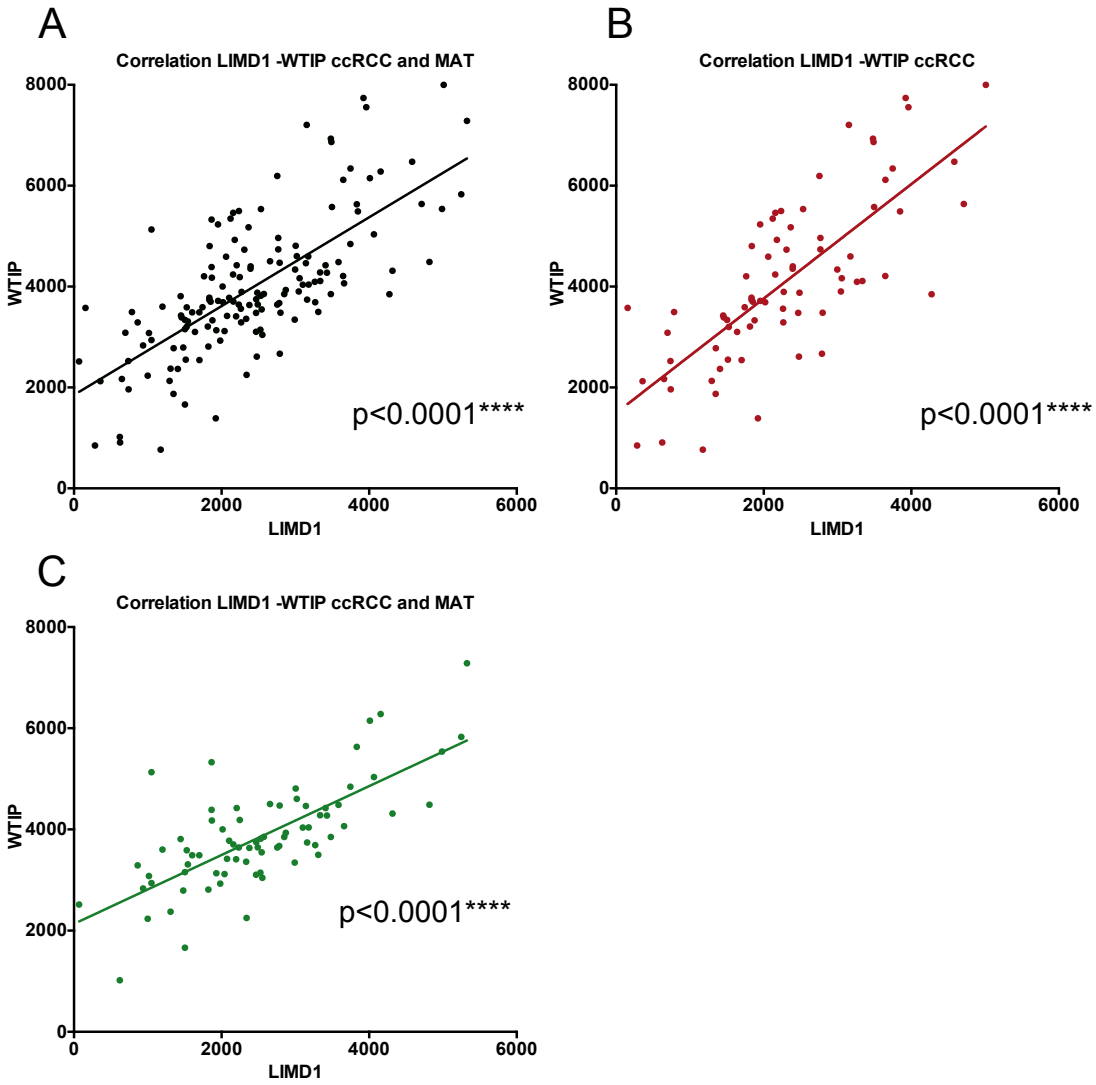

Figure 3.13 Levels of LIMD1 and WTIP expression closely correlate in ccRCC and MAT

The relationship between automated ARIOL score for LIMD1 and WTIP was plotted graphically using Prism 6 and correlation calculated using the Spearman-Rank correlation coefficient**. A** ccRCC and MAT, **B**. ccRCC and **C**. MAT

A strong positive correlation between cytoplasmic WTIP staining and LIMD1 staining in both ccRCC and MAT was observed (Spearman-Rank correlation coefficient p=0.0016** and p<0.0001*** respectively) (**Figure 3.14)**. For nuclear WTIP staining, a strong positive correlation was observed with manual LIMD1 staining in the MAT but not ccRCC histospots (Spearman-Rank correlation coefficient p=0.0044** and p=0.3366 respectively) (**Figure 3.14)**.

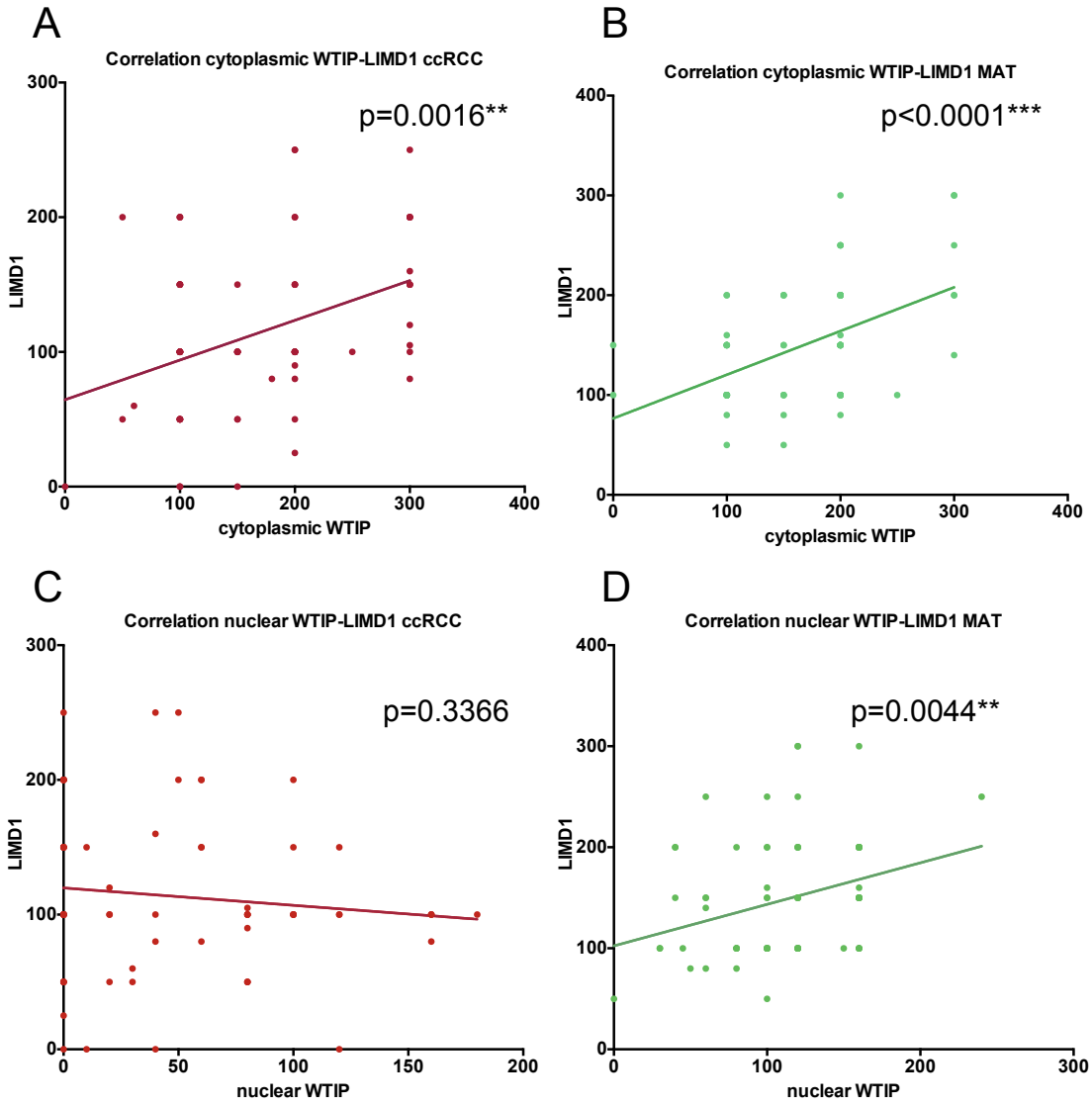

Figure 3.14 LIMD1 and WTIP correlation in ccRCC and MAT with manual scoring

The relationship between manual LIMD1 score and manual WTIP score was plotted graphically using Prism 6 and correlation calculated using the Spearman-Rank correlation coefficient**. A** correlation cytoplasmic WTIP and LIMD1 in ccRCC, **B** correlation cytoplasmic WTIP and LIMD1 in MAT, **C** correlation nuclear WTIP and LIMD1 in ccRCC, **D** correlation nuclear WTIP and LIMD1 in MAT

The strong positive correlation between LIMD1 and total WTIP in ccRCC and MAT may represent a simple association whereby tissue with more LIMD1 also express more WTIP, however the correlation between nuclear and cytoplasmic WTIP staining with LIMD1 staining suggests that the association is more complex. MAT histospots with high nuclear WTIP also have increased LIMD1 staining, and this may be a simple reflection of increased total WTIP within the tissue. In the ccRCC histospots however where 73% of the tumour samples demonstrate reduced nuclear WTIP staining compared to MAT and no association between nuclear WTIP and LIMD1 staining is observed and it was hypothesised that changes in sub-cellular WTIP localisation could be occurring independently of LIMD1 loss potentially contributing to tumourigenesis.

3.8.3 Levels of Ajuba and WTIP expression closely correlate in ccRCC but not in MAT

Staining for Ajuba and WTIP strongly associated in the ccRCC ($p=0.0317^*$) but not in the MAT histospots ($p=0.4166$) (**Figure 3.15)**.

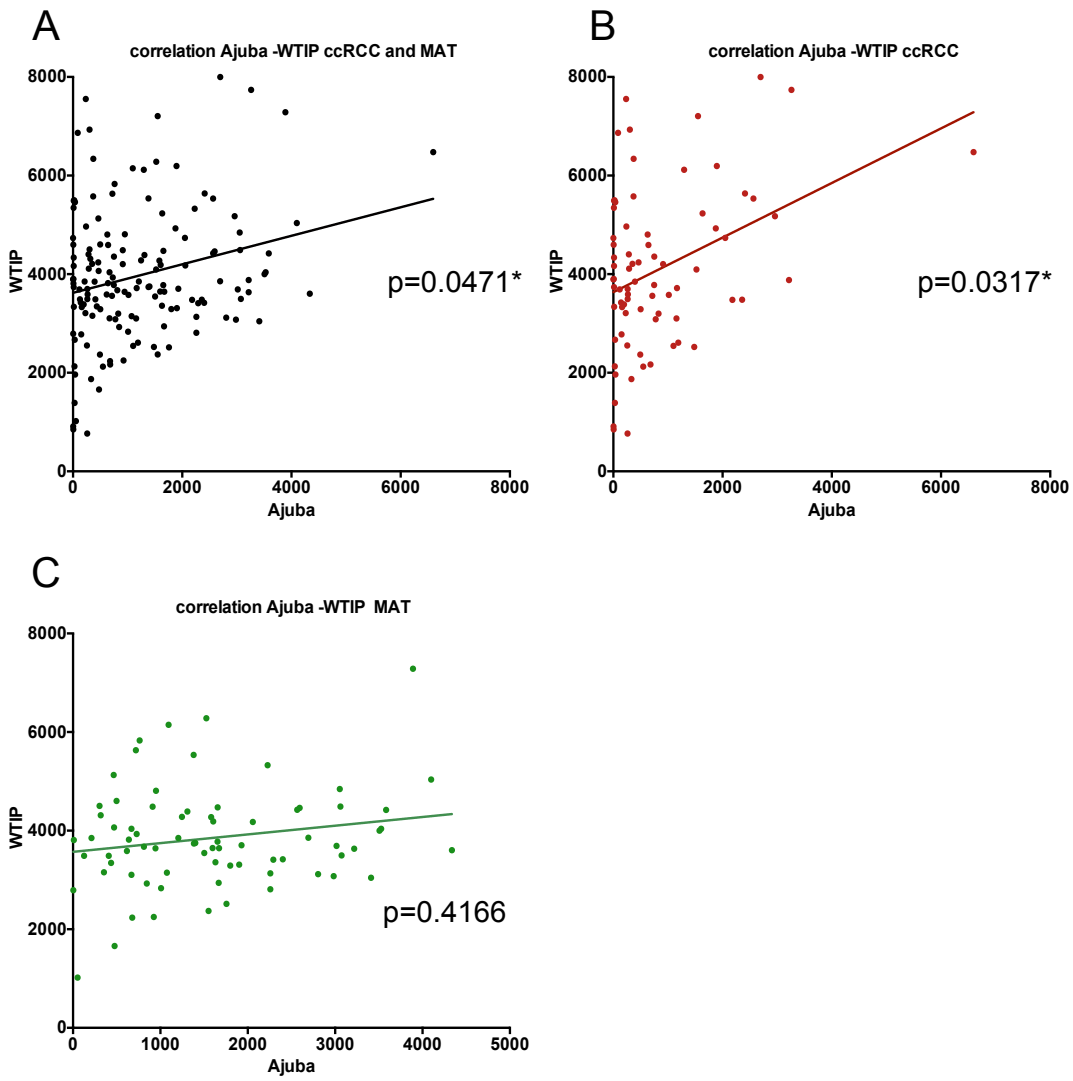

Figure 3.15 Levels of Ajuba and WTIP expression closely correlate in ccRCC but not MAT

The relationship between modified automated ARIOL score for WTIP and Ajuba was plotted graphically using Prism 6 and correlation calculated using the Spearman-Rank correlation coefficient**. A.** ccRCC and MAT, **B**. ccRCC and **C**. MAT

Again, this suggests that there is not a simple correlation whereby MAT or tumours with more Ajuba also express more WTIP and *vice versa*. In ccRCC, loss of expression of both tumour suppressors may co-exist and may function a mechanism for promoting tumourigenesis. Given the association between subcellular WTIP localisation and LIMD1 observed (**Figure 3.14**), subcellular WTIP and Ajuba staining as assessed using a manual scoring system was characterised. This demonstrated a strong correlation between cytoplasmic WTIP and Ajuba staining in both ccRCC and MAT tissue

(Spearman-Rank correlation coefficient p=0.0097** and p=0.041* respectively (**Figure 3.16)**. When nuclear WTIP and Ajuba staining was correlated, a positive correlation in the ccRCC histospots (p=0.0405*) but not MAT histospots (p=0.5889) was observed (**Figure 3.16)**. This again could imply that sub-cellular WTIP localisation may be important in driving tumourigenesis in ccRCC with a frequent reduction in Ajuba and reduced nuclear WTIP staining co-existing.

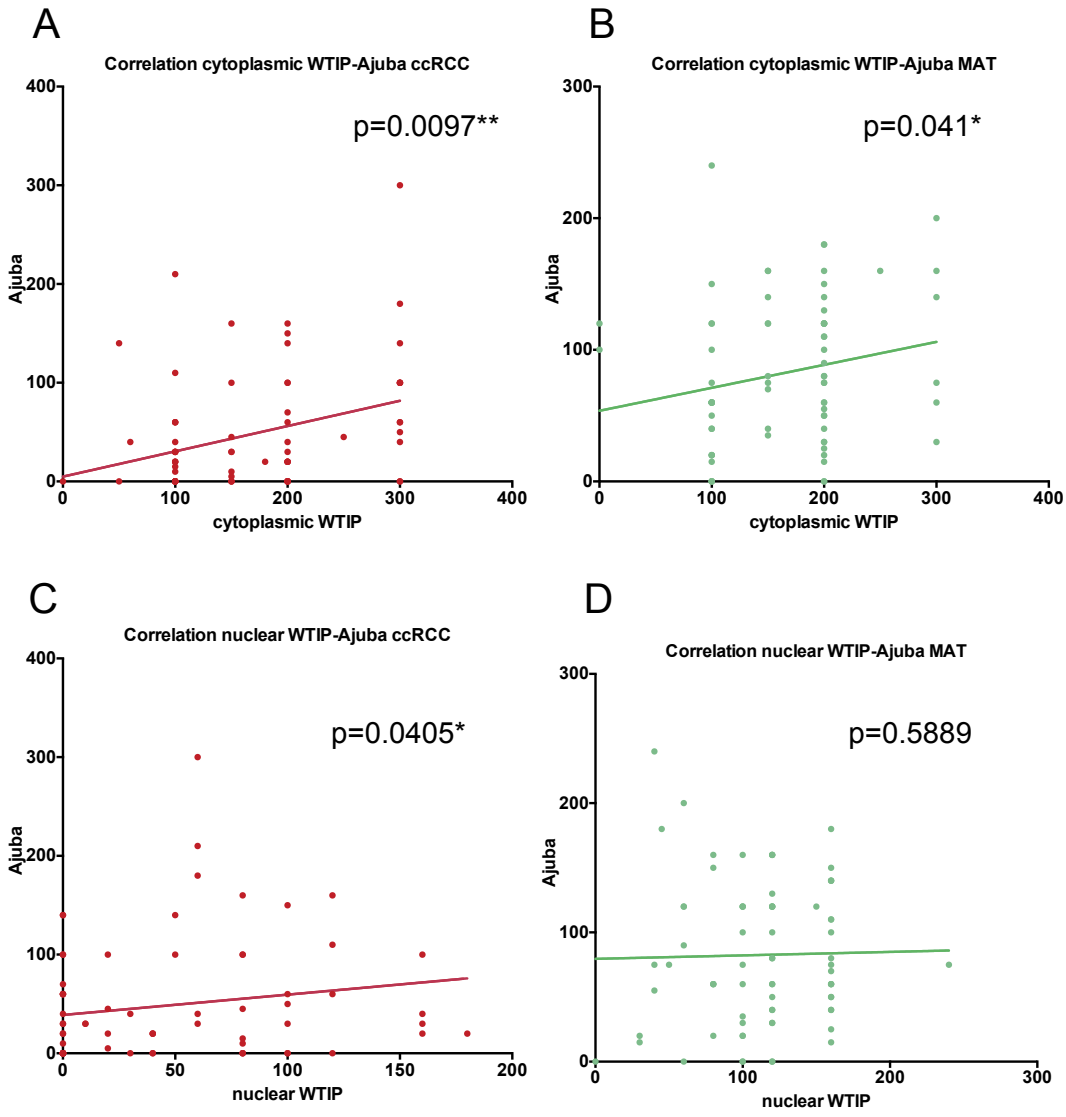

Figure 3.16 WTIP and Ajuba correlation in ccRCC and MAT with manual scoring

The relationship between manual score for WTIP and Ajuba was plotted graphically using Prism 6 and correlation calculated using the Spearman-Rank correlation coefficient. **A** correlation cytoplasmic WTIP and Ajuba in ccRCC, **B** correlation cytoplasmic WTIP and Ajuba in MAT, **C** correlation nuclear WTIP and Ajuba in ccRCC, **D** correlation nuclear WTIP and Ajuba in MAT

3.9 Immunohistochemical staining for VEGF and CD34

Given our knowledge of the role of LIMD1 in the regulation of the hypoxic response and the close homology between different LAW family members/likely overlapping functions, the relationship between staining for LAW family members and markers of angiogenesis was assessed. The TMA was stained for VEGFA, a critical mediator of angiogenesis (E, Cao et al. 2012) and CD34, an established marker for capillary endothelia in normal tissue and tumour and marker of microvascular density (MVD) (Fina, Molgaard et al. 1990).

3.9.1 Immunohistochemical staining for VEGFa and CD34 in control tissue

Positive staining for VEGFa was defined as membranous and/or cytoplasmic staining (Dorevic, Matusan-Ilijas et al. 2009). Staining obtained using an optimised manual IHC protocol was reviewed by Professor Sheaff and felt to be specific and scorable (**Figures 3.17 and 3.19)**.

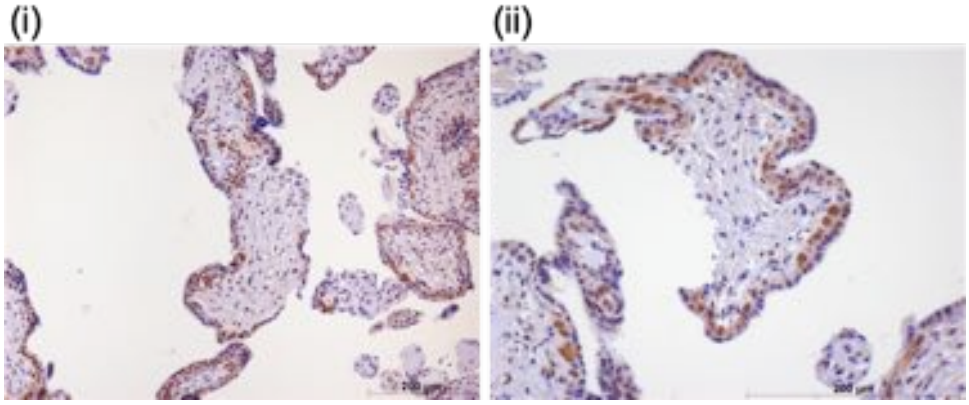

Figure 3.17 Representative control images for staining for VEGFa

A TMA printed with a range of histospots derived from normal tissues was stained using an optimised manual staining system (Ventana discovery) with visualisation using an Avidin-Biotin method to establish antibody specificity and to provide positive/negative control tissue when staining the ccRCC TMAs. Representative images of placental tissue stained with VEGFa antibody at 1:50 are shown (Figures **(i)** and **(ii**)) at 10x and 20x magnification respectively) Scale bars corresponding to 200μm are shown for size comparison

CD34 IHC was undertaken using an automated staining system (Ventana Discovery). TMAs containing a range of pre-invasive/malignant histospots were included as positive/negative controls for both CD34 and VEGFa staining (**Figures 3.17** and **3.18**),

and the primary antibody omitted as a further negative control to account for non-specific binding. Strongly positive CD34 staining was observed in the fenestrated epithelium of glomeruli in healthy renal tissue as previously described (**Figure 3.20)** (Pusztaszeri, Seelentag et al. 2006). Images were scanned and analysed using the automated Ariol system as before.

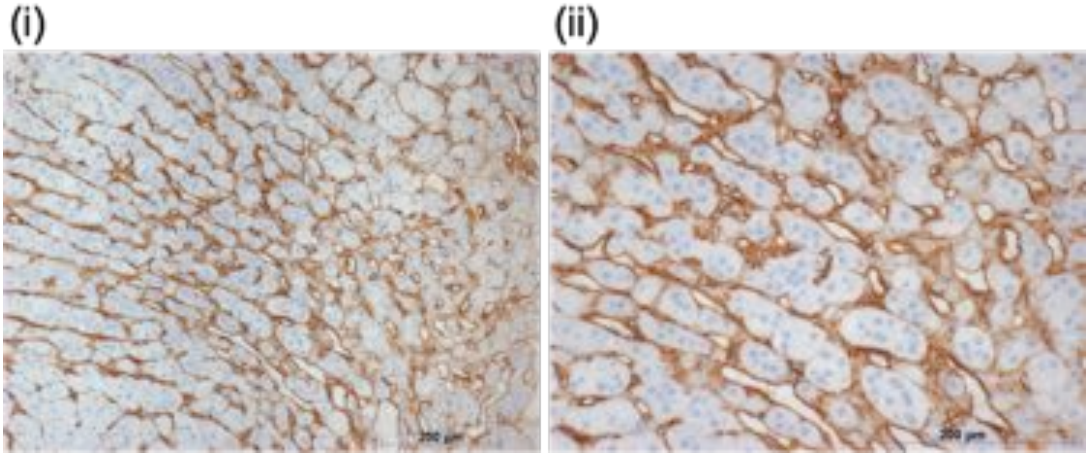

Figure 3.18 Representative control images for staining for CD34

A TMA printed with a range of histospots derived from normal tissues was stained using an automated staining system (Ventana discovery) with visualisation using an Avidin-Biotin method to establish antibody specificity and to provide positive/negative control tissue when staining the ccRCC TMAs. Representative images of highly vascularised adrenal tissue stained with CD34 antibody at 1:50 are shown (Figures **(i)** and (**ii)** at 10x and 20x magnification respectively) Scale bars corresponding to 200μm are shown

3.9.2 Immunohistochemical staining for VEGFa and CD34 in ccRCC

Having established specific and expected patterns of staining for VEGFa and CD34 in control tissue including kidney tissue, staining of the commercially available ccRCC/MAT TMA from US Biolabs was undertaken. As before, areas of tumour were manually identified with masking of the stroma and of normal/benign tissue from image analysis and exclusion of the stroma in the MAT. For VEGFa, scores were generated using the modified automated ARIOL scoring system as described. For CD34, image analysis training was undertaken using the ARIOL system to correctly identify blood vessel staining. Using this automated analysis system, the number of blood vessels within each histospot and the mean vessel area and mean lumen area were calculated. This enabled calculation of the total cross sectional area of blood vessels within each histospot.

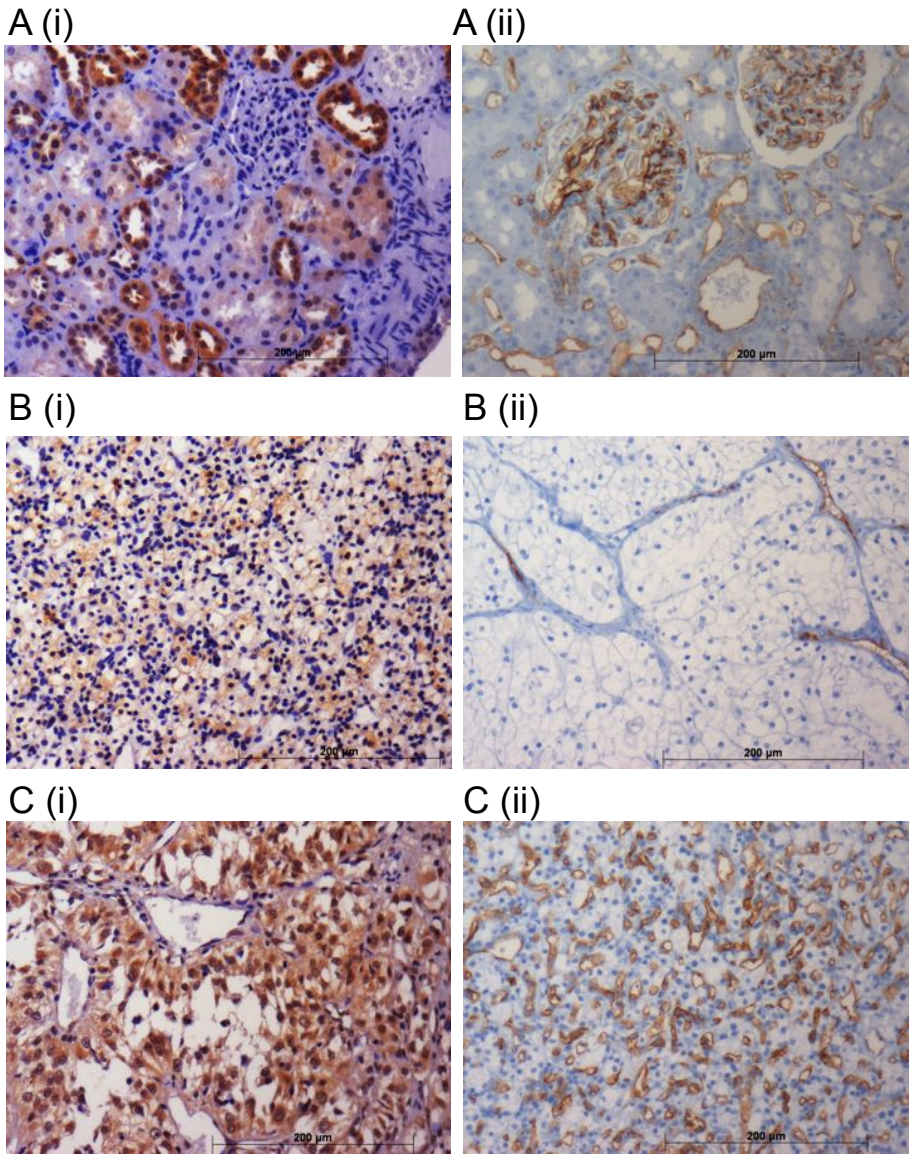

Figure 3.19 Immunohistochemistry for VEGFa and CD34 in kidney tissue and ccRCC samples

Commercially available TMAs with 75 ccRCC histospots and contiguous MAT were stained for VEGFa and CD34. Staining for VEGFa is shown in the left panel (i), with CD34 staining in the matched histospots in the right panel (ii). VEGFa staining was performed using an optimised manual protocol with antibody concentration 1:300 and visualisation using the Avidin-biotin peroxidase method. CD34 staining was undertaken using an automated system (Discovery, Ventana Medical Systems, Tucson AZ) with CD34 antibody concentration 1:50 and visualisation using the Avidin-biotin peroxidase method. **A (i)** Representative VEGFa staining in matched adjacent kidney tissue, **A (ii)** Representative CD34 staining in same MAT histospot **B (i)** Representative low level VEGFa staining in ccRCC histospot, **B (ii)**, CD34 staining in same MAT histospot **C (i)** Representative high level VEGFa staining in a ccRCC histospot, **B(iii)** CD34 staining in same matched ccRCC histospot Scale bars corresponding to 200µm are shown for size comparison.

3.9.3 Staining for LIMD1, Ajuba and WTIP does not correlate with CD34 staining

Given the role of LAW proteins in the regulation of the hypoxic response, it was hypothesised that reduced staining for LAW would be associated with increased MVD staining as assessed by CD34 staining. Comparison of LIMD1 and CD34 staining did not show any correlation ($p=0.9507$ in ccRCC histospots and $p=0.8662$ in MAT) (**Figure 3.20)**, nor was a correlation between Ajuba and CD34 staining observed ($p=0.5490$ in ccRCC histospots and $p=0.1388$ in MAT) (**Figure 3.21)**. Comparison of WTIP and CD34 staining also did not demonstrate a correlation in either ccRCC or MAT histospots, ($p=0.7362$ and $p=0.8632$ respectively) (**Figure 3.22)**.

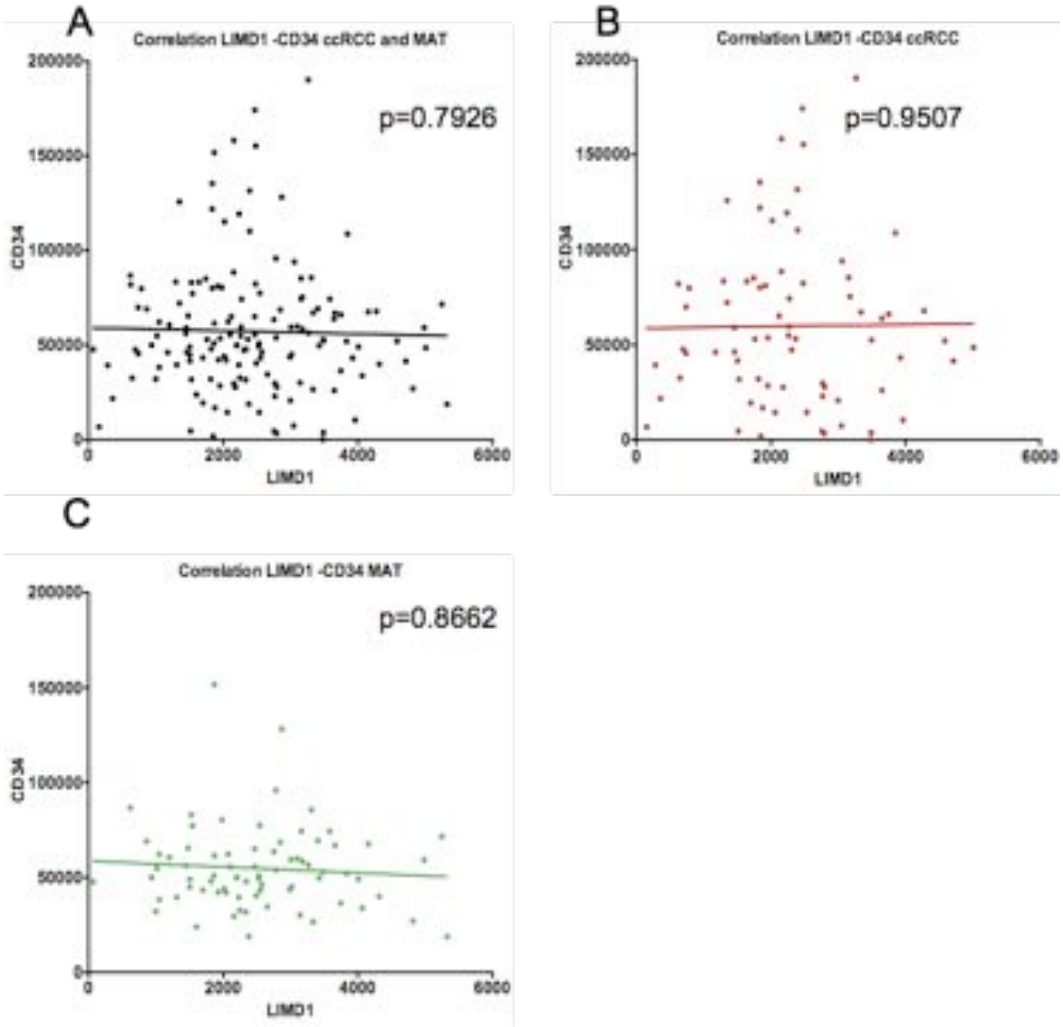

Figure 3.20 Levels of LIMD1 and CD34 assessed immunohistochemically do not correlate in either ccRCC or MAT

The relationship between modified automated ARIOL score for LIMD1 and CD34 was plotted graphically using Prism 6 and correlation calculated using the Spearman-Rank correlation coefficient**. A** ccRCC and MAT, **B**. ccRCC and **C**. MAT

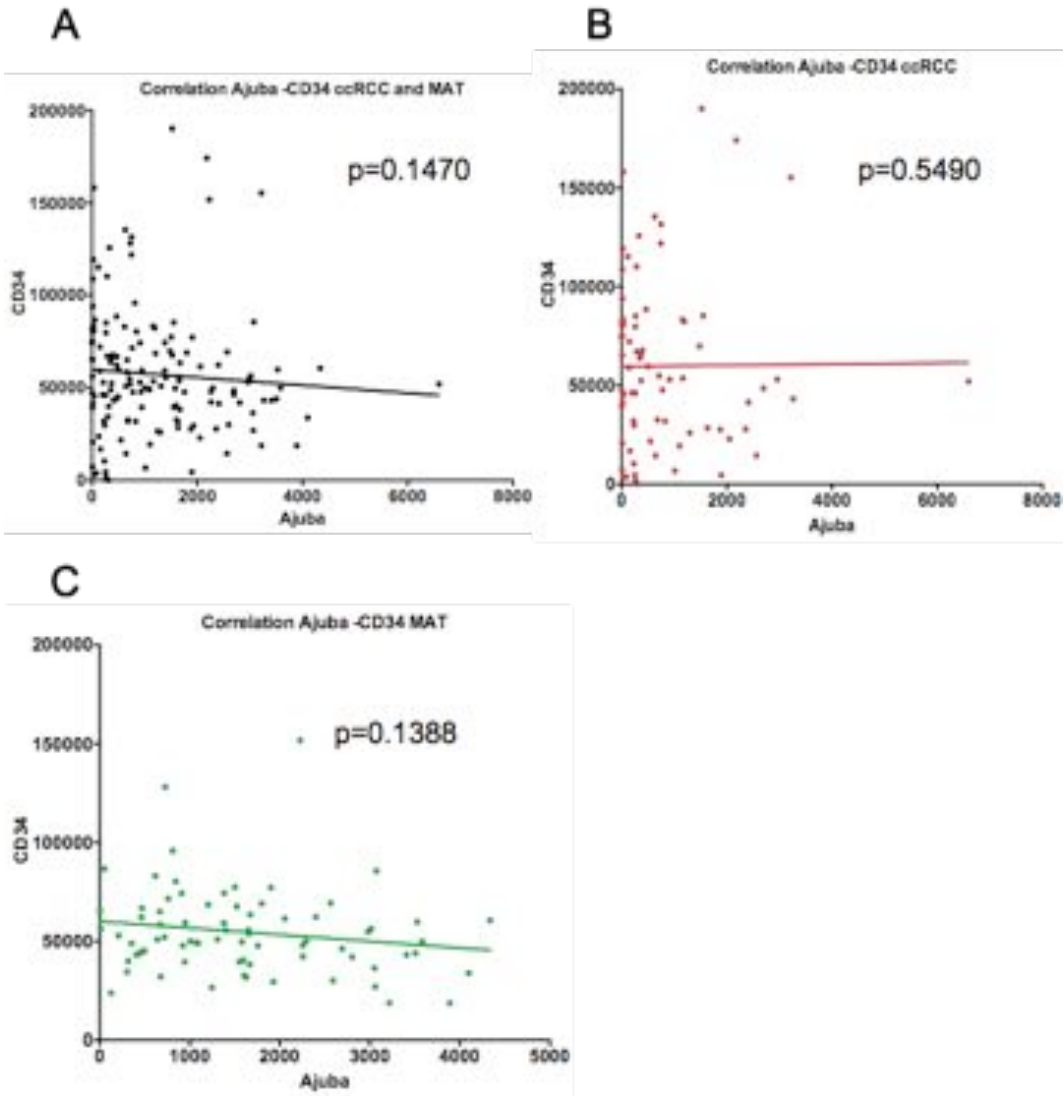

Figure 3.21 Levels of Ajuba and CD34 assessed immunohistochemically do not correlate in either ccRCC or MAT

The relationship between modified automated ARIOL score for Ajuba and CD34 staining as a measure of MVD was plotted graphically using Prism 6 and correlation calculated using the Spearman-Rank correlation coefficient**. A** ccRCC and MAT, **B** ccRCC and **C** MAT

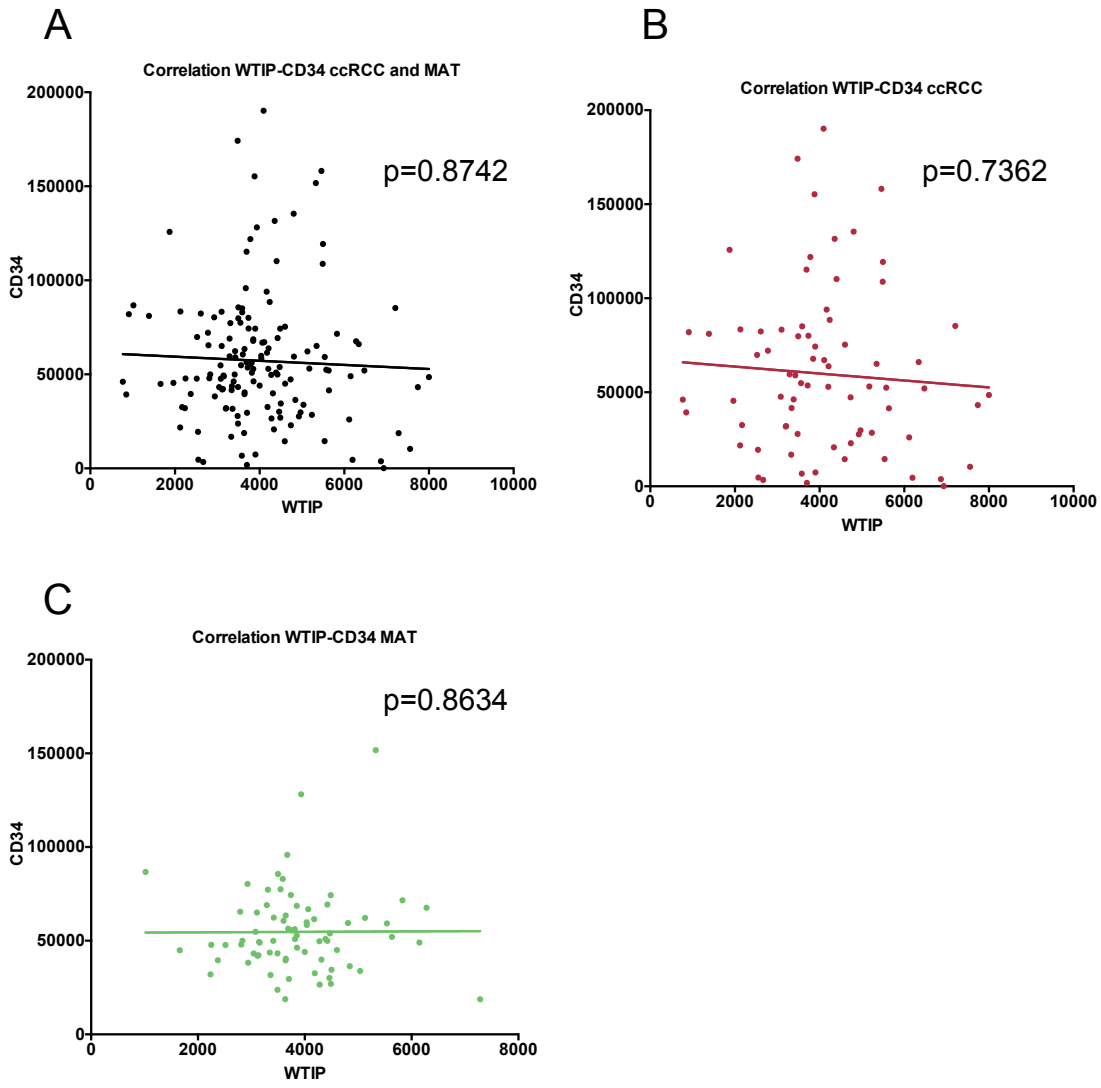

Figure 3.22 Levels of WTIP and CD34 assessed immunohistochemically do not correlate in either ccRCC or MAT

The relationship between modified automated ARIOL score for WTIP and CD34 was plotted graphically using Prism 6 and correlation calculated using the Spearman-Rank correlation coefficient**. A** ccRCC and MAT, **B**. ccRCC and **C.** MAT

3.9.4 Correlation of VEGFa staining with LIMD1, WTIP and Ajuba staining

Staining for LAW family members was correlated with that of VEGFa, a potent inducer of tumour angiogenesis in ccRCC and downstream target of HIF2α (Keith, Johnson et al. 2012). For LIMD1 a positive correlation was observed such that increasing LIMD1 expression correlated with increasing VEGFa expression in both ccRCC and MAT histospots, (Spearman Rank correlation p=0.0010** and p=0.0011** respectively) (**Figure 3.23**). For Ajuba no such correlation was observed for both ccRCC and MAT

histospots (Spearman Rank correlation p=0.9731 and p=0.1633 respectively (**Figure 3.24**). For total WTIP staining a positive association was again observed, p<0.0001**** and p=0.0009*** for ccRCC and MAT histospots respectively (**Figure 3.25**). In the first instance, this correlation may seem surprising: it had been hypothesised that low LAW expression might be associated with increasing VEGFa staining.

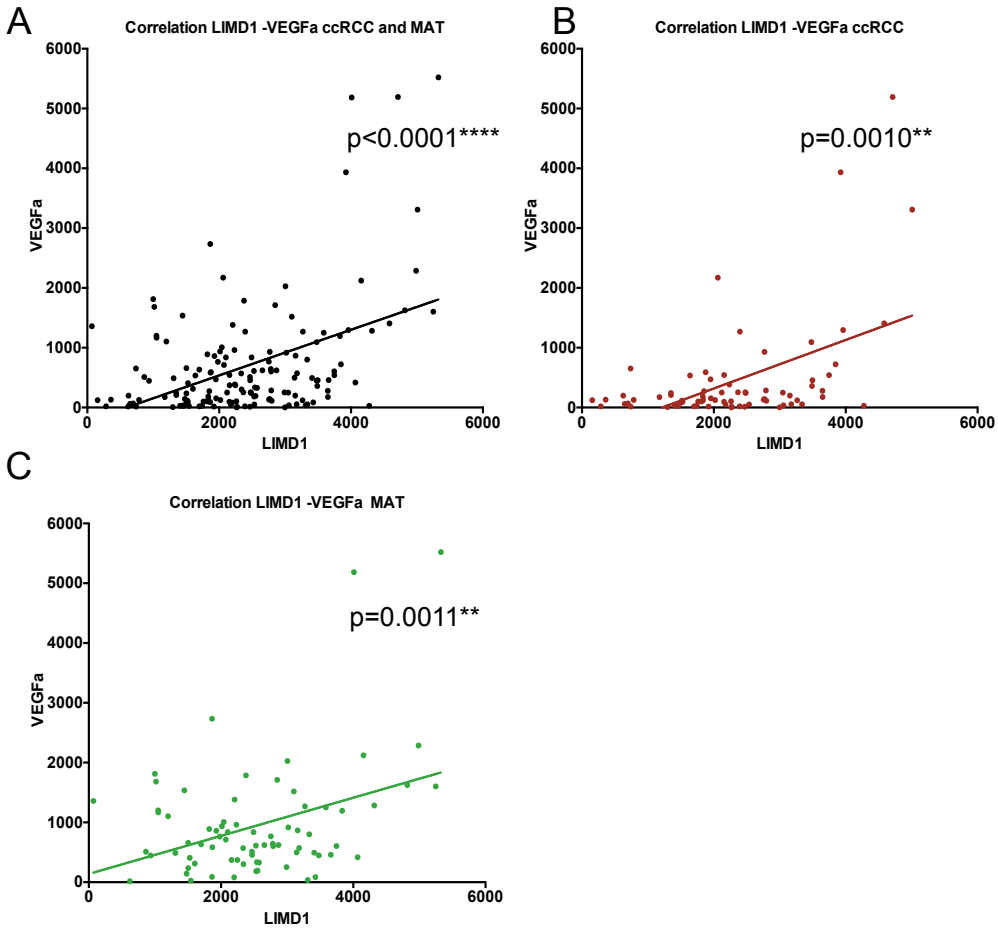

Figure 3.23 Levels of LIMD1 and VEGFa assessed immunohistochemically strongly correlate in both ccRCC and MAT

The relationship between modified automated ARIOL score for VEGFa and LIMD1 was plotted graphically using Prism 6 and correlation calculated using the Spearman-Rank correlation coefficient**. A** Correlation in combined ccRCC and MAT, **B**. Correlation in ccRCC alone and **C** Correlation in MAT alone

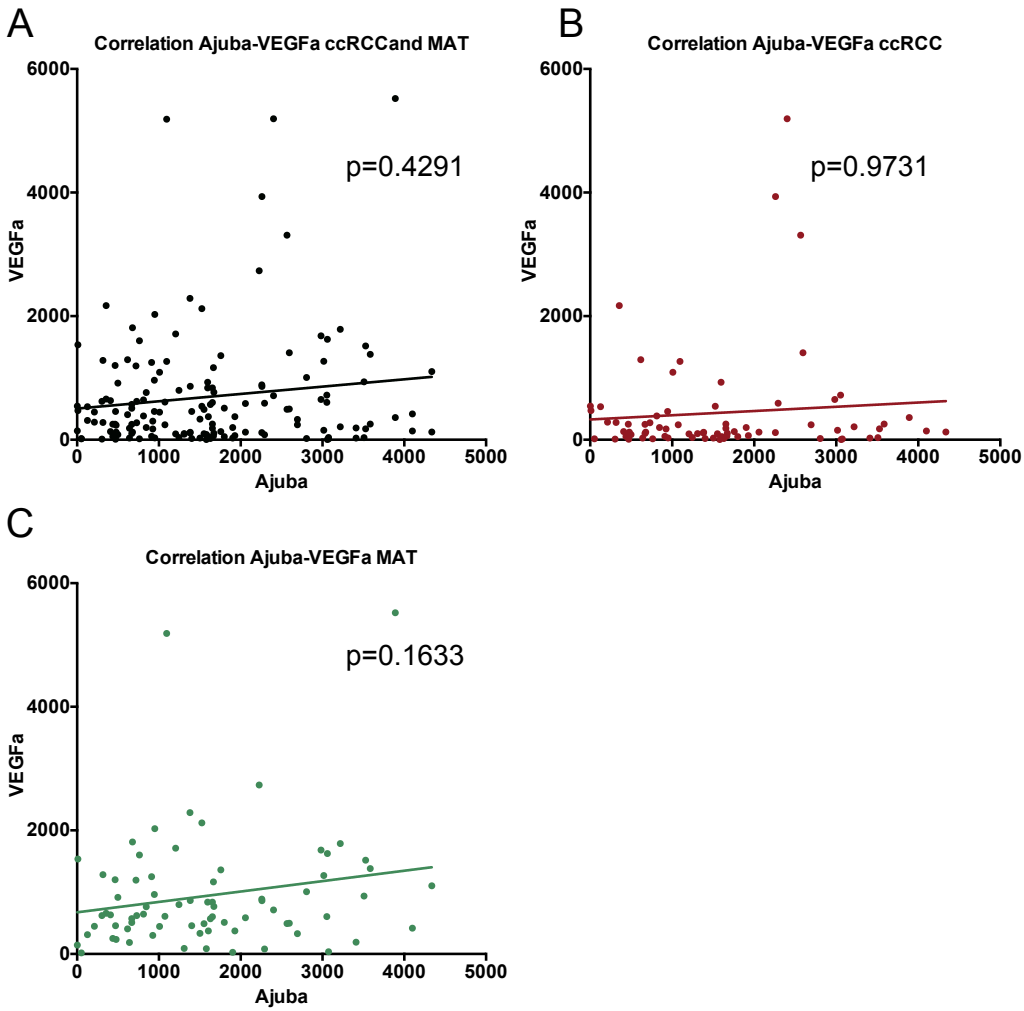

Figure 3.24 Levels of Ajuba and VEGFa assessed immunohistochemically are strongly positively correlated in both ccRCC and MAT

The relationship between modified automated ARIOL score for VEGFa and Ajuba was plotted graphically using Prism 6 and correlation calculated using the Spearman-Rank correlation coefficient**. A** Correlation in combined ccRCC and MAT, **B** Correlation in ccRCC alone and **C** Correlation in MAT alone

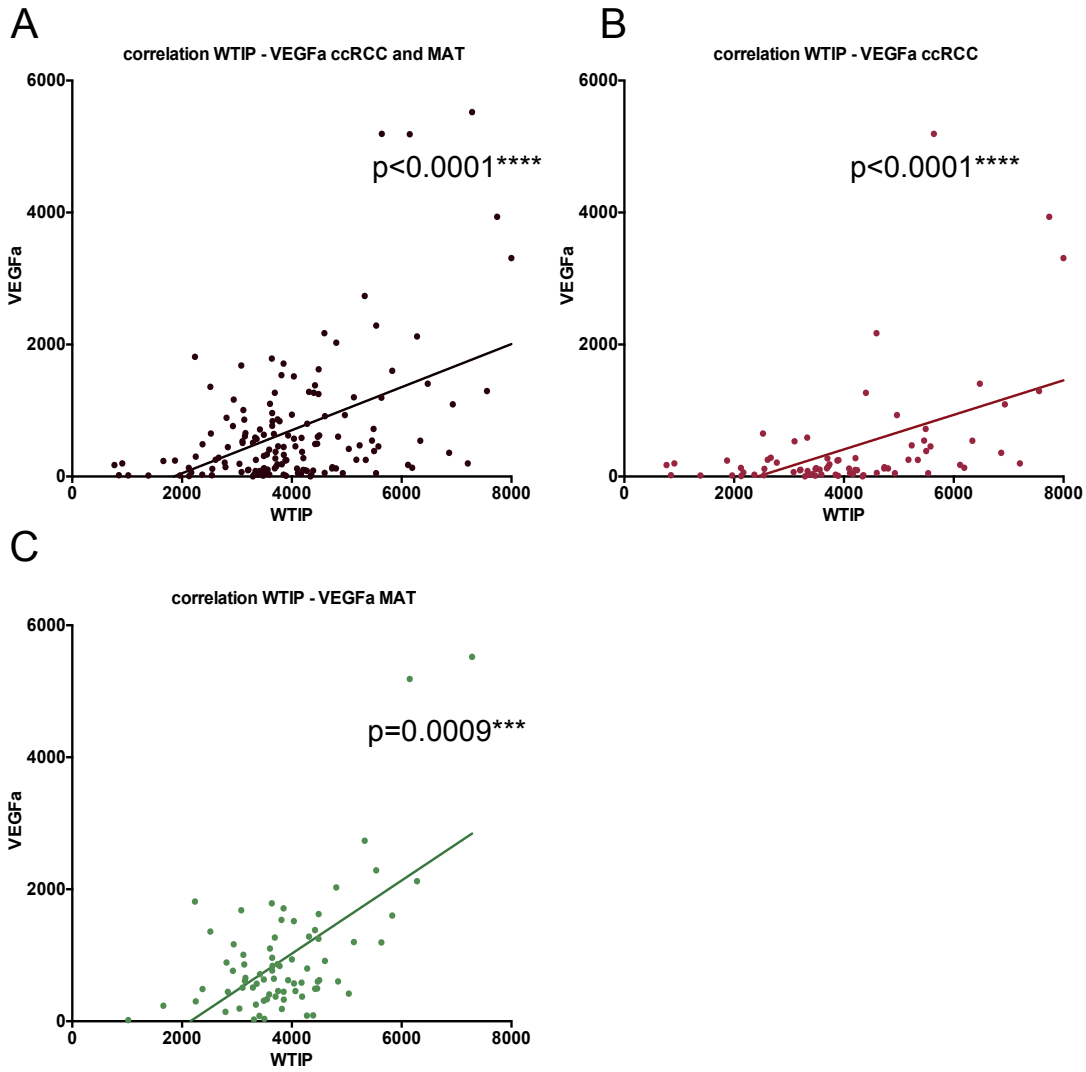

Figure 3.25 Levels of WTIP and VEGFa assessed immunohistochemically are strongly positively correlated in both ccRCC and MAT

The relationship between modified automated ARIOL score for VEGFa and WTIP was plotted graphically using Prism 6 and correlation calculated using the Spearman-Rank correlation coefficient**. A** Correlation in combined ccRCC and MAT, **B**. Correlation in ccRCC alone and **C**. Correlation in MAT alone

3.9.5 Correlation of VEGFa staining with CD34 staining

It was hypothesised that decreased LAW expression was likely to be associated with increased neo-angiogenesis and therefore increased VEGFa and CD34 staining but no association was observed between levels of LAW and CD34 staining. A positive correlation was observed between increasing LIMD1 and VEGFa staining and total

WTIP and VEGFa staining in both ccRCC and MAT histospots whilst no such correlation was observed between Ajuba and VEGFa staining in either tissue type.

Correlation of the relationship between staining for CD34 and VEGFa was undertaken (**Figure 3.26**). An inverse correlation was observed in ccRCC with increased CD34 staining associated with decreased VEGFa staining, p=0.0082**: this association was not observed in MAT p=0.4138 (**Figure 3.26**). It was hypothesised that CD34 and VEGFa staining would correlate positively in ccRCC, with increased VEGFa expression contributing to increased angiogenesis. One possible explanation may be a 'steal' effect, whereby tumours with higher total VEGFa levels in turn secrete more VEGFa, therefore promoting neo-vascularisation and resulting in paradoxically lower VEGFa staining within the tumours, but increased neo-angiogenesis. Kluger *et al* noted a similar relationship when they quantitatively assessed the relationship between vessel area and expression of VEGFR1/2 in ccRCC tumour cells (Kluger, Siddiqui et al. 2008).

The positive correlation observed between increasing LIMD1 and VEGFa staining and increasing total WTIP and VEGFa staining could therefore indicate increasing neo-angiogenesis in tumours expressing low LIMD1 or low total WTIP.

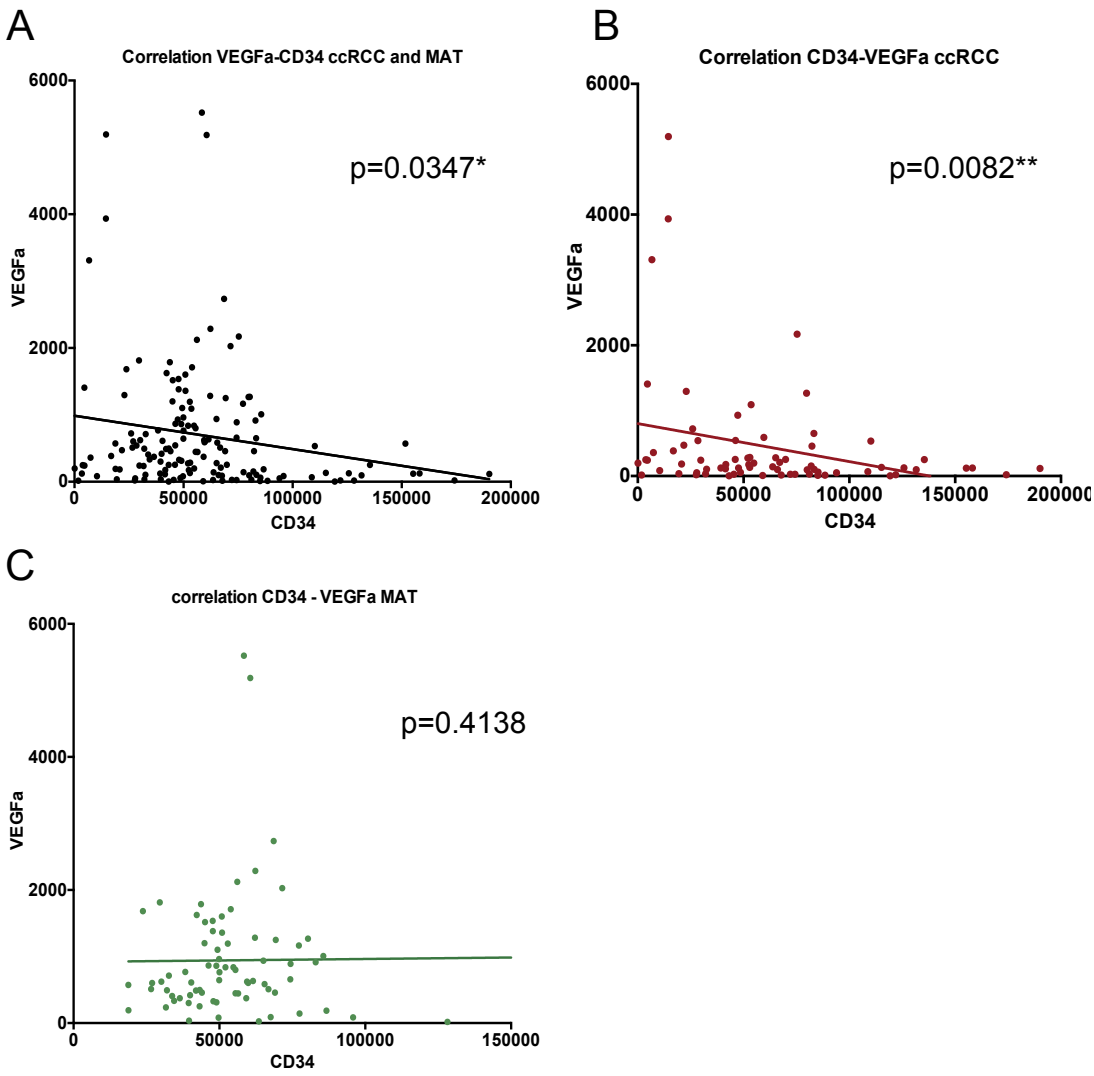

Figure 3.27 Levels of VEGFa and CD34 assessed immunohistochemically do not correlate in either ccRCC or MAT

The relationship between modified automated ARIOL score for VEGFa and CD34 was plotted graphically using Prism 6 and correlation calculated using the Spearman-Rank correlation coefficient**. A** Correlation in combined ccRCC and MAT, **B**. Correlation in ccRCC alone and **C**. Correlation in MAT alone

3.10 Summary

This chapter demonstrates the down-regulation of Ajuba and LIMD1 in most ccRCC lines *in vitro* compared to control RPTEC. WTIP expression was however only reduced in four out of twelve lines with some lines demonstrating significantly more WTIP expression. Normal immunohistochemical staining characteristics for LAW proteins are described in a range of normal/malignant tissues, and LAW staining characterised in both ccRCC samples and MAT. The relationship between staining for the three proteins is correlated in both ccRCC and MAT and staining correlated with established markers of hypoxic deregulation (**Figure 3.28**).

In vivo, loss of LIMD1 was observed in 49.3% of ccRCC tumours, with 17% demonstrating no LIMD1 staining compared to 3% of MAT (X^2 test p=0.0002**). 76% of tumours demonstrated loss of Ajuba compared to MAT, with 35% demonstrating no Ajuba staining compared to 8% of MAT (X^2 test p<0.0001***). Loss of WTIP was observed in 20% of tumours compared to MAT, with 63% of tumours actually demonstrating an increase in total WTIP staining. The subcellular localisation of WTIP appeared important with 73.3% of tumours showing reduced nuclear staining of ccRCC compared to MAT histospots and 58% of tumours demonstrated no nuclear staining compared to 9% of MAT histospots, (X^2 p=<0.0001***). For cytoplasmic staining, 4% of tumours demonstrated no cytoplasmic staining compared to 3% of MAT, X^2 test=0.344, p=0.577). This implies that sub-cellular WTIP localisation differs between tumours and MAT, with significantly less nuclear staining observed in the ccRCC samples.

Staining for LIMD1 and Ajuba and Ajuba and WTIP correlates strongly in ccRCC histospots but not in MAT, implying that co-loss frequently exists and may be relevant in tumourigenesis. Staining for LIMD1 and WTIP strongly correlated in both ccRCC and MAT histospots, which could imply a simple association whereby tissue with more LIMD1 staining also has more WTIP staining. Of note, however when sub-cellular WTIP localisation was included in the analysis, cytoplasmic WTIP staining demonstrated a strong positive correlation with LIMD1 staining in both ccRCC and MAT perhaps indicating increased total WTIP levels, whilst nuclear WTIP and LIMD1

staining demonstrated a strong positive correlation in MAT but not ccRCC, suggesting that changed in subcellular WTIP localisation may be important in driving tumourigenesis. Cytoplasmic WTIP staining positively correlated with Ajuba staining in both MAT and ccRCC, however nuclear WTIP staining correlated with Ajuba staining in ccRCC but not MAT. This could imply that sub-cellular WTIP localisation is relevant in tumourigenesis. An overview of the Spearman-Rank correlation coefficient, comparing the modified automated ARIOL score for the different proteins in the ccRCC histospots and MAT is summarised in **Figure 3.28**.

A

ccRCC	LIMD1	Ajuba	Total WTIP
LIMD1	x	p=0.0012	p<0.0001
Ajuba	p=0.0012	x	p=0.0317
Total WTIP	p<0.0001	p=0.0317	x
Cytoplasmic WTIP	p=0.0016	p=0.0097	x
Nuclear WTIP	p=0.3366	p=0.0405	x
CD34	p=0.9507	p=0.5490	p=0.7362
VEGFa	p=0.001	p=0.9731	p<0.0001

B

MAT	LIMD1	Ajuba	Total WTIP
LIMD1	x	p=0.335	p<0.0001
Ajuba	p=0.335	x	p=0.4166
Total WTIP	p<0.0001	p=0.4166	x
Cytoplasmic WTIP	p<0.0001	p=0.041	x
Nuclear WTIP	p=0.0044	p=0.5889	x
CD34	p=0.8662	p=0.1388	p=0.8634
VEGFa	p=0.0011	p=0.1633	p=0.0009

Figure 3.28 Summary overview of the Spearman-Rank correlation coefficient comparing the modified automated ARIOL score for the proteins stained immunohistochemically. **A.** ccRCC histospots and **B**. MAT

Given the importance of hypoxic deregulation in driving ccRCC and the pro-tumourigenic effects of HIF2α in ccRCC particularly through the modulation of vascular endothelial cell function, LAW expression was correlated with VEGFa and CD34 staining. LAW expression did not correlate with CD34 expression in our samples, although a strong positive association was observed between LIMD1/WTIP and VEGFa staining but not Ajuba and VEGFa staining (**Figure 3.28**). It was hypothesised that this association could actually reflect increased angiogenesis associated with reduced LIMD1/WTIP expression, whereby lower VEGFa staining resulted from increased tumour VEGFa secretion, a 'so called' steal effect.

3.11 Discussion

3.11.1 Overview of immunohistochemistry

Most of the work undertaken in this chapter has relied on the immunohistochemical detection of antigens of interest, a powerful tool for antigen identification through the visualisation of specific antigen-antibody interactions, enabling both the quantification and characterisation of the distribution and sub-cellular localisation of the antigen of interest (Yaziji and Barry 2006, Matos, Trufelli et al. 2010). IHC provides a powerful tool in diagnostic pathology, prognostication and therapeutic decision-making and given that the distribution and localisation of antigens of interest can be characterised, can provide putative information about antigen function (Matos, Trufelli et al. 2010).

IHC is a relatively low cost technique where rapid throughput is possible, particularly using automated/semi-automated systems. Multiple TMAs/slides can be processed simultaneously and more than one antigen detected simultaneously (Matos, Trufelli et al. 2010, Ramos-Vara and Miller 2014). There are however pitfalls in IHC that must be considered carefully and errors minimised (Yaziji and Barry 2006) .

3.11.2 IHC optimisation

Careful optimisation to ensure antigen-antibody specificity, to minimise variability between staining repeats and facilitate accurate quantification must be undertaken (Ramos-Vara and Miller 2014). Accurate antibody recognition is a critical step with specificity mainly dependent on the quality of the primary antibody and the ability of the antigen epitope to bind to it (Ramos-Vara and Miller 2014). In the staining protocols described some commercially available antibodies were utilised that had been widely tested and robustly validated, with suggested IHC protocols defined and positive and negative controls determined (Ramos-Vara and Miller 2014). Appropriate controls were always included and all staining reviewed by an experienced histopathologist in order to determine that staining appeared sensitive and specific, help define expected staining patterns and establish optimal antibody concentrations.

For LIMD1, Ajuba and WTIP, antibody sensitivity and specificity had been less widely evaluated immunohistochemically and had not been characterised in ccRCC. Antibody specificity had been established *in vitro* using Western Blotting techniques with si knockdown/re-expression confirming antigen specificity by the Sharp lab. Expected staining patterns and antibody specificity had been established in breast and lung tissue for LIMD1 and staining of these tissues was similar to that previously characterised (Sharp, Al-Attar et al. 2008, Spendlove, Al-Attar et al. 2008). IHC staining for Ajuba was similar to that described in online databases such as Protein Atlas and as described in the literature (Tanaka, Osada et al. 2015, Shi, Chen et al. 2016).

For all IHC, an indirect two-step method was used, which increases sensitivity since the unlabelled primary antibody retains full avidity, hence increasing the reaction intensity (Ramos-Vara and Miller 2014). For the commercially available TMAs and TMAs obtained from a clinical trial setting, standardised specimen fixation in paraffin and tissue processing was followed (Yaziji and Barry 2006, Howat and Wilson 2014), adhering to standardised Good Laboratory Guidelines. An avidin-biotin visualisation method was used, which increases sensitivity as a greater number of biotin molecules can be attached to a primary antibody (Happerfield, Bobrow et al. 1993, Ramos-Vara and Miller 2014). Background staining related to endogenous biotin activity, which is common in kidney tissue can however be problematic. Appropriate blocking steps were included and kidney tissue was always included as a negative control with omission of incubation with the primary antibody: very little staining of this control slide was consistently observed. An optimal antibody concentration was defined as the titre producing the highest ratio of 'signal' i.e. specific binding, to 'noise' i.e. minimising background labelling (Ramos-Vara and Miller 2014) (Matos, Trufelli et al. 2010). In addition, positive and negative control samples were always included which consisted of a range of tissue types represented on a TMA. Internal negative control evaluation provided an additional assurance of antibody specificity, for example ensuring that there was little stromal staining when staining for LAW proteins (Elias, Gown et al. 1989). The use of an automated IHC protocol in some cases has the potential to reduce assay-to-assay variability introduced by human variation/error and this was utilised for CD34 staining (Ramos-Vara, Kiupel et al. 2008).

3.11.3 Interpretation of IHC staining

The interpretation of IHC staining is generally qualitative and subjective and the determination of cut-off values establishing a positive or negative result often arbitrarily determined (Matos, Trufelli et al. 2010). This is particularly difficult when evaluating staining for a new antigen/biomarker where the micro-anatomic or subcellular distribution may not have been described and appropriate cut-offs for positive/negative staining determined (Seidal, Balaton et al. 2001). For example, HIF2α is generally considered to act as a nuclear transcription factor, although it is also thought to function within a protein translational initiation complex within the cytoplasm (Uniacke, Holterman et al. 2012). Kroeger *et al* demonstrated that high cytoplasmic HIF2α expression was associated with a more aggressive ccRCC phenotype (Kroeger, Seligson et al. 2014), an observation that would have been lost with conventional staining analysis that did not evaluate sub-cellular localisation.

Staining for PD-L1 and PD1 with multiple assays/antibodies within a multitude of clinical trial settings undertaken by different pharmaceutical companies has highlighted some of the problems of a lack of consistency between different assay protocols and a lack of a clear underlying biomarker definition, with different staining patterns/intensities considered positive with different IHC protocols (Kerr and Hirsch 2016).

3.11.4 Scoring systems for immunohistochemistry

A number of scoring systems are commonly used to evaluate IHC staining. The Allred quick score, is a combined score based on overall staining intensity, (typically ranging from 0-3), and the proportion of neoplastic tissue staining positively, (with grouping in to 3 categories, >75%-uniform, 25-75%-variable and 0-25% rare) (Varghese, Bukhari et al. 2014). One significant limitation of such an approach is the variability in visual perception of staining intensity related to differences in haematoxylin counter-staining and the potential for conscious or unconscious bias associated with assessing staining on contiguous tumour and matched adjacent tissue samples (Choudhury, Yagle et al. 2010). A modified version of the Allred quick score was utilised to manually evaluate

staining within the ccRCC TMAs, scoring both the staining intensity and proportion of tumour cells stained to generate a semi-quantitative score. Despite the limitations associated with manual perception of scoring, such a scoring system is generally considered accurate with good inter-observer reliability for staining observed (Zlobec, Steele et al. 2006). In addition, given that tumour and MAT tissue was represented contiguously on the same slide, no differences in haematoxylin counterstaining should have been present.

In order to obtain a more accurate objective measure of expression that better enabled comparison of staining intensity, a modified automated quantitative analysis system was used, a validated scoring system that can be more accurate than pathologist based staining (Camp, Chung et al. 2002) (Rizzardi, Johnson et al. 2012). However, in practice the use of automated systems does require significant user input with characterisation of the area of interest requiring manual input with for example exclusion of stromal tissue at least until adequate image training has been undertaken (Camp, Chung et al. 2002). An analysis of automated quantitative analysis of oestrogen receptor expression in breast carcinoma using a tissue microarray study of 3,484 cases did not demonstrate a significant difference from expert pathologist scoring (Turbin, Leung et al. 2008). Differences in staining patterns between tumour samples and the MAT were compared using both manual and automated scoring systems and good agreement observed suggesting that both methods offered a robust and comparable scoring system.

3.11.5 Changes in expression of LAW proteins in ccRCC

The Ajuba LIM proteins have not been widely characterised in mammalian tissues/malignancies although LIMD1 loss has been shown to drive tumourigenesis in breast and lung carcinoma (Sharp, Al-Attar et al. 2008, Spendlove, Al-Attar et al. 2008) and Ajuba loss implicated in malignant mesothelioma tumourigenesis (Tanaka, Osada et al. 2015). Up-regulation of Ajuba expression has been observed in oesophageal SCC samples compared to matched control tissue (Shi, Chen et al. 2016).

3.11.5. 1 Loss of LIMD1 in ccRCC histospots

Spendlove *et al* demonstrated that loss of LIMD1 was common in breast carcinoma and absent/weak nuclear staining strongly correlated with adverse prognostic indicators: worse histological subtype, increasing tumour size and tumour grade and worse cumulative-patient survival (Spendlove, Al-Attar et al. 2008). Their model proposed that loss of nuclear LIMD1 was a surrogate marker for reduced overall LIMD1 expression. Staining of lung carcinoma samples also demonstrated frequent loss of LIMD1 staining compared to control matched tissue (Sharp, Al-Attar et al. 2008).

3p LOH is common and loss of at least one *LIMD1* allele may therefore occur in many ccRCC samples. Biallelic loss of 3p is however uncommon, in one study characterising *VHL* loss, LOH of one 3p copy was observed in 94% of tumours with inactivation or hypermethylation of the remaining allele in 98% of such tumours (Gnarra, Tory et al. 1994).

In a recent study by Thiesen *et al*, copy number alterations (CNAs) in 48 ccRCC tumours were analysed. Gene losses on chromosome 3p were observed in all 48 tumours. Loss of tumour suppressor genes were common at the 3p21.31 locus, with CNAs of *LIMD1* identified in 28 of the 48 tumours analysed (58.3%): interestingly there was a correlation with loss and tumour grade with 21 of the 26 (80%) grade 1 tumours demonstrating CNA loss of *LIMD1* and only 5 of the 20 (25%) grade 3 tumours demonstrating CNA loss of *LIMD1*. This suggests that CNA of *LIMD1* occur more commonly in the lower grade, less aggressive tumour phenotype and also that higher grade tumours develop independently from the lower grade ones (Thiesen, Steinbeck et al. 2017).

The proportion of other 3p21.31 encoded tumour suppressor genes demonstrating CNA alterations was variable with loss of *SETD2* identified in 43/48 (89%) of the tumours by Thiesen *et al*. This suggests that loss of 3p21.3 genes is not simply as a result of a 'carrier' effect, i.e. tumours that have CNAs of *SETD2* for example do not demonstrate CNAs of *LIMD1* simply because they are both 3p21 encoded but that loss of genes that map close to one another can occur independently and that chromosomal

micro-deletions may be more common than previously thought (Thiesen, Steinbeck et al. 2017).

Interestingly, a study of kidneys of patients with VHL disease, i.e. germline mutations in one copy of *VHL*, has demonstrated that these patients probably have hundreds of thousands of functional VHL-null single cells or multi-centre clusters of cells, despite no evidence of ccRCC (Montani, Heinimann et al. 2010). Given that biallelic loss/inactivation of a tumour suppressor is necessary for a loss of function phenotype, CNA of 3p encoded tumour suppressors as an early initiator of tumourigenesis may occur in tissue adjacent to ccRCC samples, despite there being no evidence of tumour formation within this matched, non cancerous tissue. Using MAT as a control tissue has a number of significant advantages: staining is undertaken on tissue with the same genetic background, and therefore changes in staining for proteins of interest is likely to be associated with tumourigenesis.

However, LIMD1 staining may be reduced in such MAT histospots compared to tissue obtained from a healthy kidney without evidence of ccRCC and an even better control may therefore have consisted of contiguous MAT and distant MAT where LOH was less likely to have occurred. It was observed that LIMD1 expression was reduced in ten of the twelve (83%) ccRCC lines compared to the control RPTEC line whilst a reduction in LIMD1 staining was observed in 49.3% of ccRCC histospots compared to MAT, with 17% of the ccRCC histospots demonstrating no LIMD1 staining compared to 3% of the MAT (X^2 p=0.0002). Given the significant proportion of tumours demonstrating no LIMD1 staining, it seems likely that biallelic inactivation of *LIMD1* is occurring in a significant proportion of ccRCC samples and not MAT, further implicating *LIMD1* loss in tumourigenesis.

A recently published study characterised LIMD1 staining in 32 RCC samples and demonstrated what was described as a significant reduction in LIMD1 staining characterised as low/moderate staining compared to matched control tissue in 15.8% of tumours. It is not clear what proportion of tumours demonstrated reduced staining compared to control (Sur, Maurya et al. 2017).

Although numbers of each tumour type were low, the investigators reported that lower stage tumours, stage I were more likely to demonstrate reduced staining compared to

stage III tumours, 20.2% versus 6% leading them to hypothesise that reduced LIMD1 expression is more important in driving early disease as also hypothesised by Thiesen *et al*, although in the study by Thiesen *et al*, gene expression levels and grade were correlated (Sur, Maurya et al. 2017, Thiesen, Steinbeck et al. 2017).

However, in the study by Sur *et al* no comment is offered regarding the correlation between LIMD1 staining and grade and given the small number of tumour samples of each stage it is difficult to draw definitive conclusions regarding a correlation between more advanced tumours and loss of LIMD1 staining (Sur, Maurya et al. 2017).

Beyond the LOH of one allele, it is unclear how LIMD1 levels are down-regulated at the protein level. Huggins *et al* demonstrated that LIMD1 mRNA levels were generally unchanged compared to control tissue in breast carcinoma (Huggins, Gill et al. 2007), and only 0.85% of breast tumours had *LIMD1* mutations, suggesting at least in this tumour type that LIMD1 protein levels are regulated post-transcriptionally, for example by posttranslational modification (Huggins, Gill et al. 2007). Analysis by other investigators, using data from the TCGA Research Network analysing a data set of 450 ccRCC tumours with copy number data and 293 tumours with somatic mutation data identified 14 genes that were significantly mutated in the data set, suggestive of driver status but LIMD1 was not one of these genes characterised (Sato, Yoshizato et al. 2013).

However, as described in Chapter 1, recently as yet unpublished work by our group in lung adenocarcinoma re-analysing data from the TCGA Research Network using new data available via cBioportal suggests that LIMD1 mutation is much more common than previously described.

Analysis of 516 lung adenocarcinoma samples and 501 lung squamous cell carcinomas identified shallow and deep combined *LIMD1* deletions and this combined analysis demonstrated that deletion was much higher than previously identified and comparable to known highly mutated driver mutations (**Figure 3.28**). Both shallow and deep LIMD1 deletions are likely to contribute to loss of gene expression, albeit to different degrees.

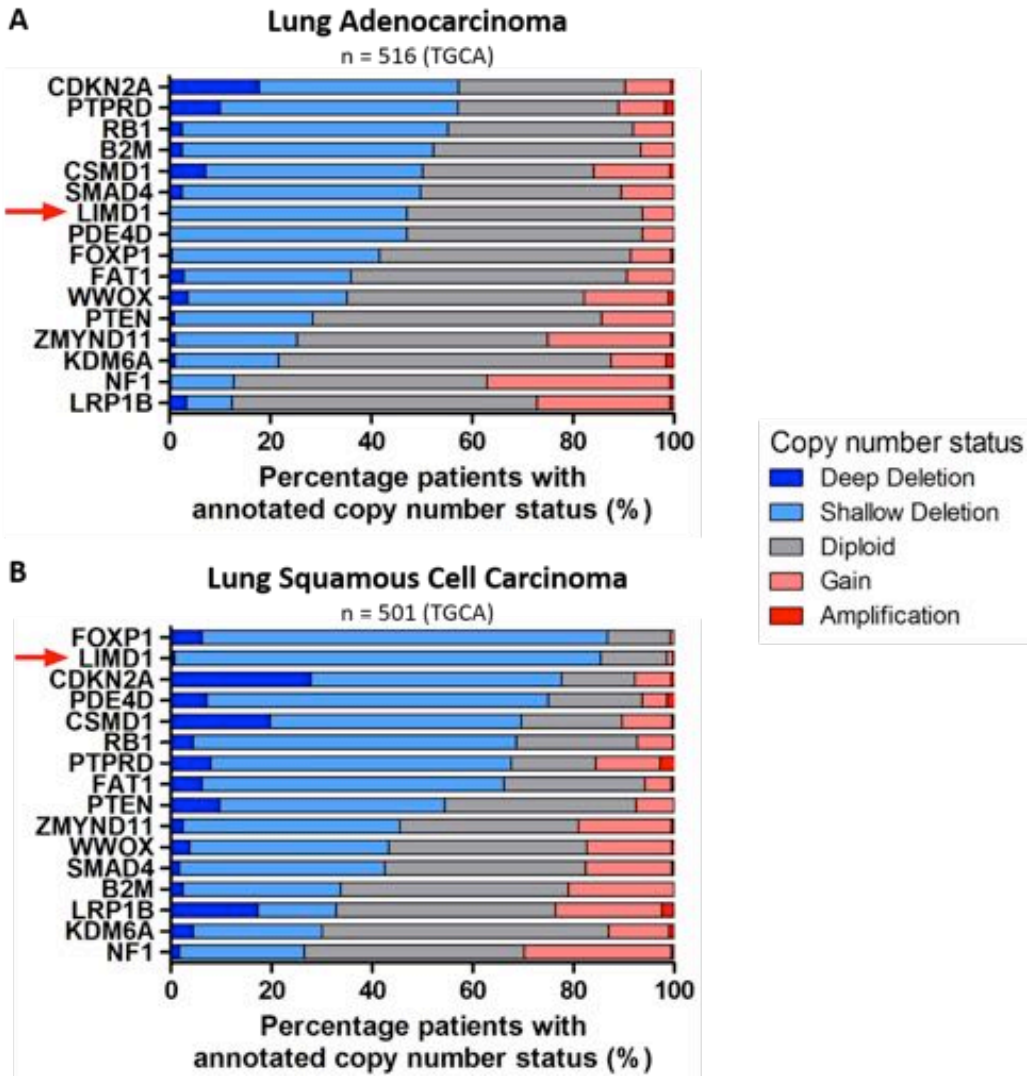

Figure 3.28 cBioPortal analysis of LIMD1 loss in adenocarcinoma and squamous cell carcinoma of the lung. Genes are ordered by percentage loss from greatest to smallest. **(A)** In lung adenocarcinoma, 0.2% of tumours contain a deep *LIMD1* deletion and 46.9% contain a shallow *LIMD1* deletion. **(B)** In squamous cell carcinoma, 0.8% of tumours contain a deep *LIMD1* deletion and 84.6% contain a shallow *LIMD1* deletion. Graphs generated by Dr John Foster (2017, unpublished).

3.11.5.2 Loss of Ajuba staining in ccRCC

The reported staining of a range of normal tissue types and tumours demonstrated as was observed that Ajuba staining is predominantly nuclear in localisation (Tanaka, Osada et al. 2015, Shi, Chen et al. 2016). Staining of twenty cases of malignant mesothelioma for Ajuba and the transcriptional co-activator and regulator of the Hippo signalling pathway YAP, which drives the transcription of target genes with consequent oncogenic transformation, demonstrated that tumours that lacked Ajuba staining had strong nuclear localisation of YAP, suggesting that Ajuba inactivation and YAP

activation correlated, providing an explanation for potential increased tumourigenesis in association with Ajuba loss (Tanaka, Osada et al. 2015).

It appears that patterns of Ajuba expression may differ significantly depending on tumour type. Interestingly in a recent study of oesophageal squamous cell carcinoma, Ajuba levels were significantly higher in the carcinoma samples, compared to adjacent control tissue and Ajuba overexpression acted oncogenically to promote cell growth and colony formation, cell migration and invasion (Shi, Chen et al. 2016). When IHC patterns were analysed in the study by Shi *et al*, tumours demonstrated predominantly cytoplasmic staining patterns, compared to the predominant nuclear staining pattern observed from matched tissue, suggesting that nuclear to cytoplasmic Ajuba transfer may drive tumourigenesis in this tumour type. When RNA sequencing was used to identify Ajuba related oncogenic pathway activation, up-regulation of MMP10 and MMP13 through the activation of ERK1/2 pathways was observed. Therefore in oesophageal SCC, Ajuba appeared to be acting as an oncogene through the up-regulation of ERK1/2 pathways (Shi, Chen et al. 2016). Shi *et al* also looked at mRNA levels of Ajuba, WTIP and LIMD1 and found in 179 paired samples that Ajuba was significantly overexpressed in tumour tissues compared to adjacent non-tumour tissue, but mRNA levels of WTIP and LIMD1 did not differ significantly (Shi, Chen et al. 2016), suggesting at least in this tumour type that Ajuba deregulation but not WTIP and LIMD1 drives tumourigenesis.

Loss of 14q in ccRCC has been associated with worse recurrence free and cancer specific survival: Kroeger *et al* hypothesised that this may be related to loss of HIF1α but other candidate genes including 14q-encoded Ajuba remain uncharacterised (Kroeger, Klatte et al. 2013). A significant proportion of tumours in our cohort demonstrated a reduction in Ajuba staining compared to MAT (76%), with 35% of tumours demonstrating no Ajuba staining compared to 8% of MAT samples (X^2 $p<0.0001$).

Kroeger *et al* demonstrated 14q LOH in around 45% of ccRCC tumours (Kroeger, Klatte et al. 2013). The reduction in Ajuba staining observed in our cohort of ccRCC tumour may in part be associated with loss of *HIF1a* through LOH at 14q with *Ajuba* loss occurring as a carrier effect. However, given that 76% of tumours demonstrated

reduced Ajuba staining compared to control, this would suggest that Ajuba downregulation occurs very frequently and is not simply a consequence of a carrier effect of *HIF1a* loss, allelic loss of *Ajuba* may be occurring independently of *HIF1a* and other mechanisms such as post-transcriptional down-regulation of protein expression may also contribute to reduced protein expression.

As was hypothesised for *LIMD1* loss, loss of one *Ajuba* allele may also be occurring in some of the MAT samples, since it would be expected that inactivation of both tumour suppressor gene copies would be required to drive tumourigenesis. Therefore Ajuba expression in MAT may be less than would be expected in healthy tissue in the absence of ccRCC. This is supported by the observation that Ajuba expression was reduced in eleven of the twelve (92%) ccRCC lines compared to the control RPTEC line (**Figure 3.1**), a figure higher than the 76% reduction in staining observed in the ccRCC samples compared to control MAT (**Figure 3.10**). Given that 35% of tumours demonstrated no Ajuba staining, compared to 8% of MAT (χ^2 $p<0.0001$), this implies that in a significant proportion of tumours, there is no or very little protein expression as a consequence of biallelic inactivation.

Work by Thiesen *et al* found that loss of 14q23.3-encoded genes was common and that weighted analysis assigned loss more commonly to high grade tumours: CNA loss of 14q11.2 encoded Ajuba was however only observed in only 4/48 tumours (8%), although CNA of other 14q encoded genes was more commonly observed, again suggesting that loss is not simply a consequence of a carrier effect. Further characterisation of CNA is therefore relevant in our cohort and further suggested experimental work described in **Section 3.12**.

3.11.5.3 Loss of WTIP staining in ccRCC

WTIP is 19q13.11 encoded and 19q loss has not been implicated in ccRCC pathogenesis. WTIP staining has not been widely characterised and a literature review failed to identify any studies characterising immunohistochemical staining in cancers. Immunofluorescence studies in *Xenopus* demonstrates that WTIP is cytoplasmically expressed and regulates ciliogenesis (Chu, Ossipova et al. 2016)

WTIP staining patterns were both nuclear and cytoplasmic in nature, which correlates with staining patterns described on Protein Atlas. Only 20% of tumours demonstrated less total WTIP staining compared to matched adjacent tissue, with 63% showing increased staining, a figure that corresponds to the *in vitro* work where 66% of ccRCC lines demonstrated increased WTIP expression compared to RPTEC control. Sub-cellular localisation however appeared important with 73% of tumours showing reduced nuclear staining compared to MAT. CNA loss of 19q13.1encoded genes including *WTIP* was only observed in a few of the 48 ccRCC samples analysed by Thiesen *et al* (Thiesen, Steinbeck et al. 2017).

It is interesting that for many tumours WTIP expression was increased compared to MAT and reasons for this remain unknown. It remains unclear why reduced nuclear WTIP staining could be associated with increased tumourigenesis and it is difficult to speculate given that changes in WTIP in malignancies have not been characterised, nor are the functions of WTIP fully understood. It could be that reduced nuclear WTIP expression in association with increased cytoplasmic expression is associated with increased microRNA silencing or could relate to WTIP's role in mitotic spindle cell orientation.

Other studies of other tumour suppressors have also shown that subcellular localisation strongly correlates with prognosis and drives tumourigenesis. As outlined, Spendlove *et al* demonstrated that subcellular LIMD1 localisation correlated with clinico-pathological outcome data, with loss of nuclear staining associated with worse outcome (Spendlove, Al-Attar et al. 2008). In addition, loss of nuclear BRCA1 expression in breast cancers is strongly associated with highly proliferative tumour phenotypes (Jarvis, Kirk et al. 1998). Kroeger *et al* characterised HIF2α staining in both cytoplasmic and nuclear compartments in ccRCC and found a strong correlation between increased cytoplasmic staining and worse clinico-pathological outcome (Kroeger, Seligson et al. 2014).

For WTIP changes in subcellular localisation may be of importance in driving tumour pathogenesis and further experiments to characterise this relationship are described in **Section 3.12**.

3.11.6 Association between patterns of LAW staining in ccRCC

It was hypothesised that given the close homology of LAW family members and characterised overlapping functions, a degree of functional redundancy is likely but that loss of all three family members was unlikely to occur, a pattern observed *in vitro* in a panel of ccRCC lines. It was also hypothesised that co-loss of one or more family member may increase tumourigenesis.

In Drosophila there is a single LAW gene orthologue *djub* and Drosophila cells that do not express *djub* are not viable. Such an association is also observed in mammalian cells, where depletion of all 3 LAW proteins in the dog kidney epithelial cell line, MDCK results in cell death (Das Thakur, Feng et al. 2010). In an analysis of MDCK cells, all three Ajuba subfamily members strongly associated with LATS1/2 suggesting that they regulate Hippo signalling in this tissue type. Depletion of both Ajuba and LIMD1 in the MDCK cells resulted in a significant increase in phospho-YAP levels, again suggesting that Ajuba and LIMD1 play a critical role in the regulation of Hippo signalling in renal cells. In the study by Das Thakur *et al*, co-depletion of Ajuba and WTIP or LIMD1 and WTIP was not undertaken (Das Thakur, Feng et al. 2010).

A strong positive correlation between LIMD1 and Ajuba staining in the ccRCC histospots but not in the MAT was observed. This suggests that LIMD1 and Ajuba down-regulation coexist in ccRCC but not in matched renal tissue and could imply that down-regulation contributes to tumourigenesis. This may in part be as a consequence of loss of heterozygosity of both 3p and 14q but as outlined, given the over-representation of ccRCC samples with no LIMD1 or no Ajuba staining compared to MAT samples, further down-regulation of both proteins appears to be occurring in at least some tumours. Information on tumour grade and stage was available for the US Biomax cohort and was correlated with LIMD1 and Ajuba levels in the ccRCC samples but did not correlate (data not shown), although the sample size was small for some of the tumour stages/grades. This does not however mean that loss of such tumour suppressors does not drive tumourigenesis, particularly if loss is an early event (Thiesen, Steinbeck et al. 2017). VHL loss and tumour grade and stage consistently fail to show any association but *VHL* loss is clearly an important driver of tumourigenesis in ccRCC (Frew and Moch 2015).

3.11.7 Relationship between LAW staining and markers of hypoxic deregulation

It was hypothesised that loss of LIMD1, Ajuba or WTIP would be associated with increased hypoxic deregulation and thus increased CD34 and VEGF staining. No correlation was observed between staining for LIMD1, Ajuba or WTIP and CD34 expression as a marker of MVD. This does not however mean that such an association does not exist.

Given the small area of histospots and inherent heterogeneity of ccRCC, analysis of MVD on TMAs may not be representative of the tumour vasculature as a whole. To date, studies assessing the prognostic value of MVD in ccRCC have shown conflicting results, with Sandlund *et al* for example finding no association with prognosis (Sandlund, Hedberg et al. 2007) whilst Iakovlev *et al* found that higher adjusted MVD was associated with shorter disease-free survival but not tumour stage (Iakovlev, Gabril et al. 2012). In addition, the distinct type of vasculature in ccRCC may be important. Yao *et al* classified intra-tumoural blood vessels based on the differential expression of blood vessel markers and identified two distinct types of microvessels: undifferentiated $CD31^{+}/CD34^{-}$ and differentiated $CD34^{+}$ vessels. Undifferentiated $CD31^{+}/CD34^{-}$ MVD only, correlated with higher tumour grade and shorter patient survival (Yao, Qian et al. 2007).

3.12 Future work

The use of histospots on TMAs for the analysis of tumour staining and correlation of such staining with clinico-pathological data has been assessed in multiple studies as valid. Histospots are however small and given the observation of tumour heterogeneity in ccRCC, concern remains they may not be representative of the tumour characteristics as a whole. The use of tissue from several areas of the same tumour and if possible metastatic sites from the same patient would establish if LAW staining is heterogeneous. Driver mutations, driving metastatic spread could for example result in similar staining characteristics in metastatic deposits but not in samples from the primary tumour. In addition, given that LOH may well be occurring in MAT adjacent to the ccRCC histospots, it would be interesting to correlate staining patterns between the ccRCC samples and contiguous and distant MAT.

Given the differences in staining for LAW proteins in ccRCC histospots compared to MAT observed it would also be interesting to analyse mRNA levels for LAW in both the ccRCC and MAT histospots, enabling the comparison of gene expression and protein levels. Huggins *et al* found that LIMD1 mRNA levels are relatively unchanged in breast tumours compared to matched controls despite protein down-regulation (Huggins, Gill et al. 2007) and this was also observed by Sharp *et al* upon interrogation of the NHGRI-sponsored tumour sequencing project dataset in lung carcinoma (Sharp, Al-Attar et al. 2008). Using the cBioportal platform to interrogate the TCGA research network would enable the identification of both shallow and deep deletions of the LAW LIMD1 proteins in ccRCC samples and control renal tissue.

Given that 3p LOH is such a common event in ccRCC, and the observations of Thiesen *et al* that CNA loss of *LIMD1* was frequent in ccRCC, it would be interesting to characterise *LIMD1* copy number in our cohort of ccRCC and MAT using Fluorescent *in situ* hybridisation (FISH). *LIMD1* LOH may also be occurring in MAT as a precursor for tumourigenesis and biallelic *LIMD1* loss/inactivation may be observed in some tumours. 14q loss is also frequently observed in ccRCC and Ajuba copy number in our ccRCC/MAT samples could also be characterised using FISH. Copy number alterations in the ccRCC samples could be correlated with contiguous and distant MAT.

Immunofluorescence (IFA) is widely used *in vitro* to characterise protein co-localisation and protein sub-cellular localisation. LAW proteins, shuttle between the cytoplasm and the nucleus with an equilibrium towards the cytoplasm (Kadrmas and Beckerle 2004). Dr. Katherine Bridge of the Sharp lab has demonstrated predominantly cytosolic LIMD1 staining in a number of ccRCC lines. Given the observation that ccRCC tumours frequently have less nuclear WTIP staining compared to MAT, it would be particularly interesting to characterise WTIP staining *in vitro* using IFA in ccRCC lines using a non-tumour cell line such as RPTEC as control. Correlation of staining patterns for LAW using IFA in such cells would characterise the relationship between sub-cellular localisation for the three family members. In addition, immunoblot of both the nuclear and cytoplasmic components of ccRCC lines could be used to characterise the sub-cellular localisation of LAW proteins.

Immunohistochemistry demonstrated no association between $CD34^+$ staining and staining for LAW proteins. As outlined however, Yao *et al* observed two distinct types of microvessel in ccRCC, undifferentiated $CD31^+/CD34^-$ and differentiated $CD34^+$ vessels with the undifferentiated $CD31^+/CD34^-$ MVD correlating with higher tumour grade and shorter patient survival in ccRCC (Yao, Qian et al. 2007) It would therefore be relevant to stain the TMAs for CD31 in addition to CD34 and correlate both CD31 and CD34 staining with that for LAW proteins and VEGF. Other investigators have found a strong correlation between VEGF staining and staining for VEGF-R1, 2 and 3 (Kluger, Siddiqui et al. 2008). Kluger *et al* found in ccRCC that staining for VEGFR-1 strongly correlated with tumour grade and VEGFR-2 staining with tumour stage but that increasing VEGF staining was neither associated with stage or grade (Kluger, Siddiqui et al. 2008). After multi-variate analysis, work by del-Puerto Nevada *et al* demonstrated that expression of phosphorylated, i.e. activated VEGFR-2 in tumour stroma might potentially be used as a predictive biomarker in RCC patients treated with first line sunitinib, and that staining correlated with both OS and PFS (del Puerto-Nevado, Rojo et al. 2014). It would therefore be interesting to correlate staining for LAW with staining for VEGFRs, in particular VEGFR1 and 2 and phosphorylated VEGFR-2.

Chapter 4

Correlation of LIMD1, WTIP and Ajuba (LAW) expression with clinico-pathological outcome data in clear cell renal cell carcinoma

4.1 Introduction

There is a continuous drive in oncology to generate better patient prognostic/predictive algorithms to improve patient outcome and help influence choice of treatment for maximum therapeutic effect. Clinical prognostic scoring systems such as the Heng scoring system can help predict patient outcome in metastatic ccRCC (Heng, Xie et al. 2013). Patient outcome within subgroups however remains highly variable and reasons for this are not fully understood. A number of biomarkers have been identified in ccRCC but biomarker validation has proved difficult and currently there are no validated predictive biomarkers, and no biomarkers used routinely in clinical practice (Gulati, Martinez et al. 2014).

In breast carcinoma, Spendlove *et al* demonstrated frequent loss of LIMD1 in tumour tissue compared to matched-control tissue. In a cohort of 459 patients, loss of nuclear staining for LIMD1 strongly correlated with reduced patient survival, increased tumour size, increased histological grade and worse Nottingham Prognostic Index, an index that stratifies patients from excellent to poor prognosis (Spendlove, Al-Attar et al. 2008).

Reduced LIMD1 staining was observed in 49.3% of ccRCC samples compared to MAT, with no staining in 17% of ccRCC samples compared to 3% of the control tissue samples. For Ajuba, a 76% reduction in staining was observed in the ccRCC samples compared to MAT, with 35% of tumour samples demonstrating no staining compared to only 8% of the control tissue samples. For WTIP, 20% of ccRCC histospots demonstrated less staining compared to control tissue, with 63% of tumours demonstrated increased staining. Subcellular WTIP localisation however appeared important, with 58% of tumours demonstrating no nuclear staining compared to only 9% of the MAT histospots.

The Experimental Cancer Medicine Network aims to help facilitate the translation of basic scientific discovery into an understanding of what drives tumourigenesis and resistance to therapeutics *in vivo* as well as to develop novel treatments for patients with cancer. Access to patient tissue from two prospective clinical trials with detailed five-year clinico-pathological outcome data represents a valuable resource, enabling the investigation of LAW staining in a large panel of tumours *in vivo* and the correlation of

staining patterns with validated clinico-pathological indices. Many studies investigating potential biomarkers in various tumour types cannot be validated and often, reporting recommendations for tumour marker prognostic studies guidelines, which state that univariate and multivariate analysis should be conducted, are not followed (Gulati, Martinez et al. 2014).

To this end, TMAs containing archived tumour samples generated from a prospective randomised clinical trial of the epidermal growth factor receptor-2 (EGFR-2) tyrosine kinase inhibitor lapatinib versus hormone therapy (Ravaud, Hawkins et al. 2008) were stained for LIMD1, Ajuba and WTIP. Staining was correlated with clinico-pathological outcome data and both univariate and multivariate analysis undertaken. LAW staining was also correlated with staining for VHL, HIF1α and HIF2α, known markers of hypoxic deregulation in ccRCC. Using TMAs generated from the phase II study investigating upfront pazopanib prior to nephrectomy in patients with metastatic ccRCC (PANTHER) study, (Powles, Sarwar et al. 2016), staining for LIMD1 was further validated immunohistochemically and staining correlated with clinico-pathological outcome data.

4.2 Aims and Objectives

- To correlate staining for LIMD1, Ajuba and WTIP in ccRCC TMAs generated from a prospective clinical trial, with clinico-pathological outcome

- To correlate LIMD1, Ajuba and WTIP staining with staining for VHL, HIF1α and HIF2α, known markers of hypoxic deregulation in ccRCC

- To validate the correlation of LIMD1 staining and clinico-pathological outcome in ccRCC by staining a further cohort of patients enrolled in a phase II clinical trial

4.3 Tumour characteristics and clinical trial information

TMAs containing archived tumour samples generated from a prospective randomised clinical trial of the epidermal growth factor receptor-2 (EGFR-2) tyrosine kinase inhibitor lapatinib versus hormone therapy (Ravaud, Hawkins et al. 2008) were stained.

This trial was published in 2008, prior to the widespread availability of targeted therapy in RCC. Eligible patients had progressed through first-line cytokine therapy and had tumours that expressed EGFR and/or its co-receptor HER-2 (Ravaud, Hawkins et al. 2008). Patients were randomised either to the active or placebo arm and stratified by Karnofsky performance status (KPS) and number of metastatic sites. Detailed clinico-pathological and 5-year follow up data was available. The trial included 460 patients but only 144 tumour samples archived locally were available for analysis. Many patients had advanced disease at the time of tumour archive: 37% had metastatic ccRCC (stage IV) and 33% Stage III disease. TMA histospots were paraffin embedded and 0.9mm in diameter, with tumours from each patient represented on the TMAs in triplicate.

A further cohort of patient samples was available, generated from a phase II study investigating upfront pazopanib prior to nephrectomy in patients with metastatic ccRCC (PANTHER) (Powles, Sarwar et al. 2016). A total of 100 patients were assessable for clinical benefit for pazopanib, with nephrectomy performed in 63 patients (61%). 82% of patients had intermediate MSKCC prognostic risk disease and 18% MSKCC poor risk disease. Tissue samples were paraffin embedded and histospots of 2mm diameter were represented on the TMAs in duplicate.

4.4 LIMD1 staining

A new batch of LIMD1 antibody was used to stain the first set of TMAs designated the GSK cohort. This antibody was generated from a new clone from the same mouse hybridoma. Over time the initial LIMD1 antibody had degraded when stored in the -20°C freezer and although it continued to give a good signal when used for immunoblotting, IHC staining intensity had diminished considerably and differences in staining intensity between histospots could not be accurately quantified using this method. In addition, obtaining consistent IHC staining using the new batch of antibody and the optimised manual IHC protocol proved very difficult.

More consistent results were however obtained when staining with this new antibody batch was undertaken using an automated staining system (Discovery System, Ventana Medical system). Staining specificity was re-established using control TMAs with histospots from a range of normal and malignant tissues. Staining of these TMAs and of paraffin embedded healthy renal tissue slides were used to determine an optimum antibody concentration and to ensure staining appeared specific. Staining patterns and intensity were observed to be consistent between the old and the new batch of antibody (**Figure 4.1**). Dr Giorgia Trevisan, a consultant histopathologist at University College London Hospital, reviewed all IHC staining.

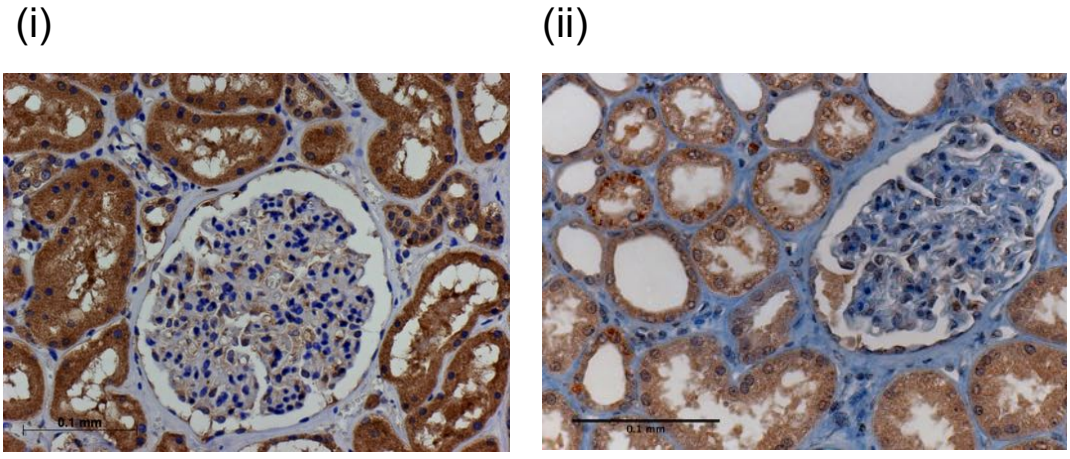

Figure 4.1. Comparison of manual and semi-automated IHC staining for LIMD1

Paraffin embedded renal tissue was stained immunohistochemically for LIMD1. Staining is cytoplasmic, with little staining of the glomeruli but staining of the distal and proximal tubules. **(i)** Representative IHC staining of renal tissue obtained using a manual IHC staining protocol and antibody concentration 1:50. **(ii)** Representative IHC staining of renal tissue obtained using a semi-automated IHC staining protocol

with antibody concentration 1:100 and a new batch of the LIMD1 antibody derived from the same hybridoma. Scale bar corresponding to 100μm is shown for size comparison.

Using the semi-automated staining system, staining patterns in ccRCC histospots and health kidney tissue were very similar to that observed with the manual IHC system with LIMD1 staining almost exclusively expressed in the cytoplasm and little stromal staining and no staining of the glomerulus observed (**Figures 4.1 and 4.2**).

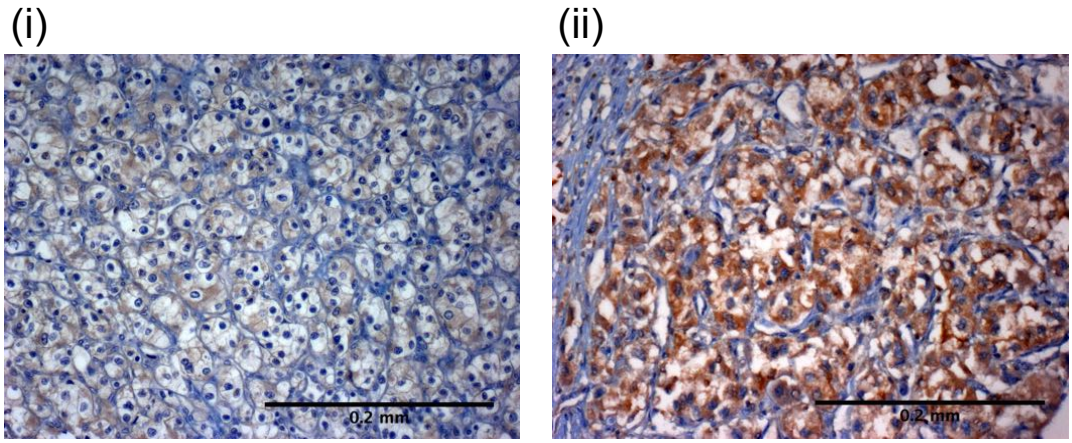

Figure 4.2 IHC staining for LIMD1 in ccRCC histospots

TMA histospots derived from a phase II clinical trial were stained immunohistochemically for LIMD1 using a semi-automated staining platform and LIMD1 antibody concentration 1:100. Histospots were represented on the TMAs in triplicate. **(i)** Low level cytoplasmic LIMD1 staining **(ii)** High level cytoplasmic LIMD1 staining.

The tumour scoring system was adapted from the scoring system used by Spendlove *et al* in the analysis of breast carcinoma (Spendlove, Al-Attar et al. 2008). Most positively staining tumours had low staining intensity and a four-point scoring system was used where zero represented no staining, one, weakly positive staining, two, moderate staining, and three, strongly positive staining. A score was generated based on the proportion of positively staining tumour cells and the intensity of staining throughout the histospot, a modified Allred scoring system (Allred, Bustamante et al. 1990). An overall score was then calculated based on the mean staining intensity for the histospots derived from the same tumour. For some tumours, samples were missing from the TMA or histospots included contained no carcinoma and such tumours were excluded. Tumours were then sub-divided into those with absent or low level LIMD1 staining, where the mean score as a function of the proportion of positive staining tumour cells and staining intensity was less than 100, and those with moderate or high LIMD1

staining, where the mean score was greater than 100. Most tumours demonstrated fairly homogeneously staining throughout the tumour histospots and this meant that defining alternative cutoffs for high versus low staining, e.g. less than the median versus more than the median was not possible as scores were too clustered. Given the low number of tumours for some staining intensity categories, this grouping was necessary in order for there to be sufficient tumours in each group to make statistical analysis meaningful.

This scoring system was used in preference to the score obtained from the automated Ariol image acquisition and analysis system as the manual LIMD1 IHC scoring had previously been validated as a robust scoring system, correlating with clinico-pathological data in a large breast carcinoma cohort (Spendlove, Al-Attar et al. 2008). In addition, the automated Ariol score did not always seem to correlate accurately with the extent of staining and staining intensity when compared to the score obtained manually. This was likely related to the small size of the histospots on the GSK TMA staining and the staining artefact present for some spots.

As before, positive and negative controls were included with the use of a TMA with histospots derived from a range of pre-invasive/invasive tumours and a negative control where the primary antibody was omitted when staining the GSK TMA. Staining patterns of control tissue and RCC samples corresponded to staining patterns observed with the previous batch of LIMD1 antibody (**Figures 4.1 and 4.2**).

Non-clear cell renal cell carcinoma samples were excluded from analysis, leaving 132 analysable ccRCC tumours. All staining was double scored by Dr Trevisan and myself, blinded to clinico-pathological outcome data and to each others scoring, although agreement had been reached as to how different staining intensities should be scored.

4.5 LIMD1 IHC of ccRCC histospots

4.5.1 Intra-class correlation coefficient analysis to assess inter-observer scoring agreement for LIMD1

In order for a scoring system to be robust, it needs to be reproducible. The intra-class correlation coefficient is the most commonly used method to assess inter-observer measurements of scoring for IHC and therefore reproducibility (Shrout and Fleiss 1979). The closer the agreement is to 1, the better the agreement between observers. Generally a score of greater than 0.75 indicates excellent agreement, between 0.4 and 0.75 good agreement and a score of less than 0.4, poor agreement (Coenraads, Van Der Walle et al. 2005, Zlobec, Steele et al. 2006). Intra-class correlation coefficient analysis was calculated using SPSS version 24. Very good correlation between scores was seen for LIMD1 staining, with an intra-class correlation coefficient of 0.743 for single measures, demonstrating that scoring was consistent and valid (**Figure 4.3**).

(i)

Case Processing Summary

		n	%
Cases	Valid	130	98.5
	Excluded	2	1.5
	Total	132	100.0

(ii)

Reliability Statistics

Cronbach's Alpha	Cronbach's Alpha Based on Standardized Items	n of Items
.852	.874	2

(iii)

Intra-class Correlation Coefficient

	Intra-class Correlation	95% Confidence Interval		F Test with True Value 0			
		Lower Bound	Upper Bound	Value	df1	df2	Sig
Single Measures	.743	.654	.811	6.770	129	129	.000
Average Measures	.852	.791	.896	6.770	129	129	.000

Figure 4.3 Very good intra-class correlation is observed for LIMD1 scoring

LIMD1 histospot staining was double scored by Dr Trevisan and myself. Staining was cytoplasmic. Histospots containing no tumour were excluded from analysis and only areas of tumour scored. A score for each histospot was generated incorporating overall staining and percentage of tumour staining positively. **(i)** Scoring by myself and Dr Trevisan was correlated with 130 valid cases included. **(ii)** Cronbach's alpha value was estimated at 0.874 suggesting very good internal consistency. **(iii)** The intra-class correlation coefficient for single measures was 0.852 for average measures, indicating very good agreement between scoring for each histospot.

4.5.2 Correlation of LIMD1 staining with tumour stage and grade

Tumour grade and tumour stage are validated prognostic indicators in ccRCC (Zisman, Pantuck et al. 2001). Spendlove *et al* had found that loss of nuclear LIMD1 staining strongly correlated with increasing tumour grade but no correlation with tumour stage was observed (Spendlove, Al-Attar et al. 2008). The association between LIMD1 staining and tumour grade and stage was characterised using the TMAs generated from the GSK study (Ravaud, Hawkins et al. 2008).

4.5.3 Tumour stage and grade do not correlate with LIMD1 staining pattern in ccRCC

Tumours were grouped in to those with absent or low LIMD1 staining and those with moderate or strong LIMD1 staining. Tumour grade did not correlate with LIMD1 staining, (X^2 test for trend p=0.658), and tumour stage did not correlate with LIMD1 staining (X^2 test for trend p=0.8492) (**Figure 4.4**)

A (i)

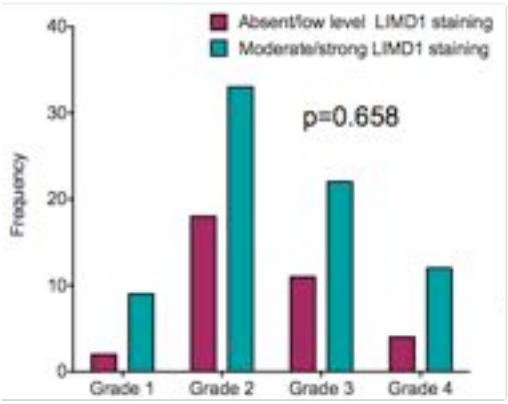

A(ii)

	No/low LIMD1 staining	Moderate/ strong LIMD1 staining
Grade 1	2/11 (18%)	9/11 (82%)
Grade 2	18/52 (35%)	33/51 (65%)
Grade 3	11/33 (33%)	22/33 (67%)
Grade 4	4/16 (25%)	12/16 (75%)

B (i)

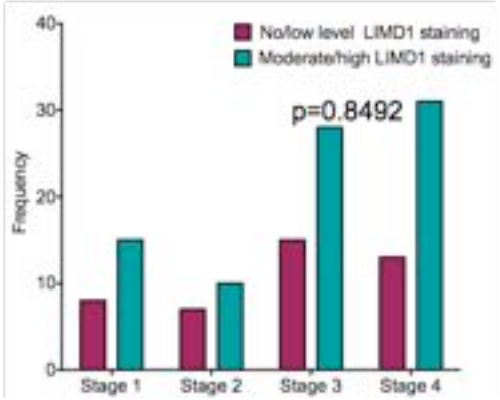

B (ii)

	No/low LIMD1 staining	Moderate/ strong LIMD1 staining
Stage 1	8/23 (35%)	15/23 (65%)
Stage 2	7/17 (41%)	10/17 (59%)
Stage 3	15/43 (35%)	28/43 (65%)
Stage 4	13/44 (30%)	31/44 (70%)

Figure 4.4 LIMD1 staining does not correlate with tumour stage and grade in ccRCC samples obtained from the GSK study

Tumours were divided in to those with no or low LIMD1 staining and those with moderate or high LIMD1 staining based on the mean staining intensity throughout the histospots derived from the same tumour. **A (i)** Bar chart illustrating the relative number of tumours with no/low LIMD1 staining versus those with moderate/high LIMD1 staining for each ccRCC tumour grade. **A (ii)** Table illustrates the relative frequency of no/low LIMD1 staining versus moderate/high LIMD1 staining for each ccRCC tumour grade. **B (i)** Bar chart illustrating the relative number of tumours with no/low LIMD1 staining versus those with moderate/high LIMD1 staining for each ccRCC tumour stage. **B (ii)** Table illustrates the relative frequency of no/low LIMD1 staining versus moderate/high LIMD1 staining for each ccRCC tumour stage. The χ^2 test for trend was calculated using Prism version 6

4.5.4 Low/absentLIMD1 staining does not correlate with overall survival

Next the relationship between LIMD1 staining and overall patient survival in the GSK cohort was examined. 28 results were censored, (patients lost to follow up or still alive at time of last follow up). Estimated median OS from start of trial commencement was 379 days with a range of 1 to 1396 days. Dr Shah Jalal of Barts Cancer Institute provided advice regarding the statistical analysis of data.

Absent/low LIMD1 staining did not correlate with OS in this cohort. The median estimated OS in patients with tumours with absent/low LIMD1 staining was 397 days compared to 351 days in patients with tumours with moderate/high LIMD1 staining (Log-rank p=0.264) (**Figure 4.5**).

(i)

Case Processing Summary

Kate LIMD1 1014 median	Total No	No. of Events	Censored	
			No.	Percent
.00	43	33	10	23.3%
1.00	87	69	18	20.7%
Overall	130	102	28	21.5%

(ii)

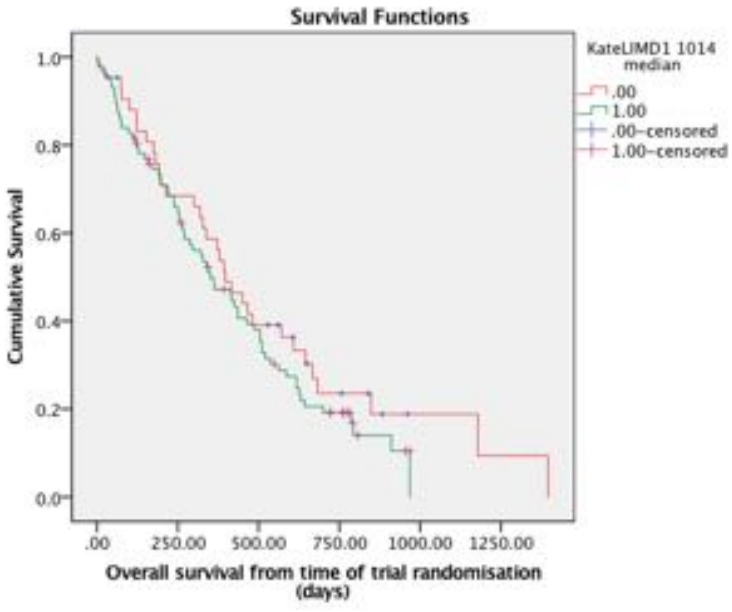

(iii)

Means and Medians for Survival Time

KateLIMD1 1014 median	Mean				Median			
			95% Confidence Interval				95% Confidence Interval	
	Estimate	Std. Error	Lower Bound	Upper Bound	Estimate	Std. Error	Lower Bound	Upper Bound
.00	534.997	70.618	396.586	673.407	397.000	49.816	299.361	494.639
1.00	419.128	33.518	353.432	484.824	351.000	57.205	238.877	463.123
Overall	467.009	36.463	395.542	538.476	379.000	35.832	308.769	449.231

(iv)

Overall Comparisons

	Chi-Square	df	Sig.
Log Rank (Mantel-Cox)	1.248	1	.264
Breslow (Generalized Wilcoxon)	.783	1	.376
Tarone-Ware	.902	1	.342

Figure 4.5 Loss of LIMD1 does not correlate with OS in ccRCC

Kaplan-Meier plot of cumulative OS in patients in the GSK cohort. OS is defined as time from randomisation to date of death or last follow up in the case of censored patients. **(i)** Summary of cases included in the analysis. **(ii)** Kaplan-Meier plots of cumulative OS in patients with ccRCC tumours with no/low total LIMD1 staining versus OS in patients with tumours with LIMD1 staining. **(iii)** Estimated

means and medians for survival time in the two groups. **(iv)** Comparison of cumulative OS with Log Rank, Breslow and Tarone-Ware Chi-Square test in the two groups. All analysis was undertaken using SPSS version 24.

4.5.5 Low/absent LIMD1 staining does not correlate with overall survival on multi-variate analysis

A Cox regression analysis was performed using SPSS Version 24. The regression model was adjusted for the validated MSKCC prognostic criteria, Karnofsky Performance status (KPS<80% or ≥80%), number of metastatic sites at screening (≤2 or >2), haemoglobin (<normal or ≥ normal), corrected serum calcium (≤10 or >10mg/dl), and age and sex which are not MSKCC prognostic criteria. These parameters were included as they were included in the initial trial Cox regression analysis (Ravaud, Hawkins et al. 2008). Information on tissue EGFR status and treatment randomisation to either lapatinib or hormone therapy was not available and therefore could not be included in the analysis. The adjusted multi-variate analysis demonstrated that absent/low LIMD1 staining was not associated with reduced OS, HR=0.911 (95% CI 0.561-1.481, p=0.708), however the validated prognostic indices of corrected calcium (HR 1.39, 95% CI 1.132-2.49, p=0.016*), number of metastatic sites (HR 2.036, 95% CI 1.239, p=0.005**) and haemoglobin (HR 1.965, 95% CI 1.218-3.175, p=0.006**) were statistically significant and correlated with worse OS as we would predict (**Figure 4.6**). This demonstrates the validity of the multivariate model used and analysis undertaken.

(i)

Omnibus Tests of Model Coefficients

-2 Log Likelihood	Overall (score)			Change From Previous Step			Change From Previous Block		
	Chi-square	df	Sig.	Chi-square	df	Sig.	Chi-square	df	Sig.
594.278	39.907	7	0.000	35.995	7	0.000	35.995	7	0.000

(ii)

Case Processing Summary

		N	Percent
Cases available in analysis	Event	82	62.1%
	Censored	22	16.7%
	Total	104	78.8%
Cases dropped	Cases with missing values	28	21.2%
	Cases with negative time	0	0.0%
	Censored cases before the earliest event in a stratum	0	0.0%
	Total	28	21.2%
Total		132	100.0%

(iii)

Risk Factor	Significance	Hazard Ratio (HR)	95% CI for HR (lower)	95% CI for HR (upper)
KPS (<80% versus > 80%)	0.052	1.866	0.993	3.506
No of metastatic sites (≤ 2versus >2)	0.005	2.036	1.239	3.355
Hb < N versus Hb> N	0.006	1.965	1.218	3.175
Corrected Ca ≤10 versus Ca >10	0.016	1.39	1.132	2.49
Age	0.070	1.026	1.027	0.998
Sex	0.523	0.840	0.492	1.434
No LIMD1 staining versus LIMD1 staining	0.708	0.911	0.561	1.481

Figure 4.6 Multi-variate Cox-regression analysis demonstrates that no/absent LIMD1 staining does not correlate with OS. There is a correlation between OS and number of metastatic sites, haemoglobin and corrected calcium.

Cox-regression analysis of OS in the GSK cohort was undertaken using SPSS version 24 to include LIMD1 staining, age, sex, KPS, number of metastatic sites, haemoglobin, and corrected calcium. **(i)** The omnibus test of model co-efficient was significant demonstrating that the new model offered an improvement over the old model **(ii)** Of the 132 patients, 104 had complete data available for all parameters and were therefore included in the analysis. **(iii)** Results of the Cox-regression analysis.

4.5.6 Low/absent LIMD1 staining does not correlate with PFS

The relationship between PFS and staining for LIMD1 was examined. PFS was defined as the time from randomisation to radiological or clinical progression as defined in the trial protocol (Ravaud, Hawkins et al. 2008). Median PFS for the cohort was 61 days with a range from 1 to 421 days. Absent/low LIMD1 staining did not correlate with PFS: estimated PFS was 67 days for patients with absent/low LIMD1 staining versus 61 days for patients with moderate/high LIMD1 staining (Log Rank (Mantel-Cox) p=0.281) (**Figure 4.7**).

(i)

Case Processing Summary

KateLIMD1 1014 median	Total n	n of Events	Censored	
			n	Percent
.00	43	43	0	0.0%
1.00	87	87	0	0.0%
Overall	130	130	0	0.0%

(ii)

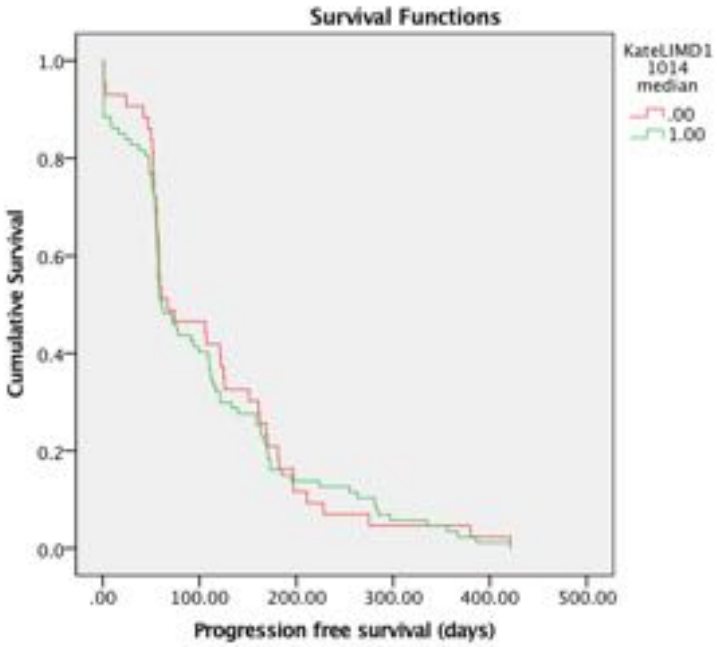

(iii)

Means and Medians for Survival Time

KateLIMD1 1014 median	Mean				Median			
			95% Confidence Interval				95% Confidence Interval	
	Estimate	Std. Error	Lower Bound	Upper Bound	Estimate	Std. Error	Lower Bound	Upper Bound
.00	113.488	14.120	85.813	141.164	67.000	31.467	5.324	128.676
1.00	107.989	10.604	87.205	128.772	61.000	9.845	41.704	80.296
Overall	109.808	8.467	93.213	126.403	61.000	7.042	47.197	74.803

(iv)

Overall Comparisons

	Chi-Square	df	Sig.
Log Rank (Mantel-Cox)	.115	1	.734
Breslow (Generalized Wilcoxon)	.437	1	.509
Tarone-Ware	.262	1	.609

Figure 4.7 Loss of LIMD1 does not correlate with PFS in ccRCC

Kaplan-Meier plot of cumulative PFS in patients in the GSK cohort. PFS is defined as time from date of randomisation to clinical or radiological progression. **(i)** Summary of cases included in the analysis **(ii)** Kaplan-Meier plots of cumulative PFS in patients with ccRCC tumours with no/low total LIMD1 staining versus PFS in patients with tumours with LIMD1 staining. **(iii)** Estimated means and medians for PFS in the two groups. **(iv)** Comparison of cumulative PFS with Log Rank, Breslow and Tarone-Ware Chi-Square test in the two groups. All analysis was undertaken using SPSS version 24.

4.5.7 Low/absent staining for LIMD1 is not statistically significant for PFS on multi-variate analysis

Multivariate Cox Regression analysis for PFS was undertaken. As before the regression model was adjusted for KPS (KPS<80% or ≥80%), number of metastatic sites at screening, haemoglobin (< normal or ≥ normal), corrected serum calcium (≤10 or >10mg/dl), age and sex. All patients had progressed at the cut off date for PFS analysis and 104 patients were included in the analysis with no cases censored. Low/absent LIMD1 staining was not associated with differences in PFS on multi-variate analysis (HR 1.179, 95% CI 0.765-1.818, p=0.457): increasing age was however associated with shorter PFS (HR 1.036, 95% CI 1.010-1.062, p=0.006*), although the other parameters included, KPS, corrected calcium, haemoglobin, number of metastatic sites and sex did not correlate (**Figure 4.8**). With the exception of sex and age these parameters, form part of the MSKCC score, a predictor of OS but not PFS and are not validated prognostic factors for PFS.

(i)

Omnibus Tests of Model Coefficients

-2 Log Likelihood	Overall (score)			Change From Previous Step			Change From Previous Block		
	Chi-square	df	Sig.	Chi-square	df	Sig.	Chi-square	df	Sig.
748.826	19.288	7	.007	18.007	7	.012	18.007	7	.012

(ii)

Case Processing Summary

		N	Percent
Cases available in analysis	Event	104	78.2%
	Censored	0	0.0%
	Total	104	78.2%
Cases dropped	Cases with missing values	29	21.8%
	Cases with negative time	0	0.0%
	Censored cases before the earliest event in a stratum	0	0.0%
	Total	29	21.8%
Total		133	100.0%

(iii)

Risk Factor	Significance	Hazard Ratio (HR)	95% CI for HR (lower)	95% CI for HR (upper)
KPS (<80% versus >80%)	0.154	1.569	0.845	2.913
No of metastatic sites (≤2 versus>2)	0.598	1.129	0.719	1.773
Hb <N versus Hb>N	0.379	1.149	1.912	1.353
Corrected Ca ≤10 versus Ca>10	0.043	1.655	1.015	2.702
Age	0.006	1.036	1.010	1.062
Sex	0.435	1.214	0.745	1.972
No/low LIMD1 staining versus moderate/high LIMD1 staining	0.457	1.179	0.765	1.818

Figure 4.8 Multi-variate Cox-regression analysis demonstrates that no/absent LIMD1 staining does not correlate with PFS. There is a correlation between age and PFS

Cox-regression analysis of PFS in the GSK cohort was undertaken using SPSS version 24 to include LIMD1 staining, age, sex, KPS, number of metastatic sites, haemoglobin, and corrected calcium. **(i)** The omnibus test of model co-efficient was significant demonstrating that the new model offered an improvement over the old model **(ii)** Of the 132 patients, 104 had complete data available for all parameters and were therefore included in the analysis. **(iii)** Results of the Cox-regression analysis.

4.6 Validation of LIMD1 staining and correlation with clinico-pathological outcome data in a further cohort of patients.

LIMD1 staining and its correlation with OS and PFS was validated by staining TMAs containing tumour samples generated from a clinical trial evaluating the role of upfront pazopanib prior to nephrectomy in mccRCC (Powles, Sarwar et al. 2016). This cohort of patients differed from those in the GSK cohort, as all patients received an upfront TKI. Histospots of 2mm derived from the same tumour were represented on the TMAs in duplicate, although for some tumours histospots were missing. The TMAs containing biopsy samples were of very poor quality as little tissue was left after staining the TMA blocks as part of the clinical trial protocol and therefore could not be used for IHC.

63 of the 100 patients evaluable for the clinical benefit of pazopanib underwent nephrectomy and patients with missing tumour samples or no tumour represented on the histospots were excluded, which left 56 tumours evaluable for IHC. Staining was undertaken as for the GSK cohort, with controls included as before and an identical scoring system used as for that described in the GSK cohort. Staining was reviewed by Professor Michael Sheaff of Barts Health NHS Trust and established to be specific and valid for analysis. Dr. Scott Shepherd and myself double scored all TMAs. The intraclass correlation coefficient for single measures was excellent at 0.834, demonstrating that the scoring system was again reliable and reproducible.

4.6.1 Correlation of LIMD1 staining and OS and PFS in the PANTHER cohort

Correlation of LIMD1 staining and OS in the PANTHER cohort, validated the findings of the GSK cohort, with no association between LIMD1 staining and OS demonstrated (Log Rank test p=0.541) (**Figure 4.9**). A similar result was obtained when LIMD1 staining and PFS was correlated in the PANTHER cohort (Log Rank test p=0.541) (**Figure 4.10**)

(i)

Case Processing Summary

LIMD1 cut off <100 versus >100	Total N	N of Events	Censored	
			N	Percent
.00	35	27	8	22.9%
1.00	21	15	6	28.6%
Overall	56	42	14	25.0%

(ii)

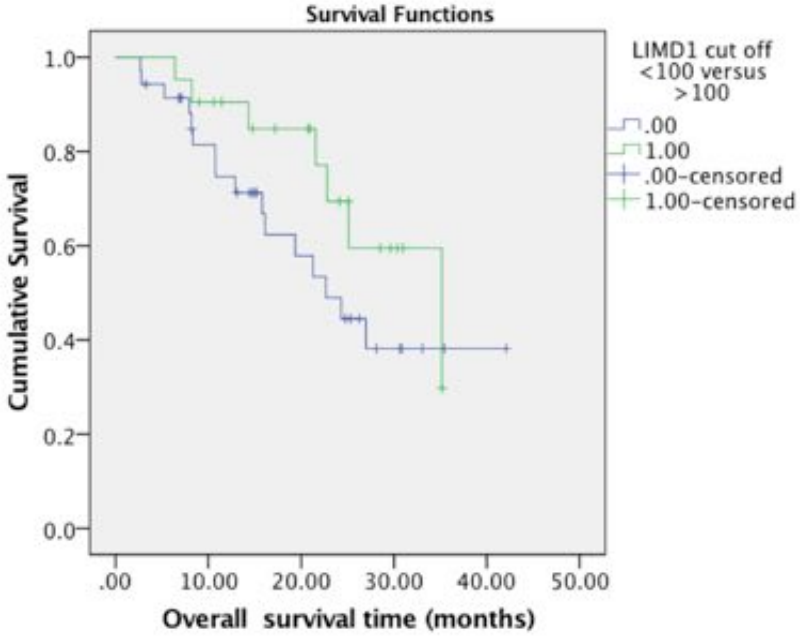

(iii)

Means and Medians for Survival Time

LIMD1 cut off <100 versus >100	Mean				Median			
			95% Confidence Interval				95% Confidence Interval	
	Estimate	Std. Error	Lower Bound	Upper Bound	Estimate	Std. Error	Lower Bound	Upper Bound
.00	25.379	2.807	19.877	30.882	22.675	3.707	15.409	29.941
1.00	28.343	2.297	23.840	32.846	35.163	7.479	20.503	49.822
Overall	27.431	2.144	23.229	31.633	26.980	4.686	17.796	36.164

(iv)

Overall Comparisons

	Chi-Square	df	Sig.
Log Rank (Mantel-Cox)	.541	1	.462
Breslow (Generalized Wilcoxon)	1.579	1	.209
Tarone-Ware	1.142	1	.285

Figure 4.9 Loss of LIMD1 does not correlate with OS in ccRCC

Kaplan-Meier plot of cumulative OS in patients in the PANTHER cohort. OS is defined as time from randomisation to date of death or last follow up in the case of censored patients. **(i)** Summary of cases included in the analysis **(ii)** Kaplan-Meier plots of cumulative OS in patients with ccRCC tumours with no/low total LIMD1 staining versus OS in patients with tumours with LIMD1 staining, **(iii)** Estimated means and medians for survival time in the two groups. **(iv)** Comparison of cumulative OS with Log Rank, Breslow and Tarone-Ware Chi-Square test in the two groups. All analysis was undertaken using SPSS version 24.

(i)

Case Processing Summary

LIMD1 cut off <100 versus >100	Total N	N of Events	Censored	
			N	Percent
.00	35	27	8	22.9%
1.00	21	15	6	28.6%
Overall	56	42	14	25.0%

(ii)

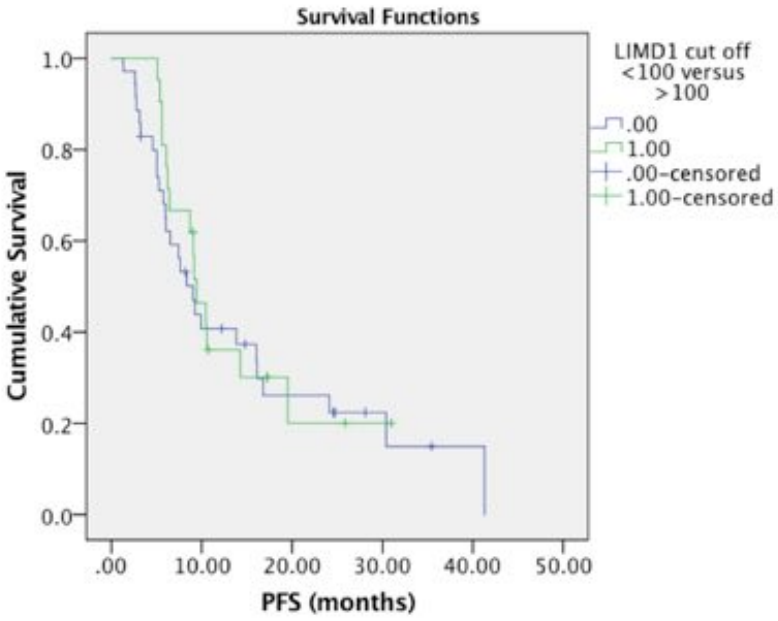

(iii)

Means and Medians for Survival Time

LIMD1 cut off <100 versus >100	Mean				Median			
			95% Confidence Interval				95% Confidence Interval	
	Estimate	Std. Error	Lower Bound	Upper Bound	Estimate	Std. Error	Lower Bound	Upper Bound
.00	14.980	2.481	10.116	19.843	9.004	1.260	6.535	11.474
1.00	13.877	2.233	9.501	18.253	9.399	.989	7.460	11.338
Overall	15.419	1.966	11.565	19.273	9.136	.637	7.887	10.384

(iv)

Overall Comparisons

	Chi-Square	df	Sig.
Log Rank (Mantel-Cox)	.541	1	.462
Breslow (Generalized Wilcoxon)	1.579	1	.209
Tarone-Ware	1.142	1	.285

Figure 4.10 Loss of LIMD1 does not correlate with PFS in ccRCC

Kaplan-Meier plot of cumulative PFS in patients in the PANTHER cohort. PFS is defined as time from randomisation to date of death or last follow up in the case of censored patients. **(i)** Summary of cases included in the analysis **(ii)** Kaplan-Meier plots of cumulative PFS in patients with ccRCC tumours with no/low total LIMD1 staining versus OS in patients with tumours with LIMD1 staining, **(iii)** Estimated means and medians for survival time in the two groups. **(iv)** Comparison of cumulative PFS with Log Rank, Breslow and Tarone-Ware Chi-Square test in the two groups. All analysis was undertaken using SPSS version 24.

4.7 Correlation of Ajuba expression with clinico-pathological indices

The association between Ajuba staining and clinico-pathological outcome data was characterised using the TMAs generated from the GSK study (Ravaud, Hawkins et al. 2008) Staining patterns were as described previously in control tissue TMAs and in healthy renal tissue and ccRCC. Staining in ccRCC tissue was predominantly nuclear with some limited cytoplasmic staining (**Figure 4.11**). As before, a TMA consisting of histospots derived from a range of pre-invasive/invasive tumours were included as positive/negative control and stomach tissue as a further positive control when staining the GSK trial TMAs. Primary antibody was omitted from one of the TMA slides as a further negative control. Professor Mike Sheaff reviewed all staining, which he felt to be specific and agreed that the optimum antibody concentration for the TMA staining was as before 1:50. As before, only nuclear staining was scored and the TMAs were double scored by Dr Scott Shepherd and myself, blinded to each others scoring and clinico-pathological outcome data, although agreement on how scoring should be undertaken had been reached. Histospots without any tumour were excluded and a score for each tumour generated based on the mean staining score for histospots from the same tumour as a function of the percentage of positively staining tumour cells and the intensity of nuclear staining (scored as before from 0-3) throughout the histospot. Such a system was used in preference to the ARIOL automated system to ensure consistency with the LIMD1 scoring.

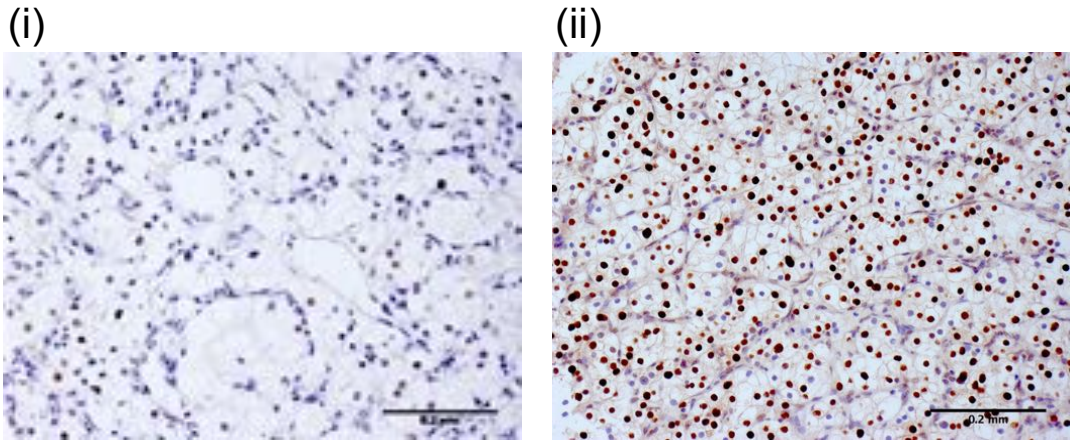

Figure 4.11 IHC staining of tumour histospots for Ajuba

TMA histospots derived from a phase II clinical trial were stained immunohistochemically for Ajuba using an optimised manual staining protocol and Ajuba antibody concentration 1:50. Histospots were represented on the TMAs in triplicate. **(i)** Low level nuclear Ajuba staining **(ii)** High level nuclear Ajuba staining. Scale bar shown for size comparison

4.7.1 Intra-class correlation coefficient analysis to assess inter-observer scoring agreement for Ajuba

The intra-class correlation coefficient analysis was calculated to assess the inter-observer scoring agreement for Ajuba. Excellent intra-class correlation of 0.943 for single measures between the two scorers was observed (**Figure 4.12**), suggesting that scoring was robust and reproducible.

(i)

Case Processing Summary

		n	%
Cases	Valid	103	100
	Excluded	0	0
	Total	103	100.0

(ii)

Reliability Statistics

Cronbach's Alpha	Cronbach's Alpha Based on Standardized Items	N of Items
.967	.967	2

(iii)

Intra-class Correlation Coefficient

	Intra-class Correlation	95% Confidence Interval		F Test with True Value 0			
		Lower Bound	Upper Bound	Value	df1	df2	Sig
Single Measures	.935	.906	.956	29.911	102	102	.000
Average Measures	.967	.951	.977	29.911	102	102	.000

Figure 4.12 Excellent intra-class correlation is observed for Ajuba scoring in the GSK TMA histospots

Ajuba histospot staining was double scored by Dr Scott Shepherd and by myself. Staining was predominantly nuclear and only nuclear staining scored. Histospots containing no tumour were excluded from analysis and only areas of tumour scored. Appropriate positive and negative controls were included. Both the proportion of positively staining tumour cells and intensity of nuclear staining was scored and a score generated by multiplying the intensity of staining by the percentage of tumour cells with positive staining. **(i)** Scoring undertaken by Dr Shepherd and myself was correlated with 103 valid cases included. **(ii)** Cronbach's alpha value was estimated at 0.964 suggesting excellent internal consistency. **(iii)** The intra-class correlation coefficient was 0.967 for average measures, indicating excellent agreement between both scorers.

4.7.2 Correlation of Ajuba staining with tumour stage and grade

Next the relationship between Ajuba staining and tumour stage and grade was examined Tumours were sub-divided into those with absent or low Ajuba staining (mean histospot score≤100) versus those with moderate or high Ajuba staining (mean histospot score >100). Analysis using alternative cutoffs for high versus low staining, e.g. score less than the median versus score greater than the median did not change the outcome of statistical analysis, including OS and PFS analysis and therefore to ensure consistency with the LIMD1 data, this cutoff was chosen. Tumour grade did not correlate with Ajuba staining, (X^2 test for trend p=0.785), however tumour stage did correlate with Ajuba staining (X^2 test for trend p=0.037*), with a significantly greater

proportion of stage 4 tumours (75%) demonstrating reduced Ajuba staining compared to stage 1 tumours (40%) (**Figure 4.13**).

A(i)

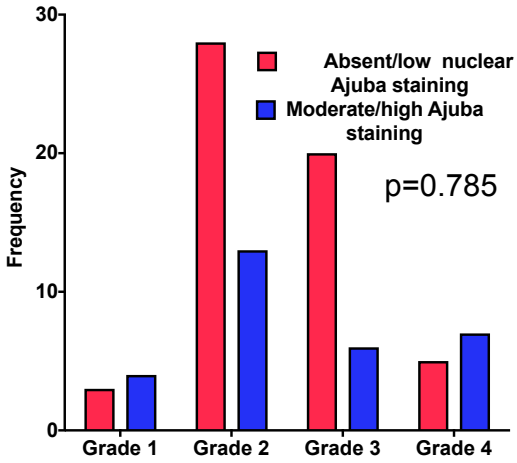

A(ii)

	Absent/low Ajuba staining	Moderate/high Ajuba staining
Grade 1	3/7 (43%)	4/7 (53%)
Grade 2	28/41 (68%)	13/41 (32%)
Grade 3	20/26 (77%)	6/26 (23%)
Grade 4	5/12 (42%)	7/12 (58%)

B(i)

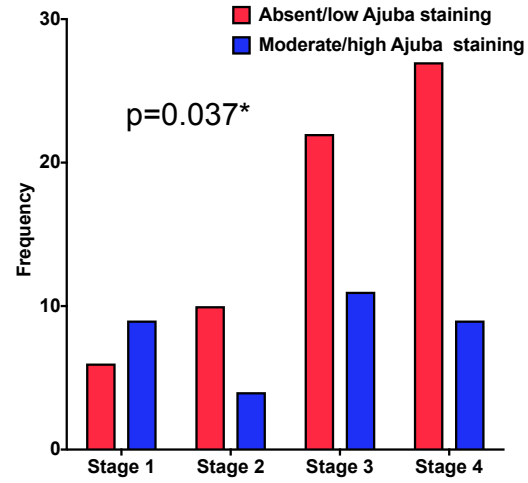

B(ii)

	Absent/low Ajuba staining	Moderate/high Ajuba staining
Stage 1	6/15 (40%)	9/15 (60%)
Stage 2	10/14 (71%)	4/14 (29%)
Stage 3	22/33 (67%)	11/33 (33%)
Stage 4	27/36 (75%)	9/36 (25%)

Figure 4.13 Ajuba staining correlates with tumour stage but not grade in ccRCC samples obtained from the GSK study

Tumours were divided in to those with no or low Ajuba staining and those with moderate or high Ajuba staining based on the mean staining intensity throughout the histospots derived from the same tumour. **A (i)** Bar chart illustrating the relative number of tumours with no/low Ajuba staining versus those with moderate/high Ajuba staining for each ccRCC tumour grade. **A (ii)** Table illustrates the relative frequency of no/low Ajuba staining versus moderate/high Ajuba staining for each ccRCC tumour grade. **B (i)** Bar chart illustrating the relative number of tumours with no/low Ajuba staining versus those with moderate/high Ajuba staining for each ccRCC tumour stage. **B (ii)** Table illustrates the relative frequency of no/low Ajuba staining versus moderate/high Ajuba staining for each ccRCC tumour stage. The χ^2 test for trend was calculated using Prism version 6

4.7.3 Ajuba staining does not correlate with OS

Univariate analysis was undertaken dividing tumours using the cutoffs described. A total of 100 patients were included in the analysis, 21 results were censored, (patients lost to follow up or still alive at time of last follow up).

Absent/low Ajuba staining did not correlate with OS in the GSK cohort. The median estimated OS in patients with tumours with absent/low Ajuba staining was 345 days compared to 379 days in patients with tumours with moderate/high Ajuba staining (Log-rank p=0.480) (**Figure 4.14**).

(i)

Case Processing Summary

Ajuba nuclear staining	Total n	n of Events	Censored	
			n	Percent
.00	66	51	15	22.7%
1.00	34	28	6	17.6%
Overall	100	79	21	21.0%

(ii)

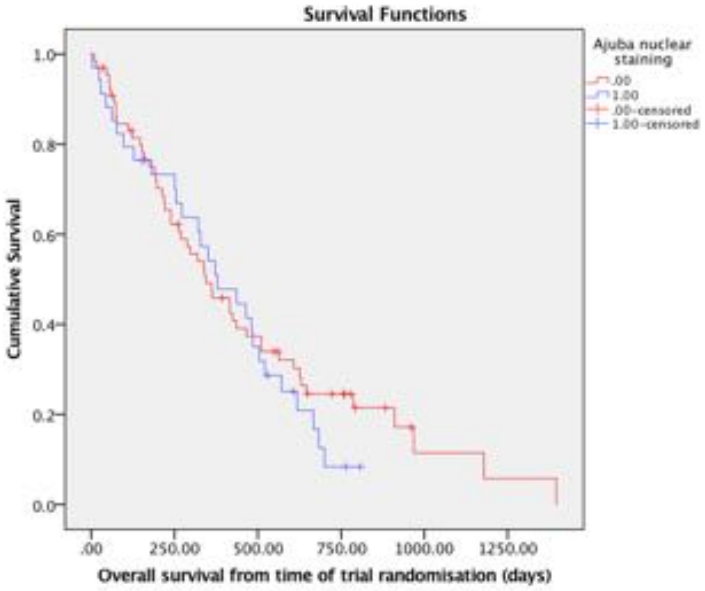

(iii)

Means and Medians for Survival Time

Ajuba nuclear staining	Mean				Median			
			95% Confidence Interval				95% Confidence Interval	
	Estimate	Std. Error	Lower Bound	Upper Bound	Estimate	Std. Error	Lower Bound	Upper Bound
.00	479.613	54.074	373.629	585.597	345.000	56.975	233.330	456.670
1.00	391.737	42.994	307.470	476.004	379.000	74.733	232.523	525.477
Overall	458.648	41.226	377.845	539.451	362.000	41.655	280.356	443.644

(iv)

Overall Comparisons

	Chi-Square	df	Sig.
Log Rank (Mantel-Cox)	.499	1	.480
Breslow (Generalized Wilcoxon)	.022	1	.883
Tarone-Ware	.124	1	.725

Figure 4.14 Loss of Ajuba does not correlate with OS in ccRCC

Kaplan-Meier plot of cumulative OS in patients in the GSK cohort. OS is defined as the time from randomisation to date of death or last follow up in the case of censored patients. **(i)** Summary of cases included in the analysis **(ii)** Kaplan-Meier plots of cumulative OS in patients with ccRCC tumours with absent/low versus moderate/high Ajuba staining **(iii)** Estimated means and medians for survival time in the two groups. **(iv)** Comparison of cumulative OS with Log Rank, Breslow and Tarone-Ware Chi-Square test in the two groups. All analysis was undertaken using SPSS version 24.

4.7.4 On multi-variate analysis, low/absent Ajuba staining does not correlate with overall survival

As before multivariate Cox regression analysis adjusting the regression model for KPS (KPS<80% or ≥80%), number of metastatic sites at screening (≤2 versus ≥2), haemoglobin (<normal/≥ normal), corrected serum calcium (≤10 or >10mg/dl), age and sex was undertaken. The adjusted multi-variate analysis demonstrated that loss of total staining for Ajuba was not statistically significant HR=1.373 (95% CI 0.774-2.435, p=0.279), however the validated prognostic markers of KPS (HR=3.804 (95% CI 1.817-7.963, p=<0.0001***), corrected calcium ((HR=1.931, (95% CI 1.070-4.553) p=0.029*), number of metastatic sites (HR=2.183, (95% CI 1.254-3.802, p=0.006*) were statistically significant and correlated as we would predict with worse OS (**Figure 4.15**). This demonstrates the validity of the multivariate model and statistical analysis.

(i)

Omnibus Tests of Model Coefficients

-2 Log Likelihood	Overall (score)			Change From Previous Step			Change From Previous Block		
	Chi-square	df	Sig.	Chi-square	df	Sig.	Chi-square	df	Sig.
437.230	40.628	7	.000	32.695	7	.000	32.695	7	.000

(ii)

Case Processing Summary

		N	Percent
Cases available in analysis	Event	65	48.9%
	Censored	18	13.5%
	Total	83	62.4%
Cases dropped	Cases with missing values	50	37.6%
	Cases with negative time	0	0.0%
	Censored cases before the earliest event in a stratum	0	0.0%
	Total	50	37.6%
Total		133	100.0%

(iii)

Risk Factor	Significance	Hazard Ratio (HR)	95% CI for HR (lower)	95% CI for HR (upper)
KPS (<80% versus >80%)	<0.0001	3.804	1.817	7.963
No of metastatic sites (>2 versus ≤2)	0.006	2.183	1.254	3.802
Hb <N versus Hb>N	0.056	1.681	0.987	2.857
Corrected Ca >10 versus ≤10	0.029	1.931	1.070	4.553
Age	0.100	1.029	0.995	1.064
Sex	0.779	1.092	0.494	1.697
No/low Ajuba staining versus moderate/high Ajuba staining	0.279	1.373	0.774	2.435

Figure 4.15 Multi-variate Cox-regression analysis demonstrates that no/absent Ajuba staining does not correlate with OS. There is a correlation between OS and number of metastatic sites, KPS, and corrected calcium.

Cox-regression analysis of OS in the GSK cohort was undertaken using SPSS version 24 to include nuclear Ajuba staining, age and sex and KPS, number of metastatic sites, haemoglobin and corrected calcium **(i)** The omnibus test of model co-efficient was significant demonstrating that the new model offered an improvement over the old model **(ii)** Of the 133 patients, 83 had complete data for all parameters and were therefore included in the analysis. (**iii)** Results of the Cox-regression analysis.

4.7.5 Ajuba staining does not correlate with PFS

The relationship between PFS and staining for Ajuba was examined. Absent/low Ajuba staining does not correlate with PFS with an estimated PFS of 59 days versus 72 days for patients with moderate/high Ajuba staining in the GSK cohort (Log Rank (Mantel-Cox) p=0.367) (**Figure 4.16**).

(i)

Case Processing Summary

Ajuba nuclear staining	Total n	n of Events	Censored	
			n	Percent
.00	66	66	0	0.0%
1.00	34	34	0	0.0%
Overall	100	100	0	0.0%

(ii)

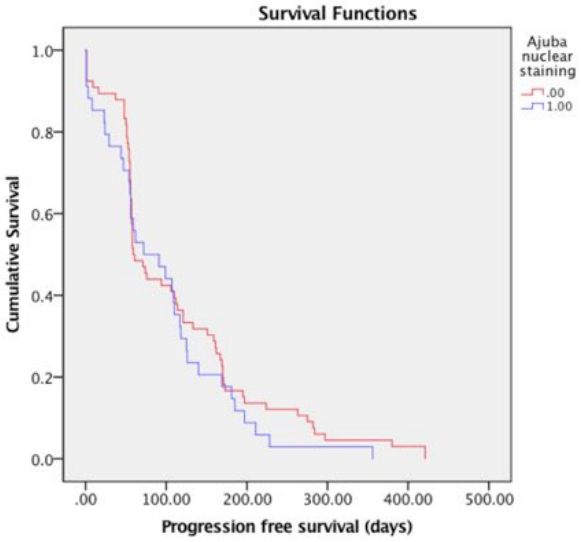

(iii)

Means and Medians for Survival Time

Ajuba nuclear staining	Mean				Median			
			95% Confidence Interval				95% Confidence Interval	
	Estimate	Std. Error	Lower Bound	Upper Bound	Estimate	Std. Error	Lower Bound	Upper Bound
.00	113.833	12.198	89.926	137.741	59.000	8.575	42.192	75.808
1.00	96.000	13.595	69.354	122.646	72.000	29.155	14.857	129.143
Overall	107.770	9.281	89.579	125.961	62.000	13.077	36.369	87.631

(iv)

Overall Comparisons

	Chi-Square	df	Sig.
Log Rank (Mantel-Cox)	.812	1	.367
Breslow (Generalized Wilcoxon)	.345	1	.557
Tarone-Ware	.466	1	.495

Figure 4.16 Loss of Ajuba does not correlate with PFS in ccRCC

Kaplan-Meier plot of cumulative PFS in patients in the GSK cohort. PFS is defined as the time from randomisation to date of death or last follow up in the case of censored patients. **(i)** Summary of cases included in the analysis **(ii)** Kaplan-Meier plots of cumulative PFS in patients with ccRCC tumours with absent/low versus moderate/high Ajuba staining **(iii)** Estimated means and medians for survival time in the two groups. **(iv)** Comparison of cumulative PFS with Log Rank, Breslow and Tarone-Ware Chi-Square test in the two groups. All analysis was undertaken using SPSS version 24.

4.7.6 Low/absent staining for Ajuba is not statistically significant for PFS on multi-variate analysis

Again multivariate Cox Regression analysis for PFS adjusting the regression model for the parameters previously described was undertaken. All patients had progressed at the cut-off date for PFS analysis and 83 patients were included in each analysis with no cases censored. Low/absent Ajuba staining was not statistically significant on multi-variate analysis for PFS (HR 1.062, 95% CI 0.642-1.754, p=0.815). Increasing age and elevated corrected calcium were associated with shorter PFS, HR 1.049, 95% CI 1.019-1.080 p=0.001**, and HR 1.730, 95% CI 1.008-2.976, p=0.047* respectively. KPS, haemoglobin, the number of metastatic sites and sex did not correlate with PFS (**Figure 4.17**)

(i)

Omnibus Tests of Model Coefficients

-2 Log Likelihood	Overall (score)			Change From Previous Step			Change From Previous Block		
	Chi-square	df	Sig.	Chi-square	df	Sig.	Chi-square	df	Sig.
551.777	27.335	7	.000	23.909	7	.001	23.909	7	.001

(ii)

Case Processing Summary

		n	Percent
Cases available in analysis	Event	83	62.4%
	Censored	0	0.0%
	Total	83	62.4%
Cases dropped	Cases with missing values	50	37.6%
	Cases with negative time	0	0.0%
	Censored cases before the earliest event in a stratum	0	0.0%
	Total	50	37.6%
Total		133	100.0%

(iii)

Risk Factor	Significance	Hazard Ratio (HR)	95% CI for HR (lower)	95% CI for HR (upper)
KPS (<80% versus >80%)	0.051	2.041	0.996	4.183
No of metastatic sites (>2 versus ≤2)	0.275	0.801	0.801	2.980
Hb <N versus Hb>N	0.216	1.359	0.836	2.210
Corrected Ca >10 versus ≤10	0.047	1.730	1.008	2.976
Age	0.001	1.049	1.019	1.080
Sex	0.641	1.138	0.661	1.960
No/low Ajuba staining versus moderate/high Ajuba staining	0.815	1.062	0.642	1.754

Figure 4.17 Multi-variate Cox-regression analysis demonstrates that no/absent Ajuba staining does not correlate with PFS. There is a correlation between age and PFS

Cox-regression analysis of PFS in the GSK cohort was undertaken using SPSS version 24 to include Ajuba nuclear staining, age and sex and KPS, number of metastatic sites, haemoglobin, and corrected calcium. **(i)** The omnibus test of model co-efficient was significant demonstrating that the new model offered an improvement over the old model **(ii)** Of the 132 patients, 83 had complete data available for all parameters and were therefore included in the analysis **(iii)** Results of the Cox-regression analysis.

4.8 Correlation of WTIP expression with clinico-pathological indices

WTIP staining was correlated with clinico-pathological outcome data using the TMAs generated from the GSK trial. Staining patterns were as described previously with both nuclear and cytoplasmic staining observed (**Figure 4.18**). As before, a TMA consisting of histospots derived from a range of pre-invasive/invasive tumours were included as positive/negative control as well as gastric tissue as a further positive control. Primary antibody was omitted from one of the TMA as a further negative control. All staining was reviewed by Professor Sheaff who felt that staining appeared specific and agreed that the optimal antibody concentration was as before 1:100. TMAs were double scored by Dr Scott Shepherd and myself, blinded to each others scoring and clinico-pathological outcome data, although agreement on how scoring should be undertaken had been reached. Histospots without any tumour were excluded and a score for each tumour generated based on the mean staining score for histospots from the same tumour as a function of the percentage of positively staining tumour cells and the intensity of nuclear staining (scored as before from 0-3) throughout the histospot. Separate scoring of both the nuclear and cytoplasmic compartments was undertaken. Again, such a system was used in preference to the Ariol automated system to ensure consistency with the LIMD1 and Ajuba scoring.

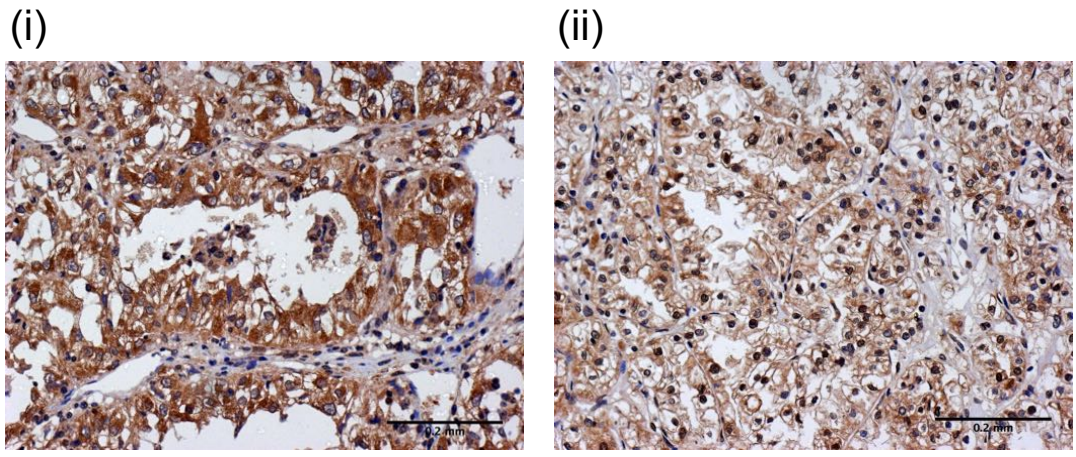

Figure 4.18 IHC staining of tumour histospots for WTIP

TMA histospots derived from a phase II clinical trial (GSK trial) were stained immunohistochemically for WTIP using an optimised manual staining protocol and WTIP antibody concentration 1:100. Histospots were represented on the TMAs in triplicate. **(i)** Strong cytoplasmic staining for WTIP in ccRCC histospot **(ii)** Strong nuclear WTIP staining in ccRCC histospot. Scale bar corresponding to 200μm is shown for size comparison.

4.8.1 Intra-class correlation coefficient analysis to assess inter-observer scoring agreement for WTIP

Intra-class correlation coefficient analysis to assess inter-observer scoring agreement for WTIP was undertaken. Excellent intra-class correlation of 0.972 for single measures between the two scorers for cytoplasmic staining was observed (**Figure 4.19A**) suggesting that scoring was robust and reproducible.

A (i)

Case Processing Summary

		N	%
Cases	Valid	81	100.0
	Excluded	0	.0
	Total	81	100.0

(ii)

Reliability Statistics

Cronbach's Alpha	N of Items
.986	2

(iii)

Intraclass Correlation Coefficient

	Intraclass Correlation	95% Confidence Interval		F Test with True Value 0			
		Lower Bound	Upper Bound	Value	df1	df2	Sig
Single Measures	.972	.957	.982	70.060	80	80	.000
Average Measures	.986	.978	.991	70.060	80	80	.000

B(i)

Case Processing Summary

		N	%
Cases	Valid	81	100.0
	Excluded	0	.0
	Total	81	100.0

(ii)

Reliability Statistics

Cronbach's Alpha	N of Items
.985	2

(iii)

Intraclass Correlation Coefficient

	Intraclass Correlation	95% Confidence Interval		F Test with True Value 0			
		Lower Bound	Upper Bound	Value	df1	df2	Sig
Single Measures	.961	.913	.980	64.744	79	79	.000
Average Measures	.980	.955	.990	64.744	79	79	.000

Figure 4.19 Excellent intra-class correlation is observed for WTIP scoring in the GSK TMA histospots

WTIP histospot staining was double scored by Dr Scott Shepherd and by myself, after review by Professor Sheath. Histospots containing no tumour were excluded from analysis and only areas of tumour scored. Appropriate positive and negative controls were included. Both the proportion of positively staining tumour cells and intensity of nuclear staining was scored and a score generated by multiplying the intensity of staining by the percentage of tumour cells with positive staining. **(i)** Scoring undertaken by Dr Shepherd and myself was correlated with 81 valid cases included. **(ii)** Cronbach's alpha value was estimated at 0.986 and 0.985 for cytoplasmic and nuclear staining respectively suggesting excellent internal consistency. **(iii)** The intra-class correlation coefficient for average measures was 0.986 and 0.980, respectively for cytoplasmic and nuclear staining respectively indicating excellent agreement between scoring.

4.8.2 WTIP staining and correlation with overall survival

Next the relationship between WTIP staining and overall patient survival was examined. A mean score for nuclear and cytoplasmic staining in each tumour based on the mean score throughout the histospots derived from the same tumour was calculated. Tumours were sub-divided into those with absent/low WTIP staining (score ≤100) versus those with moderate/high nuclear WTIP staining (score >100). Again, analysis using alternative cutoffs for high versus low staining, e.g. score less than the median versus score greater than the median did not change the outcome of statistical analysis and to ensure consistency with the LIMD1 and WTIP data, univariate analysis was undertaken subdividing tumours using these cutoffs.

For the cytoplasmic staining, a total of 97 patients were included in the analysis, 22 results were censored, (patients lost to follow up or still alive at time of last follow up).

Absent/low cytoplasmic WTIP staining did not correlate with OS in the GSK cohort. The median estimated OS in patients with tumours with absent/low cytoplasmic WTIP staining was 322 days compared to 362 days in patients with tumours with moderate/high WTIP staining (Log-rank p=0.138) (**Figure 4.20**). For nuclear WTIP staining, the median estimated OS in patients with tumours with absent/low cytoplasmic WTIP staining was 362 days compared to 338 days in patients with tumours with moderate/high nuclear WTIP staining (log-rank p=0.453) (**Figure 4.21**).

(i)

Case Processing Summary

WTIP 0-1 versus>1	Total n	n of Events	Censored	
			n	Percent
.00	31	21	10	32.3%
1.00	66	54	12	18.2%
Overall	97	75	22	22.7%

(ii)

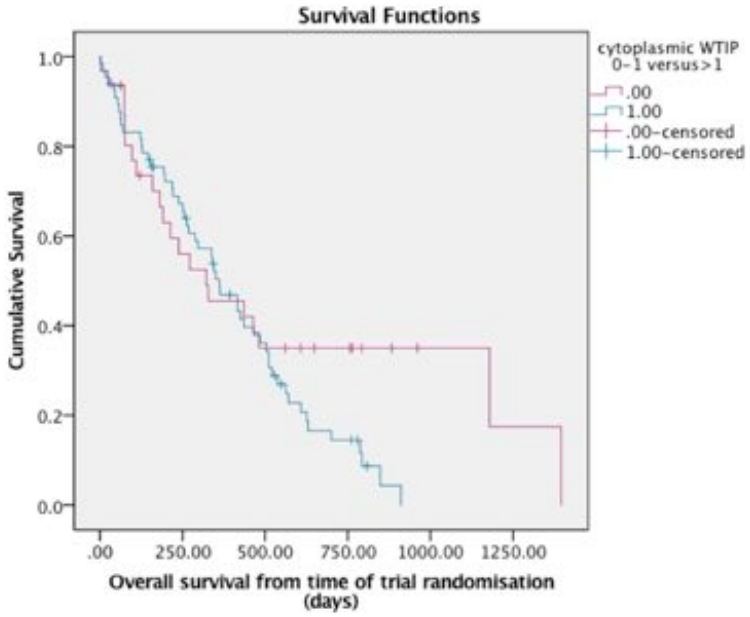

(iii)

Means and Medians for Survival Time

Cytoplasmic WTIP 0-1 versus>1	Mean				Median			
			95% Confidence Interval				95% Confidence Interval	
	Estimate	Std. Error	Lower Bound	Upper Bound	Estimate	Std. Error	Lower Bound	Upper Bound
.00	583.463	104.283	379.067	787.858	322.000	130.413	66.390	577.610
1.00	392.138	33.946	325.604	458.673	362.000	40.773	282.085	441.915
Overall	451.299	43.281	366.468	536.130	351.000	53.988	245.184	456.816

(iv)

Overall Comparisons

	Chi-Square	df	Sig.
Log Rank (Mantel-Cox)	2.198	1	.138
Breslow (Generalized Wilcoxon)	.012	1	.913
Tarone-Ware	.358	1	.550

Figure 4.20 Loss of cytoplasmic WTIP does not correlate with OS in ccRCC

Kaplan-Meier plot of cumulative OS in patients in the GSK cohort. OS is defined as the time from randomisation to date of death or last follow up in the case of censored patients. **(i)** Summary of cases included in the analysis **(ii)** Kaplan-Meier plots of cumulative OS in patients with ccRCC tumours with absent/low versus moderate/high WTIP staining **(iii)** Estimated means and medians for survival time in the two groups. **(iv)** Comparison of cumulative OS with Log Rank, Breslow and Tarone-Ware Chi-Square test in the two groups. All analysis was undertaken using SPSS version 24.

(i)

Case Processing Summary

Nuclear WTIP 0 versus 1	Total n	n of Events	Censored	
			n	Percent
.00	58	46	12	20.7%
1.00	36	27	9	25.0%
Overall	94	73	21	22.3%

(ii)

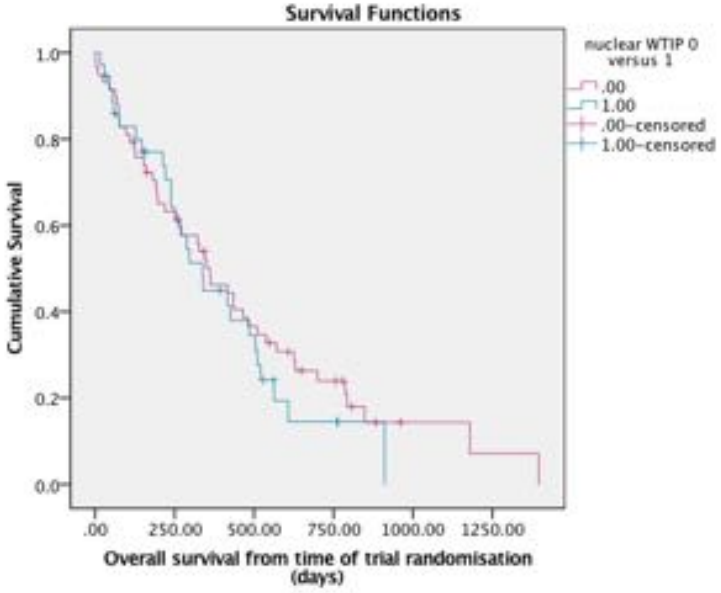

(iii)

Means and Medians for Survival Time

Nuclear WTIP 0 versus 1	Mean				Median			
			95% Confidence Interval				95% Confidence Interval	
	Estimate	Std. Error	Lower Bound	Upper Bound	Estimate	Std. Error	Lower Bound	Upper Bound
.00	474.780	58.540	360.041	589.519	362.000	55.070	254.063	469.937
1.00	390.244	49.988	292.267	488.221	338.000	48.836	242.282	433.718
Overall	447.377	43.346	362.419	532.335	345.000	52.965	241.188	448.812

(iv)

Overall Comparisons

	Chi-Square	df	Sig.
Log Rank (Mantel-Cox)	.562	1	.453
Breslow (Generalized Wilcoxon)	.050	1	.822
Tarone-Ware	.199	1	.655

Figure 4.21 Loss of nuclear WTIP does not correlate with OS in ccRCC

Kaplan-Meier plot of cumulative OS in patients in the GSK cohort. OS is defined as time from randomisation to death or date of last follow up in the case of censored patients. **(i)** Summary of cases included in the analysis **(ii)** Kaplan-Meier plots of cumulative OS in patients with ccRCC tumours with no/low total nuclear WTIP staining versus OS in patients with tumours with no/low nuclear WTIP staining, **(ii)** Estimated means and medians for OS in the two groups. **A (iii)** Comparison of cumulative OS with Log Rank, Breslow and Tarone-Ware Chi-Square test in the two groups. All analysis was undertaken using SPSS version 24.

4.8.3 Correlation of cytoplasmic WTIP staining and OS

Multivariate Cox regression analysis adjusting the OS regression model for KPS (KPS<80% versus ≥80%), number of metastatic sites at screening (≤2 versus ≥2), haemoglobin (<normal versus≥ normal), corrected serum calcium (≤10 versus >10mg/dl), age and sex was undertaken. Interestingly, the adjusted multi-variate analysis demonstrated that absent/low level cytoplasmic staining for WTIP was associated with longer survival (HR=0.438, 95% CI 0.222-0.862, p=0.017*), in contrast to the univariate model where survival was similar between the groups of patients with no/low and moderate/high cytoplasmic staining. Again, the validated prognostic markers of KPS (HR=3.367, 95% CI 1.538-7.371, p=0.002**), corrected calcium (HR=1.247, 95% CI 1.093-3.521, p=0.024*), number of metastatic sites (HR=1.852, 95% CI 1.247-3.322, p=0.039*) and Hb<N (HR 2.088, 95% CI 1.199-3.636, p=0.009**) correlated with worse OS as we would predict, again demonstrating the validity of the statistical analysis and multivariate model (**Figure 4.22**).

(i)

Omnibus Tests of Model Coefficients

-2 Log Likelihood	Overall (score)			Change From Previous Step			Change From Previous Block		
	Chi-square	df	Sig.	Chi-square	df	Sig.	Chi-square	df	Sig.
400.469	43.231	7	.000	36.347	7	.000	36.347	7	.000

(ii)

Case Processing Summary

		n	Percent
Cases available in analysis	Event	61	45.9%
	Censored	19	14.3%
	Total	80	60.2%
Cases dropped	Cases with missing values	53	39.8%
	Cases with negative time	0	0.0%
	Censored cases before the earliest event in a stratum	0	0.0%
	Total	53	39.8%
Total		133	100.0%

(iii)

Risk Factor	Significance	Hazard Ratio (HR)	95% CI for HR (lower)	95% CI for HR (upper)
KPS (<80% versus >80%)	0.002	3.367	1.538	7.371
No of metastatic sites (>2 versus ≤2)	0.039	1.852	1.247	3.322
Hb <N versus Hb>N	0.009	2.088	1.199	3.636
Corrected Ca >10 versus ≤10	0.008	1.247	1.247	4.444
Age	0.070	1.030	0.998	1.063
Sex	0.580	0.839	0.452	1.559
Absent/low cytoplasmic WTIP staining versus moderate/high cytoplasmic WTIP staining	0.017	0.438	0.222	0.862

Figure 4.22 Multi-variate Cox-regression analysis demonstrates that absent/low cytoplasmic WTIP staining correlates with OS.

Cox-regression analysis of OS in the GSK cohort was undertaken using SPSS version 24 to include LIMD1 staining, age and sex and KPS, number of metastatic sites, haemoglobin, and corrected calcium. **(i)** The omnibus test of model co-efficient was significant demonstrating that the new model offered an improvement over the old model (**ii)** Of the 133 patients, 80 patients had complete data available for all parameters and were therefore included in the analysis, 0 patients were censored. **(iii)** Results of the Cox-regression analysis.

4.8.4 Correlation of nuclear WTIP staining and OS

Multivariate Cox regression analysis for nuclear WTIP staining and OS was undertaken, adjusting the regression model for the parameters previously described. This demonstrated that absent/low nuclear WTIP staining did not correlate with OS (HR 1.441, 95% CI 0.822-2.532, p=0.202), however the validated MSKCC components of KPS, Haemoglobin and elevated corrected calcium were significantly associated with worse OS (**Figure 4.23**).

(i)

Omnibus Tests of Model Coefficients

-2 Log Likelihood	Overall (score)			Change From Previous Step			Change From Previous Block		
	Chi-square	df	Sig.	Chi-square	df	Sig.	Chi-square	df	Sig.
400.469	43.231	7	.000	36.347	7	.000	36.347	7	.000

(ii)

Case Processing Summary

		N	Percent
Cases available in analysis	Event	61	45.9%
	Censored	19	14.3%
	Total	80	60.2%
Cases dropped	Cases with missing values	53	39.8%
	Cases with negative time	0	0.0%
	Censored cases before the earliest event in a stratum	0	0.0%
	Total	53	39.8%
Total		133	100.0%

(iii)

Risk Factor	Significance	Hazard Ratio (HR)	95% CI for HR (lower)	95% CI for HR (upper)
KPS (<80% versus >80%)	0.002	3.711	1.586	8.682
No of metastatic sites (>2 versus ≤2)	0.070	1.733	0.956	3.144
Hb <N versus Hb>N	0.017	2.049	1.136	3.704
Corrected Ca >10 versus ≤10	0.025	2.012	1.089	3.717
Age	0.093	1.023	0.995	1.064
Sex	0.832	1.202	0.539	2.155
No/low nuclear WTIP staining versus moderate/high nuclear WTIP staining	0.202	1.441	0.822	2.532

Figure 4.23 Multi-variate Cox-regression analysis demonstrates that absent/low nuclear WTIP staining does not correlate with OS.

Cox-regression analysis of OS in the GSK cohort was undertaken using SPSS version 24 to include LIMD1 staining, age and sex and KPS, number of metastatic sites, haemoglobin, and corrected calcium which are components of the validated MSKCC score for predicting OS in metastatic RCC. **(i)** The omnibus test of model co-efficient was significant demonstrating that the new model offered an improvement over the old model (**ii)** Of the 133 patients, 80 patients had complete data available for all parameters and were therefore included in the analysis, no patients were censored. **(iii)** Results of the Cox-regression analysis.

4.8.5 Correlation of cytoplasmic and nuclear WTIP staining and PFS

Cox regression analysis was undertaken adjusting the regression model for the parameters described. In the adjusted multivariate model, this demonstrated that neither absent/low cytoplasmic nor absent/low nuclear WTIP staining was associated with differences in PFS compared to moderate/high expression, HR=1.245, 95% CI 0.701-2.214, p=0.455 and HR=0.800, 95% CI 0.497-1.287, p=0.358 respectively. Elevated corrected calcium and increasing age were statistically significant in both multivariate models (**Figures 4.24** and **4.25**)

(i)

Omnibus Tests of Model Coefficients

-2 Log Likelihood	Overall (score)			Change From Previous Step			Change From Previous Block		
	Chi-square	df	Sig.	Chi-square	df	Sig.	Chi-square	df	Sig.
528.115	23.797	7	.001	20.874	7	.004	20.874	7	.004

(ii)

Case Processing Summary

		n	Percent
Cases available in analysis	Event	80	60.2%
	Censored	0	0.0%
	Total	80	60.2%
Cases dropped	Cases with missing values	53	39.8%
	Cases with negative time	0	0.0%
	Censored cases before the earliest event in a stratum	0	0.0%
	Total	53	39.8%
Total		133	100.0%

(iii)

Risk Factor	Significance	Hazard Ratio (HR)	95% CI for HR (lower)	95% CI for HR (upper)
KPS (<80% versus >80%)	0.071	2.018	0.942	4.322
No of metastatic sites (>2 versus ≤2)	0.211	1.391	0.830	2.331
Hb <N versus Hb>N	0.308	1.297	0.787	2.138
Corrected Ca >10 versus ≤10	0.024	1.961	1.093	3.521
Age	0.010	1.040	1.009	1.070
Sex	0.865	1.048	0.609	1.801
No/low cytoplasmic WTIP staining versus moderate/high cytoplasmic WTIP staining	0.455	1.245	0.701	2.214

Figure 4.24 Multi-variate Cox-regression analysis demonstrates that absent/low cytoplasmic WTIP staining does not correlate with PFS. There is a correlation between age and PFS

Cox-regression analysis of PFS in the GSK cohort was undertaken using SPSS version 24 to include cytoplasmic WTIP staining, age and sex and KPS, number of metastatic sites, haemoglobin, and corrected calcium. **(i)** The omnibus test of model co-efficient was significant demonstrating that the new model offered an improvement over the old model **(ii)** Of the 133 patients, 80 had complete data available for all parameters and were therefore included in the analysis, no patients were censored. **(iii)** Results of the Cox-regression analysis.

(i)

Omnibus Tests of Model Coefficients

-2 Log Likelihood	Overall (score)			Change From Previous Step			Change From Previous Block		
	Chi-square	df	Sig.	Chi-square	df	Sig.	Chi-square	df	Sig.
502.612	23.013	7	.002	20.071	7	.005	20.071	7	.005

(ii)

Case Processing Summary

		n	Percent
Cases available in analysis	Event	77	57.9%
	Censored	0	0.0%
	Total	77	57.9%
Cases dropped	Cases with missing values	56	42.1%
	Cases with negative time	0	0.0%
	Censored cases before the earliest event in a stratum	0	0.0%
	Total	56	42.1%
Total		133	100.0%

(iii)

Risk Factor	Significance	Hazard Ratio (HR)	95% CI for HR (lower)	95% CI for HR (upper)
KPS (<80% versus >80%)	0.076	2.024	0.930	4.406
No of metastatic sites (>2 versus ≤2)	0.254	1.353	0.805	3.631
Hb <N versus Hb>N	0.415	1.236	0.743	2.055
Corrected Ca >10 versus ≤10	0.042	1.767	1.020	3.067
Age	0.012	1.039	1.007	1.008
Sex	0.996	1.002	0.562	1.788
No/low nuclear WTIP staining versus moderate/high nuclear WTIP staining	0.358	0.800	0.497	1.287

Figure 4.25 Multi-variate Cox-regression analysis demonstrates that absent/low nuclear WTIP staining does not correlate with PFS. There is a correlation between age and PFS

Cox-regression analysis of OS in the GSK cohort was undertaken using SPSS version 24 to include WTIP staining, age and sex and KPS, number of metastatic sites, haemoglobin, and corrected calcium. **(i)** The omnibus test of model co-efficient was significant demonstrating that the new model offered an improvement over the old model **(ii)** Of the 133 patients, 77 had complete data available for all parameters and were therefore included in the analysis, no patients were censored. **(iii)** Results of the Cox-regression analysis.

4.9 Staining of the TMAs for other hypoxically regulated proteins

The tumour suppressor VHL is a key component of an ubiquitin-ligase complex, targeting HIF1α for ubiquitylation and degradation. VHL loss is an early event that is near ubiquitous in both hereditary and sporadic ccRCC (Gossage, Eisen et al. 2015). Kroeger *et al* found that that high HIF2α nuclear expression was associated with lower grade and stage ccRCC tumours, whilst high cytoplasmic HIF2α was associated with a more aggressive ccRCC phenotype. Such tumours were also more likely to have positive lymph nodes and distant metastases (Kroeger, Seligson et al. 2014). HIF1α is frequently over-expressed in ccRCC and although Lidgren *et al* reported that high HIF1α expression in ccRCC was associated with better prognostic indicators, other studies have demonstrated worse survival in association with elevated HIF1α (Lidgren, Hedberg et al. 2005) (Minardi, Lucarini et al. 2015). Given the critical role of LIMD1 in the regulation of the hypoxic response and the contribution of HIF in driving tumourigenesis in ccRCC, the GSK ccRCC TMA was stained for VHL, HIF1α and HIF2α and staining correlated with staining for LIMD1

4.9.1 VHL staining of control normal kidney tissue and ccRCC tissue

In order to assess the specificity of the VHL antibody and determine an optimal antibody concentration for subsequent staining of the ccRCC TMAs, normal kidney tissue was stained using the automated Ventana discovery system with antigen visualisation using the avidin-biotin peroxidase method. VHL staining was felt to be specific and as expected stained the cytoplasm of the proximal and distal tubules with little staining of the glomeruli. After review by Dr Giorgia Trevisan, an antibody concentration of 1:100 was felt to give the best staining resolution without unacceptable background staining. In addition the TMA containing a range of pre-invasive and malignant histospots was stained in order to check expected staining patterns prior to staining the ccRCC TMAs. Normal renal tissue and the control TMA described were used as positive controls and the primary antibody omitted when staining one of the TMAs as a negative control. Of the 120-ccRCC samples, ten, 8.3% demonstrated VHL staining (**Figure 4.26**). As the proportion of tumour samples demonstrating staining for VHL was so low, it was not possible to correlate staining for VHL with that of other LAW proteins.

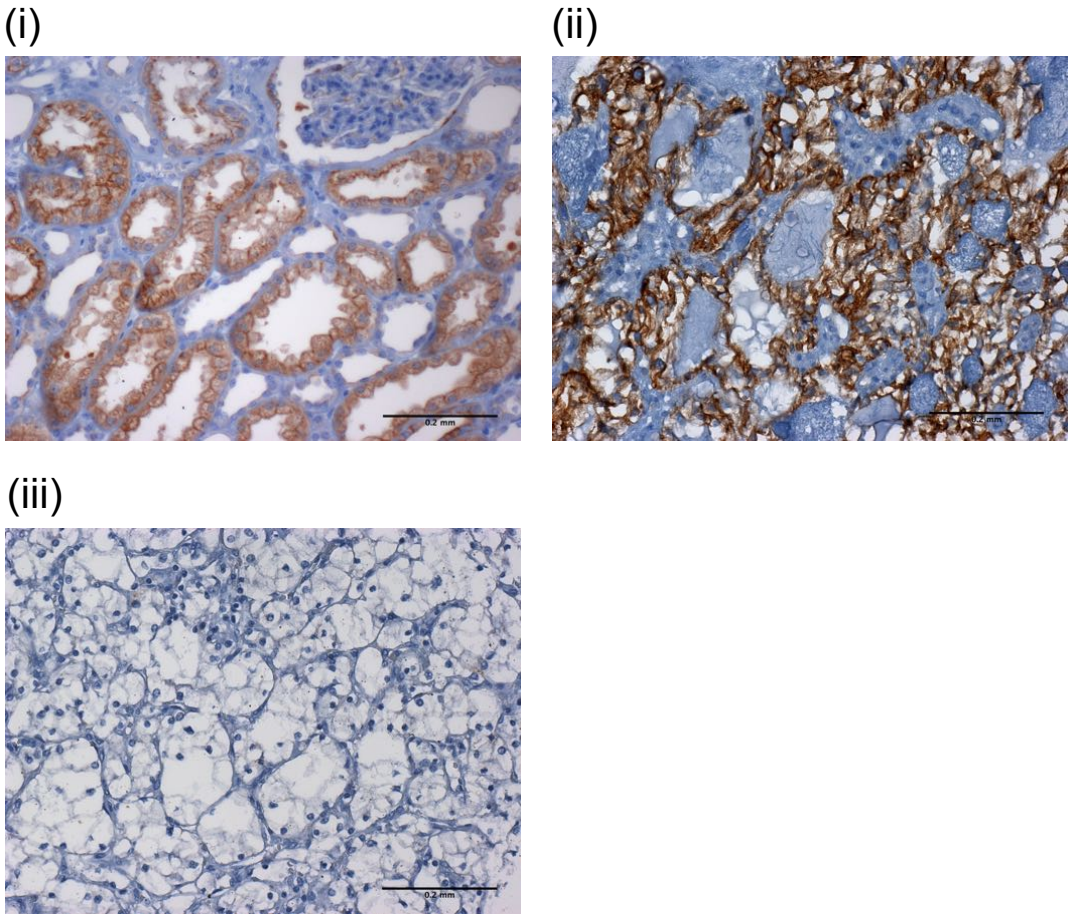

Figure 4.26: VHL staining of control normal kidney tissue and ccRCC tissue

IHC was undertaken using a semi-automated system with VHL antibody concentration 1:100 (Discovery, Ventana Medical Systems, Tucson AZ), with visualisation using the Avidin-biotin peroxidase method. (i) paraffin embedded normal kidney tissue with staining of the proximal and distal tubules but no staining of the glomerulus, **(ii**) ccRCC histospot demonstrating strong positive cytoplasmic staining, (iii) ccRCC histospot demonstrating negative staining

4.9.2 HIF-2α staining of normal kidney and clear cell renal cell carcinoma

IHC for HIF2α was performed using the automated Ventana Discovery system. As before the tissue microarray containing a range of pre-invasive/malignant histospots was stained in order to establish antibody specificity/confirm expected staining patterns and placental tissue also stained as a further control tissue. Staining was reviewed by Dr Giorgia Trevisan and felt to be specific, with no staining of the kidney glomeruli and positive cytoplasmic and nuclear staining in the proximal and distal convoluted tubules as expected (**Figure 4.27**). An antibody concentration of 1:100 was felt to provide the

greatest specificity and allow the discrimination of differences in staining intensity/pattern with little associated non-specific staining.

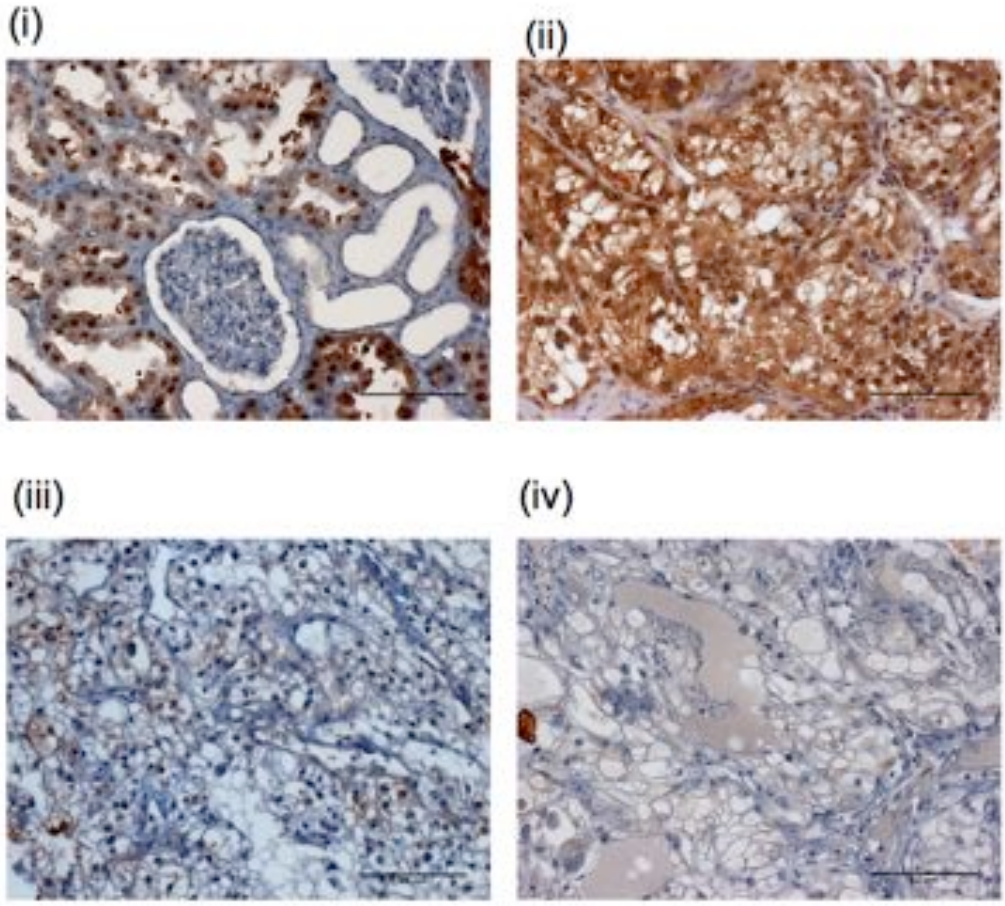

Figure 4.27. HIF2α staining of normal kidney tissue and ccRCC

IHC for HIF2α was undertaken using a semi-automated system (Discovery, Ventana Medical Systems, Tucson AZ), with antibody concentration 1:100 and visualisation using the Avidin-biotin peroxidase method. **(i)** Paraffin embedded normal kidney tissue stained with HIF2α demonstrating cytoplasmic staining and strong nuclear staining of the tubules. **(ii)** Paraffin embedded ccRCC tumour demonstrating strong nuclear and cytoplasmic HIF2α staining. **(iii)** Paraffin embedded ccRCC demonstrating weak patchy cytoplasmic and nuclear staining. **(iv)** Paraffin embedded HIF2α demonstrating neither cytoplasmic nor nuclear staining.

Representative cytoplasmic and nuclear HIF2α staining in ccRCC tissue is shown in (**Figure 4.27)**. Unfortunately, staining of the TMAs for HIF2α using the Novus Biologicals antibody was only successful if staining was undertaken immediately after the paraffin embedded sections were cut as it appeared that HIF2α antigen degradation was taking place. One of the TMAs had been sectioned in its entirety and therefore only two out of the three TMA slides could be stained. The TMAs were scored by Dr

Trevisan. The degree of reactivity was evaluated using a 3-point scale (0=negative, 1=positive, 2=strongly positive) and the percentage of tumour cells staining recorded. As before a mean score for staining was calculated based on the mean staining of all histospots derived from the same tumour. Given the findings of Kroeger *et al*, that sub-cellular HIF-2α localisation impacts on cancer-specific survival and tumour characteristics, cytoplasmic and nuclear HIF2α staining were scored separately and correlated with LIMD1 staining (Kroeger, Seligson et al. 2014).

Positive nuclear HIF2α staining was seen in 37 of the 73-ccRCC tumours evaluable (51%) and positive cytoplasmic staining in 38 of the 73-ccRCC tumours evaluable (52%). Of the tumours that expressed HIF2α in the cytoplasm, 31/38 (82%) had concomitant nuclear HIF2α staining and of the tumours that expressed HIF2α in the nucleus, 32/37 (86%) had concomitant cytoplasmic HIF2α staining.

For each tumour, the mean score for cytoplasmic and nuclear HIF2α staining was correlated with the mean score for LIMD1 staining using a manual scoring system. Calculation of the two-tailed Spearman correlation demonstrated no association between cytoplasmic HIF2α staining and LIMD1 ($p=0.5077$) nor was a correlation between nuclear HIF2α staining and staining for LIMD1 observed ($p=0.6533$). (**Figure 4.28**). In addition, there was no correlation between cytoplasmic or nuclear HIF2α staining and Ajuba staining, nor with WTIP staining, data for which is not shown.

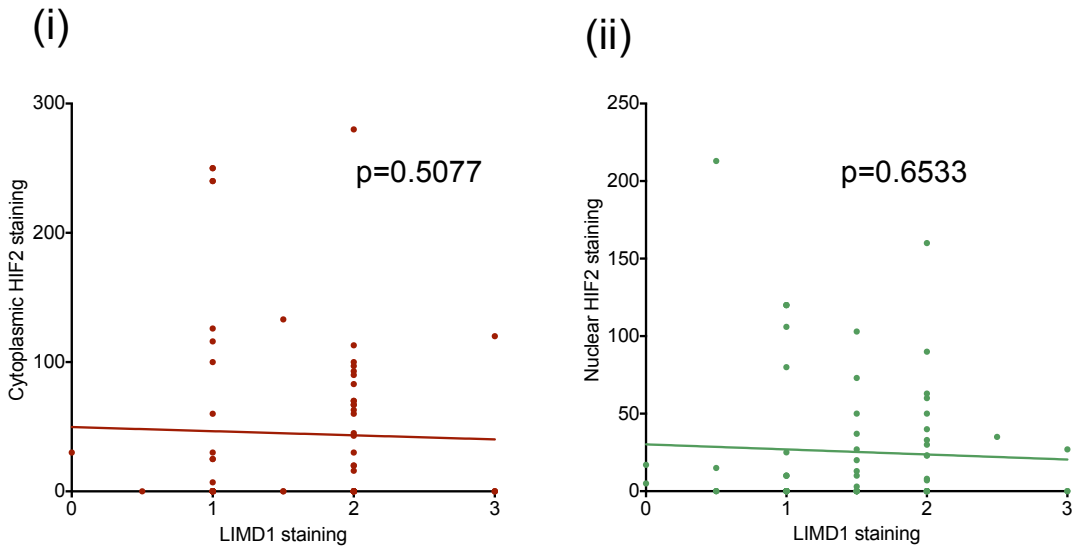

Figure 4.28 Correlation of HIF2α and LIMD1 staining

Mean HIF2α staining for all histospots from the same tumour as a function of staining intensity and proportion of tumour cells staining positively was plotted against mean LIMD1 staining. (**i)** Mean cytoplasmic HIF2α staining plotted again mean LIMD1 staining **(ii)** mean nuclear HIF2α staining plotted against mean LIMD1 staining. All analysis was undertaken in Prism 6. The two-tailed Spearman correlation is shown.

4.9.3 HIF1α staining of normal kidney and clear cell renal cell carcinoma

IHC for HIF1α using the automated Ventana system was unsuccessful and manual IHC was undertaken using an optimised protocol. After staining healthy renal tissue, placenta and tonsil tissue with a range of antibody dilution, optimal HIF1α antibody concentration was defined as 1:100. Staining in the RCC samples was predominantly cytoplasmic although some nuclear staining was observed. All staining was reviewed by Dr Giorgia Trevisan and felt to be specific.

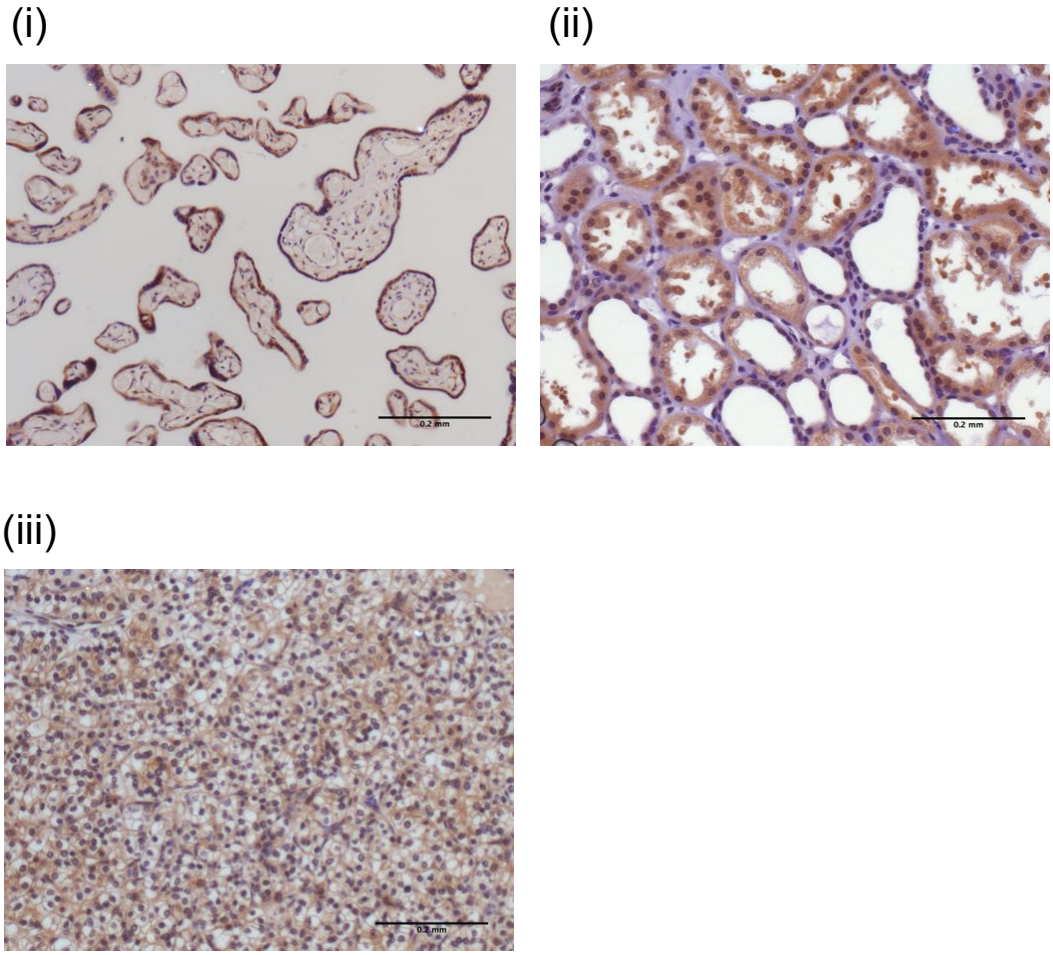

Figure 4.29 HIF1α staining of placenta, ccRCC and renal tissue

RCC samples represented in triplicate on tissue microarrays were stained using a manual IHC protocol using HIF1α antibody concentration 1:100, with visualisation using the Avidin-biotin peroxidase method. **(i)** Placenta tissue was included as a positive control **(ii)** ccRCC tumour demonstrating cytoplasmic HIF1α staining, **(iii)** HIF1α staining in renal tissue, with both cytoplasmic and nuclear staining

A total of 110 ccRCC tumours were scorable, with 20 (18%) demonstrating nuclear staining and 35 (32%) cytoplasmic staining. Generally, more cytoplasmic than nuclear staining was observed. As before, a mean score per tumour was calculated as a function of the mean staining intensity throughout the histospots from the same tumour and percentage of tumour cells staining positively, all scoring was undertaken by Dr Trevisan and endothelial cells were not scored.

All tumours with positive nuclear staining had only low levels of staining detectable and generally only in a small proportion of tumour cells: in tumours with positive HIF1α staining the mean nuclear staining of the tumours was 10% which is less than that

observed by other investigators (Ioannou, Mylonis et al. 2010). Staining for LIMD1 and both cytoplasmic and nuclear HIF1α was correlated.

Calculation of the two-tailed Spearman correlation demonstrated no association between cytoplasmic HIF1α staining and LIMD1 (p=0.0974) nor correlation between nuclear HIF1α staining and staining for LIMD1 (p=0.635) (**Figure 4.30**). However, as described the number of tumours staining positively for HIF1α particularly in the nuclear compartment was less than might have been expected and immunoassay for HIF1α can be difficult with specificity issues and variability in sensitivity with the use of different antibodies (Ioannou, Mylonis et al. 2010). There was no correlation between staining for Ajuba nor for WTIP and HIF1α staining, data for which is not shown.

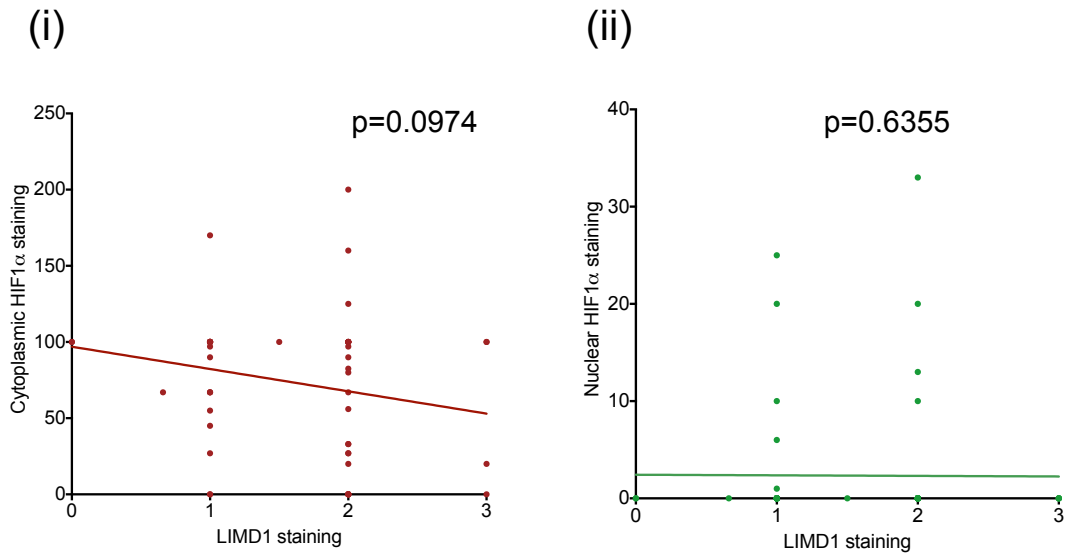

Figure 4.30 Correlation of HIF1α and LIMD1 staining

Mean HIF1α staining for all histospots from the same tumour as a function of staining intensity and proportion of tumour cells staining positively was plotted against mean LIMD1 staining. (**i)** Mean cytoplasmic HIF1α staining plotted again mean LIMD1 staining **(ii)** mean nuclear HIF1α staining plotted against mean LIMD1 staining. All analysis was undertaken in Prism 6. The two-tailed Spearman correlation is shown

4.10 Summary

Barts Cancer Institute forms part of The Experimental Cancer Medicine Network, a network that aims to facilitate the translation of basic scientific discovery into an understanding of what drives tumourigenesis and resistance to therapeutics *in vivo* as well as develop novel treatments for patients with cancer. Access to patient tissue from two prospective clinical trials with detailed five-year clinico-pathological outcome data represents a very valuable resource.

LIMD1, Ajuba and WTIP IHC staining were undertaken in ccRCC TMAs generated from a prospective phase II clinical trial of the EGFR-2 tyrosine kinase inhibitor lapatinib versus hormone therapy in patients who had progressed through first line cytokine therapy. Histospots were double scored by observers blinded to clinico-pathological outcome data and each other's scores, to ensure that scoring was valid and reliable. Excellent intra-class correlation between scorers was observed. For each patient an overall score was calculated based on the mean staining of all tumour histospots derived from that patient. For each of the three LAW proteins, tumours were divided into those expressing absent/low protein levels and those expressing moderate/high protein levels.

Often in studies investigating potential biomarkers, univariate and multivariate analysis is not undertaken. Therefore, for all three proteins, OS and PFS was correlated with levels of LIMD1, Ajuba and WTIP and in the multivariate analysis, the model modified to incorporate age, sex and components of the MSKCC score, a validated scoring system for OS in mccRCC. The clinical trial investigators also used these parameters in their multivariate analysis (Ravaud, Hawkins et al. 2008).

Tumour stage and grade were correlated with levels of LIMD1 staining and Ajuba staining. An association between loss of Ajuba staining and tumour stage was observed but no correlation between LIMD1 staining and tumour grade or stage and Ajuba staining and tumour stage. In both univariate and multivariate analysis, levels of LIMD1, Ajuba and WTIP did not correlate with OS or PFS. On multivariate analysis, components of the MSKCC score and increasing age correlating with OS, demonstrating the validity of the multivariate model. On multivariate analysis, increasing

age also corresponded with reduced PFS. The correlation of LIMD1 staining and OS and PFS, was assessed using a further cohort of patients enrolled in a clinical trial investigating the role of upfront pazopanib prior to nephrectomy in patients with mccRCC. Again no correlation between LIMD1 staining levels and OS or PFS was observed.

Hypoxic deregulation is a critical mediator of tumourigenesis in ccRCC and LAW proteins, in particular LIMD1 have been shown to play a critical role in the regulation of HIF1α levels. TMA histospots were therefore stained for the hypoxic markers, HIF1α, HIF2α and VHL and staining correlated with LIMD1 levels. No correlation was observed between staining for LIMD1/Ajuba/WTIP and HIF1α nor HIF2α.

4. 11 Discussion

4.11.1 IHC staining of ccRCC clinical trial TMAs

Staining for LIMD1 was re-optimised using an automated protocol, as manual IHC staining was no longer effective when performed with a new batch of antibody. This established very similar staining in a range of normal tissues/tumours and in ccRCC samples to that observed using the initial staining protocol, such that LIMD1 staining in the trial ccRCC TMAs was felt to be specific and valid. IHC protocol re-optimisation was not necessary when staining the trial ccRCC TMAs for Ajuba and WTIP as staining was consistent with that observed previously. Difficulties in the establishment of antibody specificity for IHC particularly for antigens not previously characterised is discussed in Chapter 3.

4.11.2 Correlating TMA staining with clinico-pathological outcome data

The use of TMAs for IHC analysis provides a number of advantages but there are limitations to such an approach. TMAs allow for the simultaneous, high-throughput analysis of multiple specimens that have been processed in the same manner and subjected to the same experimental conditions. Samples are therefore directly comparable and scoring between samples can be compared in a semi-quantitative way (Barrette, van den Oord et al. 2014). If cores are taken from pathologist-identified regions of interest as was the case for the TMAs described, staining can be reliably scored by individuals without expert training in pathology (Camp, Neumeister et al. 2008). Limited tissue is required for each TMA spot, of particular benefit in a clinical trial setting where multiple potential biomarkers may be stained and archived 'remaining' tissue, often limited in its availability is frequently used (Barrette, van den Oord et al. 2014).

Ideally TMAs should include multiple samples of the same tumour taken from as many histologically divergent sites as possible and such an approach can potentially overcome limitations associated with tumour heterogeneity, (Jensen, Riber-Hansen et al. 2011).

Intra-tumoural heterogeneity in ccRCC has been well characterised and represents an important potential barrier in the identification of tumour biomarkers (Fisher, Larkin et al. 2012) (Gulati, Martinez et al. 2014). In practice obtaining tissue from multiple tumour sites is not always possible, nor is it feasible or often appropriate to re-biopsy patients where tissue availability is limited. Insufficient samples from known spatially separated tumour regions represented in the PANTHER TMA were included as most of the tissue from the biopsy samples had been used up for the initial trial analysis and therefore assessment of inter-tumour heterogeneity for LIMD1 was not possible.

In our analysis, histospots were included in duplicate or triplicate, enabling the calculation of a mean score for staining and given the small size of the spots, minimising error in scoring. Since all TMAs were stained simultaneously for each marker, differences in staining intensity in association with variable haematoxylin counterstaining which can affect the interpretation of staining were overcome. In addition, the intra-class scoring correlation was used to demonstrate that there was excellent consistency between independent scorers and that IHC scores were therefore valid for analysis. Scorers were also blinded to clinico-pathological outcome data to minimise the likelihood for conscious or unconscious bias

Where possible TMA blocks were freshly cut prior to IHC staining although this was not possible for one TMA block in the GSK cohort where the block had been cut in its entirety. We were therefore unable to stain one of the three TMA slides for HIF-2α, as antigen degradation appeared to have occurred and staining for HIF2α in this slide was consistently negative. The loss of antigenicity in TMA FFPE tissue sections negatively impacts on staining validity (Yaziji and Barry 2006). Retention of endogenous water in tissue sections results in antigen degradation, as does exposure to high humidity during storage (Xie, Chung et al. 2011). Optimal tissue processing and storage is therefore essential. All TMA blocks were appropriately stored and processed with adherence to trial protocol Good Laboratory Practice (GLP). Although TMAs were created at the same time, they were predominantly derived from archived tumour samples of varying ages, many of which are likely to have been processed in different laboratories, where sample processing may not have been standardised. Nonetheless all hospital laboratories should adhere to GLP standards and practices should be similar. A recent European white paper on retrospective studies using archived tissues concluded that

improvements in tissue preservation and storage methods which standardised the degree of molecular degradation alongside standard operating processes make the use of archived tissue a valuable and acceptable approach within clinical trials.

4.11.3 Using archived tissue for correlation with clinico-pathological outcome data

Analysis of multiple tumour regions in primary ccRCC samples and metastatic sites reveals substantial intra-tumour heterogeneity with spatially separated sub-clones associated with distinct driver mutations and somatic copy number alterations (Gerlinger, Rowan et al. 2012, Gerlinger, Catto et al. 2015). Therefore as ccRCC tumours develop and metastasise, significant differences in tumour genotype/phenotype may be observed. Using archived tumour tissue for prognostic/predictive biomarker correlation may therefore not be representative of the tumour genotype/phenotype at the time of study enrolment, the time point at which PFS/OS correlation is undertaken. In the PANTHER cohort, tumour samples were either biopsy specimens taken at the point of clinical trial enrolment or at nephrectomy after neo-adjuvant pazopanib and therefore the issue of variation in length of time between tumour archive and study enrolment in patients was overcome. This was not the case for patients enrolled in the Phase II trial comparing lapatinib with hormonal treatment where time between study enrolment and tumour archive is likely to be highly variable. Most clinical studies do however make use of archived tissue and use of such tissue is felt to be valid in such analyses (Simon, Paik et al. 2009).

Simon *et al* propose a number of guidelines for biomarker study design using archived specimens and where possible these guidelines were followed. They stipulate that adequate amounts of archived tissue from sufficient patients are available to adequately power statistical analysis (this was the case for our study), that the potential biomarker should be analytically and pre-analytically validated for use with archived tissue (LIMD1 and Ajuba staining had been validated in previous studies using archived tissue) (Spendlove, Al-Attar et al. 2008, Shi, Chen et al. 2016)), that the plan for biomarker evaluation should be specified prior to the performance of biomarker assays on archived tissue (this was not the case) and in addition results should be validated using specimens from one or more similar studies (the staining for the GSK cohort was validated using the PANTHER tissue) (Simon, Paik et al. 2009).

4.11.4 Defining cutoffs for potential biomarkers

Defining appropriate cutoffs for potential biomarkers is an essential but difficult aspect of biomarker assessment. IHC is generally quantified using an ordinal scale using the percentage of stained tumour cells, staining intensity or a combination of both parameters such as the Allred score (Allred, Clark et al. 1993, Harvey, Clark et al. 1999), although automated quantitative systems such as the Ariol system may also be used for quantification (Bolger, Heffron et al. 2006) and such systems are discussed in Chapter 3.

In order to translate a continuous or ordinal diagnostic variable in to a meaningful stratification, appropriate cutoff determination is necessary (Mazumdar and Glassman 2000). For the initial IHC described in chapter 3, the TMAs were scored using an automated Ariol system and a score generated for IHC comparison. Scanning the clinical trial TMAs however did not seem to correlate well with the manual scores, perhaps as the histospots, particularly in the GSK cohort were small and some histospots were not intact. In addition, some background staining was present in some histospots, which could be overlooked when scoring was undertaken manually. Automated analysis and expert pathologist scoring is considered to be equivalent (Turbin, Leung et al. 2008).

For this analysis, a manual scoring system generating a combined score for each tumour was used based on the mean staining for all histospots derived from the tumour and where appropriate scoring both nuclear and cytoplasmic compartments separately using validated scoring systems were possible. Patients were then stratified in to those with no/low staining versus moderate/high staining. Spendlove *et al* used a similar stratification in their breast cancer cohort for LIMD1 staining with absent/weak nuclear LIMD1 staining strongly correlated with adverse prognostic indicators (Sharp, Al-Attar et al. 2008) and scoring system was based on this published scoring system.

Using mean or median values for defining cut-offs is frequently described (Budczies, Klauschen et al. 2012). Re-analysis of the correlation of low versus high staining for LAW proteins with clinico-pathological outcome data when cutoffs were changed, e.g. characterising low staining as staining less than the median was not possible as staining scores were too clustered. In addition when patients were stratified using a greater

number of staining intensities, for example stratifying patients in to four groups, too few samples for some staining intensities were included for data analysis to be meaningful. For Ajuba and WTIP staining where scores were less clustered, changing the cut offs e.g. to less than the median versus greater than the median did not change the outcome of the analysis, suggesting that this was a true result.

Other methods for cut-off determination are described in the literature, and underlying algorithms for determining such cut-offs are often unclear (Budczies, Klauschen et al. 2012). Established methods frequently involve the use of receiver operating characteristic (ROC) curves, a graphical plot that illustrates the performance of a binary classifier system as its discrimination threshold is varied, generally by minimising p values, or techniques to maximise combinations of test sensitivity and specificity using area under the curve calculations (Perkins and Schisterman 2006). X-tile is a validated software tool application, specialised to the analysis of survival data, which makes use of a minimal p-value approach for cut-off optimisation (Camp, Dolled-Filhart et al. 2004). Specifically, it generates plots that provide an assessment of every possible way of dividing a population into low, medium and high-level marker expression and showing the resulting population subsets alongside an associated Kaplan-Meier curve. Such analysis can provide additional information about the biological nature of a marker, such as whether there is a linear distribution related to survival. Given that it is statistically invalid to test multiple divisions and accept the best P value, initial divisions are defined in a 'training set' and then a separate patient cohort 'validation set' used for division validation (Camp, Dolled-Filhart et al. 2004). Other systems have also been developed such as Cutoff Finder, a freely available web application bundle that makes use of an R package, which offers 5 different methods for cutoff optimisation. This includes a number of methods, including stratification according to the distribution of the marker under investigation, or subdivision according to an outcome or survival variable (Budczies, Klauschen et al. 2012).

For IHC staining with LIMD1, tumour staining was fairly uniform throughout each histospot and using a system such as X-tile, where multiple cut-offs for staining are defined would not be possible.

4.11.5 Correlation of LAW staining with clinico-pathological outcome data

For a preliminary analysis assessing LAW staining and correlating with clinico-pathological outcome data we had access to two very valuable resources with clinical trial samples and detailed outcome data. For an early preliminary analysis, following the guidelines of Simon *et al* listed is rarely feasible. However, as described, where possible these guidelines were followed.

Tumour samples were missing for some patients, which became more of an issue as the TMAs were cut further. In the GSK cohort, where the bulk of IHC staining was undertaken, despite the enrolment of 460 patients in the trial, tissue from only 130 patients archived locally was available for analysis. In addition, it was not possible to obtain data as to which arm of the trial, lapatinib or placebo, patients had been randomised to and it was therefore unclear if patients in the two groups were similarly balanced with respect to arm randomisation. The clinical trial was however negative, demonstrating no difference in PFS or OS in patients randomised to either lapatinib or placebo and therefore the absence of this data is unlikely to have affected the overall analysis.

Advice regarding statistical analysis of the data was obtained. On multivariate analysis components of the validated MSKCC score, KPS, number of metastatic sites, haemoglobin concentration and corrected calcium were predictive of OS but not PFS as would be predicted. This suggests that the patient population from which samples were derived was representative of a typical cohort of patients with metastatic ccRCC and that the multivariate analysis was valid. This also implies that patient characteristics were similar in those whose tumours expressed high or low LAW levels and that the missing data, i.e. treatment arm information and EGFR status, did not significantly impact on the overall analysis. IHC analysis of LIMD1 staining in a further cohort of patients enrolled in a clinical trial, stratifying patients using the cutoffs described also did not show any difference in OS or PFS, further validating this analysis.

Given that ccRCC tumours are likely to demonstrate 3p LOH and a significant proportion 14q LOH it would be expected that many tumours would express less LIMD1 and/or Ajuba than normal renal tissue. It was hypothesised that clinico-

pathological outcome data in patients with tumours with absent/low LIMD1 expression would be worse, as had been demonstrated by Spendlove *et al* in breast carcinoma: this however was not the case (Spendlove, Al-Attar et al. 2008). The same hypothesis was also made for Ajuba. Changing the cutoff values to the mean/median or stratifying by all staining intensities was not possible for LIMD1 for the reasons described.

It is therefore possible that a statistically significant association was not identified because of too small a number of patients in one of the groups, for LIMD1 staining of the GSK cohort, 43 samples had no/low LIMD1 staining compared to 87 samples with moderate high LIMD1 staining. However visual inspection of the areas under the curve, do not look significantly different and if there had been a very significant difference in OS/PFS between the two cohorts, we would have expected to see a statistically significant difference despite the imbalance in numbers between the two groups. Changing the cutoff values for Ajuba and WTIP however did not affect the association between staining and tumour grade/stage and PFS and OS.

In the study described by Thiesen *et al* CNAs of *LIMD1* were identified in 28 of the 48 ccRCC tumours analysed (58.3%) with interestingly a correlation between lower tumour grade and loss, with 21 of the 26 (80%) grade 1 tumours demonstrating CNA compared to only 5 of the 20 (25%) grade 3 tumours. This suggests that loss of LIMD1 at least as identified by CNA could in fact be associated with a less aggressive tumour phenotype (Thiesen, Steinbeck et al. 2017). This could also fit, given our knowledge of the role of LIMD1 in the regulation of HIF1α, with the observation that HIF1α overexpression in ccRCC is often considered a positive prognostic indicator: *HIF1α* is often considered a tumour suppressor gene and that loss of *HIF1α* expression is common and may contribute to tumourigenesis (Kroeger, Klatte et al. 2013). In a recently published small cohort of 28 patients with ccRCC, loss of LIMD1 staining was common compared to MAT control tissue and more frequently observed in stage 1 tumours, 20.2% compared to 6% of stage 3 tumours, again corroborating the study by Thiesen *et al* and suggesting that LIMD1 loss may be more important in the pathogenesis of early tumours (Sur, Maurya et al. 2017).

One of the most consistently validated prognostic stratification approaches is the differentiation of ccRCC tumours into clear cell type A (ccA) and clear cell type B (ccB)

subtypes. Interestingly patients with ccA type tumours have a significant survival advantage compared to those with ccB type tumours of 8.6 versus 2 years in those with localised tumours (Brannon, Reddy et al. 2010). For ccA type tumours, the overexpression of HIF signalling components is observed, whilst for ccB type tumours, genes that regulate EMT, the cell cycle and wound healing are typically deregulated (Brannon, Reddy et al. 2010).

4.11.6 Correlation of LIMD1 staining with established markers of hypoxic deregulation

Correlation of LIMD1 staining in the GSK TMAs with staining for HIF2α in both the nuclear and cytoplasmic compartments demonstrated no significant association.

Most tumours demonstrated no HIF1α staining with fewer tumours staining positively than might have been expected (Klatte, Seligson et al. 2007, Minardi, Lucarini et al. 2015). HIF1α IHC is often difficult, with considerable variation in antibody sensitivity and specificity described (Ioannou, Mylonis et al. 2010). *In vitro* work described in chapter 5, demonstrated that LIMD1 loss was associated with increased HIF1α activity *in vitro* in two ccRCC lines as assessed using a HIF1α reporter assay. In the RCC48 cell line, HIF1α was also up-regulated in hypoxia in association with LIMD1 loss.

Given that staining was less than expected, with many tumours demonstrating no HIF1α staining, it is difficult to assess the correlation between LIMD1 and HIF1α protein levels in this cohort.

4.12 Future Work

In chapter 3, the loss of LAW is demonstrated in a significant proportion of ccRCC samples and the relationship between LAW proteins described. LAW staining and staining for markers of hypoxic deregulation are described and further IHC for CD31 and VEGF-R suggested. Further experiments characterising assessing LAW mRNA levels and copy number are suggested as well as *in vitro* work to further correlate sub-cellular localisation of LAW.

Sur *et al* stained 28 ccRCC tumours for LIMD1 expression and found that lower stage tumours were more likely to demonstrate loss of LIMD1 expression than higher stage tumours (Sur, Maurya et al. 2017). IHC was done of entire slides. TMA are considered to be a validated and appropriate method to assess tissue expression of a particular marker as a means of assessing expression of that marker in the tissue as a whole (Simon, Paik et al. 2009). Tumour heterogeneity can however be problematic and it would be interesting to score larger sections, ideally from spatially separated regions of the tumour to validate our staining findings.

The correlation of IHC staining for LAW with markers of hypoxic deregulation was difficult to characterise. As described, it was not possible to stain for HIF2α on TMAs that had been pre-cut a while previously limiting the number of tumour samples possible for analysis. It would be worthwhile to attempt to stain the recently cut commercially available TMAs described in chapter 3 for HIF2α, although some antigen degradation may also have occurred in these samples. Given the difficulties of IHC for HIF1α, characterisation of HIF1α mRNA levels by RT-PCR and correlation with staining for LAW as assessed by IHC may be a more meaningful analysis.

Chapter 5

Characterisation of the *in vitro* effects of LIMD1 loss on tumourigenesis in ccRCC

5.1 Introduction

Members of the Ajuba family function as protein adapters. Their high affinity cores enable the specific binding of multiple proteins simultaneously with subsequent regulation of a number of different pathways/processes (Kadrmas and Beckerle 2004). With both nuclear and cytoplasmic localisation domains, Ajuba family proteins function as signal transducers, mediating communication between the nucleus and the cytoplasm (Kadrmas and Beckerle 2004).

In Chapters 3 and 4, expression of LIMD1, Ajuba and WTIP was characterised in ccRCC samples and matched adjacent tissue, the relationship between the family members described and expression correlated with known markers of hypoxic deregulation. LIMD1, Ajuba and WTIP expression was also correlated with clinico-pathological outcome data.

In vitro work has identified a number of roles for Ajuba proteins. In drosophila, Djub is the sole orthologue of the Ajuba subfamily of LIM proteins and functions as an essential negative regulator of the conserved Hippo signalling pathway, a critical regulator of organ size, and cell cycle control, de-regulation of which is implicated in tumourigenesis in multiple tumour types (Huang, Wu et al. 2005). LIMD1 interacts with the retinoblastoma protein to inhibit E2F1-mediated transcription and LIMD1 loss results in the up-regulation of pro-tumourigeneic E2F1-driven transcription (Sharp, Munoz et al. 2004). LIMD1 is also a critical regulator of HIF-1 activity, acting as a molecular scaffold, bridging an association between the prolyl hydroxylases and VHL and targeting HIF1α for degradation via the proteasome (Foxler, Bridge et al. 2012). LIMD1, Ajuba and WTIP localise to cytoplasmic P-bodies, sites of miRNA/mRNA interaction, where they facilitate interactions between the core miRISC and the EIF4E/m^7GTP cap structure of mRNA, thereby blocking mRNA translation initiation (James, Zhang et al. 2010, Bridge, Shah et al. 2017).

In ccRCC, Ajuba family members have not been characterised previously *in vivo* or *in vitro* The effects of LIMD1 loss on tumourigenesis were characterised using paired ccRCC cell lines that were LIMD1 proficient or expressed low levels of LIMD1.

CRISPR-Cas-9 mediated genetic editing enables the targeted and efficient modification of eukaryotic species (Hsu, Lander et al. 2014) and has only been successfully applied to a few primary human cell types (Hendel, Bak et al. 2015). A CRISPR-Cas-9 gene editing system was used to knockout *LIMD1* and *Ajuba* in renal proximal tubular epithelial cells (RPTEC), the likely cell of origin of ccRCC. Targeted deletion of a tumour suppressor in primary cells enables the specific investigation of the effects of loss on tumourigenesis, in the absence of the deregulation of other genes/pathways.

5.2 Chapter Aims

1. To generate lentivirally transduced ccRCC cell lines with stable effective LIMD1 knockdown (shLIMD1), LIMD1-knockdown with concomitant LIMD1-rescue (rrLIMD1) and a control cell line (scr) for use in further *in vitro* assays

2. To transduce renal proximal tubular epithelial cells (RPTEC) with a B lymphoma Mo-MLV insertion region 1 homolog (BMI-1) construct

3. To utilise a CRISPR-Cas-9 gene editing system to achieve knockout of *LIMD1* and *Ajuba* in BMI-1 transduced RPTEC cell lines

4. To characterise the effects of LIMD1 loss on tumourigenesis using the lentivirally transduced cell lines

5.3 Lentiviral transduction of RCC11 and RCC48

RCC11 and RCC48 cell lines were transduced with a lentiviral construct to achieve knockdown of LIMD1 (shLIMD1), knockdown of LIMD1 with concomitant rescue (rrLIMD1) and to generate a non-targeting control cell line (scr).

The RCC11 line was selected for use in *in vitro* assays, as it expresses high levels of HIF-1α and HIF-2α. In addition, the wild type cell line expresses high levels of LIMD1 and moderate levels of Ajuba and WTIP (**Figures 3.1 and 5.1**).

In contrast the RCC48 cell line, expresses high levels of HIF-2α but lower levels of HIF1α and could therefore be considered representative of an aggressive 'hypoxically deregulated' ccRCC line, in ccRCC tumourigenesis there is often a switch from HIF1-α to HIF2-α overexpression associated with increasing tumourigenesis (Koh, Lemos et al. 2011). The RCC48 cell line expressed high levels of LIMD1 and WTIP with low Ajuba (**Figure 5.1**). Knockdown of LIMD1 in the RCC48 cell line therefore enabled the investigation of the effects of LIMD1 loss in a cell line that could be considered representative of an aggressive, 'hypoxically deregulated' ccRCC line where there was still moderate levels of expression of WTIP (**Figure 5.1**). This is in contrast to the RCC11 line, where knockdown of LIMD1 would still leave cells expressing moderate levels of Ajuba and WTIP (**Figures 3.1 and 5.1**). It was felt important that in cells where LIMD1 knockdown had been achieved, expression of either Ajuba or WTIP remained: in mammalian cells depletion of all 3 LAW proteins in the dog kidney epithelial cell line, MDCK results in cell death (Das Thakur, Feng et al. 2010). Blots kindly provided by Dr Katherine Bridge (**Figure 5.1**).

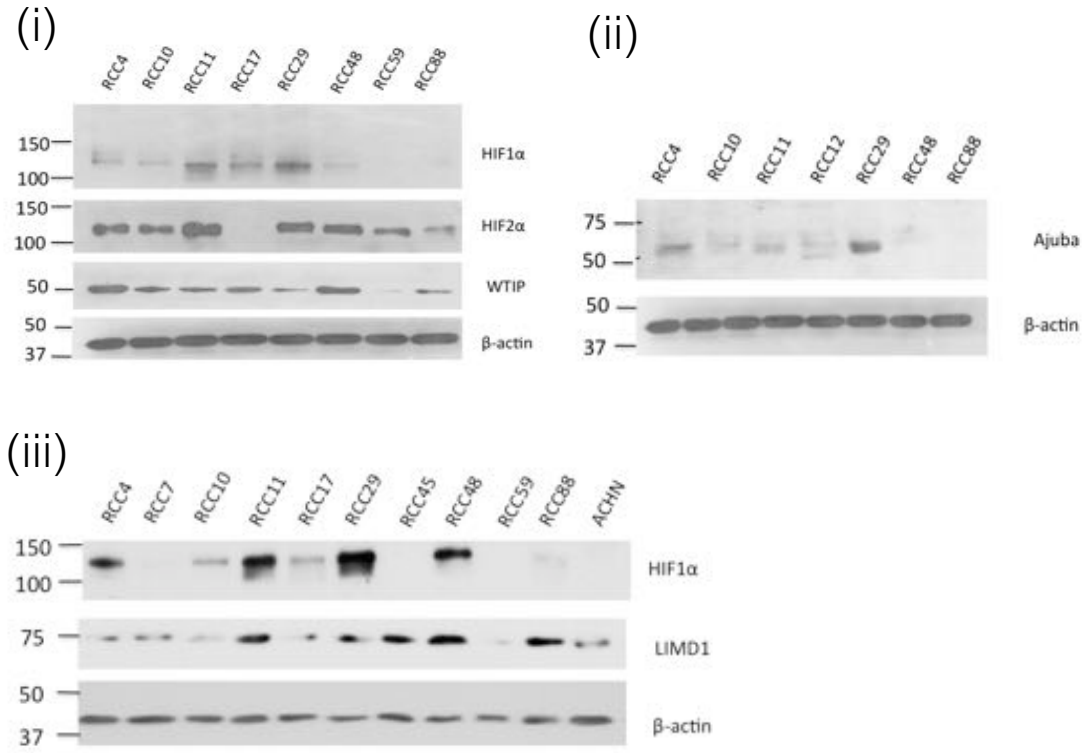

Figure 5.1. Expression levels of LIMD1, Ajuba, WTIP, HIF1α and HIF2α in a panel of ccRCC lines

(**i)** Immunoblot of HIF1α, HIF2α and WTIP in a panel of ccRCC lines with β-actin as loading control. **(ii)** Immunoblot of Ajuba in a panel of ccRCC lines with β-actin as loading control. **(iii)** Immunoblot of LIMD1 in a panel of ccRCC lines with β-actin control as loading control. Blots kindly provided by Dr Katherine Bridge of the Sharp lab.

RCC11 and RCC48 cell lines were transduced with a lentiviral construct containing (1) a LIMD1 shRNA, construct, (2) a non-targeting scr construct, or (3), a rrLIMD1 construct, with concomitant LIMD1 knockdown and rescue. All three lentiviral constructs expressed a puromycin resistance marker. Immunoblot confirmed high levels of LIMD1 expression in the non-targeting control (scr) and the rrLIMD1 lines with low levels of LIMD1 expression in the shLIMD1 line confirming successful lentiviral transduction **(Figure 5.2).**

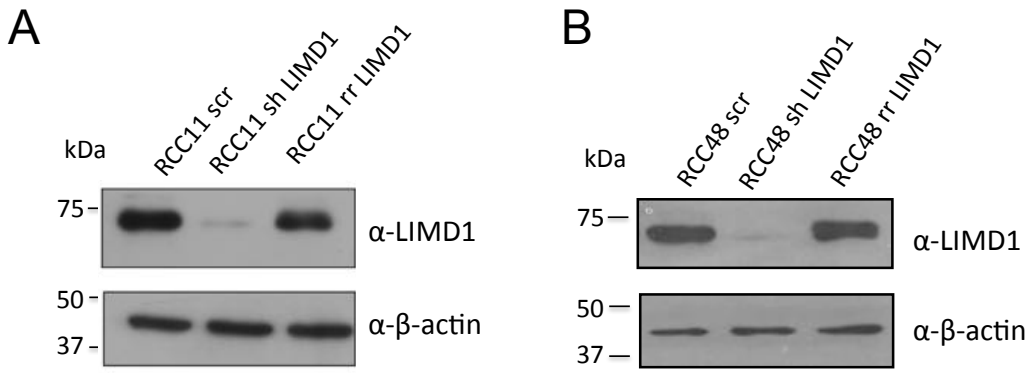

Figure 5.2. Successful lentiviral transduction of RCC11 and RCC48 ccRCC lines to create LIMD1 knockdown (shLIMD1), concomitant knockdown and rescue (rrLIMD1) and non-targeting control (scr) cell lines

RCC11 and RCC48 cells were plated in 6-well plates at a seeding density of $1x10^5$ cells/well. At 24 hours, the media was changed and concentrated virus added directly to the media. Media was changed at 48 hours and puromycin selection started at 96 hours. Once confluent, cells were passaged. Expression of LIMD1 in the scr and rrLIMD1 lines and knockdown of LIMD1 in the shLIMD1 line was confirmed by immunoblotting. **(A)** Immunoblot of LIMD1 and β-actin control in the RCC 11 line, **(B)** Immunoblot of LIMD1 and β-actin control in the RCC48 line.

5.4 Renal Proximal tubular epithelial cells (RPTEC) were effectively transduced with a BMI-1 construct

The literature predominantly supports the idea that ccRCC arises from renal proximal tubular epithelial cells (Frew and Moch 2015). One critical step in the development of a cancerous cell is the acquisition of an unlimited replicative lifespan, defined as immortalisation. ccRCC lines are very heterogeneous, with different cell lines likely to show deregulation of multiple separate genes and signalling pathways. The effects of deletion of a gene of interest in two separate cell lines may therefore be associated with significantly different experimental outcomes making generalisations about the effects of deletion of a particular gene of interest with respect to tumourigenesis difficult. The use of a primary cell line for *in-vitro* experiments overcomes these difficulties and provides an effective platform for investigating the effects of loss of a TSG on early tumourigenesis and transformation. RPTEC immortalisation was attempted by transducing RPTEC cells with a BMI-1 construct.

The transcription factor Myc can induce telomerase expression in normal human mammary epithelial cells (MEC) and normal human diploid fibroblasts through the induction of the expression of hESTs (hTRT/TP2), the limiting subunit of telomerase (Wang, Xie et al. 1998). B lymphoma Mo-MLV insertion region 1 homolog (BMI-1) is a polycomb ring finger containing protein, originally identified as a c-Myc cooperating oncoprotein. The *hTERT* promoter contains several c-Myc binding sites which can induce telomerase activity and bypass senescence in normal human mammary epithelial cells and some fibroblast cell lines (Dimri, Martinez et al. 2002) (Wang, Xie et al. 1998).

Other mechanisms drive immortalisation in MEC cells with BMI-1 acting independently of c-Myc binding sequences to upregulate hTERT expression, with the RING finger of BMI-1 and a conserved helix turn-helix-turn domain inducing telomerase with resultant MEC immortalisation (Dimri, Martinez et al. 2002). BMI-1 also can regulate cell proliferation in both MEC and fibroblasts. In BMI-1 deficient fibroblasts the tumour suppressors p16 and p19Arf, negative regulators of the cell cycle are markedly up-regulated. Overexpression of BMI-1 permits fibroblast immortalisation, by down-regulating p16 an inhibitor of CDK4 activity and $p19^{ARF}$ protein levels, a cell signal checkpoint that triggers a p53 dependent response that induces growth arrest and/or

apoptosis (Park, Park et al. 2002). This in combination with H-ras overexpression leads to neoplastic transformation of fibroblasts (Jacobs, Kieboom et al. 1999). BMI-1 over-expression also down-regulates p16 and $p19^{ARF}$ protein levels in MEC driving cell proliferation (Dimri, Martinez et al. 2002).

RPTEC lines can only be passaged a limited number of times prior to senescing, potentially reducing their usefulness for *in vitro* assays. RPTECs were transduced with a *BMI-1* construct with the aims of increasing the number of times the cells could be passaged prior to senescing and in order to generate a cell line with a greater potential for malignant transformation. In combination with the deletion of LAW proteins, it was anticipated that this would result in a cell line with a phenotype that more closely resembled that of a ccRCC line.

RPTECs were transduced with a BMI-1 construct containing a puromycin resistance gene. Following puromycin selection and passage, immunoblotting confirmed significant up-regulation of BMI-1 expression confirming that BMI-1 transduction had been successful (**Figure 5.3**).

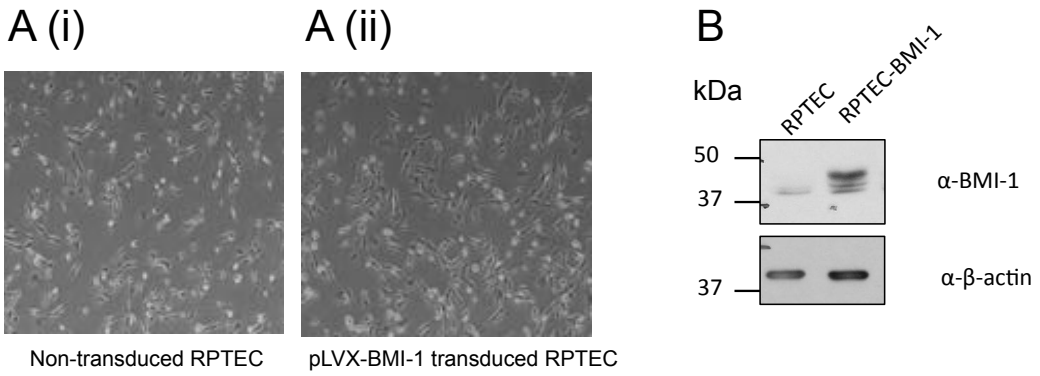

Figure 5.3. Successful lentiviral transduction of RPTECs with a BMI-1 construct

RPTEC cells were plated in 6-well plates at a seeding density of $1x10^5$ cells/well. At 24 hours, the media was changed and concentrated virus added directly to the media. Media was changed at 48 hours and puromycin selection started at 96 hours. Non-transduced RPTEC and BMI-1 transduced RPTEC were lysed and immunoblotted for BMI-1 and β-actin. **A (i), A (ii).** Representative images of non-transduced and transduced RPTEC. No difference in cell morphology was observed and both cell lines grew well. **B** Immunoblot demonstrated a significant increase in BMI-1 in the BMI-1 transduced RPTEC compared to non-transduced control.

5.5 Use of a CRISPR-Cas-9 gene editing system to knockout LIMD1 and Ajuba in BMI-1 transduced RPTEC

Cas-9-mediated gene editing enables the targeted and efficient modification of eukaryotic species (Hsu, Lander et al. 2014). In particular the use of the CRISPR system can be used to target virtually any genomic location with the use of a short RNA guide (Hsu, Lander et al. 2014). Using a CRISPR-Cas-9 system, complete and permanent cleavage of a gene of interest is possible such that no transcription of that gene will occur, with little in the way of off-target effects (Hsu, Lander et al. 2014).

An Edit-R Dharmafect™ Duo CRISPR-Cas-9 gene editing system containing a blasticidin resistance construct was used to target *LIMD1* and *AJUBA* in RPTECs. Three separate guide-RNA sequences directed against different encoding regions of *LIMD1* and *AJUBA* were used to maximise the likelihood of successful gene editing. Guide-RNAs directed against *WTIP* were not available.

Reasonable transfection efficiency of around 20% was achieved using a Dharmafect transfection system as indicated by the mKATE transfection control **(Figure 5.4A)**. Following transfection, and transient blasticidin selection, the *BMI-1* transduced RPTEC were allowed to recover and were passaged. Immunoblot for AJUBA and LIMD1 in the heterogeneous population demonstrated excellent knockout of *AJUBA* and *LIMD1* in the knockout lines compared to proficient control **(Figure 5.4B).** Unfortunately, despite repeated attempts, single colony selection of both cell lines was not possible, as cells did not survive being plated singly.

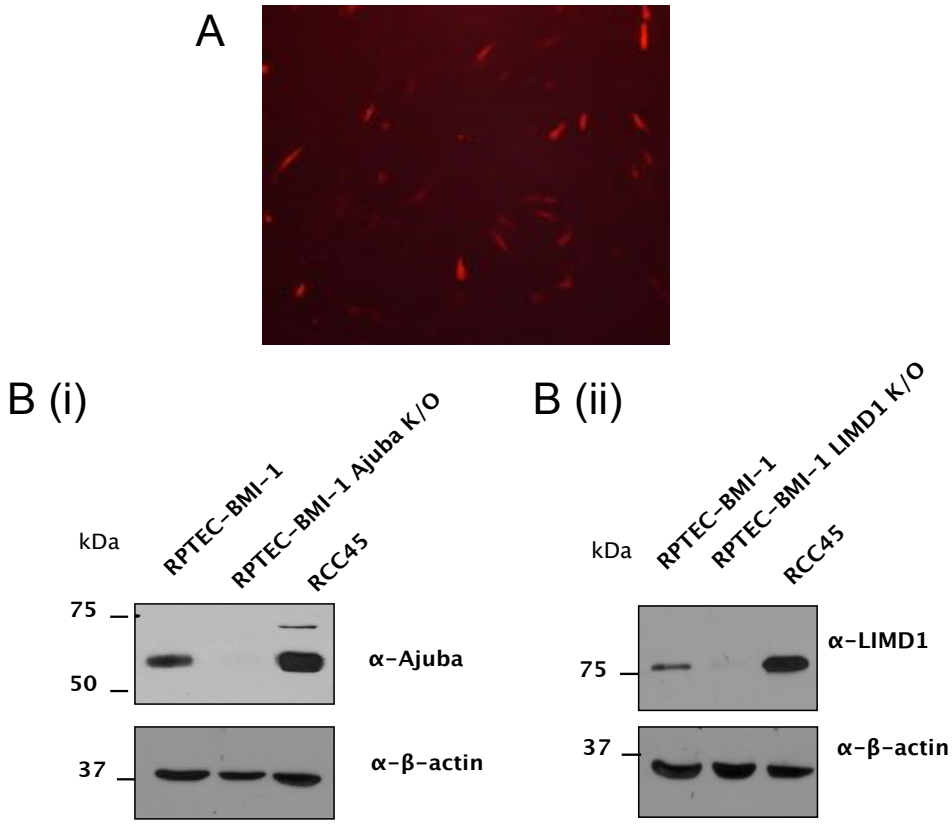

Figure 5.4. A CRISPR-Cas-9 system was used to successfully knockout Ajuba and LIMD1 in BMI-1 transducted RPTEC

BMI-1 transduced RPTEC cell lines were seeded in to a 24-well plate at a seeding density of $5x10^4$ cells/well and at 24 hours transfected using an optimised DharmaFECT™ Duo CRISPR Transfection system**.** Three crRNAs complementary to the genomic target sequence for *LIMD1*, and three for *AJUBA*, were utilised. An mKate2 fluorescent reporter with a blasticidin resistance marker and an hCMV promoter element was used to assess transfection efficiency at 48 hours. At 48 hours the transfection mix was removed and cells transiently selected with blasticidin for 72 hours before being allowed to recover and cells passaged. **(A)** A transfection efficiency of approximately 20% was achieved as assessed using the mKate2 fluorescent reporter. **B** Immunoblot of the cell lysate demonstrates very low levels of Ajuba expression in the *AJUBA* **(Bi)** and *LIMD1* **(Bii)** knockout lines compared to control following transient blasticidin selection and passage. RCC45 immunoblot is shown alongside for comparison.

5.6 Assessing the effects of LIMD1 loss on tumourigenesis in ccRCC *in vitro*

Hanahan and Weinberg proposed six critical capabilities acquired during the multistep development of cancer (Hanahan and Weinberg 2011). These capabilities include sustained proliferative signalling, evasion of growth suppressors, resistance to cell death, replicative immortality, induction of angiogenesis and activation of invasion and metastases. Underlying these capabilities is genomic instability, generating the genetic

diversity that drives the acquisition of such characteristics (Hanahan and Weinberg 2011).

The lentivirally transduced RCC11 and RCC48 lines were used to investigate the effects of LIMD1 loss on tumourigenesis, specifically the effects of LIMD1 loss on migration as a marker of invasion, sustained proliferative signalling as assessed by clonogenic assay, changes in cell cycle, indicative of changes in responsiveness to the negative regulators of cell cycle progression, and changes in angiogenesis as assessed by VEGFa ELISA and HIF1α reporter assay.

5.6.1 LIMD1 loss does not affect the migration of RCC11 and RCC48 cells as assessed by scratch assay

A simple scratch assay was used to study cell migration *in vitro*. This method is based on the observation that in a confluent cell monolayer, creation of a 'scratch' will result in cells at the edge of the gap moving to close the 'scratch', mimicking to some extent migration of cells *in vivo* (Liang, Park et al. 2007). Tumour cell migration and invasion is a clinically relevant end point as tumour metastasis impacts significantly on patient survival with 90% of cancer related patient deaths attributable to metastatic spread.

Four replicates for each experiment were carried out and three biological repeats undertaken. The mean results for each biological repeat was compared in the RCC11 and RCC48 cell lines at 24 and 48 hours. The Student's t-test was used to compare the rate of wound healing in the different lines. Loss of LIMD1 was not associated with a difference in the rate of wound healing in the RCC11 cell line at either time point (**Figure 5.4**). At 24 hours, Student's t-test p=0.136 for shLIMD1 compared to scr and p=0.947 for rrLIMD1 compared to shLIMD1 lines and at 48 hours, Student's t-test p=0.114 for shLIMD1 compared to scr and p=0.333 for rrLIMD1 compared to shLIMD1 lines.

A similar result was observed in the RCC48 cell line. At 24 hours, Student's t-test p=0.165, for shLIMD1 compared to scr lines and p=0.737 for rrLIMD1 compared to shLIMD1 lines whilst at 48 hours, Student's t-test p=0.157 for shLIMD1 compared to scr and p=0.747 for rrLIMD1 compared to shLIMD1 lines. Excellent knockdown of

LIMD1 was confirmed by immunoblot in the shLIMD1 line, with high levels of LIMD1 expression in the scr and rrLMD1 lines (**Figures 5.5 and 5.6**)

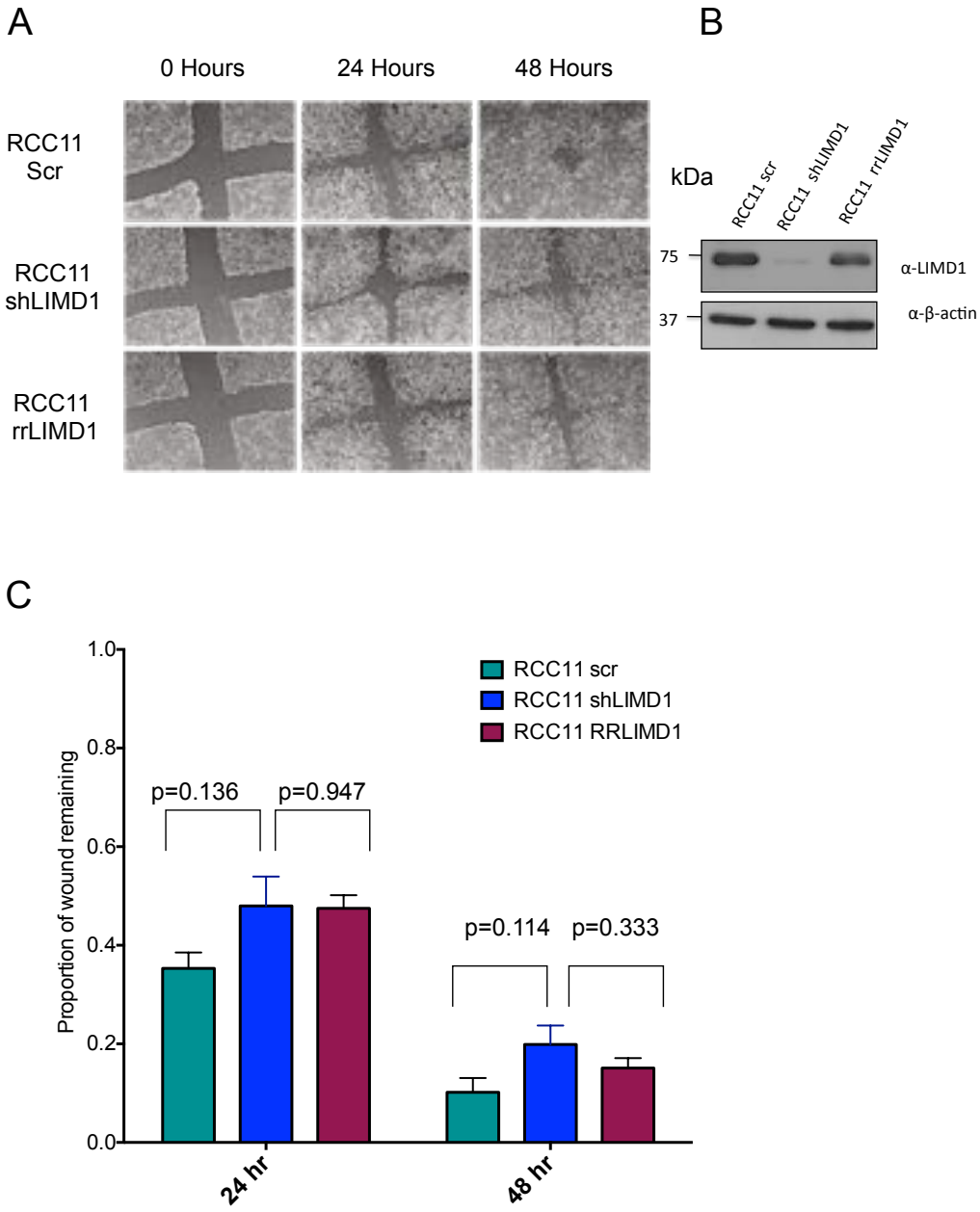

Figure 5.5. LIMD1 depletion does not affect cell migration in RCC11 cells as assessed by scratch assay

All cell lines were grown to confluency in a 6-well plate, a scratch made with the tip of a p200 prior to serum starvation with RPMI media containing 1% FCS: puromycin selection was maintained throughout. Four repeats were carried out for each scratch assay and three biological repeats undertaken. **A** Images of representative scratch at baseline and at 24 and 48 hours of RCC11 scr, shLIMD1 and rrLIMD1 cell lines. **B** Immunoblot of cells plated concurrently and lysed at 48 hours demonstrates high levels of LIMD1 expression in the scr and rrLIMD1 lines with excellent knockdown in the shLIMD1 line. **C** The mean result for each of the three experimental repeats is shown with error bars representing standard deviation. Statistical analysis shown is Student's t test. All analysis was conducted using Prism version 6.

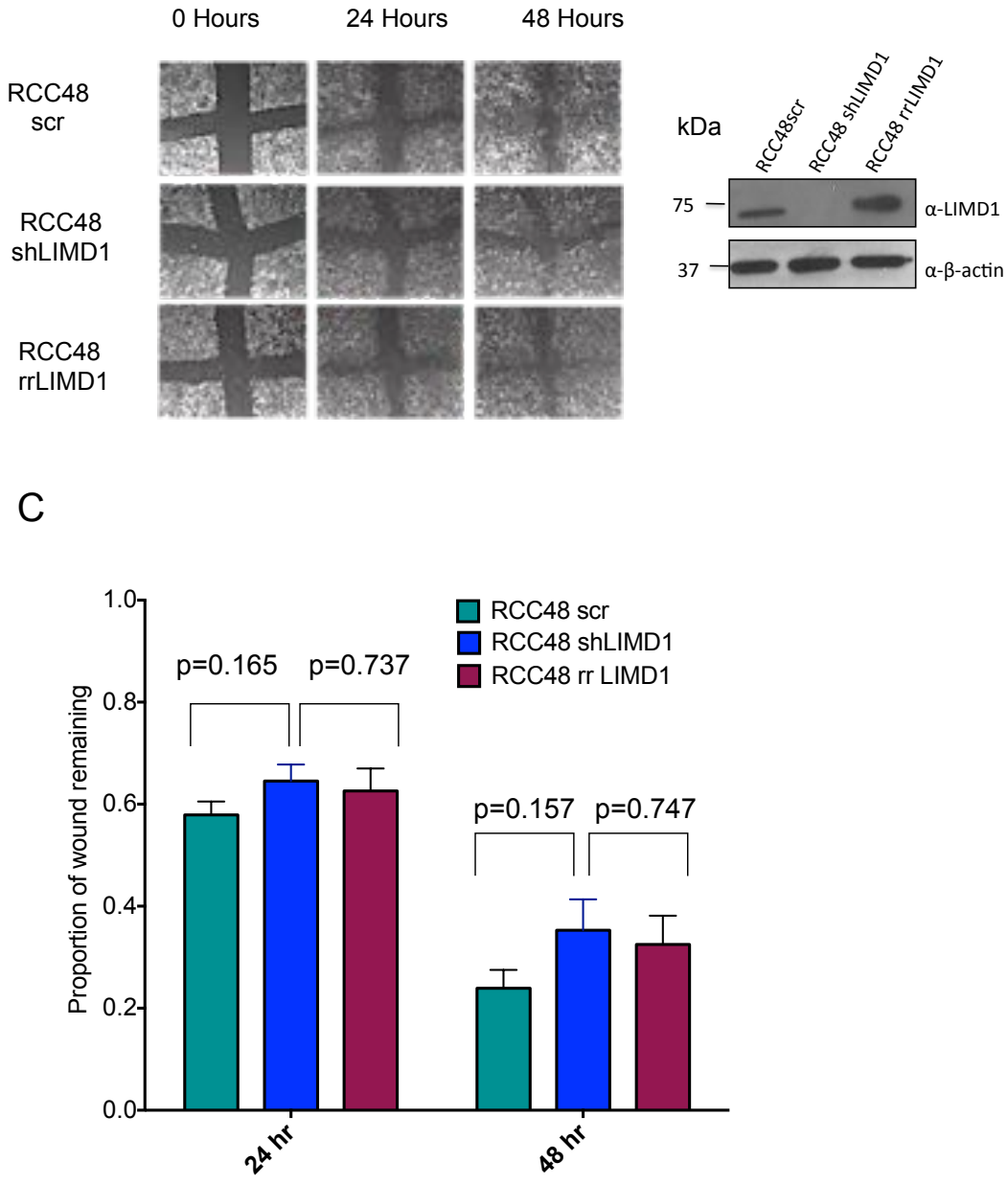

Figure 5.6. LIMD1 depletion does not affect cell migration in RCC48 cells as assessed by scratch assay

All cell lines were grown to confluency, a scratch made with the tip of a p200 prior to serum starvation with RPMI media containing 1% FCS, puromycin selection was maintained throughout. Four repeats were carried out for each scratch assay and three biological repeats undertaken. **A** Images of representative scratch at baseline and at 24 and 48 hours of RCC48 scr, shLIMD1 and rrLIMD1 cell lines. **B** Immunoblot of cells plated concurrently and lysed at 48 hours demonstrates high levels of LIMD1 expression in the scr and rrLIMD1 lines with excellent knockdown in the shLIMD1 line. **C** The mean result for each of the three experimental repeats is shown with error bars representing standard deviation. Statistical analysis shown is Student's t test. All analysis was conducted using Prism version 6.

5.6.2 LIMD1 depletion increases the number of RCC11 and RCC48 colonies formed in a clonogenic assay

Clonogenic assays are widely used assays for testing the effects of drugs/genes on the proliferative characteristics and growth of cells *in vitro* (Franken, Rodermond et al. 2006). A clonogenic survival assay determines the ability of a single cell to proliferate indefinitely, and thereby retain its ability to form a large colony or clone (Franken, Rodermond et al. 2006). The clonogenic potential of the lentiviral transduced RCC11 and RCC48 cell lines expressing LIMD1 or LIMD1 depleted was assessed. Identical numbers of cells were seeded in to a 6-well plate, and the plating efficiency (PE) calculated for each biological repeat ((Number of colonies counted/number of cells plated) before normalising the PE for the shLIMD1 and rrLIMD1 lines to that of the scr control. Six replicates were plated for each experiment, with four biological repeats undertaken.

The LIMD1 depleted RCC11 and RCC48 cell lines (shLIMD1) formed increased colonies compared to scr control as assessed by manual counting after crystal violet staining, Student's t-test p=0.0215* for RCC11 seeded at 200 cells/well. For RCC48 cells, Student's t-test p=0.0031** and p=0.0131* when seeded at 200 cells/well and 300 cells/well respectively (**Figures 5.7** and **5.8**).

The crystal violet was subsequently solubilised, an alternative method for characterising clonogenic assays (Franken, Rodermond et al. 2006). Increased absorbance was observed in the shLIMD1 lines compared to scr control. This did not quite meet statistically significant in the RCC48 lines seeded at 300 cells/well, Student's t-test p=0.1014, but was statistically significant in the RCC48 seeded at 200 cells/well, Student's t-test p<0.0001***, and for RCC11 seeded at 100 cells/well, Student's t-test p=0.0124* (**Figures 5.7** and **5.8)**.

An increased number of colonies was consistently observed in the rrLIMD1 control compared to shLMD1 line for each biological repeat, however as variability was observed in the mean number of colonies for each experiment, the shLIMD1 and rrLIMD1 data were normalised to the scr control. The resulting error bars for the

rrLIMD1 line were large and comparison of the shLIMD1/rrLIMD1 lines did not meet statistical significance.

In the RCC11 line, comparison of the LIMD1 depleted shLIMD1 (RCC11 shLIMD1) and rrLIMD1 lines did not meet statistical significance as assessed by both manual counting and reading the absorbance of the solubilised crystal violet, Student's t-test, p=0.219 and p=0.1397 respectively (**Figure 5.7**). In the RCC48 line, comparison of the LIMD1 depleted shLIMD1 and rrLIMD1 lines also did not meet statistical significance as assessed by both manual counting and reading the absorbance of the solubilised crystal violet, Student's t-test, p=0.0627 and p=0.3608 respectively for cells seeded at 200 cells/well and p=0.1565 and p=0.1562 respectively for cells seeded at 300 cells/well (**Figure 5.8**).

Taken together the increased colony formation observed in both cell lines in association with LIMD1 knockdown compared to proficient control, suggests that LIMD1 loss increases clonogenic survival in both cell lines.

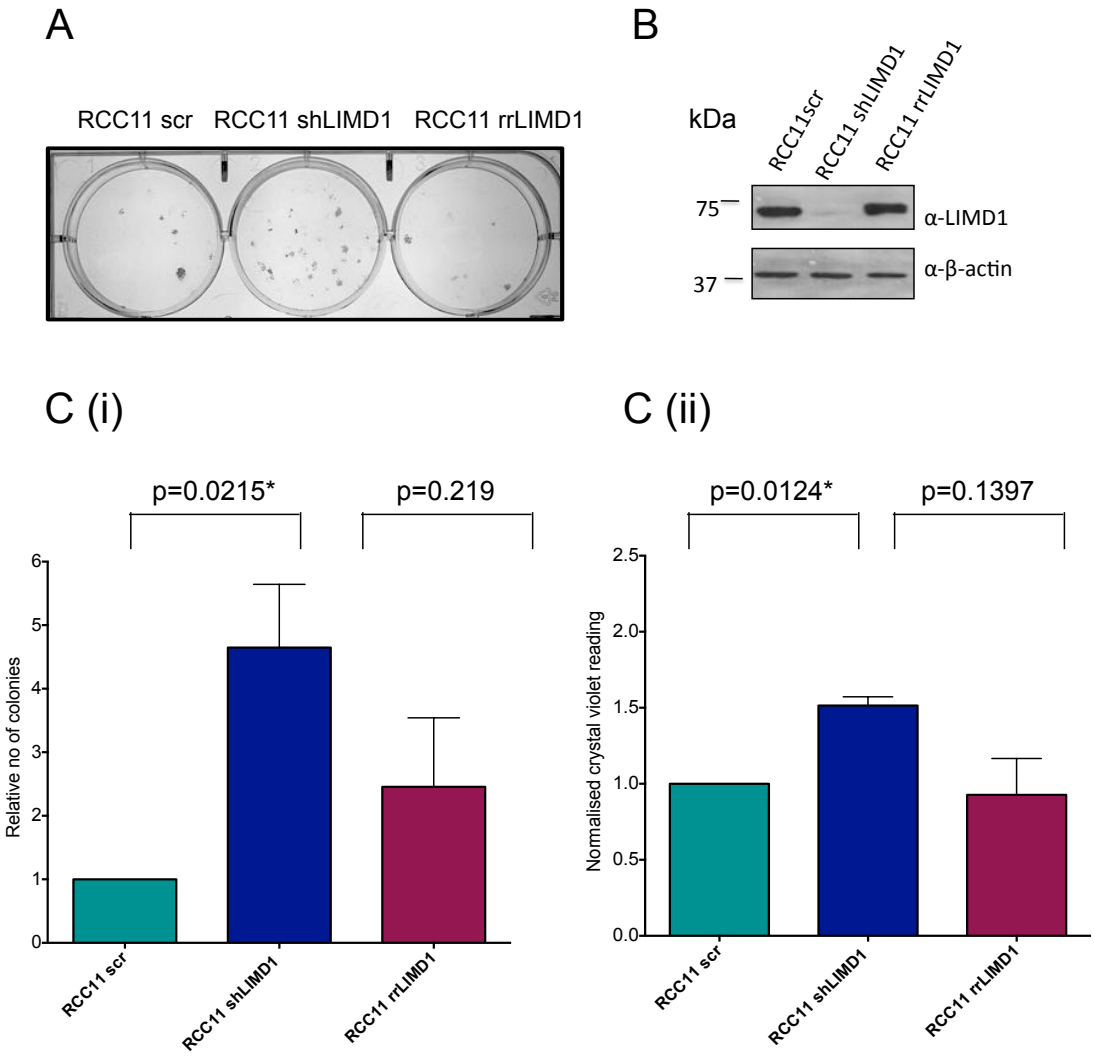

Figure 5.7. LIMD1 depletion increases RCC11 colony formation

A Representative images of colonies in the RCC11 scr, shLIMD1 and rrLIMD1 cell lines at 20 days: 100 cells of the three lentiviral transduced cell lines were seeded in to one well of a 6-well plate with six replicates for each cell line plated and cells were maintained in puromycin selection. **B** Knockdown of LIMD1 in the shLIMD1 cell line and expression in the scr and rrLIMD1 lines was confirmed at the end of the assay by Western Blot analysis. **C (i)** Results are representative of three separate biological repeats, quantifying colony number by manual counting after fixation and staining with crystal violet **C (ii)** The crystal violet was extracted and quantified by absorbance. Error bars represent standard deviation n=6, results are normalised to the scr control. Statistical analysis shown is Student's t test. All analysis was conducted using Prism version 6.

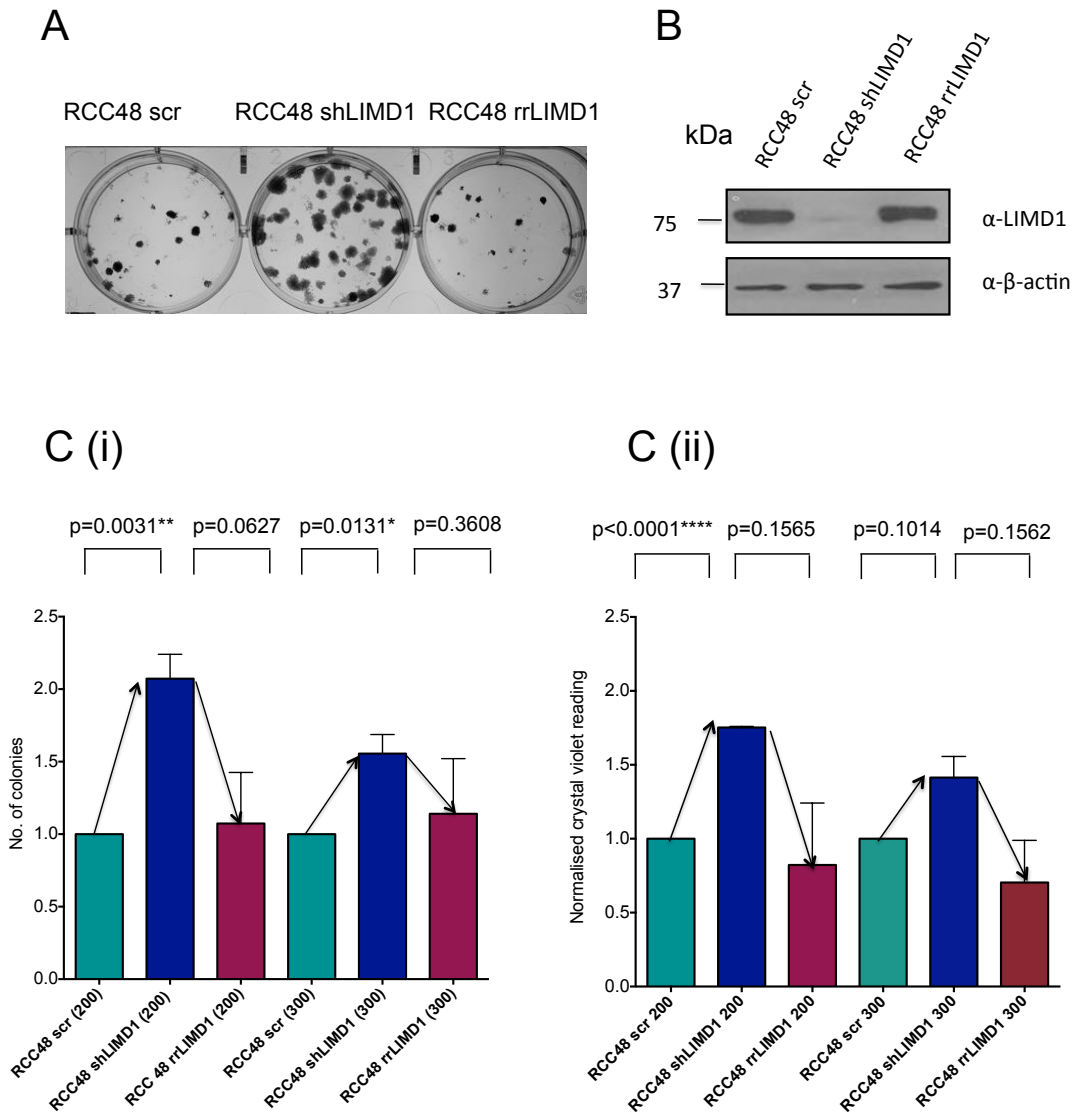

Figure 5.8. LIMD1 depletion increases RCC48 colony formation

A Representative images of colonies in the RCC11 scr, shLIMD1 and rrLIMD1 cell lines at 20 days: 200, or 300 of the three lentiviral transduced cell lines were seeded in to one well of a 6-well plate with six replicates for each cell line plated at each seeding density, cells were maintained in puromycin selection throughout. **B** Knockdown of LIMD1 in the shLIMD1 cell line and expression in the scr and rrLIMD1 lines was confirmed at the end of the assay by Western Blot analysis. **C (i)** Results are representative of three separate biological repeats quantifying colony number by manual counting after fixation and staining with crystal violet, results are normalised to the scr control. **C (ii)** The crystal violet was extracted and quantified by absorbance. Error bars represent standard deviation n=6, results are normalised to the scr control. Statistical analysis shown is Student's t test. All analysis was conducted using Prism version 6.

5.6.3 Loss of LIMD1 increases VEGFa secretion in RCC11 and RCC48 lines as assessed by ELISA

Analysis of IHC staining in the ccRCC histospots demonstrated an inverse correlation between LIMD1 and VEGFa staining, contrary to the correlation expected. It was hypothesised that this may be related to a 'steal' effect whereby tumours with higher VEGF levels in turn secrete more VEGF to promote neo-vascularisation, thereby resulting in paradoxically lower VEGF staining within the tumours, but increased neo-angiogenesis, a similar observation to that observed by Kluger *et al* (Kluger, Siddiqui et al. 2008*)*. Given this observation and the role of VEGFa as a potent mediator of angiogenesis in ccRCC, VEGFa secretion was assessed in paired LIMD1 expressing and LIMD1 depleted RCC11 and RCC48 cells.

In the RCC11 line in both normoxia and after incubation in 1% O_2 for 20 hours, increased VEGF secretion was observed in the shLIMD1 line compared to scr control, Student's t-test p=0.0418* and p=0.0434* respectively (**Figure 5.9 (Ai)**). A similar result was observed in the RCC48 line, with increased VEGF secretion in the shLIMD1 line compared to scr control: this was statistically significant in normoxia but not in hypoxia, Student's t-test p=0.0328* and p=0.0503 respectively (**Figure 5.9 (Aii)**). All assays were undertaken in duplicate and two biological repeats performed. The assay was not undertaken in the rrLIMD1 line, as insufficient ELISA kit was available.

The results of the ELISA suggests that loss of LIMD1 is associated with increased VEGF secretion *in vitro*, potentially contributing to increased angiogenesis and consistent with a role of LIMD1 in the regulation of the hypoxic response. This also supports the hypothesis that the positive correlation observed between staining for LIMD1 and VEGFa in tumour samples could be as result of increased VEGFa secretion in tumours with low LIMD1 expression, a 'steal' effect that results in those tumours having paradoxically less VEGFa staining.

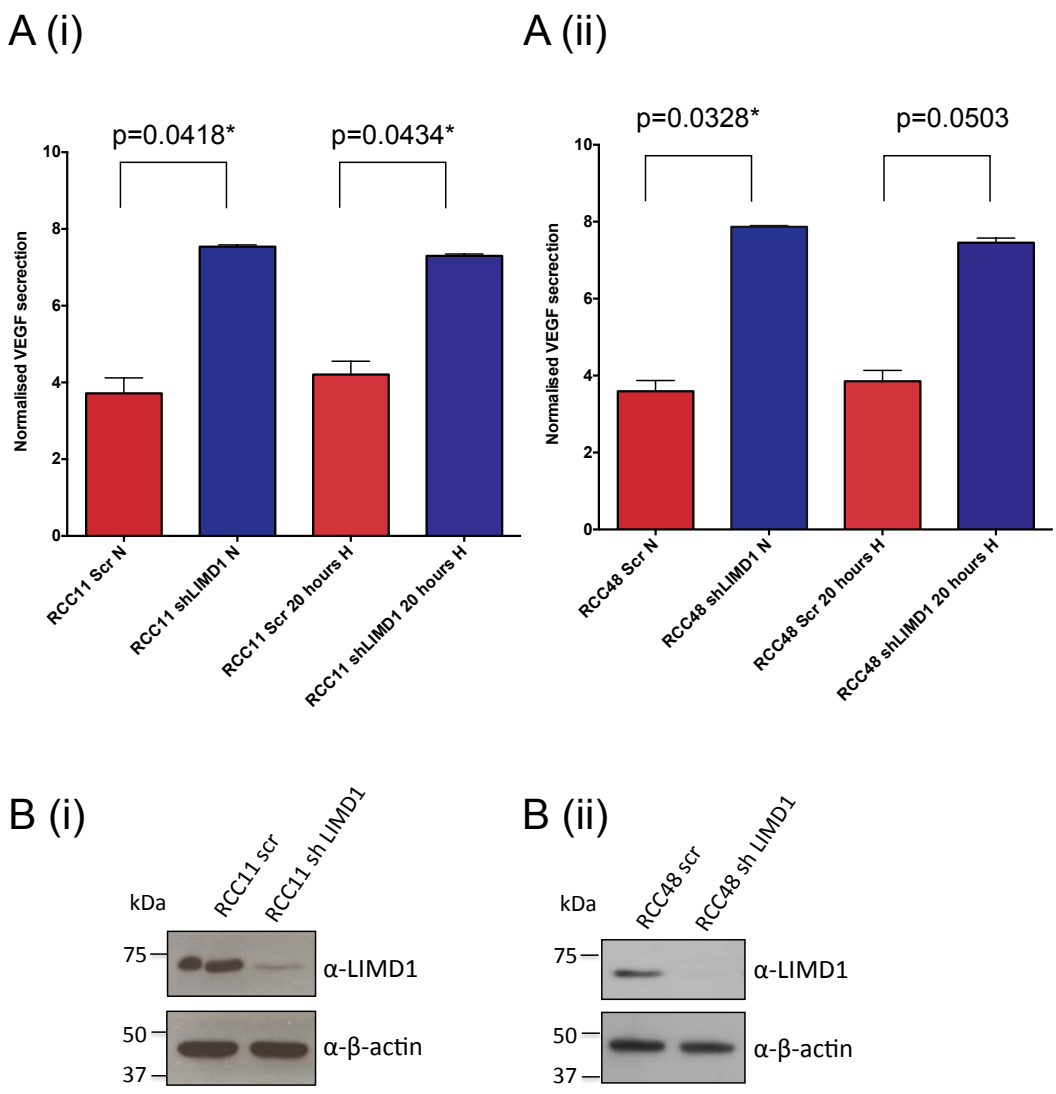

Figure 5.9 LIMD1-depletion increases VEGF secretion as assessed by ELISA in RCC11 and RCC48 cells

RCC11 and RCC48 cells were seeded at $2x10^5$ cells/well in to a 6-well plate to ensure 50-60% confluency at 36 hours. At 16 hours, RCC11 and RCC48 cells were incubated in a hypoxic chamber at 1% O_2 for 20 hours prior to lysis. Cells were also left for a further 20 hours in normoxia, (20% O_2) prior to lysis. A commercially available VEGF ELISA kit from was used to assess VEGF secretion and optical density read using a Wallac 1420 Multilabel counter plate reader. Control standards were used to determine VEGF levels. All ELISAs were measured in duplicate. Results are representative of two separate biological repeats. **(Ai)** Increased VEGF secretion is demonstrated in the RCC11 shLIMD1 cells relative to the scr control in both normoxia and hypoxia (A**ii**) Increased VEGF secretion is demonstrated in the RCC48 shLIMD1 cells relative to the scr control incubated in normoxia but not hypoxia. (**B (i)**) and **B (ii)**. Excellent knockdown of LIMD1 was observed in the shLIMD1 line upon immunoblot with high levels of LIMD1 expression in the scr line in both RCC11 (**B (i)**) and (**B (ii)**) RCC48 lines. Statistical analysis shown is Student's t test with error bars demonstrating the standard deviation. All analysis was conducted using Prism version 6.

5.6.4 HIF1α luciferase dual-reporter assay

LIMD1 functions as an adapter protein, binding PHDs and VHL simultaneously and targeting HIF1α for degradation via the proteasome. LIMD1 depletion is associated with HIF1α upregulation in HEK-293-T cells (Foxler, Bridge et al. 2012).

Luciferase dual-reporter assays are widely used to study transcriptional activation (Dyer, Ferrer et al. 2000). The two different types of luciferases commonly used have distinct substrate requirements, which produce different wavelengths of fluorescence, thus enabling quantification from a single sample. In this assay, cells were simultaneously transfected with a thymidine kinase-Renilla (TK-Renilla) luciferase reporter, thymidine kinase is constitutively expressed, and a pGL3- (6x) HRE-firefly luciferase plasmid, where the promoter response element for HIF1-α had been cloned upstream of the pGL3 basic firefly luciferase plasmid. Differences in transfection efficiency were accounted for by normalising the luminescence obtained for the experimental reporter HRE plasmid or Vo plasmid to the luminescence for the constitutive Renilla reporter. The normalised reporter luminescence in the shLIMD1 cell lines were then normalised to the scr control. Three biological repeats were carried out, with each assay conducted in triplicate. This enabled a functional read out of the effect of LIMD1 loss on the activation of a HIF1α reporter construct in both RCC11 and RCC48 cell lines.

In the RCC11 line, normalised luminescence and therefore HIF1α activity was greater in the shLIMD1 line in hypoxia compared to the scr control, Student's t-test p=0.03459*, this did not meet statistical significance in normoxia, Student's t-test p=0.3299. In RCC48, normalised luminescence and therefore HIF1α activity was greater in the shLIMD1 line in normoxia compared to the scr control, Student's t-test p=0.0040**, this did not meet statistical significance in hypoxia, p=0.0790 but a trend towards significance was observed. Excellent knockdown was observed in the shLIMD1 lines, compared to scr control as assessed by immunoblot (**Figure 5.10**).

Figure 5.10. LIMD1 depletion increases HIF1α activity as measured by a HIF1α reporter assay

$3.5x10^5$ of each cell line was seeded in to a 24-well plate, with each co-transfection carried out at 24 hours in triplicate. Cells were co-transfected with either 200 ng of the pGL3- (6x) HIF1 α HRE-firefly luciferase or 200 ng of the pGL3Vo firefly luciferase in combination with 30 ng of the TK-*Renilla* luciferase reporters. After seven hours one plate was transferred to the hypoxic workstation for sixteen

hours incubation and the second plate remained in normoxia. The luminescence was read according to the manufacturers instructions (Promega). Differences in transfection efficiency were accounted for by normalising the luminescence obtained for the experimental reporter, Firefly or Vo, to the luminescence for the constitutive reporter, Renilla. **A (i)** Increased HIF1α reporter activity is demonstrated in RCC11 shLIMD1 compared to RCC11 scr in hypoxia. **A (ii)** Increased HIF1α reporter activity is demonstrated in RCC48 shLIMD1 compared to RCC11 scr in both normoxia and hypoxia. Excellent knockdown of LIMD1 was observed in the shLIMD1 line upon immunoblot with high levels of LIMD1 expression in the scr line in both RCC11 (**B (i)**) and (**B (ii)**) RCC48 lines. Analysis was undertaken in Prism 6. Statistical analysis shown is Student's t test with error bars representing standard deviation, three biological repeats were undertaken.

5.6.6 Changes in cell cycle associated with loss of LIMD1 in RCC11

The loss of responsiveness to negative regulators of cell cycle progression, and/or the acquisition of independence from mitogenic signals is a critical change in the cell cycle associated with malignant transformation (Hanahan and Weinberg 2011). Fluorescence-associated cell sorting (FACS) is a tool used to analyse cell cycle distributions, providing a clear picture of the proportions of cells in each of the cell cycle phases.

Cell cycle phase was assessed in the RCC11 lentivirally transduced cell lines and comparison of the scr and shLIMD1 lines undertaken. Cells of similar early number passage number were used, media changed concurrently in the different lines and PI staining of cells that were approximately 50% confluent, undertaken. Three biological repeats were undertaken with each experiment conducted in triplicate. Fluorescence was read using the FACS Caliber B machine with the YG-610/20 excitation-emission filters. The appropriate gates were set around the G0/G1, S and T2/M phase peaks and analysis undertaken using Flowjo 7.6.5 software. Representative cell cycle phase peaks and gating is shown in **Figure 5.11A**. For each biological repeat, the mean for the proportion of cells in each cell cycle phase was calculated. The mean and standard deviation for the biological repeats is shown in **Figure 5.11B**. There was no difference in the proportion of cells in each phase of the cell cycle in association with loss of LIMD1.

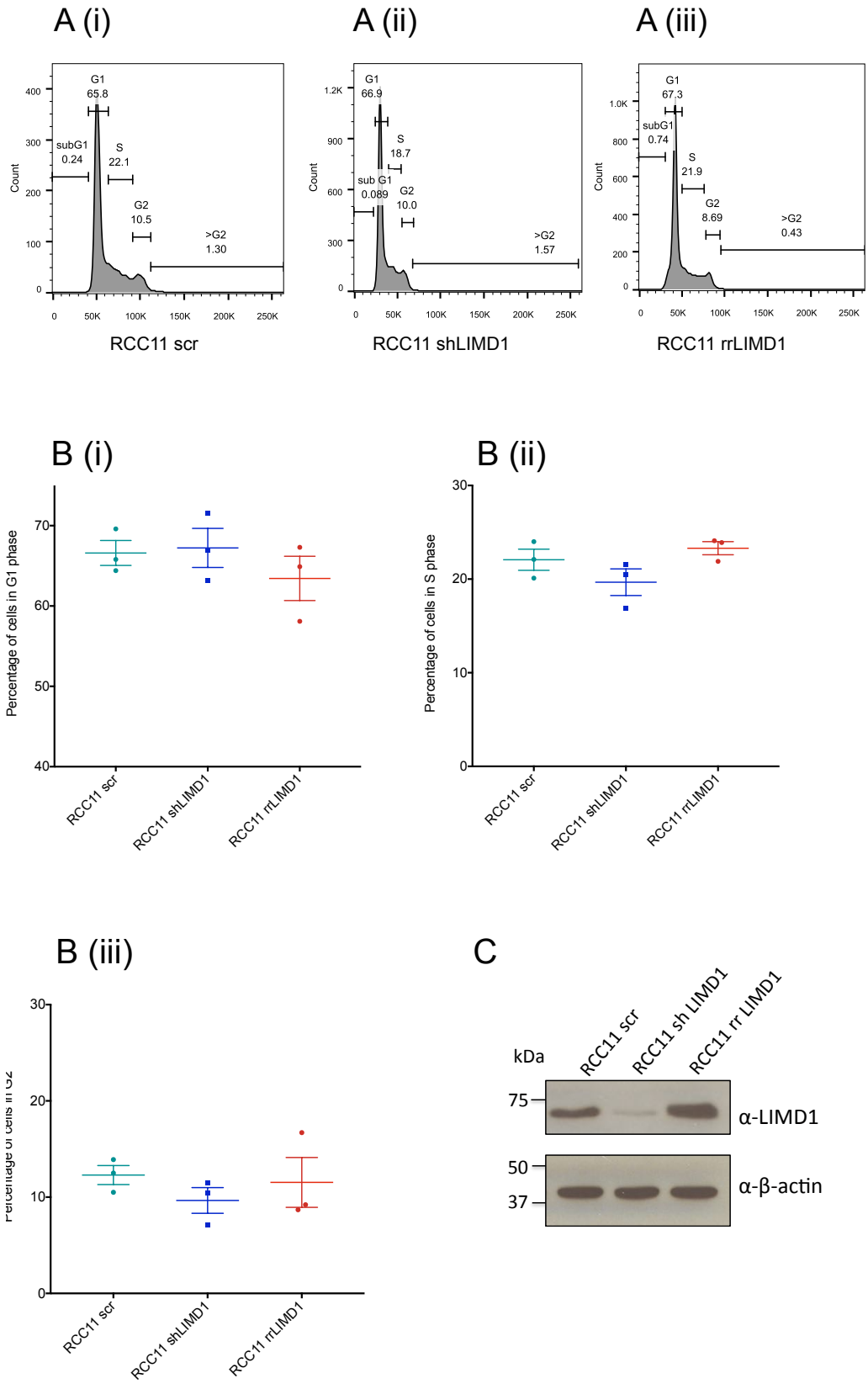

Figure 5.11. LIMD1 depletion does not affect cell cycle phase as assessed by propidium iodide staining and FACS sorting

RCC11 scr/shLIMD1 cells were seeded in to 6-well plates such that cell confluency was approximately 50% 24 hours post seeding. Cells were lysed and counted, then permeabilised and fixed prior to staining with propidium iodide. Fluorescence was read using a Fluorescence Activated Cell Sorter (FACS Caliber B) using the YG-610/20 excitation-emission filters with the appropriate gates set around the G0/G1, S and G2/M phase peaks. Results were analysed using Flowjo 7.6.5 software. Three biological repeats were undertaken with each experiment conducted in triplicate. Fluorescence was read using the FACS Caliber B machine with the YG-610/20 excitation-emission filters. (**A**) Representative cell cycle phase peaks and gating for RCC11scr, RCC11 shLIMD1 and RCC11 rrLIMD1. (**B**) For each biological repeat, the mean for the proportion of cells in each cell cycle phase was calculated and plotted using Prism 6. The mean and standard deviation for the biological repeats is shown. (C). Cells plated concurrently were also lysed and immunoblotted for LIMD1 and β-actin as loading control, high levels of LIMD1 expression were confirmed in the scr and rrLIMD1 lines with excellent knockdown in the shLIMD1 line.

5.7 Summary

In vitro work has identified a number of roles for LAW protein members including the regulation of the Hippo signalling pathway, a critical regulator of organ size and cell cycle control, de-regulation of which is implicated in tumourigenesis in multiple tumour types (Huang, Wu et al. 2005), LIMD1 interacts with the retinoblastoma protein to inhibit E2F1-mediated transcription (Sharp, Munoz et al. 2004) and functions as a critical regulator of HIF-1 activity, bridging an association between the prolyl hydroxylases and VHL and targeting HIF1α for degradation via the proteasome (Foxler, Bridge et al. 2012). In addition, LIMD1, Ajuba and WTIP localise to cytoplasmic P-bodies, sites of miRNA/mRNA interaction, where they facilitate interactions between the core miRISC and the EIF4E/m^7GTP cap structure of mRNA, thereby blocking mRNA translation initiation (James, Zhang et al. 2010)

In ccRCC, the effects of LAW protein loss on tumourigenesis have not been characterised. The effects of LIMD1 loss on tumourigenesis were investigated further. A lentiviral transduction system was used to generate non-targeting siRNA (scr) control, LIMD1 knockdown (shLIMD1), and LIMD1 knockdown with concomitant rescue (rrLIMD1) in RCC11 and RCC48 lines, chosen as they are representative of aggressive, 'hypoxically' deregulated ccRCC lines. Using these lentiviral lines, *in vitro* assays demonstrated that LIMD1 loss did not affect migration using a scratch assay as a marker of invasion, nor were changes in cell cycle observed, indicative of changes in responsiveness to the negative regulators of cell cycle progression as assessed by FACS analysis.
VEGFa ELISA and HIF1α reporter assay however suggested that LIMD1 loss in these cell lines was associated with greater hypoxic deregulation with increased VEGFa secretion and increased activity of a HIF1α reporter assay. Immunoblot of the lentivirally transduced RCC48 cell lines incubated in hypoxia also demonstrated increased HIF1α levels in association with LIMD1 knockdown.

CRISPR-Cas-9 mediated genetic editing enables the targeted and efficient modification of eukaryotic species (Hsu, Lander et al. 2014) and has only been successfully applied to

a few primary human cell types (Hendel, Bak et al. 2015). RPTEC lines were successfully transduced with a BMI-1 construct with the aim of increasing replicative lifespan and of generating cell lines that in combination with LAW protein loss more closely resembled that of a ccRCC line. A CRISPR-Cas-9 gene editing system was used to successfully knockout *LIMD1* and *AJUBA* in the BMI-1 transduced RPTEC. Single cell selection however was not possible and it was therefore not possible to use such cells in further *in vitro* assays.

5.8 Discussion

In this chapter the use of a CRISPR-Cas-9 system to selectively delete *LIMD1* and *AJUBA* in the primary renal cell line RPTEC, transduced with a BMI-1 construct was demonstrated. The effects of LIMD1 depletion on several critical features of tumourigenesis were characterised: sustained proliferative capacity using a clonogenic assay, the activation of invasion and metastases using a migration assay, sustained proliferative signalling through FACS analysis and the induction of angiogenesis using a VEGFa ELISA and HIF1α reporter assay.

5.8.1 BMI-1 transduction of RPTEC

BMI-1 can induce telomerase activity and bypass senescence in some cell lines such as mammary epithelial cells (MECs) and fibroblasts and mechanisms for this have been described (Dimri, Martinez et al. 2002) (Jacobs, Kieboom et al. 1999). However, for most epithelial cells, senescence cannot be overcome by the ectopic expression of telomerase alone, through for example BMI-1 or hTERT overexpression, and in many such cells alterations in the pRb pathway are also necessary. In a study by Lundberg *et al*, human airway epithelial cells were directly immortalised through both the successive introduction of the Simian Virus 40 Early Region (*SV40T*) and *hTERT* (Lundberg, Randell et al. 2002) and such an approach has also been used to successfully immortalise RPTEC using two lentiviral vectors carrying *hTERT* and *SV40T*, flanked by loxP sites (Kowolik, Liang et al. 2004).

Immunoblotting for hTERT was undertaken in an attempt to quantify differences in hTERT expression in association with RPTEC *BMI-1* transduction but immunoblots were of poor quality and it was difficult to assess whether *BMI-1* transduction up-regulated hTERT expression. *BMI-1* transduction did not seem to increase the replicative capacity of RPTEC, with cells undergoing senescence after a similar number of passages compared to the non-transduced cells. It is therefore likely that in the RPTECs, *BMI-1* transduction alone was not sufficient for immortalisation. This limited the use of the RPTECs for subsequent *in vitro* experiments as cell stocks underwent senescence after a few passages.

5.8.2 Use of the CRISPR-Cas-9 system to generate LIMD1 and Ajuba RPTEC knockouts

Systems such as homologous recombination-mediated targeting can generate knockin and knockout animal models, however recombination events occur extremely infrequently. RNA interference with small interfering (siRNA) or short hairpin RNAs (shRNAs) can provide good knockdown, which in the case of siRNA is transient or more permanent with an shRNA system. Very good knockdown with a lentiviral shRNA system was consistently achieved, with such a system however, levels of knockdown are variable and never complete. In addition, the lentiviral constructs used were large and sites of gene integration cannot be predicted and could vary from one cell to another, which could have unpredictable downstream consequences on the expression of other genes.

Use of CRISPR-Cas-9-mediated genetic editing enables the targeted and efficient modification of eukaryotic species (Hsu, Lander et al. 2014). In particular the use of the CRISPR system can be used to target virtually any genomic location with the use of a short RNA guide (Hsu, Lander et al. 2014). Using a CRISPR-Cas-9 system, complete and permanent cleavage of a gene of interest is possible such that no-transcription of that gene will occur with little in the way of off-target effects (Hsu, Lander et al. 2014). Given frequent 3p and 14q LOH in ccRCC, we would expect functional LIMD1 and Ajuba to be reduced in many ccRCC lines compared to primary renal lines such as RPTEC. Therefore, a system that results in biallelic permanent cleavage of LIMD1 or Ajuba allows for the clear investigation of the effects of gene loss on tumourigenesis. The Edit-R DharmaFECT^{TM} Duo CRISPR-Cas-9 system was used to successfully knock out LIMD1 and Ajuba in the BMI-1 transduced RPTEC.

CRISPR-Cas-9 technology has only been successfully applied to a few primary human cell types and predominantly cells with greater replicative potential such as human embryonic stem cells (Hendel, Bak et al. 2015). Reasons for the frequent lack of efficacy of CRISPR-Cas-9 technology in primary cells are not fully known, but some contributing factors include low transfection efficiencies, the requirement for multiple passages/proliferation, the harsh selection conditions generally required to achieve an

edited primary cell population and DNA repair fidelity (Hsu, Lander et al. 2014, Chu, Rios et al. 2015).

The use of synthesised guide RNAs is often considered to be a superior method for inducing higher levels of gene editing using a CRISPR-Cas9 system compared to for example a lentiviral construct (Hendel, Bak et al. 2015). sgRNA mediated DNA cleavage is also increased by increasing the number of sgRNAs included: three sgRNAs were used for both *LIMD1* and *Ajuba* to increase the likelihood of successful gene editing (Hendel, Bak et al. 2015). The use of a synthesised guide RNA system effectively induces targeted indels indicative of mutagenic non-homologous end joining and gene disruption, with off-target gene disruption close to background (Hendel, Bak et al. 2015). Excellent knockdown of Ajuba and LIMD1 was observed in the heterogeneous RPTEC population suggesting that this system resulted in successful biallelic gene editing in a significant proportion of cells.

FACS sorting with enrichment of cells that still express the transiently expressed mKATE2 expression plasmid two to three days days post transfection can enrich the cell population that has undergone CRISPR-Cas-9 mediated gene editing further but given the excellent knockdown in the heterogeneous population, and likely significant loss of cells associated with this approach, FACS sorting was not undertaken.

The use of single cell selection ensures that the cell population used is clonal and clearly defined. Single cell selection of the RPTEC in order to generate cells derived from a clonal population was however not possible, despite BMI-1 transduction. BMI-1 transduction did not appear to increase the number of times the cells could be passaged prior to senescing.

5.8.3. Single cell selection of primary cells

Single cell selection of primary cells is often difficult. Chu *et al* used a lentiviral CRISPR-Cas-9 system to knockout Muc01 in human epithelial cells (Chu, Rios et al. 2015). They were able to effectively grow these cells such that cells demonstrated near unlimited proliferation but did not undergo transformation. Cells were grown with the addition of a Rho-kinase (ROCK) inhibitor and using modified Schlegel culture conditions, where

cells are cultured on an irradiated fibroblast feeder layer containing specialised media additives (Chu, Rios et al. 2015). Such an approach allows near unlimited proliferation and the passage of numerous epithelial cell types without loss of primary characteristics and transformation (Liu, Ory et al. 2012). Of note single cell selection was not undertaken by Chu *et al*, but the use of modified Schlegel culture conditions in combination with puromycin selection in order to select for cells that had undergone lentiviral transduction, allowed for the selective enrichment of transduced cells. Cells grown from the heterogeneous population were then used to establish Muc01 knockout (Chu, Rios et al. 2015).

A search of the literature, failed to identify any articles detailing successful single cell selection of RPTECs. Seeding cells into a large tissue dish with the aim of single cell selecting colonies was unsuccessful, as colonies failed to grow. The use of conditioned media can also increase the likelihood of single cell selection of primary cells. Here cells are cultured in media supplemented with 25-50% media from cultured cells no more than 70% confluent. In the study by Liu *et al*, the use of modified Schlegel culture conditions, in combination with a ROCK inhibitor, caused many normal and tumour epithelial cells such as primary prostate and mammary cells to proliferate indefinitely *in vitro* (Liu, Ory et al. 2012).

It had been hoped that given the excellent LIMD1 and Ajuba knockdown in the CRISPR-Cas-9 heterogeneous RPTEC population, the heterogeneous population could be used for further *in vitro* experiments to investigate the effects of LIMD1 and Ajuba loss, but the senescence of these cell lines after a few additional passages meant that this was not possible. The use of a ROCK inhibitor and or modified Schlegel conditions may have been more successful in the RPTECs, allowing cell number to be bulked up quickly within a relatively low number of cell passages.

CRISPR-Cas-9 mediated gene editing in primary cells represents a particular challenge and has not been described in ccRCC. This work demonstrates that the Edit-R™ CRISPR-Cas9 gene-engineering platform can be used successfully to delete genes in RPTECs. Modification of the cell immortalisation protocol and techniques for bulking up cell number after CRISRP-Cas-9 mediated gene editing within a relatively few number of cell passages, could enable heterogeneous cell populations or single cell selected cells to be used in further *in vitro* assays.

5.8.4 *In vitro* work to characterise the effects of LIMD1 loss on cell migration

Simple scratch assays were undertaken in both lentiviral-transduced RCC11 and RCC48 lines, to assess the effects of LIMD1 loss on migration. It was hypothesised that LIMD1 depletion through HIF1α stabilisation might up-regulate pro-migratory cytokines such as VEGF, with consequent increased cell migration and wound healing. Loss of LIMD1 however did not increase cell migration as assessed by scratch assay in either line.

Migration is defined as the directed movement of cells on a substrate, by definition within a 2-dimensional (2-D) context, without any obstructive networks. Invasion, however is associated with the movement of cells through a 3-dimensional (3-D) matrix with associated restructuring of the 3-D environment, for example invasive cancer cells must interact and re-shape the extracellular matrix (ECM) and both migration and invasion are critical components of tumourigenesis (Liang, Park et al. 2007). Scratch assays are simple, 2-D assays that are inexpensive and easy to interpret but have some limitations. In particular it is hard to control the precise scratch area and therefore guarantee equivalence between control and experimental scratches (Liang, Park et al. 2007). With practice however, it was observed that initial scratch areas were of similar size and initial scratches that differed significantly in size from that observed typically were excluded from analysis.

A long-term wound-healing assay, defined as greater than 24 hours cannot distinguish between increased healing as a consequence of increased cell proliferation and increased cell motility. It had been observed that loss of LIMD1 did not affect the rate of cell growth in either cell line when grown in standard conditions with RPMI supplemented with 10% FCS. In the wound healing assays, cells were serum starved and grown in 1% FCS such that wound healing was more likely to be a function of cell migration and not as a result of increased cell proliferation.

Wound healing was assessed at 24 and 48 hours but wound healing was also initially assessed at 12 hours and no differences between the cell lines observed. The use of automated video microscopy in time-lapse experiments can enable the distinction

between cell migration and cell division and automated cell tracking algorithms exist that can enable the recording of several cell types simultaneously (Kramer, Walzl et al. 2013).

Scratching can damage the matrix underneath the cells and cells at the edge of the scratch are more likely to be damaged. This can result in dysfunction in their migration and the release of unidentified factors that may affect the migration of other cells. Proprietary inserts can overcome this by generating a consistent wound gap between cells and minimising the likelihood of cell damage at the wound interface. The inserts create an exclusion zone when cells are seeded, and the cell density adjusted such that cells are fully confluent (Kramer, Walzl et al. 2013). However for all cell types, particularly given the consistency of the scratch size, damage to the matrix underneath and cells at the scratch assay should have been fairly consistent.

Although our results did not show any difference in cell migration in association with LIMD1 loss, assays were only carried out in two cell lines, and further migration assays for example measuring three-dimensional migration or transwell migration assays could characterise this further.

5.8.5 Increased cell proliferation is observed in association with LIMD1 loss in ccRCC

The two-dimensional clonogenic assay demonstrated an increase in colony formation in association with LIMD1 loss suggesting that LIMD1 down-regulation may give rise to more transformed cancer cell phenotype with an increase in the cells ability to retain a proliferative capacity indefinitely.

Colony assays are simple semi-quantitative assays that are easy to read and for many years were considered the gold standard for the analysis of the proliferative/malignant potential of individual cells and their ability to resist treatment (Franken, Rodermond et al. 2006). The assay assesses the ability of individual cells to produce progeny, specifically to produce a clone defined as more than 50 cells. Typically clonogenic assays evaluate the ability of a single cell to resist treatment and grow into a colony after treatment with a chemotherapeutic agent but clonogenic assays are also used to evaluate the transforming effect of oncogenes or to investigate the effects associated with the

loss of a tumour suppressor protein (Franken, Rodermond et al. 2006).

Two separate methods were used to evaluate the number of colonies formed, a subjective manual counting approach and a more objective approach where the absorbance of the solubilised crystal violet was read. For both approaches, loss of LIMD1 was associated with increased colony formation in both cell lines. Other more quantitative approaches involve the use of an Image-J plug in to automatically assess clonogenic assay area as a function of the total well area (Guzman, Bagga et al. 2014).

Three-dimensional (3-D) colony assays measure the ability of cells to form colonies in three-dimensions, typically in soft agar. The transformations associated with this phenotype include a loss of contact inhibition and anchorage independence, i.e. cells can grow over one another, features considered critical for *in vivo* carcinogenesis. 3-D assays are often considered to represent a more stringent assay for the assessment of clonogenicity and in addition, the environment in the centre of the colony may be hypoxic or deficient in nutrients and therefore more closely resemble the *in vivo* environment (Hoffman 1991). Multiple attempts at 3-D colony assays in the lentiviral transduced RCC11 and RCC48 lines were unsuccessful and it is unclear as to why this was the case.

Both assays have some limitations in that cells that form colonies are actively dividing and are therefore considered to represent those that have the greatest potential for self-renewal and are more likely to represent the cancer stem cell population. However, cells that are reversibly non-dividing in G_0 are not assessed by such an assay and such cells may still have the potential for clonogenic growth (Hoffman 1991). In addition, the disaggregation of cells necessary for plating results in loss of normal cell interactions and such interactions may be a critical component of tumourigenesis (Hoffman 1991).

Both 2-D and 3-D colony assays have however correlated with the capacity for tumourigenesis in a number of studies *in vivo* and as such provide a good validated *in vitro* model (Niell, Soloway et al. 1983) (Freedman and Shin 1974).

5.8.6 VEGF ELISA

Correlation of VEGFa and LIMD1 staining immunohistochemically demonstrated a

positive correlation with tumours with increased LIMD1 staining also demonstrating increased VEGFa staining. VEGFa is a marker of hypoxic deregulation, up-regulated by HIF and a critical driver of ccRCC (Pouyssegur, Dayan et al. 2006) as well as representing a validated prognostic indicator in ccRCC (Patard, Rioux-Leclercq et al. 2009).

It had been hypothesised that LIMD1 and VEGFa staining would correlate negatively in ccRCC samples *in vivo*, with increasing VEGFa expression contributing to increasing angiogenesis. However an unexpected positive correlation was observed and it was hypothesised that this could be related to a 'steal' effect, whereby tumours with higher VEGFa levels in turn secrete more VEGFa to promote neo-vascularisation, thereby resulting in paradoxically lower VEGF staining within the tumours, but increased neo-angiogenesis Kluger *et al* had observed a similar relationship (Kluger, Siddiqui et al. 2008).

ELISA assays are sensitive, highly reproducible assays, which alongside the incorporation of standard controls enable the accurate quantification of the antigen or antibody of interest. As for the cell cycle analysis, cells analysed were of similar passage number and confluency, with media changed at the same time across cell lines to ensure consistency. Given the hypoxic microenvironment of ccRCC *in vivo* and the hypoxic deregulation that occurs during tumourigenesis, cells were incubated both in normoxia (20% O_2) and in hypoxia (1% O_2).

In both cell lines, VEGFa secretion was increased in the RCC11 and RCC48 cell lines in association with LIMD1 loss in both normoxia and hypoxia, although this did not quite meet statistical significance in the RCC48 line in hypoxia (**Figure 5.9**). In keeping with this observation, work by Foxler *et al* in HEK-293 cells, a human embryonal kidney derived cell line, demonstrated that depletion of endogenous LIMD1 induces the expression of endogenous HIF-1 targeted genes including VEGF as assessed by mRNA levels (Foxler, Bridge et al. 2012).

This would suggest that LIMD1 loss is not only associated with increasing VEGFa secretion as assessed by ELISA, but also fit with our hypothesis that the positive correlation observed *in vivo* was as a consequence of a 'steal' effect, whereby tumours

with greater LIMD1 in turn secreted more VEGFa, resulting in a paradoxical decrease in VEGFa staining within the tissue.

5.8.7 HIF1-α reporter assay and HIF1-α expression in hypoxia

Loss of LIMD1 in the RCC11 line was associated with an increase in HIF1α activity in hypoxia but not normoxia as assessed by an HRE-assay. In the RCC48 cell line, an increase in HIF1α activity was observed in normoxia in association with LIMD1 loss but not in hypoxia.

Loss of LIMD1 has been shown to result in the up-regulation of HIF1-α in both normoxia and hypoxia. In hypoxia, PHD2 is still active and can result in HIF1α degradation. LIMD1 depletion results in reduced PHD2 activity with consequent HIF1α up-regulation (Foxler, Bridge et al. 2012).

Although the results of the HIF1α reporter assay were inconsistent, increased HIF1α activity was observed in both cell lines (**Figure 5.9**). Error bars were however large in some of the assays and given the trend observed, further biological repeats may well result in the differences becoming statistically significant.

5.8.8 Changes in cell cycle associated with loss of LIMD1 in the ccRCC lines

Hanahan and Weinberg described the critical changes in cell cycle associated with malignant transformation: the loss of responsiveness to negative regulators of cell cycle progression and/or the acquisition of independence from mitogenic signals (Hanahan and Weinberg 2011). FACS has become a standard tool to analyse cell cycle distributions, providing a clear picture of the different proportion of cells in each of the cell cycle phases.

Work in the RCC11 line did not show differences in the proportion of cells in G1/S/G2 in association with loss of LIMD1 (**Figure 5.10**) suggesting that LIMD1 loss was not associated with changes in cell cycle as assessed with this assay.

FACS analysis provides a snapshot of the cell cycle distribution at any given point in time. Factors such as culture conditions can have a significant effect on cell cycle

progression: cells should be sub-confluent at around 50% when analysis is undertaken as over-confluency can lead to cell-cell contact and contact inhibition, although this is less critical for transformed cells (Schorl and Sedivy 2007). Media should also be changed regularly and at the same time for different cell lines undergoing analysis such that nutrient availability is consistent across lines (Schorl and Sedivy 2007).

Cells cycle can be synchronised, through for example arresting cells in G0, by growing cells to confluency and then subjecting cells to serum deprivation, although this is less critical for cells that are already transformed. A more accurate method for the determination of the fraction of cells in S phase is to pulse label an asynchronous culture with BrdU for 15-60 minutes before immediately harvesting for analysis. With this method, cells at the very beginning and end of S phase are captured which is often missed with standard FACS analysis (Schorl and Sedivy 2007).

The cell lines analysed with FACS were of a similar passage number, confluency was consistent at the time of analysis at around 50% and media was changed at the same time across the cell lines. Where possible, variables that might have affected cell cycle were kept constant.

5.9 Future work

5.9.1 Immortalisation of RPTEC

A comprehensive search of the literature did not identify any publications where a CRISPR-Cas-9 system had been used to successfully knockout gene expression in RPTEC. The use of CRISPR-Cas9 systems in primary cells is particularly difficult but provides a very powerful tool since primary cells provide a better model to investigate the effects of loss of function mutations on tumourigenesis.

BMI-1 transduction alone did not appear to result in RPTEC immortalisation, which limited their proliferative capacity, and cells that had undergone gene editing using the CRISPR-Cas-9 system underwent senescence before they could be used in *in vitro* assays. RPTECs immortalisation could be attempted through the successive introduction of the Simian Virus 40 Early Region (SV40T) and hTERT, which has been shown to effectively immortalise RPTECs without causing transformation (Kowolik, Liang et al. 2004) .

Single cell selection of BMI-1 transduced RPTECs was not possible after successful gene editing of LIMD1 and Ajuba using a CRISPR-Cas-9 mediated deletion system. Single cell selection of primary cells is difficult and although effective immortalisation may increase the likelihood of success this is not guaranteed. After single cell plating, the use of conditioned media where media is supplemented with 25-50% media obtained from cells that are approximately 70% confluent may increase the likelihood of success.

Given that it was not possible, to use the heterogeneous *LIMD1* and *AJUBA* deleted RPTEC population in further *in vitro* assays effective immortalisation may overcome this limitation. However, alongside single cell selection using conditioned media, other strategies to improve growth of the CRISPR-Cas-9 LIMD1 and Ajuba knockdown lines to enable the use of the heterogeneous population in *in vitro* assays could include the use of a Rho-kinase (ROCK) inhibitor and modified Schlegel culture conditions.

Having successfully used a CRISPR-Cas-9 system in a primary cell line, the use of such an approach in ccRCC cells is likely to be much easier, with issues such as single cell selection much easier to overcome. Using such a system, RCC45 and RCC12 cells demonstrated excellent transfection efficiencies, and the protocol could be easily optimised for a ccRCC line.

After single cell selection, the CRISPR-Cas-9 transduced cells should be subjected to a mismatch detection assay using the T-7 endonuclease assay (T7-EI) in order to confirm the presence of indels secondary to gene editing. Here genomic DNA spanning the crRNA target site is PRC amplified and analysed using the T7-EI mismatch detection assay and then run on a 2% agarose gel, with gene editing indicated by the presence of cleaved bands under the primary PCR product. Sanger sequencing can then be performed on the PCR products, to confirm whether PCR products are wild type, homozygous or heterozygous.

5.9.2 Further assays to investigate the *in vitro* effects of LIMD1 loss on tumourigenesis

5.9.2.1 Measuring the effects of LIMD1 loss on Clonogenic potential

RCC11 and RCC48 ccRCC lines were successfully lentivirally transduced to generate scr control lines, shLIMD1, and rrLIMD1 lines. A number of critical components of tumourigenesis as described by Hanahan and Weinberg were then investigated (Hanahan and Weinberg 2011).

Increased proliferative capacity was confirmed by increased colony formation in association with LIMD1 loss as assessed in a 2-D format. 3-D colony assays are however considered a more stringent assay, cells by definition must have lost of contact inhibition and be anchorage independence, features considered critical for *in vivo* carcinogenesis.

It is unclear why the 3-D assays undertaken were unsuccessful but such an approach would be worth optimising. In addition more sophisticated 3-D culture enables the

creation of an environment that more closely mimics that observed *in vivo*, for example with the inclusion of cells from the tissue microenvironment and of the basement membrane through for example the inclusion of laminin-rich basement membrane extracellular matrix (Matrigel). Recently, a novel automated method to measure clonogenic survival and proliferation of cells in a 3D matrix consisting of matrigel and more closely representing physiological *in vivo* growth conditions has been described (Eke, Hehlgans et al. 2016).

5.9.2.2 Measuring the effects of LIMD1 loss on migration and invasion

The scratch assay demonstrated that loss of LIMD1 was not associated with changes in migration. The use of more than one migration assay confirming the same result would provide additional evidence that LIMD1 loss was not associated with changes in cell migration. 2-D assays can be adapted to more closely mimic the *in-vivo* environment, for example coating plates with collagen or basal membrane extract, (Matrigel) prior to seeding. In the transwell migration assay cells are seeded in to one chamber separated by a porous membrane through which cells transmigrate. Cells are generally seeded into the upper compartment, and can then migrate vertically through pores of the membrane to the lower compartment containing an attractant or higher serum content. A variant of this, the transwell invasion assay assesses the effects of the ECM on invasion. A thin layer of ECM is overlaid on the porous filter prior to seeding cells which occludes the membrane pores and blocks non-invasive cells from migration. The IncuCyte® system for example enables the real-time visualisation and assessment of cell morphology in scratch wound assays without disrupting plates inside a tissue culture incubator.

5.9.2.3 Changes in cell cycle associated with loss of LIMD1

FACS analysis of the LIMD1 proficient and LIMD1 depleted RCC11 and RCC48 lines, was not associated with changes in cell cycle. We did not however synchronise cells prior to FACS analysis. Although such an approach is often not required in transformed cells, cell synchronisation particularly in combination with BrdU incorporation would enable the more accurate determination of cell cycle phase progression in these cell lines.

5.9.2.4 Characterising HIF in association with loss of LIMD1

Given the critical role of HIF2α in tumourigenesis in ccRCC it would be interesting to evaluate the effects of LIMD1 loss using a HIF2α reporter assay. RNA sequencing (RNA-Seq) uses high-throughput sequencing methods to provide an insight into the transcription of a cell and could be used to identify differences in the expression of genes associated with hypoxic deregulation in association with loss of LIMD1 in the cell lines described.

Chapter 6

Targeted cancer therapy in association with LIMD1 loss in ccRCC

6.1 Introduction

There is a need to selectively target cancer cells whilst minimising drug-associated toxicity in healthy cells. Multiple effective anti-cancer drugs have been identified but a particular challenge is to target cancer cells with drugs at concentrations that will not have significant effects on healthy non-cancerous tissue. Given that deletion/mutation of tumour suppressors is associated with a loss of function phenotype, targeting such genes represents a particular challenge.

Two genes are synthetically lethal if mutation/deletion of either gene is compatible with viability but mutation/deletion of both genes results in cell death, for example targeting BRCA1/2 mutated breast and ovarian cancer through PARP inhibition (Kaelin 2005, Yap, Sandhu et al. 2011). By targeting tumour cells that already have loss of function of at least one tumour suppressor, a synthetically lethal approach can be used to identify drugs that kill cells in a genotype-specific manner, targeting the protein products of genes that are synthetically lethal in association with such cancer-causing mutations (Kaelin 2005).

There is an unmet need to develop strategies by which choice of treatment is influenced by the particular characteristics of the tumour, maximising drug therapeutic effect for an individual patient. Predictive biomarkers provide information on the likely benefit of a particular treatment for an individual patient. In metastatic ccRCC however no predictive biomarkers have been consistently validated (Gulati, Martinez et al. 2014). 25% of ccRCC tumours demonstrate inherent resistance to targeted TKI therapy and resistance will almost invariably develop in the remainder of tumours (Chowdhury, Larkin et al. 2008).

49.3% of ccRCC tumours demonstrated reduced LIMD1 staining compared to matched adjacent tissue and *in vitro*, reduced LIMD1 staining was observed in ten out of twelve ccRCC lines compared to the control RPTEC line. Reduced LIMD1 staining did not correlate with the clinico-pathological indices of tumour grade, stage, PFS and OS. Nonetheless, LIMD1 loss could represent a predictive biomarker and tumours demonstrating reduced LIMD1 staining could be selectively targeted using a synthetic lethal approach.

A synthetic lethality screen was undertaken in the ccRCC cell line RCC11 and drug sensitivities in control RCC11 scr cells were compared with drug sensitivities in an RCC11 cell line where LIMD1 levels had been significantly downregulated using a knockdown lentiviral vector system (RCC11 shLIMD1). The drug library consisted of 584 FDA-approved drugs either already in clinical use as cancer-therapeutic drugs, or previously evaluated within a clinical trial setting as showing potential cancer-therapeutic effects. Such an approach should spare LIMD1-proficient cells, minimising damage to healthy normal cells and enabling the selective targeting of tumour cells with loss/low LIMD1 expression, through the targeting of an as yet uncharacterised protein product of a gene within the LIMD1-low/deficient cells.

6.2 Aims and Objectives

The aims of this chapter are:

1. To screen a drug library of 584 cancer-therapeutic drugs using a paired LIMD1 proficient ccRCC cell line (RCC11 scr) and an RCC11 cell line where LIMD1 had been significantly knocked down using a lentiviral system (RCC11 shLIMD1), in order to identify drugs that may demonstrate synthetic lethality in association with LIMD1 loss/downregulation.

2. To validate the results of the drug screen in the RCC11 scr/shLIMD1 cell lines and in a further ccRCC line, RCC48, using paired LIMD1 proficient RCC48 scr cells and LIMD1 low, RCC48 shLIMD1 cells

3. To validate the results of the drug screen in LIMD1 proficient and deficient HELA and A549 lines, where biallelic LIMD1 inactivation had been undertaken using a CRISPR-Cas-9 gene editing system

4. To establish whether reduced LIMD1 expression is associated with differences in sensitivity to the VEGF-TKI sunitinib and the mTOR inhibitor everolimus, drugs commonly used for the treatment of metastatic ccRCC

6.3 A drug screen was undertaken to identify cancer-therapeutic drugs that demonstrated synthetic lethality in association with LIMD1 loss.

Short-term cell viability assays were undertaken to assess the effects of LIMD1 depletion on the sensitivity of the ccRCC line RCC11 to a range of cancer-therapeutic drugs using a drug library obtained from the Institute of Cancer Research (ICR), with each drug represented in the drug library once. RCC11 was selected as it expresses high levels of LIMD1, Ajuba and WTIP and relatively high levels of both HIF1α and HIF2α, and is therefore representative of a relatively aggressive, hypoxically deregulated tumour line. LIMD1 depleted RCC11 cells would still be Ajuba and WTIP proficient.

The assay was performed simultaneously in the 2 lentiviral transduced cell lines RCC11 scr (control cells transduced with non-targeting siRNA (scr)) and RCC11 shLIMD1 (transduced with an shLIMD1 construct to generate effective LIMD1 knockdown). Early passage cells of identical passage were used for all assays, and cells were seeded in the absence of puromycin, and at a density to ensure confluency of between 90 and 95% on day 6, considered optimal for control wells in 2-dimensional drug viability assays. Cells were drugged at 24 hours and 72 hours such that the final drug concentration of the drug library compounds was 1μM and appropriate controls included. In addition, cells taken out of puromycin selection 24 hours prior to seeding were simultaneously plated in to six-well plates to achieve a confluency of 90-95% on day 6, and lysed and Western blotted to establish good LIMD1 expression in the scr control with effective knockdown of LIMD1 in the shLIMD1 RCC11 cell lines. Consistently high levels of LIMD1 expression were observed in the scr line, with excellent knockdown in the shLIMD1 line (**Figure 6.1**).

Drug assays were read at day 6 using the ATP-based assay, Cell-Titre Glo^{TM}. The 'Z score' method was used to compare the relative cell killing for each drug between the scr and shLIMD1 plates. This method excludes control measurements altogether under the assumption that most compounds are inactive and can serve as controls. The scoring system rescales the output of the Cell-Titre Glo^{TM} assay relative to the within plate variation by subtracting the median of the plate values from each drug assay result and dividing the difference by the median absolute deviation calculated from all

measurements within the plate. This generates a readout whereby the more negative the Z-score the greater the degree of cell killing relative to the plate as a whole and the more positive the Z-score the greater the cell viability relative to the plate as a whole and represents a validated method for the analysis of the results of a drug screening platform (Malo, Hanley et al. 2006).

The outputs of the Z-scores were plotted graphically using Prism 6. Comparison of the Z-scores for the RCC11 scr and RCC11 shLIMD1 cell lines enables the identification of drugs that are associated with more cell death in association with LIMD1 loss but not in the scr control, drugs that may demonstrate synthetic lethality in association with LIMD1 loss (**Figure 6.1**).

For most drugs there was little difference between the Z-scores for the scr and the shLIMD1 drug screens and excellent agreement between the first and the second experimental repeats. Plotting Z-scores for the drug screen in the RCC11 scr line 1st repeat against Z-scores for RCC11 scr in the 2nd repeat demonstrated excellent concordance, $p<0.0001$*** and in the RCC11 shLIMD1 line, $p<0.0001$***, for concordance. (**Figures 6.1A** and **6.1B**). This demonstrates that the drug assay repeats were consistent and suggests that where possible, inferential errors causes by procedural factors such as the format of the assay, inconsistent pipette delivery and unintended differences in compound concentration related to the evaporation of media were minimised.

Drug screen hits were likely to represent a true result when both drug screen repeats identified the same drug as a 'hit' compound. Drugs that demonstrated an increase in cell killing in the RCC11 shLIMD1 compared to the LIMD1-proficient RCC11 scr in both repeats, were designated 'hit' compounds, and are listed in Table **6.1** alongside their relative Z-scores.

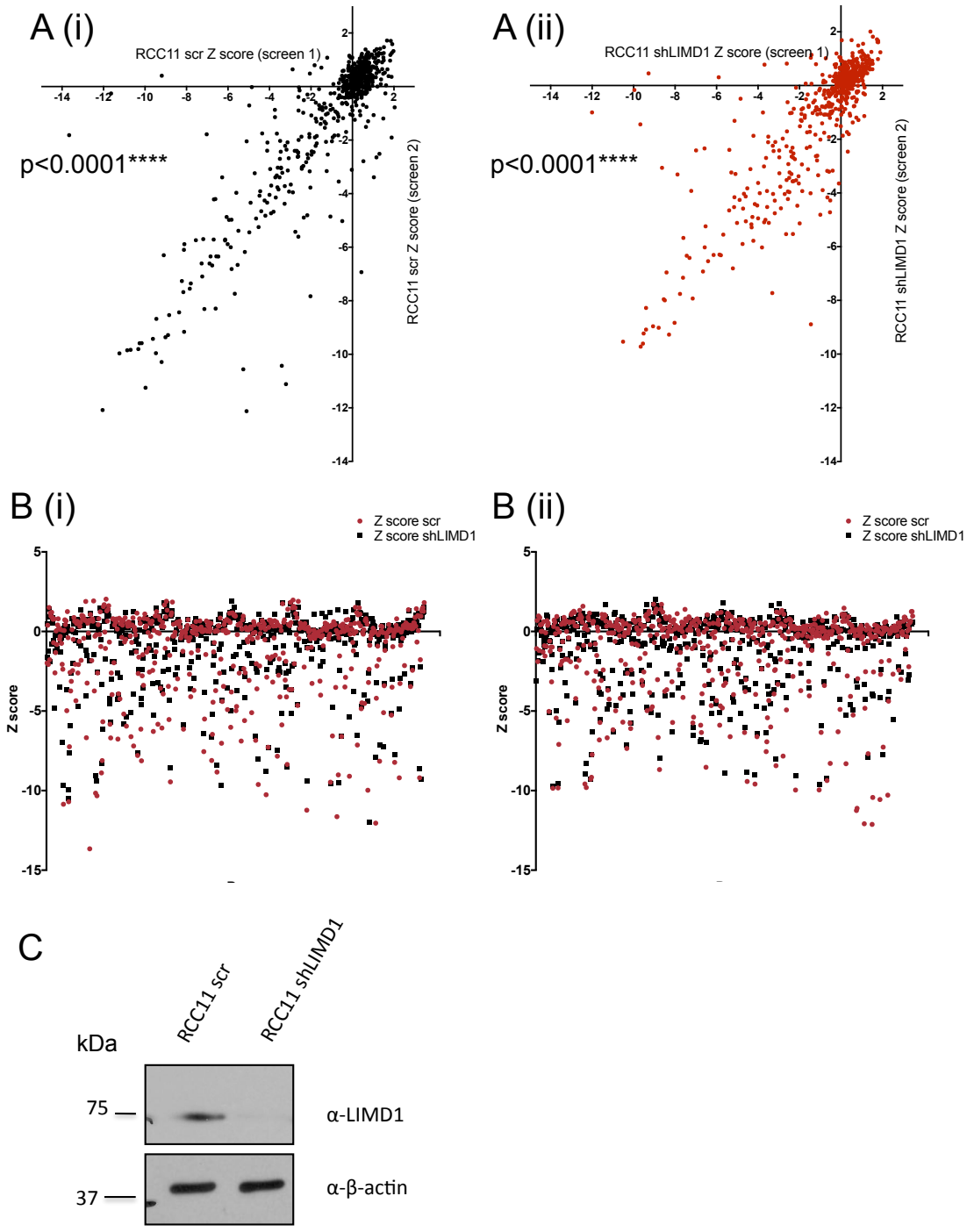

Figure 6.1: Synthetic lethality screen with drug library of 584 FDA cancer approved drugs.

RCC11 scr and shLIMD1 matched cells were plated at 1000 cells/well and 1200 cells/well respectively into 96-well plates. Cells were taken out of puromycin selection 24 hours prior to plating. Drugging with a compound library of 584 cancer approved drugs and negative controls of media only and media supplemented with 0.1% DMSO was undertaken 24 hours and 72 hours after seeding to result in a final drug concentration of the drug library compounds of 1μM. Sunitinib control wells with a final drug concentration of between 1-3μM were also included. Cell viability was assessed after 6 days using Cell

Titer-Glo Luminescent Cell Viability Assay (Promega). The 'Z score' method was used to compare the relative cell killing for each drug between the scr and shLIMD1 plates whereby the median of the plate values was subtracted from each drug assay result and then divided by the median absolute deviation calculated from all measurements within the plate. All plots were undertaken using Prism 6.

A. Graphical output of Z-scores from the 1st and 2nd drug screen repeats in matched LIMD1 proficient/low LIMD1 expressing RCC11 cells. (A (i)) Z-scores for the drug screen in the RCC11 (scr) line 1st repeat plotted against the 2nd repeat demonstrate excellent concordance ($p<0.0001$).) **(A (ii))** Z-scores for the drug screen in the RCC11 shLIMD1 1st repeat plotted against the 2nd repeat demonstrate excellent concordance ($p<0.0001$).

B (i) B (ii) Scatter plots of Z-scores for drug screen. Comparison of the Z-scores for RCC11 scr versus RCC11 shLIMD1 cell lines with both drug screens represented

C. Western blot of LIMD1 expression. Western blot analysis demonstrates high levels of expression of LIMD1 in the RCC11 scr cell line, with excellent LIMD1 knockdown in the RCC11 shLIMD1 cell line.

6.3.1 Pazopanib and irinotecan were identified as 'drug hits' in both repeats of the synthetic lethality screen

The two drugs identified as possible hits in both repeats of the drug screen were pazopanib and irinotecan with increased cell death observed in the RCC11 shLIMD1 cell line compared to RCC11 scr control (**Figure 6.2**). The difference in Z-score for these 'hit' compounds was small at around -1 and typically larger differences in Z-score are considered significant in a drug synthetic lethality drug screening platform (Malo, Hanley et al. 2006). However, both drugs have an established role in the treatment of renal cell carcinoma (Shamash, Powles et al. 2005, Sternberg, Davis et al. 2010) and differences were consistent between repeats. In addition, most treatments for ccRCC result in stable disease or a partial response at best and therefore smaller differences in Z score may be more significant in ccRCC compared to other tumour types (Escudier, Szczylik et al. 2012).

Drug	Z score (scr) 1st repeat	Z score (shLIMD1) 1st repeat	Z score (scr) 2nd repeat	Z score (shLIMD1) 2nd repeat
Pazopanib	-0.4529	-1.1557	-1.18077	-2.7898
Irinotecan	-0.4737	-1.3670	-0.1814	-1.193

Figure 6.2: Two replicates of synthetic lethality screen with drug library dosing at 1μM demonstrate increased cell death with pazopanib and irinotecan treatment in the RCC11 shLIMD1 lines compared to RCC11 scr control

Results of synthetic lethality drug screen demonstrating 'positive hits', with increased cell death in both replicates of the RCC11 shLIMD1 cell line compared to scr control. The 'Z score' method was used to compare the relative cell killing for each drug between the scr and shLIMD1 plates**.**

6.3.2 The synthetic lethality drug screen was repeated with a drug concentration of 2μM

The drug library had been stored in the -20°C freezer for over one year and it was unclear whether over this time period the potency of some of the drugs had diminished through degradation. The drug screen was therefore repeated a third time as described with the aim of drugging the cells at 24 and 72 hours with 2μM of the screen drugs within the library. Unfortunately due to evaporation of diluent within the library particularly from the plate edges, there was insufficient drug available to drug at 72 hours and drugging was therefore only carried out at 24 hours. Graphical representation of the Z-scores for this drug screen in the RCC11scr and RCC11 shLIMD1 lines is shown in **Figure 6.3**.

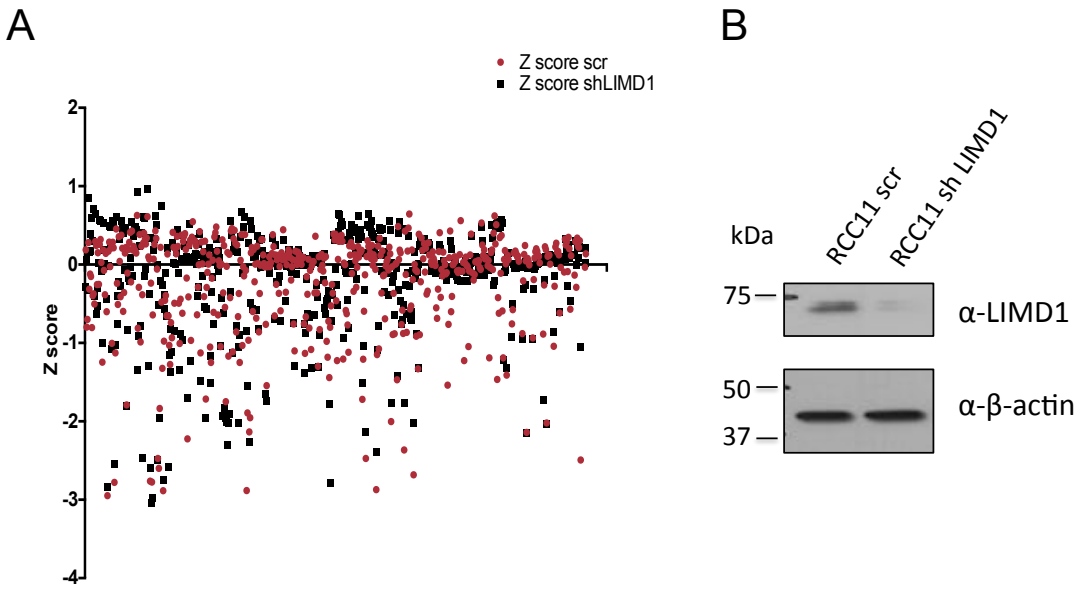

Figure 6.3: Graphical output of Z scores from the synthetic lethality drug screen with drugging with 2μM of the drug library

RCC11 scr and shLIMD1 matched cells were plated in 96 well plates. Drugging with a compound library of 584 cancer approved drugs and negative controls of media only and media supplemented with 0.1% DMSO was undertaken at 24 hours with final drug concentration of 2μM. Sunitinib control wells with a final drug concentration of between 1-3μM were also included. Cell viability was assessed after 6 days using the Cell Titer-Glo Luminescent Cell Viability Assay (Promega). The 'Z score' method was used to compare the relative cell killing for each drug between the scr and shLIMD1 plates. This rescales the output of the Cell-Titre Glo™ assay relative to the within plate variation by subtracting the average of the plate values from each drug assay result and dividing the difference by the standard deviation calculated from all measurements within the plate. All plots were undertaken using Prism 6.

A. Scatter plot of Z-scores for drug screen. Comparison of the Z-scores in RCC11 scr versus RCC11 shLIMD1 with cells drugged with 2μM of the drug library 24 hours post seeding. **B. Western blot of LIMD1 expression.** Western blot analysis demonstrates high levels of expression of LIMD1 in the RCC11 scr cell line, with excellent LIMD1 knockdown in the RCC11 shLIMD1 cell line.

6.3.3: Irinotecan was identified as a 'drug hit' in the RCC11 shLIMD1 line in the 2μM synthetic lethality screen as well as two additional drugs, selumetinib and dorzolamide

The third drug screen resulted in fewer drug compounds with very negative Z-scores (**Figure 6.3**), probably as a result of less cell killing secondary to drugging only at 24 hours. The screen did however also identify irinotecan as a potential 'selectively lethal' hit in association with LIMD1 loss: the Z-score for the shLIMD1 line was -4.811

compared to -1.1953 in the scr control (**Figure 6.4**), consistent with irinotecan demonstrating synthetic lethality in association with LIMD1 loss.

Within this screen, pazopanib resulted in increased cell death in the RCC11 scr cell line, Z-score -2.2946 versus 0.687 in the shLIMD1 line, the opposite effect to that observed in the first two drug screens. Two additional 'drug hits' were identified, the drug selumetinib, known to function as an orally available, potent, non-ATP selective MEK-1/2 inhibitor with demonstrated efficacy in K-Ras mutated non-small cell lung carcinoma (Janne, Shaw et al. 2013) and dorzolamide, a carbonic anhydrase inhibitor widely used in the treatment of glaucoma and ocular hypertension (Balfour and Wilde 1997). For selumetinib, in the 2μM drug screen, the Z-score in the shLIMD1 line was -3.4752 compared to 0.2496 in the scr control and for dorzolamide, the Z score was -1.7139 in the shLIMD1 line compared to scr control. Neither drug was identified as 'hit' compounds in the 1μM drug screens in association with LIMD1 loss (**Figures 6.3** and **6.4**).

Drug	Z score scr 2μM drug screen	Z score shLIMD1 2μM drug screen	Z score scr 1μM drug screen 1st repeat	Z score shLIMD1 1μM drug screen 1st repeat	Z score scr 2nd drug screen 2nd repeat	Z score shLIMD1 2nd drug screen 2nd repeat
Selumetinib (AZD6244)	0.2496	-3.475	-0.872	-1.190	-3.740	0.441
Dorzolamide	0.2605	-1.714	-0.050	0.576	0.450	0.176
Pazopanib	-2.2946	0.688	0.453	-1.156	-1.181	-2.790
Irinotecan	-1.1953	-4.811	-0.474	-1.367	-0.181	-1.245

Figure 6.4 Results of 'drug hits' from synthetic lethality screen with final drug concentration 2μM, alongside Z-scores from 1st and 2nd drug screen

Results of synthetic lethality drug screen demonstrating 'positive hits' with increased cell death in the shLIMD1 cell line compared to scr control with the drug library with drugging at 2μM at 24 hours, alongside Z-scores for the 1st and 2nd repeats of the drug screen with drugging at 1μM at 24 and 72 hours. The 'Z score' method was used to compare the relative cell killing for each drug between the scr and shLIMD1 plates.

6.4 Validation of hits from the synthetic-lethality drug screen

Short-term cell viability assays across a range of drug concentrations were undertaken to assess the effects of LIMD1 depletion on the sensitivity of the RCC11 and RCC48 cell lines to the 'drug hits' identified in the drug screen. The assay was performed simultaneously with early passage RCC11 and RCC48 cells transduced with a non-targeting control construct (scr), or knockdown LIMD1 construct (shLIMD1) in a 96-well plate format. As before, cells were taken out of selection 24 hours prior to seeding and seeded at a density associated with 90-95% confluency on day 6 in the control wells. Cells were also seeded in to a 6-well plate for lysis on day 6 to assess relative LIMD1 expression by immunoblot. Cells were drugged in triplicate at 24 and 72 hours for each drug concentration of between 0.1μM and 60μM and relative cell viability assessed on day 6 using the ATP based Cell-Titre Glo^{TM} assay.

6.4.1 Validation of the carbonic anhydrase inhibitor dorzolamide as a drug hit from the synthetic lethality screen.

Drugging with dorzolamide up to a concentration of 60μM resulted in almost no cell death in either the RCC11 or RCC48 cell lines (**Figure 6.5**). Although dorzolamide was identified as a 'hit' in the 2μM drug screen with a Z-score of -1.7139 in the RCC11 shLIMD1 screen compared to 0.265 in the RCC11 scr screen, almost no cell death was seen in either cell line in the 1st or 2nd drug screen at 1μM and further validation with dorzolamide was not undertaken (**Figure 6.2**). The failure of validation of drugs identified as 'hits' in a drug-screening platform is near universal. A review article by Carnero suggested that one marketable drug emerges from screening one million compounds and that only one in twenty drugs identified in a compound library as 'screening hits' are subsequently validated as 'active hits' (Carnero 2006).

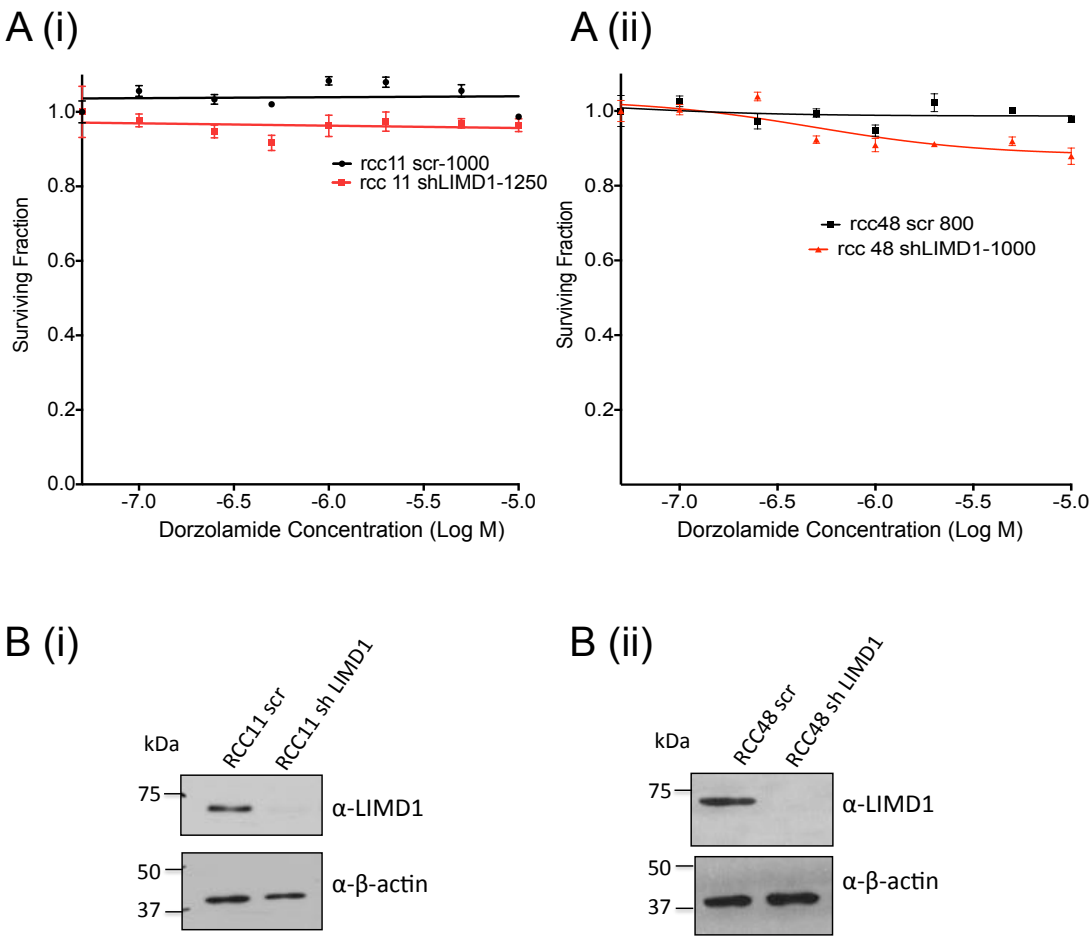

Figure 6.5: The carbonic anhydrase inhibitor dorzolamide is not associated with cell death in either RCC11 or RCC48 cell lines

RCC11 scr/shLIMD1 lines and RCC48 scr/shLIMD1 lines were taken out of puromycin selection and plated into the same 96-well plate at a seeding density associated with 90-95% confluency on day 6 and exposed to a range of dorzolamide concentrations between 0.1μM and 60μM 24 hours and 72 hours after seeding, with drugging in triplicate at each drug concentration. Cells were simultaneously plated for Western blot analysis to assess knockdown on day 6. Cell viability was assessed on day 6 using the ATP-based Cell-Titer Glo™ assay. All graphs were generated in Prism version 6, with error bars demonstrating SEM.

(A (i) Representative dorzolamide dose-response curve, RCC11 scr/shLIMD1, **(A (ii))** Representative dorzolamide dose-response curve, RCC48 scr/shLIMD1. **(B (i))** Western blot analysis demonstrates high levels of expression of LIMD1 in the RCC11 scr cell line, with good LIMD1 knockdown in the RCC11 shLIMD1 cell line. **(B (ii))** Western blot analysis demonstrates high levels of expression of LIMD1 in the RCC48 scr cell line, with good LIMD1 knockdown in the RCC11 shLIMD1 cell line.

6.4.2 Validation of selumetinib as a drug hit from the synthetic lethality screen.

Drugging with selumetinib up to a concentration of 60μM was not associated with cell death in RCC48 cells (**Figure 6.6**). In the lentiviral-transduced RCC11 scr/shLIMD1 cell lines, inconsistent results were observed with some repeats of the drug assay demonstrating increased drug sensitivity in the scr line and other repeats increased sensitivity in the shLIMD1 line, with little cell killing in either cell line up to a drug concentration of 60μM (**Figure 6.6**). Good knockdown of LIMD1 was observed in all repeats of the validation experiment **(Figure 6.6)**. In addition selumetinib sensitivity was inconsistent between repeats of the drug screen at 1μM in the RCC11 cells: increased sensitivity was observed in the shLIMD1 cell line in the 1st repeat but increased sensitivity in the scr RCC11 cell line in the 2nd repeat (**Figure 6.4**). Given the inconsistency of the drug screen results and conflicting results of the initial validation attempts, selumetinib was not felt to represent a true hit from the drug screen.

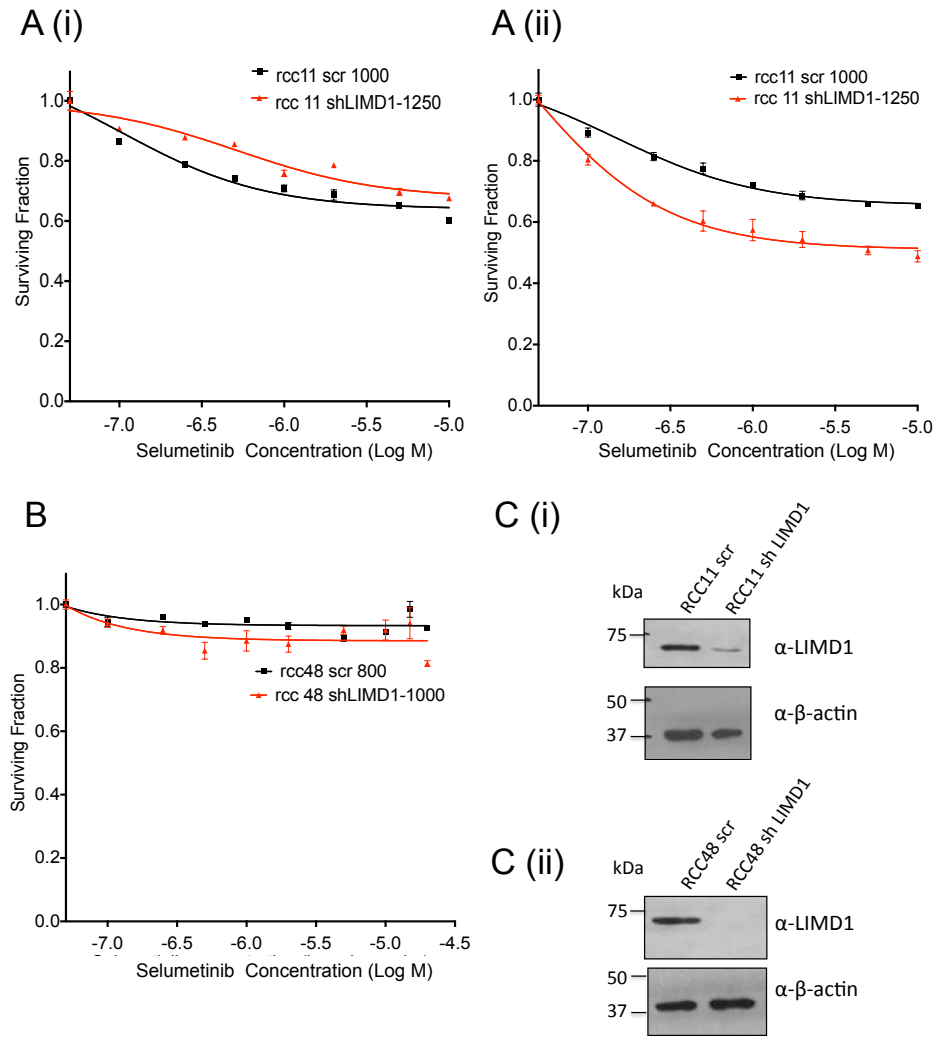

Figure 6.6: Inconsistent dose responses are observer in the RCC11 scr/shLIMD1 cell lines drugged with selumetinib and little cell death in RCC48 cells drugged with up to 60µM selumetinib

RCC11 scr/shLIMD1 lines and RCC48 scr/shLIMD1 lines were plated in the same 96 well plate at a seeding density associated with 90-95% confluency on day 6 and exposed to a range of selumetinib concentrations between 0.1µM and 60µM 24 and 72 hours after seeding, with drugging in triplicate at each drug concentration. Cells were also plated for Western blot analysis to assess knockdown on day 6. Cell viability was assessed on day 6 using the ATP-based Cell-Titer Glo™ assay. All graphs were generated in Prism version 6, with error bars demonstrating the SEM.

(A (i)-A (ii)) Selumetinib dose-response curve, RCC11 scr/shLIMD1, **B** Selumetinib dose-response curve, RCC48 scr/shLIMD1. **(B (i))** Western blot analysis demonstrates high levels of expression of LIMD1 in the RCC11 scr cell line, with excellent LIMD1 knockdown in the RCC11 shLIMD1 cell line. **(B (ii))** Western blot analysis demonstrates high levels of expression of LIMD1 in the RCC48 scr cell line, with excellent LIMD1 knockdown in the RCC11 shLIMD1 cell line.

6.4.3 Validation of the multi-targeting tyrosine kinase inhibitor pazopanib as a drug hit from the synthetic lethality screen

The multi-tyrosine kinase inhibitor pazopanib is an established first-line treatment for metastatic ccRCC, targeting VEGF, PDGF and c-Kit tyrosine kinases (Motzer, Hutson et al. 2013) (Sternberg, Davis et al. 2010). However, treating both the RCC11 scr/shLIMD1 and RCC48 scr/shLIMD1 cell lines with drug concentrations up to 60μM was associated with little cell death in either cell line, particularly for the RCC11 cell line (**Figure 6.7**). For both cell lines, no difference in relative cell death between the scr/shLIMD1 cell lines over a range of drug concentrations was observed. Excellent LIMD1 knockdown in the shLIMD1 line and high LIMD1 expression in the scr control was consistently observed (**Figure 6.7**).

The results of the drug screen repeats were also inconsistent, with the drug screen at 2μM demonstrating increased sensitivity to pazopanib in the scr line compared to shLIMD1 line (Z-score for scr line -2.2946 versus 0.68764 for shLIMD1) (**Figure 6.4**). Drugging the paired cell lines with sunitinib, a TKI also targeting VEGF, PDGF and c-KIT tyrosine kinases, demonstrated no difference in drug sensitivity between the scr/shLIMD1 cell lines, results of which are shown later in this chapter, (**Figure 6.13**).

Sunitinib and pazopanib have broadly similar tyrosine kinase targets, although some differences are noted which could explain some of the relative differences in drug sensitivity in different cell lines (Gotink and Verheul 2010). The lack of sensitivity of both cell lines to pazopanib but sensitivity to sunitinib is however surprising. Given the inconsistent results, and dose-response curves demonstrating no difference in sensitivity to sunitinib in paired RCC11 scr/shLIMD1 and RCC48 scr/shLIMD1 lines (**Figure 6.13**), pazopanib was not felt to represent a true 'hit' and was not validated further.

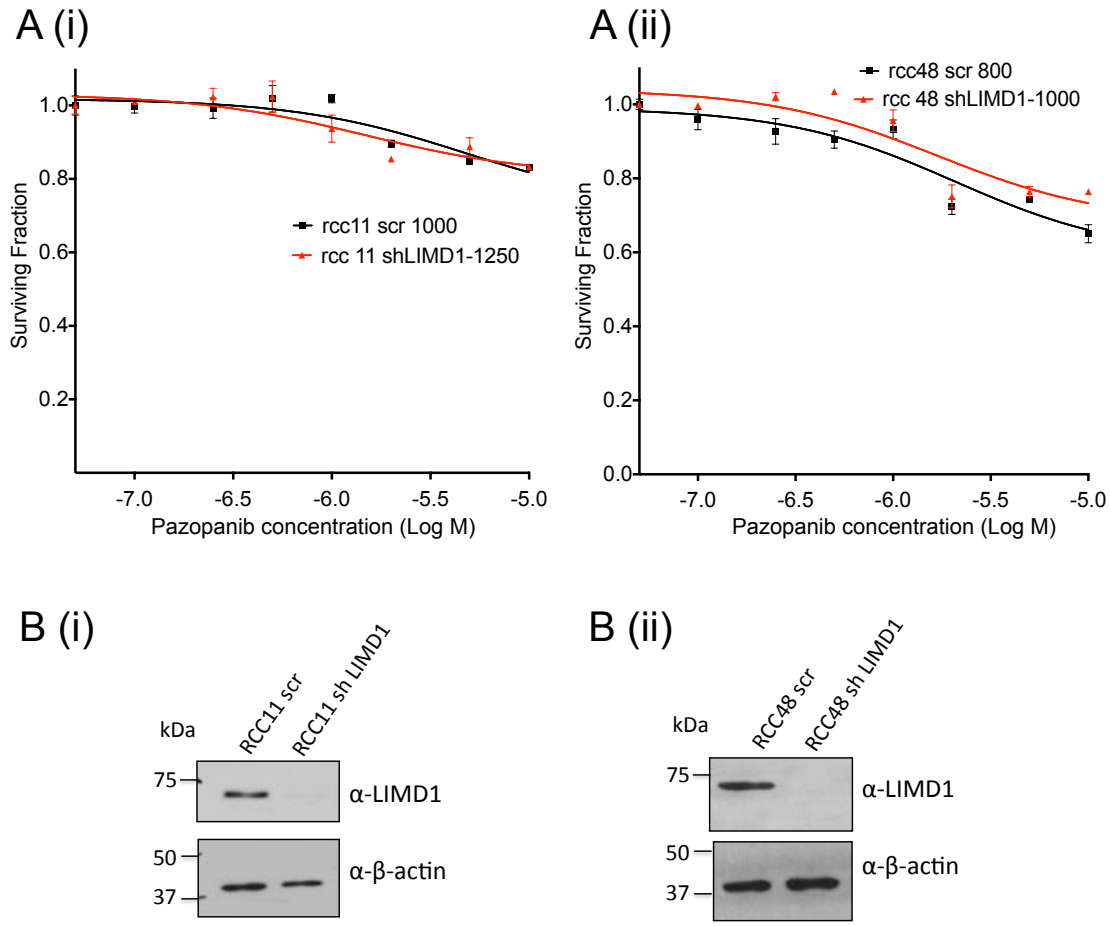

Figure 6.7. The multi-targeting targeting tyrosine kinase inhibitor pazopanib is not associated with significant cell death in RCC11 or RCC48 cell lines

RCC11 scr/shLIMD1 lines and RCC48 scr/shLIMD1 lines were plated in the same 96-well plate at a seeding density associated with 90-95% confluency on day 6 and exposed to a range of pazopanib concentrations between 0.1μM and 60μM 24 and 72 hours after seeding, with drugging in triplicate at each drug concentration. Cells were also plated for Western blot analysis to assess knockdown on day 6. Cell viability was assessed on day 6 using the ATP-based Cell-Titer Glo™ assay. All graphs were generated in Prism version 6, with error bars demonstrating the SEM. **(A (i))** Representative pazopanib dose-response curve, RCC11 scr/shLIMD1. **(A(ii))** Representative pazopanib dose-response curve RCC48 scr/shLIMD1. **(B (i))** Western blot analysis demonstrates high levels of expression of LIMD1 in the RCC11 scr cell line, with excellent LIMD1 knockdown in the RCC11 shLIMD1 cell line. **(B (ii))** Western blot analysis demonstrates high levels of expression of LIMD1 in the RCC48 scr cell line, with excellent LIMD1 knockdown in the RCC11 shLIMD1 cell line.

6.5 Validation of irinotecan as a drug hit from the synthetic lethality screen in ccRCC lines

The efficacy of chemotherapy in RCC has been disappointing and it has been suggested that this in part may be because renal cancer cells produce large amounts of a multidrug resistance protein leading to the efflux of cytotoxic drugs (Tobe, Noble-Topham et al. 1995). Relative tumour hypoxia and impaired drug delivery are also likely to contribute.

With the development of effective multi-targeting tyrosine kinase inhibitors, the role of chemotherapy in the treatment of RCC is less well defined. However, topoisomerase-I inhibitors do demonstrate efficacy *in vitro* and *in vivo*, with irinotecan demonstrating activity in renal xenografts (Miki, Nonomura et al. 1998) and topetecan resulting in increasing apoptosis in RCC cell lines compared to 5-FU (Ramp, Mahotka et al. 2001). Irinotecan efficacy has also been demonstrated *in vivo*. In a phase II trial of patients with metastatic RCC progressing after treatment with interferon alpha, a 61% symptomatic response rate was observed to combination chemotherapy with irinotecan, cisplatin and mitomycin C (Shamash, Powles et al. 2005) and activity of irinotecan alone has also been described (Fizazi, Rolland et al. 2003).

The drug screen contained a further topoisomerase-I inhibitor topetecan. No obvious differences in topetecan sensitivity between the RCC11 scr/shLIMD1 lines were observed with Z-values of -5.189 and-5.790 respectively for the first screen and -6.177 and -6.318 for the second screen respectively with the drug library at 1μM. Significant cell death was however observed in both scr/shLIMD1 lines and it may be that this drug concentration did not allow for the resolution of differences in drug sensitivity which may have been observed with drugging at lower drug concentrations. Another explanation may be that differences in drug sensitivity observed with irinotecan in the RCC11scr/shLIMD1 lines may not be related to the effects of the drug on topoisomerase-I. A number of topoisomerase-II inhibitors, etoposide, doxorubicin, daunorubicin and mitoxantrone were included in the screen. No differences in sensitivity to these drugs were observed between the scr and shLIMD1 cell lines.

Short-term cell viability assays in the paired RCC11 scr and RCC11 shLIMD1 and RCC48 scr and RCC48 shLIMD1 cell lines plated simultaneously and exposed to

increasing irinotecan concentrations were undertaken. Increased drug sensitivity in both shLIMD1 cell lines compared to scr control was observed, with a greater effect observed in the RCC48 cell line in association with LIMD1 loss (**Figures 6.8** and **6.9**).

There was some variation in the degree of cell killing at any particular irinotecan concentration between biological repeats of the assay. This variation may have been related to slight differences in final drug concentration between repeats due to for example media evaporation effects, drug dilution reproducibility and slight differences in rates of cell growth associated with cell passage/cell confluency of cells at time of seeding. Cells of similar passage were seeded for biological repeats and similar confluency/cell titre-Glo^{TM} readings for the control cells treated with DMSO alone were observed between experiments. In addition for the RCC11 cells the dose-response curves tailed off and drugging with 80 or 100μM of irinotecan did not result in increased cell death (data not shown). Drug treatment of RCC aims to reduce tumour burden or stabilise disease and complete response is unusual. Given that the dose-response curves did not consistently result in close to 100% cell death at the highest drug concentrations, calculation of the drug IC50 was difficult and therefore a drug concentration of 0.5μM was selected and sensitivity to irinotecan compared.

At this drug concentration increased cell death in association with LIMD1 loss was observed in the RCC11 shLIMD1 compared to RCC11 scr control but this did not meet statistical significance, Student's T test p=0.1161 (**Figure 6.8**). This difference was however significant in the RCC48 shLIMD1 line compared to RCC48 scr control, Student's T test p=0.0016* (**Figure 6.9**).

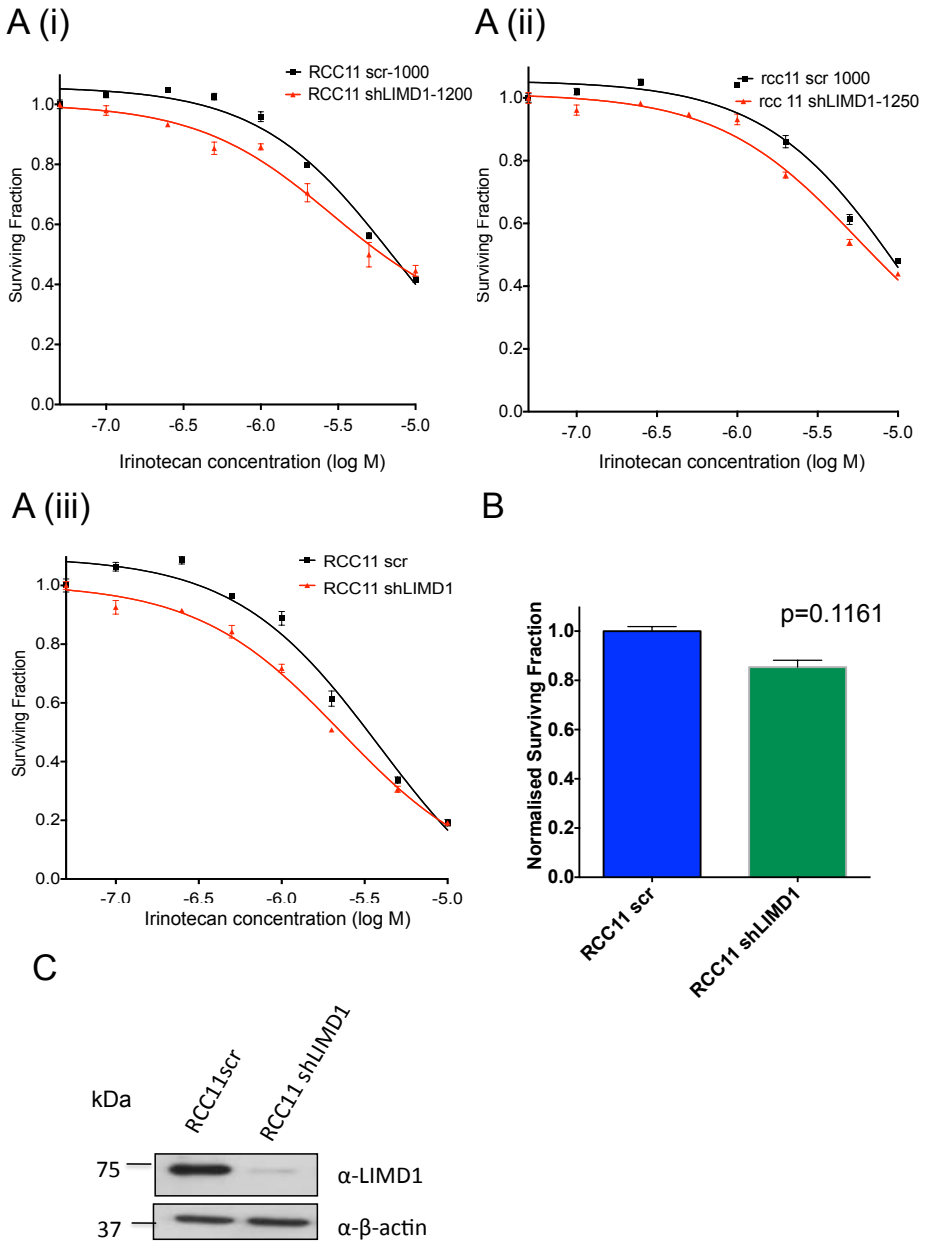

Figure 6.8: Drugging with irinotecan is associated with increased cell death in RCC11 cells with reduced LIMD1 expression (shLIMD1) compared to scr control

RCC11 scr/shLIMD1 lines were plated in a 96 well plate at a seeding density associated with 90-95% confluency on day 6 and exposed to a range of irinotecan concentrations between 0.1µM and 60µM 24 and 72 hours after seeding, with drugging in triplicate at each drug concentration. Cells were also plated for Western blot analysis to assess knockdown on day 6. Cell viability was assessed on day 6 using the ATP-based Cell-Titer Glo™ assay. All graphs were generated in Prism version 6, with error bars demonstrating the SEM. **(A (i))-A (ii))** Irinotecan dose-response curves, RCC11 scr/shLIMD1. B. An irinotecan concentration of 0.5µM was selected and relative sensitivity of RCC11 cells with high LIMD1 versus low LIMD1 expression (scr versus shLIMD1) assessed. Sensitivity to irinotecan for the shLIMD1 lines at 0.5 µM is shown relative to the scr control cells with error bars representing the SEM for the 3

biological repeats of the experiment. P value represents Students t-test value. Analysis was undertaken using Prism 6.

C. Immunoblot demonstrating high levels of LIMD1 expression in the scr control with good knockdown in the shLIMD1 cell lines.

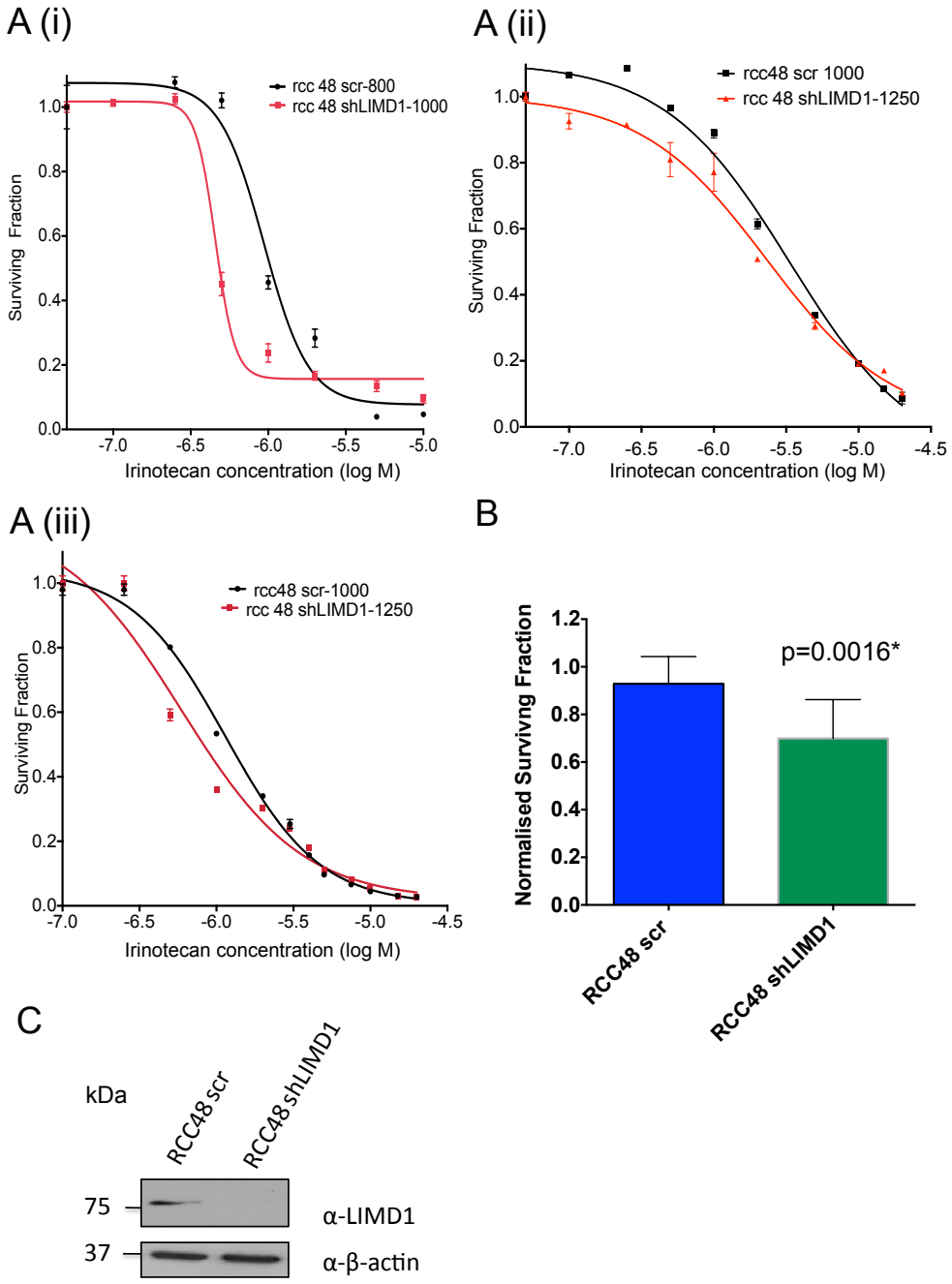

Figure 6.9: Drugging with the topoisomerase-I inhibitor irinotecan is associated with increased cell death in RCC48 cells with reduced LIMD1 expression (shLIMD1) compared to scr control

RCC48 scr/shLIMD1 lines were plated in a 96 well plate at a seeding density associated with 90-95% confluency on day 6 and exposed to a range of irinotecan concentrations between 0.1µM and 60µM 24

and 72 hours after seeding, with drugging in triplicate at each drug concentration. Cells were also plated for Western blot analysis to assess knockdown on day 6. Cell viability was assessed on day 6 using the ATP-based Cell-Titer Glo™ assay. All graphs were generated in Prism version 6, with error bars demonstrating the SEM. **(A (i))-A (ii))** Irinotecan dose-response curves, RCC48 scr/shLIMD1. **B.** An irinotecan concentration of 0.5μM was selected and relative sensitivity of RCC48 cells with high LIMD1 versus low LIMD1 expression (scr versus shLIMD1) assessed. Sensitivity to irinotecan for the shLIMD1 lines at 0.5 μM is shown relative to the scr control cells with error bars representing the SEM for the 3 biological repeats of the experiment. P value represents Students t-test value. Analysis was undertaken using Prism 6. **C.** Immunoblot demonstrating high levels of LIMD1 expression in the scr control with good knockdown in the shLIMD1 cell line

6.6 Validation of irinotecan as a drug hit from the synthetic lethality screen in non-ccRCC lines in association with LIMD1 loss

Dr Daniel Foxler of the Sharp group had used a CRISPR-Cas-9 system to biallelically inactivate LIMD1 in the lung adenocarcinoma line, A549 and in HELA cells. Cell viability in CRISPR-Cas-9 LIMD1$^{-/-}$ cells and LIMD1 proficient Cas-9 control cells exposed to increasing irinotecan concentration was compared. It was hypothesised that as the CRISPR-Cas-9 LIMD1 knockout cell lines expressed no LIMD1, in comparison to the RCC11/RCC48 shLIMD1 lines where some LIMD1 expression remained, a greater difference in cell viability between the Cas-9 LIMD1 proficient and CRISPR-Cas-9 LIMD1 deficient cell lines might be observed.

Increased sensitivity to irinotecan in the LIMD1$^{-/-}$ HELA/A549 CRISPR-Cas 9 cells compared to LIMD1 proficient controls was observed in all three biological repeats of the irinotecan dose-response assays in both cell lines (**Figures 6.10** and **6.11**). Again some variation in the degree of cell killing at any particular irinotecan concentration between biological repeats of the assay in both proficient and deficient cell lines was observed. Cells of similar passage were seeded for biological repeats and similar confluency/cell titre-Glo^{TM} readings for the control cells treated with DMSO alone were observed between experiments.

A concentration of 2μM irinotecan was selected and irinotecan sensitivity in both the A549 LIMD1$^{-/-}$ and HELA LIMD1$^{-/-}$ cells compared to proficient control. This concentration was selected as differences in irinotecan drug sensitivity in the LIMD1

deficient compared to proficient A549 and HELA cells was greatest at this drug concentration. Again, calculation of the drug IC50 was not possible, as at the highest irinotecan drug concentrations, cell death close to 100% was not consistently observed. Pooled analysis of the biological repeats demonstrated a significant increase in sensitivity to irinotecan with on average a 25% increase in cell death in the LIMD1 deficient A549 cells compared to proficient control drugged with 2μM irinotecan, Student's T test, p=0.0232* (**Figure 6.11**). This figure was even greater in HELA cells, where 60% more cell death occurred in the LIMD1 deficient HELA cells compared to proficient control at this drug concentration, Student's T test p=0.0196* (**Figure 6.11**).

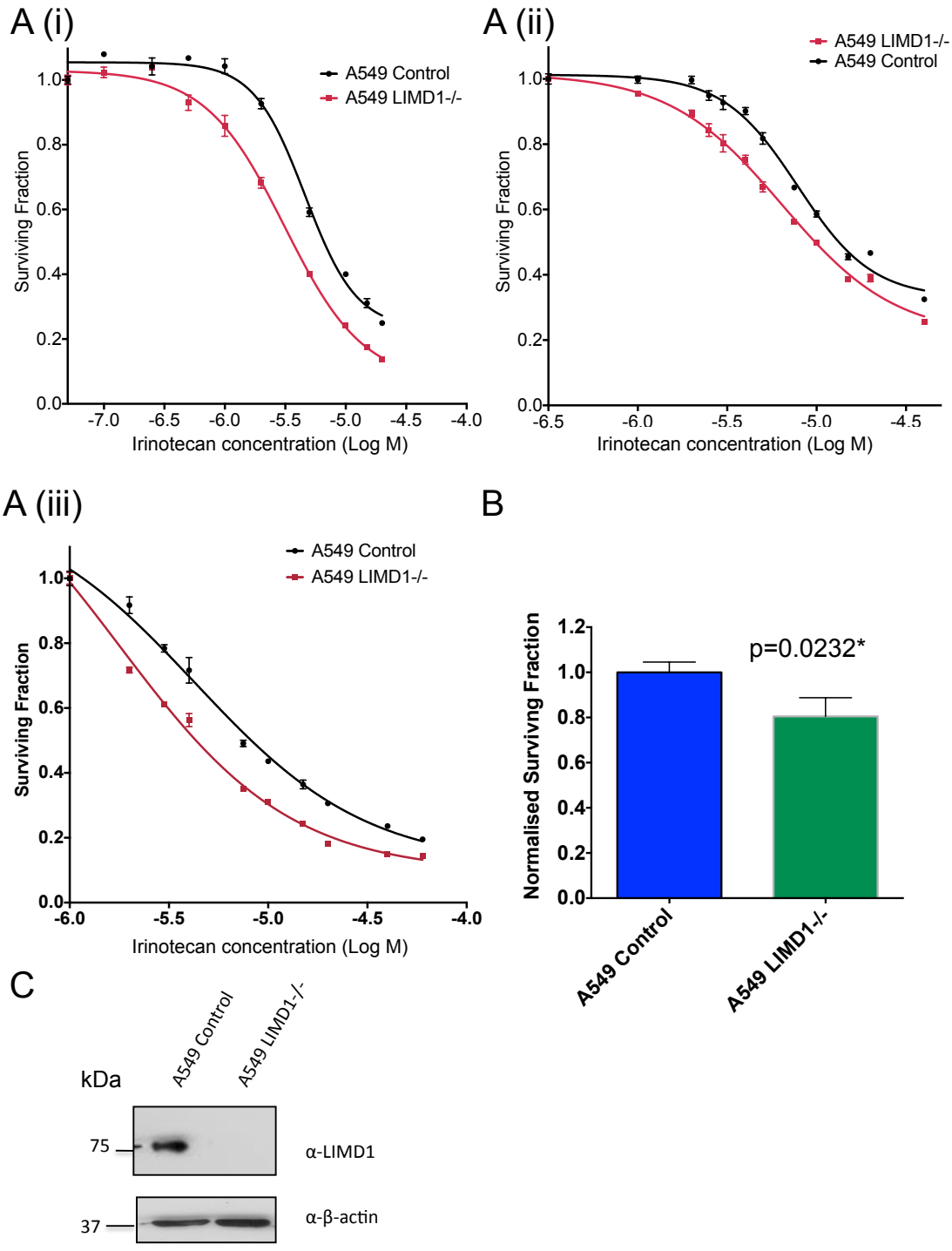

Figure 6.10: The topoisomerase-I inhibitor irinotecan is associated with increased cell death in LIMD1 deficient compared to matched LIMD1-proficient control A549 cells

A549 CRISPR/Cas-9 LIMD1$^{+/+}$ and CRISPR/Cas-9 LIMD1$^{-/-}$ cells were plated simultaneously in a 96-well plate at a seeding density associated with 90-95% confluency on day 6 and exposed to a range of irinotecan concentrations between 0.1μM and 60μM 24 and 72 hours after seeding, with drugging in triplicate at each drug concentration. Cells were also plated for Western blot analysis to assess LIMD1

expression on day 6. Both cell lines were plated simultaneously on the same 96 well plate and exposed to a range of irinotecan concentrations between 0.1μM and 60μM 24 hours after seeding, with drugging in triplicate at each drug concentration. Cell viability was assessed on day 6 using the ATP-based Cell-Titer Glo™ assay. All graphs were generated in Prism version 6, with error bars demonstrating the SEM**. (A(i))-A(iii))** Irinotecan dose-response curves, for A549 LIMD1$^{+/+}$ and A549 LIMD1$^{-/-}$ lines. **B.** An irinotecan concentration of 2μM was selected and the relative sensitivity of HELA and A549 LIMD1$^{-/-}$ cells generated by a CRISPR-Cas-9 LIMD1 knockout system compared to CRISPR-Cas-9 LIMD1$^{+/+}$ control assessed. Sensitivity to irinotecan at 2μM is shown relative to the CRISPR-Cas-9LIMD1$^{+/+}$ control cells with error bars representing the SEM for the 3 biological repeats. P value represents Students t-test value. All analysis was undertaken using Prism 6. **C.** Immunoblot demonstrating high levels of LIMD1 expression in the A549 LIMD1$^{+/+}$ control with no LIMD1 expression in the A549 LIMD1$^{-/-}$.

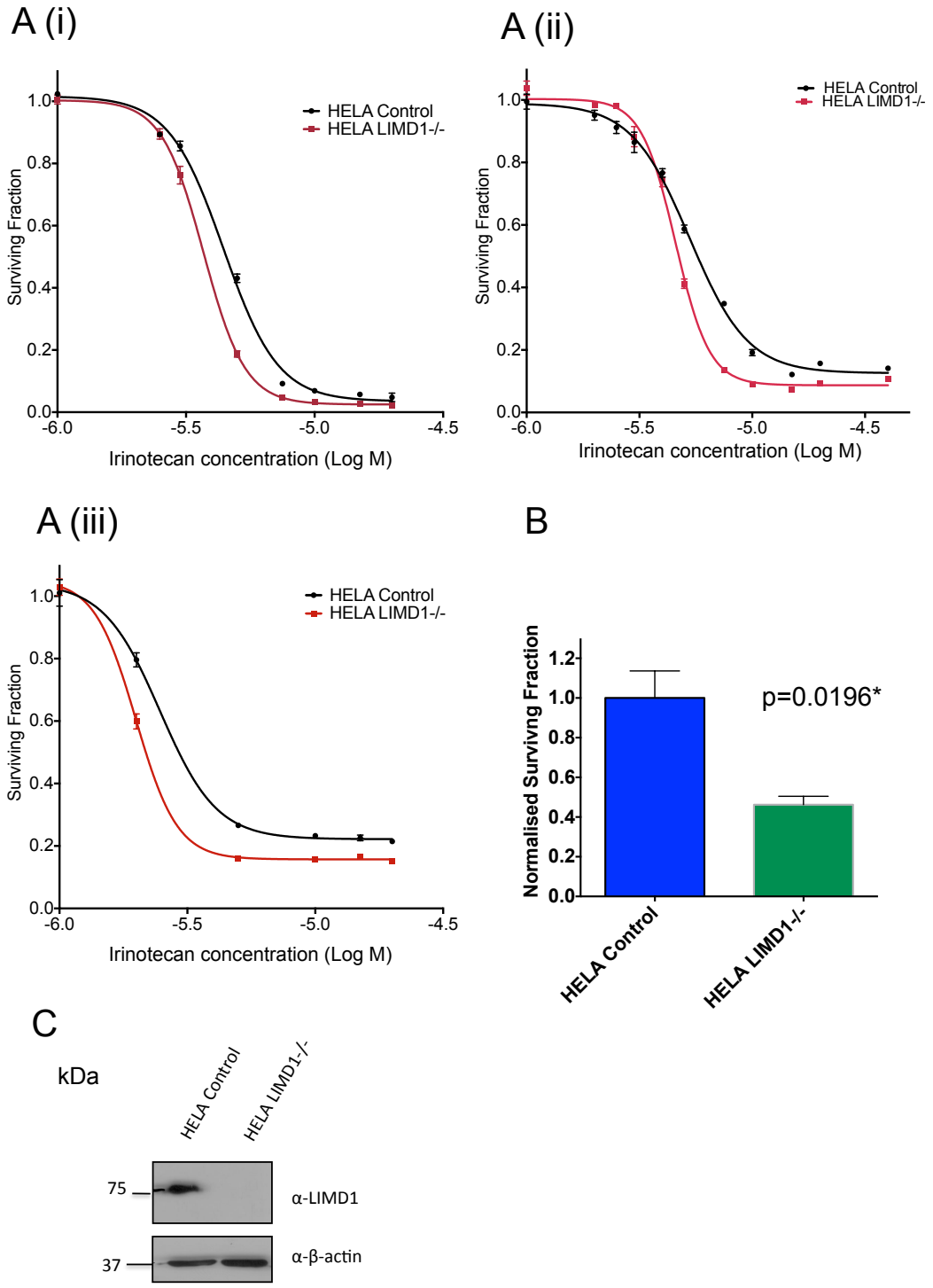

Figure 6.11: The topoisomerase-I inhibitor irinotecan is associated with increased cell death in LIMD1 deficient compared to matched LIMD1-proficient control HELA cells

HELA CRISPR/Cas-9 LIMD1$^{+/+}$ and CRISPR/Cas-9 LIMD1$^{-/-}$ cells were plated simultaneously in a 96 well plate at a seeding density associated with 90-95% confluency on day 6 and exposed to a range of irinotecan concentrations between 0.1µM and 60µM 24 and 72 hours after seeding, with drugging in triplicate at each drug concentration. Cells were also plated for Western blot analysis to assess LIMD1

expression on day 6. Cell viability was assessed on day 6 using the ATP-based Cell-Titer Glo™ assay. All graphs were generated in Prism version 6, with error bars demonstrating the SEM. **(A(i))-A(iii))** Irinotecan dose-response curves, for HELA LIMD1$^{+/+}$ and HELA LIMD1$^{-/-}$ lines. **B.** An irinotecan concentration of 2μM was selected and the relative sensitivity of HELA LIMD1$^{-/-}$ cells generated by a CRISPR-Cas-9 LIMD1 knockout system compared to CRISPR-Cas-9 LIMD1$^{+/+}$ control assessed. Sensitivity to irinotecan at 2μM is shown relative to the CRISPR-Cas-9LIMD1$^{+/+}$ control cells with error bars representing the SEM for the 3 biological repeats. P value represents Students t-test value. All analysis was undertaken using Prism 6. **C.** Immunoblot demonstrating high levels of LIMD1 expression in the HELA LIMD1$^{+/+}$ control with no LIMD1 expression in the HELA LIMD1$^{-/-}$.

6.7 Levels of endogenous LAW expression correlate with sensitivity to irinotecan in a panel of ccRCC cell lines.

LAW expression was evaluated in a panel of ccRCC cell lines with Western Blotting and is described in chapter 3. Given the overlapping functions of LAW family members particularly in the regulation of the hypoxic response and microRNA silencing, the relationship between expression of LAW family members and sensitivity to irinotecan was explored.

Five ccRCC cell lines were selected, two with high levels of expression of all three family members, RCC11 and CAKI2, and three with lower levels of expression of LAW family members, RCC4, RCC12 and RCC912 (**Figure 6.12B**). Irinotecan dose-response was characterised in these cell lines by Ms Kathryn Davidson. As before, cells were seeded into 96- well plates such that they were at between 90-95% confluency on day 6 in the control wells containing DMSO 0.1% only. Drugging at a range of irinotecan concentrations was undertaken at 24 and 72 hours and the plates read on day 6 using an ATP based assay (Cell-Titer-Glo™). Cell lines with low levels of endogenous LAW expression RCC4, RCC12 and RCC912 demonstrated increased sensitivity to irinotecan compared to CAKI2 and RCC11, cell lines that express high levels of LAW proteins, suggesting that loss of LAW expression is associated with increased irinotecan sensitivity in ccRCC (**Figure 6.12A**).

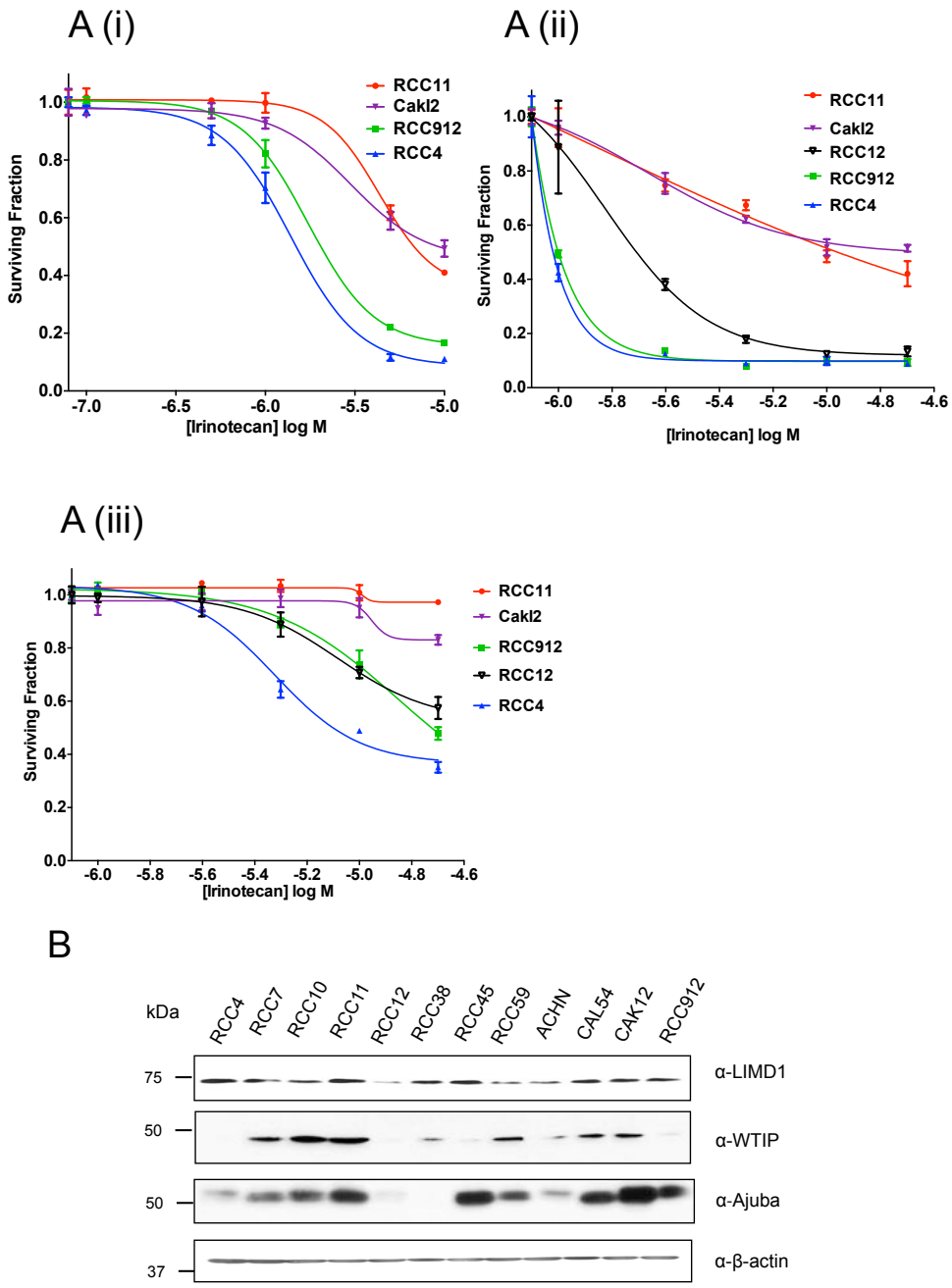

Figure 6.12. Levels of endogenous LAW expression correlates with sensitivity to irinotecan in a panel of ccRCC cell lines

RCC4, RCC11, RCC12, CAKI2 and RCC912 cells were plated in a 96 well plate at a seeding density associated with 90-95% confluency on day 6 and exposed to a range of irinotecan concentrations between 0.1µM and 60µM 24 and 72 hours after seeding, with drugging in triplicate at each drug concentration. Cell viability was assessed on day 6 using the ATP-based Cell-Titer Glo™ assay. All graphs were generated in Prism version 6, with error bars demonstrating the SEM. **(A)** Irinotecan dose-response curves, for RCC4, RCC11, RCC12, CAKI2 and RCC912 cell lines. **B.** Immunoblot demonstrating levels of LAW expression in a panel of ccRCC cell lines with β-actin included as a loading control.

6.8 LIMD1 loss does not affect the sensitivity of RCC11 or RCC48 to the tyrosine-kinase inhibition sunitinib or the mTOR inhibitor temsirolimus

Short-term cell viability assays were undertaken to assess the effects of LIMD1 depletion on the sensitivity of the ccRCC lines RCC11 and RCC48 to the multi-tyrosine kinase inhibitor sunitinib. Sunitinib is a TKI which acts predominantly to inhibit VEGF, PDGF and c-kit tyrosine kinases and is used first-line in the treatment of ccRCC (Albiges, Choueiri et al. 2015). The effects of LIMD1 depletion on sensitivity to temsirolimus, an mTOR inhibitor used after the failure of TKI were also characterised (Albiges, Choueiri et al. 2015).

Work by del Peurto-Nevado *et al*, demonstrated that phosphorylated KDR staining (phosphorylated VEGFR2) is a predictor of clinical benefit to sunitinib-based therapy and hence that active angiogenesis predicts response to therapy (del Puerto-Nevado, Rojo et al. 2014). Given the known function of LIMD1 in the regulation of the hypoxic response, the effects of LIMD1 loss on sunitinib sensitivity were investigated. In the RCC11/RCC48 cell lines, loss of LIMD1 was not however associated with differences in sensitivity to the multi-TKI pazopanib (**Figure 6.7**).

As before, the assay was performed in the RCC11/48 scr and shLIMD1 lentiviral transduced cell lines plated simultaneously in the same 96-well plates. Cells were taken out of puromycin selection 24 hours prior to seeding and seeded at the cell densities previously described. Cells were also plated in a 6-well plate and lysed on day 6 to check for LIMD1 expression in the scr control and LIMD1 knockdown in the shLIMD1 line. Drug assays were read at day 6 using the Cell-Titre Glo^{TM}. LIMD1 depletion did not affect the sensitivity of either cell lines to sunitinib when compared to control LIMD1 proficient cell lines (**Figures 6.13** and **6.14**).

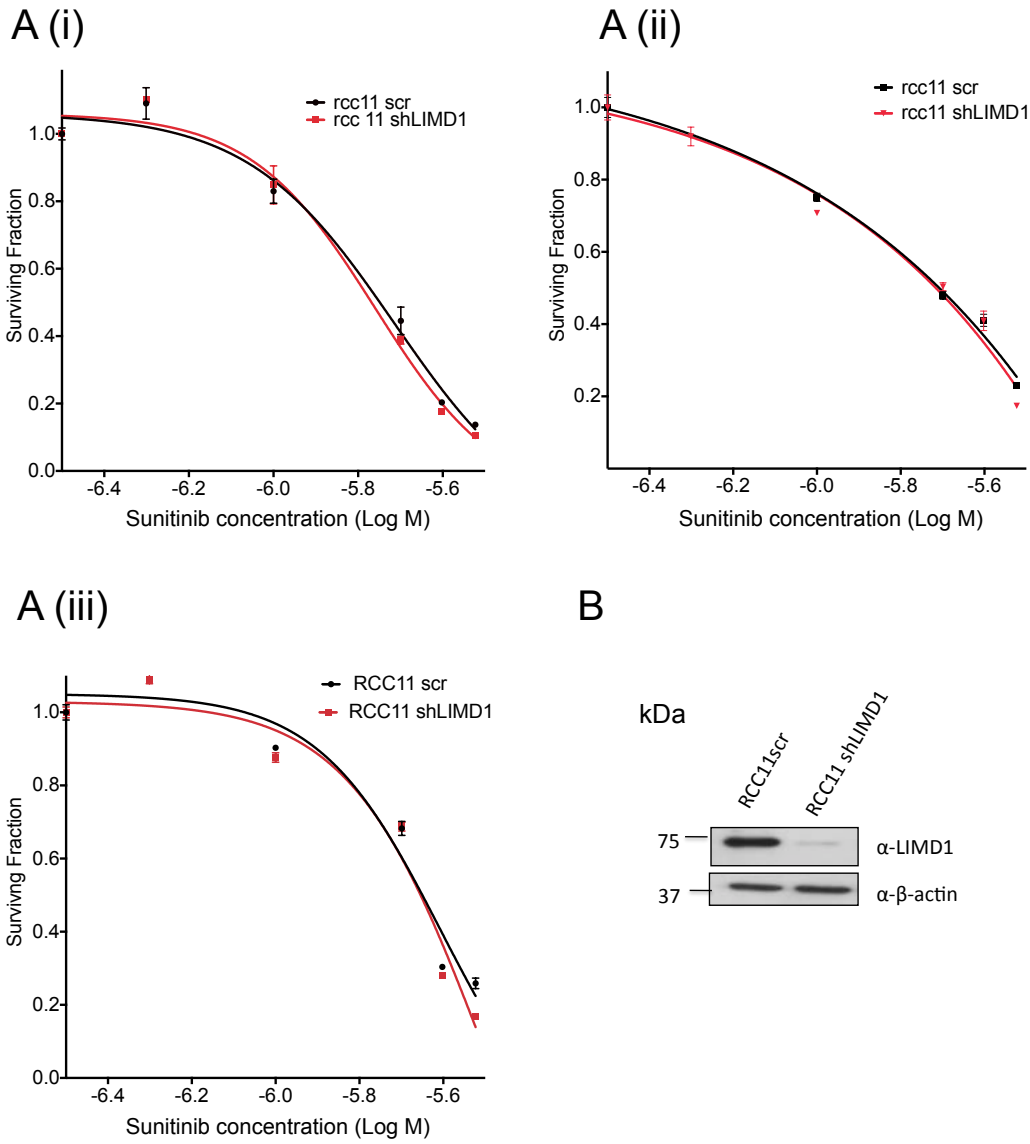

Figure 6.13 LIMD1-depletion does not affect the sensitivity of RCC11 to the multi-tyrosine kinase inhibitor sunitinib

RCC11 scr/shLIMD1 cells were plated in to a 96 well plate at a seeding density association with 90-95% confluency on day 6. Cells were also plated for Western blot analysis to assess LIMD1 knockdown on day 6. Scr/shLIMD1 cells were plated simultaneously on the same 96 well plate and exposed to a range of sunitinib concentrations between 0.1μM and 10μM 24 and 72 hours after seeding, with drugging in triplicate at each drug concentration. Cell viability was assessed on day 6 using the ATP-based Cell-Titer Glo™ assay. All graphs were generated in Prism version 6, with error bars demonstrating the SEM**. (A (i)-A (iii))** Sunitinib dose-response curve, RCC11 scr/shLIMD1, **B** Expression of LIMD1 in the scr line and knockdown of LIMD1 in the shLIMD1 line was confirmed by Western Blotting

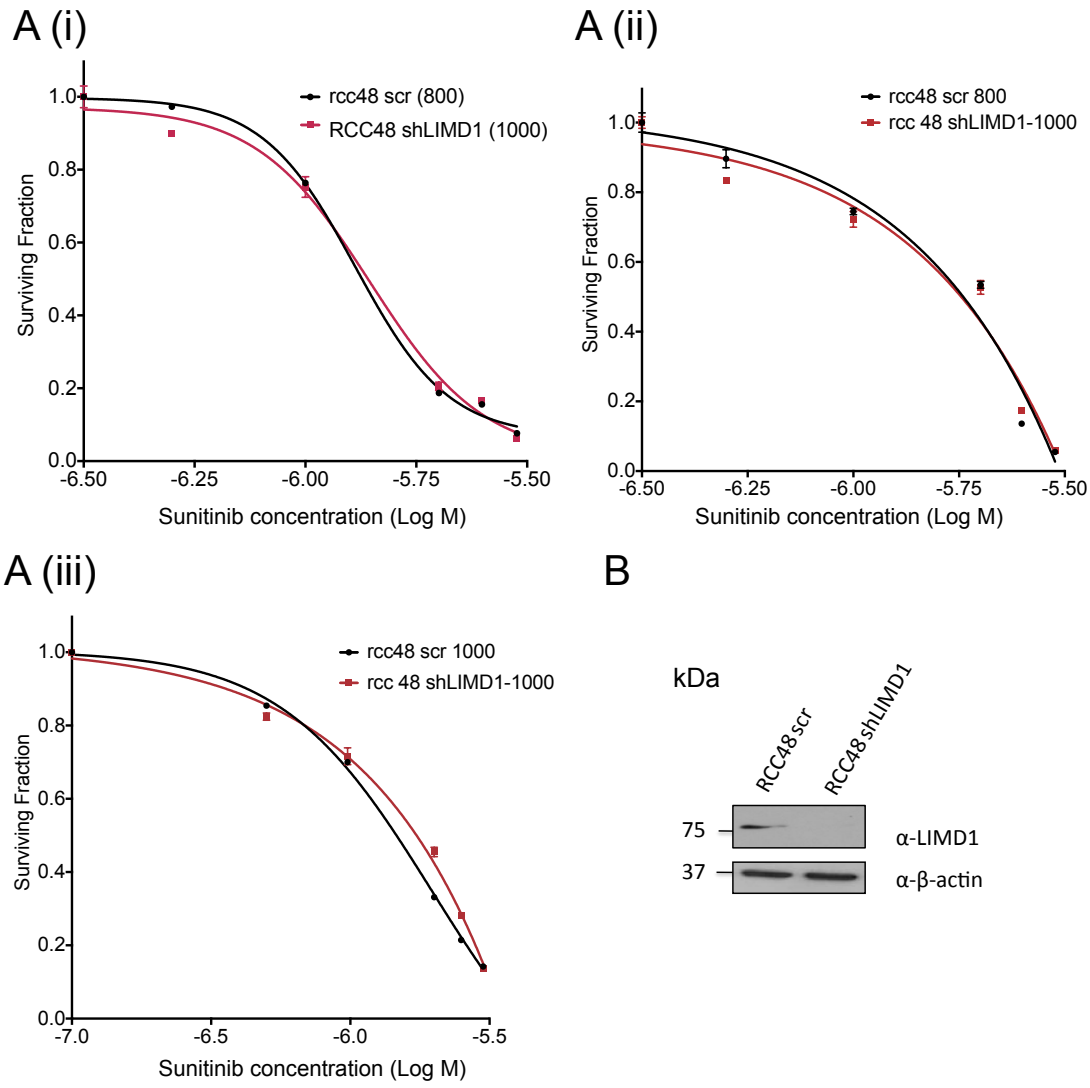

Figure 6.14 LIMD1-depletion does not affect the sensitivity of RCC48 to the multi-tyrosine kinase inhibitor sunitinib

RCC48 scr/shLIMD1 cells were plated in to a 96 well plate at a seeding density association with 90-95% confluency on day 6. Cells were also plated for Western blot analysis to assess LIMD1 knockdown on day 6. Scr/shLIMD1 cells were plated simultaneously on the same 96 well plate and exposed to a range of sunitinib concentrations between 0.1μM and 10μM 24 and 72 hours after seeding, with drugging in triplicate at each drug concentration. Cell viability was assessed on day 6 using the ATP-based Cell-Titer Glo™ assay. All graphs were generated in Prism version 6, with error bars demonstrating the SEM. **(A (i)-A (iii))** Sunitinib dose-response curve, RCC11 scr/shLIMD1, **B** Expression of LIMD1 in the scr line and knockdown of LIMD1 in the shLIMD1 line was confirmed by Western Blotting

Temsirolimus is a serine-threonine kinase inhibitor targeting mTOR (Mackenzie, Rini et al. 2011). The mTOR pathway is a convergence point for multiple signalling pathways, including the PI3K/Akt pathways, the insulin-like growth factor pathways and the

MAP-kinase pathways and mTOR functions to elicit the response of tumour cells to numerous growth and survival signals. Phosphorylation of the downstream targets of mTOR, S6K and 4EBP1 results in increased translation of a range of specific proteins that allow cell cycle progression and increased translation of components of the hypoxia-inducible pathway, in particular HIF1α (Mackenzie, Rini et al. 2011). Temsirolimus demonstrates OS benefit versus IFN-α in poor-prognosis metastatic RCC patients (Hudes, Carducci et al. 2007) and retrospective data suggests some efficacy after progression with VEGFR inhibitors (Mackenzie, Rini et al. 2011).

The assay was undertaken as described for sunitinib in the RCC11 and RCC48 scr/shLIMD1 lines. LIMD1 depletion did not affect the sensitivity of either cell line to temsirolimus when compared to control LIMD1 proficient cell lines (**Figures 6.14** and **6.15**).

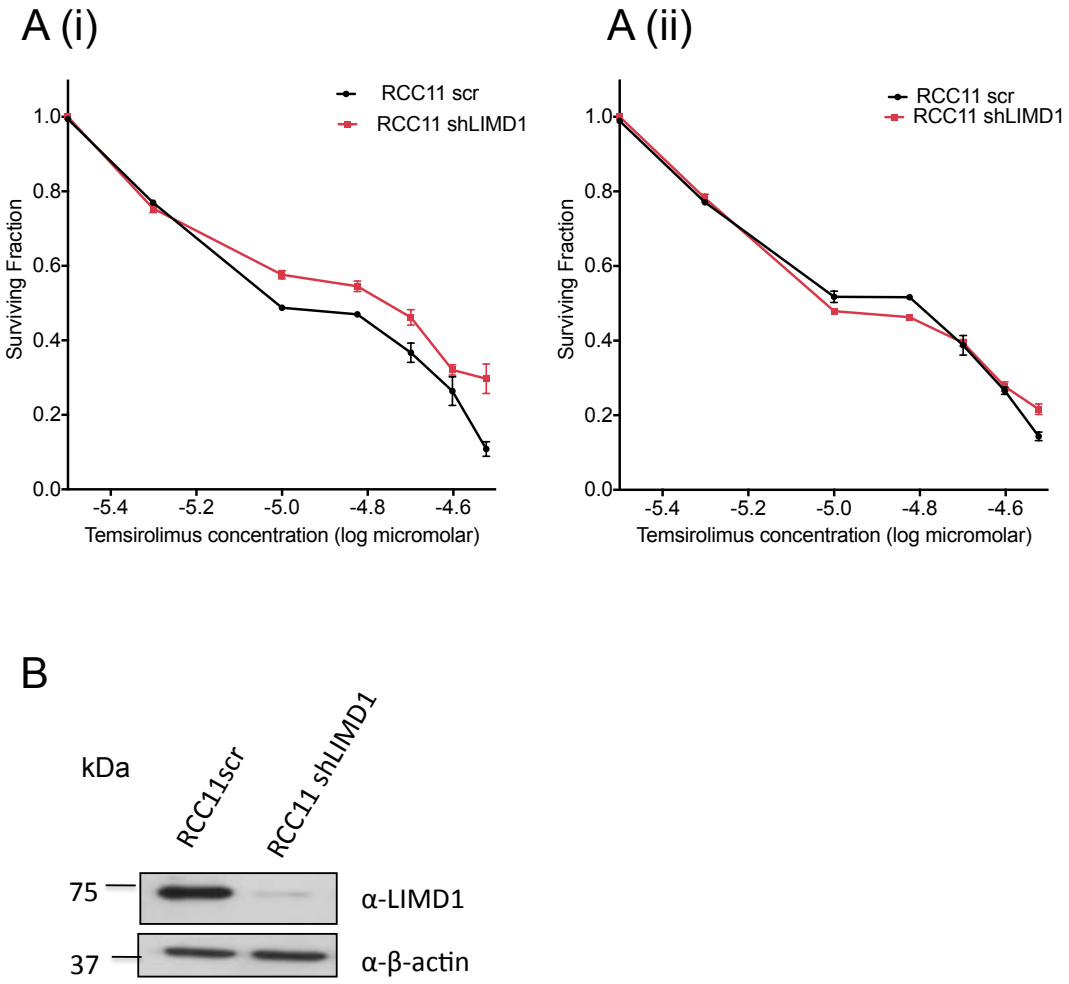

Figure 6.14 LIMD1-depletion does not affect the sensitivity of RCC11 cells to the multi-tyrosine kinase inhibitor temsirolimus

RCC111 scr/shLIMD1 cells were plated in to a 96 well plate at a seeding density association with 90-95% confluency on day 6. Cells were also plated for Western blot analysis to assess LIMD1 knockdown on day 6. Scr/shLIMD1 cells were plated simultaneously on the same 96 well plate and exposed to a range of sunitinib concentrations between 5μM and 40μM 24 and 72 hours after seeding, with drugging in triplicate at each drug concentration. Cell viability was assessed on day 6 using the ATP-based Cell-Titer Glo™ assay. All graphs were generated in Prism version 6, with error bars demonstrating the SEM. **(A (i)-A (iii))** Temsirolimus dose-response curve, RCC11 scr/shLIMD1, **B** Expression of LIMD1 in the scr line and knockdown of LIMD1 in the shLIMD1 line was confirmed by Western Blotting

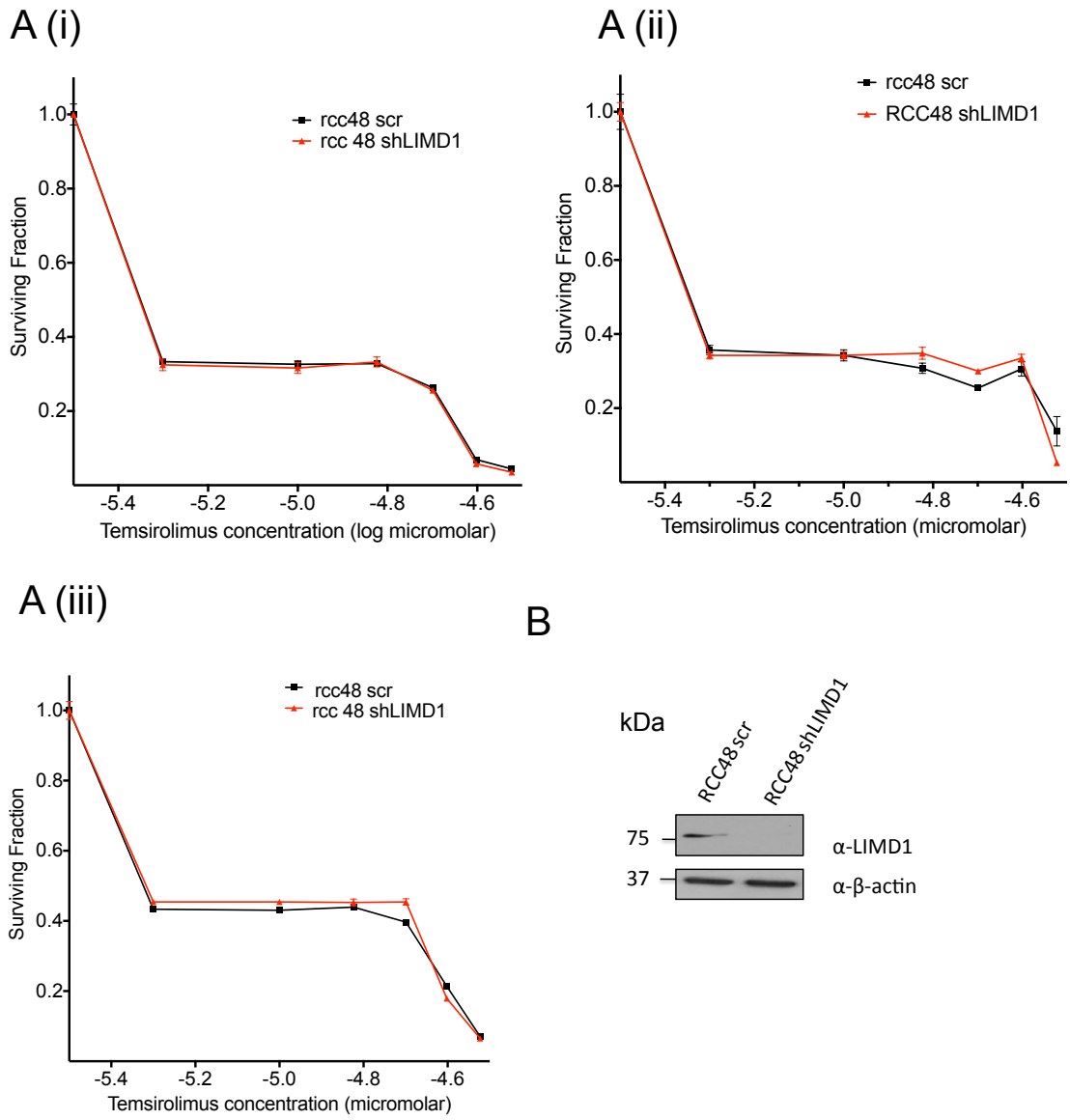

Figure 6.15 LIMD1-depletion does not affect the sensitivity of RCC48 to the multi-tyrosine kinase inhibitor temsirolimus

RCC48 scr/shLIMD1 cells were plated in to a 96 well plate at a seeding density association with 90-95% confluency on day 6. Cells were also plated for Western blot analysis to assess LIMD1 knockdown on day 6. Scr/shLIMD1 cells were plated simultaneously on the same 96 well plate and exposed to a range of sunitinib concentrations between 5μM and 40μM 24 hours after seeding, with drugging in triplicate at each drug concentration. Cell viability was assessed on day 6 using the ATP-based Cell-Titer Glo™ assay. All graphs were generated in Prism version 6, with error bars demonstrating the SEM. **(A (i)-A (iii))** Temsirolimus dose-response curve, RCC11 scr/shLIMD1, **B** Expression of LIMD1 in the scr line and knockdown of LIMD1 in the shLIMD1 line was confirmed by Western Blotting

6.9 Summary

Ten out of twelve ccRCC lines characterised *in vitro* demonstrated reduced LIMD1 expression compared to LIMD1 proficient primary cells (RPTEC) and 49.3% of ccRCC samples compared to MAT *in vivo* (results shown in Chapter 3). Consequently the selective targeting of tumours demonstrating LIMD1 loss/down-regulation represents an attractive novel therapeutic approach and the identification of a drug demonstrating synthetic lethality in association with loss of this tumour suppressor would enable the selective targeting of a significant proportion of ccRCC tumours with relative sparing of non-tumour LIMD1 proficient cells.

A synthetic lethality screen was undertaken in paired RCC11 proficient (scr) compared to RCC11 deficient (shLIMD1) cell lines using a compound library of 584 FDA approved drugs with demonstrated anti-cancer activity or evaluated as potential anti-cancer drugs. This identified a number of 'hits' that resulted in increased cell death in the LIMD1 deficient compared to proficient cells. With the exception of the topoisomerase-I inhibitor irinotecan, validation of the 'hits' from the drug screen across a range of drug concentrations in RCC11scr/RCC11 shLIMD1 cells was not successful.

In both RCC11 shLIMD1 and RCC48 shLIMD1 cell lines and in the non-ccRCC cell lines, HELA and A549, where LIMD1 had been deleted using a CRISPR-Cas-9 gene editing system, dose-response curves demonstrated increased irinotecan sensitivity in the LIMD1 low/deficient cell lines compared to LIMD1 proficient control.

In a panel of five ccRCC cell lines, two with high levels of LAW expression, CAKI2 and RCC11, and three with lower levels of LAW expression, RCC4, RCC12 and RCC912, increased sensitivity to irinotecan was observed in cell lines with low LAW expression compared to cell lines with high LAW expression. Taken together, this indicates that LAW expression levels and in particular LIMD1 loss may act as a predictive biomarker for irinotecan sensitivity in ccRCC lines and perhaps non-ccRCC lines *in vitro*, although further validation is required.

The sensitivity of the paired RCC11scr/shLIMD1 cell lines and RCC48 scr/shLIMD1 cell lines to the multi-TKI sunitinib used in the first line treatment of ccRCC, and the mTOR inhibitor temsirolimus, used after failure of primary TKI therapy demonstrated no differences in sensitivity to either drug in association with LIMD1 loss compared to the LIMD1 proficient cells.

6.10 Discussion

6.10. 1 Drug screening platforms in oncology

This chapter demonstrates the use of a drug-screening platform to identify drugs with established anti-cancer activity, which may act in a synthetically lethal manner in association with LIMD1 loss. Irinotecan was validated as a 'drug hit' across a range of concentrations in two ccRCC and two non-ccRCC cell lines and an association between lower LAW expression and increased irinotecan sensitivity was observed in a panel of 5 ccRCC lines. Given our observation that loss of LIMD1 is a feature of 50% of ccRCC cell lines *in vitro* and reduced LIMD1 expression is observed in 49.3% of ccRCC tumours, targeting LIMD1 low/deficient or LAW low/deficient tumours with irinotecan may represent an attractive biomarker driven treatment strategy.

In oncology, drug screening offers a powerful tool for identifying novel anti-cancer drugs or identifying novel uses for existing anti-cancer drugs (Sharma, Haber et al. 2010). A key challenge in drug candidate screening is the accurate determination of human efficacy: toxicity and lack of clinical efficacy are the commonest causes of drug failure during drug development (Kola 2008) with fewer than 10% of novel cancer drugs identified in drug screening platforms progressing successfully through clinical development (Arrondeau, Gan et al. 2010). In addition, nearly 3% of all drugs that make it into the clinical setting are subsequently withdrawn due to adverse side effects (Kola and Landis 2004).

The use of drug-libraries containing FDA-approved drugs with known cancer-therapeutic efficacy and clearly identified toxicity profiles overcomes many of these problems and such an approach is likely to lead to a much higher hit rate. More recently, synthetically lethal approaches have been utilised to identify novel therapeutic drugs, or characterise the role of drugs within biomarker driven populations, such as the use of PARP inhibitors in patients with breast and ovarian cancers in association with BRCA1 or BRCA2 mutations (Yap, Sandhu et al. 2011). Such an approach is particularly attractive as it minimises toxicity to healthy, non-cancer cells (Chan and Giaccia 2011).

6.10.2 Two-dimensional drug screening platforms.

The use of a two dimensional drug-screening platform has a number of advantages. Such assays are amenable to automated/semi-automated high throughput screening, which can reduce screening cost and time and particularly with automated platforms can quickly generate accurate screen information, allowing a potential drug to be quickly evaluated as a drug of interest or disregarded as unlikely to demonstrate efficacy (Chen, Huang et al. 2011). Such early-stage *in vitro* cell-based assays, can provide a multitude of information on relevant biological end-points, including drug sensitivity, proliferation, motility, differentiation, cell shape, metabolism and protein expression/localisation (Chen, Huang et al. 2011).

However, there are a number of limitations to such an approach. In our assays in a 96-well plate, only 800-2500 cells per well were plated and cells were plated manually. Seeding density may have a significant impact on the end point of drug sensitivity with small variations in seeding density significantly impacting on drug sensitivity. Errors may be caused by poor pipette delivery, and unintended differences in compound concentrations as a result of evaporation of the solvent. In addition, systematic across-plate and within-plate column or row biases, typically known as edge effects are common (Malo, Hanley et al. 2006). When using 2μM of the drug library, drugging at 24 and 72 hours could not be undertaken due to insufficient drug availability, particularly for drugs at the edges of the plates, where presumably greater evaporation had taken place.

Once technical and procedural efficiencies have been optimised, the only way to minimise variability further is to take averages (the mean or median) across replicate measurements. Excellent reproducibility between the two repeats of the drug screen at 1μM (**Figure 6.1**) was observed, however without further repeated measurements, activity estimates are difficult to quantify. In addition, further replicate measurements can provide estimates of variability and therefore be used in power analysis, to determine the likely probability of detecting a 'true hit' (Malo, Hanley et al. 2006). Increasing the number of replicates will reduce the number of false positives, without increasing the number of false negatives (Malo, Hanley et al. 2006).

Using a single drug dose has a number of limitations. The topoisomerase-I inhibitor topetecan resulted in significant death and very negative Z-scores in both RCC11 scr and shLIMD1 lines. Topetecan may still demonstrate synthetic lethality in association with LIMD1 loss in this cell line but the toxicity observed in both lines at this drug concentration with almost all cells killed may have obscured any association and it would be relevant to conduct a topetecan dose-response curve with the RCC11scr/shLIMD1 lines.

Drugging with the drug library was undertaken at 24 and 72 and cell viability output read on day 6 using an ATP based Cell-Titer Glo™ assay. Different drugs within the library will have different pharmacokinetics and the optimal timing of both dosing and reading output is likely to vary from one drug to another. By varying both the dosing schedules and timing of output reading, different 'hits' from the screen may well have been identified.

Another limitation is that the drug screen was undertaken in one paired cell line alone. This line was selected as it is VHL mutated, expresses high levels of all 3 LAW family members, high HIF1α and moderate HIF2α. It was therefore felt that to be representative of an aggressive 'hypoxically deregulated' ccRCC LIMD1 tumour phenotype. In addition, given that all 3 LAW family members are expressed, lentiviral knockdown of LIMD1 allowed for the effects of LIMD1 loss alone on drug sensitivity to be investigated.

6.10.3 Statistical analysis of two-dimensional drug-screening platforms.

Statistical analysis of the assay performance is critical in assessing such screen data. Recent articles have expressed concern about a lack of reproducibility of drug testing methodology and suggested standardisation of laboratory protocols (Hatzis, Bedard et al. 2014). The screen undertaken used the commonly held assumption that the data from the screen is normally distributed and a log transformation was then applied to achieve a better fit to the normal distribution. A more robust Z-score method was then calculated for each compound, which normalises each compound to the median value and median absolute deviation as opposed to the mean and the standard deviation. Such

an approach is commonly used and in particular is attractive as it diminishes the effects of outliers on the final analysis result (Chung, Zhang et al. 2008).

Another method is to use the B score, sometimes considered a more robust analogue of the Z score (Brideau, Gunter et al. 2003). This method applies a two-way median polish to account for row and column effects of the plate, and the resulting residuals within each plate are divided by their median absolute deviations to standardise for plate-to plate variability. This approach has the advantage that it is non-parametric and therefore makes minimal distribution assumptions, minimises measurement biases related to position and is resistant to statistical outliers (Malo, Hanley et al. 2006, Mpindi, Swapnil et al. 2015).

Mpindi *et al* concluded that for high throughput screening experiments with high hit rates, it is best to scatter controls throughout the plate and normalise using a polynomial least squares fit method, to reduce edge effects (Mpindi, Swapnil et al. 2015). For the drug library described most controls were within column seven of twelve on the 96-well plate and given that the library was already plated prior to use, it would not have been possible to change the location of the control wells.

6.10.4 Three-dimensional assays to more closely mimic the *in-vivo* environment.

2-D *in vitro* assays offer a number of advantages, but as outlined, do not provide sufficient data for understanding drug performance *in vivo* (Astashkina, Mann et al. 2012). In particular an *in vitro* assay should produce reliable, biomedically relevant information that mimics the phenotype of cells within the target tissue (Mazzoleni, Di Lorenzo et al. 2009). By using a more *in vivo*-like, three-dimensional environment, a more robust screening platform that more closely resembles the *in vivo* environment can be created. For example cells grown in 2D versus 3D environments demonstrate significant differences in cell morphology, proliferation, gene expression, signalling and differentiation (Schmeichel and Bissell 2003). Organotypic, organ/explant and 3-D cultures can overcome some of these limitations (Astashkina, Mann et al. 2012). High throughput methods for 3-D models can be employed although are less straightforward than for 2-D models. For example using 3D microarray culture for drug assays, where

microarray spots are printed on a modified glass microscope slide or chip (Meli, Jordan et al. 2012).

6.10.5 Genomic heterogeneity and its impact on drug screening

Genomic heterogeneity has a significant impact on drug sensitivity and in ccRCC this may related to both intra-patient and inter-patient heterogeneity, reflecting heterogeneity both within the primary tumour and within metastatic deposits (Gerlinger, Catto et al. 2015). In non-small cell lung cancer (NSCLC) for example, the EGFR TKIs gefitinib and erlotinib, demonstrate significant efficacy in patients with activating EGFR mutations, however only around 10% of patients with adenocarcinomas have such mutations (Kris, Natale et al. 2003). In metastatic ccRCC, driver mutations not shared by the primary tumour may drive metastatic spread and contribute to resistance to targeted therapy (Gerlinger, Rowan et al. 2012).

6.10.6 Irinotecan as a drug demonstrating synthetic lethality in association with LIMD1 loss

Despite the limitations of the drug screen outlined, the identification of irinotecan as a potential hit appears to represent a true result. The difference in irinotecan drug sensitivity between the RCC11 scr and shLIMD1 line did not quite meet statistical significance when validated across a range of drug concentrations (**Figures 6.8** and **6.10**) but the differences were statistically significant in the RCC48 shLIMD1 cells compared to RCC48 scr line (**Figures 6.9 and 6.10**) and in both the HELA CRISPR-Cas-9 LIMD1 and A549 CRISRP-Cas-9 LIMD1 proficient and deficient cell lines, where LIMD1 loss was consistently associated with increased irinotecan sensitivity (**Figures 6.11**, **6.12**). Additional work undertaken by Miss Katy Davidson demonstrated that in the RCC lines CAKI2 and RCC11 where LAW expression is high, reduced sensitivity to irinotecan is observed compared to the RCC lines RCC4, RCC12 and RCC912, where LAW expression is low (**Figure 6.13**).

Irinotecan is a semisynthetic analogue of captothecin that causes S-phase specific cell killing through its interaction with cellular Topo-I-DNA complexes (Xu and Villalona-

Calero 2002). Specifically, topoisomerases cleave and reseal the phosphodiester backbone of DNA by forming covalent enzyme-DNA linkages, allowing the passage of single and double strand DNA breaks through the nick. Topo-1 binds to single strand DNA breaks and the Topo-1 DNA complex leads to irreversible arrest of the replication fork and cell death upon collision with the advancing replication form, as well as signalling the presence of DNA damage to an S-phase checkpoint mechanism and G2 arrest/delay (Solary, Bertrand et al. 1994, Webb and Ebeler 2003). Multiple mechanisms determine irinotecan sensitivity, including cellular drug accumulation, related to active drug efflux, levels of Topo-1 expression, variations in enzyme levels involved in the conversion of irinotecan to its more active form SN-38, alterations in cellular response to drug-Topo-1-DNA complex formation and variations in the activation of the transcription factor NFκB by DNA damage (Xu and Villalona-Calero 2002).

It is difficult to know why increased irinotecan sensitivity is seen in association with LIMD1 loss/depletion. Several studies have identified an association between hypoxia and chemo-resistance in a number of tumour types, mediated through the Ajuba signalling pathway. In hepatocellular carcinoma (HCC), under conditions of hypoxia, HCC cells are highly resistant to topoisomerase inhibitors including the active metabolite of irinotecan, SN38 (Cai, Liu et al. 2014). It had previously been demonstrated that HIF1 plays a critical role in chemo-resistance in HCC cells (Jiao and Nan 2012, Tong, Li et al. 2013). Dai *et al* however showed that the Yes-Associated Protein (YAP), an oncoprotein closely correlated with the development of HCC (Xu, Yao et al. 2009) played a critical role in mediating resistance to SN38, with hypoxia inhibiting LATS1 mediated phosphorylation of YAP in a HIF1 independent manner, in turn inducing YAP nuclear translocation and YAP accumulation with subsequent activation of its downstream target genes, (Dai, Zhuang et al. 2016) including genes that promote tumour progression and or metastasis (Zeng and Hong 2008). Notably in association with nuclear YAP translocation in hypoxia, HCC cells were much less sensitive to SN38 in hypoxia compared to normoxia, and this effect was abrogated upon YAP depletion (Dai, Zhuang et al. 2016). In addition, Dai *et al* used statins, which inhibit the mevalonate metabolic pathway and are used to treat hypercholesterolaemia to inhibit YAP nuclear translocation which in turn re-sensitised HCC cells to SN38 in hypoxia (Dai, Zhuang et al. 2016).

The Ajuba LIM proteins are negative regulators of the Hippo signaling pathway (Das Thakur, Feng et al. 2010). Ajuba, LIMD1 and WTIP strongly associate with LATS1/2 and in mammalian cells antagonise the phosphorylation of YAP (Das Thakur, Feng et al. 2010). Work by Zhao *et al* has demonstrated that in sub-confluent non-contacted cells, Ajuba LIM proteins are predominantly cytosolic, whilst YAP is nuclear and cells proliferate but once confluent, YAP is phosphorylated and is translocated to the cytosol whilst Ajuba proteins are recruited to adherens junctions (Zhao, Wei et al. 2007) potentially releasing LATS and enabling Hippo pathway mediated YAP phosphorylation with subsequent cell inactivation and growth arrest. Therefore LAW depletion can potentially increase active YAP, with increased YAP nuclear translocation and downstream oncogene target activation. Given the observation of reduced sensitivity to SN38 in association with nuclear YAP translocation in HCC, it might however be hypothesised that LAW depletion might reduce irinotecan sensitivity in ccRCC, the opposite of the results observed.

One explanation for increased irinotecan sensitivity in LIMD1 depleted cells may come from work by Chen *et al* in colorectal cell lines. In a study evaluating multi-drug resistance (MDR) in the colorectal carcinoma cell lines Colo205 and HCT-8, established by exposure of the primary cell lines to increasing doses of 5-fluorouracil (5-FU) over a year, LIMD1 expression was found to be increased in the MDR cell lines compared to their respective parental cell line. LIMD1 siRNA constructs transfected into these MDR cell lines were able to abrogate some aspects of the MDR phenotype, almost completely re-sensitising the cells to 5-FU and significantly increasing the proportion of cells undergoing apoptosis compared to the MDR cell lines. The authors had previously demonstrated that resistance of these MDR cell lines was mediated through the expression of the multidrug transporter gene MRP1 (ABCC1). The association between LIMD1 upregulation and multi-drug resistance was not explored but the authors hypothesised that this was related to the function of LIMD1 as an adapter-linker protein, shuttling between the nucleus and cytoplasm and perhaps contributing to increasing cell drug efflux (Chen, Zhu et al. 2014).

6.11 Future work

6.11.1 Further experiments to investigate the role of irinotecan as a potentially synthetic lethal drug in association with LIMD1 loss

Further experiments are required to investigate the role of irinotecan as a potentially synthetic lethal drug in association with LIMD1 loss. We have looked at a small panel of five ccRCC cell lines and correlated irinotecan sensitivity with LAW expression. This should be extended to include a larger panel with variable LAW expression. In addition we have cell lines in which a CRISPR-Cas-9 system has been used to selectively delete Ajuba and WTIP expression and this will provide a useful screening platform to further investigate the effects of loss of LAW on irinotecan sensitivity and assess if Ajuba/WTIP loss results in a similar phenotype. Additional assays measuring irinotecan effects on cell growth can also be undertaken such as colony assay formation, which determines the ability of a cell to proliferate indefinitely and thereby retain its reproductive ability to form a large colony or clone (Riss, Moravec et al. 2004). Short-term cell viability assays, using an ATP based assay of cell viability, such as Cell Titer-Glo™ or the MTT assay which measures the ability of cells to convert MTT into a purple coloured formazan product as a result of reduced NADH activity (Riss, Moravec et al. 2004) rely predominantly on mitotic linked death for differences in cell viability to be observed but many drugs may affect proliferation/cell cycle block but have no impact on clonogenic capacity after drug-withdrawal (Citrin 2016), this may be of particular relevance for RCC where disease stabilisation/control is often the main aim of treatment.

Irinotecan is a known inhibitor of topoisomerase-I but it is not clear that in this screen differences in sensitivity associated with LIMD1 loss were as a consequence of topoisomerase-I activity. The expression of topoisomerase-I in the paired LIMD1 proficient/deficient cell lines should be compared. Although we attempted to characterise expression, difficulties with optimising the antibody for Western Blot analysis meant that levels were not characterised. mRNA levels could also be compared using RT-PCR.

The topoisomerase-I inhibitor topetecan was associated with significant cell death in both RCC11 scr and RCC11 shLIMD1 lines in the drug screen with similar Z-scores in both cell lines. This however, as outlined, does not mean that topetecan does not potentially demonstrate synthetically lethal in association with LIMD1 loss and dose-response assays should be undertaken in paired LIMD1 proficient/deficient cell lines. Validation with topetecan would strongly suggest that the mechanism of synthetic lethality is related to topoisomerase-I inhibition. In addition, by using siRNAs to knockdown topoisomerase I and assays where topoisomerase-I is knocked down and re-expressed in LIMD1 deficient/proficient cell lines, with and without irinotecan drugging, topoisomerase-I as a likely target for synthetic lethality in association with LIMD1 loss can be further investigated.

No topoisomerase-II inhibitors were identified as hits in the synthetic lethality screen. Topoisomerase II cuts both strands of a double stranded DNA molecule in an ATP-dependent manner to repair double strand breaks (Nitiss 2009). Topoisomerase-II inhibitors act to increase levels of covalent topoisomerase II-cleaved DNA complexes acting either as therapeutic poisons or inhibitors, through the disruption of the catalytic turnover of the complex (Burden and Osheroff 1998). Given the limitations of a drug screen and the high potential for missing drug therapeutic hits, it would be relevant to carry out drug-response curves in paired LIMD1 proficient/deficient ccRCC lines with topoisomerase-II inhibitors.

Other relevant assays include the assessment of topoisomerase-I activity in the paired LIMD1 proficient/deficient cell lines. Topoisomerase I facilitates the relaxation of supercoiled DNA, which has a different electrophoretic mobility from DNA that is completely relaxed, i.e. not supercoiled. Using *E.coli* plasmid DNA, which is negatively supercoiled, the amount of active topoisomerase-I can be determined on an agarose gel with ethidium bromide staining (Nitiss, Soans et al. 2012).

Given the effects of topoisomerase-I activity on cell cycle, with the Topo1-DNA complex initiating activation of an S-phase checkpoint mechanism and G2 arrest/delay (Solary, Bertrand et al. 1994) it would be interesting to investigate the effects of irinotecan on cell cycle in the LIMD1 proficient/deficient cell pairs using for example

propidium iodide staining and FACS analysis. In addition, given that abnormal cellular replication is associated with the accumulation of replication-associated double strand DNA breaks (DSB) and the close association between cell cycle control and the DNA damage response pathway (Shaltiel, Krenning et al. 2015), it would be relevant to look at phosphorylation of H2AX (γH2Ax), considered one of the earliest indications of a DSB (Paull, Rogakou et al. 2000), in combination with cell cycle analysis.

Final discussion

Final Discussion

Representing 5% and 3% of all adult malignancies in men and women respectively (Levi, Ferlay et al. 2008, Ljungberg, Campbell et al. 2011) (Rathmell and Godley 2010), the incidence of RCC is continuing to increase particularly in the Western World where environmental factors such as hypertension and obesity increase relative risk (Ljungberg, Campbell et al. 2011). RCC incidence trends worldwide have started to show signs of plateau and more strikingly, cancer mortality rates have levelled or shown signs of decline in some western countries (Ljungberg, Campbell et al. 2011). Whilst this is in part related to an increase in the proportion of small tumours diagnosed incidentally and a downward shift in tumour stage, all stage mortality has started to fall (Gill, Aron et al. 2010, Ljungberg, Campbell et al. 2011). Nonetheless, the prognosis for many patients with metastatic RCC remains poor (Heng, Xie et al. 2013).

The commonest RCC subtype, ccRCC represents around 80% of all RCC types (Frew and Moch 2015). Greater understanding of tumour biology has shown that beyond the seminal genetic alteration of *VHL*, ccRCC tumours are extremely heterogeneous. Notably, three of the most commonly deregulated genes *PBRMI*, *BAP1* and *SETD2* are located close to *VHL* on chromosome 3p and mutation of *BAP1* or *SETD2* is associated with worse clinico-pathological outcomes (Hakimi, Pham et al. 2013, Sato, Yoshizato et al. 2013, Frew and Moch 2015). Indeed ccRCC cancers are increasingly referred to as 'diseases of chromosome 3p.'

The sequential use of TKIs that target angiogenesis and/or mTOR inhibitors can significantly improve progression free survival and overall survival in metastatic ccRCC such that median overall survival now stands at around 40-months (Heng, Xie et al. 2013) and novel therapies may increase this further. Despite this progress, durable responses are exceedingly rare. Some of the escape mechanisms, particularly cMET upregulation and FGF activation have driven the development of novel targeting strategies that target these pathways with cabozantinib targeting both cMET and VEGF TKI pathways and lenvatinib inhibiting VEGF and FGF pathways (Karakashev and Reginato 2015).

The paucity of durable responses to targeted therapies stimulated interest in the development of immune modulators for effective targeting of RCC. Observations that circulating cytokines, chemokines and tumour infiltrating lymphocytes were commonly observed in ccRCC confirmed a complex interaction between the tumour and host immune system (Porta, Bonomi et al. 2007). RCC can effectively subvert the host immune response, particularly through the increased expression of immunosuppressive cytokines and the upregulation of immuno-suppressive T-regulatory cells (Noessner, Brech et al. 2012). Complex feedback mechanisms involving immune checkpoint molecules inhibit immune system activation of both the innate and adaptive systems (Topalian, Drake et al. 2015). RCC can up-regulate cell surface immune checkpoint ligands that block T cell function in response to inflammation, a process known as adaptive immune resistance (Noessner, Brech et al. 2012).

The use of high dose IL-2 confirmed that modulating the immune response in metastatic RCC could be used to effect tumour response, although durable responses are observed in only a small subset of patients and in clinical trials this did not translate to an increase in overall OS. In addition toxicity is very significant (Coppin, Porzsolt et al. 2005). Checkpoint blockade with PD-1 and PDL-1/2 blocking drugs alone or in combination with CTLA-4 blockade offers an exciting new therapeutic avenue (Topalian, Drake et al. 2015). Results from the Checkmate 214 Study presented at ESMO in September 2017 demonstrated a significant improvement in PFS for poor and intermediate prognosis patients with PDL-1 positive tumours receiving combination immunotherapy with nivolumab, a PD-1 inhibitor, and ipilumimab, a CTLA-4 inhibitor, compared to VEGF-targeted therapy with sunitinib (22.8 months versus 5.9 months) (Rexer, Steiner et al. 2017).

Despite these successes, many patients present with primary resistance to VEGF targeted therapies and immunotherapy and most initial responders will ultimately develop progressive disease (Powles, Chowdhury et al. 2011, Escudier, Porta et al. 2014). The use of clinical prognostic groups such as the Heng criteria stratifies patients into prognostic groups but does not predict response to therapy (Heng, Xie et al. 2013). Robust predictive biomarkers are required to help clinicians identify drugs demonstrating maximal benefit for individual patients whilst minimising toxicity.

Many potential biomarkers have been identified in ccRCC but most do not help patient selection. Most biomarkers were assessed after patients had started treatment and most targeted therapies for metastatic RCC were approved on the basis of clinical trials of an unselected patient population and not using a molecularly stratified biomarker guided approach (Gulati, Martinez et al. 2014). Much of the published biomarker data is retrospective, based on small studies and results from such studies are often contradictory.

A further difficulty in the identification of biomarkers is tumour heterogeneity, particularly of relevance in the development of drug resistance, where drug selection pressures may facilitate the faster growth of drug resistance clones, ultimately resulting in further metastasis and treatment failure. (Gerlinger, Rowan et al. 2012)

LIMD1 is a 3p21.3 encoded tumour suppressor with a range of established functions including the regulation of the hypoxic response through HIF1α regulation (Foxler, Bridge et al. 2012), and regulation of miRNA silencing (Bridge, Shah et al. 2017). Given LIMD1's critical role in the regulation of pathways commonly deregulated in ccRCC and location on 3p, it was hypothesised that loss could be an important driver of tumourigenesis in ccRCC. Recent work by Thiesen *et al* has demonstrated that CNA of LIMD1 are common, occurring in 58.3% of ccRCC tumours analysed and occurring independently of CNA at other 3p loci (Thiesen, Steinbeck et al. 2017).

Ajuba and WTIP are closely homologous LIM-domain proteins with overlapping roles identified (Kadrmas and Beckerle 2004): both for example play a role in the regulation of the hypoxic response and microRNA silencing (Foxler, Bridge et al. 2012, Bridge, Shah et al. 2017). Ajuba is an important regulator of the Hippo signalling pathway, deregulation of which is frequently implicated in tumourigenesis (Das Thakur, Feng et al. 2010, Tanaka, Osada et al. 2015). All three proteins have not been characterised in ccRCC.

Initial work demonstrated that LIMD1 loss was common both *in vitro* and *in vivo*, in 88% of cell lines and in 49% of ccRCC samples compared to matched adjacent tissue. Even higher rates of Ajuba loss were observed: in 92% of cell lines analysed and in 76% of ccRCC samples. Interestingly WTIP loss was not common either *in vitro*, or *in vivo*. *In*

vitro, 33% of cell lines demonstrated less WTIP staining and *in vivo* 63% of tumours actually demonstrated an increase in total WTIP staining. Subcellular WTIP localisation however did appear to be relevant with 49% of tumours demonstrating no nuclear staining compared to matched control tissue.

Staining tissue samples derived from a large clinical trial failed to demonstrate any association between LIMD1 levels and tumour grade/stage, nor was an association between staining and PFS or OS observed. For Ajuba an association between tumour stage and reduced staining was observed, whilst for WTIP no association between staining and tumour stage/grade or PFS/OS was observed. Thiesen *et al* demonstrated that CNA alterations of *LIMD1* were more commonly observed in lower grade tumours (Thiesen, Steinbeck et al. 2017).

Although LIMD1, Ajuba and WTIP levels did not appear to be prognostic in this cohort with the exception of Ajuba staining and tumour stage, loss of expression could still be predictive of response to therapy. The concept of synthetic lethality is being exploited in oncology to identify drugs that specifically target cancer cells. In cancer cells where a particular cancer-specific gene inactivation has occurred, targeting a second gene may result in cancer-specific cell death whilst sparing non-cancerous cells (Nijman 2011).

Using a drug library containing 584-cancer therapeutic drugs, paired LIMD1 proficient and deficient ccRCC lines were screened for drugs that demonstrated synthetic lethality in association with LIMD1 loss. This identified irinotecan as a potential synthetically lethal drug hit, associated with increased death in the LIMD1 deficient compared to proficient control and further validated as demonstrating increased cell death in association with LIMD1 loss in two ccRCC lines across a range of drug concentrations as well as in HELA cells and a lung adenocarcinoma line, A549. Using a panel of 6 ccRCC lines, ccRCC lines with reduced LAW expression demonstrated increased sensitivity to irinotecan compared to those expressing higher levels of LAW proteins.

Sequencing strategies in mccRCC remain to be fully defined and the paradigm for treating ccRCC is constantly being re-evaluated. Given the molecular complexity of this tumour type, a 'one size' fits all approach is not appropriate and our understanding of

this complex tumour type is increasing all the time. Chemotherapy currently plays a relatively limited role in the treatment of metastatic ccRCC: most ccRCC tumours demonstrate a degree of chemotherapy resistance (Tobe, Noble-Topham et al. 1995, Karakashev and Reginato 2015) and novel targeted agents that are associated with superior efficacy have largely replaced such a treatment modality. Nonetheless, chemotherapy does have a limited role particularly for aggressive tumour types with sarcomatoid differentiation and a study evaluating combination chemotherapy with irinotecan, cisplatin and mitomycin-C demonstrated a response rate of 64% (Shamash, Powles et al. 2005).

Based on our data so far, it could be hypothesised that loss of LAW family members could increase sensitivity to irinotecan chemotherapy in ccRCC and perhaps in other tumour types. Irinotecan is an attractive drug to investigate further in a clinical setting in association with loss of LAW family members, as it is a commonly used chemotherapy drug with a well-understood toxicity profile. In addition in several colorectal cell lines, LIMD1 upregulation is associated with chemotherapy resistance and this resistance was abrogated by transfection with siRNA LIMD1 constructs (Chen, Zhu et al. 2014).

This data presented is preliminary and significant further *in vitro* validation is required as well as further experiments to determine the potential mechanism associated with synthetic lethality in association with LIMD1 loss. Moving forward, animal studies with *in vivo* xenografts analysis demonstrating a reduction in tumour volume in LIMD1 knockout/low-expressing xenografts compared to control would be required and patient derived xenografts (PDX) models could be used to demonstrate that endogenous LIMD1 levels determine irinotecan sensitivity *in vivo*. Funding has been obtained for such work.

Perhaps given the efficacy of novel targeted agents including immunotherapy agents, if irinotecan is evaluated in a clinical setting, a more rational approach would be to combine it with VEGF-targeting agents such as sunitinib or to give it in combination with a drug targeting the PD-1/PDL-1 axis such as nivolumab in patients stratified for low LAW expression. Another approach could be to target patients with reduced LAW expression who had progressed through multiple lines of therapy including VEGF targeting drugs and immunotherapy agents. It would be important to investigate genetic

heterogeneity with respect to LAW expression in such a patient cohort and what effect this heterogeneity had on sensitivity to irinotecan: the use of circulating blood biomarkers such as circulating tumour cells and cell-free plasma DNA may however provide a non-invasive real time surrogate for tissue based biomarkers and overcome some of the issues associated with tumour heterogeneity.

Given the need for effective biomarker identification and paucity of both prognostic and predictive biomarkers that have been externally validated in ccRCC, our preliminary results are encouraging and with further validation experiments and clinical trial evaluation could represent a further stratified approach for the treatment of mccRCC. Given our validation of the drug screen demonstrating increasing response to irinotecan in HELA and the lung adenocarcinoma line A549 as well as in ccRCC lines in association with LIMD1 loss, such an approach could suggest that LIMD1 loss could predict the response to a target therapy independently of the tumour histology. Targeted therapy for such mutations/molecular markers are being evaluated in 'Basket trials', screening patients across tumour types for targetable mutations/deregulated pathways and treating with drugs targeting such pathways.

References

References

Al Sarakbi, W., W. Sasi, W. G. Jiang, T. Roberts, R. F. Newbold and K. Mokbel (2009). "The mRNA expression of SETD2 in human breast cancer: correlation with clinico-pathological parameters." BMC Cancer **9**: 290.

Albiges, L., T. Choueiri, B. Escudier, M. Galsky, D. George, F. Hofmann, T. Lam, R. Motzer, P. Mulders, C. Porta, T. Powles, C. Sternberg and A. Bex (2015). "A systematic review of sequencing and combinations of systemic therapy in metastatic renal cancer." Eur Urol **67**(1): 100-110.

Allred, D. C., M. A. Bustamante, C. O. Daniel, H. V. Gaskill and A. B. Cruz, Jr. (1990). "Immunocytochemical analysis of estrogen receptors in human breast carcinomas. Evaluation of 130 cases and review of the literature regarding concordance with biochemical assay and clinical relevance." Arch Surg **125**(1): 107-113.

Allred, D. C., G. M. Clark, R. Elledge, S. A. Fuqua, R. W. Brown, G. C. Chamness, C. K. Osborne and W. L. McGuire (1993). "Association of p53 protein expression with tumor cell proliferation rate and clinical outcome in node-negative breast cancer." J Natl Cancer Inst **85**(3): 200-206.

An, J. and M. B. Rettig (2005). "Mechanism of von Hippel-Lindau protein-mediated suppression of nuclear factor kappa B activity." Mol Cell Biol **25**(17): 7546-7556.

Appelhoff, R. J., Y. M. Tian, R. R. Raval, H. Turley, A. L. Harris, C. W. Pugh, P. J. Ratcliffe and J. M. Gleadle (2004). "Differential function of the prolyl hydroxylases PHD1, PHD2, and PHD3 in the regulation of hypoxia-inducible factor." J Biol Chem **279**(37): 38458-38465.

Arrondeau, J., H. K. Gan, A. R. Razak, X. Paoletti and C. Le Tourneau (2010). "Development of anti-cancer drugs." Discov Med **10**(53): 355-362.

Aso, T., W. S. Lane, J. W. Conaway and R. C. Conaway (1995). "Elongin (SIII): a multisubunit regulator of elongation by RNA polymerase II." Science **269**(5229): 1439-1443.

Astashkina, A., B. Mann and D. W. Grainger (2012). "A critical evaluation of in vitro cell culture models for high-throughput drug screening and toxicity." Pharmacol Ther **134**(1): 82-106.

Aydin, H. and M. Zhou (2008). "The changing face of renal cell carcinoma pathology." Curr Oncol Rep **10**(3): 235-244.

Balfour, J. A. and M. I. Wilde (1997). "Dorzolamide. A review of its pharmacology and therapeutic potential in the management of glaucoma and ocular hypertension." Drugs Aging **10**(5): 384-403.

Barrette, K., J. J. van den Oord and M. Garmyn (2014). "Tissue microarray." J Invest Dermatol **134**(9): e24.

Bellocco, R., E. Pasquali, M. Rota, V. Bagnardi, I. Tramacere, L. Scotti, C. Pelucchi, P. Boffetta, G. Corrao and C. La Vecchia (2012). "Alcohol drinking and risk of renal cell carcinoma: results of a meta-analysis." Ann Oncol **23**(9): 2235-2244.

Bex, A., P. Mulders, M. A. S. Jewett, J. Wagstaff, R. van Velthoven, P. M. Laguna Pes, L. Wood, H. H. E. van Melick, P. Soetekouw, J. B. Lattouf, T. Powles, E. Boleti, I. J. de Jong, S. Rottey, B. Tombal, S. Marreaud, L. Collette, S. Collette, C. U. Blank and J. B. Haanen (2017). "LBA35Immediate versus deferred cytoreductive nephrectomy (CN) in patients with synchronous metastatic renal cell carcinoma (mRCC) receiving sunitinib (EORTC 30073 SURTIME)." Annals of Oncology **28**(suppl_5): mdx440.030-mdx440.030.

Biswas, S., H. Troy, R. Leek, Y. L. Chung, J. L. Li, R. R. Raval, H. Turley, K. Gatter, F. Pezzella, J. R. Griffiths, M. Stubbs and A. L. Harris (2010). "Effects of HIF-1alpha and HIF2alpha on Growth and Metabolism of Clear-Cell Renal Cell Carcinoma 786-0 Xenografts." J Oncol **2010**: 757908.

Blankenship, C., J. G. Naglich, J. M. Whaley, B. Seizinger and N. Kley (1999). "Alternate choice of initiation codon produces a biologically active product of the von Hippel Lindau gene with tumor suppressor activity." Oncogene **18**(8): 1529-1535.

Block, K., Y. Gorin, P. Hoover, P. Williams, T. Chelmicki, R. A. Clark, T. Yoneda and H. E. Abboud (2007). "NAD(P)H oxidases regulate HIF-2alpha protein expression." J Biol Chem **282**(11): 8019-8026.

Bolger, N., C. Heffron, I. Regan, M. Sweeney, S. Kinsella, M. McKeown, G. Creighton, J. Russell and J. O'Leary (2006). "Implementation and evaluation of a new automated interactive image analysis system." Acta Cytol **50**(5): 483-491.

Boshoff, C. and R. Weiss (2002). "AIDS-related malignancies." Nat Rev Cancer **2**(5): 373-382.

Bott, M., M. Brevet, B. S. Taylor, S. Shimizu, T. Ito, L. Wang, J. Creaney, R. A. Lake, M. F. Zakowski, B. Reva, C. Sander, R. Delsite, S. Powell, Q. Zhou, R. Shen, A. Olshen, V. Rusch and M. Ladanyi (2011). "The nuclear deubiquitinase BAP1 is commonly inactivated by somatic mutations and 3p21.1 losses in malignant pleural mesothelioma." Nat Genet **43**(7): 668-672.

Brahimi-Horn, M. C. and J. Pouyssegur (2007). "Hypoxia in cancer cell metabolism and pH regulation." Essays Biochem **43**: 165-178.

Brannon, A. R., A. Reddy, M. Seiler, A. Arreola, D. T. Moore, R. S. Pruthi, E. M. Wallen, M. E. Nielsen, H. Liu, K. L. Nathanson, B. Ljungberg, H. Zhao, J. D. Brooks, S. Ganesan, G. Bhanot and W. K. Rathmell (2010). "Molecular Stratification of Clear Cell Renal Cell Carcinoma by Consensus Clustering Reveals Distinct Subtypes and Survival Patterns." Genes Cancer **1**(2): 152-163.

Braun, J. E., E. Huntzinger and E. Izaurralde (2013). "The role of GW182 proteins in miRNA-mediated gene silencing." Adv Exp Med Biol **768**: 147-163.

Brideau, C., B. Gunter, B. Pikounis and A. Liaw (2003). "Improved statistical methods for hit selection in high-throughput screening." J Biomol Screen **8**(6): 634-647.

Bridge, K. S., K. M. Shah, Y. Li, D. E. Foxler, S. C. K. Wong, D. C. Miller, K. M. Davidson, J. G. Foster, R. Rose, M. R. Hodgkinson, P. S. Ribeiro, A. A. Aboobaker, K. Yashiro, X. Wang, P. R. Graves, M. J. Plevin, D. Lagos and T. V. Sharp (2017). "Argonaute Utilization for miRNA Silencing Is Determined by Phosphorylation-Dependent Recruitment of LIM-Domain-Containing Proteins." Cell Rep **20**(1): 173-187.

Budczies, J., F. Klauschen, B. V. Sinn, B. Gyorffy, W. D. Schmitt, S. Darb-Esfahani and C. Denkert (2012). "Cutoff Finder: a comprehensive and straightforward Web application enabling rapid biomarker cutoff optimization." PLoS One **7**(12): e51862.

Bui, M. H., H. Visapaa, D. Seligson, H. Kim, K. R. Han, Y. Huang, S. Horvath, E. J. Stanbridge, A. Palotie, R. A. Figlin and A. S. Belldegrun (2004). "Prognostic value of carbonic anhydrase IX and KI67 as predictors of survival for renal clear cell carcinoma." J Urol **171**(6 Pt 1): 2461-2466.

Burden, D. A. and N. Osheroff (1998). "Mechanism of action of eukaryotic topoisomerase II and drugs targeted to the enzyme." Biochim Biophys Acta **1400**(1-3): 139-154.

Cai, T. Y., X. W. Liu, H. Zhu, J. Cao, J. Zhang, L. Ding, J. S. Lou, Q. J. He and B. Yang (2014). "Tirapazamine sensitizes hepatocellular carcinoma cells to topoisomerase I inhibitors via cooperative modulation of hypoxia-inducible factor-1alpha." Mol Cancer Ther **13**(3): 630-642.

Camp, R. L., G. G. Chung and D. L. Rimm (2002). "Automated subcellular localization and quantification of protein expression in tissue microarrays." Nat Med **8**(11): 1323-1327.

Camp, R. L., M. Dolled-Filhart and D. L. Rimm (2004). "X-tile: a new bio-informatics tool for biomarker assessment and outcome-based cut-point optimization." Clin Cancer Res **10**(21): 7252-7259.

Camp, R. L., V. Neumeister and D. L. Rimm (2008). "A decade of tissue microarrays: progress in the discovery and validation of cancer biomarkers." J Clin Oncol **26**(34): 5630-5637.

Campbell, P. J., S. Yachida, L. J. Mudie, P. J. Stephens, E. D. Pleasance, L. A. Stebbings, L. A. Morsberger, C. Latimer, S. McLaren, M. L. Lin, D. J. McBride, I. Varela, S. A. Nik-Zainal, C. Leroy, M. Jia, A. Menzies, A. P. Butler, J. W. Teague, C. A. Griffin, J. Burton, H. Swerdlow, M. A. Quail, M. R. Stratton, C. Iacobuzio-Donahue and P. A. Futreal (2010). "The patterns and dynamics of genomic instability in metastatic pancreatic cancer." Nature **467**(7319): 1109-1113.

Cancer Genome Atlas Research, N. (2013). "Comprehensive molecular characterization of clear cell renal cell carcinoma." Nature **499**(7456): 43-49.

Carnero, A. (2006). "High throughput screening in drug discovery." Clin Transl Oncol **8**(7): 482-490.

Carroll, V. A. and M. Ashcroft (2005). "Targeting the molecular basis for tumour hypoxia." Expert Rev Mol Med **7**(6): 1-16.

Cassidy, L. D. and M. Narita (2015). "CELL BIOLOGY. GATA get a hold on senescence." Science **349**(6255): 1448-1449.

Chakraborty, S. B., S. Dasgupta, A. Roy, A. Sengupta, B. Ray, S. Roychoudhury and C. K. Panda (2003). "Differential deletions in 3p are associated with the development of head and neck squamous cell carcinoma in Indian patients." Cancer Genet Cytogenet **146**(2): 130-138.

Chan, D. A. and A. J. Giaccia (2011). "Harnessing synthetic lethal interactions in anticancer drug discovery." Nat Rev Drug Discov **10**(5): 351-364.

Chan, D. A., P. D. Sutphin, P. Nguyen, S. Turcotte, E. W. Lai, A. Banh, G. E. Reynolds, J. T. Chi, J. Wu, D. E. Solow-Cordero, M. Bonnet, J. U. Flanagan, D. M. Bouley, E. E. Graves, W. A. Denny, M. P. Hay and A. J. Giaccia (2011). "Targeting GLUT1 and the Warburg effect in renal cell carcinoma by chemical synthetic lethality." Sci Transl Med **3**(94): 94ra70.

Chekulaeva, M., H. Mathys, J. T. Zipprich, J. Attig, M. Colic, R. Parker and W. Filipowicz (2011). "miRNA repression involves GW182-mediated recruitment of CCR4-NOT through conserved W-containing motifs." Nat Struct Mol Biol **18**(11): 1218-1226.

Chekulaeva, M., R. Parker and W. Filipowicz (2010). "The GW/WG repeats of Drosophila GW182 function as effector motifs for miRNA-mediated repression." Nucleic Acids Res **38**(19): 6673-6683.

Chen, J., D. Zhang, W. Zhang, Y. Tang, W. Yan, L. Guo and B. Shen (2013). "Clear cell renal cell carcinoma associated microRNA expression signatures identified by an integrated bioinformatics analysis." J Transl Med **11**: 169.

Chen, P. C., Y. Y. Huang and J. L. Juang (2011). "MEMS microwell and microcolumn arrays: novel methods for high-throughput cell-based assays." Lab Chip **11**(21): 3619-3625.

Chen, Y., A. Boland, D. Kuzuoglu-Ozturk, P. Bawankar, B. Loh, C. T. Chang, O. Weichenrieder and E. Izaurralde (2014). "A DDX6-CNOT1 complex and W-binding pockets in CNOT9 reveal direct links between miRNA target recognition and silencing." Mol Cell **54**(5): 737-750.

Chen, Z., X. Zhu, T. Xie, J. Xie, K. Quo and X. Liu (2014). "Drug resistance reversed by silencing LIM domain-containing protein 1 expression in colorectal carcinoma." Oncol Lett **8**(2): 795-798.

Cho, D., S. Signoretti, S. Dabora, M. Regan, A. Seeley, M. Mariotti, A. Youmans, A. Polivy, L. Mandato, D. McDermott, E. Stanbridge and M. Atkins (2007). "Potential histologic and molecular predictors of response to temsirolimus in patients with advanced renal cell carcinoma." Clin Genitourin Cancer **5**(6): 379-385.

Cho, D., S. Signoretti, M. Regan, J. W. Mier and M. B. Atkins (2007). "The role of mammalian target of rapamycin inhibitors in the treatment of advanced renal cancer." Clin Cancer Res **13**(2 Pt 2): 758s-763s.

Choudhury, K. R., K. J. Yagle, P. E. Swanson, K. A. Krohn and J. G. Rajendran (2010). "A robust automated measure of average antibody staining in immunohistochemistry images." J Histochem Cytochem **58**(2): 95-107.

Choueiri, T. K., B. Escudier, T. Powles, N. M. Tannir, P. N. Mainwaring, B. I. Rini, H. J. Hammers, F. Donskov, B. J. Roth, K. Peltola, J. L. Lee, D. Y. C. Heng, M. Schmidinger, N. Agarwal, C. N. Sternberg, D. F. McDermott, D. T. Aftab, C. Hessel, C. Scheffold, G. Schwab, T. E. Hutson, S. Pal, R. J. Motzer and M. investigators (2016). "Cabozantinib versus everolimus in advanced renal cell carcinoma (METEOR): final results from a randomised, open-label, phase 3 trial." Lancet Oncol **17**(7): 917-927.

Choueiri, T. K., S. Halabi, B. L. Sanford, O. Hahn, M. D. Michaelson, M. K. Walsh, D. R. Feldman, T. Olencki, J. Picus, E. J. Small, S. Dakhil, D. J. George and M. J. Morris (2017). "Cabozantinib Versus Sunitinib As Initial Targeted Therapy for Patients With Metastatic Renal Cell Carcinoma of Poor or Intermediate Risk: The Alliance A031203 CABOSUN Trial." J Clin Oncol **35**(6): 591-597.

Choueiri, T. K., M. M. Regan, J. E. Rosenberg, W. K. Oh, J. Clement, A. M. Amato, D. McDermott, D. C. Cho, M. B. Atkins and S. Signoretti (2010). "Carbonic anhydrase IX and pathological features as predictors of outcome in patients with metastatic clear-cell renal cell carcinoma receiving vascular endothelial growth factor-targeted therapy." BJU Int **106**(6): 772-778.

Chow, W. H., L. M. Dong and S. S. Devesa (2010). "Epidemiology and risk factors for kidney cancer." Nat Rev Urol **7**(5): 245-257.

Chowdhury, S., J. M. Larkin and M. E. Gore (2008). "Recent advances in the treatment of renal cell carcinoma and the role of targeted therapies." Eur J Cancer **44**(15): 2152-2161.

Chu, C. W., O. Ossipova, A. Ioannou and S. Y. Sokol (2016). "Prickle3 synergizes with Wtip to regulate basal body organization and cilia growth." Sci Rep **6**: 24104.

Chu, H. W., C. Rios, C. Huang, A. Wesolowska-Andersen, E. G. Burchard, B. P. O'Connor, T. E. Fingerlin, D. Nichols, S. D. Reynolds and M. A. Seibold (2015). "CRISPR-Cas9-mediated gene knockout in primary human airway epithelial cells reveals a proinflammatory role for MUC18." Gene Ther **22**(10): 822-829.

Chung, N., X. D. Zhang, A. Kreamer, L. Locco, P. F. Kuan, S. Bartz, P. S. Linsley, M. Ferrer and B. Strulovici (2008). "Median absolute deviation to improve hit selection for genome-scale RNAi screens." J Biomol Screen **13**(2): 149-158.

Citrin, D. E. (2016). "Short-Term Screening Assays for the Identification of Therapeutics for Cancer." Cancer Res **76**(12): 3443-3445.

Clement, J. M. and D. F. McDermott (2009). "The high-dose aldesleukin (IL-2) "select" trial: a trial designed to prospectively validate predictive models of response to high-dose IL-2 treatment in patients with metastatic renal cell carcinoma." Clin Genitourin Cancer **7**(2): E7-9.

Clifford, S. C., A. H. Prowse, N. A. Affara, C. H. Buys and E. R. Maher (1998). "Inactivation of the von Hippel-Lindau (VHL) tumour suppressor gene and allelic losses at chromosome arm 3p in primary renal cell carcinoma: evidence for a VHL-independent pathway in clear cell renal tumourigenesis." Genes Chromosomes Cancer **22**(3): 200-209.

Coenraads, P. J., H. Van Der Walle, K. Thestrup-Pedersen, T. Ruzicka, B. Dreno, C. De La Loge, M. Viala, S. Querner, T. Brown and M. Zultak (2005). "Construction and validation of a photographic guide for assessing severity of chronic hand dermatitis." Br J Dermatol **152**(2): 296-301.

Coppin, C., F. Porzsolt, A. Awa, J. Kumpf, A. Coldman and T. Wilt (2005). "Immunotherapy for advanced renal cell cancer." Cochrane Database of Systematic Reviews(1).

Coppin, C., F. Porzsolt, A. Awa, J. Kumpf, A. Coldman and T. Wilt (2005). "Immunotherapy for advanced renal cell cancer." Cochrane Database Syst Rev(1): CD001425.

Crossey, P. A., K. Foster, F. M. Richards, M. E. Phipps, F. Latif, K. Tory, M. H. Jones, E. Bentley, R. Kumar, M. I. Lerman and et al. (1994). "Molecular genetic investigations of the mechanism of tumourigenesis in von Hippel-Lindau disease: analysis of allele loss in VHL tumours." Hum Genet **93**(1): 53-58.

Cummins, J. M., Y. He, R. J. Leary, R. Pagliarini, L. A. Diaz, Jr., T. Sjoblom, O. Barad, Z. Bentwich, A. E. Szafranska, E. Labourier, C. K. Raymond, B. S. Roberts, H. Juhl, K. W. Kinzler, B. Vogelstein and V. E. Velculescu (2006). "The colorectal microRNAome." Proc Natl Acad Sci U S A **103**(10): 3687-3692.

Dai, X. Y., L. H. Zhuang, D. D. Wang, T. Y. Zhou, L. L. Chang, R. H. Gai, D. F. Zhu, B. Yang, H. Zhu and Q. J. He (2016). "Nuclear translocation and activation of YAP by hypoxia contributes to the chemoresistance of SN38 in hepatocellular carcinoma cells." Oncotarget **7**(6): 6933-6947.

Dalgliesh, G. L., K. Furge, C. Greenman, L. Chen, G. Bignell, A. Butler, H. Davies, S. Edkins, C. Hardy, C. Latimer, J. Teague, J. Andrews, S. Barthorpe, D. Beare, G. Buck, P. J. Campbell, S. Forbes, M. Jia, D. Jones, H. Knott, C. Y. Kok, K. W. Lau, C. Leroy, M. L. Lin, D. J. McBride, M. Maddison, S. Maguire, K. McLay, A. Menzies, T. Mironenko, L. Mulderrig, L. Mudie, S. O'Meara, E. Pleasance, A. Rajasingham, R. Shepherd, R. Smith, L. Stebbings, P. Stephens, G. Tang, P. S. Tarpey, K. Turrell, K. J. Dykema, S. K. Khoo, D. Petillo, B. Wondergem, J. Anema, R. J. Kahnoski, B. T. Teh, M. R. Stratton and P. A. Futreal (2010). "Systematic sequencing of renal carcinoma reveals inactivation of histone modifying genes." Nature **463**(7279): 360-363.

Daniel, C. R., K. L. Schwartz, J. S. Colt, L. M. Dong, J. J. Ruterbusch, M. P. Purdue, A. J. Cross, N. Rothman, F. G. Davis, S. Wacholder, B. I. Graubard, W. H. Chow and R. Sinha (2011). "Meat-cooking mutagens and risk of renal cell carcinoma." Br J Cancer **105**(7): 1096-1104.

Das Thakur, M., Y. Feng, R. Jagannathan, M. J. Seppa, J. B. Skeath and G. D. Longmore (2010). "Ajuba LIM proteins are negative regulators of the Hippo signaling pathway." Curr Biol **20**(7): 657-662.

de Vries, C., J. A. Escobedo, H. Ueno, K. Houck, N. Ferrara and L. T. Williams (1992). "The fms-like tyrosine kinase, a receptor for vascular endothelial growth factor." Science **255**(5047): 989-991.

del Puerto-Nevado, L., F. Rojo, S. Zazo, C. Carames, G. Rubio, R. Vega, C. Chamizo, V. Casado, J. Martinez-Useros, R. Rincon, M. Rodriguez-Remirez, A. Borrero-Palacios, I. Cristobal, J. Madoz-Gurpide, O. Aguilera and J. Garcia-Foncillas (2014). "Active angiogenesis in metastatic renal cell carcinoma predicts clinical benefit to sunitinib-based therapy." Br J Cancer **110**(11): 2700-2707.

Deprimo, S. E., C. L. Bello, J. Smeraglia, C. M. Baum, D. Spinella, B. I. Rini, M. D. Michaelson and R. J. Motzer (2007). "Circulating protein biomarkers of pharmacodynamic activity of sunitinib in patients with metastatic renal cell carcinoma: modulation of VEGF and VEGF-related proteins." J Transl Med **5**: 32.

Dimova, D. K. and N. J. Dyson (2005). "The E2F transcriptional network: old acquaintances with new faces." Oncogene **24**(17): 2810-2826.

Dimri, G. P., J. L. Martinez, J. J. Jacobs, P. Keblusek, K. Itahana, M. Van Lohuizen, J. Campisi, D. E. Wazer and V. Band (2002). "The Bmi-1 oncogene induces telomerase activity and immortalizes human mammary epithelial cells." Cancer Res **62**(16): 4736-4745.

Dong, Z., M. A. Venkatachalam, J. Wang, Y. Patel, P. Saikumar, G. L. Semenza, T. Force and J. Nishiyama (2001). "Up-regulation of apoptosis inhibitory protein IAP-2 by hypoxia. Hif-1-independent mechanisms." J Biol Chem **276**(22): 18702-18709.

Dorai, T., I. Sawczuk, J. Pastorek, P. H. Wiernik and J. P. Dutcher (2006). "Role of carbonic anhydrases in the progression of renal cell carcinoma subtypes: proposal of a unified hypothesis." Cancer Invest **24**(8): 754-779.

Dorevic, G., K. Matusan-Ilijas, E. Babarovic, I. Hadzisejdic, M. Grahovac, B. Grahovac and N. Jonjic (2009). "Hypoxia inducible factor-1alpha correlates with vascular endothelial growth factor A and C indicating worse prognosis in clear cell renal cell carcinoma." J Exp Clin Cancer Res **28**: 40.

Dueck, A., C. Ziegler, A. Eichner, E. Berezikov and G. Meister (2012). "microRNAs associated with the different human Argonaute proteins." Nucleic Acids Res **40**(19): 9850-9862.

Dyer, B. W., F. A. Ferrer, D. K. Klinedinst and R. Rodriguez (2000). "A noncommercial dual luciferase enzyme assay system for reporter gene analysis." Anal Biochem **282**(1): 158-161.

E, G., Y. Cao, S. Bhattacharya, S. Dutta, E. Wang and D. Mukhopadhyay (2012). "Endogenous vascular endothelial growth factor-A (VEGF-A) maintains endothelial cell homeostasis by regulating VEGF receptor-2 transcription." J Biol Chem **287**(5): 3029-3041.

Eales, K. L., K. E. Hollinshead and D. A. Tennant (2016). "Hypoxia and metabolic adaptation of cancer cells." Oncogenesis **5**: e190.

Edge, S. B. and C. C. Compton (2010). "The American Joint Committee on Cancer: the 7th edition of the AJCC cancer staging manual and the future of TNM." Ann Surg Oncol **17**(6): 1471-1474.

Eke, I., S. Hehlgans, V. Sandfort and N. Cordes (2016). "3D matrix-based cell cultures: Automated analysis of tumor cell survival and proliferation." Int J Oncol **48**(1): 313-321.

Elias, J. M., A. M. Gown, R. M. Nakamura, D. C. Wilbur, G. E. Herman, E. S. Jaffe, H. Battifora and D. J. Brigati (1989). "Quality control in immunohistochemistry. Report of a workshop sponsored by the Biological Stain Commission." Am J Clin Pathol **92**(6): 836-843.

Escudier, B., T. Eisen, W. M. Stadler, C. Szczylik, S. Oudard, M. Staehler, S. Negrier, C. Chevreau, A. A. Desai, F. Rolland, T. Demkow, T. E. Hutson, M. Gore, S. Anderson,

G. Hofilena, M. Shan, C. Pena, C. Lathia and R. M. Bukowski (2009). "Sorafenib for treatment of renal cell carcinoma: Final efficacy and safety results of the phase III treatment approaches in renal cancer global evaluation trial." J Clin Oncol **27**(20): 3312-3318.

Escudier, B., C. Porta, P. Bono, T. Powles, T. Eisen, C. N. Sternberg, J. E. Gschwend, U. De Giorgi, O. Parikh, R. Hawkins, E. Sevin, S. Negrier, S. Khan, J. Diaz, S. Redhu, F. Mehmud and D. Cella (2014). "Randomized, controlled, double-blind, cross-over trial assessing treatment preference for pazopanib versus sunitinib in patients with metastatic renal cell carcinoma: PISCES Study." J Clin Oncol **32**(14): 1412-1418.

Escudier, B., C. Porta, M. Schmidinger, F. Algaba, J. J. Patard, V. Khoo, T. Eisen, A. Horwich and E. G. W. Group (2014). "Renal cell carcinoma: ESMO Clinical Practice Guidelines for diagnosis, treatment and follow-up." Ann Oncol **25 Suppl 3**: iii49-56.

Escudier, B., C. Porta, M. Schmidinger, F. Algaba, J. J. Patard, V. Khoo, T. Eisen, A. Horwich and E. G. W. Group (2014). "Renal cell carcinoma: ESMO Clinical Practice Guidelines for diagnosis, treatment and follow-updagger." Ann Oncol **25 Suppl 3**: iii49-iii56.

Escudier, B., C. Szczylik, C. Porta and M. Gore (2012). "Treatment selection in metastatic renal cell carcinoma: expert consensus." Nat Rev Clin Oncol **9**(6): 327-337.

Eubank, T. D., J. M. Roda, H. Liu, T. O'Neil and C. B. Marsh (2011). "Opposing roles for HIF-1alpha and HIF-2alpha in the regulation of angiogenesis by mononuclear phagocytes." Blood **117**(1): 323-332.

Facciabene, A., G. T. Motz and G. Coukos (2012). "T-regulatory cells: key players in tumor immune escape and angiogenesis." Cancer Res **72**(9): 2162-2171.

Faivre, S., G. Kroemer and E. Raymond (2006). "Current development of mTOR inhibitors as anticancer agents." Nat Rev Drug Discov **5**(8): 671-688.

Fan, Y., H. Li, X. Ma, Y. Gao, L. Chen, X. Li, X. Bao, Q. Du, Y. Zhang and X. Zhang (2015). "Prognostic Significance of Hypoxia-Inducible Factor Expression in Renal Cell Carcinoma: A PRISMA-compliant Systematic Review and Meta-Analysis." Medicine (Baltimore) **94**(38): e1646.

Feng, Y., H. Zhao, H. F. Luderer, H. Epple, R. Faccio, F. P. Ross, S. L. Teitelbaum and G. D. Longmore (2007). "The LIM protein, Limd1, regulates AP-1 activation through an interaction with Traf6 to influence osteoclast development." J Biol Chem **282**(1): 39-48.

Feuerstein, R., X. Wang, D. Song, N. E. Cooke and S. A. Liebhaber (1994). "The LIM/double zinc-finger motif functions as a protein dimerization domain." Proc Natl Acad Sci U S A **91**(22): 10655-10659.

Filipowicz, W., S. N. Bhattacharyya and N. Sonenberg (2008). "Mechanisms of post-transcriptional regulation by microRNAs: are the answers in sight?" Nat Rev Genet **9**(2): 102-114.

Fina, L., H. V. Molgaard, D. Robertson, N. J. Bradley, P. Monaghan, D. Delia, D. R. Sutherland, M. A. Baker and M. F. Greaves (1990). "Expression of the CD34 gene in vascular endothelial cells." Blood **75**(12): 2417-2426.

Fiore, C., D. Bailey, N. Conlon, X. Wu, N. Martin, M. Fiorentino, S. Finn, K. Fall, S. O. Andersson, O. Andren, M. Loda and R. Flavin (2012). "Utility of multispectral imaging in automated quantitative scoring of immunohistochemistry." J Clin Pathol **65**(6): 496-502.

Fisher, R., J. Larkin and C. Swanton (2012). "Inter and intratumour heterogeneity: a barrier to individualized medical therapy in renal cell carcinoma?" Front Oncol **2**: 49.

Fizazi, K., F. Rolland, C. Chevreau, J. P. Droz, D. Mery-Mignard, S. Culine and B. Escudier (2003). "A phase II study of irinotecan in patients with advanced renal cell carcinoma." Cancer **98**(1): 61-65.

Foxler, D. E., K. S. Bridge, V. James, T. M. Webb, M. Mee, S. C. Wong, Y. Feng, D. Constantin-Teodosiu, T. E. Petursdottir, J. Bjornsson, S. Ingvarsson, P. J. Ratcliffe, G. D. Longmore and T. V. Sharp (2012). "The LIMD1 protein bridges an association between the prolyl hydroxylases and VHL to repress HIF-1 activity." Nat Cell Biol **14**(2): 201-208.

Frank, I., M. L. Blute, J. C. Cheville, C. M. Lohse, A. L. Weaver and H. Zincke (2002). "An outcome prediction model for patients with clear cell renal cell carcinoma treated with radical nephrectomy based on tumor stage, size, grade and necrosis: the SSIGN score." J Urol **168**(6): 2395-2400.

Franken, N. A., H. M. Rodermond, J. Stap, J. Haveman and C. van Bree (2006). "Clonogenic assay of cells in vitro." Nat Protoc **1**(5): 2315-2319.

Freedman, V. H. and S. I. Shin (1974). "Cellular tumorigenicity in nude mice: correlation with cell growth in semi-solid medium." Cell **3**(4): 355-359.

Frew, I. J. and H. Moch (2015). "A clearer view of the molecular complexity of clear cell renal cell carcinoma." Annu Rev Pathol **10**: 263-289.

Fuhrman, S. A., L. C. Lasky and C. Limas (1982). "Prognostic significance of morphologic parameters in renal cell carcinoma." Am J Surg Pathol **6**(7): 655-663.

Gana, S., P. Veggiotti, G. Sciacca, C. Fedeli, A. Bersano, G. Micieli, M. Maghnie, R. Ciccone, E. Rossi, K. Plunkett, W. Bi, V. R. Sutton and O. Zuffardi (2012). "19q13.11 cryptic deletion: description of two new cases and indication for a role of WTIP haploinsufficiency in hypospadias." Eur J Hum Genet **20**(8): 852-856.

Gao, J., B. A. Aksoy, U. Dogrusoz, G. Dresdner, B. Gross, S. O. Sumer, Y. Sun, A. Jacobsen, R. Sinha, E. Larsson, E. Cerami, C. Sander and N. Schultz (2013). "Integrative analysis of complex cancer genomics and clinical profiles using the cBioPortal." Sci Signal **6**(269): pl1.

Garcia-Donas, J., L. J. Leandro-Garcia, A. Gonzalez Del Alba, M. Morente, I. Alemany, E. Esteban, J. A. Arranz, M. A. Climent, E. Gallardo, D. E. Castellano, J. Bellmunt, B. Mellado, J. Puente, F. Moreno, A. Font, S. Hernando, M. Robledo and C. Rodriguez-Antona (2013). "Prospective study assessing hypoxia-related proteins as markers for the outcome of treatment with sunitinib in advanced clear-cell renal cell carcinoma." Ann Oncol **24**(9): 2409-2414.

Gerlinger, M., J. W. Catto, T. F. Orntoft, F. X. Real, E. C. Zwarthoff and C. Swanton (2015). "Intratumour heterogeneity in urologic cancers: from molecular evidence to clinical implications." Eur Urol **67**(4): 729-737.

Gerlinger, M., A. J. Rowan, S. Horswell, J. Larkin, D. Endesfelder, E. Gronroos, P. Martinez, N. Matthews, A. Stewart, P. Tarpey, I. Varela, B. Phillimore, S. Begum, N. Q. McDonald, A. Butler, D. Jones, K. Raine, C. Latimer, C. R. Santos, M. Nohadani, A. C. Eklund, B. Spencer-Dene, G. Clark, L. Pickering, G. Stamp, M. Gore, Z. Szallasi, J. Downward, P. A. Futreal and C. Swanton (2012). "Intratumor heterogeneity and branched evolution revealed by multiregion sequencing." N Engl J Med **366**(10): 883-892.

Gerszten, P. C., S. A. Burton, C. Ozhasoglu and W. C. Welch (2007). "Radiosurgery for spinal metastases: clinical experience in 500 cases from a single institution." Spine (Phila Pa 1976) **32**(2): 193-199.

Ghosh, S., A. Ghosh, G. P. Maiti, N. Alam, A. Roy, B. Roy, S. Roychoudhury and C. K. Panda (2008). "Alterations of 3p21.31 tumor suppressor genes in head and neck squamous cell carcinoma: Correlation with progression and prognosis." Int J Cancer **123**(11): 2594-2604.

Gill, I. S., M. Aron, D. A. Gervais and M. A. Jewett (2010). "Clinical practice. Small renal mass." N Engl J Med **362**(7): 624-634.

Gimenez-Bachs, J. M., A. S. Salinas-Sanchez, F. Sanchez-Sanchez, J. G. Lorenzo-Romero, M. J. Donate-Moreno, H. Pastor-Navarro, D. C. Garcia-Olmo, J. Escribano-Martinez and J. A. Virseda-Rodriguez (2006). "Determination of vhl gene mutations in sporadic renal cell carcinoma." Eur Urol **49**(6): 1051-1057.

Gnarra, J. R., K. Tory, Y. Weng, L. Schmidt, M. H. Wei, H. Li, F. Latif, S. Liu, F. Chen, F. M. Duh and et al. (1994). "Mutations of the VHL tumour suppressor gene in renal carcinoma." Nat Genet **7**(1): 85-90.

Gnarra, J. R., S. Zhou, M. J. Merrill, J. R. Wagner, A. Krumm, E. Papavassiliou, E. H. Oldfield, R. D. Klausner and W. M. Linehan (1996). "Post-transcriptional regulation of

vascular endothelial growth factor mRNA by the product of the VHL tumor suppressor gene." Proc Natl Acad Sci U S A **93**(20): 10589-10594.

Golay, J., L. Basilico, L. Loffarelli, S. Songia, V. Broccoli and M. Introna (1996). "Regulation of hematopoietic cell proliferation and differentiation by the myb oncogene family of transcription factors." Int J Clin Lab Res **26**(1): 24-32.

Goldenson, B. and J. D. Crispino (2015). "The aurora kinases in cell cycle and leukemia." Oncogene **34**(5): 537-545.

Gordan, J. D., J. A. Bertout, C. J. Hu, J. A. Diehl and M. C. Simon (2007). "HIF-2alpha promotes hypoxic cell proliferation by enhancing c-myc transcriptional activity." Cancer Cell **11**(4): 335-347.

Gordan, J. D., P. Lal, V. R. Dondeti, R. Letrero, K. N. Parekh, C. E. Oquendo, R. A. Greenberg, K. T. Flaherty, W. K. Rathmell, B. Keith, M. C. Simon and K. L. Nathanson (2008). "HIF-alpha effects on c-Myc distinguish two subtypes of sporadic VHL-deficient clear cell renal carcinoma." Cancer Cell **14**(6): 435-446.

Gossage, L., T. Eisen and E. R. Maher (2015). "VHL, the story of a tumour suppressor gene." Nat Rev Cancer **15**(1): 55-64.

Gossage, L., M. Murtaza, A. F. Slatter, C. P. Lichtenstein, A. Warren, B. Haynes, F. Marass, I. Roberts, S. J. Shanahan, A. Claas, A. Dunham, A. P. May, N. Rosenfeld, T. Forshew and T. Eisen (2014). "Clinical and pathological impact of VHL, PBRM1, BAP1, SETD2, KDM6A, and JARID1c in clear cell renal cell carcinoma." Genes Chromosomes Cancer **53**(1): 38-51.

Gotink, K. J. and H. M. Verheul (2010). "Anti-angiogenic tyrosine kinase inhibitors: what is their mechanism of action?" Angiogenesis **13**(1): 1-14.

Graeber, T. G., C. Osmanian, T. Jacks, D. E. Housman, C. J. Koch, S. W. Lowe and A. J. Giaccia (1996). "Hypoxia-mediated selection of cells with diminished apoptotic potential in solid tumours." Nature **379**(6560): 88-91.

Gulati, S., P. Martinez, T. Joshi, N. J. Birkbak, C. R. Santos, A. J. Rowan, L. Pickering, M. Gore, J. Larkin, Z. Szallasi, P. A. Bates, C. Swanton and M. Gerlinger (2014). "Systematic Evaluation of the Prognostic Impact and Intratumour Heterogeneity of Clear Cell Renal Cell Carcinoma Biomarkers." Eur Urol.

Gulati, S., P. Martinez, T. Joshi, N. J. Birkbak, C. R. Santos, A. J. Rowan, L. Pickering, M. Gore, J. Larkin, Z. Szallasi, P. A. Bates, C. Swanton and M. Gerlinger (2014). "Systematic evaluation of the prognostic impact and intratumour heterogeneity of clear cell renal cell carcinoma biomarkers." Eur Urol **66**(5): 936-948.

Gumbiner, B. M. and N. G. Kim (2014). "The Hippo-YAP signaling pathway and contact inhibition of growth." J Cell Sci **127**(Pt 4): 709-717.

Guttridge, D. C., C. Albanese, J. Y. Reuther, R. G. Pestell and A. S. Baldwin, Jr. (1999). "NF-kappaB controls cell growth and differentiation through transcriptional regulation of cyclin D1." Mol Cell Biol **19**(8): 5785-5799.

Guzman, C., M. Bagga, A. Kaur, J. Westermarck and D. Abankwa (2014). "ColonyArea: an ImageJ plugin to automatically quantify colony formation in clonogenic assays." PLoS One **9**(3): e92444.

Hakimi, A. A., C. G. Pham and J. J. Hsieh (2013). "A clear picture of renal cell carcinoma." Nat Genet **45**(8): 849-850.

Han, J., Y. Lee, K. H. Yeom, J. W. Nam, I. Heo, J. K. Rhee, S. Y. Sohn, Y. Cho, B. T. Zhang and V. N. Kim (2006). "Molecular basis for the recognition of primary microRNAs by the Drosha-DGCR8 complex." Cell **125**(5): 887-901.

Hanahan, D. and R. A. Weinberg (2011). "Hallmarks of cancer: the next generation." Cell **144**(5): 646-674.

Happerfield, L. C., L. G. Bobrow, R. Bains and K. D. Miller (1993). "Peroxidase labelling immunocytochemistry: a comparison of eleven commercially-available avidin-biotin systems." Br J Biomed Sci **50**(1): 21-26.

Harvey, J. M., G. M. Clark, C. K. Osborne and D. C. Allred (1999). "Estrogen receptor status by immunohistochemistry is superior to the ligand-binding assay for predicting response to adjuvant endocrine therapy in breast cancer." J Clin Oncol **17**(5): 1474-1481.

Harvey, K. F., X. Zhang and D. M. Thomas (2013). "The Hippo pathway and human cancer." Nat Rev Cancer **13**(4): 246-257.

Hatzis, C., P. L. Bedard, N. J. Birkbak, A. H. Beck, H. J. Aerts, D. F. Stem, L. Shi, R. Clarke, J. Quackenbush and B. Haibe-Kains (2014). "Enhancing reproducibility in cancer drug screening: how do we move forward?" Cancer Res **74**(15): 4016-4023.

He, L. and G. J. Hannon (2004). "MicroRNAs: small RNAs with a big role in gene regulation." Nat Rev Genet **5**(7): 522-531.

Hendel, A., R. O. Bak, J. T. Clark, A. B. Kennedy, D. E. Ryan, S. Roy, I. Steinfeld, B. D. Lunstad, R. J. Kaiser, A. B. Wilkens, R. Bacchetta, A. Tsalenko, D. Dellinger, L. Bruhn and M. H. Porteus (2015). "Chemically modified guide RNAs enhance CRISPR-Cas genome editing in human primary cells." Nat Biotechnol **33**(9): 985-989.

Heng, D. Y., W. Xie, M. M. Regan, L. C. Harshman, G. A. Bjarnason, U. N. Vaishampayan, M. Mackenzie, L. Wood, F. Donskov, M. H. Tan, S. Y. Rha, N. Agarwal, C. Kollmannsberger, B. I. Rini and T. K. Choueiri (2013). "External validation and comparison with other models of the International Metastatic Renal-Cell Carcinoma Database Consortium prognostic model: a population-based study." Lancet Oncol **14**(2): 141-148.

Heng, D. Y., W. Xie, M. M. Regan, M. A. Warren, A. R. Golshayan, C. Sahi, B. J. Eigl, J. D. Ruether, T. Cheng, S. North, P. Venner, J. J. Knox, K. N. Chi, C. Kollmannsberger, D. F. McDermott, W. K. Oh, M. B. Atkins, R. M. Bukowski, B. I. Rini and T. K. Choueiri (2009). "Prognostic factors for overall survival in patients with metastatic renal cell carcinoma treated with vascular endothelial growth factor-targeted agents: results from a large, multicenter study." J Clin Oncol **27**(34): 5794-5799.

Herbst, R. S., J. C. Soria, M. Kowanetz, G. D. Fine, O. Hamid, M. S. Gordon, J. A. Sosman, D. F. McDermott, J. D. Powderly, S. N. Gettinger, H. E. Kohrt, L. Horn, D. P. Lawrence, S. Rost, M. Leabman, Y. Xiao, A. Mokatrin, H. Koeppen, P. S. Hegde, I. Mellman, D. S. Chen and F. S. Hodi (2014). "Predictive correlates of response to the anti-PD-L1 antibody MPDL3280A in cancer patients." Nature **515**(7528): 563-567.

Hirota, T., N. Kunitoku, T. Sasayama, T. Marumoto, D. Zhang, M. Nitta, K. Hatakeyama and H. Saya (2003). "Aurora-A and an interacting activator, the LIM protein Ajuba, are required for mitotic commitment in human cells." Cell **114**(5): 585-598.

Hockel, M. and P. Vaupel (2001). "Tumor hypoxia: definitions and current clinical, biologic, and molecular aspects." J Natl Cancer Inst **93**(4): 266-276.

Hoffman, R. M. (1991). "In vitro sensitivity assays in cancer: a review, analysis, and prognosis." J Clin Lab Anal **5**(2): 133-143.

Howat, W. J. and B. A. Wilson (2014). "Tissue fixation and the effect of molecular fixatives on downstream staining procedures." Methods **70**(1): 12-19.

Hsi, E. D. (2001). "A practical approach for evaluating new antibodies in the clinical immunohistochemistry laboratory." Arch Pathol Lab Med **125**(2): 289-294.

Hsu, P. D., E. S. Lander and F. Zhang (2014). "Development and applications of CRISPR-Cas9 for genome engineering." Cell **157**(6): 1262-1278.

Hu, C. J., A. Sataur, L. Wang, H. Chen and M. C. Simon (2007). "The N-terminal transactivation domain confers target gene specificity of hypoxia-inducible factors HIF-1alpha and HIF-2alpha." Mol Biol Cell **18**(11): 4528-4542.

Hu, C. J., L. Y. Wang, L. A. Chodosh, B. Keith and M. C. Simon (2003). "Differential roles of hypoxia-inducible factor 1alpha (HIF-1alpha) and HIF-2alpha in hypoxic gene regulation." Mol Cell Biol **23**(24): 9361-9374.

Huang, J., S. Wu, J. Barrera, K. Matthews and D. Pan (2005). "The Hippo signaling pathway coordinately regulates cell proliferation and apoptosis by inactivating Yorkie, the Drosophila Homolog of YAP." Cell **122**(3): 421-434.

Huang, Y., Y. Dai, J. Yang, T. Chen, Y. Yin, M. Tang, C. Hu and L. Zhang (2009). "Microarray analysis of microRNA expression in renal clear cell carcinoma." Eur J Surg Oncol **35**(10): 1119-1123.

Hudes, G., M. Carducci, P. Tomczak, J. Dutcher, R. Figlin, A. Kapoor, E. Staroslawska, J. Sosman, D. McDermott, I. Bodrogi, Z. Kovacevic, V. Lesovoy, I. G. Schmidt-Wolf, O. Barbarash, E. Gokmen, T. O'Toole, S. Lustgarten, L. Moore, R. J. Motzer and A. T. Global (2007). "Temsirolimus, interferon alfa, or both for advanced renal-cell carcinoma." N Engl J Med **356**(22): 2271-2281.

Huggins, C. J., M. Gill and I. L. Andrulis (2007). "Identification of rare variants in the hLIMD1 gene in breast cancer." Cancer Genet Cytogenet **178**(1): 36-41.

Hutson, T. E., V. Lesovoy, S. Al-Shukri, V. P. Stus, O. N. Lipatov, A. H. Bair, B. Rosbrook, C. Chen, S. Kim and N. J. Vogelzang (2013). "Axitinib versus sorafenib as first-line therapy in patients with metastatic renal-cell carcinoma: a randomised open-label phase 3 trial." Lancet Oncol **14**(13): 1287-1294.

Iakovlev, V. V., M. Gabril, W. Dubinski, A. Scorilas, Y. M. Youssef, H. Faragalla, K. Kovacs, F. Rotondo, S. Metias, A. Arsanious, A. Plotkin, A. H. Girgis, C. J. Streutker and G. M. Yousef (2012). "Microvascular density as an independent predictor of clinical outcome in renal cell carcinoma: an automated image analysis study." Lab Invest **92**(1): 46-56.

Iliopoulos, O., A. P. Levy, C. Jiang, W. G. Kaelin, Jr. and M. A. Goldberg (1996). "Negative regulation of hypoxia-inducible genes by the von Hippel-Lindau protein." Proc Natl Acad Sci U S A **93**(20): 10595-10599.

Iliopoulos, O., M. Ohh and W. G. Kaelin, Jr. (1998). "pVHL19 is a biologically active product of the von Hippel-Lindau gene arising from internal translation initiation." Proc Natl Acad Sci U S A **95**(20): 11661-11666.

Ioannou, M., I. Mylonis, E. Kouvaras, R. Papamichali, A. Daponte, E. Paraskeva, G. Simos and G. K. Koukoulis (2010). "Validated analysis of HIF-1alpha expression in cancer cells using a controlled and comparative immunoassay." Oncol Rep **24**(1): 161-169.

Israel, G. M. and M. A. Bosniak (2005). "How I do it: evaluating renal masses." Radiology **236**(2): 441-450.

Iyer, N. V., L. E. Kotch, F. Agani, S. W. Leung, E. Laughner, R. H. Wenger, M. Gassmann, J. D. Gearhart, A. M. Lawler, A. Y. Yu and G. L. Semenza (1998). "Cellular and developmental control of O2 homeostasis by hypoxia-inducible factor 1 alpha." Genes Dev **12**(2): 149-162.

Jaakkola, P., D. R. Mole, Y. M. Tian, M. I. Wilson, J. Gielbert, S. J. Gaskell, A. von Kriegsheim, H. F. Hebestreit, M. Mukherji, C. J. Schofield, P. H. Maxwell, C. W. Pugh and P. J. Ratcliffe (2001). "Targeting of HIF-alpha to the von Hippel-Lindau ubiquitylation complex by O2-regulated prolyl hydroxylation." Science **292**(5516): 468-472.

Jacobs, J. J., K. Kieboom, S. Marino, R. A. DePinho and M. van Lohuizen (1999). "The oncogene and Polycomb-group gene bmi-1 regulates cell proliferation and senescence through the ink4a locus." Nature **397**(6715): 164-168.

Jacobsen, J., T. Rasmuson, K. Grankvist and B. Ljungberg (2000). "Vascular endothelial growth factor as prognostic factor in renal cell carcinoma." J Urol **163**(1): 343-347.

James, V., S. C. Wong and T. V. Sharp (2012). "MicroRNA-mediated gene silencing: are we close to a unifying model?" Biomol Concepts **3**(1): 29-40.

James, V., Y. Zhang, D. E. Foxler, C. H. de Moor, Y. W. Kong, T. M. Webb, T. J. Self, Y. Feng, D. Lagos, C. Y. Chu, T. M. Rana, S. J. Morley, G. D. Longmore, M. Bushell and T. V. Sharp (2010). "LIM-domain proteins, LIMD1, Ajuba, and WTIP are required for microRNA-mediated gene silencing." Proc Natl Acad Sci U S A **107**(28): 12499-12504.

Janne, P. A., A. T. Shaw, J. R. Pereira, G. Jeannin, J. Vansteenkiste, C. Barrios, F. A. Franke, L. Grinsted, V. Zazulina, P. Smith, I. Smith and L. Crino (2013). "Selumetinib plus docetaxel for KRAS-mutant advanced non-small-cell lung cancer: a randomised, multicentre, placebo-controlled, phase 2 study." Lancet Oncol **14**(1): 38-47.

Jarvis, E. M., J. A. Kirk and C. L. Clarke (1998). "Loss of nuclear BRCA1 expression in breast cancers is associated with a highly proliferative tumor phenotype." Cancer Genet Cytogenet **101**(2): 109-115.

Jensen, T. O., R. Riber-Hansen, H. Schmidt, S. J. Hamilton-Dutoit and T. Steiniche (2011). "Tumor and inflammation markers in melanoma using tissue microarrays: a validation study." Melanoma Res **21**(6): 509-515.

Jiao, M. and K. J. Nan (2012). "Activation of PI3 kinase/Akt/HIF-1alpha pathway contributes to hypoxia-induced epithelial-mesenchymal transition and chemoresistance in hepatocellular carcinoma." Int J Oncol **40**(2): 461-468.

Jonasch, E., P. Corn, L. C. Pagliaro, C. L. Warneke, M. M. Johnson, P. Tamboli, C. Ng, A. Aparicio, R. G. Ashe, J. J. Wright and N. M. Tannir (2010). "Upfront, randomized, phase 2 trial of sorafenib versus sorafenib and low-dose interferon alfa in patients with advanced renal cell carcinoma: clinical and biomarker analysis." Cancer **116**(1): 57-65.

Jung, M., H. J. Mollenkopf, C. Grimm, I. Wagner, M. Albrecht, T. Waller, C. Pilarsky, M. Johannsen, C. Stephan, H. Lehrach, W. Nietfeld, T. Rudel, K. Jung and G. Kristiansen (2009). "MicroRNA profiling of clear cell renal cell cancer identifies a robust signature to define renal malignancy." J Cell Mol Med **13**(9B): 3918-3928.

Kadrmas, J. L. and M. C. Beckerle (2004). "The LIM domain: from the cytoskeleton to the nucleus." Nat Rev Mol Cell Biol **5**(11): 920-931.

Kaelin, W. G., Jr. (2005). "The concept of synthetic lethality in the context of anticancer therapy." Nat Rev Cancer **5**(9): 689-698.

Kaelin, W. G., Jr. (2007). "The von Hippel-Lindau tumor suppressor protein and clear cell renal carcinoma." Clin Cancer Res **13**(2 Pt 2): 680s-684s.

Kansanen, E., S. M. Kuosmanen, H. Leinonen and A. L. Levonen (2013). "The Keap1-Nrf2 pathway: Mechanisms of activation and dysregulation in cancer." Redox Biol **1**: 45-49.

Kanu, N., E. Gronroos, P. Martinez, R. A. Burrell, X. Yi Goh, J. Bartkova, A. Maya-Mendoza, M. Mistrik, A. J. Rowan, H. Patel, A. Rabinowitz, P. East, G. Wilson, C. R. Santos, N. McGranahan, S. Gulati, M. Gerlinger, N. J. Birkbak, T. Joshi, L. B. Alexandrov, M. R. Stratton, T. Powles, N. Matthews, P. A. Bates, A. Stewart, Z. Szallasi, J. Larkin, J. Bartek and C. Swanton (2015). "SETD2 loss-of-function promotes renal cancer branched evolution through replication stress and impaired DNA repair." Oncogene **34**(46): 5699-5708.

Karakashev, S. V. and M. J. Reginato (2015). "Progress toward overcoming hypoxia-induced resistance to solid tumor therapy." Cancer Manag Res **7**: 253-264.

Karam, J. A., B. I. Rini, L. Varella, J. A. Garcia, R. Dreicer, T. K. Choueiri, E. Jonasch, S. F. Matin, S. C. Campbell, C. G. Wood and N. M. Tannir (2011). "Metastasectomy after targeted therapy in patients with advanced renal cell carcinoma." J Urol **185**(2): 439-444.

Ke, Q. and M. Costa (2006). "Hypoxia-inducible factor-1 (HIF-1)." Mol Pharmacol **70**(5): 1469-1480.

Keith, B., R. S. Johnson and M. C. Simon (2012). "HIF1alpha and HIF2alpha: sibling rivalry in hypoxic tumour growth and progression." Nat Rev Cancer **12**(1): 9-22.

Kerr, K. M. and F. R. Hirsch (2016). "Programmed Death Ligand-1 Immunohistochemistry: Friend or Foe?" Arch Pathol Lab Med **140**(4): 326-331.

Kholodnyuk, I., M. Kost-Alimova, V. Kashuba, R. Gizatulin, A. Szeles, E. J. Stanbridge, E. R. Zabarovsky, G. Klein and S. Imreh (1997). "A 3p21.3 region is preferentially eliminated from human chromosome 3/mouse microcell hybrids during tumor growth in SCID mice." Genes Chromosomes Cancer **18**(3): 200-211.

Kibel, A., O. Iliopoulos, J. A. DeCaprio and W. G. Kaelin, Jr. (1995). "Binding of the von Hippel-Lindau tumor suppressor protein to Elongin B and C." Science **269**(5229): 1444-1446.

Kim, S. P., A. L. Alt, C. J. Weight, B. A. Costello, J. C. Cheville, C. Lohse, C. Allmer and B. C. Leibovich (2011). "Independent validation of the 2010 American Joint Committee on Cancer TNM classification for renal cell carcinoma: results from a large, single institution cohort." J Urol **185**(6): 2035-2039.

Kim, W. Y., S. Perera, B. Zhou, J. Carretero, J. J. Yeh, S. A. Heathcote, A. L. Jackson, P. Nikolinakos, B. Ospina, G. Naumov, K. A. Brandstetter, V. J. Weigman, S. Zaghlul, D.

N. Hayes, R. F. Padera, J. V. Heymach, A. L. Kung, N. E. Sharpless, W. G. Kaelin, Jr. and K. K. Wong (2009). "HIF2alpha cooperates with RAS to promote lung tumorigenesis in mice." J Clin Invest **119**(8): 2160-2170.

Klatte, T., D. B. Seligson, S. B. Riggs, J. T. Leppert, M. K. Berkman, M. D. Kleid, H. Yu, F. F. Kabbinavar, A. J. Pantuck and A. S. Belldegrun (2007). "Hypoxia-inducible factor 1 alpha in clear cell renal cell carcinoma." Clin Cancer Res **13**(24): 7388-7393.

Kluger, H. M., S. F. Siddiqui, C. Angeletti, M. Sznol, W. K. Kelly, A. M. Molinaro and R. L. Camp (2008). "Classification of renal cell carcinoma based on expression of VEGF and VEGF receptors in both tumor cells and endothelial cells." Lab Invest **88**(9): 962-972.

Knudson, A. G., Jr. (1971). "Mutation and cancer: statistical study of retinoblastoma." Proc Natl Acad Sci U S A **68**(4): 820-823.

Koh, M. Y., R. Lemos, Jr., X. Liu and G. Powis (2011). "The hypoxia-associated factor switches cells from HIF-1alpha- to HIF-2alpha-dependent signaling promoting stem cell characteristics, aggressive tumor growth and invasion." Cancer Res **71**(11): 4015-4027.

Koh, M. Y. and G. Powis (2009). "HAF : the new player in oxygen-independent HIF-1alpha degradation." Cell Cycle **8**(9): 1359-1366.

Koh, M. Y. and G. Powis (2012). "Passing the baton: the HIF switch." Trends Biochem Sci **37**(9): 364-372.

Kola, I. (2008). "The state of innovation in drug development." Clin Pharmacol Ther **83**(2): 227-230.

Kola, I. and J. Landis (2004). "Can the pharmaceutical industry reduce attrition rates?" Nat Rev Drug Discov **3**(8): 711-715.

Kondo, K., M. Yao, M. Yoshida, T. Kishida, T. Shuin, T. Miura, M. Moriyama, K. Kobayashi, N. Sakai, S. Kaneko, S. Kawakami, M. Baba, N. Nakaigawa, Y. Nagashima, Y. Nakatani and M. Hosaka (2002). "Comprehensive mutational analysis of the VHL gene in sporadic renal cell carcinoma: relationship to clinicopathological parameters." Genes Chromosomes Cancer **34**(1): 58-68.

Koshiji, M., Y. Kageyama, E. A. Pete, I. Horikawa, J. C. Barrett and L. E. Huang (2004). "HIF-1alpha induces cell cycle arrest by functionally counteracting Myc." EMBO J **23**(9): 1949-1956.

Kost-Alimova, M. and S. Imreh (2007). "Modeling non-random deletions in cancer." Semin Cancer Biol **17**(1): 19-30.

Koul, H., J. S. Huh, K. O. Rove, L. Crompton, S. Koul, R. B. Meacham and F. J. Kim (2011). "Molecular aspects of renal cell carcinoma: a review." Am J Cancer Res **1**(2): 240-254.

Kowolik, C. M., S. Liang, Y. Yu and J. K. Yee (2004). "Cre-mediated reversible immortalization of human renal proximal tubular epithelial cells." Oncogene **23**(35): 5950-5957.

Kramer, N., A. Walzl, C. Unger, M. Rosner, G. Krupitza, M. Hengstschlager and H. Dolznig (2013). "In vitro cell migration and invasion assays." Mutat Res **752**(1): 10-24.

Kris, M. G., R. B. Natale, R. S. Herbst, T. J. Lynch, Jr., D. Prager, C. P. Belani, J. H. Schiller, K. Kelly, H. Spiridonidis, A. Sandler, K. S. Albain, D. Cella, M. K. Wolf, S. D. Averbuch, J. J. Ochs and A. C. Kay (2003). "Efficacy of gefitinib, an inhibitor of the epidermal growth factor receptor tyrosine kinase, in symptomatic patients with non-small cell lung cancer: a randomized trial." JAMA **290**(16): 2149-2158.

Kroeger, N., T. Klatte, K. Chamie, P. N. Rao, F. D. Birkhauser, G. A. Sonn, J. Riss, F. F. Kabbinavar, A. S. Belldegrun and A. J. Pantuck (2013). "Deletions of chromosomes 3p and 14q molecularly subclassify clear cell renal cell carcinoma." Cancer **119**(8): 1547-1554.

Kroeger, N., D. B. Seligson, S. Signoretti, H. Yu, C. E. Magyar, J. Huang, A. S. Belldegrun and A. J. Pantuck (2014). "Poor prognosis and advanced clinicopathological features of clear cell renal cell carcinoma (ccRCC) are associated with cytoplasmic subcellular localisation of Hypoxia inducible factor-2alpha." Eur J Cancer **50**(8): 1531-1540.

LaGory, E. L. and A. J. Giaccia (2016). "The ever-expanding role of HIF in tumour and stromal biology." Nat Cell Biol **18**(4): 356-365.

Langer, E. M., Y. Feng, H. Zhaoyuan, F. J. Rauscher, 3rd, K. L. Kroll and G. D. Longmore (2008). "Ajuba LIM proteins are snail/slug corepressors required for neural crest development in Xenopus." Dev Cell **14**(3): 424-436.

Latif, F., K. Tory, J. Gnarra, M. Yao, F. M. Duh, M. L. Orcutt, T. Stackhouse, I. Kuzmin, W. Modi, L. Geil and et al. (1993). "Identification of the von Hippel-Lindau disease tumor suppressor gene." Science **260**(5112): 1317-1320.

Le Tourneau, C., S. Faivre, M. Serova and E. Raymond (2008). "mTORC1 inhibitors: is temsirolimus in renal cancer telling us how they really work?" Br J Cancer **99**(8): 1197-1203.

Leibovich, B. C., M. L. Blute, J. C. Cheville, C. M. Lohse, I. Frank, E. D. Kwon, A. L. Weaver, A. S. Parker and H. Zincke (2003). "Prediction of progression after radical nephrectomy for patients with clear cell renal cell carcinoma: a stratification tool for prospective clinical trials." Cancer **97**(7): 1663-1671.

Lerman, M. I. and J. D. Minna (2000). "The 630-kb lung cancer homozygous deletion region on human chromosome 3p21.3: identification and evaluation of the resident candidate tumor suppressor genes. The International Lung Cancer Chromosome 3p21.3 Tumor Suppressor Gene Consortium." Cancer Res **60**(21): 6116-6133.

Levi, F., J. Ferlay, C. Galeone, F. Lucchini, E. Negri, P. Boyle and C. La Vecchia (2008). "The changing pattern of kidney cancer incidence and mortality in Europe." BJU Int **101**(8): 949-958.

Li, L., C. Shen, E. Nakamura, K. Ando, S. Signoretti, R. Beroukhim, G. S. Cowley, P. Lizotte, E. Liberzon, S. Bair, D. E. Root, P. Tamayo, A. Tsherniak, S. C. Cheng, B. Tabak, A. Jacobsen, A. A. Hakimi, N. Schultz, G. Ciriello, C. Sander, J. J. Hsieh and W. G. Kaelin, Jr. (2013). "SQSTM1 is a pathogenic target of 5q copy number gains in kidney cancer." Cancer Cell **24**(6): 738-750.

Li, M., Y. Wang, Y. Song, R. Bu, B. Yin, X. Fei, Q. Guo and B. Wu (2015). "MicroRNAs in renal cell carcinoma: a systematic review of clinical implications (Review)." Oncol Rep **33**(4): 1571-1578.

Liang, C. C., A. Y. Park and J. L. Guan (2007). "In vitro scratch assay: a convenient and inexpensive method for analysis of cell migration in vitro." Nat Protoc **2**(2): 329-333.

Liang, X. H., G. X. Zhang, Y. B. Zeng, H. F. Yang, W. H. Li, Q. L. Liu, Y. L. Tang, W. G. He, Y. N. Huang, L. Zhang, L. N. Yu and X. C. Zeng (2014). "LIM protein JUB promotes epithelial-mesenchymal transition in colorectal cancer." Cancer Sci **105**(6): 660-666.

Lidgren, A., Y. Hedberg, K. Grankvist, T. Rasmuson, J. Vasko and B. Ljungberg (2005). "The expression of hypoxia-inducible factor 1alpha is a favorable independent prognostic factor in renal cell carcinoma." Clin Cancer Res **11**(3): 1129-1135.

Lin, J., Y. Horikawa, P. Tamboli, J. Clague, C. G. Wood and X. Wu (2010). "Genetic variations in microRNA-related genes are associated with survival and recurrence in patients with renal cell carcinoma." Carcinogenesis **31**(10): 1805-1812.

Liu, X., V. Ory, S. Chapman, H. Yuan, C. Albanese, B. Kallakury, O. A. Timofeeva, C. Nealon, A. Dakic, V. Simic, B. R. Haddad, J. S. Rhim, A. Dritschilo, A. Riegel, A. McBride and R. Schlegel (2012). "ROCK inhibitor and feeder cells induce the conditional reprogramming of epithelial cells." Am J Pathol **180**(2): 599-607.

Livraghi, L. and J. E. Garber (2015). "PARP inhibitors in the management of breast cancer: current data and future prospects." BMC Med **13**: 188.

Ljungberg, B., K. Bensalah, S. Canfield, S. Dabestani, F. Hofmann, M. Hora, M. A. Kuczyk, T. Lam, L. Marconi, A. S. Merseburger, P. Mulders, T. Powles, M. Staehler, A. Volpe and A. Bex (2015). "EAU Guidelines on Renal Cell Carcinoma: 2014 Update." Eur Urol.

Ljungberg, B., S. C. Campbell, H. Y. Choi, D. Jacqmin, J. E. Lee, S. Weikert and L. A. Kiemeney (2011). "The epidemiology of renal cell carcinoma." Eur Urol **60**(4): 615-621.

Loboda, A., A. Jozkowicz and J. Dulak (2010). "HIF-1 and HIF-2 transcription factors--similar but not identical." Mol Cells **29**(5): 435-442.

Luderer, H. F., S. Bai and G. D. Longmore (2008). "The LIM protein LIMD1 influences osteoblast differentiation and function." Exp Cell Res **314**(15): 2884-2894.

Lughezzani, G., C. Jeldres, H. Isbarn, P. Perrotte, S. F. Shariat, M. Sun, H. Widmer, P. Arjane, F. Peloquin, D. Pharand, J. J. Patard, M. Graefen, F. Montorsi and P. I. Karakiewicz (2009). "Tumor size is a determinant of the rate of stage T1 renal cell cancer synchronous metastasis." J Urol **182**(4): 1287-1293.

Lundberg, A. S., S. H. Randell, S. A. Stewart, B. Elenbaas, K. A. Hartwell, M. W. Brooks, M. D. Fleming, J. C. Olsen, S. W. Miller, R. A. Weinberg and W. C. Hahn (2002). "Immortalization and transformation of primary human airway epithelial cells by gene transfer." Oncogene **21**(29): 4577-4586.

Mackenzie, M. J., B. I. Rini, P. Elson, A. Schwandt, L. Wood, M. Trinkhaus, G. Bjarnason and J. Knox (2011). "Temsirolimus in VEGF-refractory metastatic renal cell carcinoma." Ann Oncol **22**(1): 145-148.

MacLennan, S., M. Imamura, M. C. Lapitan, M. I. Omar, T. B. Lam, A. M. Hilvano-Cabungcal, P. Royle, F. Stewart, G. MacLennan, S. J. MacLennan, S. E. Canfield, S. McClinton, T. R. Griffiths, B. Ljungberg, J. N'Dow, U. S. R. R. Group and E. A. U. R. C. G. Panel (2012). "Systematic review of oncological outcomes following surgical management of localised renal cancer." Eur Urol **61**(5): 972-993.

Malo, N., J. A. Hanley, S. Cerquozzi, J. Pelletier and R. Nadon (2006). "Statistical practice in high-throughput screening data analysis." Nat Biotechnol **24**(2): 167-175.

Maroto, P. and B. Rini (2014). "Molecular biomarkers in advanced renal cell carcinoma." Clin Cancer Res **20**(8): 2060-2071.

Massari, F., M. Santoni, C. Ciccarese, D. Santini, S. Alfieri, G. Martignoni, M. Brunelli, F. Piva, R. Berardi, R. Montironi, C. Porta, S. Cascinu and G. Tortora (2015). "PD-1 blockade therapy in renal cell carcinoma: current studies and future promises." Cancer Treat Rev **41**(2): 114-121.

Mataraza, J. and P. Gotwals (2016). "Recent advances in immuno-oncology and the application to urological cancers." BJU Int.

Matos, L. L., D. C. Trufelli, M. G. de Matos and M. A. da Silva Pinhal (2010). "Immunohistochemistry as an important tool in biomarkers detection and clinical practice." Biomark Insights **5**: 9-20.

Mazumdar, M. and J. R. Glassman (2000). "Categorizing a prognostic variable: review of methods, code for easy implementation and applications to decision-making about cancer treatments." Stat Med **19**(1): 113-132.

Mazzoleni, G., D. Di Lorenzo and N. Steimberg (2009). "Modelling tissues in 3D: the next future of pharmaco-toxicology and food research?" Genes Nutr **4**(1): 13-22.

McCormick, R. I., C. Blick, J. Ragoussis, J. Schoedel, D. R. Mole, A. C. Young, P. J. Selby, R. E. Banks and A. L. Harris (2013). "miR-210 is a target of hypoxia-inducible factors 1 and 2 in renal cancer, regulates ISCU and correlates with good prognosis." Br J Cancer **108**(5): 1133-1142.

McDermott, D. F., J. A. Sosman, M. Sznol, C. Massard, M. S. Gordon, O. Hamid, J. D. Powderly, J. R. Infante, M. Fasso, Y. V. Wang, W. Zou, P. S. Hegde, G. D. Fine and T. Powles (2016). "Atezolizumab, an Anti-Programmed Death-Ligand 1 Antibody, in Metastatic Renal Cell Carcinoma: Long-Term Safety, Clinical Activity, and Immune Correlates From a Phase Ia Study." J Clin Oncol **34**(8): 833-842.

Mejean, A., A. Ravaud, S. Thezenas, S. Colas, J. B. Beauval, K. Bensalah, L. Geoffrois, A. Thiery-Vuillemin, L. Cormier, H. Lang, L. Guy, G. Gravis, F. Rolland, C. Linassier, E. Lechevallier, C. Beisland, M. Aitchison, S. Oudard, J. J. Patard, C. Theodore, C. Chevreau, B. Laguerre, J. Hubert, M. Gross-Goupil, J. C. Bernhard, L. Albiges, M. O. Timsit, T. Lebret and B. Escudier (2018). "Sunitinib Alone or after Nephrectomy in Metastatic Renal-Cell Carcinoma." N Engl J Med **379**(5): 417-427.

Mekhail, T. M., R. M. Abou-Jawde, G. Boumerhi, S. Malhi, L. Wood, P. Elson and R. Bukowski (2005). "Validation and extension of the Memorial Sloan-Kettering prognostic factors model for survival in patients with previously untreated metastatic renal cell carcinoma." J Clin Oncol **23**(4): 832-841.

Meli, L., E. T. Jordan, D. S. Clark, R. J. Linhardt and J. S. Dordick (2012). "Influence of a three-dimensional, microarray environment on human cell culture in drug screening systems." Biomaterials **33**(35): 9087-9096.

Miki, T., N. Nonomura, N. Takaha, K. Nishimura, Y. Kojima, M. Sawada and A. Okuyama (1998). "Antitumor effect of irinotecan hydrochloride (CPT-11) on human renal tumors heterotransplanted in nude mice." Int J Urol **5**(4): 370-373.

Millauer, B., S. Wizigmann-Voos, H. Schnurch, R. Martinez, N. P. Moller, W. Risau and A. Ullrich (1993). "High affinity VEGF binding and developmental expression suggest Flk-1 as a major regulator of vasculogenesis and angiogenesis." Cell **72**(6): 835-846.

Minardi, D., G. Lucarini, M. Santoni, R. Mazzucchelli, L. Burattini, A. Conti, E. Principi, M. Bianconi, M. Scartozzi, G. Milanese, R. Di Primio, R. Montironi, S. Cascinu and G. Muzzonigro (2015). "Survival in patients with clear cell renal cell carcinoma is predicted by HIF-1alpha expression." Anticancer Res **35**(1): 433-438.

Montani, M., K. Heinimann, A. von Teichman, T. Rudolph, A. Perren and H. Moch (2010). "VHL-gene deletion in single renal tubular epithelial cells and renal tubular cysts: further evidence for a cyst-dependent progression pathway of clear cell renal carcinoma in von Hippel-Lindau disease." Am J Surg Pathol **34**(6): 806-815.

Moon, S., S. J. Um and E. J. Kim (2015). "Role of Asxl1 in kidney podocyte development via its interaction with Wtip." Biochem Biophys Res Commun **466**(3): 560-566.

Motzer, R. J., J. Bacik, B. A. Murphy, P. Russo and M. Mazumdar (2002). "Interferon-alfa as a comparative treatment for clinical trials of new therapies against advanced renal cell carcinoma." J Clin Oncol **20**(1): 289-296.

Motzer, R. J., B. Escudier, P. Tomczak, T. E. Hutson, M. D. Michaelson, S. Negrier, S. Oudard, M. E. Gore, J. Tarazi, S. Hariharan, C. Chen, B. Rosbrook, S. Kim and B. I. Rini (2013). "Axitinib versus sorafenib as second-line treatment for advanced renal cell carcinoma: overall survival analysis and updated results from a randomised phase 3 trial." Lancet Oncol **14**(6): 552-562.

Motzer, R. J., T. E. Hutson, D. Cella, J. Reeves, R. Hawkins, J. Guo, P. Nathan, M. Staehler, P. de Souza, J. R. Merchan, E. Boleti, K. Fife, J. Jin, R. Jones, H. Uemura, U. De Giorgi, U. Harmenberg, J. Wang, C. N. Sternberg, K. Deen, L. McCann, M. D. Hackshaw, R. Crescenzo, L. N. Pandite and T. K. Choueiri (2013). "Pazopanib versus sunitinib in metastatic renal-cell carcinoma." N Engl J Med **369**(8): 722-731.

Motzer, R. J., T. E. Hutson, P. Tomczak, M. D. Michaelson, R. M. Bukowski, S. Oudard, S. Negrier, C. Szczylik, R. Pili, G. A. Bjarnason, X. Garcia-del-Muro, J. A. Sosman, E. Solska, G. Wilding, J. A. Thompson, S. T. Kim, I. Chen, X. Huang and R. A. Figlin (2009). "Overall survival and updated results for sunitinib compared with interferon alfa in patients with metastatic renal cell carcinoma." J Clin Oncol **27**(22): 3584-3590.

Motzer, R. J., T. E. Hutson, P. Tomczak, M. D. Michaelson, R. M. Bukowski, O. Rixe, S. Oudard, S. Negrier, C. Szczylik, S. T. Kim, I. Chen, P. W. Bycott, C. M. Baum and R. A. Figlin (2007). "Sunitinib versus interferon alfa in metastatic renal-cell carcinoma." N Engl J Med **356**(2): 115-124.

Motzer, R. J., M. Mazumdar, J. Bacik, W. Berg, A. Amsterdam and J. Ferrara (1999). "Survival and prognostic stratification of 670 patients with advanced renal cell carcinoma." J Clin Oncol **17**(8): 2530-2540.

Motzer, R. J., B. I. Rini, D. F. McDermott, B. G. Redman, T. M. Kuzel, M. R. Harrison, U. N. Vaishampayan, H. A. Drabkin, S. George, T. F. Logan, K. A. Margolin, E. R. Plimack, A. M. Lambert, I. M. Waxman and H. J. Hammers (2015). "Nivolumab for Metastatic Renal Cell Carcinoma: Results of a Randomized Phase II Trial." J Clin Oncol **33**(13): 1430-1437.

Mpindi, J. P., P. Swapnil, B. Dmitrii, S. Jani, K. Saeed, K. Wennerberg, T. Aittokallio, P. Ostling and O. Kallioniemi (2015). "Impact of normalization methods on high-throughput screening data with high hit rates and drug testing with dose-response data." Bioinformatics **31**(23): 3815-3821.

Niell, H. B., M. S. Soloway, C. A. Wood, L. W. McCallum and K. Webster (1983). "The use of a tumor colony assay in predicting chemotherapeutic drug response in murine bladder cancer." Cancer **52**(4): 619-625.

Nijman, S. M. (2011). "Synthetic lethality: general principles, utility and detection using genetic screens in human cells." FEBS Lett **585**(1): 1-6.

Ning, S., K. Trisler, B. W. Wessels and S. J. Knox (1997). "Radiobiologic studies of radioimmunotherapy and external beam radiotherapy in vitro and in vivo in human renal cell carcinoma xenografts." Cancer **80**(12 Suppl): 2519-2528.

Nitiss, J. L. (2009). "DNA topoisomerase II and its growing repertoire of biological functions." Nat Rev Cancer **9**(5): 327-337.

Nitiss, J. L., E. Soans, A. Rogojina, A. Seth and M. Mishina (2012). "Topoisomerase assays." Curr Protoc Pharmacol **Chapter 3**: Unit 3 3.

Nix, D. A., J. Fradelizi, S. Bockholt, B. Menichi, D. Louvard, E. Friederich and M. C. Beckerle (2001). "Targeting of zyxin to sites of actin membrane interaction and to the nucleus." J Biol Chem **276**(37): 34759-34767.

Noessner, E., D. Brech, A. N. Mendler, I. Masouris, R. Schlenker and P. U. Prinz (2012). "Intratumoral alterations of dendritic-cell differentiation and CD8(+) T-cell anergy are immune escape mechanisms of clear cell renal cell carcinoma." Oncoimmunology **1**(8): 1451-1453.

Nola, S., R. Daigaku, K. Smolarczyk, M. Carstens, B. Martin-Martin, G. Longmore, M. Bailly and V. M. Braga (2011). "Ajuba is required for Rac activation and maintenance of E-cadherin adhesion." J Cell Biol **195**(5): 855-871.

O'Farrell, A. M., T. J. Abrams, H. A. Yuen, T. J. Ngai, S. G. Louie, K. W. Yee, L. M. Wong, W. Hong, L. B. Lee, A. Town, B. D. Smolich, W. C. Manning, L. J. Murray, M. C. Heinrich and J. M. Cherrington (2003). "SU11248 is a novel FLT3 tyrosine kinase inhibitor with potent activity in vitro and in vivo." Blood **101**(9): 3597-3605.

O'Reilly, A. and J. Larkin (2017). "Lenvatinib for use in combination with everolimus for the treatment of patients with advanced renal cell carcinoma following one prior anti-angiogenic therapy." Expert Rev Clin Pharmacol **10**(3): 251-262.

Oka, H., Y. Chatani, R. Hoshino, O. Ogawa, Y. Kakehi, T. Terachi, Y. Okada, M. Kawaichi, M. Kohno and O. Yoshida (1995). "Constitutive activation of mitogen-activated protein (MAP) kinases in human renal cell carcinoma." Cancer Res **55**(18): 4182-4187.

Onder, T. T., P. B. Gupta, S. A. Mani, J. Yang, E. S. Lander and R. A. Weinberg (2008). "Loss of E-cadherin promotes metastasis via multiple downstream transcriptional pathways." Cancer Res **68**(10): 3645-3654.

Oosterwijk, E., W. K. Rathmell, K. Junker, A. R. Brannon, F. Pouliot, D. S. Finley, P. F. Mulders, Z. Kirkali, H. Uemura and A. Belldegrun (2011). "Basic research in kidney cancer." Eur Urol **60**(4): 622-633.

Pal, S. K. and R. A. Figlin (2011). "Unraveling the role of hypoxia-inducible factor in renal cell carcinoma: a biological and therapeutic perspective." Cancer Discov **1**(3): 198-199.

Palapattu, G. S., B. Kristo and J. Rajfer (2002). "Paraneoplastic syndromes in urologic malignancy: the many faces of renal cell carcinoma." Rev Urol **4**(4): 163-170.

Pantuck, A. J., G. Zeng, A. S. Belldegrun and R. A. Figlin (2003). "Pathobiology, prognosis, and targeted therapy for renal cell carcinoma: exploiting the hypoxia-induced pathway." Clin Cancer Res **9**(13): 4641-4652.

Paradis, V., N. B. Lagha, L. Zeimoura, P. Blanchet, P. Eschwege, N. Ba, G. Benoit, A. Jardin and P. Bedossa (2000). "Expression of vascular endothelial growth factor in renal cell carcinomas." Virchows Arch **436**(4): 351-356.

Park, Y. B., M. J. Park, K. Kimura, K. Shimizu, S. H. Lee and J. Yokota (2002). "Alterations in the INK4a/ARF locus and their effects on the growth of human osteosarcoma cell lines." Cancer Genet Cytogenet **133**(2): 105-111.

Pasanen, A., M. Heikkila, K. Rautavuoma, M. Hirsila, K. I. Kivirikko and J. Myllyharju (2010). "Hypoxia-inducible factor (HIF)-3alpha is subject to extensive alternative splicing in human tissues and cancer cells and is regulated by HIF-1 but not HIF-2." Int J Biochem Cell Biol **42**(7): 1189-1200.

Patard, J. J., H. L. Kim, J. S. Lam, F. J. Dorey, A. J. Pantuck, A. Zisman, V. Ficarra, K. R. Han, L. Cindolo, A. De La Taille, J. Tostain, W. Artibani, C. P. Dinney, C. G. Wood, D. A. Swanson, C. C. Abbou, B. Lobel, P. F. Mulders, D. K. Chopin, R. A. Figlin and A. S. Belldegrun (2004). "Use of the University of California Los Angeles integrated staging system to predict survival in renal cell carcinoma: an international multicenter study." J Clin Oncol **22**(16): 3316-3322.

Patard, J. J., E. Leray, A. Rodriguez, N. Rioux-Leclercq, F. Guille and B. Lobel (2003). "Correlation between symptom graduation, tumor characteristics and survival in renal cell carcinoma." Eur Urol **44**(2): 226-232.

Patard, J. J., N. Rioux-Leclercq, D. Masson, S. Zerrouki, F. Jouan, N. Collet, C. Dubourg, B. Lobel, M. Denis and P. Fergelot (2009). "Absence of VHL gene alteration and high VEGF expression are associated with tumour aggressiveness and poor survival of renal-cell carcinoma." Br J Cancer **101**(8): 1417-1424.

Paull, T. T., E. P. Rogakou, V. Yamazaki, C. U. Kirchgessner, M. Gellert and W. M. Bonner (2000). "A critical role for histone H2AX in recruitment of repair factors to nuclear foci after DNA damage." Curr Biol **10**(15): 886-895.

Pawson, T. and P. Nash (2003). "Assembly of cell regulatory systems through protein interaction domains." Science **300**(5618): 445-452.

Pearson, G., F. Robinson, T. Beers Gibson, B. E. Xu, M. Karandikar, K. Berman and M. H. Cobb (2001). "Mitogen-activated protein (MAP) kinase pathways: regulation and physiological functions." Endocr Rev **22**(2): 153-183.

Pennacchietti, S., P. Michieli, M. Galluzzo, M. Mazzone, S. Giordano and P. M. Comoglio (2003). "Hypoxia promotes invasive growth by transcriptional activation of the met protooncogene." Cancer Cell **3**(4): 347-361.

Perkins, N. J. and E. F. Schisterman (2006). "The inconsistency of "optimal" cutpoints obtained using two criteria based on the receiver operating characteristic curve." Am J Epidemiol **163**(7): 670-675.

Petursdottir, T. E., U. Thorsteinsdottir, J. G. Jonasson, P. H. Moller, C. Huiping, J. Bjornsson, V. Egilsson, S. Imreh and S. Ingvarsson (2004). "Interstitial deletions including chromosome 3 common eliminated region 1 (C3CER1) prevail in human solid tumors from 10 different tissues." Genes Chromosomes Cancer **41**(3): 232-242.

Phuoc, N. B., H. Ehara, T. Gotoh, M. Nakano, S. Kamei, T. Deguchi and Y. Hirose (2008). "Prognostic value of the co-expression of carbonic anhydrase IX and vascular endothelial growth factor in patients with clear cell renal cell carcinoma." Oncol Rep **20**(3): 525-530.

Polakis, P. (2012). "Wnt signaling in cancer." Cold Spring Harb Perspect Biol **4**(5).

Poon, E., A. L. Harris and M. Ashcroft (2009). "Targeting the hypoxia-inducible factor (HIF) pathway in cancer." Expert Rev Mol Med **11**: e26.

Porta, C., L. Bonomi, B. Lillaz, C. Paglino, B. Rovati, I. Imarisio, P. Morbini, C. Villa, M. Danova, M. Mensi and B. Rovereto (2007). "Renal cell carcinoma-induced immunosuppression: an immunophenotypic study of lymphocyte subpopulations and circulating dendritic cells." Anticancer Res **27**(1A): 165-173.

Pouyssegur, J., F. Dayan and N. M. Mazure (2006). "Hypoxia signalling in cancer and approaches to enforce tumour regression." Nature **441**(7092): 437-443.

Powles, T., S. Chowdhury, R. Jones, M. Mantle, P. Nathan, A. Bex, L. Lim and T. Hutson (2011). "Sunitinib and other targeted therapies for renal cell carcinoma." Br J Cancer **104**(5): 741-745.

Powles, T., N. Sarwar, A. Stockdale, S. J. Sarker, E. Boleti, A. Protheroe, R. Jones, S. Chowdhury, J. Peters, G. Oades, T. O'Brien, M. Sullivan, M. Aitchison, L. Beltran, D. Worth, K. Smith, C. Michel, G. Trevisan, E. Harvey-Jones, A. Wimalasingham, A. Sahdev, C. Ackerman and S. Crabb (2016). "Safety and Efficacy of Pazopanib Therapy Prior to Planned Nephrectomy in Metastatic Clear Cell Renal Cancer." JAMA Oncol.

Powles, T., N. Sarwar, A. Stockdale, S. J. Sarker, E. Boleti, A. Protheroe, R. Jones, S. Chowdhury, J. Peters, G. Oades, T. O'Brien, M. Sullivan, M. Aitchison, L. Beltran, D. Worth, K. Smith, C. Michel, G. Trevisan, E. Harvey-Jones, A. Wimalasingham, A. Sahdev, C. Ackerman and S. Crabb (2016). "Safety and Efficacy of Pazopanib Therapy Prior to Planned Nephrectomy in Metastatic Clear Cell Renal Cancer." JAMA Oncol **2**(10): 1303-1309.

Purdue, M. P., M. Johansson, D. Zelenika, J. R. Toro, G. Scelo, L. E. Moore, E. Prokhortchouk, X. Wu, L. A. Kiemeney, V. Gaborieau, K. B. Jacobs, W. H. Chow, D. Zaridze, V. Matveev, J. Lubinski, J. Trubicka, N. Szeszenia-Dabrowska, J. Lissowska, P. Rudnai, E. Fabianova, A. Bucur, V. Bencko, L. Foretova, V. Janout, P. Boffetta, J. S. Colt, F. G. Davis, K. L. Schwartz, R. E. Banks, P. J. Selby, P. Harnden, C. D. Berg, A. W. Hsing, R. L. Grubb, 3rd, H. Boeing, P. Vineis, F. Clavel-Chapelon, D. Palli, R. Tumino, V. Krogh, S. Panico, E. J. Duell, J. R. Quiros, M. J. Sanchez, C. Navarro, E. Ardanaz, M. Dorronsoro, K. T. Khaw, N. E. Allen, H. B. Bueno-de-Mesquita, P. H. Peeters, D. Trichopoulos, J. Linseisen, B. Ljungberg, K. Overvad, A. Tjonneland, I. Romieu, E. Riboli, A. Mukeria, O. Shangina, V. L. Stevens, M. J. Thun, W. R. Diver, S. M. Gapstur, P. D. Pharoah, D. F. Easton, D. Albanes, S. J. Weinstein, J. Virtamo, L. Vatten, K. Hveem, I. Njolstad, G. S. Tell, C. Stoltenberg, R. Kumar, K. Koppova, O. Cussenot, S. Benhamou, E. Oosterwijk, S. H. Vermeulen, K. K. Aben, S. L. van der Marel, Y. Ye, C. G. Wood, X. Pu, A. M. Mazur, E. S. Boulygina, N. N. Chekanov, M. Foglio, D. Lechner, I. Gut, S. Heath, H. Blanche, A. Hutchinson, G. Thomas, Z. Wang, M. Yeager, J. F. Fraumeni, Jr., K. G. Skryabin, J. D. McKay, N. Rothman, S. J. Chanock, M. Lathrop and P. Brennan (2011). "Genome-wide association study of renal cell carcinoma identifies two susceptibility loci on 2p21 and 11q13.3." Nat Genet **43**(1): 60-65.

Pusztaszeri, M. P., W. Seelentag and F. T. Bosman (2006). "Immunohistochemical expression of endothelial markers CD31, CD34, von Willebrand factor, and Fli-1 in normal human tissues." J Histochem Cytochem **54**(4): 385-395.

Ramos-Vara, J. A., M. Kiupel, T. Baszler, L. Bliven, B. Brodersen, B. Chelack, S. Czub, F. Del Piero, S. Dial, E. J. Ehrhart, T. Graham, L. Manning, D. Paulsen, V. E. Valli, K. West and I. American Association of Veterinary Laboratory Diagnosticians Subcommittee on Standardization of (2008). "Suggested guidelines for immunohistochemical techniques in veterinary diagnostic laboratories." J Vet Diagn Invest **20**(4): 393-413.

Ramos-Vara, J. A. and M. A. Miller (2014). "When tissue antigens and antibodies get along: revisiting the technical aspects of immunohistochemistry--the red, brown, and blue technique." Vet Pathol **51**(1): 42-87.

Ramp, U., C. Mahotka, T. Kalinski, E. Ebel, H. E. Gabbert and C. D. Gerharz (2001). "Topotecan (Hycamtin) responsiveness in human renal carcinoma cell lines of the clear cell and papillary types." Anticancer Res **21**(5): 3509-3517.

Ratcliffe, P. J. (2003). "New insights into an enigmatic tumour suppressor." Nat Cell Biol **5**(1): 7-8.

Ratheesh, A., R. Priya and A. S. Yap (2013). "Coordinating Rho and Rac: the regulation of Rho GTPase signaling and cadherin junctions." Prog Mol Biol Transl Sci **116**: 49-68.

Rathmell, W. K. and P. A. Godley (2010). "Recent updates in renal cell carcinoma." Curr Opin Oncol **22**(3): 250-256.

Raval, R. R., K. W. Lau, M. G. Tran, H. M. Sowter, S. J. Mandriota, J. L. Li, C. W. Pugh, P. H. Maxwell, A. L. Harris and P. J. Ratcliffe (2005). "Contrasting properties of hypoxia-inducible factor 1 (HIF-1) and HIF-2 in von Hippel-Lindau-associated renal cell carcinoma." Mol Cell Biol **25**(13): 5675-5686.

Ravaud, A., R. Hawkins, J. P. Gardner, H. von der Maase, N. Zantl, P. Harper, F. Rolland, B. Audhuy, J. P. Machiels, F. Petavy, M. Gore, P. Schoffski and I. El-Hariry (2008). "Lapatinib versus hormone therapy in patients with advanced renal cell carcinoma: a randomized phase III clinical trial." J Clin Oncol **26**(14): 2285-2291.

Reddy, A. and W. G. Kaelin, Jr. (2002). "Using cancer genetics to guide the selection of anticancer drug targets." Curr Opin Pharmacol **2**(4): 366-373.

Renfranz, P. J., S. E. Siegrist, B. E. Stronach, T. Macalma and M. C. Beckerle (2003). "Molecular and phylogenetic characterization of Zyx102, a Drosophila orthologue of the zyxin family that interacts with Drosophila Enabled." Gene **305**(1): 13-26.

Rexer, H. (2015). "[Therapy of untreated local advanced or metastatic renal cell carcinoma. Phase III, randomized, open-label study of nivolumab combined with ipilimumab versus sunitinib monotherapy in subjects with previously untreated, local advanced or metastatic renal cell carcinoma (CheckMate 214 - AN 36/15 of the AUO)]." Urologe A **54**(10): 1443-1445.

Rexer, H., T. Steiner and L. Bergmann (2017). "[Nivolumab combined with ipilimumab versus sunitinib monotherapy-SUNNIFORECAST AN 41/16 of the AUO : A phase 2, randomized, open-label study in subjects with previously untreated and advanced (unresectable or metastatic) non-clear cell renal cell carcinoma]." Urologe A **56**(6): 802-803.

Rini, B. I. (2011). "Targeted therapy for patients with renal-cell carcinoma." Lancet Oncol **12**(12): 1085-1087.

Rini, B. I., S. Halabi, J. E. Rosenberg, W. M. Stadler, D. A. Vaena, L. Archer, J. N. Atkins, J. Picus, P. Czaykowski, J. Dutcher and E. J. Small (2010). "Phase III trial of bevacizumab plus interferon alfa versus interferon alfa monotherapy in patients with

metastatic renal cell carcinoma: final results of CALGB 90206." J Clin Oncol **28**(13): 2137-2143.

Riss, T. L., R. A. Moravec, A. L. Niles, H. A. Benink, T. J. Worzella and L. Minor (2004). Cell Viability Assays. Assay Guidance Manual. G. S. Sittampalam, N. P. Coussens, H. Nelson et al. Bethesda (MD).

Rizzardi, A. E., A. T. Johnson, R. I. Vogel, S. E. Pambuccian, J. Henriksen, A. P. Skubitz, G. J. Metzger and S. C. Schmechel (2012). "Quantitative comparison of immunohistochemical staining measured by digital image analysis versus pathologist visual scoring." Diagn Pathol **7**: 42.

Robinson, M. J. and M. H. Cobb (1997). "Mitogen-activated protein kinase pathways." Curr Opin Cell Biol **9**(2): 180-186.

Rodriguez, A., J. J. Patard and B. Lobel (2002). "Renal cell carcinoma in young adults: incidence, disease outcome and review of the literature." Arch Esp Urol **55**(8): 969-975.

Roldo, C., E. Missiaglia, J. P. Hagan, M. Falconi, P. Capelli, S. Bersani, G. A. Calin, S. Volinia, C. G. Liu, A. Scarpa and C. M. Croce (2006). "MicroRNA expression abnormalities in pancreatic endocrine and acinar tumors are associated with distinctive pathologic features and clinical behavior." J Clin Oncol **24**(29): 4677-4684.

Sakamoto, S., A. J. Ryan and N. Kyprianou (2008). "Targeting vasculature in urologic tumors: mechanistic and therapeutic significance." J Cell Biochem **103**(3): 691-708.

Samaan, S., H. W. Khella, A. Girgis, A. Scorilas, E. Lianidou, M. Gabril, S. N. Krylov, M. Jewett, G. A. Bjarnason, H. El-said and G. M. Yousef (2015). "miR-210 is a prognostic marker in clear cell renal cell carcinoma." J Mol Diagn **17**(2): 136-144.

Sandlund, J., Y. Hedberg, A. Bergh, K. Grankvist, B. Ljungberg and T. Rasmuson (2007). "Evaluation of CD31 (PECAM-1) expression using tissue microarray in patients with renal cell carcinoma." Tumour Biol **28**(3): 158-164.

Sato, Y., T. Yoshizato, Y. Shiraishi, S. Maekawa, Y. Okuno, T. Kamura, T. Shimamura, A. Sato-Otsubo, G. Nagae, H. Suzuki, Y. Nagata, K. Yoshida, A. Kon, Y. Suzuki, K. Chiba, H. Tanaka, A. Niida, A. Fujimoto, T. Tsunoda, T. Morikawa, D. Maeda, H. Kume, S. Sugano, M. Fukayama, H. Aburatani, M. Sanada, S. Miyano, Y. Homma and S. Ogawa (2013). "Integrated molecular analysis of clear-cell renal cell carcinoma." Nat Genet **45**(8): 860-867.

Schermer, B., C. Ghenoiu, M. Bartram, R. U. Muller, F. Kotsis, M. Hohne, W. Kuhn, M. Rapka, R. Nitschke, H. Zentgraf, M. Fliegauf, H. Omran, G. Walz and T. Benzing (2006). "The von Hippel-Lindau tumor suppressor protein controls ciliogenesis by orienting microtubule growth." J Cell Biol **175**(4): 547-554.

Schito, L. and G. L. Semenza (2016). "Hypoxia-Inducible Factors: Master Regulators of Cancer Progression." Trends Cancer **2**(12): 758-770.

Schmeichel, K. L. and M. J. Bissell (2003). "Modeling tissue-specific signaling and organ function in three dimensions." J Cell Sci **116**(Pt 12): 2377-2388.

Schoenfeld, A., E. J. Davidowitz and R. D. Burk (1998). "A second major native von Hippel-Lindau gene product, initiated from an internal translation start site, functions as a tumor suppressor." Proc Natl Acad Sci U S A **95**(15): 8817-8822.

Schoenfeld, A. R., E. J. Davidowitz and R. D. Burk (2000). "Elongin BC complex prevents degradation of von Hippel-Lindau tumor suppressor gene products." Proc Natl Acad Sci U S A **97**(15): 8507-8512.

Schorl, C. and J. M. Sedivy (2007). "Analysis of cell cycle phases and progression in cultured mammalian cells." Methods **41**(2): 143-150.

Schutte, U., S. Bisht, L. C. Heukamp, M. Kebschull, A. Florin, J. Haarmann, P. Hoffmann, G. Bendas, R. Buettner, P. Brossart and G. Feldmann (2014). "Hippo signaling mediates proliferation, invasiveness, and metastatic potential of clear cell renal cell carcinoma." Transl Oncol **7**(2): 309-321.

Sedor, J. R., S. M. Madhavan, J. H. Kim and M. Konieczkowski (2011). "Out on a LIM: chronic kidney disease, podocyte phenotype and the Wilm's tumor interacting protein (WTIP)." Trans Am Clin Climatol Assoc **122**: 184-197.

Seidal, T., A. J. Balaton and H. Battifora (2001). "Interpretation and quantification of immunostains." Am J Surg Pathol **25**(9): 1204-1207.

Shaltiel, I. A., L. Krenning, W. Bruinsma and R. H. Medema (2015). "The same, only different - DNA damage checkpoints and their reversal throughout the cell cycle." J Cell Sci **128**(4): 607-620.

Shamash, J., T. Powles, P. Wilson, W. Ansell and T. Oliver (2005). "Prognostic factors in cytokine-refractory renal cell carcinoma treated with irinotecan, Cisplatin, and mitomycin chemotherapy." J Clin Oncol **23**(6): 1323-1325.

Sharma, S. V., D. A. Haber and J. Settleman (2010). "Cell line-based platforms to evaluate the therapeutic efficacy of candidate anticancer agents." Nat Rev Cancer **10**(4): 241-253.

Sharp, T. V., A. Al-Attar, D. E. Foxler, L. Ding, A. V. T. Q. de, Y. Zhang, H. S. Nijmeh, T. M. Webb, A. G. Nicholson, Q. Zhang, A. Kraja, I. Spendlove, J. Osborne, E. Mardis and G. D. Longmore (2008). "The chromosome 3p21.3-encoded gene, LIMD1, is a critical tumor suppressor involved in human lung cancer development." Proc Natl Acad Sci U S A **105**(50): 19932-19937.

Sharp, T. V., F. Munoz, D. Bourboulia, N. Presneau, E. Darai, H. W. Wang, M. Cannon, D. N. Butcher, A. G. Nicholson, G. Klein, S. Imreh and C. Boshoff (2004). "LIM domains-containing protein 1 (LIMD1), a tumor suppressor encoded at

chromosome 3p21.3, binds pRB and represses E2F-driven transcription." Proc Natl Acad Sci U S A **101**(47): 16531-16536.

Sheehan, J. P., M. H. Sun, D. Kondziolka, J. Flickinger and L. D. Lunsford (2003). "Radiosurgery in patients with renal cell carcinoma metastasis to the brain: long-term outcomes and prognostic factors influencing survival and local tumor control." J Neurosurg **98**(2): 342-349.

Shen, C., R. Beroukhim, S. E. Schumacher, J. Zhou, M. Chang, S. Signoretti and W. G. Kaelin, Jr. (2011). "Genetic and functional studies implicate HIF1alpha as a 14q kidney cancer suppressor gene." Cancer Discov **1**(3): 222-235.

Shi, X., Z. Chen, X. Hu, M. Luo, Z. Sun, J. Li, S. Shi, X. Feng, C. Zhou, Z. Li, W. Yang, Y. Li, P. Wang, F. Zhou, Y. Gao and J. He (2016). "AJUBA promotes the migration and invasion of esophageal squamous cell carcinoma cells through upregulation of MMP10 and MMP13 expression." Oncotarget.

Shrout, P. E. and J. L. Fleiss (1979). "Intraclass correlations: uses in assessing rater reliability." Psychol Bull **86**(2): 420-428.

Simon, R. M., S. Paik and D. F. Hayes (2009). "Use of archived specimens in evaluation of prognostic and predictive biomarkers." J Natl Cancer Inst **101**(21): 1446-1452.

Solary, E., R. Bertrand and Y. Pommier (1994). "Apoptosis induced by DNA topoisomerase I and II inhibitors in human leukemic HL-60 cells." Leuk Lymphoma **15**(1-2): 21-32.

Song, T., X. Zhang, C. Wang, Y. Wu, W. Cai, J. Gao and B. Hong (2011). "MiR-138 suppresses expression of hypoxia-inducible factor 1alpha (HIF-1alpha) in clear cell renal cell carcinoma 786-O cells." Asian Pac J Cancer Prev **12**(5): 1307-1311.

Spendlove, I., A. Al-Attar, O. Watherstone, T. M. Webb, I. O. Ellis, G. D. Longmore and T. V. Sharp (2008). "Differential subcellular localisation of the tumour suppressor protein LIMD1 in breast cancer correlates with patient survival." Int J Cancer **123**(10): 2247-2253.

Srichai, M. B., M. Konieczkowski, A. Padiyar, D. J. Konieczkowski, A. Mukherjee, P. S. Hayden, S. Kamat, M. A. El-Meanawy, S. Khan, P. Mundel, S. B. Lee, L. A. Bruggeman, J. R. Schelling and J. R. Sedor (2004). "A WT1 co-regulator controls podocyte phenotype by shuttling between adhesion structures and nucleus." J Biol Chem **279**(14): 14398-14408.

Srigley, J. R., B. Delahunt, J. N. Eble, L. Egevad, J. I. Epstein, D. Grignon, O. Hes, H. Moch, R. Montironi, S. K. Tickoo, M. Zhou, P. Argani and I. R. T. Panel (2013). "The International Society of Urological Pathology (ISUP) Vancouver Classification of Renal Neoplasia." Am J Surg Pathol **37**(10): 1469-1489.

Stebbins, C. E., W. G. Kaelin, Jr. and N. P. Pavletich (1999). "Structure of the VHL-ElonginC-ElonginB complex: implications for VHL tumor suppressor function." Science **284**(5413): 455-461.

Stein, A., J. Bellmunt, B. Escudier, D. Kim, S. G. Stergiopoulos, W. Mietlowski, R. J. Motzer and R.-T. S. Group (2013). "Survival prediction in everolimus-treated patients with metastatic renal cell carcinoma incorporating tumor burden response in the RECORD-1 trial." Eur Urol **64**(6): 994-1002.

Sternberg, C. N., I. D. Davis, J. Mardiak, C. Szczylik, E. Lee, J. Wagstaff, C. H. Barrios, P. Salman, O. A. Gladkov, A. Kavina, J. J. Zarba, M. Chen, L. McCann, L. Pandite, D. F. Roychowdhury and R. E. Hawkins (2010). "Pazopanib in locally advanced or metastatic renal cell carcinoma: results of a randomized phase III trial." J Clin Oncol **28**(6): 1061-1068.

Sudarshan, S. and W. M. Linehan (2006). "Genetic basis of cancer of the kidney." Semin Oncol **33**(5): 544-551.

Sur, S., A. K. Maurya, A. Roy, T. V. Sharp, D. K. Pal and C. K. Panda (2017). "Over expression of HIF1alpha is associated with inactivation of both LimD1 and VHL in renal cell carcinoma: Clinical importance." Pathol Res Pract **213**(12): 1477-1481.

Tahiliani, M., K. P. Koh, Y. Shen, W. A. Pastor, H. Bandukwala, Y. Brudno, S. Agarwal, L. M. Iyer, D. R. Liu, L. Aravind and A. Rao (2009). "Conversion of 5-methylcytosine to 5-hydroxymethylcytosine in mammalian DNA by MLL partner TET1." Science **324**(5929): 930-935.

Tanaka, I., H. Osada, M. Fujii, A. Fukatsu, T. Hida, Y. Horio, Y. Kondo, A. Sato, Y. Hasegawa, T. Tsujimura and Y. Sekido (2015). "LIM-domain protein AJUBA suppresses malignant mesothelioma cell proliferation via Hippo signaling cascade." Oncogene **34**(1): 73-83.

Tanaka, Y., S. Nakayamada and Y. Okada (2005). "Osteoblasts and osteoclasts in bone remodeling and inflammation." Curr Drug Targets Inflamm Allergy **4**(3): 325-328.

Tang, P. A., M. M. Vickers and D. Y. Heng (2011). "Clinical and molecular prognostic factors in renal cell carcinoma: what we know so far." Hematol Oncol Clin North Am **25**(4): 871-891.

Tannir, N. M., G. Schwab and V. Grunwald (2017). "Cabozantinib: an Active Novel Multikinase Inhibitor in Renal Cell Carcinoma." Curr Oncol Rep **19**(2): 14.

Thiery, J. P. (2003). "Epithelial-mesenchymal transitions in development and pathologies." Curr Opin Cell Biol **15**(6): 740-746.

Thiesen, H. J., F. Steinbeck, M. Maruschke, D. Koczan, B. Ziems and O. W. Hakenberg (2017). "Stratification of clear cell renal cell carcinoma (ccRCC) genomes by gene-directed copy number alteration (CNA) analysis." PLoS One **12**(5): e0176659.

Thoma, C. R., A. Toso, K. L. Gutbrodt, S. P. Reggi, I. J. Frew, P. Schraml, A. Hergovich, H. Moch, P. Meraldi and W. Krek (2009). "VHL loss causes spindle misorientation and chromosome instability." Nat Cell Biol **11**(8): 994-1001.

Thompson, R. H., H. Dong, C. M. Lohse, B. C. Leibovich, M. L. Blute, J. C. Cheville and E. D. Kwon (2007). "PD-1 is expressed by tumor-infiltrating immune cells and is associated with poor outcome for patients with renal cell carcinoma." Clin Cancer Res **13**(6): 1757-1761.

Thornburg, N. J., W. Kulwichit, R. H. Edwards, K. H. Shair, K. M. Bendt and N. Raab-Traub (2006). "LMP1 signaling and activation of NF-kappaB in LMP1 transgenic mice." Oncogene **25**(2): 288-297.

Tobe, S. W., S. E. Noble-Topham, I. L. Andrulis, R. W. Hartwick, K. L. Skorecki and E. Warner (1995). "Expression of the multiple drug resistance gene in human renal cell carcinoma depends on tumor histology, grade, and stage." Clin Cancer Res **1**(12): 1611-1615.

Tong, Y., Q. G. Li, T. Y. Xing, M. Zhang, J. J. Zhang and Q. Xia (2013). "HIF1 regulates WSB-1 expression to promote hypoxia-induced chemoresistance in hepatocellular carcinoma cells." FEBS Lett **587**(16): 2530-2535.

Topalian, S. L., C. G. Drake and D. M. Pardoll (2015). "Immune checkpoint blockade: a common denominator approach to cancer therapy." Cancer Cell **27**(4): 450-461.

Toschi, A., E. Lee, N. Gadir, M. Ohh and D. A. Foster (2008). "Differential dependence of hypoxia-inducible factors 1 alpha and 2 alpha on mTORC1 and mTORC2." J Biol Chem **283**(50): 34495-34499.

Tran, H. T., Y. Liu, A. J. Zurita, Y. Lin, K. L. Baker-Neblett, A. M. Martin, R. A. Figlin, T. E. Hutson, C. N. Sternberg, R. G. Amado, L. N. Pandite and J. V. Heymach (2012). "Prognostic or predictive plasma cytokines and angiogenic factors for patients treated with pazopanib for metastatic renal-cell cancer: a retrospective analysis of phase 2 and phase 3 trials." Lancet Oncol **13**(8): 827-837.

Turbin, D. A., S. Leung, M. C. Cheang, H. A. Kennecke, K. D. Montgomery, S. McKinney, D. O. Treaba, N. Boyd, L. C. Goldstein, S. Badve, A. M. Gown, M. van de Rijn, T. O. Nielsen, C. B. Gilks and D. G. Huntsman (2008). "Automated quantitative analysis of estrogen receptor expression in breast carcinoma does not differ from expert pathologist scoring: a tissue microarray study of 3,484 cases." Breast Cancer Res Treat **110**(3): 417-426.

Turcotte, S., D. A. Chan, P. D. Sutphin, M. P. Hay, W. A. Denny and A. J. Giaccia (2008). "A molecule targeting VHL-deficient renal cell carcinoma that induces autophagy." Cancer Cell **14**(1): 90-102.

Uniacke, J., C. E. Holterman, G. Lachance, A. Franovic, M. D. Jacob, M. R. Fabian, J. Payette, M. Holcik, A. Pause and S. Lee (2012). "An oxygen-regulated switch in the protein synthesis machinery." Nature **486**(7401): 126-129.

van der Veldt, A. A., K. Eechoute, H. Gelderblom, J. Gietema, H. J. Guchelaar, N. P. van Erp, A. J. van den Eertwegh, J. B. Haanen, R. H. Mathijssen and J. A. Wessels (2011). "Genetic polymorphisms associated with a prolonged progression-free survival in patients with metastatic renal cell cancer treated with sunitinib." Clin Cancer Res **17**(3): 620-629.

van Wijk, N. V., F. Witte, A. C. Feike, A. Schambony, W. Birchmeier, S. Mundlos and S. Stricker (2009). "The LIM domain protein Wtip interacts with the receptor tyrosine kinase Ror2 and inhibits canonical Wnt signalling." Biochem Biophys Res Commun **390**(2): 211-216.

Vanharanta, S., W. Shu, F. Brenet, A. A. Hakimi, A. Heguy, A. Viale, V. E. Reuter, J. J. Hsieh, J. M. Scandura and J. Massague (2013). "Epigenetic expansion of VHL-HIF signal output drives multiorgan metastasis in renal cancer." Nat Med **19**(1): 50-56.

Varela, I., P. Tarpey, K. Raine, D. Huang, C. K. Ong, P. Stephens, H. Davies, D. Jones, M. L. Lin, J. Teague, G. Bignell, A. Butler, J. Cho, G. L. Dalgliesh, D. Galappaththige, C. Greenman, C. Hardy, M. Jia, C. Latimer, K. W. Lau, J. Marshall, S. McLaren, A. Menzies, L. Mudie, L. Stebbings, D. A. Largaespada, L. F. Wessels, S. Richard, R. J. Kahnoski, J. Anema, D. A. Tuveson, P. A. Perez-Mancera, V. Mustonen, A. Fischer, D. J. Adams, A. Rust, W. Chan-on, C. Subimerb, K. Dykema, K. Furge, P. J. Campbell, B. T. Teh, M. R. Stratton and P. A. Futreal (2011). "Exome sequencing identifies frequent mutation of the SWI/SNF complex gene PBRM1 in renal carcinoma." Nature **469**(7331): 539-542.

Varghese, F., A. B. Bukhari, R. Malhotra and A. De (2014). "IHC Profiler: an open source plugin for the quantitative evaluation and automated scoring of immunohistochemistry images of human tissue samples." PLoS One **9**(5): e96801.

Wang, J., L. Y. Xie, S. Allan, D. Beach and G. J. Hannon (1998). "Myc activates telomerase." Genes Dev **12**(12): 1769-1774.

Wang, L., M. E. A. Howell, B. McPeak, K. Riggs, C. Kohne, J. U. Yohanon, D. E. Foxler, T. V. Sharp, J. P. Moorman, Z. Q. Yao and S. Ning (2018). "LIMD1 is induced by and required for LMP1 signaling, and protects EBV-transformed cells from DNA damage-induced cell death." Oncotarget **9**(5): 6282-6297.

Wang, L., Z. Q. Yao, J. P. Moorman, Y. Xu and S. Ning (2014). "Gene expression profiling identifies IRF4-associated molecular signatures in hematological malignancies." PLoS One **9**(9): e106788.

Wang, Y., J. Shi, K. Chai, X. Ying and B. P. Zhou (2013). "The Role of Snail in EMT and Tumorigenesis." Curr Cancer Drug Targets **13**(9): 963-972.

Webb, J. D., M. L. Coleman and C. W. Pugh (2009). "Hypoxia, hypoxia-inducible factors (HIF), HIF hydroxylases and oxygen sensing." Cell Mol Life Sci **66**(22): 3539-3554.

Webb, M. R. and S. E. Ebeler (2003). "A gel electrophoresis assay for the simultaneous determination of topoisomerase I inhibition and DNA intercalation." Anal Biochem **321**(1): 22-30.

Wright, G., B. Tan, A. Rosenwald, E. H. Hurt, A. Wiestner and L. M. Staudt (2003). "A gene expression-based method to diagnose clinically distinct subgroups of diffuse large B cell lymphoma." Proc Natl Acad Sci U S A **100**(17): 9991-9996.

Wu, R., K. Durick, Z. Songyang, L. C. Cantley, S. S. Taylor and G. N. Gill (1996). "Specificity of LIM domain interactions with receptor tyrosine kinases." J Biol Chem **271**(27): 15934-15941.

Xie, R., J. Y. Chung, K. Ylaya, R. L. Williams, N. Guerrero, N. Nakatsuka, C. Badie and S. M. Hewitt (2011). "Factors influencing the degradation of archival formalin-fixed paraffin-embedded tissue sections." J Histochem Cytochem **59**(4): 356-365.

Xu, M. Z., T. J. Yao, N. P. Lee, I. O. Ng, Y. T. Chan, L. Zender, S. W. Lowe, R. T. Poon and J. M. Luk (2009). "Yes-associated protein is an independent prognostic marker in hepatocellular carcinoma." Cancer **115**(19): 4576-4585.

Xu, Q., C. Tan, S. Ni, Q. Wang, F. Wu, F. Liu, X. Ye, X. Meng, W. Sheng and X. Du (2015). "Identification and validation of a two-gene expression index for subtype classification and prognosis in Diffuse Large B-Cell Lymphoma." Sci Rep **5**: 10006.

Xu, Y. and M. A. Villalona-Calero (2002). "Irinotecan: mechanisms of tumor resistance and novel strategies for modulating its activity." Ann Oncol **13**(12): 1841-1851.

Yang, J. C., M. Hughes, U. Kammula, R. Royal, R. M. Sherry, S. L. Topalian, K. B. Suri, C. Levy, T. Allen, S. Mavroukakis, I. Lowy, D. E. White and S. A. Rosenberg (2007). "Ipilimumab (anti-CTLA4 antibody) causes regression of metastatic renal cell cancer associated with enteritis and hypophysitis." J Immunother **30**(8): 825-830.

Yang, Q., G. Yoshimura, I. Mori, T. Sakurai and K. Kakudo (2002). "Chromosome 3p and breast cancer." J Hum Genet **47**(9): 453-459.

Yao, X., C. N. Qian, Z. F. Zhang, M. H. Tan, E. J. Kort, X. J. Yang, J. H. Resau and B. T. Teh (2007). "Two distinct types of blood vessels in clear cell renal cell carcinoma have contrasting prognostic implications." Clin Cancer Res **13**(1): 161-169.

Yap, T. A., S. K. Sandhu, C. P. Carden and J. S. de Bono (2011). "Poly(ADP-ribose) polymerase (PARP) inhibitors: Exploiting a synthetic lethal strategy in the clinic." CA Cancer J Clin **61**(1): 31-49.

Yaziji, H. and T. Barry (2006). "Diagnostic Immunohistochemistry: what can go wrong?" Adv Anat Pathol **13**(5): 238-246.

Yildiz, E., G. Gokce, H. Kilicarslan, S. Ayan, O. F. Goze and E. Y. Gultekin (2004). "Prognostic value of the expression of Ki-67, CD44 and vascular endothelial growth factor, and microvessel invasion, in renal cell carcinoma." BJU Int **93**(7): 1087-1093.

Zbar, B., H. Brauch, C. Talmadge and M. Linehan (1987). "Loss of alleles of loci on the short arm of chromosome 3 in renal cell carcinoma." Nature **327**(6124): 721-724.

Zeng, Q. and W. Hong (2008). "The emerging role of the hippo pathway in cell contact inhibition, organ size control, and cancer development in mammals." Cancer Cell **13**(3): 188-192.

Zhang, H., P. Gao, R. Fukuda, G. Kumar, B. Krishnamachary, K. I. Zeller, C. V. Dang and G. L. Semenza (2007). "HIF-1 inhibits mitochondrial biogenesis and cellular respiration in VHL-deficient renal cell carcinoma by repression of C-MYC activity." Cancer Cell **11**(5): 407-420.

Zhao, B., K. Tumaneng and K. L. Guan (2011). "The Hippo pathway in organ size control, tissue regeneration and stem cell self-renewal." Nat Cell Biol **13**(8): 877-883.

Zhao, B., X. Wei, W. Li, R. S. Udan, Q. Yang, J. Kim, J. Xie, T. Ikenoue, J. Yu, L. Li, P. Zheng, K. Ye, A. Chinnaiyan, G. Halder, Z. C. Lai and K. L. Guan (2007). "Inactivation of YAP oncoprotein by the Hippo pathway is involved in cell contact inhibition and tissue growth control." Genes Dev **21**(21): 2747-2761.

Zhou, L., X. D. Liu, M. Sun, X. Zhang, P. German, S. Bai, Z. Ding, N. Tannir, C. G. Wood, S. F. Matin, J. A. Karam, P. Tamboli, K. Sircar, P. Rao, E. B. Rankin, D. A. Laird, A. G. Hoang, C. L. Walker, A. J. Giaccia and E. Jonasch (2016). "Targeting MET and AXL overcomes resistance to sunitinib therapy in renal cell carcinoma." Oncogene **35**(21): 2687-2697.

Zigeuner, R., G. Hutterer, T. Chromecki, A. Imamovic, K. Kampel-Kettner, P. Rehak, C. Langner and K. Pummer (2010). "External validation of the Mayo Clinic stage, size, grade, and necrosis (SSIGN) score for clear-cell renal cell carcinoma in a single European centre applying routine pathology." Eur Urol **57**(1): 102-109.

Zisman, A., A. J. Pantuck, F. Dorey, J. W. Said, O. Shvarts, D. Quintana, B. J. Gitlitz, J. B. deKernion, R. A. Figlin and A. S. Belldegrun (2001). "Improved prognostication of renal cell carcinoma using an integrated staging system." J Clin Oncol **19**(6): 1649-1657.

Zlobec, I., R. Steele, R. P. Michel, C. C. Compton, A. Lugli and J. R. Jass (2006). "Scoring of p53, VEGF, Bcl-2 and APAF-1 immunohistochemistry and interobserver reliability in colorectal cancer." Mod Pathol **19**(9): 1236-1242.